Acta Geodaetica, Geophysica et Montanistica Hungarica

VOLUME 22, NUMBERS 1–2, 1987

Akadémiai Kiadó, Budapest
AGGM 22 (1–2) 1–332 (1987) HU ISSN 0236-5758

ACTA GEODAETICA, GEOPHYSICA et MONTANISTICA HUNGARICA
A Quarterly Journal of the Hungarian Academy of Sciences

Acta Geodaetica, Geophysica et Montanistica (AGGM) publishes original reports on geodesy, geophysics and minings in English.

AGGM is published in yearly volumes of four numbers by

AKADÉMIAI KIADÓ
Publishing House of the Hungarian Academy of Sciences
H-1054 Budapest, Alkotmány u. 21.

Manuscripts and editorial correspondence should be addressed to

AGGM Editorial Office
H-9401 Sopron P.O. Box 5

Subscription information

Orders should be addressed to

KULTURA Foreign Trading Company
H-1389 Budapest P.O. Box 149

INSTRUCTIONS TO AUTHORS

Manuscripts should be sent to the editors (MTA Geodéziai és Geofizikai Kutató Intézete, AGGM Editorial Office, H-9401 Sopron, P.O.Box 5, HUNGARY). Only articles not submitted for publication elsewhere are accepted.

Manuscripts should be typewritten in duplicate, double-spaced, 25 lines with 50 letters each. The papers generally include the following components, which should be presented in the order listed.

1. Title, name of author(s), affiliation, dateline, abstract, keywords
2. Text, acknowledgements
3. References
4. Footnotes
5. Legends
6. Tables and illustrations

1. The *affiliation* should be as concise as possible and should include the complete mailing address of the authors. The *date of receipt* of the manuscript will be supplied by the editors. The abstract should not exceed 250 words and should clearly and simply summarize the most important methods and results. 5–10 significant expressions describing the content are used as *keywords*. Authors may recommend these keywords.

2. The *text* should be generally in English and as short and clear as possible. From Hungarian authors papers are also accepted in Hungarian.

The section heading should *not* be underlined or in capitals.

Please note that underlining denotes special types:

– single underlining: italics
— double underlining: bold-face roman

ACTA GEODAETICA, GEOPHYSICA et MONTANISTICA HUNGARICA

A Quarterly Journal of the Hungarian Academy of Sciences

VOLUME 22

Akadémiai Kiadó, Budapest
1987

CONTENTS

Book Reviews

AUTHOR INDEX

KEYWORD INDEX

CONTENTS

Foreword

In this number of Acta Geodaetica, Geophysica et Montanistica Hungarica papers are published which were presented at the first seminar devoted to the problems of ionospheric irregularities and aeronomy of the upper atmosphere in Sopron, Hungary, April 9-13, 1985. The seminar was sponsored by the Committee on Planetary Geophysics (KAPG) working in the framework of the academies of sciences in the Socialist countries. The topics discussed at the seminar covered the structure of ionospheric irregularities, the study of the sporadic E layer, wind systems in the upper atmosphere, atmospheric waves, turbulence and aeronomical processes, origin and transformation of the irregularities in the ionosphere, as well as origin of the sporadic E layer. For the introduction of the most important problems discussed at the seminar papers were invited. In these invited papers the irregular structure of the F region and of the outer ionosphere and related phenomena, the turbulence and aeronomic processes in the lower thermosphere were reviewed. Besides these three invited review papers 25 contributed papers were presented in 5 half-day sessions.

It was obviously not possible to discuss all aspects of ionospheric irregularities and problems related to their formation. Thus, the papers dealt mainly with the ground based observations of ionospheric irregularities and related phenomena, which limited in advance the topic. Nevertheless, this collection of papers gives an overview of the present situation in the investigation of ionospheric irregularities and also shows those trends which developed in these countries. Thus, it indicates also those problems which will be studied in the next years.

P Bencze

Geodetic and Geophysical Research Institute, Hungarian Academy of Sciences, Sopron, Hungary

Acta Geod. Geoph. Mont. Hung., Vol. 22 (1-2), pp. 5-45 (1987)

THE IRREGULAR STRUCTURE OF THE F REGION AND THE OUTER IONOSPHERE

M N Fatkullin

Institute of Geomagnetism, Ionosphere and Radio Wave Propagation (IZMIRAN),
Academy of Sciences of the USSR, 142092 Troitsk,
Moskovskaya oblast, USSR

The present state of the investigation concerning the irregular structure of the F region and the outer ionosphere is reviewed. The review deals with questions as the experimental methods, results of the measurements carried out by radiophysical and in-situ methods, occurrence of irregularities in the different plasmaparameters, models of the electron density irregularities and physical mechanisms of the formation of irregularities at the heights studied here. Tasks of future investigations are also discussed.

Keywords: irregularities; plasma instabilities; radiophysical methods

1. INTRODUCTION

The plasma in the ionosphere is an irregular and non-stationary medium concerning its spatial structure with a broad spectrum of characteristic space and time scales. During the last 10 to 15 years it became clear that these irregularities appear not only in the electron concentration (n_e), but also in other parameters of the ionized and neutral component, although the occurrence of the irregularities in the different parameters has not been uniformly studied. The characteristic spatial scales of the electron density irregularities vary from a meter to some thousands of kilometers depending on different conditions.

Let X be the local value of a certain parameter of the ionosphere in a certain moment and $X_0(\underline{r}, t)$ the space and time average or the background value of $X(\underline{r}, t)$. By an irregularity of the parameter X the quantity $\Delta X = X(\underline{r}, t) - X_0(\underline{r}, t)$ is understood and as a measure of the irregularity the mean square fluctuation of the parameter X is generally used, i.e. the

quantity $\overline{(\Delta X^2)} = \overline{(X^2)} - \overline{(X)^2}$, where the overbar indicates mean value and also the relative fluctuation $\delta X = \left[\overline{(\Delta X)^2}\right]^{1/2} / X_0$ is calculated, i.e. the relative error obtained by replacing X by its mean value X_0. In such an approximation $X_0(\underline{r}, t)$ comprises the "regular" large scale irregular structure of the ionosphere, e.g. regular height, latitudinal and longitudinal variations of its parameters.

The investigation of the irregular structure of the ionosphere by radiophysical methods, especially by the bottomside vertical sounding began in the mid-thirties after the discovery of the spread-F and sporadic E layers in the equatorial ionosphere (Berkner and Wells 1934, Booker and Wells 1938).

In the last years the interest in the study of the irregular structure of the F region and of the outer ionosphere increased from both experimental and theoretical points of view. As a consequence of the intense studies concerning the irregular structure of the ionosphere in the height region considered, a series of monographs, reviews and numerous original papers were published in the last years.

Considering the irregular structure of the ionosphere a very important aspect is the study of the conditions connected with artificial disturbances of the ionospheric plasma, when the disturbing factor is controlled and the initial conditions are known. The artificial disturbance of the ionospheric plasma can be produced by different procedures: heating by radio waves, injection of bundles of energetic particles, nuclear and industrial explosions, aerodynamic effect of rockets and satellites, release of chemically active and inactive materials. Effects in the ionosphere connected with earthquakes and volcanic eruptions belong to this circle of phenomena, too. Individual aspects of the irregular structure of the ionosphere in the presence of artificial effects of different origins are discussed e.g. in the reviews by Davis (1979), Karlov et al. (1980), Winkler (1980) and in the collection of papers "Non-linear thermal phenomena in the plasma" (1979).

Here, attention is devoted to the results of investigation of the irregular F region and the outer ionosphere in natural conditions. An attempt is made to generalize the up-to-

-date results and to discuss unsolved problems. Because of the great number of papers concerning this problem it will be referred only to papers in which detailed reviews of original studies can be found.

2. EXPERIMENTAL METHODS FOR THE STUDY OF THE IRREGULAR STRUCTURE OF THE IONOSPHERE

The known and relatively new methods used at present for the investigation of the irregular structure of the ionosphere, first of all for the study of the irregularities of the electron density can be devided into direct, in-situ measurements carried out by means of rockets and satellites, and into radiophysical methods. In other words, the irregular structure of the ionosphere is studied practically by the same methods which are generally used in ionospheric investigations. Merits and deficiencies of each method are known well enough. Therefore, here only some comments will be made which may be useful in the estimation of the completeness and adequacy of the experimental information concerning the parameters characterizing the irregular structure of the ionosphere.

2.1 Methods of the direct measurement of the ionospheric parameters

The direct methods are discussed in detail by Bauer and Nagy (1975) and by Fejer and Kelley (1980). By direct measurements, as it is known, experiments are meant, which enable the determination of the parameters of the medium in the vicinity of the flying object carrying the measuring tool.*

At present in-situ methods are used for the measurement of such important parameters of the ionospheric plasma as the concentration, temperature, chemical composition and the velocity of the ordered motion of the ionized and neutral components, as well as electric and magnetic fields. For the measurement of the concentration and temperature (T_e and T_i) of the charged

*This does not refer to the remote sounding of the ionosphere by satellites.

particles Langmuir-probes, retarding potential analyzers and high frequency methods with different modifications are used. The ion composition is measured by means of mass spectrometers of different types (Bennett type radiofrequency, with magnetic deflection and quadrupole). The density, temperature and chemical composition of the neutral upper atmosphere is determined by the measurement of the drag of satellites and by means of microphon detectors and mass spectrometers, respectively.

When measuring in-situ the absolute values of different ionospheric parameters, a number of uncertainties and difficulties arise. As regards the irregular structure of the ionosphere, when mainly the relative quantities of the type δn_e are of interest, these uncertainties in the absolute values are insignificant.

In-situ measurements of the parameters of the ionospheric irregularities by means of satellites are certainly valuable and useful. Nevertheless, it is useful to consider some shortcomings of these methods (Gdalevich 1980, Fatkullin 1982).

1. Probe measurements on board of satellites enable the determination of characteristics of the irregularities along the satellite's orbit, in addition, as it is known the satellite intersects the geomagnetic field lines in different latitudes at different angles. Therefore, it is not always possible to identify this type of data with the physical concepts of the transverse (to the Earth's magnetic field) and longitudinal (along the magnetic field) dimensions of the ionospheric irregularities. Because of the conditions mentioned above, the dimensions of the irregularities are according to the data of in-situ satellite measurements smaller at high latitudes and larger at low latitudes than in reality (Gdalevich 1980).

2. It is not possible to distinguish the spatial (latitude, longitude, height) characteristics of the irregularities from their time variations considering individual transitions of a satellite. If the height of the satellite is also fixed, different physical phenomena are recorded at different latitudes because of the variation of the physical conditions (especially that of the ion composition) with latitude, with

hour of the day etc.

3. The scale of the irregularities along the satellite's orbit is determined by "the resolving power", i.e. by the speed of sampling of the actual instrument. Therefore, if at the time of an in-situ satellite measurement irregularities with characteristic dimension $l \geqslant l_0$ along the satellite's orbit were observed, then this does not mean the absence of irregularities $l_0 \geqslant l$ under the conditions of this experiment.

4. Ion traps with electrodes of constant potential are used in some satellite experiments for the investigation of the characteristics of irregularities and the changes of the ion current $j_i = en_i\,(\underline{u}_S + \underline{v}_i)$ are mesured where n_i is the total ion density, $\underline{u}_S$ is the velocity of the satellite and $\underline{v}_i$ is the velocity of motion of the irregularities (or that of the wave propagation causing the irregularities of the concentration of charged particles). Obviously the dimensions of the irregularities obtained at the analysis of the data of in-situ satellite measurements cannot correspond to the real conditions in case of $(\tilde{\underline{v}}_i) \gtrsim (\underline{u}_S)$. An analysis of the data of the measurements carried out on board of the satellite IK-8 has shown that at low latitudes changes of the ion current are mainly due to corresponding variations of the total ion density (i.e. $\delta j \sim \delta n_i$) and at high latitudes the change of the velocity $\delta \tilde{v}_i$ contributes also to δj_i (Serafimov et al. 1976).

5. The frequency characteristics of the ionospheric irregularities depend on the Doppler-effect: $f_H = \left| f - \frac{1}{2\pi} (\underline{k}\ \underline{u}_S) \right|$, where f_H is the frequency of the oscillations observed at the satellite, $k = (2\pi/\lambda)$ is the wave number (λ is the wave length of the observed oscillations).

2.2 Radiophysical methods of the investigation of ionospheric irregularities

The different radiophysical methods of the investigation of the ionosphere have been described in details (Davies 1962, Evans 1969, Eccles and King 1970, Farley 1971, Galkin et al. 1971, Migulin 1973, Evans 1974, 1975, Namazov et al. 1975, Migulin et al. 1978, Fejer and Kelley 1980, Afraymovich 1982,

Hanuise 1983). Here they are discussed from the point of view of their applicability for the investigation of the irregular structure of the ionosphere.

Radiophysical methods are based on the solution of the inverse problem, where the parameters of the ionosphere affecting the propagation of radio waves are determined on the basis of the characteristics of radio signals reflected, scattered or transmitted by the ionosphere. Such parameters are the amplitude, phase, the time of retardation, the angle of incidence, the polarization and the diffuse character of the signals received.

The ground based radiophysical methods can be summarized in the followings.

1. Standard vertical sounding. By this method an ionogram, i.e. the virtual height of the reflections at a fixed frequency $h'(f = \text{const}, t)$ is recorded. The measurement of $h'(f = \text{const}, t)$ enables the study of travelling ionospheric disturbances (TID) and in case of measurements at three or more points the estimation of the velocity and direction of TID-s. Different types of the spread-F phenomenon and disturbances of the electron density appearing on ionograms in form of slopes or hooks are investigated. The analysis of multiple reflections enables the study of medium scale irregularities taking into account the intensity of the different multiple reflections.

2. Oblique incidence and back scatter soundings especially in case of transmission paths of great lengths do not have sufficient spatial resolution for an investigation of the irregular structure of the ionosphere (Namazov and Novikov 1980).

3. Vertical sounding of the ionosphere by signals intricately modulated and compressed in time or in frequency. A resolution of 0.75-1.5 km in the virtual height can be reached in this case while the resolution in virtual height amounts to 15 km with standard ionosondes in case of a duration of 100 μs of the impulses.

4. Measurement of the Doppler shift of fixed frequency radio waves incident vertically, slightly obliquely and obliquely. Measurements at a single frequency do not enable the

determination of the location of the irregularities and the study of their vertical displacement. Soundings at many frequencies enhance the possibilities of this method (Bertel et al. 1984).

5. Incoherent scatter of radio waves are a powerful means of the investigation of the irregular structure of the ionosphere, but it has no sufficient spatial and time resolution yet, except in individual equipments. Sometimes the development of the irregular structure producing among others spread-F can be observed by means of this method.

6. Forward scatter of radar signals in the HF band by ionospheric irregularities. Among others, irregularities of $l = 3$ m can be observed by the radar station at Jicamarca which is used for the study of the equatorial spread-F. The radar system at the island of Kwajalein is designed to the study of irregularities with $l = 1.93$, 0.36 and 0.11 m.

7. Phase (Doppler) and polarization (Faraday) measurements of monochromatic signals in the range from some tens to some hundreds of MHz carried out by both low orbiting and geostationary satellites. Sometimes discreet sources of cosmic radio emissions are observed. For the investigation of the irregular structure of the ionosphere fluctuations of the signals received are used.

This method enables, when used as remote sounding of the ionosphere by satellites, to study the conditions at heights $h > h_mF$ being inaccessible for ground based radiophysical methods. Du Castel and Faynot (1964) called attention already in 1965 to the presence of characteristic curved traces in ionograms identified with travelling disturbances when analyzing the data of the topside sounding satellite Alouette-1. At present the experimental material obtained by this method is used for the investigation of the irregular structure of the ionosphere at heights of $h_mF2 \lesssim h \lesssim 3000$ km producing scattered reflections on the ionograms (spread-F) (Calvert and Schmid 1964, Dyson 1968, Maruyama and Matuura 1980). One of the basic merits of the method is the possibility that a global "snapshot" of the outer ionosphere can be obtained from pole to pole in

relative short intervals, moreover - what is very important in certain heliophysical and geophysical conditions - the local-character of the irregular structure of the ionosphere can be observed (Fig. 1). The use of topside sounding data presented

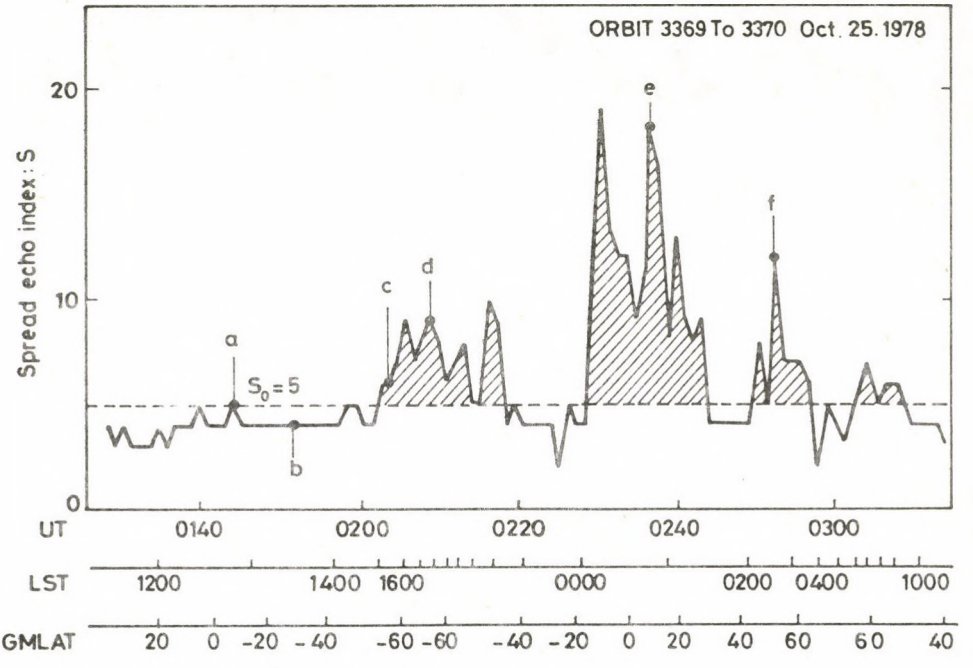

Fig. 1. Variation of the spread-F index S along the orbit of the satellite ISS-b constructed on the basis of 100 ionograms (Maruyama and Matuura 1980). Individual points denoted by a - f correspond to ionograms published in that paper

in form of $n_e(h)$ profiles began in the last years for the study of medium and small - scale irregularities of the electron density and of corresponding wave-like disturbances in the outer ionosphere (Solodovnikov et al. 1981, Fatkullin et al. 1984, Solodovnikov et al. 1984). This is so far useful as it is possible to determine the height and latitude dependence of the irregular structure along the satellite's orbit in the given case. However, there are two limitations. The first is that the spatial, latitudinal-longitudinal scale of the observable

electron density irregularities is limited in case of ionospheric stations of small power. For instance in case of the satellite Alouette-1 (frequency range of the sounding 1-12 MHz, speed of the frequency sweeping 1 $MHzs^{-1}$), only irregularities with spatial scales of the order not less than some hundred kilometers, i.e. medium - or large - scale irregularities can be revealed. The second limitation is connected with the accuracy of the computation of $n_e(h)$ profiles on the basis of topside sounding ionograms. This accuracy makes the determination of local electron density irregularities impossible.

3. RESULTS OF EXPERIMENTAL AND MORPHOLOGICAL INVESTIGATIONS

There are many discussions on the results of the experimental and morphological investigations of irregular structures in the electron density at the height of the F region and in the outer ionosphere, obtained by means of different methods (Herman 1966, Aarons et al. 1971, Gershman 1976, Crane 1977, Alimov and Rakhlin 1979, Erukhimov et al. 1980, Fejer and Kelley 1980, Gdalevich 1980, Ovezgeldiev and Muradov 1980, Kelley and McClure 1981, Vsekhsvyatskaya 1981, Fatkullin 1982, Hanuise 1983, Pancheva and Samardzhiev 1983, Gershman et al. 1984).

3.1 The irregular structure of the electron density distribution

The characteristic spatial scales of the electron density irregularities vary from a meter to some thousand kilometers depending on different conditions (e.g. the linear dimensions of the irregularities causing the spread-F phenomenon and the scintillation of the radio signals from cosmic sources and of satellites range from some hundred meters to some kilometers). Some examples are presented in Figs 2, 3 and 4 showing the spectral distribution of the linear dimensions of the electron density irregularities in individual cases. As a rule the broad spectrum of the characteristic dimensions of the electron density irregularities is divided into certain ranges, though such a division is in want of a generally accepted terminology.

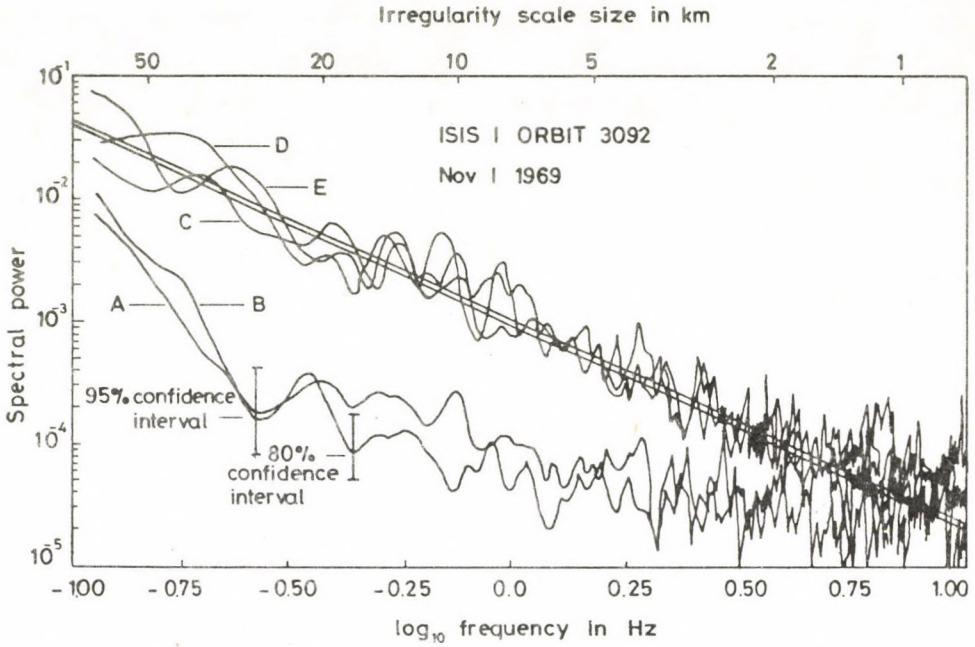

Fig. 2. The power spectrum of the electron density irregularities of different scale according to measurements carried out by means of the satellite ISIS-1 November 1, 1969 (orbit no 3092).
A-$\Lambda \simeq 60.1^{O}$N, h $\simeq$ 1374 km, 13 30 MLT, B-$\Lambda \simeq 65.8^{O}$N, h $\simeq$ 1517 km, 13 14 MLT, C-$\Lambda \simeq 76.4^{O}$N, h $\simeq$ 1810 km, 12 13 MLT, D-$\Lambda \simeq 80.8^{O}$N, h $\simeq$ 1957 km, 11 09 MLT, E-$\Lambda \simeq 83.7^{O}$N, h $\simeq$ 2103 km, 9 23 MLT (Phelps and Sagalyn 1976)

For instance, the following division of the scales of irregularities in the equatorial F region was suggested by Livingston et al. (1981): $l > 1000$ km planetary scale, $10 \leq l \leq 1000$ km medium-scale, $0.1 \leq l \leq 10$ km intermediate scale and $l < 10$ m short wave length. The electron density irregularities of $l <$ 1-10 km belong (after Erukhimov et al. 1980) to small scale irregularities. Troitsky (1980) distinguishes two groups, medium-scale and large-scale irregularities, considering the electron density irregularities related to travelling ionospheric disturbances. In case of large-scale perturbations the

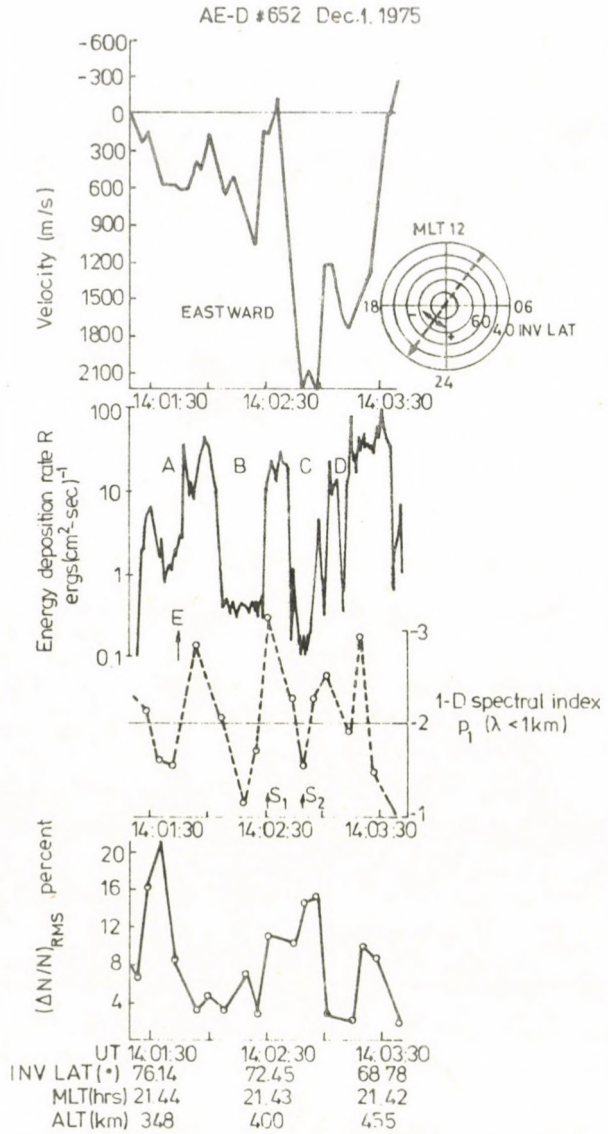

Fig. 3. Data of the orbit no 652 of the satellite AE-D between 14 01, 30 s, and 14 03, 30 s UT December 1, 1975 showing the zonal component (E-W) of the velocity of the plasma drift, the velocity of the energy input, the onedimensional spectral index of the irregularities with scale $l < 1$ km and the amplitude of the electron density irregularities. In the regions of precipitating electrons large spectral indices appear and the spectral index decreases, where in strongly structured irregularities large amplitudes of ionospheric irregularities occur (Basu et al. 1984)

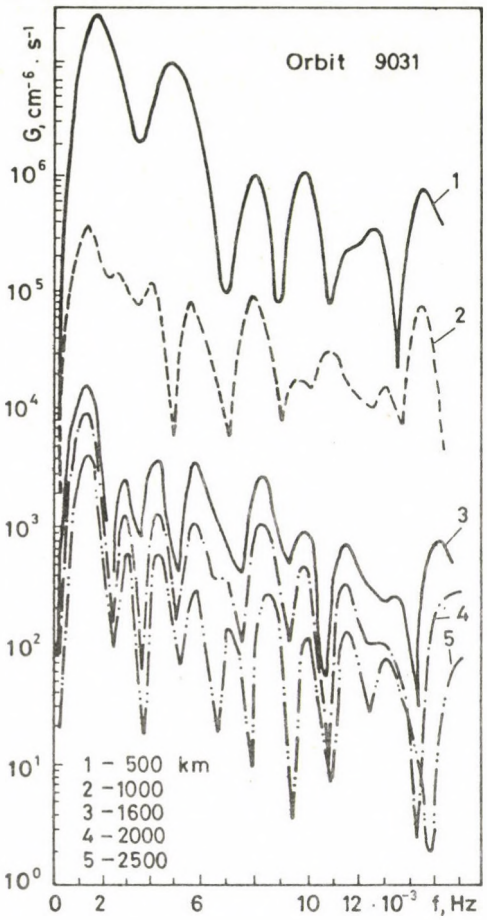

Fig. 4. Energy spectra of medium- and large-scale fluctuations of the electron density in the outer ionosphere at fixed heights from an analysis of topside sounding data of the satellite Alouette-1 (December 30, 1967, orbit no 9031, φ = 74.8-4.9°N, λ = 134.4-166.5°E, 00 20-03 00 LT, Kp = 3, $F_{10.7}$ = 159)

horizontal wave length is $l \gtrsim 1000$ km, the period $T > 30$ min, the horizontal component of the phase velocity $V \simeq$ 400-1000 ms^{-1}. In case of medium-scale irregularities, l amounts to ten or hundred kilometers, $T \simeq$ 10-60 min and $V \simeq$ 100-250 ms^{-1}.

3.11 The spread-F phenomenon

One of the indicators of the F region's irregular structure is on bottomside vertical soundings of the ionosphere, as well as in topside soundings by satellites, the increase of the duration of the signal reflected from the ionosphere as com-

pared to the duration of the sounding impulse. This phenomenon is called spread-F. Based on the experience of many years of bottomside vertical sounding, four types of spread-F are distinguished: 1. range spreading (spread in height or distance), 2. frequency spreading, 3. mixed type spreading (the traces of the reflections are broadened both in virtual height and in frequency), 4. spur (all transitional types of the spread which correspond to none of the definitions mentioned above).

Numerous reviews were devoted to the study of the spread-F phenomenon (e.g. reviews by Herman 1966, Booker 1979, Ovezgeldiev and Muradov 1980, Kelley and McClure 1981, Gershman et al. 1984). As characteristics of the spread-F phenomenon, the intensity and the probability of its occurrence $P(F_{sp})$ are used. $P(F_{sp})$ depends on latitude, longitude, local time, season, on solar and geomagnetic activities. The basic regularities of the different variations of $P(F_{sp})$ are well enough documented by the tabulated data of the network of vertical sounding stations. They are investigated by means of the topside sounding of the ionosphere on board of different satellites, too (Calvert and Schmid 1964, Dyson 1968, Maruyama and Matuura 1980). One example is shown in Fig. 5. Some properties of the occurrence of the spread-F determined by statistical analysis are the followings: 1. spread-F is basically a night-time phenomenon except of magnetic latitudes $\Phi > 60^{o}$, 2. in the period of high solar activity intense spread-F is only observed within the zone $\Phi = \pm 20^{o}$ and at high latitudes ($\Phi > 60^{o}$), in case of low solar activity it is observed at mid-latitudes, 3. range spread-F, characteristic of the low and equatorial latitudes, appears immediately after sunset, the maximum of $P(F_{sp})$ occurs before local midnight; the daily maximum occurrence of the frequency spread-F, characteristic of the high and mid-latitudes, appears after local midnight; at transitional latitudes mixed type spread-F is observed, 4. at mid-latitudes ($\Phi \simeq 25^{o}$-55^{o}) the probability $P(F_{sp})$ is small. The minimum of $P(F_{sp})$ is at $\Phi \simeq \pm 40^{o}$.

In spite of a great number of papers devoted to study of the global, regional and local morphology of the spread-F on

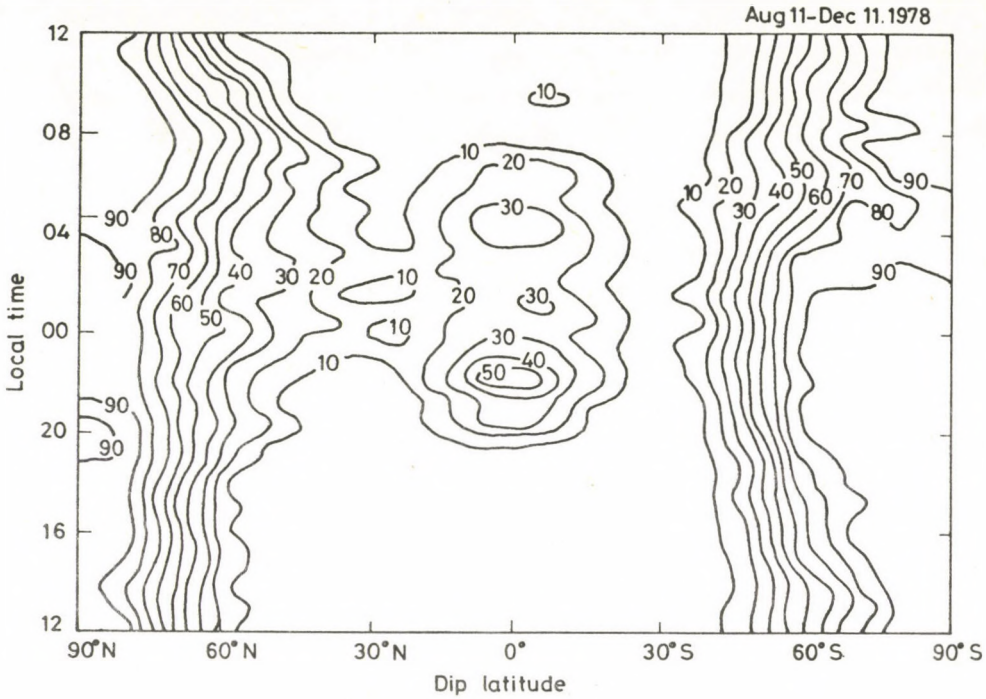

Fig. 5. Distribution of the occurrence probability of scattered reflections on the topside sounding ionograms (satellite ISS-b) as a function of local time and magnetic dip latitude for the period August-December, 1978 (Maruyama and Matuura 1980)

the basis of the network of vertical sounding stations, this phenomenon remained uncleared to the beginning of the seventies because of the lack of independent measurements under conditions when on vertical sounding ionograms spread-F is observed. It was not clear, to what extent it can be concluded from the observations of spread-F on the quantitative characteristics of the irregular structure of the F region at different latitudes.

Results obtained in the study of spread-F in the last years are due to the investigation of the relation between the occurrence of spread-F and the different parameters of the F region (foF2, total electron content, half width, height of the layer, velocity of the vertical motions, temperatures of charged and neutral particles), to the correlation to other phenomena

(scintillation of the signals of discrete sources and different satellites, night air glow at the wave length 6300 Å, VLF emission), to complex measurements using rockets, satellites and incoherent scatter equipments, to the measurement of the scintillation of satellite signals to Doppler observations etc.

The most significant results in the experimental investigation of the structure of the ionosphere under spread-F conditions have been achieved in the last years at equatorial latitudes, because of two facts. On the one hand a relatively narrow band of intense spread-F can be found there, on the other up-to-date measuring equipments are located there. Some results of these studies can be summarized as follows (Figs 6 and 7).

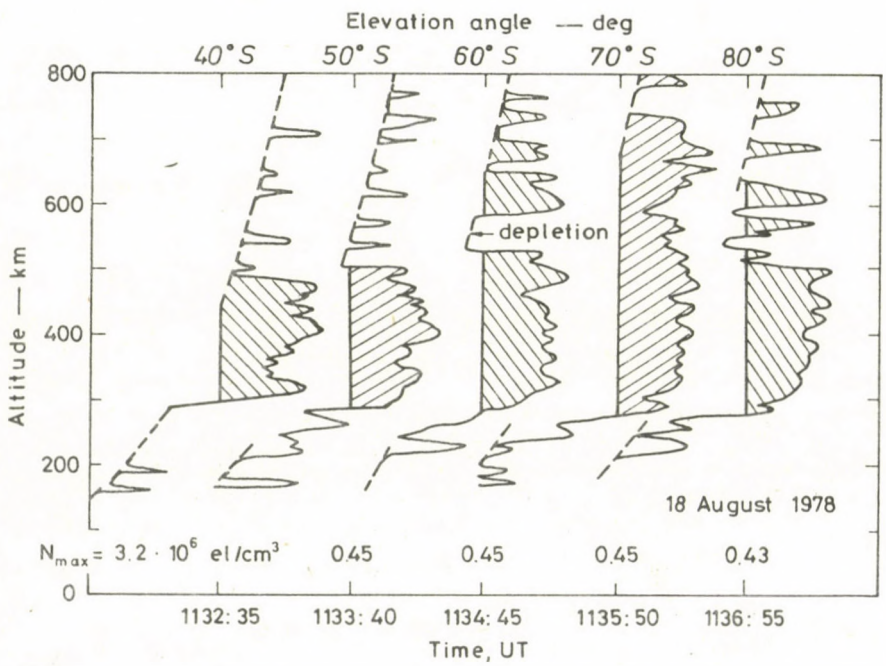

Fig. 6. $n_e(h)$ profiles in the equatorial ionosphere for different elevation angles of the radar beam on the basis of the data of incoherent scatter measurements in Altair (Marshall Islands, geomagnetic latitude 4.3°N) August 18, 1978 (Tsunoda 1980)

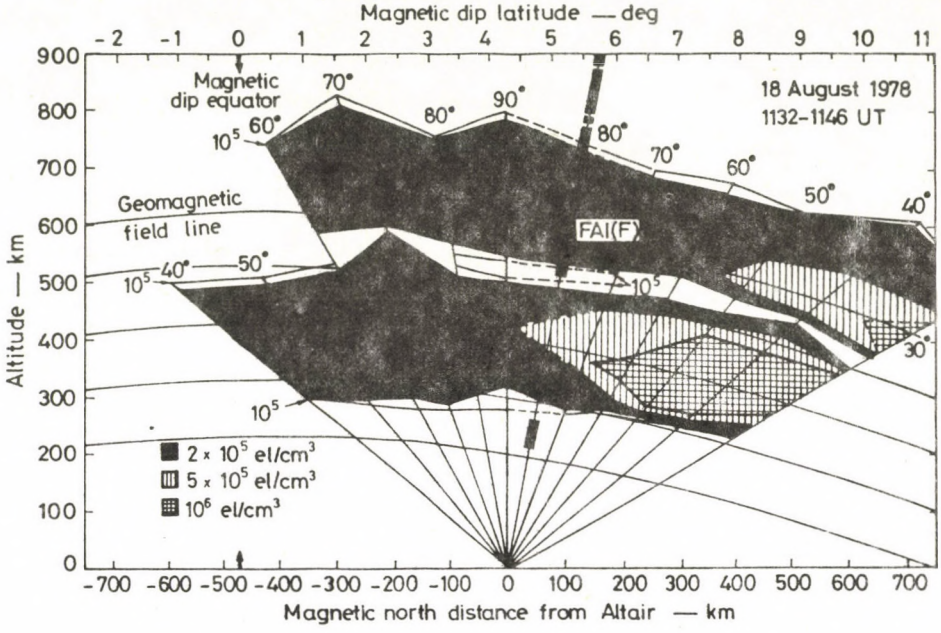

Fig. 7. Contour maps of the latitudinal distribution of the electron density ($n_e \geq 2.10^5$ cm^{-3}) and regions of decreased plasma density elongated along the geomagnetic field lines according to the data of incoherent scatter measurements in Altair August 18, 1978 in the interval 11 32-11 46 UT. On the horizontal axis (bottom) the distance is plotted from the measuring site FAI(F) to the field-aligned irregularity in the F region (Tsunoda 1980)

Firstly, range spread-F occurs in the equatorial ionosphere only when the velocity of the vertical drift remains in the F region after sunset upwards directed. However, the maximum intensity of the spread-F is observed when the drift velocity is small or even it is directed downwards (see e.g. Rastogi 1984). In the beginning the range spread-F appears at the bottom of the F region or even below it, than it propagates through the whole F region because of the downward motion of the whole region or in consequence of the upward motion of the irregularities. The vertical motion of the scattering layers may occur independently of the general motion of the main F layer. Sometimes these motions are of opposite directions. The altitude of the height scattered echo on the ionogram corresponds

very well to the height of the maximum intensity of the scattered echo in VHF back scatter records, contrary to the virtual height of vertically reflected signals. This means that the range spread-F phenomenon recorded on HF sounding ionograms and back scatter echos indicate in the equatorial ionosphere at frequencies exceeding the plasma frequency the same process of scattering by layers with steep gradient of the plasma density. The frequency spread-F is unable to reflections at VHF.

According to complex experiments irregularities of small dimension with l equal to about some meters and those with $l \simeq 0.1$-1 km coexist in the equatorial ionosphere in the dusk hours. However, later (about one hour after the occurrence) the small irregularities disappear, but the irregularities with $l \simeq 0.1$-1 km remain. At about midnight eastward drifting irregularities of the electron density appear causing scintillation of VHF radio waves (f = 413 and 1239 MHz) but leaving radar signals unaffected. This indicates that in the late night hours the spectrum of irregularities ends between 100 m and 3 m.

An increase of the velocity of the downward plasma drift is observed in the night-time F region according to the data of the measurements carried out by the incoherent scatter method, in case of the presence of spread-F on ground based vertical sounding ionograms at mid-latitudes (Namazov and Dzyubanov 1979).

At high latitudes spread-F is nearly always present. It was shown by complex experiments (Kelley et al. 1980) that the spectrum of variations determined from ionospheric sounding and from scintillation observations is usually less steep then k^{-2}. In the layer with a thickness of the order of some hundred kilometers, $|\Delta n_e|$ is $\geqq 1.0 \cdot 10^3$ cm^{-3} in the phase of development of an auroral substorm.

3.12 In-situ satellite measurements

Results of satellite measurement concerning the spectral characteristics of electron density irregularities can be found in a lot of papers. Some of these publications are listed in Table I., where comments are also made. Moreover, in Figs 2, 3,

Table I

Authors	Comments
1	2
Dyson (1969)	Autumn, 1966, satellite Alouette-2, irregularities of the electron density with scales l from 100 m to some hundred km measured by Langmuir probe. Height $500 \leq h \leq 3000$ km and $5 \lesssim \delta n_e \lesssim 70$ %. The comparison of the probe measurements with simultaneously taken ionograms shows that at the height of the satellite spread-F is observed whenever fine structure occurs. Nevertheless, spread-F is recorded in the height of the satellite especially at mid-latitudes, if the probe measurements do not show any irregular structures. In cases when spread-F is observed, but the probe measurements do not indicate irregular structure, $\delta n_e < 5$ % (resolving power of the Langmuir probe).
Getmantzev et al. (1973)	December, 1970, satellite "Kosmos-381", latitude $40^0 \leq \varphi \leq 74^0$N, irregularities of the electron density with scales from 0.5 to 120 km measured by high frequency impedance sonde. Altitude about 1000 km. The ratio $\Delta n_e/n_e$ increases with increasing linear dimensions of the irregularities.
Dyson et al. (1974)	Satellite OGO-6, scales l = 70 m - 7 km, n = 0.92 $\pm$ 0.06 (polar latitudes) and l = 70 m - - 4 km, n = 1.08 $\pm$ 0.28 (equatorial zone). The index n does not depend on latitude and amplitude of the irregularities. Quasi-periodic irregularities were observed and also irregularities, where a harmonic component has been found in the power spectrum in the dependence of l. The distribution of the intensity corresponding to scales $l \lesssim 3$ km is sometimes of a random character in the spectra of the irregularities.

Table I (cont.)

1	2
Phelps and Sagalyn (1976)	February, 1969 - April, 1972, satellite ISIS-1, irregularities with scales l = 200 m-100 km, n = 1.5 - 2.5 measured by a spherical electrostatic probe. Altitude $547 \leq h \leq 3523$ km, λ (invariant latitude) $> 40^{o}$. In the day-time cusp n = 2.1 at Kp >3 and n = 1.8 at Kp ≤ 3. In the auroral zone at the night side of the Earth n = 2 in case of Kp >3 and n = 1.8 at Kp ≤ 3. In the polar cap n = 2.05 and 1.9 in case of Kp >3 and Kp <3 respectively.
Basu (1978)	November, 1969 - February 1970, satellite OGO-6, the scale l of the irregularities changes from hundreds of meters to some kilometers. The relation of small-scale irregularities to steep gradients of the plasma density perpendicular to the L-shells at the height of the F region has been studied for $2 \leq L \leq 4$. The small scale irregularities connected with gradients of $n(O^{+})$ correlate with low frequency electrostatic fluctuations, but not with some significant variations of the temperature.
Maier et al. (1978)	Satellite ISIS-2, in the region of the cusp of the northern hemisphere at a height of 1400 km; small scale irregularities are analyzed. In the sector 8-16 hour local geomagnetic time irregularities of the thermal plasma having a broad spectrum with typical scales $l \simeq 0.7$ km are found at $76^{o} \leq \Lambda \leq 82^{o}$, further irregularities of electrons with energies $E > 20$ keV at $75^{o} \leq \Lambda \leq 80^{o}$. The amplitude of the irregularities of the thermal plasma is ~ 10 %, but in individual cases reaches a factor of 2. Ionospheric irregularities correlate better with low energy electrons and auroras than with energetic electrons.
Komrakov and Skrebkova (1980)	1973, satellite "Interkosmos-Kopernik-500", the scales of the irregularities l = 0.5-100 km measured by high frequency impedance probe, $n = 1.5 \pm 0.12$, height $180 \leq h \leq 1400$ km. The

Table I (cont.)

1	2
	spectra of the irregularities with $3 \leq l \leq 10$-20 km change according to a power function. At $l > 10$-20 km the slope of the spectrum decreases. For the height region $180 \leq h \leq 500$ km the value of n is somewhat larger (0.1-0.14) than for altitudes $600 \leq h \leq 1400$. At mid-latitudes $(40 \pm 2)^{o}$N, $n = 1.85 \pm 0.12$ in average in the midday hours.
Komrakov et al. (1983)	January, 1971, satellite "Kosmos-381", $\Delta n_e/n_e$ = 2-4 % at $0 \leq Kp \leq 8$ and $47 \leq R \leq 83$, where R is the sunspot number. Any systematic variations of n depending on Kp and R could not be shown, though, the mean value of the spectral index depends on the mean level of solar activity.
Rodriguez and Szuszczewich (1984)	Summer, 1978, satellite S3-4, scales of the irregularities l = 75-150 km in the high-latitude ionosphere at the height of the lower part of the F region ($170 \leq h \leq 200$ km). During moderate geomagnetic activity (Kp = 2-3, AE $\simeq$ 100) for the day-time auroral oval and the polar cusp irregularities with scales $l > 7.5$ km are the most characteristic ones. In the polar cap at the twilight side a strengthening of the irregular structure of the ionosphere is recorded.

4, 8 and 9 examples are shown.

The results of satellite measurements refer to different heliophysical and geophysical conditions as height, latitude, longitude, local time, levels of the solar and geomagnetic activities. They are related to irregularities of different scales. Therefore, it is obvious that experiments to summarize them in form of some qualitative and quantitative scheme cannot be always unambiguous.

The main results of these measurements can be summarized as follows. 1. There are two known zones, the high latitude and the equatorial zone in the latitudinal variation of the probability of electron density irregularities at the height of the F region and in the outer ionosphere (Fig. 10). The low latitude boundary of the high latitude zone coincides approximately with the poleward edge of the mid-latitude trough. The most

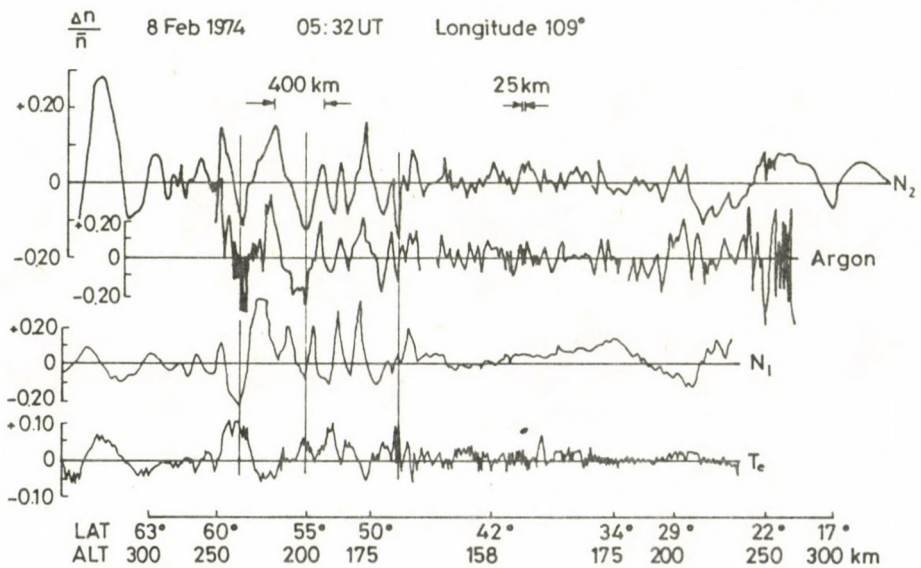

Fig. 8. Variations of the relative values of $n(N_2)$, $n(Ar)$, n_i and T_e along the orbit no 594 according to the measurements carried out by the satellite AE-C February 8, 1974. The relative scales along the orbit are shown and the vertical lines indicate the phase relations between the parameters (Reber et al. 1975)

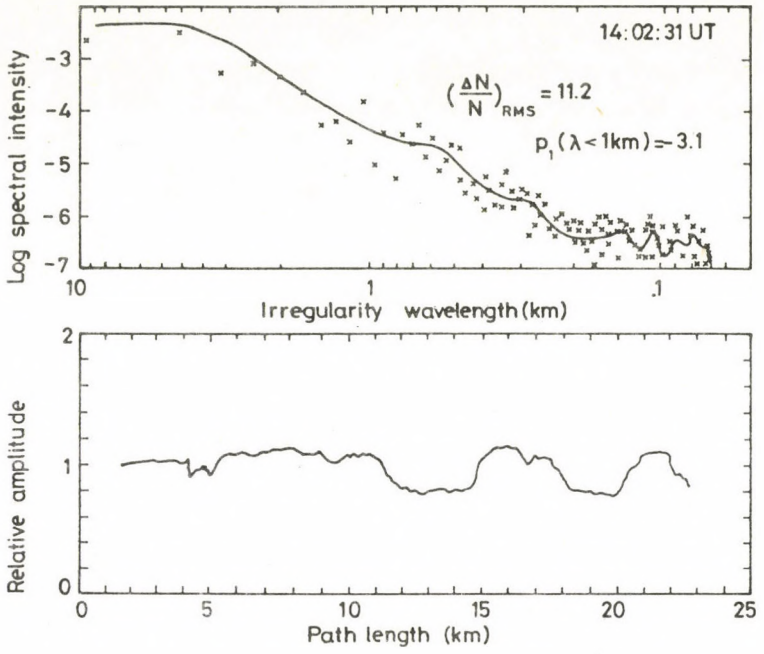

Fig. 9. Relative amplitude (δn_i = 11.2 %, bottom) and spectral distribution of the dimensions of the ion density irregularities (top) on the basis of high resolution measurements carried out on board of the satellite AE-D (orbit no 652). The measurements correspond to the point denoted in Fig. 3 by the point S_1 (Basu et al. 1984)

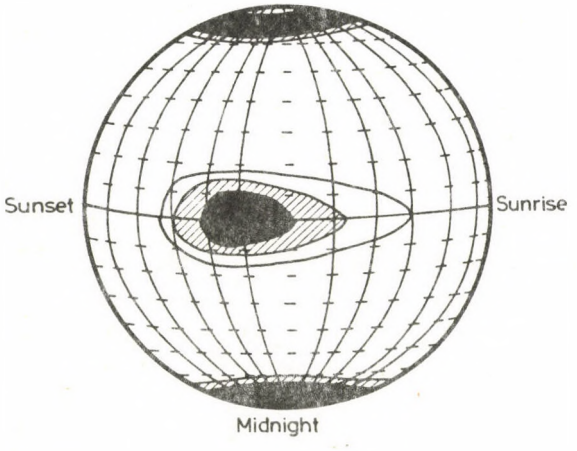

Fig. 10. Schematic representation of the distribution of electron density irregularities as a function of latitude and local time causing scintillation of satellite signals (the density of the lines indicates qualitatively the occurrence frequency of deep fadings) (Aarons et al. 1971)

intense irregularities are observed in the auroral zone. There is an asymmetry in the high latitude zone of irregularities between the two hemispheres. During disturbances the equatorial boundary of the high latitude zone of irregularities is shifted to lower latitudes. 2. The probability of the irregularities depends on local time, season, longitude, solar and geomagnetic activity. The probability of irregularities at all latitudes is greater during night than during the day. The seasonal variation of the characteristics of the irregularities is hardly studied. According to certain data during geomagnetic storms the probability of irregularities and their intensity increases at all latitudes.

A detailed investigation of the characteristics of the irregularities with scales of $10 \leq l \leq 150$ km along the noon-midnight meridian on the basis of the satellite "Cosmos-900" ($h \simeq 500$ km) in case of $1 \leq Kp \leq 6$ (Gdalevich et al. 1980) shows that according to the character of the variations $\delta n_i \simeq \delta n_e = (\overline{\Delta n_i^2}/n_{io}^2)^{1/2}$ at the height of the F region in both hemispheres five latitudinal zones can be distinguished in the dependence on the geomagnetic activity 1. auroral zone 2. polar caps 3. mid-latitude region ($\Phi \simeq 25\text{-}50^o$) 4. pre equatorial zone 5. geomagnetic equator ($\Phi = \pm 3^o$). In case of Kp = 1 at latitudes near the cusp $\delta n_i \lesssim 10$ % in the day-time hours. In case of $Kp > 3$, irregularities with $l \simeq 10\text{-}150$ km are observed at all latitudes.

3.13 Vertical distribution of ionospheric irregularities

The vertical distribution of irregular electron density structures can be inferred under different heliophysical and geophysical conditions from studies by e.g. Gupta (1980), Kelley et al. (1980), Tsunoda (1980), Bakay et al. (1981), Narcisi and Szuszczewicz (1981), Kelley et al. (1982). Some examples are presented in Fig. 6.

Rocket measurements of the electron density, temperature and ion composition of the equatorial ionosphere were carried out by Narcisi and Szuszczevicz (1981) in the presence of spread-F. The first rocket was launched during the final phase

of spread-F and the second experiment was carried out during the presence of a well defined spread-F. At the first experiment significant troughs (bubbles) were found in the electron density profile in the whole F region from 260 to 500 km (Fig. 11). During the second experiment electron density irregularities were observed only in the lower part of the F region (Fig. 11). The ion composition in the irregularities is characterized by the reduction of the concentration of N^+ and O^+ ions, as well as by small changes in the concentration of the molecular ions NO^+ and O_2^+, and of the metal ions Fe^+ and Mg^+, too. The ratio $n(N^+)/n(O^+)$ decreases in the "bubbles". The lack of significant changes of the molecular ion concentrations with height in "bubbles" shows that atmospheric turbulence does not play a significant role in the lower part of the equatorial F region in the formation of electron density irregularities.

3.14 Empirical models of the irregularities of the electron density

Three kinds of models of the different parameters are developed for the regular structure of the ionosphere namely empirical, theoretical and semi-empirical or hybrid models (Fatkullin 1975). The aim of the empirical modeling is to synthetize in a model presentation the basic parameters based on analysis and generalization of the often scanty experimental data which would indicate originally the situation in the ionosphere under this or that conditions. A number of models of different parameters are suggested for the regular structure of the ionosphere (Fatkullin et al. 1981). For the parameters of the electron density irregularities there are no general empirical models spanning the broad spectrum of the parameters of the irregularities in typical heliophysical and geophysical conditions if the whole problem is to be considered (Erukhimov et al. 1977, Gershman et al. 1984). Individual attempts have been made to construct empirical models of the irregularities on the basis of the scintillation of satellite signals and the study of spread-F (Fig. 12).

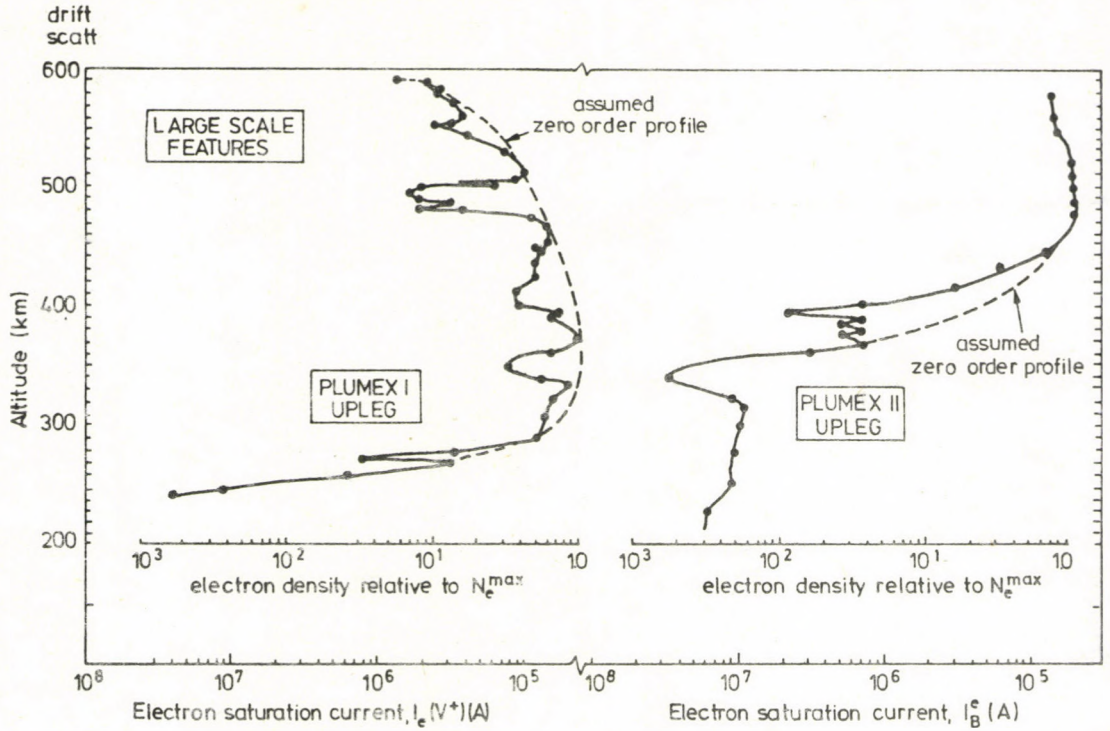

Fig. 11. Large scale structures in the normalized profiles $n_e(h)/N_mF2$ measured (continuous line) during the rocket experiments PLUMEX-1 and PLUMEX-2 on the atoll Kwajalein (geomagnetic latitude 4.3°N). The assumed zero order profiles $n_e(h)/N_mF2$, i.e. without the large scale structure are denoted by dotted lines (Narcisi and Szuszczewicz 1981)

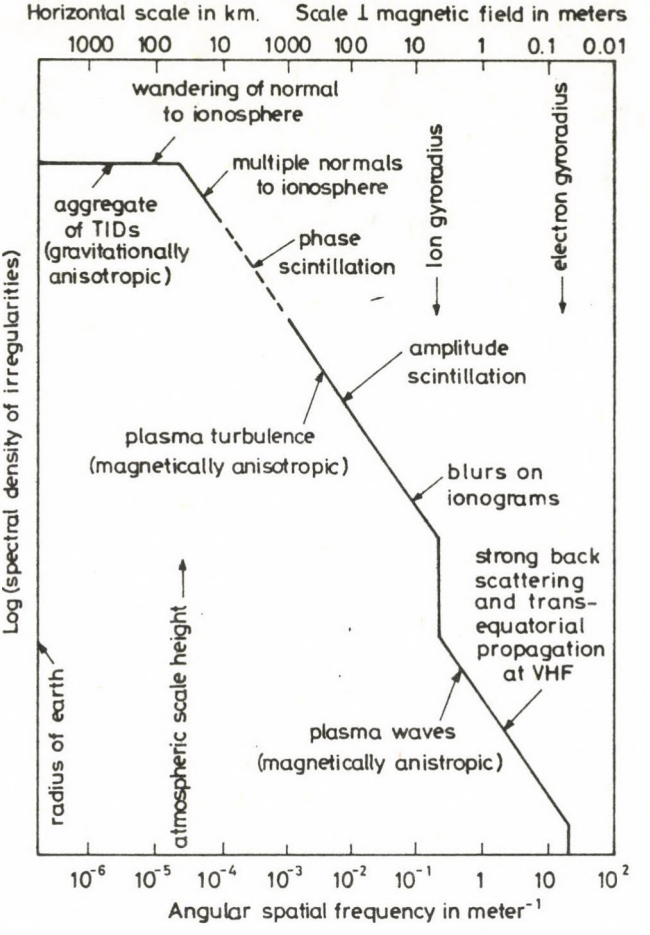

Fig. 12. Schematic representation of the spectrum of ionospheric plasma fluctuations as a function of the angular spatial frequency generalizing the up-to-date state of the investigations (Booker 1979)

Model of the electron density irregularities producing scintillation of signals in the VHF/UHF bands

Several reviews deal with the scintillation of signals produced by non-stationary processes in the ionosphere and with experiments to estimate the parameters of ionospheric irregularities on the basis of these data (Aarons et al. 1971, Crane

1977, Alimov and Rakhlin 1979). Fremouw and Rino (1973) made an attempt to construct empirical models of the electron density irregularities. They assume that the electron density irregularities of the F region, causing the scintillation of signals are concentrated at a height of 350 km, the thickness of the layer containing the irregularities amounts to 100 km and the ratio of the longitudinal to the transverse dimensions of the irregularities is 10. This model of the electron density irregularity is presented in the form

$$\Delta n_e = \Delta n_e (R, D, \Phi, t)_{eq} + \Delta n_e (\Phi, t)_{mid} + \\ + \Delta n_e (R, \Phi, t)_{hi} + \Delta n_e (R, \Phi, t)_{aur}, \tag{1}$$

where

$$\Delta n_e (R, D, \Phi, t)_{eq} = (5.5 \cdot 10^9)(1 + 0.05R) \cdot \\ \cdot \left[1 - 0.4 \cos \pi \left(\frac{D + 10}{91.25}\right)\right] \left\{\exp\left[-\left(\frac{t}{4}\right)^2\right] + \right. \\ \left. + \exp\left[-\left(\frac{t - 23.5}{3.5}\right)^2\right]\right\} \cdot \\ \cdot \left\{\exp\left[-\left(\frac{\Phi}{12}\right)^2\right]\right\} \quad el/m^3 \tag{2}$$

$$\Delta n_e (\Phi, t)_{mid} = (6.0 \cdot 10^8)\left(1 + 0.4 \cos \frac{\pi t}{12}\right) \\ \left\{\exp\left[-\left(\frac{\Phi - 32.5}{10}\right)^2\right]\right\} el/m^3 \tag{3}$$

$$\Delta n_e (R, \Phi, t)_{hi} = (2.7 \cdot 10^9) \left\{1 + \right. \\ \left. + \operatorname{erf}\left[\frac{\Phi - \Phi_b (R, t)}{0.02 \Phi_b (R, t)}\right]\right\} el/m^3 \tag{4}$$

$$\Delta n_e\,(R, \Phi, t)_{aur} = (5.0 \cdot 10^7)\, R \cdot \cdot \left\{ \exp\left[- \left(\frac{\Phi - 70 + 2\cos(\pi t/12)}{0.03R} \right) \right] \right\} \text{el/m}^3 \tag{5}$$

$$\Phi_b = 79 - 0.13R - (5 + 0.04R) \cdot \cdot \cos(\pi t/12) \text{ degrees.} \tag{6}$$

Φ is the geomagnetic latitude, t the local time (in hour), D the number of the day in the year and R the sunspot number.

According to Fremouw and Rino (1973) the mean value of the transverse scale of the irregularity corresponding to a reduction to its e-th part multiplied by the spatial autocorrelation function of the scintillations can be given in the form

$$l_\perp = 300 + 600\left\{ 1 + \text{erf}\left[(\Phi - 12)/3 \right] \right\} - 450\left\{ 1 + \text{erf}\left[(\Phi - 62)/3 \right] \right\} + 200\left\{ 1 + \text{erf}\left[(\Phi - 69)/3 \right] \right\} \text{ m} . \tag{7}$$

In Eq. (1) the first term describes the maximum of the scintillations at the equator at midnight, the reduction of the intensity of the scintillations in the early morning hours, a simple harmonical seasonal variation with maxima at the equinoxes, linear dependence on the solar activity and the latitudinal dependence in the form of a Gaussian distribution with reduction of the intensity by e^{-1} in 12^o at both sides of the geomagnetic equator. Simple diurnal and latitudinal variations of the scintillations at mid-latitudes are given by the second term. The third term in Eq. (1) describes the scintillation at high latitudes not directly related to auroral disturbances. Scintillations connected with the auroral activity in the vicinity of the auroral oval are represented by the fourth term.

The comparison of this model with experimental data gives quite satisfactory results concerning the scintillation of satellite signals under different heliophysical and geophysical

treble underlining: bold-face italics
red underlining: Greek letters
green underlining: script letters.

Rules for mathematical-physical notations:

trigonometric, logarithmic, analytic symbols, symbols for units and functions are in roman type (not underlined)

letter symbols in mathematical and physical formulas, scalars, and subscripts of algebraic and physical quantities are in italics (underlined)

vectors, matrices, operators in probability theory are in bold-face roman type (double underlining)

tensors, operators and some special functions are in script letters (green underlining). These cannot be bold.

Greek letters (red underlining) cannot be bold or extra bold type (thus they cannot be used for vectors or tensors)

void upper lines e.g. for vectors

avoid possible confusion between o (letter) and 0 (zero), l (letter) and 1 (one), ν (Greek nu) and v, u (letters) etc.

explain ambiguous or uncommon symbols by making marginal notes in pencil

be careful about superscripts and subscripts

formulae must be numbered consecutively with the number in parentheses to the right of the formula. References in text to the equations may then usually be made by the number in parenthesis. When the word equation is used with a number, it is to be abbreviated, Eq. or Eqs in the plural

the International System of Units (SI) should be used.

Authors are liable for the cost of alteration in the *proofs*. It is, therefore, the responsibility of the author to check the text for errors of facts before submitting the paper for publication.

3. *References* are accepted only in the Harvard system. Citations in the text should be as:

...(Bomford 1971)...or Bomford (1971)

...(Brosche and Sündermann 1976)...

...(Gibbs et al. 1976b)...

The list of references should contain names and initials of all authors (the abbreviation et al. is not accepted here); for *journal articles* year of publication, the title of the paper, title of the journal abbreviated, volume number, first and last page.

For *books* or *chapters in books*, the title is followed by the publisher and place of publication.

All items must appear both in the text and references.

Examples:

Bomford G 1971: Geodesy. Clarendon Press, Oxford

Brosche P, Sündermann J 1976: Effects of oceanic tides on the rotation of the earth. Manuscript. Univ. of Bonn

Buntebarth G 1976: Temperature calculations on the Hungarian seismic profile-section NP-2. In: *Geoelectric and Geothermal Studies (East-Central Europe, Soviet Asia), KAPG Geophysical Monograph*. Akadémiai Kiadó, Budapest, 561–566.

Gibbs N E, Poole W G, Stockmeyer P K 1976a: An algorithm for reducing the bandwidth and profile of a sparse matrix. *SIAM J. Number. Anal.*, 13, 236–250.

Gibbs N E, Poole W G, Stockmeyer P K 1976b: A comparison of several bandwidth and profile reduction algorithms. *ACM Trans. on Math. Software*, 2, 322–330.

Szarka L 1980: Potenciáltérképezés analóg modellezéssel (Analogue modeling of potential mapping). *Magyar Geofizika*, 21, 193–200.

4. *Footnotes* should be typed on separate sheets.

5. *Legends* should be short and clear. The place of the tables and figures should be indicated in the text, on the margin.

6. *Tables* should be numbered serially with Roman numerals. Vertical lines are not used.

All the illustrations should contain the figure number and author's name in pencil on the reverse.

Figures will be redrawn. Therefore the most important point is clearness of the figures, even pencil-drawings are accepted (with a duplicate).

Photographs and *half-tone* illustrations should be sharp and well contrasted.

If a specific reduction or enlargement is required, please indicate this in blue pencil on the figure.

The editors will send information to the first author about the *arrival* and acceptance of the papers. A galley proof is also sent to the first author for *correction*. Hundred *offprints* are supplied free of charge.

Periodicals of the Hungarian Academy of Sciences are obtainable at the following addresses:

AUSTRALIA
C B D LIBRARY AND SUBSCRIPTION SERVICE
Box 4886, G P O *Sydney N S W 2001*
COSMOS BOOKSHOP, 145 Ackland Street
St Kilda (Melbourne), Victoria 3182

AUSTRIA
GLOBUS, Hochstadtplatz 3 *1206 Wien XX*

BELGIUM
OFFICE INTERNATIONAL DE LIBRAIRIE
30 Avenue Marnix *1050 Bruxelles*
LIBRAIRIE DU MONDE ENTIER
162 rue du Midi *1000 Bruxelles*

BULGARIA
HEMUS, Bulvar Ruszki 6 *Sofia*

CANADA
PANNONIA BOOKS, P O Box 1017
Postal Station 'B' *Toronto, Ontario M5T 2T8*

CHINA
CNPICOR, Periodical Department, P O Box 50
Peking

CZECHOSLOVAKIA
MAĎARSKÁ KULTURA, Národní třída 22
115 66 Praha
PNS DOVOZ TISKU, Vinohradská 46 *Praha 2*
PNS DOVOZ TLAČE, *Bratislava 2*

DENMARK
EJNAR MUNKSGAARD, Norregade 6
1165 Copenhagen K

FEDERAL REPUBLIC OF GERMANY
KUNST UND WISSEN ERICH BIEBER
Postfach 46, *7000 Stuttgart 1*

FINLAND
AKATEEMINEN KIRJAKAUPPA, P O Box 128 *SF-00101 Helsinki 10*

FRANCE
DAWSON-FRANCE S A, B P 40 *91121 Palaiseau*
EUROPERIODIQUES S A, 31 Avenue de Versailles *78170 La Celle St Cloud*
OFFICE INTERNATIONAL DE DOCUMENTATION ET LIBRAIRIE, 48 rue Gay-Lussac
75240 Paris Cedex 05

GERMAN DEMOCRATIC REPUBLIC
HAUS DER UNGARISCHEN KULTUR
Karl Liebknecht Straße 9, *DDR-102 Berlin*
DEUTSCHE POST ZEITUNGSVERTRIEBSAMT, Straße der Pariser Kommune 3-4, *DDR-104 Berlin*

GREAT BRITAIN
BLACKWELL'S PERIODICALS DIVISION
Hythe Bridge Street, *Oxford OX1 2ET*
BUMPUS, HALDANE AND MAXWELL LTD
Cowper Works, *Olney, Bucks MK46 4BN*
COLLET'S HOLDINGS LTD., Denington Estate, *Wellingborough, Northants NN8 2QT*
WM. DAWSON AND SONS LTD., Cannon House, *Folkstone, Kent CT19 5EE*
H. K. LEWIS AND CO., 136 Gower Street
London WC1E 6BS

GREECE
KOSTARAKIS BROTHERS INTERNATIONAL BOOKSELLERS, 2 Hippokratous Street, *Athens-143*

HOLLAND
MEULENHOFF-BRUNA B. V., Beulingstraat 2
Amsterdam
MARTINUS NIJHOFF B.V.
Lange Voorhout 9-11, *Den Haag*
SWETS SUBSCRIPTION SERVICE
347b Heereweg, *Lisse*

INDIA
ALLIED PUBLISHING PRIVATE LTD., 13-14
Asaf Ali Road, *New Delhi 110001*
150 B-6 Mount Road, *Madras 600002*
INTERNATIONAL BOOK HOUSE PVT. LTD.
Madame Cama Road, *Bombay 400039*
THE STATE TRADING CORPORATION OF INDIA LTD., Books Import Division, Chandralok 36 Janpath, *New Delhi 110001*

ITALY
INTERSCIENTIA, Via Mazzè 28, *10149 Torino*
LIBRERIA COMMISSIONARIA SANSONI, Via Lamarmora 45, *50121 Firenze*
SANTO VANASIA, Via M. Macchi 58
20124 Milano
D. E. A., Via Lima 28, *00198 Roma*

JAPAN
KINOKUNIYA BOOK STORE CO., LTD.
17-7 Shinjuku 3-chome, Shinjuku-ku, *Tokyo 160-91*
MARUZEN COMPANY LTD., Book Department, P.O. Box 5050 Tokyo International, *Tokyo 100-31*
NAUKA LTD. IMPORT DEPARTMENT
2-30-19 Minami Ikebukuro, Toshima-ku, *Tokyo 171*

KOREA
CHULPANMUL, *Phenjan*

NORWAY
TANUM-TIDSKRIFT-SENTRALEN A.S., Karl Johansgatan 41-43, *1000 Oslo*

POLAND
WĘGIERSKI INSTYTUT KULTURY, Marszałkowska 80, *00-517 Warszawa*
CKP-I W, ul. Towarowa 28, *00-958 Warszawa*

ROUMANIA
D. E. P., *Bucuresti*
ILEXIM, Calea Grivitei 64-66, *Bucuresti*

SOVIET UNION
SOJUZPECHAT - IMPORT, *Moscow*
and the post offices in each town
MEZHDUNARODNAYA KNIGA, *Moscow G-200*

SPAIN
DIAZ DE SANTOS, Lagasca 95, *Madrid 6*

SWEDEN
GUMPERTS UNIVERSITETSBOKHANDEL AB
Box 346, *401 25 Goteborg 1*

SWITZERLAND
KARGER LIBRI AG, Petersgraben 31, *4011 Basel*

USA
EBSCO SUBSCRIPTION SERVICES
P.O. Box 1943, *Birmingham, Alabama 35201*
F. W. FAXON COMPANY, INC.
15 Southwest Park, *Westwood Mass. 02090*
READ-MORE PUBLICATIONS, INC.
140 Cedar Street, *New York, N.Y. 10006*

YUGOSLAVIA
JUGOSLOVENSKA KNJIGA, Terazije 27, *Beograd*
FORUM, Vojvode Mišića 1, *21000 Novi Sad*

Index 26 031

Acta Geodaetica, Geophysica et Montanistica Hungarica

VOLUME 22, NUMBERS 3–4, 1987

Akadémiai Kiadó, Budapest

AGGM 22 (3–4) 333–473 (1987) HU ISSN 0236-5758

ACTA GEODAETICA, GEOPHYSICA et MONTANISTICA HUNGARICA
A Quarterly Journal of the Hungarian Academy of Sciences

Acta Geodaetica, Geophysica et Montanistica (AGGM) publishes original reports on geodesy, geophysics and minings in English.

AGGM is published in yearly volumes of four numbers by

AKADÉMIAI KIADÓ
Publishing House of the Hungarian Academy of Sciences
H–1054 Budapest, Alkotmány u. 21.

Manuscripts and editorial correspondence should be addressed to

AGGM Editorial Office
H–9401 Sopron P.O. Box 5

Subscription information

Orders should be addressed to KULTURA Foreign Trading Company
H–1389 Budapest P.O. Box 149

Acta Geodaetica, Geophysica et Montanistica Hungarica is abstracted/indexed in Geographical Abstracts, GeoRef Information System, Science Abstracts

INSTRUCTIONS TO AUTHORS

Manuscripts should be sent to the editors (MTA Geodéziai és Geofizikai Kutató Intézete, AGGM Editorial Office. H–9401 Sopron, P.O. Box 5. HUNGARY) Only articles not submitted for publication elsewhere are accepted.

Manuscripts should be typewritten in duplicate, double-spaced, 25 lines with 50 letters each. The papers generally include the following components, which should be presented in the order listed.

1. Title, name of author(s), affiliation, dateline, abstract, keywords
2. Text, acknowledgements
3. References
4. Footnotes
5. Legends
6. Tables and illustrations

1. The *affiliation* should be as concise as possible and should include the complete mailing address of the authors. The *date of receipt* of the manuscript will be supplied by the editors. The abstract should not exceed 250 words and should clearly and simply summarize the most important methods and results. 5–10 significant expressions describing the content are used as *keywords*. Authors may recommend these keywords.

2. The *text* should be generally in English and as short and clear as possible. From Hungarian authors papers are also accepted in Hungarian.

The section heading should *not* be underlined or in capitals.

Please note that underlining denotes special types:

– single underlining: italics
– double underlining: bold-face roman

CONTENTS

conditions.

Models of irregularities causing spread-F

At present two procedures are used for this purpose though, both are based on the same relation

$$(\Delta n_e/n_{eo}) \simeq 2 (\Delta f/f_o) , \qquad (8)$$

where n_{eo} and f_o are the background values of the electron concentration and the critical frequency of the F2 layer respectively, Δn_e and Δf are the deviations of n_e and f_oF2 from the background value. In case of $(\Delta n_e/n_e) \ll 1$ and $(\Delta f/f_o) \ll 1$ this relation can easily be obtained from the formula $n_e = 1.24 \cdot 10^4 (f^2, \text{MHz}) \text{ cm}^{-3}$.

In the first procedure some model of the global distribution of f_oF2 and Δn_e is used as a basis and Δf is computed for the frequency spread-F. For instance Singleton (1975) constructed a model for the global distribution of the occurrence probability of spread-F applying the empirical model of the global distribution of f_oF2 and the model of the global distribution of Δn_e according to Fremouw and Rino (1973). For latitudes below 70^o this model corresponds well to the observations.

In the second procedure a determination of Δn_e is attempted by taking f_oF2 and Δf data referring to spread-F conditions. Kutimskaya and Gudkova (1983) analyzed the global distribution of the indices S = 1, 2 and 3 for spread-F which correspond to Δf = 0.25, 0.5 and more than 0.5 MHz. For the analysis the authors used the S indices of 45 ionospheric stations located at low, middle and high latitudes. The results of the calculations of Δn_e are quite satisfactory.

3.15 The irregular structure of the ionosphere and low frequency electromagnetic waves

Useful informations concerning the relation between the irregular structure of the ionosphere and low frequency electromagnetic waves can be found in the articles by Kelley (1972),

Holtet et al. (1977), Kelley et al. (1979), Likhter et al. (1980), Kelley et al. (1982). The observation of ELF electromagnetic waves on board of the OGO-6 satellite in the equatorial ionosphere at altitudes below the maximum of the F2 layer shows that steep gradients of the plasma density are not stable against processes producing equatorial spread-F in the region where the electromagnetic waves are observed. Simultaneous rocket (with probes) and radar measurements of the irregularities with characteristics dimensions of 10-100 m and less than 10 m were made in the equatorial F region by Kelley et al. (1982) when intensive reflections from the F region were observed, the strength of which gradually diminished. According to the data of the rocket measurements the spectrum of the electron density fluctuations varies as k^{-5} above 200 km while the spectrum of the fluctuations of the electric field as k^{-3}. At lower heights the power spectrum for wave lengths of the order of some ten meters is less steep.

n_i, T_e and the fields of ELF and VLF emissions were measured on board of the satellite "Interkosmos-14" by Likhter et al. (1980) in the region of the mid-latitude trough. The phase of the fluctuations of T_e is opposite to that of n_i. The connection of the fluctuations of n_i and T_e with the fluctuations of the electric field of the emissions is of a complicated character, however, there are indications accounting for the local generation of the VLF waves within the trough in the zone of irregularities.

3.2 The appearance of irregularities in other parameters of the ionospheric plasma

Irregularities can also be observed in the temperatures of electrons (T_e), ions (T_i) and neutral particles (T_n), in the velocities of electrons ($\underline{v}_e$), ions ($\underline{v}_i$) and neutral particles ($\underline{v}_n$), in the concentration of the different ions (O^+, NO^+, O_2^+, N^+, N_2^+, H^+, He^+) and neutrals (O, N_2, O_2, H, He, Ar).

It is to be noted that variations of the parameters mentioned above are hardly studied under conditions, when electron density irregularities of different spatial and time

scales occur.

In Fig. 8 an example showing the wave like structure of $n(N_2)$, $n(Ar)$, n_i and T_e is presented on the basis of simultaneous measurements of the AE-C satellite (Reber et al. 1975). An analysis of the fluctuations of n_e and T_e has shown along the orbit of the Aeros-B satellite (h_s = 200-870 km, July, 1974 - September, 1975) that the global distributions of Δn_e and ΔT_e are analogous, but of different amplitude (Münther et al. 1978). Maximum fluctuations of n_e and T_e are observed in the auroral zone of the northern hemisphere in November, and in the southern hemisphere in June. At mid-latitudes the fluctuations of n_e and T_e are weak during the day and considerable at night. Intense fluctuations of n_e and T_e are observed which do not correlate with the Kp indices.

Hanson and Sanatani (1971) published data indicating the increased concentration of metal ions (Fe^+) in the equatorial ionosphere during spread-F.

4. PHYSICAL MECHANISMS OF THE FORMATION OF IONOSPHERIC IRREGULARITIES

A number of reviews is devoted to the discussion of the results of investigations about different formation mechanisms of irregularities at the height of the F region (Herman 1966, Gershman 1974, D'Angelo 1977, Gelberg 1977, Gershman and Grigorev 1978, Ossakow 1978, Booker 1979, Erukhimov et al. 1980, Fejer and Kelley 1980, Gershman 1980, Ovezgeldiev and Muradov 1980, Ossakow 1981, Fatkullin 1982, Keskinen and Ossakow 1983, Pancheva and Samardzhiev 1983, Gershman et al. 1984).

All investigators agree that the broad spectrum of irregularities from some meters to some thousands of kilometers cannot be explained by one mechanism. This is so far obvious as on the one hand depending on height and latitude the physical conditions in the ionosphere change quickly, on the other hand there are a number of factors independent of each other which can generate irregularities.

Some data concerning the fundamental parameters of the ionospheric plasma as the free mean path (λ) and gyroradius

(r) of charged particles are listed below. At the height of the F region ($h \gtrsim 160$ km) and in the outer ionosphere ($h \leq 1000$ km) the mean free path is $0.3 \lesssim \lambda_e \lesssim 81$ km for electrons and for O^+ ions $0.02 \lesssim \lambda_{O^+} \lesssim 27$ km, for NO^+ ions $0.03 \lesssim \lambda_{NO^+} \lesssim 30$ km, for H^+ ions $0.04 \lesssim \lambda_H \lesssim 40$ km. The values for the gyroradius, in the same height interval are $2 \lesssim r_e \lesssim 6$ cm, $3 \lesssim r_{O^+} \lesssim 8$ m, $4.2 \lesssim r_{NO^+} \lesssim 10$ m and $0.8 \lesssim r_{H^+} \lesssim 2.0$ m (Fatkullin et al. 1981).

Basic processes of the formation of irregularities at the altitudes in question (neglecting the interaction among them) can be divided into three groups. 1. Plasma instabilities produced by the irregularity of the concentration, temperature or any other parameters of the charged particles, by fluxes of precipitating energetic charged particles, by electric fields, currents and so on. 2. Processes connected with the redistribution of charged particles due to the motion of the neutral component produced by the propagation of waves of different types in the upper atmosphere. 3. Magnetospheric processes and ion-acoustic waves with frequencies $\omega \lesssim 10^{-2}$ s^{-1} at $h \simeq 1000$ km generated by the former as a result of the transformation of hydromagnetic waves.

Formation mechanisms of irregularities at the height of the F region and in the outer ionosphere related to magnetospheric processes are quantitatively not yet studied. Some indications of the presence of medium- and large-scale irregularities in the outer ionosphere ($500 \lesssim h \lesssim 3000$ km) were found by Solodovnikov et al. (1984) analyzing the data of the satellite sounding of the ionosphere the formation of which is connected with ion-acoustic waves.

A lot of papers deal with the study of the perturbations of the ionized component due to the propagation of waves of different types in the upper atmosphere (e.g. Hooke 1968, Francis 1974, Gershman 1974, Gershman and Grigorev 1978). Travelling ionospheric disturbances (TID) are usually brought into connection with this mechanism. The sources of atmospheric gravity waves are the auroral and equatorial electrojets, strong explosions, earthquakes, volcanic eruptions, tornadoes, storms, solar eclipses, jet streams in the lower atmosphere,

the terminator, meteor impacts, launches of large rockets etc.

Travelling ionospheric disturbances are usually divided into large-scale, medium-scale and small-scale TID's (Drobzhev 1980, Troitsky 1980). There are many indications that the formation of large-scale TID's with $l \gtrsim 1000$ km and $T > 30$ min is due to auroral phenomena. The sources of medium-scale TID's with l of the order of some hundred kilometers and $T \simeq 10$-60 min are not well understood. The situation is rendered more difficult by the fact that depending on the given conditions some of the sources of the atmospheric gravity waves mentioned above may be absent, but others may act simultaneously. In the study of the medium-scale TID's at mid-latitudes preference is given to the sources located in the lower layers of the atmosphere and connected with the dynamics of the atmosphere. The small--scale TID's with $T \simeq 15$-50 s and 3-5 min do not show correlation with the geomagnetic and solar activities. This type of TID is geographycally localized.

The procedure of the investigation of the effect of atmospheric gravity waves on the ionosphere is well known (see e.g. Gershman and Grigorev 1978). Here, it is to emphasize that this question is seldom considered in self-consistent form, i.e. the corresponding equations of both the charged and the neutral particles are not simultaneously considered but the dynamics of the neutral particles itself depends on the state of the ionosphere. The parameters of the ionized component are often taken from independent sources in the study of the generation and propagation of gravity waves in the upper atmosphere.

In the ionosphere different types of plasma instabilities may occur. One of the basic tasks of the investigation of the plasma instabilities in the ionosphere consists of a) clearing the question, where and in which heliophysical and geophysical conditions one mechanism (or several mechanisms) is predominant as compared to other possible mechanisms b) to connect by quantitative relations the quantities characterizing the formation of instabilities with basic parameters of the ionosphere in an undisturbed condition.

The majority of the papers on mechanisms of the iono-

spheric plasma instabilities deals with small perturbations in a quasi-hydrodynamical approach. Naturally, the small perturbation approximation cannot characterize the whole process of development of the instabilities. However, the question cannot always be answered till which phase of the development of the disturbances the perturbations may be considered as small and linear ones. In the initial phases of the development the linear approximation yields quite acceptable results. On the other hand, the quasi-hydrodynamic description is applicable only if the dimensions of the irregularities are much greater than the mean free path of the charged particles. In case of smaller dimensions of the irregularities, the kinetic approach is needed.

The formalism of the investigation of plasma instabilities in the F region of the ionosphere, presented in detail by Gershman et al. (1984) and the individual computations are omitted, here the results obtained can be summarized as follows.

Three regions are considered separately the equator, middle and high latitudes.

1. At present the situation is the best studied in the equatorial ionosphere. Numerous investigations (see e.g. Ossakow 1981) show that spread-F is caused here by irregularities of the electron density, the dimensions of which cover 3-6 orders of magnitude. In the vicinity of the lower boundary of the night-time equatorial F region irregularities with dimensions of many kilometers are produced by the Rayleigh-Taylor instability. In connection with these irregularities, bubbles of decreased electron density are formed at the lower boundary of the F region which result in the irregular structure of the F region by rising due to an $\underline{E} \times \underline{B}$ drift. The spectral density of the electron density fluctuations with scales mentioned above is proportional to $k_{\perp}^{-2}$, where $\underline{k}_{\perp}$ is the wave number vector perpendicular to the geomagnetic field. Theoretical results show that irregularities with dimension less or of the order of 10 m are generated by kinetic drift instabilities of different types. The instabilities are formed by a two step process. They are generated by steep height gradients of the electron density,

which on the other hand are produced by primary instabilities of the Rayleigh-Taylor type.

In the ionospheric plasma with the characteristic property of the presence of all kinds of TID's, instabilities, among them the Rayleigh-Taylor instability occur seldom in a "pure" form. In realistic conditions the situation is more complicated. The presence of TID's can result in spatial resonance and serve then as a mechanism inducing plasma instability if their phase velocities are equal to the velocity of the electromagnetic drift in the direction of the TID.

2. In the mid-latitude F region the situation concerning the predominant mechanisms of plasma instabilities is not clear. In the presence of gradients (e.g. in the vertical direction) of the electron density the gradient-drift instability arising from the drift of charged particles in transverse electric and magnetic fields is not effective (Gershman 1980). However, plasma convergence connected with the spatially irregular motion of charged particles is possible. In this case the increment of the instability $\gamma \simeq \operatorname{div} \underline{U}_{io}$, where $\underline{U}_{io}$ is the velocity of the ions in the "background" state of the ionosphere.

3. The results of theoretical investigations concerning the mechanisms of the irregular structure of the ionosphere at high latitudes are reviewed by Keskinen and Ossakow (1983). The basic mechanisms of the generation of irregularities in the high latitude F region are convective-current and gradient--drift instabilities.

5. COMMENTS CONCERNING FURTHER DEVELOPMENTS

In the present phase of the experimental and theoretical investigations of electron density irregularities at the height of the F region and in the outer ionosphere, there are many unsolved problems. An attempt is made here to list some of them.

1. Determination of the longitudinal and transverse dimensions of the irregularities, or of their ratio is one of the most important tasks of the experiments. Livingston et al. (1982) used at Poker-Flat (Alaska) the measurement of the spatial coherence of signals transmitted by the satellite Wideband

for the determination of the characteristics of the anisotropy in electron density irregularities with transverse scales of about 1 km in the auroral F region. Three types of the anisotropy of the irregularities have been distinguished a) plate-like irregularities elongated along the magnetic field and L-shells, b) cylindrical type irregularities also elongated along the geomagnetic field, c) irregularities of elliptical cross section. The study of the dependence of the irregularities on geomagnetic latitude in night-time conditions indicates the influence of the auroral convection on the form of the irregularities. Plate-like irregularities are observed at the equatorial side of the auroral zone in the region of the east-west plasma drift, cylindrical irregularities are found at the northern boundary of the auroral zone and irregularities of elliptical cross section occur in the vicinity of the Harang-discontinuity.

2. It is a consequence of the historical development that the irregularities of the electron density are meant as irregular structure of the ionosphere. From a practical point of view, e.g. for the propagation of radio waves of different frequencies the knowledge of the irregular structure of the electron density distribution in the ionosphere is very important. However, from a physical point of view, especially for the study of the formation mechanisms of the irregularities and their concretization, simultaneous measurements of the characteristics of the irregularities have special significance not only those of the electron density, but also of other parameters of the ionospheric plasma (T_e, T_i, T_n, ion and neutral composition, velocities of the charged and neutral particles).

3. The ionosphere is a region of the atmosphere where many processes are of local or regional character. This refers fully to the irregular structure, too. Therefore, estimates of the spatial and time characteristics of the different irregularities are urgently needed. It should be cleared e.g. for spread-F by spaced vertical sounding stations located in different distance from each other and by simultaneous measurements how far identical or how different are the properties of the occur-

rence of this phenomenon on ionograms recorded at a given time.

4. At present as it has been already mentioned a significant quantity of data has accumulated concerning the parameters of the irregularities obtained by means of satellites in different heliophysical and geophysical conditions. They remained so far incomplete. Therefore, it would be necessary to attempt a synthesis of some empirical models of electron density irregularities on the basis of these data taking into account basic heliophysical and geophysical factors.

5. In the last years the interest in the ionospheric effects of lithospheric processes (earthquakes, tsunamis, volcanic eruptions), as well as of underground and surface processes, increased significantly, though, according to the few available data, these effects appear superposed on the irregular structure of the ionosphere. This problem is of interest on the one hand due to its practical significance, i.e. due to the search for precursors of earthquakes, on the other hand because of the necessity of quantitative estimates of changes in the ionosphere being independent of the effect of the Sun on the upper atmosphere and ionosphere.

6. Experimental determination of the characteristic time of formation and dispersal of irregularities of different scales.

7. The question has been discussed in the fifties and sixties whether there are isolated ionospheric irregularities or the structure of the ionosphere itself is cloudy. In addition the existence of electron density irregularities of the most diverse forms (cylindrical, spherical etc.) was suggested. In the seventies the formation of electron density irregularities was brought into connection with wave perturbations of the neutral upper atmosphere. In realistic ionospheric conditions, both types of electron density irregularities exist simultaneously. The question is where and when this or that type of the irregularities predominates.

8. Further clarification of the role of plasma instabilities and of the basic formation mechanisms of irregularities in typical heliophysical and geophysical conditions. Consideration of non-linear effects in the development of plasma in-

stabilities.

9. Numerical modeling of ionospheric irregularities.

10. Investigation of the role of wave motions in the neutral atmosphere and their formation mechanisms.

11. Questions related to the effect of irregularities of different scale on the large scale structure of the ionosphere.

REFERENCES

Aarons J, Whitney H E, Allen R S 1971: Proc. IEEE, 59, 159-172.

Alimov V A, Rakhlin A V 1979: N. i radiofiz. int. Gorkiy, preprint No 132, 52.

Afraymovich E L 1982: Interference methods of the radio sounding of the ionosphere (in Russian). Nauka, Moscow

Bakay A S, Russkin V M, Solodovnikov G K, Fatkullin M N 1981: Geomagn. i aeronomiya, 21, 545-547.

Basu S 1978: J. Geophys. Res., A83, 182-190.

Basu S, Basu S, Aarons J, McClure J P, Cousins M D 1978: J. Geophys. Res., A83, 4219-4226.

Basu S, Basu S, MacKenzie E, Coley W R, Hanson W B, Lin C S 1984: J. Geophys. Res., 89, 5554-5564.

Bauer S J, Nagy A F 1975: Proc. IEEE, 63, 230-249.

Berkner L V, Wells H W 1934: Terr. Magn. and Atmos. Electr., 39, 215.

Bertel L, Guyader P, Lassudrie-Duchesne P 1984: Radio Sci., 19, 879-890.

Booker H G 1979: J. Atmos. and Terr. Phys., 41, 501-515.

Booker H G, Wells H W 1938: Terr. Magn. and Atmos. Electr., 43, 249-256.

Calvert W, Schmid C W 1964: J. Geophys. Res., 69, 1839-1852.

Crane R K 1977: Proc. IEEE, 65, 180-199.

D'Angelo N 1977: Revs. Geophys. and Space Phys., 15, 299-307.

Davies K 1962: Proc. IRE, 50, 1544.

Davis T N 1979: Repts. Progr. Phys., 42, 1565-1604.

Drobzhev V I 1980: Ionosfernie issledovaniya, No 30, 62-68.

Du Castel F, Faynot J M 1964: Nature, 204, 984-985.

Dyson P L 1968: J. Geophys. Res., 73, 2441-2446.

Dyson P L 1969: J. Geophys. Res., 74, 6291-6303.

Dyson P L, McClure J P, Hanson W B 1974: J. Geophys. Res., 79, 1497-1502.

Eccles D, King J W 1970: J. Atmos. and Terr. Phys., 32, 517-538.

Erukhimov L M, Kazimirovsky E S, Kokourov V D 1977: Issledovaniya po geomagnetizmu, aeronomii i fizike Solntsa, 41, 3-6.

Erukhimov L M, Maksimenko O I, Myasnikov E N 1980: Ionosphernie issledovaniya, No 30, 27-53.

Evans J V 1969: Proc. IEEE, 57, 496-530.

Evans J V 1974: J. Atmos. and Terr. Phys., 36, 2183-2234.

Evans J V 1975: Proc. IEEE, 63, 1636-1650.

Farley D T 1971: In: Methods of Experimental Physics, v. 9B, chap. 14, edited by R H Lovberg and H R Grien, Academic, New York

Fatkullin M N 1975: In: Itogi nauki i tekhniki. Geomagnetizm i visokie sloi atmosferi 2. VINITI, Moscow, 102-168.

Fatkullin M N 1982: In: Itogi nauki i tekhniki. Geomagnetizm i visokie sloi atmosferi 6. VINITI, Moscow, 224.

Fatkullin M N, Zelenova T I, Kozlov V K, Legenka A D, Soboleva T N 1981: Empirical models of the mid-latitude ionosphere (in Russian), Moscow

Fatkullin M N, Solodovnikov G K, Legenka A D, Drukarenko S P 1984: Geomagn. i aeronomiya, 24, 191-195.

Fejer B G, Kelley M C 1980: Rev. Geophys. and Space Phys., 18, 401-454.

Francis S H 1974: J. Geophys. Res., 79, 5245-5260.

Fremouw E J. Rino C L 1973: Radio Sci., 8, 213-222.

Galkin A I, Erofeev N M, Kazimirovksy E S, Kokourov V D 1971: Ionospheric measurements (in Russian). Nauka, Moscow

Gdalevich G L 1980: Artificial Satellites, 15, 165-178.

Gdalevich G L, Ozerov V D, Vsekhsvyatskaya I S, Novikova L N, Soboleva T N 1980: Geomagn. i. aeronomiya, 20, 809-816.

Gelberg M G 1977: Rasprostraneniya radiovoln v polyarnoy ionosfere, Kolsky filial AN, Apatiti, 157-172.

Gershman B N 1974: Dynamics of the ionospheric plasma (in Russian). Nauka, Moscow

Gershman B N 1976: In: Itogi nauki i tekhniki. Geomagnetizm i visokie sloi atmosferi 3. VINITI, Moscow, 62-87.

Gershman B N 1980: Ionosfernie issledovaniya, No 30, 17-26.

Gershman B N, Grigorev G I 1978: Ionosfernie issledovaniya, No 25, 5-15.

Gershman B N, Kazimirovsky E S, Kokourov V D, Chernobrovkina N A 1984: The phenomenon spread-F in the ionosphere (in Russian). Nauka, Moscow

Getmantsev G G, Komrakov G P, Ivanov V P, Popkov I V, Tyukin V N 1973: Kosmicheskie issledovaniya, 11, 335-337.

Gupta S P 1980: Space Res., 20, 127-130.

Hanson W B, Sanatani S 1971: J. Geophys. Res., 76, 7761-7768.

Hanuise C 1983: Radio Sci., 18, 1093-1121.

Herman J R 1966: Rev. Geophys., 4, 255-299.

Holtet J A, Maynard N C, Heppner J P 1977: J. Atmos. and Terr. Phys., 39, 247-257.

Hooke W H 1968: J. Atmos. and Terr. Phys., 30, 795-823.

Karlov V D, Kozlov S I, Tkachev G N 1980: Kosmicheskie issledovaniya, 18, 266-277.

Kelley M C 1972: J. Geophys. Res., 77, 1327-1334.

Kelley M C, McClure J P 1981: J. Atmos. and Terr. Phys., 43, 427-435.

Kelley M C, Holtet J A, Tsurutani B T 1979: Plat. and Space Sci., 27, 127-130.

Kelley M C, Baker K D, Ulwick J C, Rino C L, Baron M J 1980: Radio Sci., 15, 491-505.

Kelley M C, Pfaff R, Baker K D, Ulwick J C, Livingston R, Rino C, Tsunoda R 1982: J. Geophys. Res., A87, 1575-1588.

Keskinen M J, Ossakow S L 1983: Radio Sci., 18, N6.

Komrakov G P, Skrebkova L A 1980: Ionosfernie issledovaniya, No 30, 49-52.

Komrakov G P, Lerner A M, Skrebkova L A 1983: Izv. vuzov. Radiofizika, 26, 770-772.

Kutimskaya M A, Gudkova T V 1983: Empirical model of spread-F for mid-latitudes taking into account solar activity (in Russian). Irkut. un., Irkutsk

Likhter Ya M, Gdalevich G L, Afonin V V, Larkina V I, Mikhaylov Yu M, Ozerov V D, Serafimov K B, Bankov L G, Dachev Tz P, Trendafilov N S, Chapkanov S K, Triska P, Jiricek F, Smilauer J 1980: Artificial satellites, 15, 184-193.

Livingston R C, Rino C L, McClure J P, Hanson W B 1981: J. Geophys. Res., A86, 2421-2428.

Livingston R C, Rino C L, Owen J, Tsunoda R T 1982: J. Geophys. Res., A87, 10519-10562.

Maier E J, Brace L H, Kayser S E 1978: J. Geophys. Res., A83, 2533-2542.

Maruyama T, Matuura N 1980: J. Rad. Res. Labs. Japan, 27, 201-206.

Migulin V V 1973: Vestn. AN SSSR, No 8, 9-15.

Migulin V V, Lobachevskiy L A, Namazov S A, Novikov V D 1978: Izv. AN Turkm. SSR, ser. fiz-tekhn., khim, i geol. nauk, 46, 46-63.

Münther C H, Spenner K, Neske E 1978: Geophys. and Astrophys. Fluid Dyn., 11, 141-150.

Namazov S A, Dzyubanov D A 1979: Ionosfernie issledovaniya,

No 27, 115-118.

Namazov S A, Novikov V D 1980: Ionosfernie issledovaniya, No 30, 87-94.

Namazov S A, Novikov V D, Khmelnitsky I A 1975: Izv. vuzov. Radiofizika, 18, 473-501.

Narcisi R S, Szuszczewicz E P 1981: J. Atmos. and Terr. Phys., 43, 463-471.

Ossakow S L 1978: In: Wave Instabilities in Space Plasmas. Proc. Symp., Helsinki, 265-289.

Ossakow S L 1981: J. Atmos. and Terr. Phys., 43, 437-452.

Ovezgeldiev O G, Muradov A 1980: Izv. AN Turkm. SSR, ser. fiz.--tekhn., khim. i geol. nauk., No 5, 43-67.

Pancheva D, Samardzhiev D 1983: Bulg. geofiz. spisanie, 9, 3-24.

Phelps A D R, Sagalyn R C 1976: J. Geophys. Res., 81, 515-523.

Rastogi R G 1984: Indian Journal of Radio and Space Physics, 13, 84-93.

Reber C A, Hedin A E, Pelz D T, Potter W E, Brace L H 1975: J. Geophys. Res., 80, 4576-4580.

Rodriguez P, Szuszczewicz E P 1984: J. Geophys. Res., A89, 5575-5580.

Serafimov K B, Kutiev I S, Bochev A Z, Dachev Ts P, Gringauz K I, Afonin V V, Gdalevich G L, Gubsky V F, Ozerov V D, Smilauer J 1976: Space Res., 16, 465-469.

Singleton D G 1975: J. Atmos. and Terr. Phys., 37, 1535-1544.

Solodovnikov G K, Bakay A S, Russkin V M, Fatkullin M N 1981: Geomagn. i aeronomiya, 21, 1009-1017.

Solodovnikov G K, Fatkullin M N, Russkin V M, Krokhmalnikov E B 1984: In: Modeling of the irregular structure of the ionosphere (in Russian). IZMIRAN, Moscow, 5-41.

Thermal non-linear phenomena in plasmas (in Russian). Sb. nauchn. tr. int. prikl. fiz. AN SSSR, Gorkiy, 216.

Troitsky B V 1980: Ionosfernie issledovaniya, No 30, 57-66.

Tsunoda R T 1980: J. Atmos. Terr. Phys., 42, 743-752.

Villadares C E, Hanson W B, McClure J P, Cragin B L 1983: J. Geophys. Res., A88, 8025-8042.

Vsekhsvyatskaya I S 1981: In: Fizika i struktura ekvatorialnoy ionosferi. Nauka, Moscow, 62-76.

Winkler T R 1980: Rev. Geophys. and Space Phys., 18, 659-682.

Yeh K C, Liu C H 1974: Rev. Geophys. and Space Phys., 12, 193-216.

Acta Geod. Geoph. Mont. Hung., Vol. 22 (1-2), pp. 47-59 (1987)

EXPERIMENTAL INVESTIGATION OF THE IRREGULAR STRUCTURE OF THE IONOSPHERE

E P Datsko[1], O I Maksimenko[1], V I Moskalyuk[1], N M Boguta[1]

[1]Main Astronomical Observatory, Academy of Sciences of the Ukr. SSR
252127 Kiev, Goloseevo, USSR

In this paper results of an experimental investigation of the following large scale irregular structures in the ionosphere at mid-latitudes are presented: sporadic E layer and the absence of the F2 layer (G condition according to the Handbook of Ionogram Interpretation, Pigott and Rawer 1972).

Data obtained by processing ionograms of the bottomside sounding of the ionosphere are used in the period 1964-1976 within the latitude range 46--60°N.

Morphological characteristics of the occurrence of the above mentioned structures are determined. A parameter characterizing the screening density of a sporadic E layer is introduced and its properties are studied in case of mid-latitude Es types as a function of the level of solar and geomagnetic activities. The occurrence of the condition G increases with latitude without a simultaneous change of the shape of the diurnal variation.

The obtained irregularity characteristics are to be considered in modeling and prediction of the propagation of radio waves in the ionosphere.

Keywords: effects of solar and geomagnetic activities; G condition; irregular structure of the ionosphere; sporadic E layers

The method of vertical sounding of the ionosphere by means of automatic ionospheric stations is widely used for the investigation of large scale irregular structures at mid-latitudes. There are large height gradients of the electron density both in the lower ionosphere- - that is sporadic formations in the form of thin Es layers of high electron density - and in the upper ionosphere- - sporadic vanishing of the main electron density maximum F2.

It is known that sporadic E layers have extensions of hundreds and thousands of kilometers in N-S and E-W directions (Chavdarov et al. 1978) and the G condition can be observed at different latitudes (Datsko et al. 1984). For the description of these phenomena probabilistic relations are used. Large

scale irregular structures with large electron density gradients play a substantial role in the determination of the path and in the prediction of the propagation of radio waves. The formation of dense Es layers alters the path of the ionospheric propagation of radio waves, and the vanishing of the F2 layer may contribute to the degeneration of existing ionospheric channels (Shlionsky et al. 1979). At the same time small scale irregularities of the electron density also exist which produce by scattering the radio waves ionospheric wave guides or remove waves from them (Gurevich and Tsedilina 1979).

DIURNAL, SEASONAL AND SOLAR CYCLE VARIATIONS OF Es

Diurnal, seasonal and solar cycle variations of the percentual occurrence of sporadic E layers are considered which differ from each other in the degree of reflection of radio signals. These are so called screening layers not transmitting the incident signals, and they are characterized by the almost complete coincidence of the screening frequency fbEs with the boundary frequency foEs, i.e. the range of their semitransparency is $\Delta fbEs = foEs - fbEs \leq 0.5$ MHz. Semitransparent layers are characterized by the range of semitransparency $0.5 \text{ MHz} < \Delta fbEs < 2$ MHz and the transparent layers by $\Delta fbEs > 2$ MHz (Chavdarov et al. 1978).

As it can be seen in Fig. 1, where diurnal variations of the percentage occurrence PE % of the screening (1), semitransparent (2) and transparent (3) Es layers are presented for three seasons of the year of solar activity minimum (1964) and that of a year of solar activity maximum (1969) at the station Kiev, the screening layer predominates in all seasons. The character of the diurnal variation shown by the percentage occurrence of the screening Es layer changes with season. The single winter maximum of the occurrence (PEs ~ 40-50 %), which appears about noon, is substituted in the equinoctial and summer months by two maxima of PEs (10 LT and 18 LT). Meanwhile, the magnitude of the occurrence somewhat increases (PEs ~ 70 %) and in summer the maxima are displaced forming an additional maximum at noon. In the year of solar activity maximum the morning

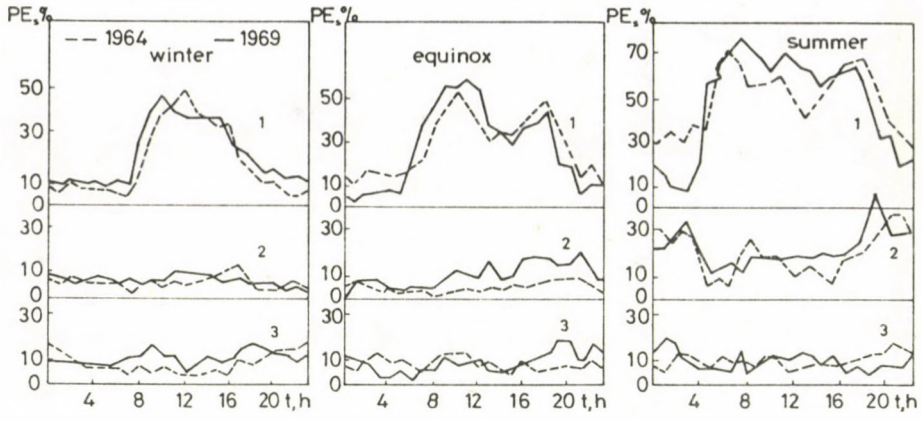

Fig. 1. Diurnal variations of the percentage occurrence of the screening, semitransparent and transparent Es layers in winter, summer and equinoxes of the solar activity minimum (-----) and maximum (———) at the ionospheric station Kiev

maximum increases in all seasons and simultaneously the evening maximum is reduced. Contrary to the screening layer, the diurnal variation of the percentage occurrence of the transparent Es layer does not show characteristic properties and amounts to ~10 % in winter and at equinoxes. At the same time the diurnal variation of the semitransparent Es layer shows night-time and morning maxima of ~30 %.

Seasonal variations of the percentage occurrence of the screening and semitransparent Es layers at mid-latitudes have similar character. In the year of solar activity minimum, a maximum PEs of the screening layer is observed from May to October, i.e. during the greater part of the year, but the semitransparent layer appears less often than in 1969, especially at equinoxes. Thus the character of the diurnal and seasonal variations of the Es occurrence is determined at mid-latitudes by the screening properties of the layer. The effect of the solar activity on the diurnal and seasonal variation of the screening Es occurrence is more definite in the evening hours and in autumn respectively.

RELATION OF Es TO GEOMAGNETIC ACTIVITY

As it has been shown earlier (Datsko et al. 1978), the occurrence of screening Es layers is inversely proportional to the geomagnetic activity in the afternoon and night hours, at the latitude of Kiev. In the winter months such a relation does not exist. Moreover, there is a negative correlation between the occurrence of Es and daily mean value of the geomagnetic horizontal component during increased solar activity. An increase of the occurrence of intense Es layers with increasing geomagnetic disturbance SD has been revealed. More detailed results concerning the relation of Es to geomagnetic activity have been obtained by analysing the seasonal change of the diurnal variation of Es occurrence in case of the four mid-latitude types f, l, c and h in 1964 and 1969 for two levels of the geomagnetic activity characterized by the geomagnetic index C (Fig. 2). The clearest inverse relation is observed between the percentage occurrence of the types f, l and geomagnetic activity during equinoxes at 18-19 LT in the period of the daily maximum and in summer at 20-22 LT. Besides the reduction of the percentage occurrence of the types f, l the magnetic disturbance results at the equinoxes in a change of the diurnal variation of PEs, due to the strengthening of the second night-time maximum of Es occurrence at 3 LT. In the years of increased solar activity analogous features are observed at 7 LT in the morning. The high types of the sporadic E layer are more often found in the period of weak geomagnetic activity in day-time hours. In summer an increase of the evening maximum is experienced. At equinoxes during the day the effect of the geomagnetic activity is insignificant, though the winter day-time behaviour is characterized by an increase of the percentage occurrence of the high types in geomagnetically disturbed periods what is especially significant afternoon in the year of minimum solar activity.

Thus, at low solar activity disturbances of the geomagnetic field which reduce PEs in summer, enable the appearance of a maximum of the c type Es in winter and that of the night type l at equinoxes. In years of increased solar activity especially

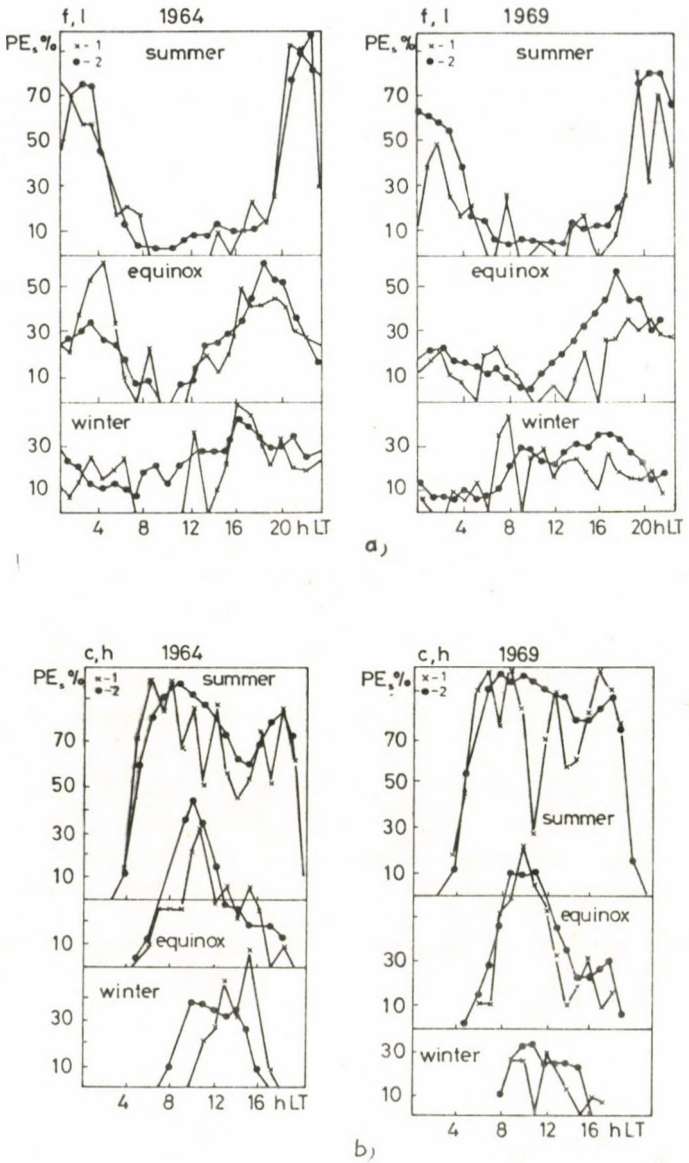

Fig. 2. Seasonal changes in the diurnal variation of the percentage occurrence of the midlatitude Es types f, l (Fig. 2a) and c, h in the years of the solar activity minimum (1964) and maximum (1969) for geomagnetically disturbed (1) and quiet (2) periods

in the evening hours the negative correlation between the occurrence of Es and the geomagnetic activity is strengthened, though the appearance of an additional morning maximum of the l type Es is also observed.

SOME PROPERTIES OF Es

Datsko et al. (1978) have determined the parameter screening density in the form of the ratio fbEs/foEs for mid-latitude Es types. In Fig. 3 diurnal variations of the density of the Es types f, l and c, h are plotted for different seasons of the years of minimum (1964) and maximum (1969) solar activity. The most dense layers are observed during the day. In the evening and night hours the density is substantially less and a great difference is found between the screening density in the years 1969 and 1964. The density of f and l type Es decreases significantly with increasing solar activity in all seasons in the morning and afternoon and it

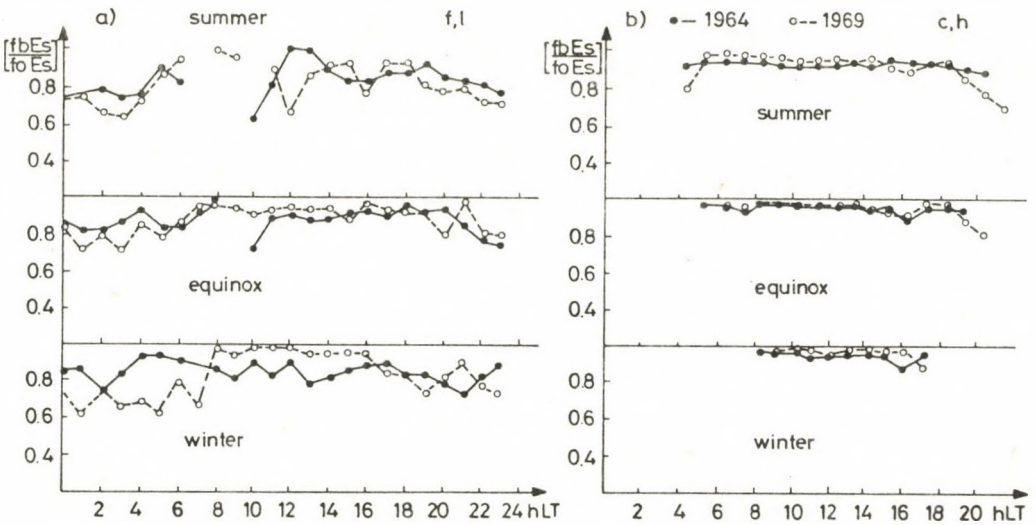

Fig. 3. Diurnal variations of the monthly mean values of the screening density fbEs/foEs for the Es types f, l (a) and c, h (b) in three seasons of 1964 and 1969

increases in the day-time hours in winter, as well as at equinoxes. The density of the high Es layers (c, h) is the largest, which almost did not change during the whole period of observations, somewhat decreasing after 1618 LT. In the year of high solar activity in winter and summer the day-time Es types are also characterized by a decrease of the density. Thus, the effect of the solar activity is larger on the magnitude of the density in case of the lower lying sporadic E layers.

Seasonal variations of the screening density of the Es layer are shown in Fig. 4 for given hours of the day, corresponding to the time of the daily maxima in the occurrence of the mid-latitude Es types f, l, c, h in the years of maximum

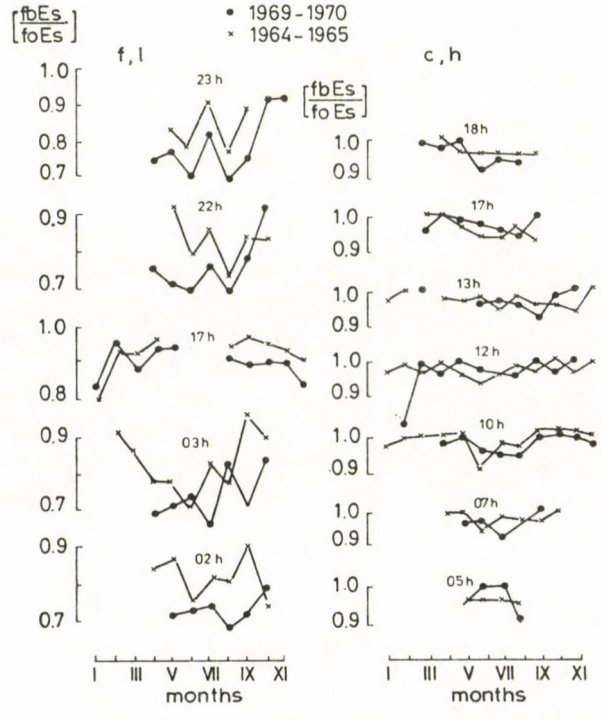

Fig. 4. Seasonal variations of the screening density of the Es types f, l, c, h for individual hours of the day in the periods 1964-65 and 1969-70

and minimum solar activity. The screening density of the Es types c and h hardly changes during the year. Only a tendency of decreasing screening density in the summer months can be observed, being more stable about noon. In case of the low lying Es layers another behaviour can be observed. Basically, it is an irregular seasonal variation of the density in form of an increase of fbEs/foEs at equinoxes. Contrary to the day-time high Es types in the years of minimum and maximum solar activity the character of the density variation about midnight remains approximately the same. In case of night-time low lying Es layers a higher negative correlation is found between the screening density and the solar activity. Because of the large scattering of the values, the analysis of the diurnal variation of fbEs/foEs of the f, l and c, h type sporadic E layers did not show any definite clear relation between the magnitude of the screening density and the level of geomagnetic activity (Fig. 5) in geomagnetically quiet and disturbed conditions of the years of minimum and maximum solar activity. Small changes of the screening density have been observed in case of the types c, h during the day, by the types f, l at night. At equinoxes in geomagnetically quiet periods they amount to 0.15, while the changes of density with geomagnetic activity are significantly less, i.e. 0.05, especially in the year of solar activity minimum. Thus, it could be shown that the screening density (or the irregularity) of the sporadic E layer is determined by its type, its height, varies during the year with the level of solar and geomagnetic activities. It has also been demonstrated that in case of the low Es types the irregularity is largest in the night hours in all seasons. At mid-latitudes the irregularity of the Es types f, l is more sensitive to changes of the solar activity, than to that of the geomagnetic activity.

STRUCTURAL IRREGULARITIES IN THE F REGION OF THE IONOSPHERE

Changes of the structure of the ionosphere (sporadic layers, stratifications, especially the displacement of the height of the electron density maxima) prove to be often of crucial

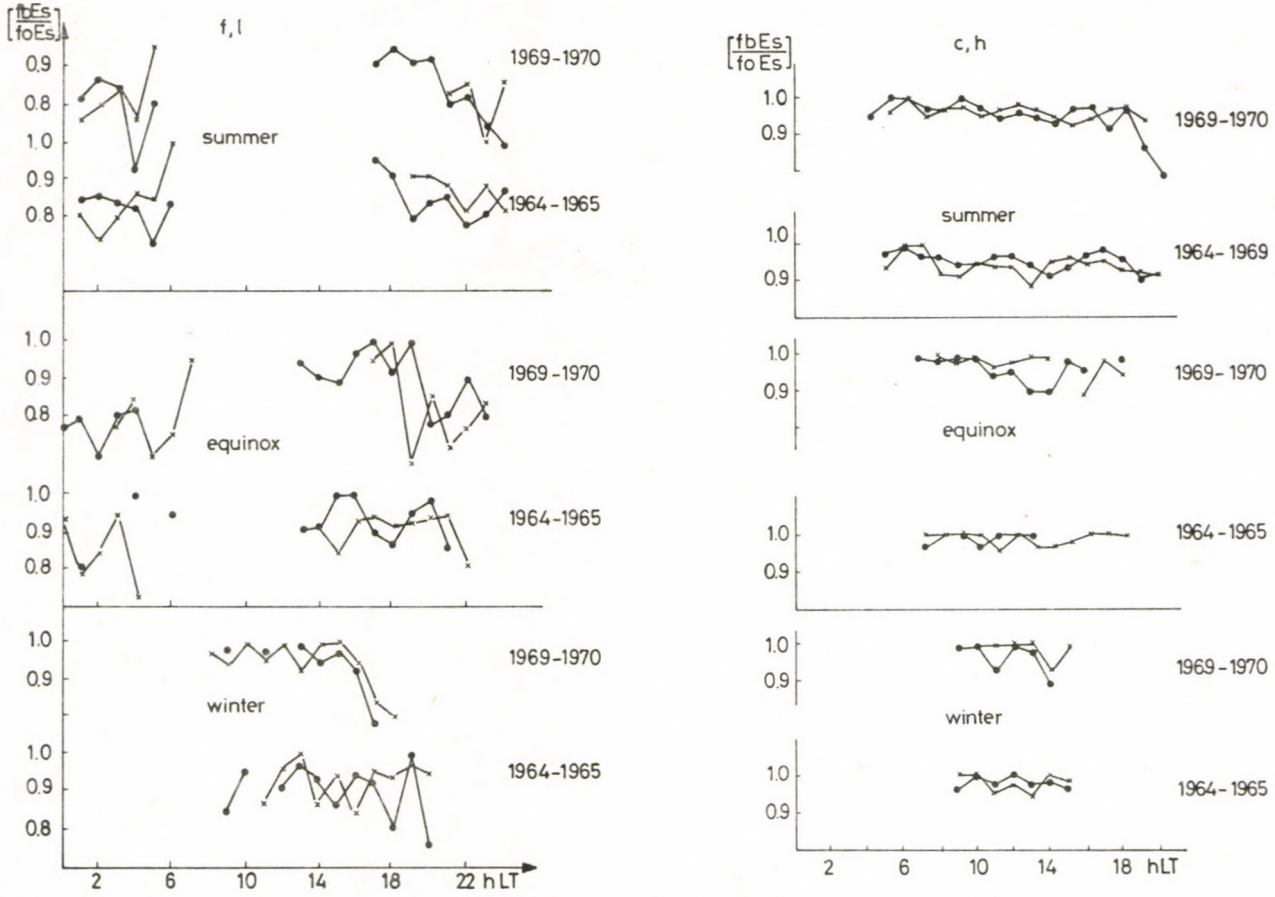

Fig. 5a-b. Diurnal variations of the density of the Es types f, l (Fig. 5a) and c, h in case of 5 geomagnetically quiet (•) and disturbed (×) days in each season of the solar activity minimum and maximum

importance in the prediction of the long-distance HF propagation. Therefore, the gradual decrease of the electron density in the F2 layer to the electron density should be studied at the maximum of the F1 layer and less. According to the Handbook of Ionogram Interpretation and Reduction (Piggott and Rawer 1972) this is the so called "G condition".

In the followings the results of a study of the G condition morphology are discussed based on the data of vertical sounding of the ionosphere at stations of the northern hemisphere in the latitudinal zone 45-60°. For the mid-latitude station Kiev the diurnal and seasonal variations of the percentage occurrence of G were determined in each month of the years 1963-65, 1974-77. It has been found that in 40 % of the cases the G condition is observed for a short time (5-15 min) and only in 1 % of the cases it exists for 5 hours or more. In Fig. 6 the diurnal variation of the percentage occurrence of G is presented in summer and equinoxes in the vicinity of the solar activity minimum. In summer the occurrence has two maxima,

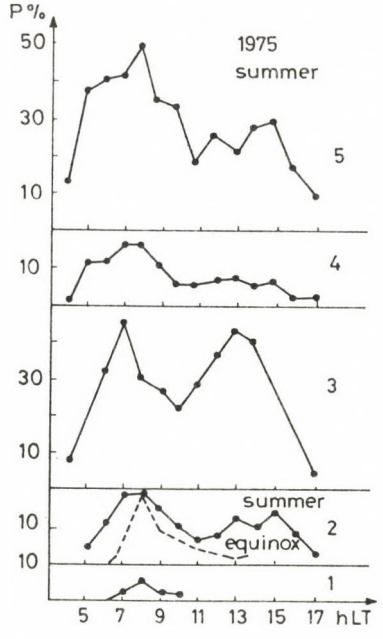

Fig. 6. Diurnal variations of the percentage occurrence of the G condition at mid-latitude stations: 1 - Rostov, 2 - Kiev, 3 - Kaliningrad, 4 - Moscow, 5 - Leningrad

one in the morning at 8 LT and a second in the afternoon at 1415 LT, but at equinoxes only one in the morning appears. Besides, the morning maximum is usually predominant. In addition to the diurnal variations the seasonal variation of the occurrence of G has also been studied at different latitudes. In the years of the solar activity minimum the characteristic feature of the seasonal variation is maximum occurrence in July. A clear 11 year period of the occurrence of G has also been found with maxima in 1975 (86 %) and 1964 (68 %) as compared to 26 % in 1976 and 32 % in 1965. In the period of maximum occurrence of G, July 1975 the latitudinal variation of the phenomenon, has been investigated in more detail. Data of the mid-latitude stations Rostov, Kiev, Kaliningrad, Moscow and Leningrad have been used. In Fig. 7. the seasonal variations of the monthly mean occurrence of G are plotted at the individual stations. Except an increase of the occurrence of G with latitude in all seasons there is no definite change of the character of

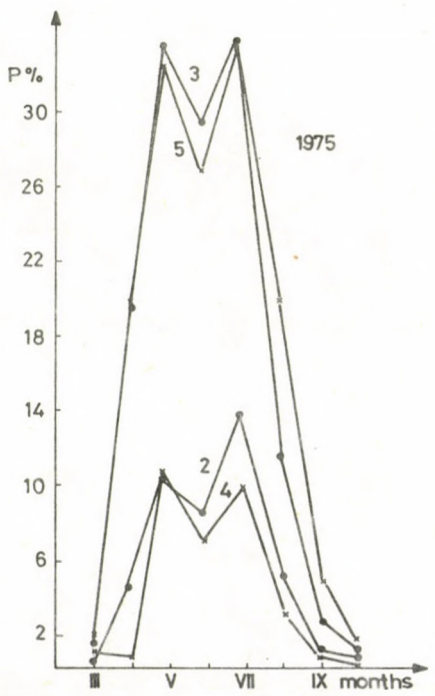

Fig. 7. Seasonal variations of the monthly mean percentage occurrence of the G condition at mid-latitude stations

the diurnal variation and that of the seasonal variation with latitude. A clear dependence of the occurrence on the parameter L could also not been shown.

Examples of the variation of the electron density at fixed heights in the ionosphere during G condition are presented in Fig. 8 and the corresponding height variation of the lines of equal concentration obtained on the basis of the computed N(h) profiles are also given. The vanishing of the F2 layer maximum is preceded by sharp decreases of the concentration at altitudes below 200 km. The development of the G condition is followed by a rise of the F1 layer by 30 km, however, during this process significant changes in the E layer are not observed. From this analysis it follows that the downward displacement of

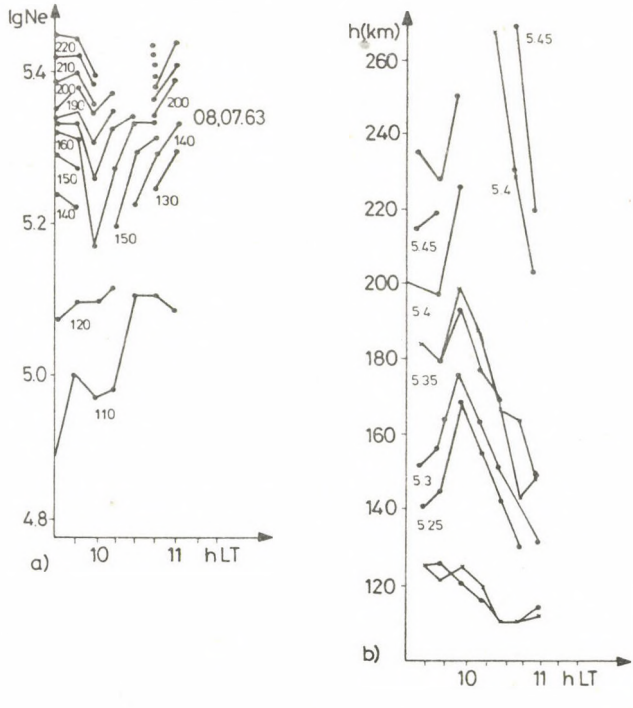

Fig. 8. Variations of the parameters of N(h) profiles during G condition: a) electron density at constant heights, b) hE, hF1 and hF2 in case of constant electron densities

the main ionization maximum to the height of the F1 layer is simultaneously observed in a large area of the northern hemisphere developing mainly during minimum solar activity in the period of moderate geomagnetic activity. The speed of the change of concentration seems to depend on latitude. Nevertheless, the displacement of the maximum can also be of local character often occurring at high latitudes.

Besides a gradual change of the structure (G condition) the fast vanishing of reflections from the F region (from the levels of the F1 and F2 layers) called as phenomenon "lacuna" in the Handbook of Ionogram Interpretation and Reduction is often observed at high latitudes. The lacunas are considered to be the result of processes related to the precipitation of particles from the dayside cusp, to magnetospheric phenomena (Sylvain and Carton 1979). The influence of both the lacuna and the G condition producing sharp gradients of the electron density in the ionosphere are of decisive importance for the propagation of short wave signals. Nevertheless, the mechanism of the development of these phenomena may be different.

REFERENCES

Chavdarov S S, Chasovitin Yu K, Chernishev S P, Sheftel V M 1978: Mid-latitude sporadic E layer of the ionosphere (in Russian). Nauka, Moscow

Datsko E P, Maksimenko O I, Moskalyuk V I 1978: In: Particle Acceleration and Plasma Effects in Space (in Russian). Sb. Nauchn. Tr. Naukova dumka, 141-154.

Datsko E P, Maksimenko O I, Moskalyuk V I 1984: In: Abstracts of papers, 17. Symposium for solar-terrestrial Physics, KAPG, Nauka, 146-147.

Gurevich A V, Tsedilina E E 1979: Long-distance propagation of short radio waves (in Russian). Moscow, Nauka

Piggott W R, Rawer K 1972: Handbook of ionogram interpretation and reduction. Warsaw

Shlionsky A G 1979: Long-distance propagation of radio waves in the ionosphere (in Russian), Nauka, Moscow

Sylvain M, Carton S 1979: Planetary Space Science, 27, 1293--1301.

Acta Geod. Geoph. Mont. Hung., Vol. 22 (1-2), pp. 61-71 (1987)

SPREAD-F AS A SPECIFIC MANIFESTATION OF THE IRREGULAR STRUCTURE OF THE IONOSPHERE

O G Ovezgeldiev[1], A Muradov[1], A Mukhametnazarova[1], Yu Karadzhaev[1]

[1]Physical and Technical Institute of the Academy of Sciences of the Turkmen SSR, 744000 Ashkhabad, Gogol al. 15, USSR

Basic morphological properties are shown and a statistical model of the spread-F phenomenon is constructed. The quantitative characteristics of this phenomenon are studied by means of the method of spectral analysis. It is assumed that internal gravity waves can play the initiative role in the generation of the irregularities responsible for the phenomenon spread-F.

Keywords: internal gravity waves; irregular structure of the ionosphere; spread-F

The F region of the ionosphere is a dynamical, unstable formation subjected to different regular and irregular variations. The regular variations of the parameters of the F region have been studied in detail, empirical and theoretical models suitably describing these variations were constructed. The irregular variations of the F region parameters, produced by a number of factors of so far unknown physical nature are less studied. Therefore, the investigation of these variations is of scientific and practical interest in order to construct models of their spatial and temporal distribution and for the clarification of the physical mechanisms of their formation.

One of the most frequently occurring irregular phenomena in the ionosphere is the spread F appearing in vertical sounding ionograms in form of a dimmed trace of the reflected signal. In earlier phases of the investigation of the ionosphere, spread F has been only a factor making the interpretation of ionograms more difficult and the physical character of this phenomenon has been considered only marginally. Nevertheless, with the development of the ideas concerning the physical processes in the upper atmosphere the opinion has gradually

been confirmed that this phenomenon is due to the scattering of radio waves by small scale irregularities of the ionosphere. Experimental investigations have shown that in consequence of the scattering on irregularities in the region of reflection the reflected impulse is of a much greater duration than the transmitted one. As a result of this the trace on the ionograms becomes dimmed, diffuse, consisting of more scattered reflections.

The study of the spatial and temporal characteristics of the spread-F led to information on the regularities of the distribution of ionospheric irregularities responsible for this phenomenon and to recognition of their formation mechanisms.

In the last years the study of spread-F draws growing attention due to broadening of the possibilities of making experiments by means of both ground based and satellite methods. Scattered reflections have been recorded on topside sounding ionograms, on the basis of which a model of the spatial and temporal distribution of spread-F has been constructed in the outer ionosphere well agreeing with the results of the bottom side sounding. It became clear that the irregularities responsible for the spread-F are located in a large height interval both below and above the maximum of the F region of the ionosphere. Valuable information on the fine structure of the spread-F has been obtained by means of the incoherent scatter stations. Briefly, many experimental methods are used at present for the study of the spread-F by means of which experimental data are obtained for processing and quantitative interpretation.

It has to be noted that radio waves are subjected in case of spread-F at the reflection from the ionosphere to the largest fluctuations if the dimensions of the scattering irregularities are equal to the magnitude of the first Fresnel zone. Therefore, the study of the spread-F phenomenon in the ionosphere is of great practical importance.

The analysis of the results of systematical observations concerning spread-F based on the experimental data of the network of ionospheric stations enabled to establish the basic morphological properties of the spatial and temporal distribu-

tion of this phenomenon (Ovezgeldiev and Muradov 1980). Considering the geographical distribution of the occurrence frequency of spread-F according to the geomagnetic latitude of the observing station three basic zones are distinguished. The first zone is constituted by the equatorial region between the geomagnetic latitudes $\pm 20^{o}$. Here spread-F occurs steadily in the night-time hours, predominantly in the evening and pre-sunrise hours. This is the zone of maximum spread-F occurrence frequency.

The second zone of the maximum spread-F occurrence frequency starts at a geomagnetic latitude of about 40^{o} and approaching the poles, the percentage of its occurrence frequency increases to 100 %. The high latitude spread-F is observed basically at night, but it occurs frequently during the day, too. At latitudes above 70^{o} spread-F appears during the day, this zone is called the region of the "steady maximum". The mid-latitude spread-F is similar to the high-latitude one but it is of a much lower probability of occurence and of a less intensity.

The third zone is constituted by the geomagnetic latitudes from 20^{o} to 40^{o}, this is the zone of minimum spread-F occurrence frequency. On the basis of many experimental data of the station Ashkhabad located in this zone a statistical, empirical model of spread-F has been constructed (Muradov and Mukhametnazarova 1981). Diurnal seasonal and solar cycle variations of spread-F have been determined in geomagnetically quiet and disturbed conditions. Scattered reflections appear in this zone exclusively in the night-time hours (Fig. 1) and their characteristics are similar to the equatorial spread-F.

At equatorial and transitional latitudes the maximum probability of the occurrence of scattered reflections is in summer months, but at middle and high latitudes in winter months.

Spread-F varies also with solar and geomagnetic activities. The correlation between scattered reflections and the solar and geomagnetic activities depends on the latitude of the observing station.

Spread-F occurs more frequently at equatorial stations in the year of solar activity maximum. The probability of the

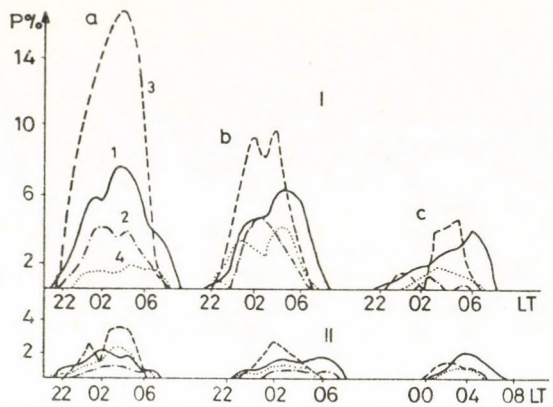

Fig. 1. Empirical model of spread-F obtained on the basis of the data of the station Ashkhabad
I - quiet conditions; II - disturbed conditions; a,b,c - minimum, medium and maximum solar activity; 1,2,3,4 - spring, autumn, summer and winter

occurrence of scattered reflections is at high latitudes also higher in the year of solar activity maximum.

At the latitude of Ashkhabad the probability of the occurrence of scattered reflections decreases with increasing solar activity. Thus, according to our results the percentage occurrence of scattered reflections is almost three times greater in the year of solar activity minimum than in the year of solar activity maximum (Fig. 1).

The correlation between spread-F occurrence and geomagnetic activity is negative at equatorial latitudes (lower than 20^{o} geomagnetic latitude), at middle and high latitudes it is positive.

At the station Ashkhabad the percentage occurrence of scattered reflections is substantially higher in geomagnetically quiet conditions than in disturbed times. Thus, the situation is at these latitudes the same as at equatorial latitudes.

Moving from high to equatorial latitudes the correlation between spread-F occurrence and geomagnetic activity changes to the opposite.

Here it should be reminded that the latitudinal variation of ionospheric disturbances. As a rule negative ionospheric disturbances are transformed into positive disturbances when moving from high to equatorial latitudes at a certain transitional latitude of $30-40^{o}$ geomagnetic latitude and retain

their sign till the equator. There is certain similarity between the latitudinal variation of ionospheric disturbances and the dependence of spread-F on the level of geomagnetic activity. An explaination of this experimental fact should be attempted later.

Besides the generally accepted basic quantitative characteristic of the spread-F, i.e. the probability of its occurrence (the ratio of the number of cases with scattered reflections to the number of observations) new quantitative characteristics of this phenomenon have been introduced (Muradov and Mukhametnazarova 1982): the height range of the scattering, proportional to the duration of the reflected impulse and the parameter $\Delta f/f$ being the quantitative measure of the mean amplitude of the electron density irregularity (Δf is the frequency range of the scattering).

For the quantitative interpretation of the experimental regularities of the spread-F further investigations are needed concerning the formation mechanism of this phenomenon. In the last years more and more attention is devoted to the wave mechanism of the spread-F formation related to the effect of acoustic-gravity waves (Booker 1979). According to up-to-date theoretical considerations steep gradients in the F region of the ionosphere due to acoustic gravity waves can result in the development of a Rayleigh-Taylor instability and in the formation of zones of decreased electron density ("bubbles") the presence of which is in many cases followed by the formation of small scale irregularities elongated along the direction of the geomagnetic field and they are responsible for the phenomenon spread-F and the ionospheric scintillation of satellite signals.

Acoustic-gravity waves in the ionosphere have been recorded by direct satellite measurements (Trinks and Mayr 1976, Mayr and Hedin 1977). According to recent data acoustic-gravity waves extend over a broad range of the frequency spectrum beginning with the Brunt-Vaisala frequency to frequencies including the diurnal variations of the atmosphere. The horizontal dimensions of the acoustic-gravity waves extend from sizes corresponding to the scale height of the neutral atmosphere at

the altitude of the F region to dimensions of the order of the Earth's radius, the vertical dimensions are of the order of the scale height (Booker 1979).

Acoustic-gravity waves are generated primarily in the neutral atmosphere. As a result of the collision of neutral particles with charged particles the latter are forced to oscillate along the geomagnetic field lines. Because of the magnetization of the plasma at the height of the F region the neutral particles cannot move the plasma perpendicular to the geomagnetic field lines and undergo a damping known as "ion drag". The resulting motion of the plasma is called travelling ionospheric disturbance (TID).

It was already in the fifties that the phenomenon spread-F was related to TID's (Uyeda and Ogata 1954, Mc Nicol and Bowman 1957). Further investigations have shown that ionospheric scintillations of satellite signals and of discreet radio sources correlate also with spread-F. This result hints at the joint formation of the phenomena mentioned above.

For the experimental proof of the existing conception concerning the wave origin of spread-F a special experiment was carried out by the simultaneous vertical sounding of the ionosphere at two sites with different distances between them and the distance having different orientation. Such experimental data as the non-simultaneity of the occurrence of scattered reflections at different sites, the shift concerning their occurrence and ceasing at different sites, as well as their dependence on the distance between the sites and its orientation, the similarity in the distribution of the newly introduced quantitative spread-F characteristics at the different points prove the wave origin of this phenomenon (Muradov and Mukhametnazarova 1983).

Periodical components have to be present in case of the wave origin of the irregularities in the acoustic-gravity wave range of the spectrum of the fluctuations. Thus, periodical components from 15 min to 85 min have been revealed (Titheridge 1971) on the basis of the spectrum of total electron content fluctuations obtained by the Faraday rotation of the polariza-

tion plane of satellite signals, where the lower limit corresponds to the Brunt-Vaisala frequency at the height of the F region and the upper limit is determined by the filter used in the spectral analysis.

For the quantitative study of the structure of spread-F spectral analysis was used by the authors, after an investigation of its use for time series of ionospheric parameters carried out by Karadzhaev (1982). Concerning the interrelation between spread-F and sporadic E layer it was assumed that the sporadic E layer could be the source of middle scale internal gravity waves generated by turbulence in the turbopause region which could play a role in the production of irregularities responsible for spread-F by propagating to the F region of the ionosphere. In these investigations synchronous power spectra of the quantitative spread-F parameter ($\Delta f/f$) (Muradov and Mukhametnazarova 1982) and of the frequency parameters of the sporadic E layer were computed. For this purpose data of the continuous vertical sounding of the ionosphere were used. On the basis of the data obtained with continuous spaced sounding of the ionosphere simultaneously, coherence spectra were calculated at two pairs of stations with distances of 18 and 120 km from each other. The results of 12 series were analyzed, each lasted from 2 to 4 hours.

The power spectra were computed by the maximum entropy method while the coherence spectra were obtained by means of the method of Blackman-Tukey. The critical frequencies of the Es layer and of the F region (foEs and foF2), the blanketing frequency (fbEs), the quantitative spread-F parameter ($\Delta f/f$) and the ratio ΔfbEs/fbEs being an indicator of the turbulence in the zone of Es formation were submitted to spectral analysis. At the computation of the spectra components with periods greater than 1 hour were eliminated by a sliding average filter (Karadzhaev 1982).

The computation of time spectra of the ionospheric parameters mentioned above was carried out in the frequency range of 1-6 cycles/h. The results of the computations have shown that the spectra obtained are characterized by one maximum.

From 9 power spectra of the spread-F parameter $\Delta f/f$ determined from sounding data of the station Ashkhabad, there are in 7 cases maxima distributed in the range from ~13 min to ~30 min with a mean value of about 20 min (Fig. 2). This period appears in the range of acoustic-gravity waves observed in the height of the F region of the ionosphere and according to the opinion of the present authors it is a quantitative proof of the wave origin of the spread-F (Muradov et al. 1984).

A single steady maximum appears also in the power spectra of the other ionospheric parameters during spread F. This may be an evidence of the similarity between the structure of the F region and that of the Es layer. In all cases considered here strong turbulence was observed, the value of Δf_{bEs} varied on

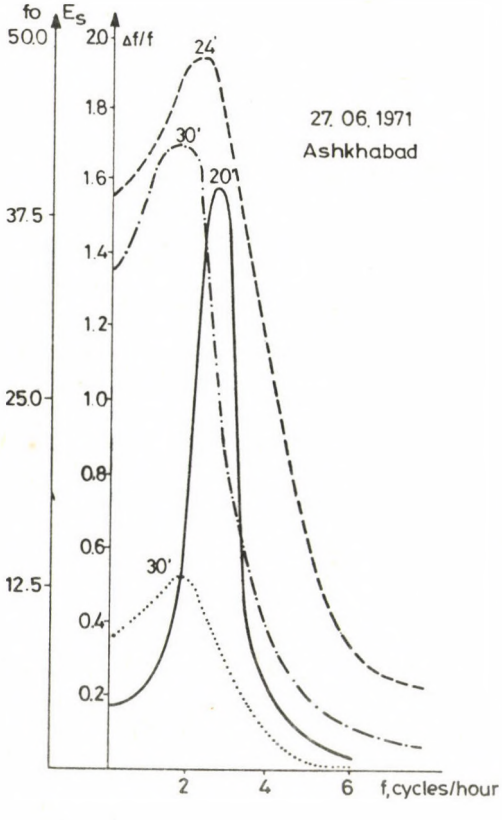

Fig. 2. Power spectra of the frequency parameters of the F region and of the Es layer during spread-F ($\Delta f/f$ ——— , foF2 -.-.-, foEs -----, fbEs .....)

the average from 1 MHz to 2.8 MHz. The maxima of the power spectra of foEs occur on the average at a period of 21 min changing within the range from 20 min to 30 min.

The wave origin of the spread-F is indicated also by the spectra of spaced sounding data. Spectra obtained in case of small distances (Ashkhabad-Vanovsky 18 km) (Fig.3) have maxima at the same period. In case of greater distances (Ashkhabad--Bakharden) in the spectra of only one of the stations (Ashkhabad) occurs a maximum (Fig. 4).

The above mentioned results are supported by the coherence spectra obtained for the stations in question. Coherence is found in case of short bases (Fig. 5a), the coherence ceases in case of long bases (Fig. 5b). The mechanism discussed here

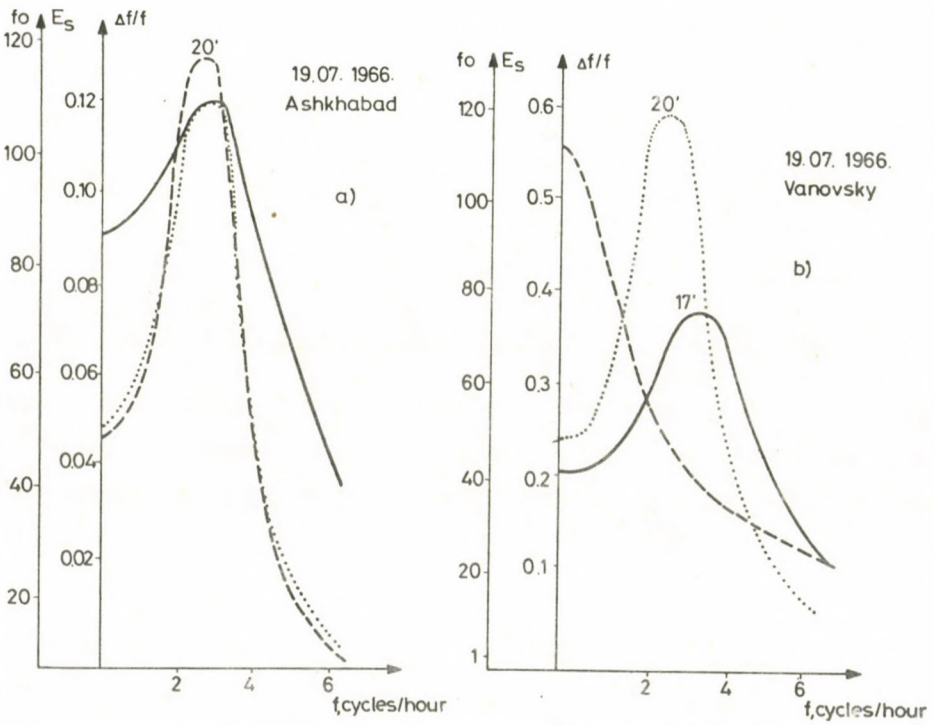

Fig. 3. Power spectra of the parameters in question in case of short bases for the station pair Ashkhabad-Vanovsky (18 km). Notation as in Fig. 2

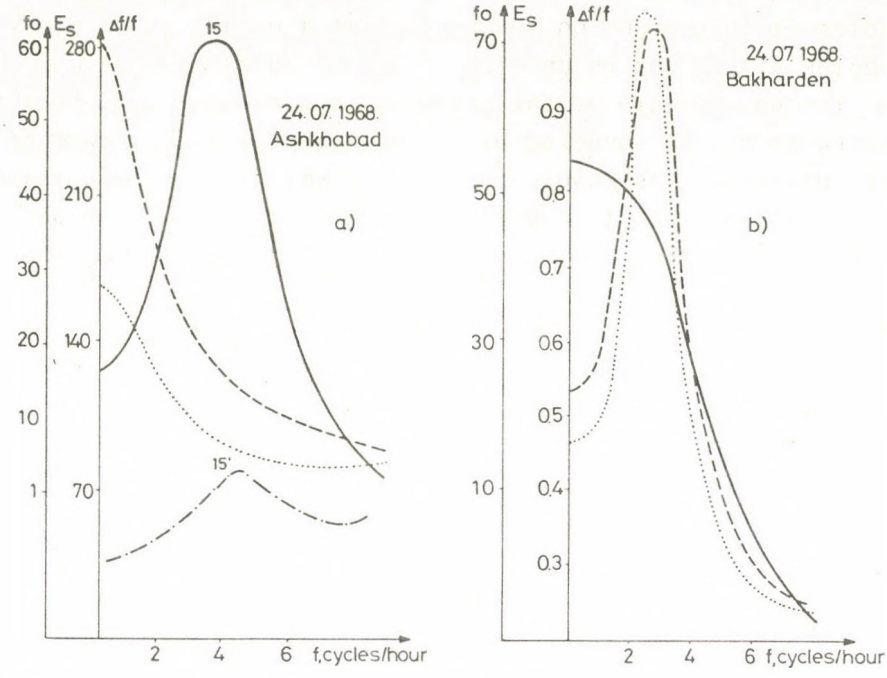

Fig. 4. Power spectra of the parameters in question in case of long bases for the pair of stations Ashkhabad-Bakharden (120 km). Notation as in Fig. 2

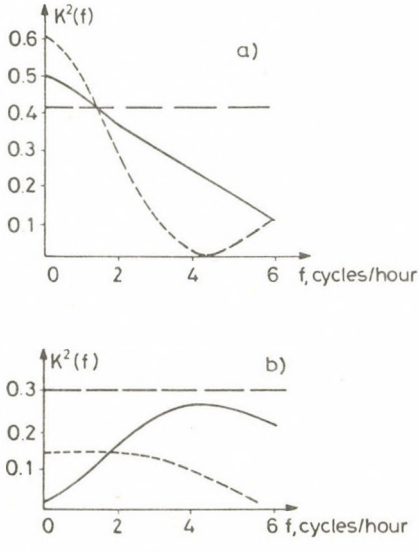

Fig. 5. Spectra of coherence between the frequency parameters of the F region and of the Es layer on the basis of continuous spaced sounding for pairs of stations with short (a) and long (b) base. Notations as in Fig. 2

enables to explain the similarity of the latitudinal variation of ionospheric disturbances to the dependence of spread-F on the level of geomagnetic activity.

REFERENCES

Booker H G 1979: J. Atmos. Terr. Phys., 41, 501-515.

Karadzhayev Yu 1982: Proc. Acad. Sci. of the TSSR, Ser. Phys.-Techn., Chem. and Geol. Sci., 94-97.

Mayr H G, Hedin A E 1977: J. Geophys. Res., 82, 1227.

McNicol R W E, Bowman G G 1957: Aust. J. Phys., 10, 588.

Muradov A, Mukhametnazarova A 1981: Proc. Acad. Sci. of the TSSR, Ser. Phys.-Techn., Chem. and Geol. Sci., 107-110.

Muradov A, Mukhametnazarova A 1982: Issledovaniya po geomagnetizmu, aeronomii i fizike solntsa, "Nauka", Moscow, 59, 24-28.

Muradov A, Mukhametnazarova A 1983: Phys. Solariterr., No 20, 86-92.

Muradov A, Mukhametnazarova A, Karadzhaev Yu 1984: Extended Abstracts, Symposium KAPG, Praha, 55

Ovezgeldiev O G, Muradov A 1980: Proc. Acad. Sci. of the TSSR, Ser. Phys.Techn., Chem. and Geol. Sci., 43-67.

Titheridge J E 1971: Planet. Space Sci., 19, 1593.

Trinks H, Mayr H G 1976: J. Geophys. Res., 81, 4023.

Uyeda H, Ogata Y 1954: Rep. Ionosphere and Space Res. Japan, 8, 103-107.

Acta Geod. Geoph. Mont. Hung., Vol. 22 (1-2), pp. 73-85 (1987)

MAGNETOSPHERIC AND IONOSPHERIC IRREGULARITIES CONNECTED WITH GEOMAGNETIC STORMS

D Pancheva[1] and Ts Ralchovsky[1]

[1]Geophysical Institute, Bulgarian Academy of Sciences, 1113 Sofia, Acad. G. Bonchev str. Block 3, Bulgaria

In the present paper the influence of meridional winds, generated at auroral latitudes by Joule heating is investigated on the electron distribution in the ionosphere-magnetosphere system during geomagnetic storms. The electron concentration obtained from ground based whistler measurements as well as data of the ionospheric station in Sofia have been used. It is shown that the magnetospheric irregularities found near the equator for $1.5 < L < 2.5$ are connected with the positive reaction of the day-time mid-latitude F region.

Keywords: F region of the ionosphere; geomagnetic storm; ionospheric irregularities; magnetospheric irregularities

INTRODUCTION

During geomagnetic disturbances, energy provided by the solar wind is consumed in the magnetosphere-ionosphere system by three main mechanisms (Akasofu 1981) a) particle injection into the inner magnetosphere with an energy Q_R proportional to $\partial D_{st}/\partial t$, b) Joule heating Q_J due to the dissipation of auroral electrojet currents and c) energy deposited in the auroral ionosphere by precipitating particles. During the main phase of the geomagnetic storm $Q_R \geqq Q_J$, i.e. the Joule heating is usually the second energy sink after the ring current. During the recovery phase, however, because of increased single or sequential magnetic substorms, Q_J exceeds often significantly Q_R, i.e. the Joule heating becomes the most important energy sink. In the paper of Davies (1981) the role of the precipitating particles in auroral latitudes is discussed. It is established that 30 % of the mean energy is due to them and the remaining 70 % is due to Joule heating. As a result of this significant

heating of the ionosphere at auroral latitudes, a meridional wind directed to the equator is generated. These winds move the plasma upwards along geomagnetic field lines. The upward drift delays the ambipolar diffusion, being normally directed downwards. As a result the F2 maximum is formed at greater heights, where the recombination coefficient is smaller. Therefore meridional winds induced by the Joule heating are responsible for the increase of the electron concentration in the mid-latitude F region (or the occurrence of a positive phase can be attributed to them). These electron density enhancements can propagate upwards along the geomagnetic field lines to the equator. Thus, the enhancements of the electron concentration near the equator shown by ground based whistler observations can be the result of the increased electron density at all altitudes along geomagnetic field lines from the mid-latitude F2 maximum to the equator, i.e. the result of the positive phase in the reaction of the mid-latitude F region. This means that such an increase in the magnetospheric electron concentration during geomagnetic storms can also be an indication of the occurrence of a positive phase in the reaction of the mid-latitude F region.

In the present paper the influence of the neutral wind on the electron distribution in the ionosphere-magnetosphere system during geomagnetic storms is studied. It is shown that the magnetospheric irregularities observed near the equator at $1.5 < L < 2.5$ are connected with the positive reaction of the day-time mid-latitude F region. The electron concentration determined on the basis of ground based whistler observations as well as data of the ionospheric station Sofia have been used.

The occurrence of irregularities in the electron concentration at ionospheric and magnetospheric heights during geomagnetic storms depends significantly on the intensity of the induced meridional wind. Thus, it is closely connected with the rate of Joule heating at auroral latitudes. Therefore, in order to understand the energy transfer or the connection of the solar wind with the magnetosphere-ionosphere system, it is important to establish good estimates of the global Joule heating rates. For that purpose as an approximate measure of the global Joule heating rate the auroral AE-index is used (Baumjohann and

Kamide 1984). It was found that: $Q_J = 0.32$ AE, where Q_J is measured in [GW] and AE in [nT]. If the electron irregularities at magnetospheric altitudes near the equator indicated by whistler measurements in Sofia and the positive phases of the day-time F region reaction revealed by the ionospheric station are due to meridional winds, clearly expressed peaks in the AE index coinciding or preceding the measurements should exist. The increase of the auroral activity leads to a change of the geomagnetic field recorded in low-latitude observatories (Gonzales et al. 1979). Consequently, significant changes in the AE-indices should be accompanied by disturbances in the equatorial D_{st}-index. The present work consideres four cases of magnetospheric irregularities observed near the equator at $1.5 < L < 2.5$ and in the afternoon and night hours. In two cases both AE- and D_{st}-indices are available. The AE variations have actually some effect on the D_{st}-index. This allows us to use the variation of D_{st}-indices as an indication of Joule heating in the auroral region, if the AE-index is missing.

EXPERIMENTAL RESULTS

Data of the Sofia ionospheric station, as well as ground based whistler observations also carried out in Sofia during geomagnetic storms have been used. The results are given in UT.

1. March 19-20, 1971

Figure 1 presents the 3-hourly Kp-indices, the AE-indices, the critical frequencies of the F2 layer (f_0F2) with the monthly median value and the magnetospheric irregularities obtained by whistler observations for the interval 1.8-1.9 L together with the background electron density respectively. The storm considered starts with a sudden commencement (SC) on March 19 1150 UT. The whistler measurements were made on the same day in the interval 2050-2052 UT indicating irregularities with concentrations of $6.1 \cdot 10^3$ cm^{-3} and $1.2 \cdot 10^4$ cm^{-3}, while the background concentration in this height interval was $(1 \text{ to } 2) \cdot 10^3$cm^{-3}. The midlatitude F region shows a well defined two-phase reaction, positive in the afternoon and night hours of March 19 and strong negative reaction during the next day. At the time of

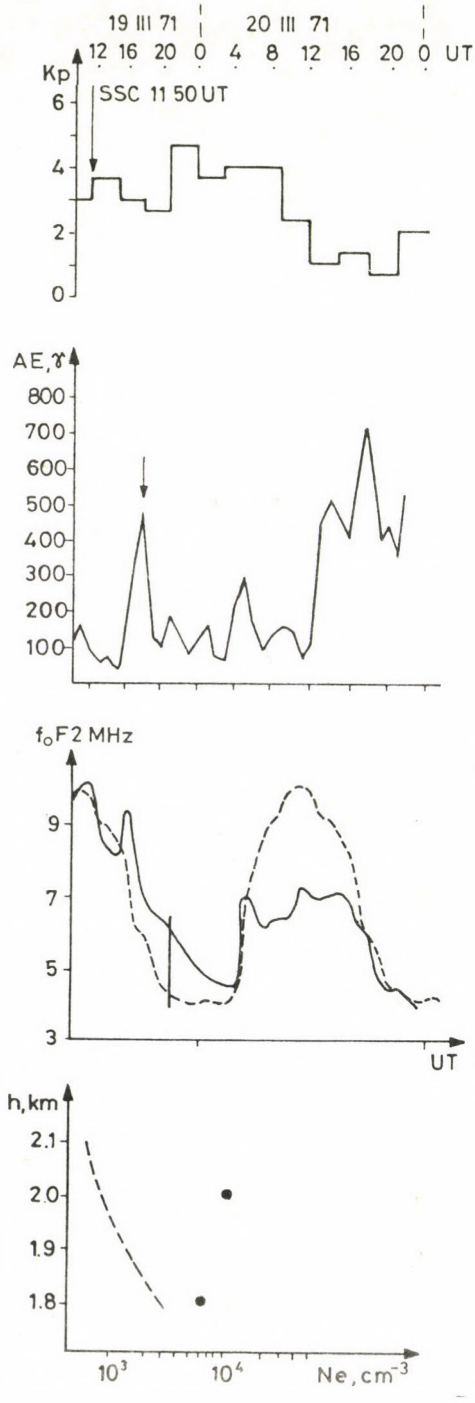

Fig. 1. a) three hourly geomagnetic planetary Kp index, b) auroral electrojet magnetic activity index AE, c) f_0F2 (continuous line) compared with the monthly median value (dashed line), d) observed irregularities in the equatorial magnetospheric electron concentration compared with background electron density (dashed line) for March 19-20, 1971

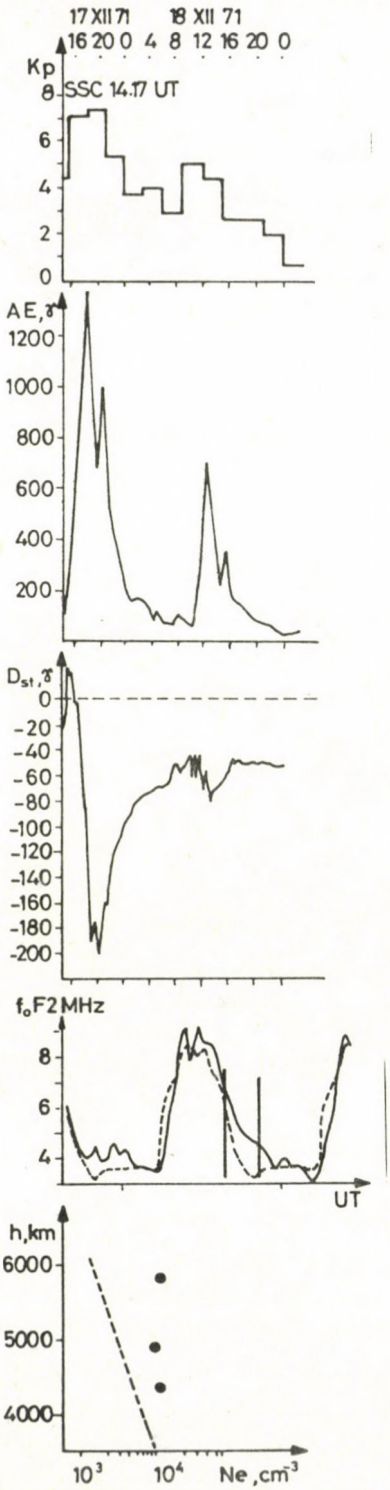

the whistler measurements $\Delta f_0F2 = f_0F2 - (f_0F2)_{med} = 2$ MHz or $\Delta N_mF2 \simeq 5 \cdot 10^4$ cm^{-3}. The change of h'F was $\Delta h'F \simeq 20$ km, i.e. due to the effect of the wind the F region maximum has been formed at a greater height.

2. December 17-19, 1971

This is a double geomagnetic storm with two sudden commencements at 1904 UT on December 16 and at 1417 UT on December 17. Figure 2 presents the Kp, AE, D_{st} indices, f_0F2 and the results of whistler measurements after the second SC as the big D_{st} decrease (-202 γ) occurred after it. This figure demonstrates the well defined synchronism of the geomagnetic indices used here. The auroral activity is characterized by two peaks which may be responsible for the double, two-phase reaction of the F region. The whistler measurements were carried out in the interval 1500--2000 UT on December 18, i.e. during the recovery phase of the D_{st}-index. The electron concentration determined is $\sim 10^4$ cm^{-3}, i.e. almost an order of magnitude higher than the corresponding background electron density. In this period

Fig. 2. a) three hourly Kp index, b) AE index, c) equatorial D_{st} index, d) f_0F2 compared with the monthly-median value, e) revealed equatorial magnetospheric irregularities for December 17-19, 1971

$\Delta f_0F2 \simeq 1.5$ MHz, or $\Delta N_mF2 \simeq 2.8 \cdot 10^4$ cm^{-3} and $\Delta h'F \simeq 20$ km.

3. October 12-14, 1972

This is not a strong geomagnetic storm. It is distinguished by the strengthening of auroral activity which continues during the three days considered (Fig. 3). The mid-latitude F region reaction shows four consecutive two-phase cycles due to the auroral activity. The whistler measurements were made on October 14 in the interval 1200-1400 UT. The maximum electron concentration observed is $2.7 \cdot 10^4$ cm^{-3}, i.e. by one order of magnitude higher than the background electron density. In the period of the whistler measurements $\Delta f_0F2 \simeq 1.7$ MHz, or $\Delta N_mF2 \simeq$ $\simeq 3.6 \cdot 10^4$ cm^{-3} and $\Delta h'F \simeq 40$ km.

4. December 12-14, 1977

Figure 4 shows that this storm is also not a strong one and is characterized by intense auroral activity, well illustrated by the recovery phase of the D_{st}-index. It is possible that exactly this activity gives rise to the consecutive two-phase cycles in the reaction of the mid-latitude F region. The whistler measurements were made on December 13-14 in the interval 1250-0352 UT, again during the recovery phase. Irregularities with a concentration of $3 \cdot 10^3$ cm^{-3} are observed at mid-night at altitudes 1.8 L and 2.0 L. After mid-night irregularities at 1.9 L determined on the basis of whistlers have a concentration of about $4.5 \cdot 10^3$ cm^{-3}. During this period $\Delta f_0F2 \simeq 2$ MHz, or $\Delta N_mF2 \simeq 5 \cdot 10^4$ cm^{-3} and $\Delta h'F \simeq 30$ km, i.e. in this case the F2-maximum is formed higher than under quiet geomagnetic conditions.

DISCUSSION AND CONCLUSIONS

In the above mentioned four geomagnetic storms (detailed description in Pancheva (1985)) there is a close relation between auroral activity, characterized by the AE-index, positive mid-latitude F region reaction and the magnetospheric irregularities revealed near the equator at $1.5 < L < 2.5$. Because of this and due to the fact that the magnetospheric irregularities have been observed during the recovery phase (except in the first case), if the large-scale convective electric

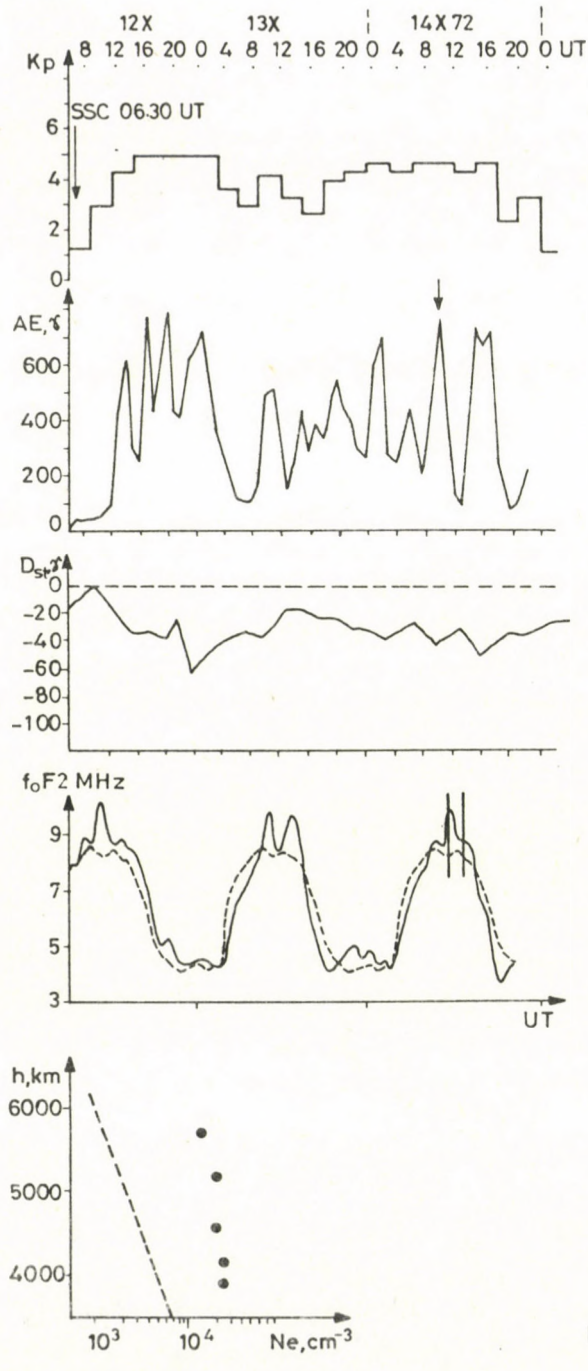

Fig. 3. Same as Fig. 2 but for October 12-14, 1972

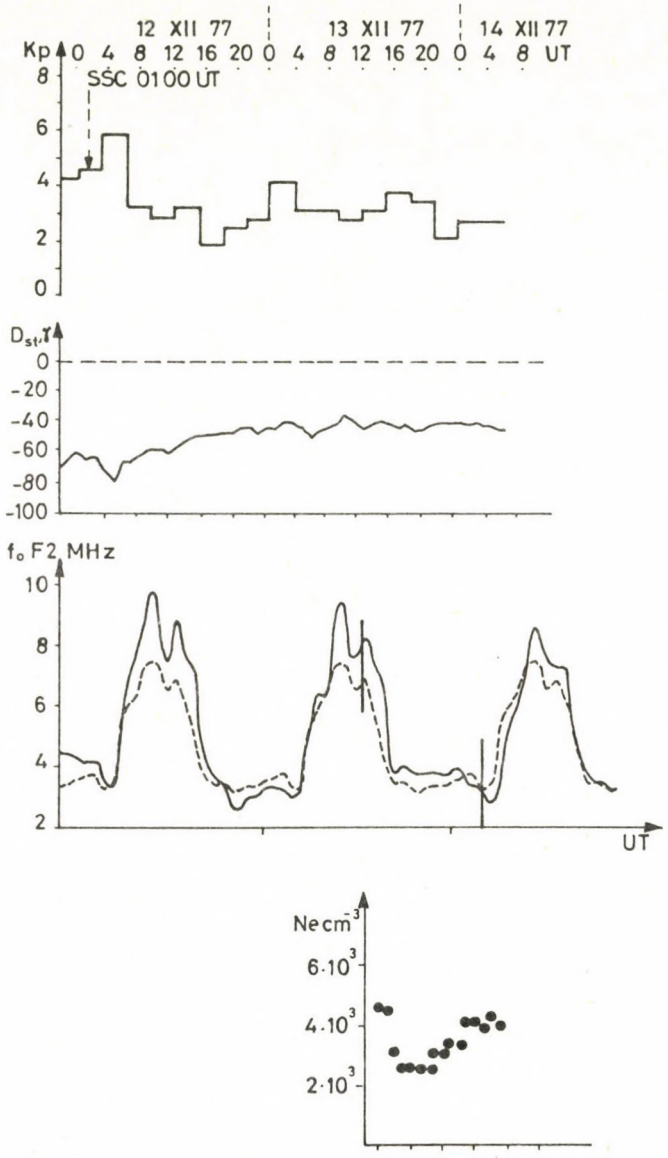

Fig. 4. a) three hourly Kp index, b) D_{st} index, c) f_oF2 compared with the monthly median value, d) equatorial magnetospheric irregularities December 12-14, 1977

fields decrease quickly, the conclusion may be drawn that the meridional wind, generated during auroral substorms is the main link connecting the positive reaction of the mid-latitude F region in the afternoon hours with the magnetospheric irregularities, found near the equator (Pancheva 1985). The positive reaction of the F region during geomagnetic storms can also be associated with the penetration of electric fields which originate from the magnetosphere. Maynard and Chen (1975) present more than 15 cases of magnetospheric irregularities observed near the equator the appearance of which they attribute to magnetospheric convection.

In order to decide which of the two mechanisms (neutral winds or electric fields) predominate in the present case, it is necessary to see how these two mechanisms work.

During geomagnetic substorms and storms, energy supplied by Joule heating and precipitating particles is deposited in the auroral ionosphere. This energy results in temperature increase which in turn affects the neutral composition (Mayr and Harris 1983). Temperature and density variations change the pressure gradient and drive meridional winds directed to the equator. The meridional wind appears almost immediately after the energy deposition in the auroral zones. Neutral winds carry the plasma along the geomagnetic field lines, i.e. they raise it to heights, where the recombination is less. This explains the positive reaction of the F region. Due to the wind the energy is redistributed by adiabatic heat transfer. This leads to an increase of the low-latitude temperature, i.e. to the decrease of the temperature gradient. Simultaneously another process influencing mainly neutral composition takes place. The wind-induced diffusion - a considerably slower process - accomplishes the following composition changes: an increase in the heavier constituents N_2, Ar, O_2 at high-latitudes, as well as that of the lighter components He and O at low-latitudes. Therefore, in the mid-latitude F region the ratio O/N_2 changes (usually decreases on the second day of the storm). This leads to an increase of the recombination and consequently to a negative reaction of the F region. The observed succession of posi-

tive and negative phases in ionospheric reaction can be explained by the different time-scales of the two processes, wind generation and composition changes. If the neutral wind is the main cause of the positive reaction of the F region then it is necessarily followed by a negative one. Besides due to the opposite effect of the composition change on the wind and temperature fields the two phases are interrelated. The increase of O and He densities at low-latitudes affects significantly the total atmospheric pressure and is the main cause of the decrease of the pressure gradient. This immediately leads to the decrease of wind which reduces the adiabatic heat transfer, or increases the temperature difference between high- and low-latitudes.

Strong electrostatic fields of magnetospheric origin penetrating into the polar ionosphere drive by Lorenz force neutral winds with velocities up to 1 km/s. The wind systems generated by heat (Joule heating) and momentum (Lorenz force) sources differ considerably, the former are divergent, the latter vortical. Although the winds created by the latter can reach high velocities, they do not affect considerably the composition, because they do not drive vertical motion. Therefore, when electric fields produce the positive reaction of the F region, it is not necessarily followed by a negative phase causally connected with the preceding positive phase.

In order to prove that this wind mechanism predominates it is necessary 1. to show that in case of the above mentioned geomagnetic storms we have to deal with a really two-phase reaction, 2. to find a definite connection between the two phases. This can be achieved by the investigation of the intensity of the ionospheric reaction, defined by $\delta f_0F2 = f_0F2 - (f_0F2)_m/(f_0F2)_m \cdot 100$ %. Figure 5 shows the variation of δf_0F2 for four geomagnetic storms. The main features of the variation of δf_0F2 are the succession of positive and negative phases, i.e. their junction in so called two-phase cycles of the reaction of the mid-latitude F region, and a reverse connection between them. In order to compare the two phases of each cycle, both the intensity and the duration of the iono-

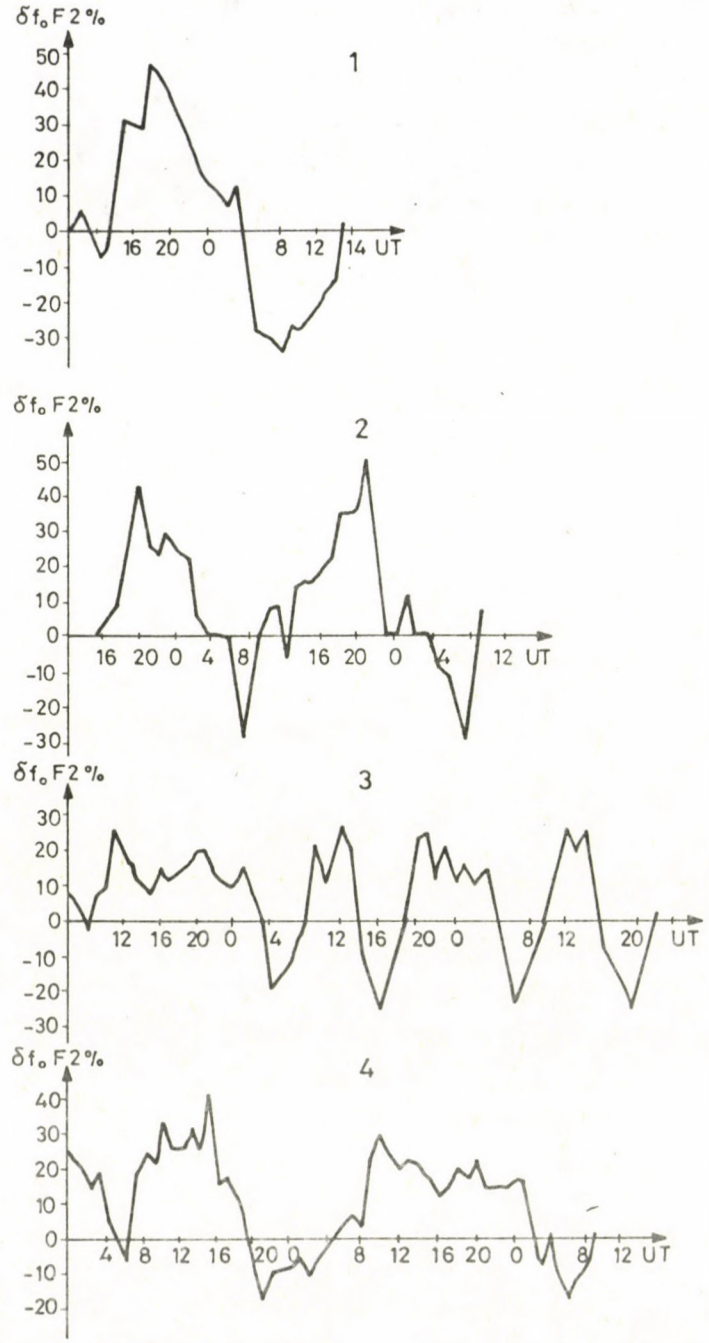

Fig. 5. The variation of $\delta f_0 F2$ in case of the four geomagnetic storms

spheric disturbance must be considered. The product of these two values is proportional to the energy of the process. For that purpose the areas under the curve of δf_0F2 in the figure were studied. Table I shows areas of the two-phase cycles, corresponding to the four geomagnetic storms. They are marked by S_{ij} where i = 1, 2, 3, 4 and give the number of the investigated storm, while j corresponds to the number of the cycle in each storm. Figure 6 shows the connection between S^+_{ij} and S^-_{ij}.

Table I

Number of the storm	Number of the cycle	S^+_{ij}	S^-_{ij}
1	1	S^+_{11}=343	S^-_{11}=271
2	1	S^+_{21}=225	S^-_{21}= 60
	2	S^+_{22}=221	S^-_{22}= 77
3	1	S^+_{31}=232	S^-_{31}= 57
	2	S^+_{32}= 86	S^-_{32}= 79
	3	S^+_{33}=136	S^-_{33}= 75
	4	S^+_{34}=100	S^-_{34}= 88
4	1	S^+_{41}=268	S^-_{41}= 64
	2	S^+_{42}=298	S^-_{42}= 55

The inverse relation between them is well expressed. This is an indication that the mechanisms causing these phases are interrelated. The inverse relation is a direct result of the feed-back coupling between composition changes (result of wind-induced diffusion) and wind and temperature fields. Only the first storm„ during which the whistler measurements have been carried out in course of the main phase of the storm, differs considerably. This can probably mean that the effect of the neutral wind, driven by Joule heating is combined with the influence of electric fields of magnetospheric origin.

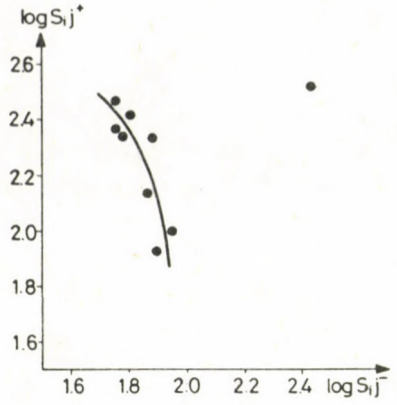

Fig. 6. Connection between S^{+}_{ij} and S^{-}_{ij} for the geomagnetic storms studied here

The complex ionospheric reaction during geomagnetic substorms and storms is due to circulation, electrodynamical and wave processes. In order to estimate the relative importance of the different processes, it is necessary to have a large base of solar, geomagnetic, magnetospheric and ionospheric data, as well as improved analytical and numerical models.

REFERENCES

Akasofu S I 1981: Space Sci. Rev., 28, 121-190.

Baumjohann W, Kamide Y 1984: J. Geophys. Res., 89, 383-388.

Davies R 1981: Radio Sci., 16, 1407-1430.

Gonzales C A, Kelley M C, Fejer B G, Vickrey J F, Woodman R F 1979: J. Geophys. Res., 84, 5803-5812.

Maynard N C, Chen A J 1975: J. Geophys. Res., 80, 1009-1013.

Mayr H, Harris I 1983: Composition variations in high-latitude thermosphere due to winds. Exploration of the polar upper atmosphere.

Pancheva D 1985: Bulg. Geoph. Journ., 11, No 4.

Acta Geod. Geoph. Mont. Hung., Vol. 22 (1-2), pp. 87-95 (1987)

DYNAMICS OF IONOSPHERIC DISTURBANCES AT HIGH LATITUDES

O M Pirog[1], G A Zherebtzov[1], B G Dolgoarshinnikh[1]

[1]Sibirian Institute of Geomagnetism, Ionosphere and Radio Wave Propagation (SibIZMIR), 664033 Irkutsk, P.O.Box 4, USSR

A statistical analysis of the ionospheric disturbances poleward of the main trough of ionization has been carried out. Data of a chain of ionospheric stations working along the meridian of Norilsk in the period December 1982 - February 1983 and also data of the ionosondes in Arkhangelsk and Heiss Island were used. At each station for each hour of the day the probability of ionospheric disturbances of different types has been determined at different Kp values. On the basis of the probabilities obtained, schemes of the development of the ionospheric substorm were constructed at different latitudes in LT-Kp coordinates. An analytical relation determining the invariant latitude of the main ionization trough as a function of LT and Kp has been established.

Keywords: ionospheric disturbances; main ionization trough

When investigating the ionospheric disturbances at high latitudes, the large scale structure of the ionosphere has to be considered. Its basic feature is the main ionization trough. Poleward of the trough the auroral plasma penetrates into the ionosphere and due to it the formation of the northward edge of the trough and of sporadic ionization in the E region, characteristic only of high latitudes, an increased absorption in the lower ionosphere take place (Liszka 1967, Khalipov et al. 1977, Besprozvannaya et al. 1982).

The dynamics of ionospheric disturbances north of the trough has been investigated by Benkova et al. (1984) on the basis of data from stations located at different latitudes and longitudes. The analysis has been carried out for the winter months of the years 1975 and 1976, i.e. for the solar activity minimum. Regularities of the variations appearing in the development of an ionospheric substorm indicated at stations

ordered according to increasing latitude, that longitudinal variations are insignificant and do not distort the general scheme determined by the latitude of the station, by the local time and the geomagnetic activity.

The expedition "Taymir-82" enabled to get a lot of experimental data for the investigation of the dynamics of ionospheric disturbances on the basis of a meridional chain and the possibility of a comparison with the results of Benkova et al. (1984) for the explaination of the solar activity effect. Besides 5 stations located along the meridian of Norilsk, data from Heiss Island and Arkhangelsk were also used for the better latitudinal resolution. The coordinates of the stations are shown in Table I.

Table I. Coordinates of stations

Station name	Geographical coordinates Latitude	Longitude	Invariant latitude	L
Heiss Island	80.6°	58.0°	73.8°	12.9
Sterlegova	75.4°	89.0°	69.4°	8.1
Ust-Taree	73.3°	90.5°	67.4°	6.9
Norilsk	69.3°	88.2°	63.6°	5.02
Igarka	67.2°	89.2°	62.0°	4.5
Arkhangelsk	64.6°	40.5°	60.1°	4.02
P-Tunguska	61.6°	90.0°	55.8°	3.2

For each station a statistical analysis of the ionospheric disturbances has been made as a function of the Kp value and local time. In this procedure the probability of the different disturbance types has been determined for each hour of the day and Kp value. Comparing the probabilities obtained, in an LT--Kp coordinate system for each station schemes of the development of an ionospheric substorm has been constructed, which show what type of the disturbances is most probable in case of

a given station, for a given hour and given value of Kp. These maps are shown in Fig. 1. The following notations are used: N--regular day-time F2 layer; F--anomalous ionization in the F region produced by a flux of low energy electrons ($E < 1$ keV) in the diffuse zone of precipitation (Liszka 1967, Khalipov et al. 1977); R--r type sporadic E layer, the appearance of which is due to the precipitation of electrons of energies up to ~ 3 keV or that of ring current protons (Eather et al. 1976, Besprozvannaya and Shchuka 1977, Kukushkina 1982); D--sporadic E layers of other types, generally types a and f accompanying discrete auroras the energy of the electrons being in this case 5-10 keV (Eather et al. 1976, Kukushkina 1982); A--absence of reflections from the F region due to screening by an Es layer indicating the redistribution inside the energy spectrum of the fluxes towards higher energies; B--total absorption produced by the enhanced ionization in the D region due to the precipitation of electrons of energies more than 40 keV (Driatsky 1974).

The boundary of the region of occurrence for each disturbance type is given by $P \geqq 0.5$ (probability more than 50 %).

Figure 1 shows how the onset time of the disturbance and its type varies at the same Kp value depending on latitude. The unhatched areas in the evening and morning hours indicate that under these conditions any type of the disturbances is equally probable.

In P-Tunguska the regular F2 layer is observed during the whole night in case of $Kp < 4$. With the increase of Kp and the latitude of the station, the area of its occurrence is reduced, displaced to the midday hours and at Heiss Island it disappears completely. In P-Tunguska anomalous ionization in the F region (F) appears after midnight at $Kp \geqq 4$ connected with the motion of the northern edge of the trough. With increasing geomagnetic activity and latitude the zone of F extends gradually toward evening and morning hours and is displaced to lower values of Kp. At Heiss Island, where solar radiation is completely absent in winter the anomalous ionization in the F region can be observed round the clock in form of scattered and inclined reflections.

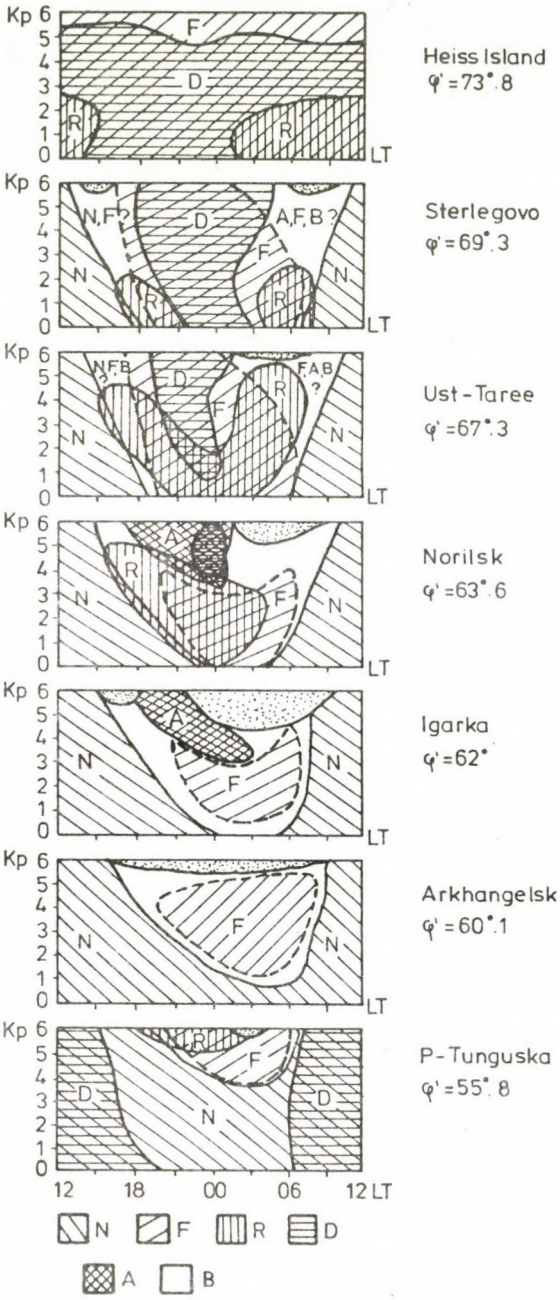

Fig. 1. Illustrations of the development of an ionospheric substorm in LT-Kp coordinate system in the winter 1982/83 (near the solar activity maximum)

The $F2_s$ layer disappears in Norilsk and Igarka at $Kp \geq 4$ because of absorption and screening of the F region by the Es layer in Norilsk and Igarka in the evening and midnight hours. The screening (A) is observed with the highest probability. At high-latitude stations in the morning hours the occurrence of $F2_s$ layers, screening and absorption are equally probable. Long-lived periods of total absorption are observed only in Igarka in case of $Kp > 4$ and in Arkhangelsk at $Kp > 5$. At stations located more to the north or more to the south, the probability of absorption decreases.

Es_r is observed with the highest probability in Norilsk and Ust-Taree. In Norilsk the area of occurrence of Es_r expands symmetrically from midnight if Kp increases from 0 to 3. At $Kp > 3$ Es_r is mainly observed in the evening hours. In Ust-Taree the r type predominates during the whole night at $Kp \leq 2$, at $Kp > 2$ two intervals of occurrence of the type r with probabilities higher than 50 % develop in the evening and morning hours, which are displaced with increasing activity in opposite directions. In Sterlegovo there are two zones of $P(R) > 50$ % in the morning and evening hours at $Kp < 3$. In Heiss Island Es_r is observed morning and during the day at $Kp < 3$. From 15 00 to 01 00 LT the probability of its occurrence is less than 10 %. Both Es_r and $F2_s$ are again observed in Igarka and Arkhangelsk at $P(R) < 50$ %, in P-Tunguska at $Kp \geq 5$ with high probability. In case of very high activity it appears in the trough and in the mid-latitude zone. The regularities of the occurrence of Es_r at high-latitude stations, Heiss Island included are consistent with the structure of precipitation of electron fluxes in the auroral zone. Obviously the Es_r layer in P-Tunguska differs from that observed at auroral stations. For its appearance ring current protons are most probably responsible.

The zone of observation of other Es layer types is located around midnight displaced somewhat towards the evening hours and expands with increasing latitude. In Heiss Island Es layers are steadily present, but their frequency exceeds rarely 2 MHz, whereas in the zone the most probable values of fbEs fall into the range 3-4 MHz.

In P-Tunguska flat Es layers are observed in the day-time

hours and the zone of their occurrence is gradually reduced with increasing Kp. Such a behaviour is characteristic of mid--latitude Es layers and differs strongly from the morphology of Es layers at high latitude stations.

Illustrations of the development of the ionospheric disturbance show which type of perturbations predominates in case of a given Kp at the given station in particular hour of the day. Unfortunately, the irregularity of the structure of the ionosphere to the north of the trough renders more difficult the analytical description of the boundaries separating areas of the occurrence of the different disturbance types. Moreover, the structure of the ionosphere within the auroral zones depends on the solar activity. The schemes of the ionospheric substorm development are shown in Fig. 2 for comparison at the stations Dixon, Norilsk and Arkhangelsk in the winter of 1975/76. Common features are at the three stations the substantial decrease of

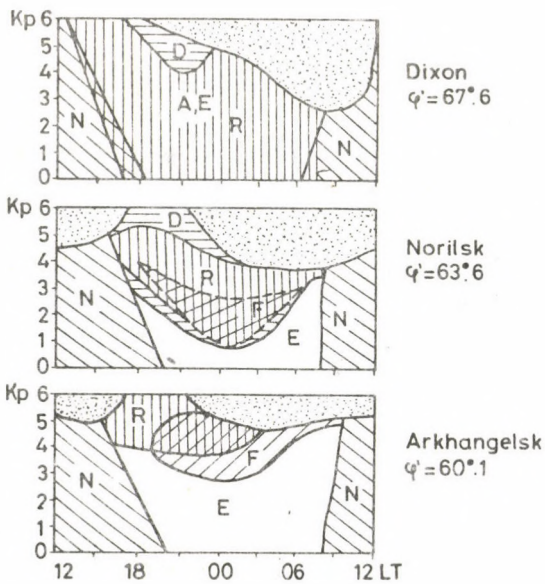

Fig. 2. Illustrations of the development of an ionospheric substorm in the winter of 1975/76 (solar activity minimum)

the zone of $F2_s$ occurrence in the year of solar activity minimum, the broadening of the area of Es_r occurrence and the existence of a zone, where due to the low level of the ionization reflections are absent (E conditions, i.e. foF2 $<$ 1 MHz). The zone of Es_r is present during the whole night at Dixon (see Ust-Taree) in the year of solar activity minimum (hereby it screens the F region) and the duration of the total absorption is significantly increased. In Norilsk and Arkhangelsk the same changes are observed. Similar changes can probably be attributed both to the lower level of the background ionization in the year of solar activity minimum and to the decrease of the intensity of diffuse precipitation. Thus, even a slight enhancement of the discrete fluxes can result in a total absorption or in the appearance of screening Es layers. Boundaries of the area of the regular F2 layer occurrence are more stable depending on the level of solar activity. This boundary corresponds to the main ionization trough, inasmuch as it separates the undisturbed ionosphere from the disturbed one. Using the changes of the boundary P(N) = 50 % with LT and Kp at the different stations shown in Fig. 1 and taking the coordinates of the stations, the equation of a parabola is obtained, by which the location of the main ionization trough is described in time and space as a function of Kp:

$$\tilde{\Phi}' = 0.16\,\tilde{t} - 0.4\,Kp^2 + 1.3$$

where $\tilde{\Phi}'$ and $\tilde{t}$ determine the displacements of the axis of the parabola as compared to the midnight meridian

$$\Phi' = \Phi' - 60^o - \frac{t - 2.5}{5}$$

$$\tilde{t} = t - 2.5 + \frac{\Phi' - 60^o}{5}$$

where $\tilde{\Phi}'$ and $\tilde{t}$ are the invariant latitude and local time. The locations of the trough, obtained by the authors are compared in Φ', LT coordinate system for Kp = 1, 3, 5 with locations of the boundary of the diffuse electron precipitation (Khalipov et al. 1977), with determinations of the trough by satellites

(Spiro et al. 1978) and with data of the Yakutsk meridional chain (Benkova and Zikrach 1983) (Fig. 3).

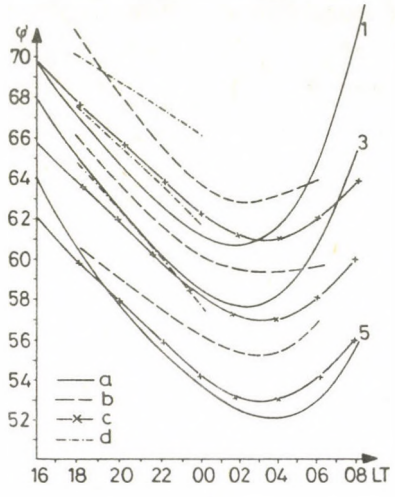

Fig. 3. Variations of the location of the main ionization trough in Φ-LT coordinates for Kp = 1, 3 and 5, as shown by a) the data of the Norilsk meridional chain, b) satellite measurements (Spiro et al. 1978), c) the data of the Yakutsk meridional chain (Benkova et al. 1984), d) location of the boundary of the diffuse precipitation (Khalipov et al. 1977)

REFERENCES

Benkova N P, Zikrach E K 1983: In: Physical processes in the region of the main ionospheric trough. Prague, 7-18.

Benkova N P, Kozlov E F, Pirog O M, Samorokin N I 1984: J. Phys. Solari-Terrestr., (in press)

Besprozvannaya A S, Shchuka T I 1977: Geomagn. i aeronomiya, 17, 35-39.

Besprozvannaya A S, Shirochkov A V, Shchuka T I 1982: In: Ionosfernoe prognozirovanie, Moscow, Nauka, 49-66.

Driatsky V M 1974: The nature of anomalous absorption of the cosmic radio noise in the high-latitude lower ionosphere (in Russian). Leningrad, Gidrometeoizdat

Eather R H, Mende S B, Judge J R 1976: J. Geophys. Res., 81, 2805-2824.

Khalipov V Ya, Galperin Yu I, Lisakov Yu V, Krapier J, Nikolaenko L M, Sinitin V M, Sovo J-A 1977: Kosmicheskie issledovaniya, 15, 708-724.

Kukushkina R S 1982: In: Issledovaniya visokoshirotnoy ionosferi i magnitosferi Zemli. Leningrad, Nauka, 101-111.

Liszka L 1967: J. Atmos. Terr. Phys., 29, 1243-1249.

Spiro R W, Hulis R A, Hanson W B 1978: J. Geophys. Res., 83, 4255-4263.

Acta Geod. Geoph. Mont. Hung., Vol. 22 (1-2), pp. 97-106 (1987)

LARGE LATITUDINAL IONIZATION GRADIENTS IN THE SUBAURORAL F REGION DURING RAPID ION DRIFTS

Yu I Galperin[1], V L Khalipov[2], V M Filippov[2], D D Reshetnikov[2]

[1]Institute for Space Research, Academy of Sciences of the USSR, Moscow, Profsoyuznaya ul. 84/32, USSR

[2]Institute for Cosmophysical Research and Aeronomy, Yakutsk, Lenin ul. 31, USSR

In many satellite and ground based experiments in the subauroral ionosphere a narrow band of very large westward ion drifts has been observed due to intense local electric fields directed to the pole. In this paper changes are studied in the structure of the high latitude ionosphere during the development of narrow bands of rapid drift. The results show that narrow (~100-200 km) and deep troughs of the latitudinal distribution of N_e are formed in the subauroral F region of the ionosphere in the vicinity of the zenith of the observing station at this time.

Keywords: band of rapid westward ion drift (SAID); polarization jet; spaced receiver method; vertical and oblique incidence sounding (DI)

The most important part of the convection pattern in the subauroral zone during a substorm is a jet of very rapid westward plasma drift which is formed in the vicinity of the polar edge of the trough. This has been shown on the basis of measurements on board of the satellites Kosmos-184, S3-2, OGO-6 and AE-C in the last years (Galperin et al. 1973, 1974, Smiddy et al. 1977, Maynard 1978, Spiro et al. 1979).

The narrow jet of rapid westward drift has been first observed at an invariant latitude of $\Lambda_0 \sim 60^0$ in the measurements on board of the satellite "Kosmos-184" in November 1967 and described in detail by Galperin et al. (1973, 1974), who called it "polarization jet". Direct measurements of the drift velocity have shown that a "polarization jet" of velocities to 1.9 km s^{-1} is formed during a large flare of a substorm in the midnight sector at the equatorial edge, broadening and intensifying the bands of westward drift along the auroral oval in the evening sector (MLT ~ 21) almost at the same invariant latitude, but in the southern hemisphere. After 40 min the

satellite "Kosmos-184" traversed again an analogous narrow jet of rapid westward drift which was also located at the equatorial edge of the broad band of eastward drift in the subauroral zone and was probably the continuation of the "polarization jet" in the evening sector.

These observations of the narrow jet of rapid westward drift at L shells near the plasmapause have later been confirmed and extended on the basis of other satellite measurements (Smiddy et al. 1977, Maynard 1978, Spiro et al. 1979). Smiddy et al. (1977) reported cases of observation of intense local, poleward electric fields, measured by the satellite S3-2 in the vicinity of the projection of the plasmapause. These fields have sporadically been observed in a latitude zone from L = 2.4 to L = 4 and they have always been found in the vicinity of the local electron density minimum with spatial scales less than 100 km.

The same intense local fields near the minimum of the main trough have also been revealed by the analysis of measurements carried out on board of the satellite OGO-6 in the premidnight sector at latitudes 60^{o} in 1969 (Maynard 1978). The author assumes that such fields can be produced during substorms as a result of an extension towards low latitudes of the region affected by convection maintaining the low conductivity of the ionosphere in the area of the main ionization trough. Spiro et al. (1979) reported on the basis of measurements of the satellite AE-C observations of rapid westward subauroral ion drifts. Based on a large statistics of data resulting from 5 year operation of the satellite, the character and morphology of this phenomenon have been studied. As a characteristic of subauroral ion drifts the coincidence of narrow bands of large velocities with those of sudden ion concentration gradients at altitudes 180-600 km is considered. They note that in all cases of narrow jets in the trough, the drift velocity was directed to west until local morning hours. Spiro et al. (1979) have shown that in spite of the fact that 85 % of rapid ion drifts were found in connection with a well defined trough in the F region ionization, jets with rapid ion drifts have been recorded only in

20 % of the observations of mid-latitude troughs. As a possible formation mechanism of jets of rapid drifts, a polarization electric field is considered which is produced by gradient drift at the separation of positive and negative energetic charged particles of the plasma layer in the vicinity of the inner boundary of the Alfven layer during substorms (Southwood and Wolf 1978). This mechanism does not demand an anomalous resistance at the equatorial edge of the negative electrojet as it has been assumed in the interpretation of the phenomenon "polarization jet" (Galperin et al. 1973, 1974) on the basis of the polarization mechanism suggested by Coroniti and Kennel (1972):

The results of model calculations concerning the parameters of the subauroral lower F region (Spiro et al. 1978) and E region (Banks and Yasuhara 1978) have shown that an additional narrow concentration "subtrough" is formed in the band of the "polarization jet" due to the transport of ions connected with the increase of the effective recombination coefficient. Regarding the F region this conclusion is in qualitative agreement with the measurements (Spiro et al. 1978, 1979).

Recently additional data of both satellite (Bythrow et al. 1980, Rich et al. 1980, Maynard et al. 1980) and ground based measurements (Mikkelsen et al. 1981, Bourdillon et al. 1982, Robinson et al. 1982) have been published concerning the "polarization jet" which confirmed the important role of this phenomenon in substorm processes at L shells near the plasmapause.

The small latitudinal extent of this band and the large gradients of the electron density at its edges cause difficulties in its exploration. It is noted that according to model calculations (Spiro et al. 1978, Banks and Yasuhara 1978) the most definite changes in the characteristics of the subauroral ionosphere occur below the F region maximum, therefore, for a topside sounder on board of a satellite the chance of finding such a narrow structure in the vicinity of the polar edge of the trough is low. At the same time, the role of this feature of the convection is certainly very important in the latitudinal concentration profile at the polar edge of the trough in

the production of electron density irregularities, of air glow effects etc.

In order to discover a "polarization jet" on the basis of a large number of ionosonde data, its development on the ionogram of a subauroral station must be known. In order to reconstruct this development, Sivtzeva et al. (1982, 1983) considered three characteristic events in detail, when a reliable identification and localization of the "jet" as relative to the station is possible by means of published direct satellite observations of the "polarization jet" above the region of Yakutsk and based on ionograms of a meridional chain of ionospheric stations.

Filippov et al. (1984) constructed a quantitative model of the high electron density distribution in the subauroral F region during the occurrence of a narrow band of rapid drift in the vicinity of the zenith of the observing station and on the basis of it, model ionograms similar to that observed at a subauroral ionospheric station in the vicinity of the band were computed.

In this paper another case of simultaneous observation of rapid ion drift bands is studied based on the data of the satellite DE-2 (Sugiura et al. 1983) referring to the vicinity of the meridional chain of vertical and oblique incidence sounding stations and on the variations in the structure of the ionosphere according to the data of bottomside sounding stations. The observations were carried out on October 7, 1981. For this purpose at the stations Zhigansk and Yakutsk the horizontal rhombic antenna was reversed what enabled sounding to the "north" and to the "south" and to get substantially new experimental data on the electron density distribution with the ionosonde located below the band of intense northward electric fields. The experimental equipment is described by Mamrukov et al. (1982). In Fig. 1 a succession of ionograms of vertical and oblique incidence sounding obtained are shown in case of sounding to the "north" and to the "south" at the stations Tixie, Zhigansk and Yakutsk. Bottom right the magnetogram of Tixie is also presented where the times of soundings are denoted by arrows. Figure 1 shows that an additional reflection of a lower

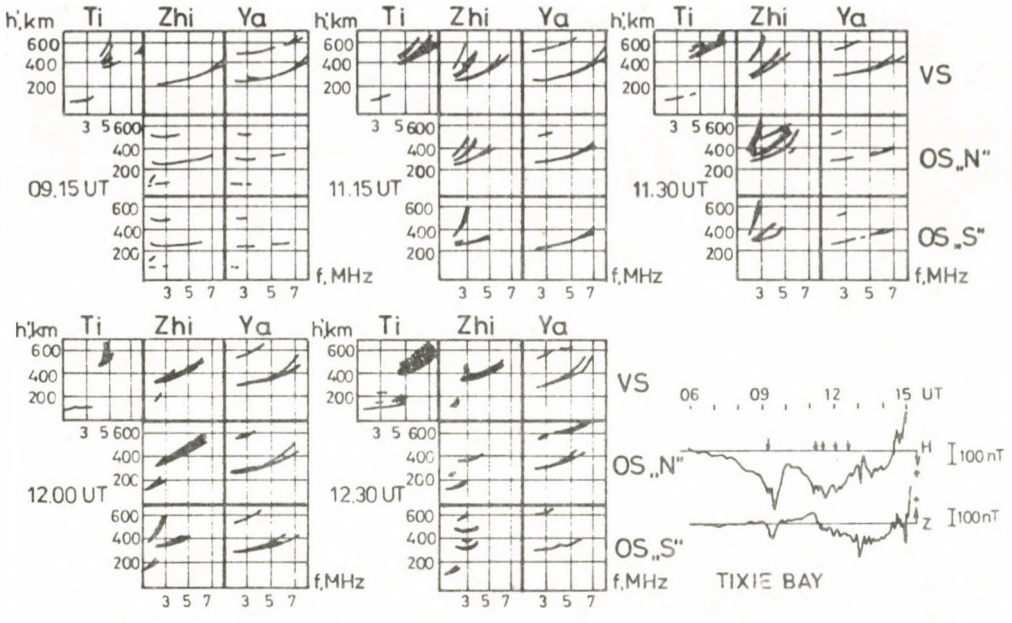

Fig. 1. Succession of vertical and oblique incidence sounding ionograms at the stations Tixie, Zhigansk and Yakutsk during the occurrence of a narrow band of rapid drift on October 7, 1981. The magnetogram of Tixie is also shown

critical frequency and in a distance larger than the trace of the regular F2 layer appears at time of the development of the substorm active phase (09 15 UT) in the vertical sounding ionogram of Tixie. This reflection is characteristic of the occurrence of a rapid westward drift band and corresponds to the decrease of the electron density in the zenith of the observing station (Sivtzeva et al. 1982, 1983). Later above the station Tixie this trace disappeared and at 11 15 UT it appeared above the station Zhigansk, however, at the station Tixie reflections corresponding to the location of the station below the diffuse zone of precipitation are observed (Halipov et al. 1977). Traces in a distance of ~ 500 km characteristic of the approach to the boundary of diffuse precipitation appeared at 11 30 UT (20 30 LT) by the oblique incidence sounding to the "north" from station Zhigansk, at 12 00 UT station Zhigansk got to the

diffuse zone, though reflections of the type $F3_s$ can be seen yet at the oblique incidence sounding to the "south" (Sivtzeva et al. 1982, 1983) proving the motion of the narrow trough to the south of station Zhigansk. At 12 30 UT reflections showing the approach of the polar edge of the trough already to the latitude of station Yakutsk appeared by the oblique incidence sounding to the "north" from station Yakutsk.

In Fig. 2 maps of the lines of equal ionization corresponding to consecutive ionograms of the vertical and oblique incidence sounding presented in Fig. 1 are shown. Bottom right in Fig. 2 results of electric field and field aligned current measurements on board of the satellite DE-2 are plotted, where the observation time of a narrow band of intense poleward electric

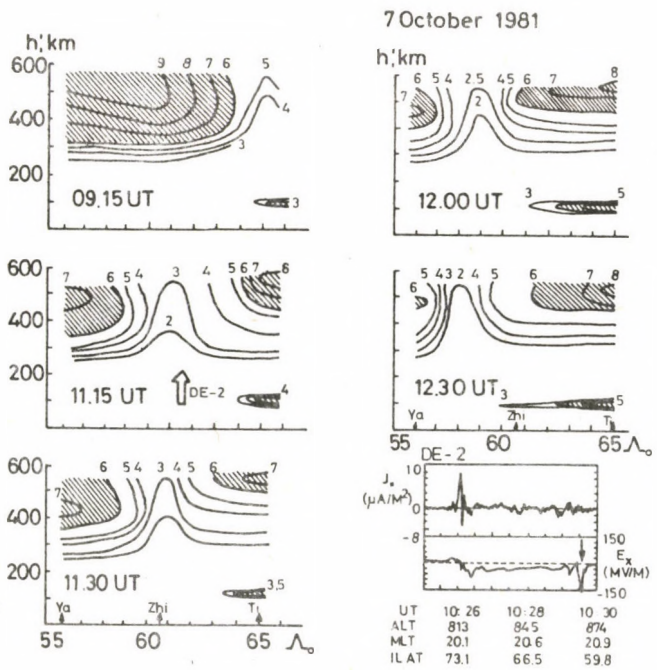

Fig. 2. Succession of maps of equal ionization lines obtained on the basis of ionograms of Fig. 1 and a sudden jump of the northward electric field recorded on board of the satellite DE-2 (Sugiura et al. 1983)

field (>150 mV m^{-1}) is denoted by an arrow, on the map of lines of equal ionization the time of the jump in the electric field at 11 15 UT is denoted by a thick arrow. The satellite measurements were carried out 45 min earlier than the narrow trough appeared above the station Zhigansk, but displaced approximately just as much in MLT to the east from the meridian of the ground based measurements. It should be noted that the map of equal ionization lines was constructed with invariant latitude and virtual height coordinates using traces in the ionograms which correspond to the narrow trough of ionization and to motion of the polar edge of the trough. In this procedure the knowledge of the directional antenna pattern allows to get information concerning the angles of reception of the reflected signals and to use them in the construction of isolines. In Fig. 2 the numbers on the curves indicate the plasma frequency in MHz. The narrow ionization trough is located at the equatorial edge of the diffuse precipitation.

In the following parameters of a narrow band of rapid drift recorded by means of the spaced receiver method (D1) are discussed. For the identification of a band occurring in the vicinity of the observing station, its development in the structure of the subauroral ionosphere indicated by characteristic reflections has also been used. The observational results on November 26, 1983 are shown in Fig. 3. Top the sucession of ionograms obtained with vertical and oblique incidence sounding to the "north" and "south" at station Tixie, bottom the drift velocity measured by means of method D1 and the magnetogram of station Tixie are presented. In the vertical sounding ionograms small circles denote regions of the ionosphere, at the reflection from which the drift velocity was determined by method D1, further, numbers around the small circles correspond to the number of the drift velocity vector. The simultaneous occurrence of traces characteristic of a station with all three antennas (vertical sounding, oblique incidence sounding "north" and "south") below the band of the "polarization jet" and their uniformity indicate that the narrow ionization trough is located at the zenith of the observing station and it is of a small

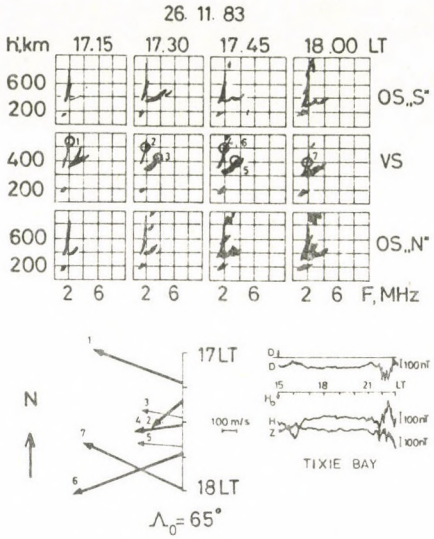

Fig. 3. Drift velocities measured by means of the method D1 during the occurrence of a narrow band of rapid drift on November 26, 1983 at the station Tixie. The magnetogram of Tixie is also shown

spatial extent (~ 100-200 km). The results of the experiment show that in the region of the ionosphere affected by the band of rapid ion drift at the beginning and at the end of the observations large (up to 700 ms^{-1}) westward drift velocities are recorded, though in the centre of the observation period drift velocities in the regular F2 layer and in type $F3_s$ reflections (Filippov et al. 1984) are approximately equal and directed to the west (compare arrows Nos 2, 3, 4 and 5). Similarly high drift velocities were measured under analogous conditions in Zhigansk on February 8, 1982 by means of the method D1. Thus, results of the measurements carried out by the method D1 show that through the structural properties of the ionosphere accomplished by a band of rapid westward ion drift substantially large valocities of westward plasma convection are observed.

CONCLUSIONS

The experimental results presented in this paper show that in the subauroral F region, during the development of a narrow band of rapid drift narrow and deep ionization troughs are formed, which are produced partly by rapid westward transport

of the ionization, partly by the change of the speed of photochemical reactions in strong electric fields, resulting trough recombination processes in a sudden reduction of ionization in this region of the ionosphere (Schunk et al. 1976).

According to measurements carried out by means of the method DI in the region of the "polarization jet", high westward drift velocities of the ionospheric plasma are recorded (up to 700 ms^{-1}).

From the measurements of a meridional chain of ionosondes a characteristic succession of vertical and oblique incidence sounding ionograms observed during the development of the "polarization jet" is presented.

REFERENCES

Banks P M, Yasuhara F 1978: Geophys. Res. Lett., 5, 1047-1052.

Bourdillon A, Nicollet M, Parent J 1982: Geophys. Res. Lett., 9, 696-699.

Bythrow P F, Heelis R A, Hanson W B, Power R A 1980: J. Geophys. Res., 85, 151-159.

Coroniti F V, Kennel C F 1972: J. Geophys. Res., 77, 2835-2841.

Filippov V M, Galperin Yu I, Shestakova L V 1984: Kosmich. issled., 22, 557-564.

Galperin Yu I, Ponomarev V N, Zosimova A G 1973: Kosmich. issled., 11, 273-296.

Galperin Yu I, Ponomarev V N, Zosimova A G 1974: Geophys., 30, 1-7.

Halipov V L, Galperin Yu I, Lisakov Yu V, Krane Zh, Nikolaenko L M, Sinitzin V M, Sovo Zh-A 1977: Kosmich, issled., 15, 708.

Mamrukov A P, Kiselev V A, Neustroev E M, Filippov L D 1982: In: Izd. Ya F SO AN SSSR, Yakutsk, 24-25.

Maynard N C 1978: Geophys. Res. Lett., 5, 617-618.

Maynard N C, Aggson T L, Heppner J P 1980: Geophys. Res. Lett., 7, 881-887.

Mikkelsen I S, Horgensen T S, Kelley M C, Larsen M F, Pereira E, Vickrey J 1981: J. Geophys. Res., 86, 1513-1524.

Rich F J, Burke W, Kelley M, Smiddy M 1980: J. Geophys. Res., 85, 2335-2340.

Robinson R M, Vondrak R R, Potemra T A 1982: J. Geophys. Res., 87, 731-741.

Schunk B W, Banks P M, Raitt W F 1976: J. Geophys. Res., 81, 3271.

Sivtzeva L D, Filippov V M, Halipov V L, Galperin Yu I, Ershova V A, Nikolaenko L M, Ponomarev Yu N, Simitzin V M 1982: Reprint No Pr-724 IKI AN SSSR, 1-56.

Sivtzeva L D, Filippov V M, Halipov V L, Galperin Yu I, Ershova V A, Nikolaenko L M, Ponomarev Yu N, Sinitzin V M 1983: Kosmich issled., 21, 584-608.

Smiddy M, Kelley M C, Burke W, Rich F, Sagalyn R, Shuman B, Hays R, Lai S 1977: Geophys. Res. Lett., 4, 543.

Southwood D J, Wolf R A 1978: J. Geophys. Res., 83, 5227-5232.

Spiro R W, Heelis R A, Hanson W B 1978: J. Geophys. Res., 83, 4255-4267.

Spiro R W, Heelis R A, Hanson W B 1979: Geophys. Res. Lett., 6, 660-675.

Sugiura M, Lyemori T, Hoffman R A, Maynard N C, Burch J L, Winningham J D 1983: Relationships between field-aligned currents, electric fields, and particle precipitation as observed by dynamics Explorer-2. NASA Technical Memorandum 85025

Acta Geod. Geoph. Mont. Hung., Vol. 22 (1-2), pp. 107-114 (1987)

IRREGULARITIES IN THE DISTRIBUTION OF O^+ AND H^+ IONS IN THE SUBAURORAL IONOSPHERE

V A Ershova[1], L D Sivtseva[2], V M Filippov[2], V L Khalipov[2], A P Yaichnikov[3]

[1]Institute for Space Research, Academy of Sciences of the USSR, Moscow, Profsoyuznaya ul. 84/32, USSR

[2]Institute for Cosmosphysical Research and Aeronomy, Yakutsk, Lenin ul. 31, USSR

[3]Institute for Applied Geophysics, Moscow, Gleborskaya ul. 20b, USSR

In this paper experimental data are presented concerning the distribution of O^+ and H^+ ions in the subauroral ionosphere at altitudes from 400 to 1000 km for night hours of the winter solstice measured on board of the satellites "Intercosmos-12" "Oreol-1, 2" and "Meteor".

Irregularities of characteristic scales of 200 km in the latitudinal distribution of O^+ and H^+ ions are observed both in geomagnetically quiet and disturbed conditions in the region of the midlatitude trough.

For the interpretation of the results, data of a chain of vertical and oblique incidence sounding stations have also been used. The possible mechanism is discussed which leads to the observed irregularities in the latitudinal distribution of O^+ and H^+ ions in the subauroral ionosphere.

Keywords: ionospheric irregularities; mid-latitude trough; subauroral ionosphere

Investigation of the ion distribution in the subauroral outer ionosphere has been carried out by means of a number of satellites, and of known data concerning the location and dynamics of the mid-latitude trough in concentrations of the ions O^+ and H^+ (Köhnlein and Raitt 1977, Brinton et al. 1978, Ahmed et al. 1979, Ivanov et al. 1980, Moffet and Quegan 1983). The mechanisms leading to formation of the mid-latitude trough in the outer ionosphere could be identified by the study of the simultaneous distributions of different ions in the region of the trough, as well as investigation of the irregularities in the distribution of different ions directly in the trough.

Only a few recent reports can be found about observations of irregularities of the dimension of 100-200 km in the region of the mid-latitude trough. According to Miller and Grebowsky

(1977), structures of increased electron concentration have been observed on the basis of the data measured on board of "ISIS-2". They presented cases of the occurrence of irregularities in concentration of the ions O^+ and H^+ with characteristic dimensions of ~ 200 km in the region of the mid-latitude trough recorded by the satellites "Intercosmos-12" (Gdalevich et al. 1979), "Oreol-1 and 2" (Ershova and Sivtseva 1974, Grechnev et al. 1977) and "Meteor" (Ivanov et al. 1980) at altitudes between 400 and 1000 km in the night hours of the winter solstice and in the electron concentration found on the basis of data of bottom side soundings. All satellites except "Meteor" were unoriented.

In Fig. 1 cases of localized irregularities are shown in the distribution of the O^+ concentration at the bottom of the trough at invariant latitudes Λ_0 $\sim 60\text{-}67^0$ recorded on the satellites "Oreol-2" and "Meteor" under quiet conditions (K_p = 1-, K_p = 0 respectively) after midnight. Here peaks of uniform structure of the O^+ concentration can be seen within

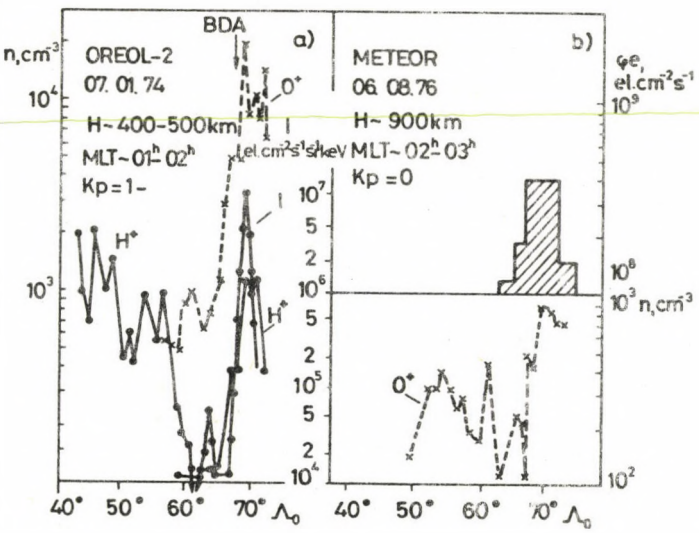

Fig. 1. Examples of irregularities in the concentration of O^+ ions in the area of the mid-latitude trough from the measurements of the satellites "Oreol-2" (a) and "Meteor" (b). In Fig. 1a I corresponds to the flux of electrons of energy ~ 2 keV. In Fig. 1b the integral flux of electrons of energy $E > 350$ eV measured simultaneously by the satellite "Meteor" is shown by the histogram

the trough both at 450 km (data of the satellite "Oreol-2") and at 900 km (data of the satellite "Meteor"). Simultaneous measurements of precipitating particles on board of these satellites indicate their absence in the area of occurrence of the irregularities. The O^+ concentration increases by a factor of 2-3. Thus, the irregularities revealed in the distribution of the O^+ concentration at the bottom of the trough are not connected with precipitation.

In Fig. 2 examples of the occurrence of irregularities in the distribution of H^+ ions are shown in the area of the light ion trough; they have been recorded by the satellites "Oreol-1" and "Intercosmos-12" at altitudes between 450 and 650 km in the

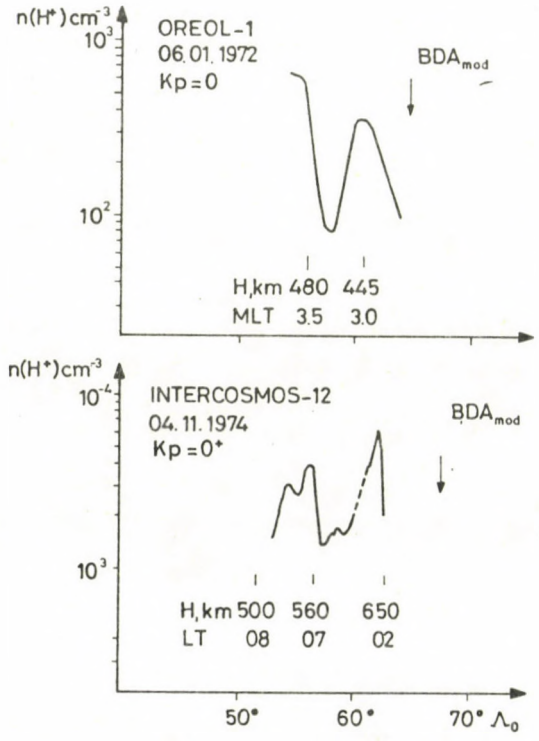

Fig. 2. Examples of irregularities in the distribution of H^+ ions within the light ion trough recorded by the satellites "Oreol-1" and "Intercosmos-12". The location of the boundary of diffuse aurora obtained by means of the model Gussenhoven et al. (1983) is indicated by arrows

post-midnight period under quiet conditions (K_p = 0). In these cases the location of the polar edge of the trough is shown by arrows indicating the location of the diffuse auroral boundary (BDA) determined on the basis of a model for the morning sector (Gussenhoven et al. 1983). Thus, the increase of H^+ concentration in the vicinity of the invariant latitude 60^o takes place within the light ion trough at both satellites.

However, if the angular characteristics of the H^+ ions is sufficiently broad (both satellites were unoriented), it is impossible to determine with certainty, whether the given accumulation of H^+ ions corresponds to the increase of H^+ concentration, or in these cases fluxes of H^+ ions are recorded by the mass-spectrometer. If it is supposed that fluxes have been recorded then they will be directed to the east in the morning sector corresponding to the pattern of convection in the post-midnight sector.

In Fig. 3 another case of irregularities in the distribution of H^+ is shown at the bottom of the trough which was observed by the satellite "Oreol-2" in a height of 800 km at

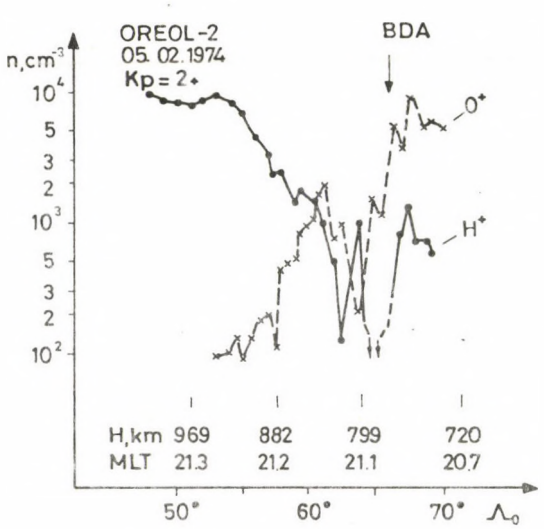

Fig. 3. Latitudinal distribution of the ions O^+ and H^+ measured by means of the satellite "Oreol-2" February 5, 1974 during a substorm

21 MLT and K_p = 2+. These measurements were carried out in the initial phase of a substorm (according to the Kiruna magnetogram), occurring after a quiet period of three days. Here, a sudden and localized (~ 100 km) increase of the H^+ concentration can be seen at the bottom of the light ion trough. In this case the measurements were made along field lines at pitch-angles near zero. It is possible that this irregularity in the distribution of H^+ indicates a downward flux of H^+ ions along the field lines.

The ionosphere's structure in the area of the main ionization trough is studied by the data of bottomside sounding stations. Figure 4 shows the ionograms of the station Zhigansk ($\Lambda_0 = 61^0$) for December 27, 1977. Vertical and oblique incidence soundings of the ionosphere have been carried out by means of an aerial of the type "horizontal rhombus". The directional patterns of the antenna for the oblique incidence sounding have the characteristic feature that at 2-3 MHz its effectivity to receive signals from the region near to the zenith of the station is approximately equal to that of the antenna for vertical sounding.

In Fig. 4 the ionogram of the oblique incidence sounding to the north is denoted by OS "N", while that of the vertical sounding by VS. It can be seen from the figure that an additional reflection having a critical frequency exceeding that of a regular layer appeared at 01 00 LT in altitudes above the regular F2 layer. The traces appearing at high virtual heights can simultaneously be seen both in the ionograms of the vertical sounding and in the ionograms of the oblique incidence sounding showing that this reflecting region is located near the zenith of the station. This is also confirmed by the form of the trace having additional reflections characteristic of the vertical reflections. This night such reflections were observed only at the station Zhigansk, at the stations Yakutsk and Tixie they were absent. From the latitudinal profile of ionization it follows that the station Zhigansk is located at this time on the day-side of the main ionization trough. At the time in question the polar edge of the trough was above Tixie

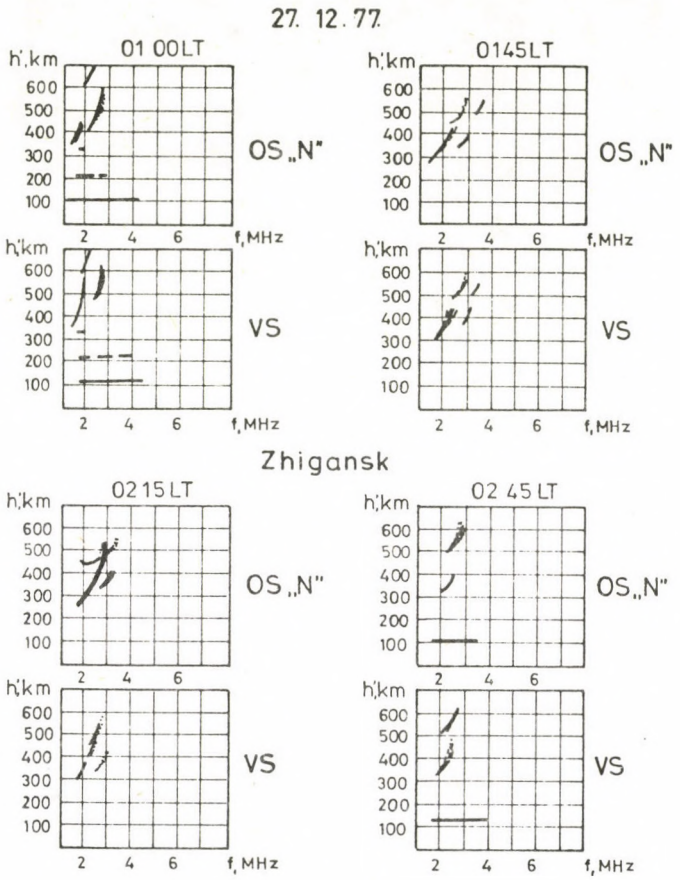

Fig. 4. Successive ionograms of the station Zhigansk for 27. 12. 1977 at the time of additional reflection recordings in the area of the main ionization trough

($\Lambda_0 = 65.5^0$). According to the magnetogram, in Tixie a negative disturbance with an amplitude of ~150 nT was recorded.

An analysis of successive ionograms shows that the disturbance develops within ~2 hours and the station Zhigansk gets into the zone of diffuse aurora. It is suggested that the additional vertical reflections at heights ~500 km shown in Fig. 4 correspond to the increase of electron concentration at these heights in the area of the main trough and to the appearance of

the effect "release" of ionization from the plasmasphere into the ionosphere.

Similar ionograms have also been recorded in a number of cases.

Taylor (1973) presented results of the measurement of ionization height profiles obtained by the method of incoherent scatter of radio waves in Malvern where an additional electron density maximum was observed in the area of the main ionization trough at heights ~600 km, wich descended gradualy to the height of the regular F2 layer.

The results presented here shaw that irregularities in the latitudinal concentration distribution of the O^+ ions and electrons are observed in a broad range of altitudes from the F region maximum to 1000 km. It is possible that in case of these irregularities one of the formation mechanisms is localized fluxes of thermal H^+ ions from the plasmasphere into the ionosphere in the initial phase of substorms.

REFERENCES

Ahmed N, Sagalin R C, Wildman S L, Behrke W J 1979: J. Geophys. Res., 84, 489-497.

Brinton H C, Grebowsky J M, Brace L H 1978: J. Geophys. Res., 83, 4767-4776.

Ershova V A, Sivtseva L D 1974: Kosmicheskie issled., 12, 572-576.

Gdalevich G L, Grechnev K V, Ershova V A, Istomin V G, Ozerov V D, Dachev I P, Kutiev I S, Ivanova T N, Chereji I, Marcea V, Ristoin D, Taderjan G, Rustenbach J, Schmilauer J 1979: Space Res. in Bulgaria, Sofia, 2, 44-50.

Grechnev K V, Ershova V A, Shulchishin Iu A, Sivtseva L D, Vasyukov S V, Krane Zh, Blan E, Sovo Zh A 1977: Kosmicheskie issled., 15, 274-285.

Gussenhoven M S, Hardy D A, Heineman N 1983: J. Geophys. Res., 88, 5696-5708.

Ivanov G V, Perkov I A, Pogulyaevskiy L I, Romanovsky Iu A, Rilov Iu P, Yaichnikov A P 1980: Kosmicheskie issled., 18, 384-391.

Köhnlein W, Raitt W J 1977: Planet. Space Sci., 25, 600-602.

Miller M J, Grebowsky J M 1977: Geophys. Res. Lett.,4, 369-372.

Moffett R J, Quegan S 1983: J. Atmos. Terr. Phys., 45, 315-343.
Taylor G N 1973: J. Atmos. Terr. Phys., 35, 647-656.

Acta Geod. Geoph. Mont. Hung., Vol. 22 (1-2), pp. 115-125 (1987)

ON SOME CHARACTERISTICS OF SPREAD-F AND THE NIGHT ENHANCEMENTS OF f_0F2 AT LOW LATITUDES

D Samardzhiev[1] and S Uzunova[1]

[1]Geophysical Institute, Bulgarian Academy of Sciences, Akad. G. Bonchev str., bl. 13, Sofia 1113, Bulgaria

Based on vertical sounding data of the African stations Dakar, Ouagadougou and Djibouti for the period 1976-81, characteristics of the anomalous night enhancement of f_0F2 and spread-F are investigated. The results obtained support the conclusion that the two phenomena are closely but inversely related. A joint study of the characteristics and properties of both events mutually supplementing each other is needed.

Keywords: geomagnetic anomaly; night enhancement of f_0F2; spread-F

INTRODUCTION

The purpose of the present work is to determine some characteristics of the anomalous night enhancements of the critical frequency f_0F2 (Δf_0) and that of the spread-F (F_{spr}) of the ionosphere over the African zone. For the period 1976-1981 data from three stations have been used. These are

Dakar - $\varphi = 14^o46'N$, $\lambda = 17^o25'W$, $\Phi = 21.7^oN$

Ouagadougou - $\varphi = 12^o22'N$, $\lambda = 01^o32'E$, $\Phi = 16.6^oN$

Djibouti - $\varphi = 11^o31'N$, $\lambda = 42^o50'E$, $\Phi = 07.0^oN$.

The dependence of the two phenomena on solar activity is traced from R_{min} in 1976 to the years after the maximum in 1979. The parallel investigation allows to determine interrelations and their variations (Samardzhiev and Smaradzhiev 1985).

RESULTS

A) Night enhancements of f_0F2

A common characteristic of the African zone is the very small number of enhancements as compared to the number of cases

observed in the American and Asian zones (Samardzhiev and Samardzhiev 1981, Samardzhiev and Uzunova 1984). For the sake of objectivity when comparing the characteristics at the different stations and for the different periods the parameter "frequency of occurrence" has been used.

The first parameter considered is the frequency of occurrence $\nu\ \% = \frac{m}{w}$, where m is the number of nights in the month when Δf_0 was observed and w is the number of nights with measurements. In this region two cases per night are very rarely recorded. In Fig. 1a the monthly means of ν are shown at the three stations for each year of the period investigated. The curves show a very well defined yearly variation with a minimum in summer and a maximum in winter. The character of the yearly variation at the three stations is similar but differences are observed too which are obviously determined by the location of the stations with respect to the geomagnetic equator. The largest difference between the values of ν for the winter and summer periods occurs in Dakar at the site being most distant from the geomagnetic equator and the smallest difference is found in Djibouti at the southernmost point.

In Fig. 2 the hourly distribution of the f_0F2 night enhancements are plotted expressed by the parameter $\alpha = \frac{n}{w}$, where n is the number of cases with Δf_0 in the given hour of the night of the month investigated and w is the number of observations. The figure shows values averaged for two seasons: a - summer and b - winter. It is known (Pancheva et al. 1983) that at low latitudes the year is to be divided into two seasons, into summer including the period from April to September and winter lasting from October to March. Since during the summer period the number of the observed Δf_0 is much smaller than in winter, the ratio of the scales of the two seasons summer/winter is given by 1:5.

As seen from the figures in the occurrence of the night enhancements mostly one maximum is observed. In the different years the time of the maximum is different, and a definite dependence on solar activity is evident. In summer at the stations Ouagadougou and Djibouti this maximum is shifted from foremidnight at low solar activity to the post-midnight hours

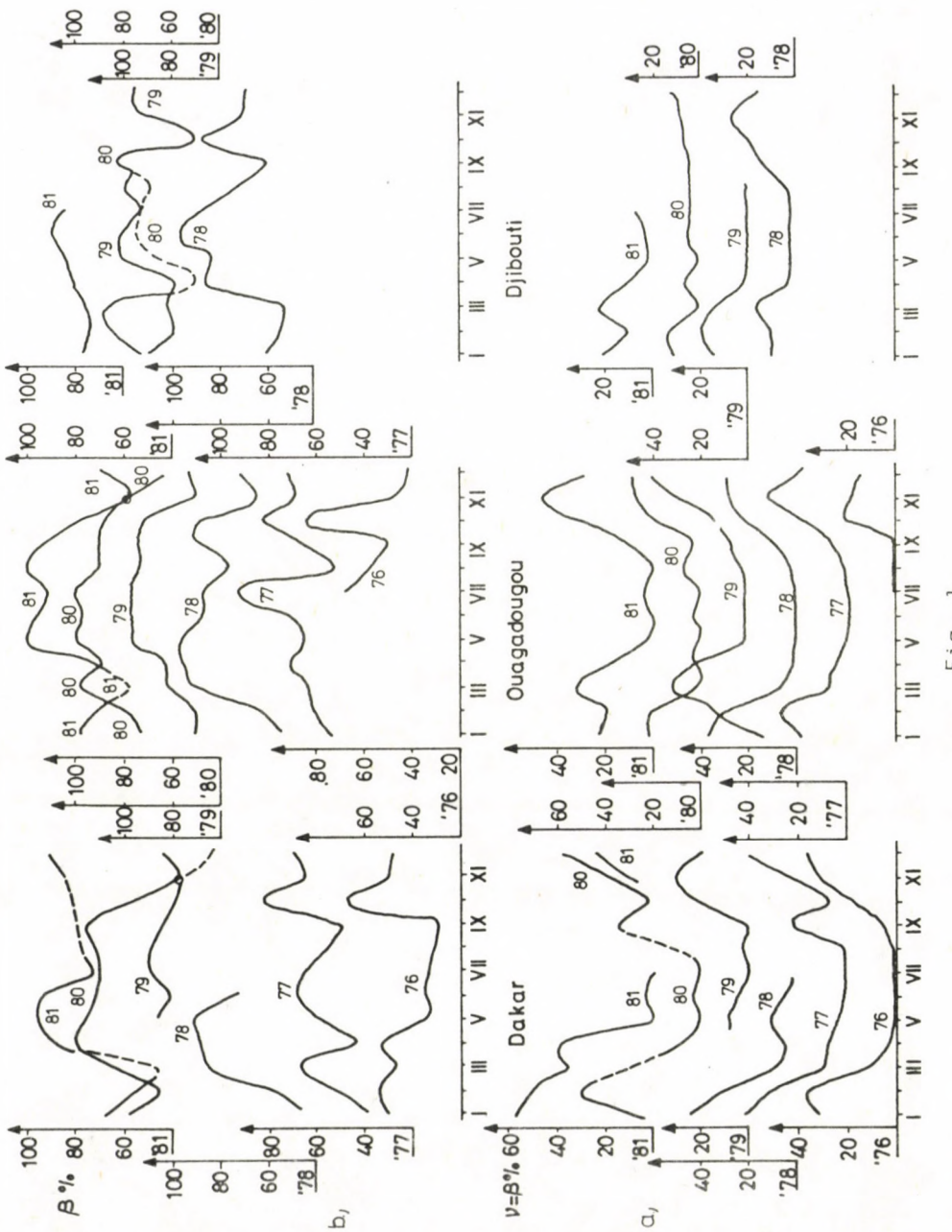

Fig. 1.

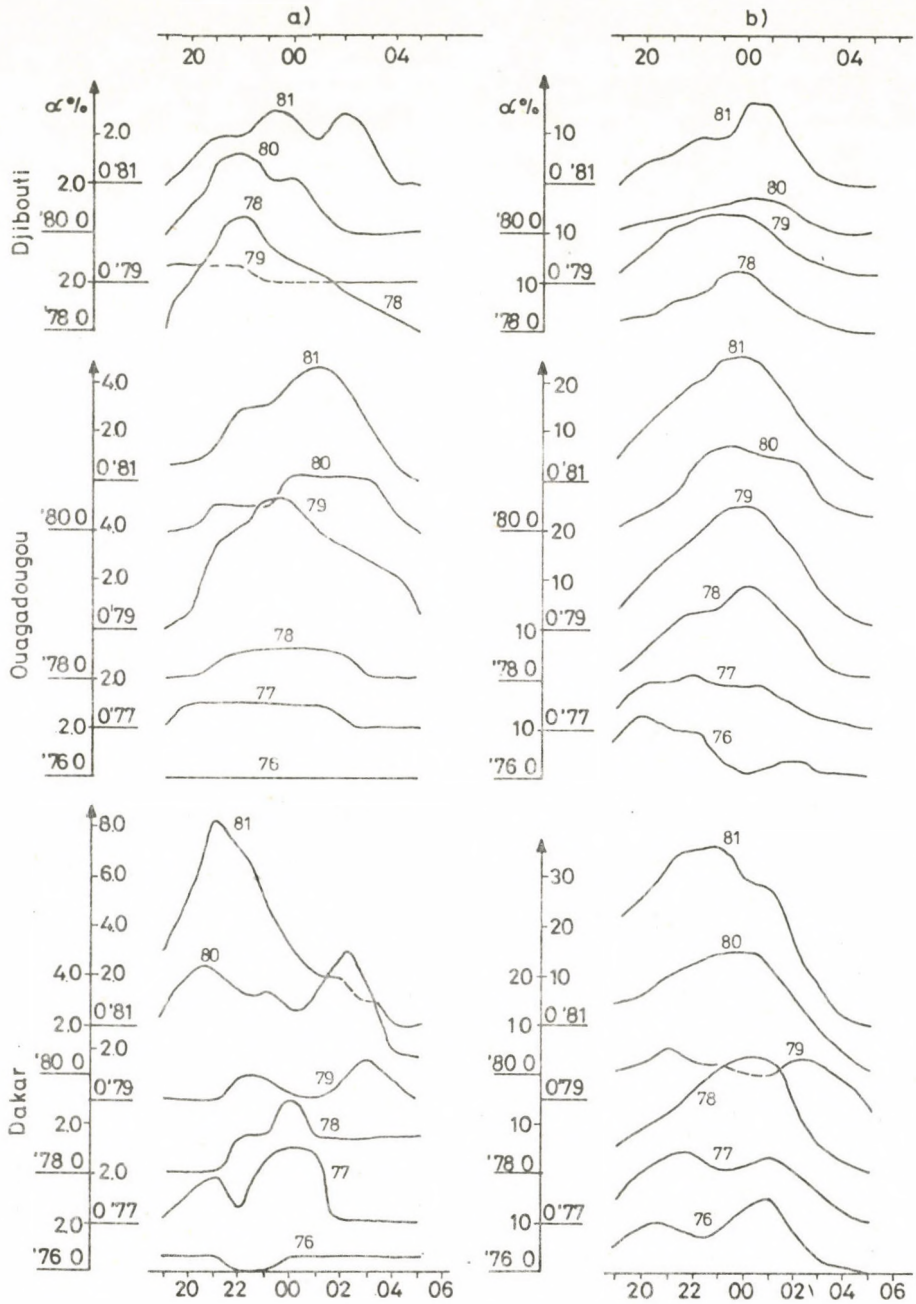
a)
b)
20
00
04
α%
Djibouti
Ouagadougou
Dakar
81
80
79
78
77
76
0'81
'80 0
0'79
'78 0
0'77
'76 0
22
02
06

Fig. 2.

at high solar activity. The data from the station Dakar show an inverse relationship, at high R the maximum in the occurrence of Δf_0 moves even to early night hours (about 21^h). During the winter period the distribution of α has also one maximum except some years at the station Dakar. Here a tendency similar to the summer and a change of the time of maximum occurrence during the solar activity cycle are found. At the same time the data from the other two stations show that the time of maximum occurring in the midnight hours does not change essentially.

Figure 3a gives the night variations of α_y averaged for one year. From the curves a definite spatial dependence of the night enhancements and the influence of the solar activity on their occurrence is well established. The general increase of the number of Δf_0 enhancements with the increase of R is observed at the stations Dakar and Ouagadougou except the years 1979-80. This does not refer to Djibouti where the determination of a corresponding dependence is hampered by the lack of data for 1976 and 1977 and by the availability of a smaller number of observed events during the remaining years.

In Fig. 4a seasonal average values of the frequency of occurrence ν are given. Here the dependence of the events on the solar activity cycle can be seen. The results obtained for the occurrence of the night enhancements are mostly analogous to those obtained for the Asian and American zones (Samardzhiev and Samardzhiev 1981, Samardzhiev and Uzunova 1984).

b) Spread-F

In the investigation of the spread-F phenomenon the same characteristic has been used as in case of the night enhancements of f_0F2, i.e. the frequency of occurrence β %.

In Fig. 1b the montly average frequency of occurrence β is given for each year. The yearly curves in this figure are of different type, but there is still a tendency for higher values of the parameter during summer months than during winter months. This, however, is not valid for the station Dakar in 1976 and partly in 1977 (low R). For the period of high solar activity during many of the months in 90-95 % of the hours

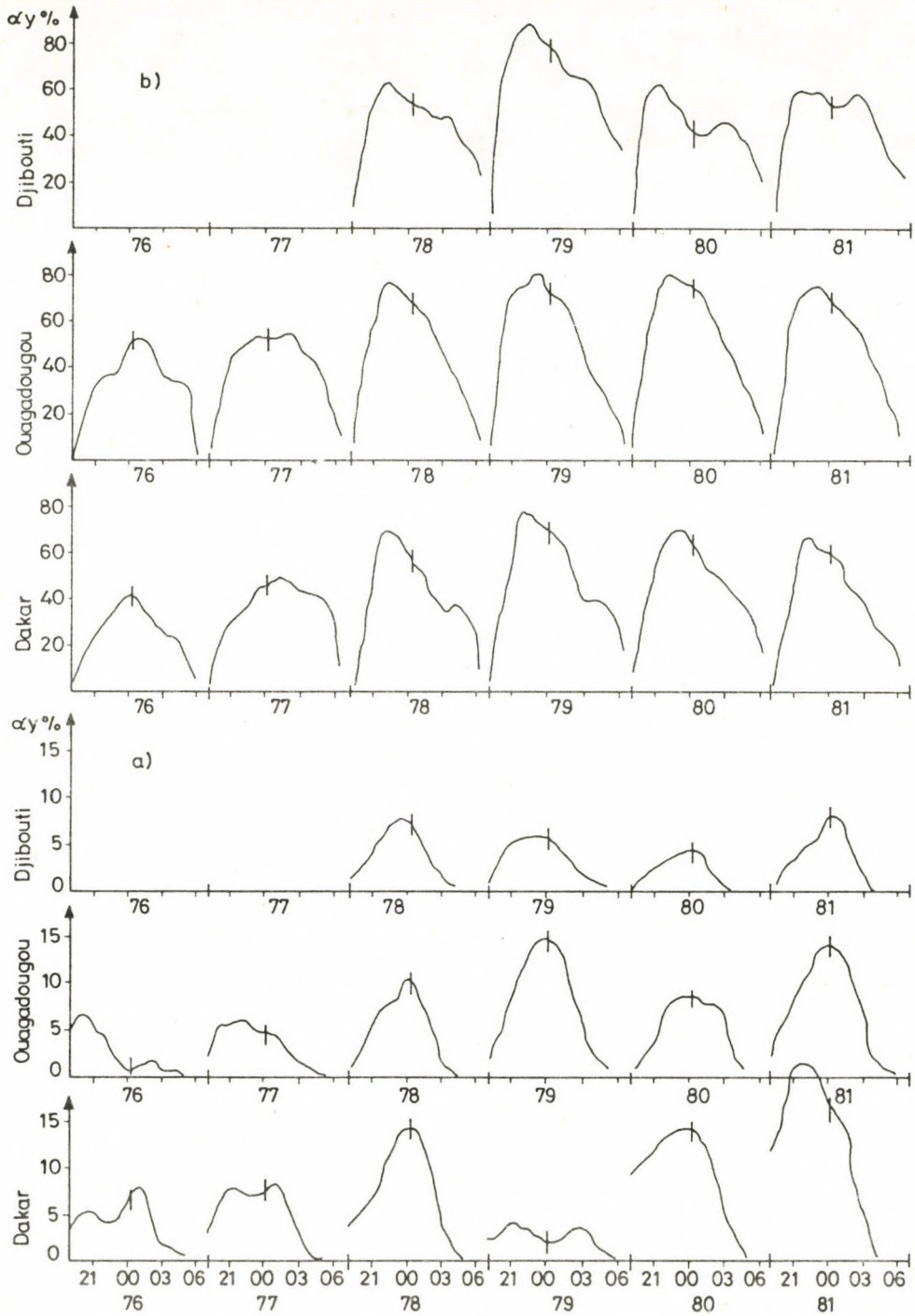

Fig. 3.

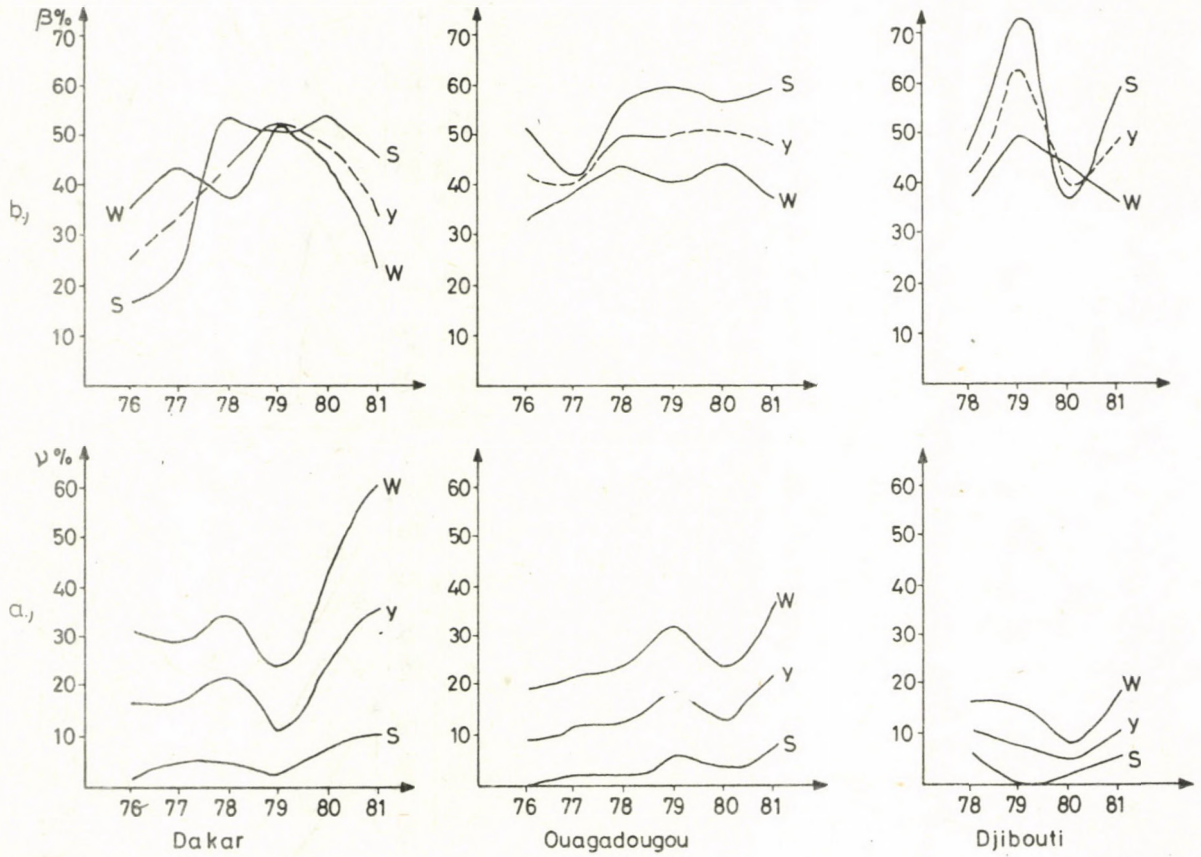
β%
b_j
70
60
50
40
30
20
10
W
S
y
76 77 78 79 80 81
ν%
a_j
Dakar
Ouagadougou
Djibouti

Fig. 4 .

F_{spr} is observed, and in 7 of the summer months F_{spr} can always be observed ($\beta_{\%}$ = 100 %). These are in Dakar April, 1980; in Ouagadougou May and July, 1980 and May and August 1981, and in Djibouti May and June 1979.

A better idea of F_{spr} occurrence is obtained from the hourly distribution of the frequency of occurrence. In Fig. 5 the seasonal averages are shown for summer (a) and winter (b) in each year. Here the scales for the two seasons are the same, thus the results may be directly compared. At all the three stations and in almost each year the proportion of disturbed hours is higher during summer, i.e. F_{spr} is a more frequent phenomenon during summer.

On the whole the curves show one maximum type α distribution. The maximum in winter is very characteristic and abrupt and occurs at all the three stations before midnight, between 21 and 23h. In summer in the years with increasing (1978) and high (1979-80) R, the most disturbed hours are around midnight. The most apparent deviations from the general behaviour of the distribution can be found in Djibouti in summer of 1980 (the number of cases of F_{spr} is less and maxima occur at 21 and 03h) and 1981 (maximum at 02h). At the station Dakar another peculiarity has been observed: in the period 1976-77 the number of hours with E_{spr} is less in summer than in winter, and in the winter months of 1979 this number is significantly larger than that in 1980, although in the two years the level of solar activity was the same.

An idea about the hourly distribution of α_y can be obtained from Fig. 3b where the variations averaged for the years in question are shown. At all the three stations in the period 1978-81 the maximum number of cases occurs in the premidnight hours. In 1976-77 the phenomenon is less frequent and the hourly distribution is different from that of the remaining years. It is very interesting that at all three stations 1979 is the year with the largest number of hours with F_{spr}. The other characteristic of the distributions is that in case of the station Djibouti-besides the very low level of disturbance in 1980 - the hourly distribution has definitely two maxima at

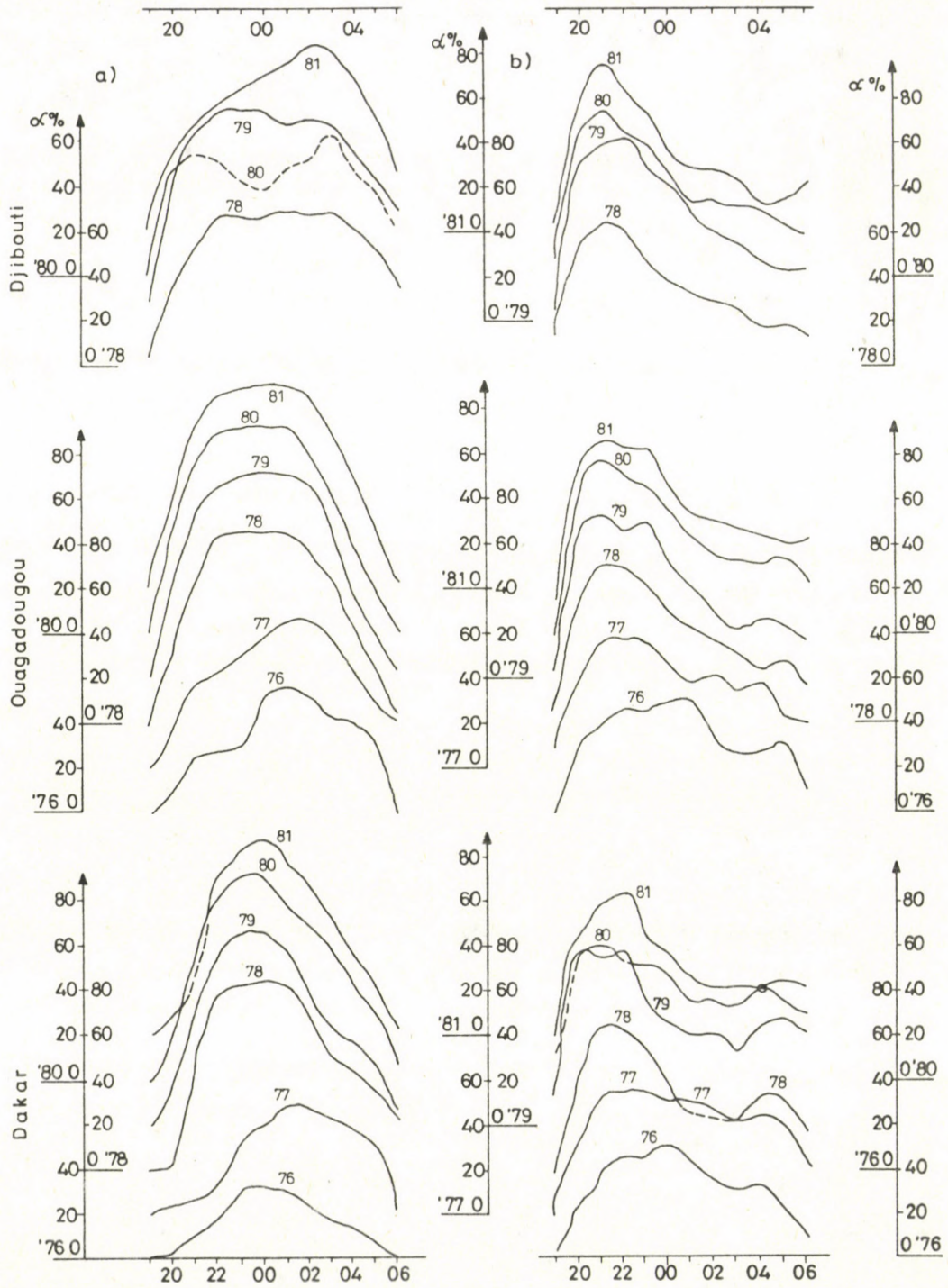
a)
b)
Djibouti
Ouagadougou
Dakar
α%
20
00
04
22
02
06
81
80
79
78
77
76
'80 0
'81 0
'78 0
'77 0
'76 0
0 '78
0 '79
0 '80
0'76

Fig. 5.

21 and 03h and a minimum exactly at midnight in the period after R_{max}.

The best survey of β is given in Fig. 4b where for the different years seasonal averages are presented. The variation from year to year at the station Dakar is well expressed and considering the variation with R, logical and the variations of the seasonal values are of opposite sense, reciprocal (with the exception of 1981). For the other two stations the relation of β to R as well as the connection between the seasonal values are only partial.

COMPARISON OF THE CHARACTERISTICS OF THE TWO PHENOMENA

A stable dependence of the f_0F2 enhancement on season can be seen in Fig. 1a with minimum occurrence frequency of the phenomenon in summer and maximum in winter. The variation of these frequencies is shown in Fig. 2. The F_{spr} curves in Fig. 1b have no so well defined yearly variation, while the hourly distribution (Fig. 5) is characterized by the same type of curves in both seasons at all the three stations. The rough comparison of the two series of curves shows that the frequency of occurrence of F_{spr} is higher in summer, especially for the hours after midnight. Therefore, it may be quite definitely stated that the night-time anomalous enhancement of f_0F2 is a winter phenomenon, and the spread-F a summer one.

Figure 3 presents the spatial variation of the two phenomena. The number of Δf_0 is larger at the stations lying nearer to the northern crest of the equatorial anomaly than at the near equatorial station Djibouti, while in case of F_{spr} the reverse ratio is observed both at R_{min} and R_{max}, the lowest frequency of occurrence is found at the station most distant from the equator, i.e. in Dakar. This observation is confirmed by Fig. 4.

CONCLUSIONS

On the basis of vertical sounding data of three African stations for the period 1976-81 some characteristics of the

anomalous night enhancements of f_0F2 and spread-F have been studied. The following results were obtained:

1. The anomalous night enhancements of f_0F2 occur more frequently during the winter period than in summer. At the stations near to the equatorial anomaly the number of cases is larger. The frequency of occurrence is directly proportional to the solar activity.

2. The spread-F phenomenon occurs more often during the summer period than in winter. A certain although less expressed dependence on geomagnetic activity is observed. More definite is the connection between F_{spr} and solar activity - maximum values are observed in 1979.

3. The results obtained support the conclusion that the two phenomena are closely, but inversely related. Therefore, a joint study of the characteristics and properties of the two phenomena mutually supplementing each other is needed for the purpose of a complex investigation.

REFERENCES

Pancheva D, Samardzhiev D, Samardzhiev T 1983: Bulg. Geophys. J., 9, 51.

Pancheva D, Samardzhiev D, Uzunova S 1984: Bulg. Geophys. J., 10, 34.

Samardzhiev D, Samardzhiev T 1981: Bulg. Geophys., J. 7, 36.

Samardzhiev D, Uzunova S 1984: Bulg. Geophys., J., 10, 48.

Samardzhiev D, Samardzhiev T 1985: Bulg. Geophys., J. (in press)

Acta Geod. Geoph. Mont. Hung., Vol. 22 (1-2), pp. 127-133 (1987)

SPATIAL CHARACTERISTICS OF THE IRREGULARITIES IN THE MID-LATITUDE IONOSPHERE

O N Boytman[1], I I Varshavskiy[1], B O Vugmeyster[1], N N Klimov[1]

[1]Sibirian Institute of Geomagnetism Ionosphere and Radio Wave Propagation (SibIZMIR), 664 033 Irkutsk 33, P.O.Box 4, USSR

In this paper the results of investigations are described about a method for the prediction of the irregular structure of the ionosphere. In the prediction the virtual height as a function of the frequency, the Doppler velocity and the angle of incidence at the vertical sounding of the ionosphere are used as initial data.

Keywords: irregular structure of the ionosphere; prediction; propagation of radio waves

Parameters of the signal at the receiving site can be computed only if the refractive index of the medium n (r, t) is known in the region between the transmitter and the receiver. The determination of the parameters of the medium on the basis of the results of sounding is problematic even assuming that the medium consists of plane layers (basic assumption in the computation of N(h)-profiles), and it has often no unambiguous solution. The reconstruction of a three-dimensionally irregular medium can only be realized on the basis of measurements in a single point with severe assumptions concerning the model, the validity of which is doubtful. Additional difficulties arise from the fact that the state of the medium cannot directly be determined, indirect (radiophysical) methods are only available, for which algorithms are necessary concerning the reconstruction of the medium from the parameters of the reflected signal.

In general, the problem of the prediction of state of the ionosphere consists of the construction of suitable models, by which the reconstruction of the parameters of the ionospheric

disturbance is possible from measured parameters of the signal. In this procedure the undisturbed concentration of the ionospheric plasma is assumed to be known, i.e. the density of the plasma is expressed in the form

$$N(\underline{r}, t) = N_0(z)\left[1 + \varepsilon(\underline{r}, t)\right]. \quad (1)$$

In the prediction the virtual height as a function of the frequency $h'(f)$ and a series of Doppler velocities v_p and angles of incidence of the signal at the vertical sounding are used as initial parameters. The undisturbed part of the electron density $N_0(z)$ is computed on the basis of ionograms.

The algorithms developed in SIBIZMIR for the prediction of the irregular structure of the ionosphere have been controlled by a measurement program of the digital ionosonde "Basis" and by the computation program IVK-2. The scheme of the measurements is presented in Fig. 1.

The software (SW) consists of two parts namely of standard and special programs. The standard SW includes the operational system RAFOS adapted to the configuration required by the hardware. The special SW consists of a program library controlling the experiment and collecting and preprocessing the data of ionospheric sounding. The modules of the library are programs executing the following tasks:

- control and collection of information with the ionosonde "Basis",
- control and collection of information with the equipment PRK-3M,
- preparation of files and computation of electron density profiles,
- preparation of data files and computation of the Doppler frequency and the angle of incidence.

Moreover, the special SW comprises programs which enable the direct prediction of the electron density on the basis of results of the data preprocessing. The decisive phase of the prediction is the construction of certain rules or decisive functions F enabling the estimation of the predicted quantity from the predictors.

As predictors the time series of Doppler velocities, of

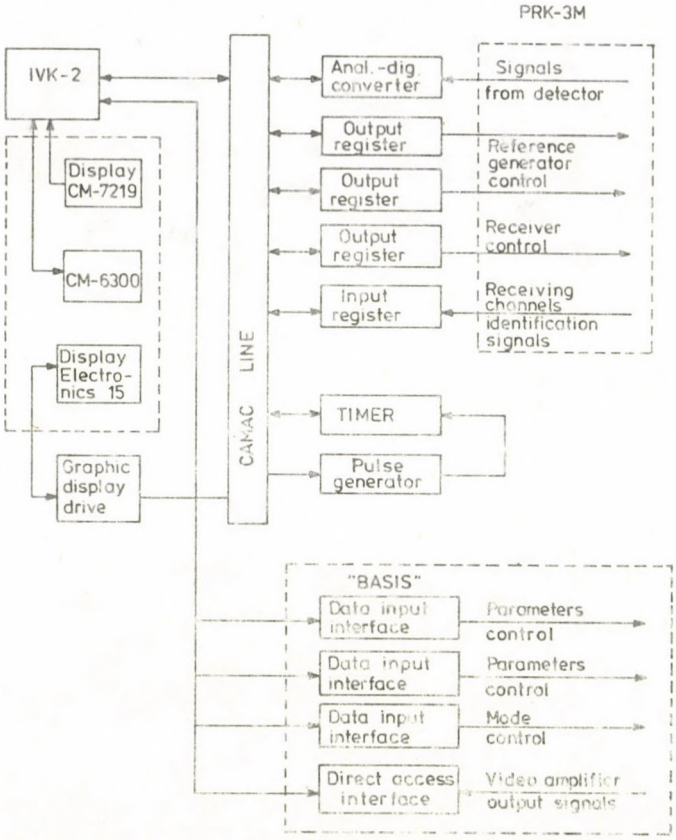

Fig. 1. Functional diagram of the ionospheric measuring complex

angles of incidence and electron density profiles, obtained from ionograms of the vertical sounding of the ionosphere were selected. The predicted quantity is a function describing variations of the electron density in time and space.

The error of the prediction is indirectly estimated by comparing the observed characteristics of the oblique incidence transmission path with those of trajectories in the medium computed by the predicted quantity.

In general, the decisive function is a model consisting of the superposition of determined and random quantities.

The deterministic function is a Fourier series, i.e. it is

assumed that

$$\varepsilon(\underline{r},\ t) = \sum_{i=1}^{N} \sigma_i \cos\left(\omega_i(t-t_o) + \underline{k}_i\ (\underline{r}-\underline{r}_o) + \varphi_i\right) \qquad (2)$$

where $\underline{r}_o$, t_o are the space and time coordinates of the transmitter. The model assumes that the perturbation of the electron density is the sum of traveling plane waves of amplitudes much less than the bakcground value $N_o(z)$.

In the second step of the prediction the unknown parameters of the model σ_i, ω_i, $\underline{k}_i$ and φ_i are to be estimated, than the relation between these parameters and the observed time series of Doppler frequencies ($f_D(t)$) in the direction of the angle of incidence $[\alpha_x(t),\ \alpha_y(t)]$ should be established. The x axis of the coordinate system is directed to east, the y axis to north and the z axis vertically upwards.

It is assumed in agreement with Varshavskiy and Kalikhman (1984) that the change of the phase path due to deviation of the trajectory from the vertical is small in case of vertical sounding. Then neglecting the effect of the geomagnetic field and excluding vertical perturbations from the discussion the relations

$$f_D(t) = \frac{2b}{\lambda_o} \sum_{i=1}^{N} \sigma_i \omega_i \cos\left(\omega_i\ (t-t_o) + \varphi_i + \frac{\pi}{2}\right)$$

$$\sin\alpha_x(t) = b \sum_{i=1}^{N} \sigma_i\ k_{xi} \cos\left(\omega_i\ (t-t_o) + \varphi_i + \frac{\pi}{2}\right) \qquad (3)$$

$$\sin\alpha_y(t) = b \sum_{i=1}^{N} \sigma_i\ k_{yi} \cos\left(\omega_i\ (t-t_o) + \varphi_i + \frac{\pi}{2}\right)$$

$$b = \frac{2}{3}\frac{df_p^2}{a} \qquad \lambda_o = \frac{C}{f_p}$$

are obtained, where C is the velocity of light, f_p is the applied frequency, a is the gradient of the bakcground electron density in the reflection point and $d = 1.24 \cdot 10^4$ MHz^{-2}m^{-3}.

Fourier analysis of the initial time series yields estimates of the most significant spectral components.

For the time series of Doppler frequencies F_j, AX_j and AY_j denote components of the power spectrum, and α_x, α_y and ΦF_j components of the phase spectrum. Then, for each of N waves included in the initial model the amplitude δ_j of the perturbation, the module of the phase velocity V_j, the wave length λ_j and the azimuth ψ_j of the propagation and the phase φ_j of the wave can be computed by the following formulas:

$$\delta_j = \frac{\lambda_o F_j}{2b\,\omega_j}; \quad V_j = \frac{F_j}{2\sqrt{AX_j^2 + AY_j^2}}; \quad \lambda_j = \frac{\pi F_j}{\omega_j \sqrt{AX^2 + AY_j^2}};$$

$$\psi_j = \arctan(AX_j/AY_j); \quad \varphi_j = -\Phi F_j - \frac{\pi}{2}. \tag{4}$$

Equations (2)-(4) enable to construct a scheme of the deterministic prediction of the electron density perturbation.

In order to determine time and space limits of the effectivity of the prediction scheme, a correlation analysis of the initial time series was carried out. In this procedure the time interval is estimated in which the correlation function of the initial series decreases to 0.5 and this value is called the radius of inertia. Then the scheme enables to prepare the prediction based on the inertia for a period not exceeding the radius of inertia. In case of predictions for periods greater than the radius of inertia the decisive function (model) should be supplemented with a stochastic component. This will be developed later.

If the period of prediction is greater than the time interval, in which the correlation function becomes zero, then an electron density profile computed on the basis of certain global ionospheric models (e.g. Polyakov et al. 1978) can be used as predictors.

For an estimation of the errors attributed to the scheme of the deterministic inertial prediction, a comparison of predicted and observed data is necessary, after removing errors as errors of measurement of the reconstruction of $N_o(z)$ and

others. For this purpose a model experiment was carried out. Time series were synthetized for a three dimensionally irregular reference medium by means of trajectory computations (Varshavskiy and Kalikhman 1984) both for vertical propagation and for four oblique transmission parths of 100 km lengths.

By means of the method presented here and on the basis of the series $f_0(t)$, $\alpha_x(t)$ and $\alpha_y(t)$ parameters of the electron density waves were estimated and the ionospheric box has been predicted (Varshavskiy and Kalikhman 1984). Further some parameters of the radio signal, as the azimuth ψ and angle of deviation of the ray from the vertical Θ were compared for the reference and the predicted media at four selected transmission paths.

In order to estimate the degree of perturbation of the azimuth and the angle of incidence, mean square deviations of these quantities ($\overline{\Delta}\,\psi$ and $\overline{\Delta}\,\Theta$) were calculated. It can be shown on the basis of these parameters how large the error of the prediction would be if it would be prepared on the basis of the background part of the electron density profile.

The error of the method in question is given by the mean square deviations $\delta\psi$, $\delta\Theta$ of the reference parameters ψ and Θ from the predicted values. The corresponding estimates are presented in Table I.

Table I. Estimates of the mean square deviations of the reference parameters ψ and Θ

Test number	$\overline{\Delta}\,\psi$ (degree)	$\overline{\Delta}\,\Theta$ (degree)	$\delta\psi$ (degree)	$\delta\Theta$ (degree)
1	12.88	1.276	2.31	0.085
2	6.84	0.905	2.42	0.404
3	5.7	1.17	1.88	0.18
4	4.04	1.1	3.11	0.22

The investigations carried out allow us to formulate a method for the deterministic inertial prediction of the irregular ionospheric structure. The model experiment proves the effectivity of the suggested prediction scheme.

Further improvement of the method would consist of the determination of the radii of inertia for the predicted parameters and of their temporal and spatial variations on the basis of experimental data.

REFERENCES

Polyakov V I, Sukhodolskaya V E, Ivelskaya M K, Shapranova G V 1978: Semiempirical model of the ionosphere (in Russian). Materiali MCD-B, Moscow

Varshavskiy I I, Kalikhman A D 1984: In: Issl. Geomagn. Aeron. Fiz. Solntza, No 67, 165-172.

Acta Geod. Geoph. Mont. Hung., Vol. 22 (1-2), pp. 135-154 (1987)

NON-STATIONARY QUASI-HYDRODYNAMICS OF CHARGED PARTICLES IN THE IRREGULAR IONOSPHERE (E AND F REGIONS)

A S Minkin[1] and M N Fatkullin[1]

[1]Institute of Geomagnetism, Ionosphere and Radio Wave Propagation, Academy of Sciences of the USSR, 142092 Troitsk, Moskovskaya oblast, USSR

Non-stationary quasi-hydrodynamics of electrons and ions is studied considering time varying electric fields, the velocity of neutral wind, as well as gradients of charged particle concentration and temperature. For the electrons and ions their collision with neutral particles is taken into account. Allowance is made for the departure of the geographical coordinate system from the geomagnetic coordinate system. Different special cases are discussed.

Keywords: ionospheric plasma instabilities; plasma dynamics; physics of the ionosphere; wave perturbations in the ionosphere

INTRODUCTION

The dynamics of charged particles in the ionosphere of the Earth has been discussed in a number of papers (e.g. Gershman 1974, Fatkullin 1982). This problem is important from the point of view of questions as structure of the ionosphere, currents in the ionosphere and their geomagnetic effects, wave perturbations in the ionosphere, ionospheric plasma instabilities etc. In theoretical studies the starting point is generally the quasi-hydrodynamic equation of motion of charged particles

$$m_\alpha n_\alpha \left[\frac{\partial \underline{v}_\alpha}{\partial t} + (\underline{v}_\alpha \cdot \nabla)\,\underline{v}_\alpha\right] = e_\alpha n_\alpha \underline{E} + \frac{e_\alpha n_\alpha}{c}(\underline{v}_\alpha \times \underline{B}) -$$

$$- \operatorname{grad} p_\alpha + m_\alpha n_\alpha \underline{g} - n_\alpha \sum_{\beta \neq \alpha} n_\beta \Theta_{\alpha\beta}(\underline{v}_\alpha - \underline{v}_\beta) - \qquad (1)$$

$$- n_\alpha \sum_n n_n \Theta_{\alpha n}(\underline{v}_\alpha - \underline{v}_n) \ ,$$

Acta Geod. Geoph. Mont. Hung. 22, 1987
Akadémiai Kiadó, Budapest

where m_α, n_α, $\underline{v}_\alpha$, p_α and e_α are the mass, concentration, velocity, pressure and charge of the particle of type α, $\underline{E}$ and $\underline{B}$ are the electric and magnetic fields, respectively, g is the acceleration due to gravity, $\underline{v}_n$ the velocity of neutral particles and c the velocity of light. Furthermore

$$\Theta_{\alpha\beta} = \frac{\nu_{\alpha\beta}}{n_\beta} \mu_{\alpha\beta} \qquad (2)$$

where $\nu_{\alpha\beta}$ is the collision frequency and $\mu_{\alpha\beta}$ the reduced mass. In ionospheric investigations the stationary solutions of Eq. (1) are sufficiently well understood (Gershman 1974) and some of them will be considered as special cases below.

As regards ionospheric conditions, nonstationary solutions of Eq. (1) have not been studied so far taking into account the time dependence of the forcing factors ($\underline{E}$, $\underline{v}_n$, ∇p_α), as far as it is known for the authors. In the physics of ionized gases such problems have been considered for some cases by a number of authors (Landau and Lifshitz 1960, Boguslavskiy 1961, Schuman 1963, Alfven and Fälthämmar 1967).

In this paper an attempt is made to study the nonstationary solution of Eq. (1) for electrons and positive ions in real ionospheric conditions and taking into account arbitrarily time dependent electric fields, velocity of neutrals and concentration gradients of charged particles, This has importance as under ionospheric conditions some parameters of the medium undergo variations of characteristic periods ranging from fraction of a second to some tens of minutes.

INITIAL CONDITIONS

1. In case of the positive ions and electrons only collisions with neutral particles are taken into account.

2. It is assumed that the ion-neutral and the electron--neutral collision frequencies do not depend on time.

3. The problem is studied in the geographical coordinate system, where $\underline{r}$ is the radius vector, Θ is the colatitude, λ is the geographical longitude. The following notations will be

used:

$$\nabla_r \equiv \frac{\partial}{\partial r}\,, \quad \nabla_\Theta \equiv \frac{1}{r}\,\frac{\partial}{\partial \Theta}\,, \quad \nabla_\lambda \equiv \frac{1}{r\,\sin\Theta}\,\frac{\partial}{\partial \lambda} \tag{3}$$

4. In the geographical coordinate system the magnetic field of the Earth has the following coordinates

$$B_r = |\underline{\underline{B}}|\,(\mp \sin I), \quad B_\Theta = |\underline{\underline{B}}|\cos I \cos D\,, \quad B_\lambda = |\underline{\underline{B}}|\cos I \sin D\,, \tag{4}$$

where I is the dip angle, D the magnetic declination and the upper sign refers to the northern hemisphere, the lower one to the southern hemisphere. The same notation will be applied below.

5. In Eq. (1) the term $m_\alpha\, n_\alpha\, (\underline{\underline{v}}_\alpha \cdot \nabla)\, \underline{\underline{v}}_\alpha$ is neglected.

Satisfying the conditions mentioned above the initial system of equations is for particles of type α

$$\begin{aligned}
\frac{\partial w_\alpha}{\partial t} &= -a_\alpha w_\alpha + \Omega_\alpha \cos I \sin D u_\alpha - \Omega_\alpha \cos I \cos D v_\alpha + W_\alpha(t)\,,\\
\frac{\partial u_\alpha}{\partial t} &= -\Omega_\alpha \cos I \sin D w_\alpha - a_\alpha u_\alpha \mp \Omega_\alpha \sin I v_\alpha + U_\alpha(t)\,,\\
\frac{\partial v_\alpha}{\partial t} &= \Omega_\alpha \cos I \cos D w_\alpha \pm \Omega_\alpha \sin I u_\alpha - a_\alpha v_\alpha + V_\alpha(t)\,,
\end{aligned} \tag{5}$$

where w_α, u_α and v_α are the vertical, meridional and zonal velocity components of the charged particles of type α, $W_\alpha(t)$, $U_\alpha(t)$ and $V_\alpha(t)$ are the forcing factors

$$a_\alpha = \frac{n_n\, \Theta_{\alpha n}}{m_\alpha}\,, \qquad \Omega_\alpha = \frac{e_\alpha\, B}{m_\alpha\, C}\,, \tag{6}$$

$$\begin{aligned}
W_\alpha(t) &= \frac{e_\alpha}{m_\alpha} E_r + a_\alpha w_n + g_r - \frac{\nabla_r P_\alpha}{m_\alpha n_\alpha}\,, \quad U_\alpha(t) = \frac{e_\alpha}{m_\alpha} E_\Theta + \\
&+ a_\alpha u_n - \frac{\nabla_\Theta P_\alpha}{m_\alpha n_\alpha}\,, \quad V_\alpha(t) = \frac{e_\alpha}{m_\alpha} E_\lambda + a_\alpha v_n - \frac{\nabla_\lambda P_\alpha}{m_\alpha n_\alpha}\,,
\end{aligned} \tag{7}$$

where w_n, u_n and v_n are the vertical, meridional and zonal components of the neutral wind.

SOLUTIONS FOR DIFFERENT CASES

The general solution of the initial system of equations has a lengthy form. It is presented in Appendix I. Moreover,

in Appendix II solutions referring to the initial conditions $t = t_0$, $w_\alpha = w_{\alpha 0}$, $u_\alpha = u_{\alpha 0}$ and $v_\alpha = v_{\alpha 0}$ are given.

Here a more detailed discussion of a number of more specific cases is attempted.

1. Considering high latitudes, where $I \simeq \frac{\pi}{2}$, the relations

$$w_\alpha(t) = e^{-a_\alpha t}\left[\int e^{a_\alpha t} W_\alpha(t)\, dt + C_1\right], \tag{8}$$

$$u_\alpha(t) = e^{-a_\alpha t}\left[\cos\Omega_\alpha t \int e^{a_\alpha t}\left(U_\alpha(t)\cos\Omega_\alpha t \pm V_\alpha(t)\sin\Omega_\alpha t\right) dt + \right.$$
$$+ \sin\Omega_\alpha t \int e^{a_\alpha t}\left(U_\alpha(t)\sin\Omega_\alpha t \mp V_\alpha(t)\cos\Omega_\alpha t\right) dt + \tag{9}$$
$$\left. + C_2\cos\Omega_\alpha t \mp C_3\sin\Omega_\alpha t\right],$$

$$v_\alpha(t) = e^{-a_\alpha t}\left[\sin\Omega_\alpha t \int e^{a_\alpha t}\left(V_\alpha(t)\sin\Omega_\alpha t \pm U_\alpha(t)\cos\Omega_\alpha t\right) dt + \right.$$
$$+ \cos\Omega_\alpha t \int e^{a_\alpha t}\left(V_\alpha(t)\cos\Omega_\alpha t \mp U_\alpha(t)\sin\Omega_\alpha t\right) dt \pm \tag{10}$$
$$\left. \pm C_2\sin\Omega_\alpha t + C_3\cos\Omega_\alpha t\right],$$

are obtained, where C_1, C_2 and C_3 are integration constants.

At the time $t = t_0$, it should be $w_\alpha(t) = w_{\alpha 0}$, $u_\alpha(t) = u_{\alpha 0}$ and $v_\alpha(t) = v_{\alpha 0}$. In case of these initial conditions Eqs (8)-(10) take the following forms

$$w_\alpha(t) = e^{-a_\alpha t}\int_{t_0}^{t} e^{a_\alpha t} W_\alpha(t)\, dt + w_{\alpha 0}\cdot e^{-a_\alpha \tau}, \tag{11}$$

$$u_\alpha(t) = e^{-a_\alpha t}\left[\cos\Omega_\alpha t \int_{t_0}^{t} e^{a_\alpha t}\left(U_\alpha(t)\cos\Omega_\alpha t \pm V_\alpha(t)\sin\Omega_\alpha t\right) dt + \right.$$
$$\left. + \sin\Omega_\alpha t \int_{t_0}^{t} e^{a_\alpha t}\left(U_\alpha(t)\sin\Omega_\alpha t \mp V_\alpha(t)\cos\Omega_\alpha t\right) dt\right] + \tag{12}$$
$$+ q\, e^{-a_\alpha \tau}\sin\left(\Omega_\alpha \tau \mp \psi\right),$$

$$v_\alpha(t) = e^{-a_\alpha t}\left[\sin\Omega_\alpha t \int_{t_0}^{t} e^{a_\alpha t}\,(V_\alpha(t)\sin\Omega_\alpha t \pm U_\alpha(t)\cos\Omega_\alpha t)\,dt + \right.$$

$$\left. + \cos\Omega_\alpha t \int_{t_0}^{t} e^{a_\alpha t}\,(V_\alpha(t)\cos\Omega_\alpha t \mp U_\alpha(t)\sin\Omega_\alpha t)\,dt\right] + \qquad (13)$$

$$+ q\, e^{-a_\alpha \tau}\sin(\Omega_\alpha \tau \pm \varphi)\ ,$$

where

$$\tau = t - t_0,\quad \tan\psi = \frac{u_{\alpha 0}}{v_{\alpha 0}},\quad \tan\varphi = \frac{v_{\alpha 0}}{u_{\alpha 0}},\quad q = \sqrt{u_{\alpha 0}^2 + v_{\alpha 0}^2}\ . \qquad (14)$$

If the forcing factors do not depend on time, then Eqs (11)-(13) can be written as

$$w_\alpha(t) = \frac{W_\alpha}{a_\alpha}\,(1 - e^{-a_\alpha\tau}) + w_{\alpha 0}\, e^{-a_\alpha\tau}\ , \qquad (15)$$

$$u_\alpha(t) = \frac{1 - e^{-a_\alpha\tau}}{a_\alpha^2 + \Omega_\alpha^2}\,(a_\alpha U_\alpha \mp \Omega_\alpha V_\alpha) + q\, e^{-a_\alpha\tau}\sin(\Omega_\alpha\tau \mp \psi), \qquad (16)$$

$$v_\alpha(t) = \frac{1 - e^{-a_\alpha\tau}}{a_\alpha^2 + \Omega_\alpha^2}\,(a_\alpha V_\alpha \pm \Omega_\alpha U_\alpha) + q\, e^{-a_\alpha\tau}\sin(\Omega_\alpha\tau \pm \varphi). \qquad (17)$$

In case of $\tau \gg \frac{1}{a_\alpha}\ e^{-a_\alpha\tau} \longrightarrow 0$ Eqs (15)-(17) lead to

$$w_\alpha = \frac{W_\alpha}{a_\alpha}\ , \qquad (18)$$

$$u_\alpha = \frac{a_\alpha U_\alpha \mp \Omega_\alpha V_\alpha}{a_\alpha^2 + \Omega_\alpha^2}\ , \qquad (19)$$

$$v_\alpha = \frac{a_\alpha V_\alpha \pm \Omega_\alpha U_\alpha}{a_\alpha^2 + \Omega_\alpha^2}\ . \qquad (20)$$

The forcing factors should vary with time according to the following relation

$$W_\alpha(t) = W_{\alpha 0} + \sum_{k=1}^{\infty} W_{\alpha k} \sin(k\omega\tau + \alpha_k), \quad U_\alpha(t) = U_{\alpha 0} + \sum_{k=1}^{\infty} U_{\alpha k} \sin(k\omega\tau + \alpha_k), \quad V_\alpha(t) = V_{\alpha 0} + \sum_{k=1}^{\infty} V_{\alpha k} \sin(k\omega\tau + \alpha_k). \tag{21}$$

Then, the initial conditions, being $\tau = 0$, $w_\alpha = w_{\alpha 0}$, $u_\alpha = u_{\alpha 0}$ and $v_\alpha = v_{\alpha 0}$ the equations for the velocity components of the charged particles take the form

$$w_\alpha(t) = \frac{W_{\alpha 0}}{a_\alpha}(1 - e^{-a_\alpha\tau}) + \sum_{k=1}^{\infty} \frac{W_{\alpha k}}{\sqrt{a_\alpha^2 + (k\omega)^2}} \left[\sin(k\omega\tau + \alpha_k - \Theta_k) - e^{-a_\alpha\tau} \sin(\alpha_k - \Theta_k)\right] + w_{\alpha 0} e^{-a_\alpha\tau}, \tag{22}$$

$$u_\alpha(t) = \frac{1-e^{-a_\alpha\tau}}{a_\alpha^2 + \Omega_\alpha^2}(a_\alpha U_{\alpha 0} \mp \Omega_\alpha V_{\alpha 0}) + \frac{1}{2} \sum_{k=1}^{\infty} \sqrt{U_{\alpha k}^2 + V_{\alpha k}^2} \cdot$$

$$\cdot \left\{ \frac{\sin(k\omega\tau + \alpha_k - \varkappa_k \mp A_k)}{\sqrt{a_\alpha^2 + (k\omega + \Omega_\alpha)^2}} + \frac{\sin(k\omega\tau + \alpha_k - \vartheta_k \pm A_k)}{\sqrt{a_\alpha^2 + (k\omega + \Omega_\alpha)^2}} - e^{-a_\alpha\tau} \left[\frac{\sin(\alpha_k - \varkappa_k \mp A_k)}{\sqrt{a_\alpha^2 + (k\omega + \Omega_\alpha)^2}} + \frac{\sin(\alpha_k - \vartheta_k \pm A_k)}{\sqrt{a_\alpha^2 + (k\omega - \Omega_\alpha)^2}} \right] \right\} + \tag{23}$$

$$+ q\, e^{-a_\alpha\tau} \sin(\Omega_\alpha\tau \mp \psi),$$

$$v_\alpha(t) = \frac{1-e^{-a_\alpha\tau}}{a_\alpha^2 + \Omega_\alpha^2}(a_\alpha V_{\alpha 0} \pm \Omega_\alpha U_{\alpha 0}) \pm \frac{1}{2} \sum_{k=1}^{\infty} \sqrt{U_{\alpha k}^2 + V_{\alpha k}^2} \cdot$$

$$\cdot \left\{ \frac{\cos(k\omega\tau + \alpha_k - \varkappa_k \mp A_k)}{\sqrt{a_\alpha^2 + (k\omega + \Omega_\alpha)^2}} - \frac{\cos(k\omega\tau + \alpha_k - \vartheta_k \pm A_k)}{\sqrt{a_\alpha^2 + (k\omega - \Omega_\alpha)^2}} - \right. \tag{24}$$

$$- e^{-a_\alpha \tau}\left[\frac{\cos(\alpha_k - \chi_k \mp A_k)}{\sqrt{a_\alpha^2 + (k\omega + \Omega_\alpha)^2}} - \frac{\cos(\alpha_k - \vartheta_k \pm A_k)}{\sqrt{a_\alpha^2 + (k\omega - \Omega_\alpha)^2}}\right]\Bigg\} +$$

$$+ q\, e^{-a_\alpha \tau} \sin(\Omega_\alpha \tau \pm \ell) ,$$

where

$$\tan \Theta_k = \frac{k\omega}{a_\alpha} , \quad \tan \chi_k = \frac{k\omega + \Omega_\alpha}{a_\alpha} , \quad \tan \vartheta_k = \frac{k\omega - \Omega_\alpha}{a_\alpha} ,$$

$$\tan A_k = \frac{V_{\alpha k}}{U_{\alpha k}} . \qquad (25)$$

2. Now the case should be considered when $I \simeq 0$ (equatorial latitudes); however, the geographical coordinate system does not coincide with the geomagnetic coordinate system ($D \neq 0$). In this case following equations of the velocity components are obtained for the initial conditions $w_\alpha = w_{\alpha 0}$, $u_\alpha = u_{\alpha 0}$ and $v_\alpha = v_{\alpha 0}$ at the time $t = t_0$:

$$w_\alpha(t) = e^{-a_\alpha t}\left\{-\left[\cos\Omega t \int_{t_0}^{t} e^{a_\alpha t} W_\alpha(t) \cos\Omega_\alpha t\, dt + \right.\right.$$

$$\left. + \sin\Omega_\alpha t \int_{t_0}^{t} e^{a_\alpha t} W_\alpha(t) \sin\Omega_\alpha t\, dt\right] +$$

$$+ S_D\left[\sin\Omega_\alpha t \int_{t_0}^{t} e^{a_\alpha t} U_\alpha(t) \cos\Omega_\alpha t\, dt - \right. \qquad (26)$$

$$\left. - \cos\Omega_\alpha t \int_{t_0}^{t} e^{a_\alpha t} U_\alpha(t) \sin\Omega_\alpha t\, dt\right] -$$

$$- C_D\left[\sin\Omega_\alpha t \int_{t_0}^{t} e^{a_\alpha t} V_\alpha(t) \cos\Omega_\alpha t\, dt - \right.$$

$$\left.\left. - \cos\Omega_\alpha t \int_{t_0}^{t} e^{a_\alpha t} V_\alpha(t) \sin\Omega_\alpha t\, dt\right\} + q' e^{-a_\alpha \tau} \sin(\Omega_\alpha \tau + \xi) ,\right.$$

$$u_\alpha(t) = e^{-a_\alpha t}\left\{C_D\int_{t_o}^{t} e^{a_\alpha t}\left[C_D U_D(t) + S_D V_\alpha(t)\ dt\right] -\right.$$

$$- S_D\left[\sin\Omega_\alpha t\int_{t_o}^{t} e^{a_\alpha t} W_\alpha(t)\cos\Omega_\alpha t\ dt -\right.$$

$$\left. - \cos\Omega_\alpha t\int_{t_o}^{t} e^{a_\alpha t} W_\alpha(t)\sin\Omega_\alpha t\ dt\right] +$$

$$+ S_D^2\left[\cos\Omega_\alpha t\int_{t_o}^{t} e^{a_\alpha t} U_\alpha(t)\cos\Omega_\alpha t\ dt +\right.$$

$$\left. + \sin\Omega_\alpha t\int_{t_o}^{t} e^{a_\alpha t} U_\alpha(t)\sin\Omega_\alpha t\ dt\right] - \qquad (27)$$

$$- S_D C_D\left[\cos\Omega_\alpha t\int_{t_o}^{t} e^{a_\alpha t} V_\alpha(t)\cos\Omega_\alpha t\ dt +\right.$$

$$\left.\left. + \sin\Omega_\alpha t\int_{t_o}^{t} e^{a_\alpha t} V_\alpha(t)\sin\Omega_\alpha t\ dt\right]\right\} + e^{-a_\alpha\tau}\left[C_D(C_D u_{\alpha o} + S_D v_{\alpha o}) +\right.$$

$$\left. + q' S_D\cos(\Omega_\alpha\tau + \xi)\right],$$

$$v_\alpha(t) = e^{-a_\alpha t}\left\{S_D\int_{t_o}^{t} e^{a_\alpha t}\left[C_D U_\alpha(t) + S_D V_\alpha(t)\right]dt\ +\right.$$

$$+ C_D\left[\sin\Omega_\alpha t\int_{t_o}^{t} e^{a_\alpha t} W_\alpha(t)\cos\Omega_\alpha t\ dt -\right.$$

$$\left. - \cos\Omega_\alpha t\int_{t_o}^{t} e^{a_\alpha t} W_\alpha(t)\sin\Omega_\alpha t\ dt\right] -$$

$$- S_D C_D\left[\cos\Omega_\alpha t\int_{t_o}^{t} e^{a_\alpha t} U_\alpha(t)\cos\Omega_\alpha t\ dt +\right.$$

$$\left. + \sin\Omega_\alpha t\int_{t_o}^{t} e^{a_\alpha t} U_\alpha(t)\sin\Omega_\alpha t\ dt\right] + \qquad (28)$$

$$+ C_D^2\left[\sin\Omega_\alpha t\int_{t_o}^{t} e^{a_\alpha t} V_\alpha(t)\sin\Omega_\alpha t\ dt +\right.$$

$$+ \cos\Omega_\alpha t \int_{t_0}^{t} e^{a_\alpha t} V_\alpha(t) \cos\Omega_\alpha t \, dt \Bigg] \Bigg\}$$

$$+ e^{-a_\alpha \tau} \Big[S_D (C_D u_{\alpha o} + S_D v_{\alpha o}) - q' \cdot C_D \cos(\Omega_\alpha \tau + \xi) \quad ,$$

where

$$S_D = \sin D, \; C_D = \cos D, \; q' = \sqrt{w_{\alpha o}^2 + (S_D u_{\alpha o} - C_D v_\alpha)^2} \; , \qquad (29)$$

$$\tan \xi = \frac{w_{\alpha o}}{S_D u_{\alpha o} - C_D v_{\alpha o}} \; .$$

If the geographical coordinate system coincides with the geomagnetic coordinate system (D = 0), one gets

$$w_\alpha(t) = e^{-a_\alpha t} \Bigg[-\cos\Omega_\alpha t \int_{t_0}^{t} e^{a_\alpha t} W_\alpha(t) \cos\Omega_\alpha t \, dt -$$

$$- \sin\Omega_\alpha t \int_{t_0}^{t} e^{a_\alpha t} W_\alpha(t) \sin\Omega_\alpha t \, dt -$$

$$- \sin\Omega_\alpha t \int_{t_0}^{t} e^{a_\alpha t} V_\alpha(t) \cos\Omega_\alpha t \, dt + \qquad (30)$$

$$+ \cos\Omega_\alpha t \int_{t_0}^{t} e^{a_\alpha t} V_\alpha(t) \sin\Omega_\alpha t \, dt \Bigg] + q'' e^{-a_\alpha \tau} \sin(\Omega_\alpha \tau - \xi'),$$

$$u_\alpha(t) = e^{-a_\alpha t} \int_{t_0}^{t} e^{a_\alpha t} U_\alpha(t) \, dt + u_{\alpha o} e^{-a_\alpha \tau} \quad , \qquad (31)$$

$$v_\alpha(t) = e^{-a_\alpha t} \Bigg[\sin\Omega_\alpha t \int_{t_0}^{t} e^{a_\alpha t} W_\alpha(t) \cos\Omega_\alpha t \, dt -$$

$$- \cos\Omega_\alpha t \int_{t_0}^{t} e^{a_\alpha t} W_\alpha(t) \sin\Omega_\alpha t \, dt + \qquad (32)$$

$$+ \sin\Omega_\alpha t \int_{t_0}^{t} e^{a_\alpha t} V_\alpha(t) \sin\Omega_\alpha t \, dt +$$

$$+ \cos \Omega_\alpha t \int_{t_0}^{t} e^{a_\alpha t} V_\alpha(t) \cos \Omega_\alpha t \, dt \Big] - q'' e^{-a_\alpha \tau} \cos(\Omega_\alpha \tau - \xi'),$$

where

$$q'' = \sqrt{w_{\alpha o}^2 + v_{\alpha o}^2}, \quad \tan \xi' = \frac{w_{\alpha o}}{v_{\alpha o}}. \tag{33}$$

If the forcing factors W_α, U_α and V_α are independent of time, then in case of $D \neq 0$

$$w_\alpha(t) = \frac{-a_\alpha W_\alpha + \Omega_\alpha (S_D U_\alpha - C_D V_\alpha)}{a_\alpha^2 + \Omega_\alpha^2} -$$

$$- e^{-a_\alpha \tau} \sqrt{\frac{W_\alpha^2 + (S_D U_\alpha - C_D V_\alpha)^2}{a_\alpha^2 + \Omega_\alpha^2}} \sin(\Omega_\alpha \tau + \beta - \gamma) + \tag{34}$$

$$+ q' e^{-a_\alpha \tau} \sin(\Omega_\alpha \tau + \xi),$$

$$u_\alpha(t) = \frac{1}{a_\alpha} C_D (C_D U_\alpha + S_D V_\alpha)(1 - e^{-a_\alpha \tau}) +$$

$$+ \frac{S_D [-\Omega_\alpha W_\alpha + a_\alpha (S_D U_\alpha - C_D V_\alpha)]}{a_\alpha^2 + \Omega_\alpha^2} -$$

$$- e^{-a_\alpha \tau} S_D \sqrt{\frac{W_\alpha^2 + (S_D U_\alpha - C_D V_\alpha)^2}{a_\alpha^2 + \Omega_\alpha^2}} \cos(\Omega_\alpha \tau + \beta + \gamma) + \tag{35}$$

$$+ e^{-a_\alpha \tau} [S_D \cdot q' \cos(\Omega_\alpha \tau + \xi) + C_D u_{\alpha o} + S_D v_{\alpha o})],$$

$$v_\alpha(t) = \frac{1}{a_\alpha} S_D (C_D U_\alpha + S_D V_\alpha)(1 - e^{-a_\alpha \tau}) +$$

$$+ \frac{C_D [\Omega_\alpha W_\alpha - a_\alpha (S_D U_\alpha - C_D V_\alpha)]}{a_\alpha^2 + \Omega_\alpha^2} -$$

$$- e^{-a_\alpha \tau} C_D \sqrt{\frac{W_\alpha^2 + (S_D U_\alpha - C_D V_\alpha)^2}{a_\alpha^2 + \Omega_\alpha^2}} \cos(\Omega_\alpha \tau + \beta - \gamma) + \tag{36}$$

$$+ e^{-a_\alpha \tau} [S_D (C_D U_{\alpha o} + S_D v_{\alpha o}) - C_D \cdot q' \cos(\Omega_\alpha \tau + \xi),$$

where

$$\tan\gamma = \frac{W_\alpha}{S_D U_\alpha - C_D V_\alpha}, \quad \tan\beta = \frac{\Omega_\alpha}{a_\alpha}. \tag{37}$$

In case of D = 0, from Eqs (34)-(36) the relations

$$w_\alpha(t) = -\frac{a_\alpha W_\alpha + \Omega_\alpha V_\alpha}{a_\alpha^2 + \Omega_\alpha^2} - e^{-a_\alpha\tau}\sqrt{\frac{W_\alpha^2 + V_\alpha^2}{a_\alpha^2+\Omega_\alpha^2}}\sin(\Omega_\alpha\tau + \beta + \gamma') + \tag{38}$$
$$+ e^{-a_\alpha\tau} q'' \sin(\Omega_\alpha\tau + \xi'),$$

$$u_\alpha(t) = \frac{U_\alpha}{a_\alpha}(1 - e^{-a_\alpha\tau}) + u_{\alpha o} e^{-a_\alpha\tau}, \tag{39}$$

$$v_\alpha(t) = \frac{\Omega_\alpha W_\alpha + a_\alpha V_\alpha}{a_\alpha^2 + \Omega_\alpha^2} - e^{-a_\alpha\tau}\sqrt{\frac{W_\alpha^2 + V_\alpha^2}{a_\alpha^2+\Omega_\alpha^2}}\cos(\Omega_\alpha\tau + \beta + \gamma') - \tag{40}$$
$$- e^{-a_\alpha\tau} q'' \cos(\Omega_\alpha\tau + \xi'),$$

are obtained, where $\tan\gamma' = \frac{W_\alpha}{V_\alpha}$.

The forcing factors should be given by relations of the type (21). Then, from Eqs (26)-(28) for D ≠ 0 one gets the relations

$$w_\alpha(t) = \frac{-a_\alpha W_{\alpha o} + \Omega_\alpha(S_D U_{\alpha o} - C_D V_{\alpha o})}{a_\alpha^2 + \Omega_\alpha^2} -$$
$$- e^{-a_\alpha\tau}\sqrt{\frac{W_{\alpha o}^2 + (S_D U_{\alpha o} - C_D V_{\alpha o})^2}{a_\alpha^2 + \Omega_\alpha^2}}\sin(\Omega_\alpha\tau + \beta - \gamma_o) +$$
$$+ \frac{1}{2}\sum_{k=1}^{\infty}\sqrt{W_{\alpha k}^2 + (S_D U_{\alpha k} - C_D V_{\alpha k})^2}\left\{\frac{\cos(k\omega\tau + \alpha_k - \lambda_k + \gamma_k)}{\sqrt{a_\alpha^2 + (k\omega + \Omega_\alpha)^2}} - \right. \tag{41}$$
$$- \frac{\cos(k\omega\tau + \alpha_k - \vartheta_k - \gamma_k)}{\sqrt{a_\alpha^2 + (k\omega - \Omega_\alpha)^2}} - e^{-a_\alpha\tau}\left[\frac{\cos(\alpha_k - \lambda_k + \gamma_k)}{\sqrt{a_\alpha^2 + (k\omega + \Omega_\alpha)^2}} - \right.$$
$$\left.\left. - \frac{\cos(\alpha_k - \vartheta_k - \gamma_k)}{\sqrt{a_\alpha^2 + (k\omega - \Omega_\alpha)^2}}\right]\right\} + q' e^{-a_\alpha\tau}\sin(\Omega_\alpha\tau + \xi),$$

$$u_\alpha(t) = \frac{1}{a_\alpha} C_D (C_D U_{\alpha o} + S_D V_{\alpha o}) (1 - e^{a_\alpha \tau}) -$$

$$- \frac{S_D [\Omega_\alpha W_{\alpha o} - a_\alpha (S_D U_{\alpha o} - C_D V_{\alpha o})]}{a_\alpha^2 + \Omega_\alpha^2} -$$

$$- e^{-a_\alpha \tau} S_D \sqrt{\frac{W_{\alpha o}^2 + (S_D U_{\alpha o} - C_D V_{\alpha o})^2}{a_\alpha^2 + \Omega_\alpha^2}} \cos(\Omega_\alpha \tau + \beta + \gamma_o) +$$

$$+ \sum_{k=1}^{\infty} \left\{ \frac{C_D (C_D U_{\alpha k} + S_D V_{\alpha k})}{\sqrt{a_\alpha^2 + (k\omega)^2}} [\sin(k\omega\tau + \alpha_k - \Theta_k) - \right. \tag{42}$$

$$- e^{-a_\alpha \tau} \sin(\alpha_k - \Theta_k)] + \frac{1}{2} S_D \sqrt{W_{\alpha k}^2 + (S_D U_{\alpha k} - C_D V_{\alpha k})^2}$$

$$\left[\frac{\sin(k\omega\tau + \alpha_k - \chi_k - \gamma_k)}{\sqrt{a_\alpha^2 + (k\omega + \Omega_\alpha)^2}} + \frac{\sin(k\omega\tau + \alpha_k - \vartheta_k - \gamma_k)}{\sqrt{a_\alpha^2 + (k\omega - \Omega_\alpha)^2}} - \right.$$

$$\left. \left. - e^{-a_\alpha \tau} \left[\frac{\sin(\alpha_k - \chi_k - \gamma_k)}{\sqrt{a_\alpha^2 + (k\omega + \Omega_\alpha)^2}} + \frac{\sin(\alpha_k - \vartheta_k - \gamma_k)}{\sqrt{a_\alpha^2 + (k\omega - \Omega_\alpha)^2}} \right] \right] \right\} +$$

$$+ e^{-a_\alpha \tau} [C_D (C_D U_{\alpha o} + S_D V_{\alpha o}) + S_D q' \cos(\Omega_\alpha \tau + \xi)],$$

$$v_\alpha(t) = \frac{1}{a_\alpha} S_D (C_D U_{\alpha o} + S_D V_{\alpha o}) (1 - e^{-a_\alpha \tau}) +$$

$$+ \frac{C_D [\Omega_\alpha W_{\alpha o} - a_\alpha (S_D U_{\alpha o} - C_D V_{\alpha o})]}{a_\alpha^2 + \Omega_\alpha^2} -$$

$$- e^{-a_\alpha \tau} C_D \sqrt{\frac{W_{\alpha o}^2 + (S_D U_{\alpha o} - C_D V_{\alpha o})^2}{a_\alpha^2 + \Omega_\alpha^2}} \cos(\Omega_\alpha \tau + \beta - \gamma_o) +$$

$$+ \sum_{k=1}^{\infty} \left\{ \frac{S_D (C_D U_{\alpha k} + S_D V_{\alpha k})}{\sqrt{a_\alpha^2 + (k\omega)^2}} [\sin(k\omega\tau + \alpha_k - \Theta_k) - \right. \tag{43}$$

$$- e^{-a_\alpha \tau} \sin(\alpha_k - \Theta_k)] - \frac{1}{2} C_D \sqrt{W_{\alpha k}^2 + (S_D U_{\alpha k} - C_D V_{\alpha k})^2}$$

$$\left[\frac{\sin(k\omega\tau + \alpha_k - \chi_k - \gamma_k)}{\sqrt{a^2 + (k\omega + \Omega_\alpha)^2}} + \frac{\sin(k\omega\tau + \alpha_k - \vartheta_k + \gamma_k)}{\sqrt{a^2 + (k\omega - \Omega_\alpha)^2}} - \right.$$

$$- e^{-a_\alpha \tau} \left[\frac{\sin(\alpha_k - x_k - \gamma_k)}{\sqrt{a_\alpha^2 + (k\omega + \Omega_\alpha)^2}} + \frac{\sin(\alpha_k - \vartheta_k + \gamma_k)}{\sqrt{a_\alpha^2 + (k\omega - \Omega_\alpha)^2}} \right] \Bigg\} +$$

$$+ e^{-a_\alpha \tau} \left[S_D (C_D u_{\alpha o} + S_D v_{\alpha o}) - C_D q' \cos(\Omega_\alpha \tau + \xi) \right],$$

where

$$\tan \gamma_o = \frac{W_{\alpha o}}{S_D U_{\alpha o} - C_D V_{\alpha o}}, \quad \tan \gamma_k = \frac{W_{\alpha k}}{S_D U_{\alpha k} - C_D V_{\alpha k}}. \tag{44}$$

If the geographical coordinate system coincides with the geomagnetic coordinate system ($D = 0$), Eqs (41)-(43) take the form

$$w_\alpha(t) = -\frac{a_\alpha W_{\alpha o} + \Omega_\alpha V_{\alpha o}}{a_\alpha^2 + \Omega_\alpha^2} - e^{-a_\alpha \tau} \sqrt{\frac{W_{\alpha o}^2 + V_{\alpha o}^2}{a_\alpha^2 + \Omega_\alpha^2}} \sin(\Omega_\alpha \tau + \beta + \gamma_o') +$$

$$+ \frac{1}{2} \sum_{k=1}^{\infty} \sqrt{W_{\alpha k}^2 + V_{\alpha k}^2} \left\{ \frac{\cos(k\omega\tau + \alpha_k - x_k - \gamma_k')}{\sqrt{a_\alpha^2 + (k\omega + \Omega_\alpha)^2}} - \right. \tag{45}$$

$$- \frac{\cos(k\omega\tau + \alpha_k - \vartheta_k + \gamma_k')}{\sqrt{a_\alpha^2 + (k\omega - \Omega_\alpha)^2}} - e^{-a_\alpha \tau} \left[\frac{\cos(\alpha_k - x_k - \gamma_k')}{\sqrt{a_\alpha^2 + (k\omega + \Omega_\alpha)^2}} - \right.$$

$$\left. \left. - \frac{\cos(\alpha_k - \vartheta_k + \gamma_k')}{\sqrt{a_\alpha^2 + (k\omega - \Omega_\alpha)^2}} \right] \right\} + q'' e^{-a_\alpha \tau} \sin(\Omega_\alpha \tau - \xi'),$$

$$u_\alpha(t) = \frac{U_{\alpha o}}{a_\alpha} (1 - e^{-a_\alpha \tau}) + \sum_{k=1}^{\infty} \frac{U_{\alpha k}}{\sqrt{a_\alpha^2 + (k\omega)^2}}$$

$$\left[\sin(k\omega\tau + \alpha_k - \Theta_k) - e^{-a_\alpha \tau} \sin(\alpha_k - \Theta_k) \right] + \tag{46}$$

$$+ u_{\alpha o} e^{-a_\alpha \tau},$$

$$v_\alpha(t) = \frac{\Omega_\alpha W_{\alpha o} + a_\alpha V_{\alpha o}}{a_\alpha^2 + \Omega_\alpha^2} - e^{-a_\alpha \tau} \sqrt{\frac{W_{\alpha o}^2 + V_{\alpha o}^2}{a_\alpha^2 + \Omega_\alpha^2}} \cos(\Omega_\alpha \tau + \beta + \gamma_o') -$$

$$- \sum_{k=1}^{\infty} \frac{1}{2} \sqrt{W_{\alpha k}^2 + V_{\alpha k}^2} \left[\frac{\sin (k\omega\tau + \alpha_k - \varkappa_k + \gamma_k')}{\sqrt{a_\alpha^2 + (k\omega + \Omega_\alpha)^2}} + \right. \tag{47}$$

$$+ \frac{\sin (k\omega\tau + \alpha_k - \vartheta_k - \gamma_k')}{\sqrt{a_\alpha^2 + (k\omega - \Omega_\alpha)^2}} - e^{-a_\alpha \tau} \left[\frac{\sin (\alpha_k - \varkappa_k + \gamma_k')}{\sqrt{a_\alpha^2 + (k\omega + \Omega_\alpha)^2}} + \right.$$

$$\left. \left. + \frac{\sin (\alpha_k - \vartheta_k - \gamma_k')}{\sqrt{a_\alpha^2 + (k\omega - \Omega_\alpha)^2}} \right] \right] - q'' e^{-a_\alpha \tau} \cos (\Omega_\alpha \tau - \xi') ,$$

where

$$\tan \gamma_0' = \frac{W_{\alpha o}}{V_{\alpha o}} , \qquad \tan \gamma_k' = \frac{W_{\alpha k}}{V_{\alpha k}} . \tag{48}$$

DISCUSSION

If the forcing factors are independent of time, then in the general case (Appendix I) for $\tau \gg \frac{1}{a}$ the solutions are transformed into known relations of the stationary case (Klevtzur and Fatkullin 1983).

In all equations obtained for the velocity of charged particles the factor $e^{-a_\alpha \tau}$ appears. Estimating the value of this function for real ionospheric conditions, in Fig. 1 for electrons and ions $e^{-a_\alpha \tau}$ is presented as a function of time and for different fixed heights. The values $a_e = \nu_{en}$ and $a_i = \frac{\nu_{in}}{2}$ for summer day-time conditions in the mid-latitude ionosphere and for low solar activity are taken from Fatkullin et al. (1981). At heights of the F region and in case of $\tau \simeq$ 10 s the contribution of the factor $e^{-a_\alpha \tau}$ may be significant.

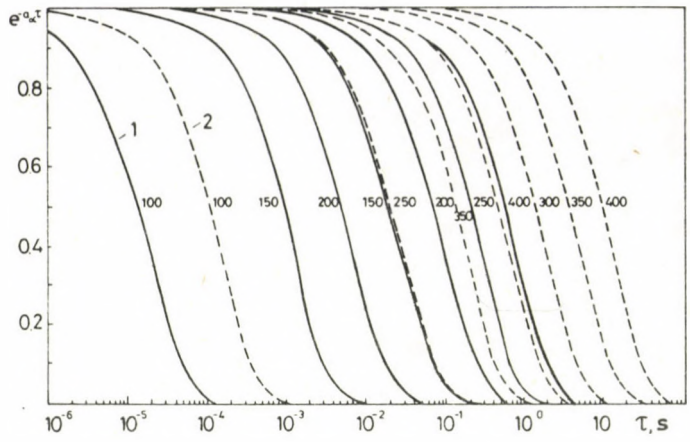

Fig. 1. The variation of $e^{-a_\alpha \tau}$ as a function of τ for fixed heights, 1 - for electrons, 2 - for ions

APPENDIX I

General solution of the initial system of equations is:

$$
\begin{aligned}
W_\alpha(t) = e^{-a_\alpha t}\Big\{ & \mp S_I \int e^{a_\alpha t}\big[\mp S_I W_\alpha(t) + C_I(C_D U_\alpha(t) + \\
& + S_D V_\alpha(t))\big]dt - C_I^2\big[\cos\Omega_\alpha t \int e^{a_\alpha t} W_\alpha(t)\cos\Omega_\alpha t\, dt + \\
& + \sin\Omega_\alpha t \int e^{a_\alpha t} W_\alpha(t)\sin\Omega_\alpha t\, dt\big] + C_I(S_D \sin\Omega_\alpha t \pm \\
& \pm S_I C_D \cos\Omega_\alpha t)\int e^{a_\alpha t} U_\alpha(t)\cos\Omega_\alpha t\, dt - C_I(S_D\cos\Omega_\alpha t \mp \\
& \mp S_I C_D \sin\Omega_\alpha t)\int e^{a_\alpha t} U_\alpha(t)\sin\Omega_\alpha t\, dt - C_I(\mp S_I S_D\cos\Omega_\alpha t + \\
& + C_D \sin\Omega_\alpha t)\int e^{a_\alpha t} V_\alpha(t)\cos\Omega_\alpha t\, dt - C_I(\mp S_I S_D \sin\Omega_\alpha t - \\
& - C_D\cos\Omega_\alpha t)\int e^{a_\alpha t} V_\alpha(t)\sin\Omega_\alpha t\, dt \mp C_1\frac{S_I}{C_I S_D} -
\end{aligned}
\tag{I.1}
$$

$$- C_2 \frac{C_I (\mp S_I S_D \cos\Omega_\alpha t + C_D \sin\Omega_\alpha t)}{1 - C_I^2 S_D^2} -$$

$$- C_3 \frac{C_I (\mp S_I S_D \sin\Omega_\alpha t - C_D \cos\Omega_\alpha t)}{1 - C_I^2 S_D^2} \Bigg\},$$

$$u_\alpha(t) = e^{-a_\alpha t} \Bigg\{ C_I C_D \int e^{a_\alpha t} \left[\mp S_I W_\alpha(t) + C_I (C_D U_\alpha(t) + \right.$$

$$\left. + S_D V_\alpha(t)) \right] dt - C_I (\mp S_I C_D \cos\Omega_\alpha t + S_D \sin\Omega_\alpha t) \int e^{a_\alpha t} W_\alpha(t) \cos\Omega_\alpha t \, dt +$$

$$+ C_I (\mp S_I C_D \sin\Omega_\alpha t + S_D \cos\Omega_\alpha t) \int e^{a_\alpha t} W_\alpha(t) \sin\Omega_\alpha t \, dt +$$

$$+ (1 - C_I^2 C_D^2) (\cos\Omega_\alpha t \int e^{a_\alpha t} U_\alpha(t) \cos\Omega_\alpha t \, dt +$$

$$+ \sin\Omega_\alpha t \int e^{a_\alpha t} U_\alpha(t) \sin\Omega_\alpha t \, dt - (C_I^2 S_D C_D \cos\Omega_\alpha t \pm$$

$$\pm S_I \sin\Omega_\alpha t) \int e^{a_\alpha t} V_\alpha(t) \cos\Omega_\alpha t \, dt - (C_I^2 S_D C_D \sin\Omega_\alpha t \mp$$

$$\mp S_I \cos\Omega_\alpha t) \int e^{a_\alpha t} V_\alpha(t) \sin\Omega_\alpha t \, dt + C_1 \frac{C_D}{S_D} -$$

$$- C_2 \frac{C_I^2 S_D C_D \cos\Omega_\alpha t \pm S_I \sin\Omega_\alpha t}{1 - C_I^2 S_D^2} - C_3 \frac{C_I^2 S_D C_D \sin\Omega_\alpha t \mp S_I \cos\Omega_\alpha t}{1 - C_I^2 S_D^2} \Bigg\}, \tag{I.2}$$

$$v_\alpha(t) = e^{-a_\alpha t} \Bigg\{ C_I S_D \int e^{a_\alpha t} \left[\mp S_I W_\alpha(t) + C_I (C_D U_\alpha(t) + S_D V_\alpha(t)) \right] dt +$$

$$+ C_I (C_D \sin\Omega_\alpha t \pm S_I S_D \cos\Omega_\alpha t) \int e^{a_\alpha t} W_\alpha(t) \sin\Omega_\alpha t \, dt -$$

$$- C_I (C_D \cos\Omega_\alpha t \mp S_I S_D \sin\Omega_\alpha t) \int e^{a_\alpha t} W_\alpha(t) \sin\Omega_\alpha t \, dt -$$

$$- (C_I^2 S_D C_D \cos\Omega_\alpha t \mp S_I \sin\Omega_\alpha t) \int e^{a_\alpha t} U_\alpha(t) \cos\Omega_\alpha t \, dt +$$

$$+ (\mp S_I \cos\Omega_\alpha t - C_I^2 S_D C_D \sin\Omega_\alpha t) \int e^{a_\alpha t} U_\alpha(t) \sin\Omega_\alpha t \, dt + \tag{I.3}$$

$$+ (1 - C_I^2 S_D^2) (\sin\Omega_\alpha t \int e^{a_\alpha t} V_\alpha(t) \sin\Omega_\alpha t \, dt +$$

$$+ \cos\Omega_\alpha t \int e^{a_\alpha t} V_\alpha(t) \cos\Omega_\alpha t \, dt) + C_1 + C_2 \cos\Omega_\alpha t + C_3 \sin\Omega_\alpha t \ ,$$

where C_1, C_2 and C_3 are integration constants, $C_I = \cos I$, $S_I = \sin I$, $C_D = \cos D$, $S_D = \sin D$.

APPENDIX II

Solution of the initial system of differential equations with initial conditions at the time $t = t_0$.

$$w_\alpha(t) = w_{\alpha 0}, \quad u_\alpha(t) = u_{\alpha 0}, \quad v_\alpha(t) = v_{\alpha 0}.$$

$$\begin{aligned}
w_\alpha(t) = e^{-a_\alpha t} \Bigg\{ & \mp S_I \int_{t_0}^{t} e^{a_\alpha t} \left[\mp S_I W_\alpha(t) + C_I (C_D U_\alpha(t) + S_D V_\alpha(t)) \right] dt - \\
& - C_I^2 \Big(\cos\Omega_\alpha t \int_{t_0}^{t} e^{a_\alpha t} W_\alpha(t) \cos\Omega_\alpha t \, dt + \\
& + \sin\Omega_\alpha t \int_{t_0}^{t} e^{a_\alpha t} W_\alpha(t) \sin\Omega_\alpha t \, dt \Big) + C_I \Big(S_D \sin\Omega_\alpha t \pm \\
& \pm S_I C_D \cos\Omega_\alpha t \Big) \int_{t_0}^{t} e^{a_\alpha t} U_\alpha(t) \cos\Omega_\alpha t \, dt - C_I \Big(S_D \cos\Omega_\alpha t \mp \\
& \mp S_I C_D \sin\Omega_\alpha t \Big) \int_{t_0}^{t} e^{a_\alpha t} U_\alpha(t) \sin\Omega_\alpha t \, dt - C_I \Big(C_D \sin\Omega_\alpha t \mp \\
& \mp S_I S_D \cos\Omega_\alpha t \Big) \int_{t_0}^{t} e^{a_\alpha t} V_\alpha(t) \cos\Omega_\alpha t \, dt + C_I \Big(C_D \cos\Omega_\alpha t \pm \\
& \pm S_I S_D \sin\Omega_\alpha t \Big) \int_{t_0}^{t} e^{a_\alpha t} V_\alpha(t) \sin\Omega_\alpha t \, dt \Bigg\} + \\
& + e^{-a_\alpha \tau} \left[\mp S \cdot A + B \cdot \sin(\Omega_\alpha \tau + \delta) \right]^{t_0},
\end{aligned} \tag{II.1}$$

$$u_\alpha(t) = e^{-a_\alpha t}\left\{C_I C_D \int_{t_0}^{t} e^{a_\alpha t}\left[\mp S_I W_\alpha(t) + C_I(C_D U_\alpha(t) + S_D V_\alpha(t))\right]dt - \right.$$

$$- C_I\,(S_D \sin\Omega_\alpha t \mp S_I C_D \cos\Omega_\alpha t)\int_{t_0}^{t} e^{a_\alpha t} W_\alpha(t)\cos\Omega_\alpha t\,dt +$$

$$+ C_I\,(S_D \cos\Omega_\alpha t \mp S_I C_D \sin\Omega_\alpha t)\int_{t_0}^{t} e^{a_\alpha t} W_\alpha(t)\sin\Omega_\alpha t\,dt +$$

$$+ (1 - C_I^2 C_D^2)\,(\cos\Omega_\alpha t \int_{t_0}^{t} e^{a_\alpha t} U_\alpha(t)\cos\Omega_\alpha t\,dt +$$

$$+ \sin\Omega_\alpha t \int_{t_0}^{t} e^{a_\alpha t} U_\alpha(t)\sin\Omega_\alpha t\,dt\,) - (C_I^2 S_D C_D \cos\Omega_\alpha t \pm$$

$$\pm S_I \sin\Omega_\alpha t)\int_{t_0}^{t} e^{a_\alpha t} V_\alpha(t)\cos\Omega_\alpha t\,dt - (C_I^2 S_D C_D \sin\Omega_\alpha t \mp$$

$$\left.\mp S_I \cos\Omega_\alpha t)\int_{t_0}^{t} e^{a_\alpha t} V_\alpha(t)\sin\Omega_\alpha t\,dt\right\} + e^{-a_\alpha \tau}\left[C_I C_D A + \right. \tag{II.2}$$

$$\left. + F\sin(\Omega_\alpha \tau + \eta)\right],$$

$$v_\alpha(t) = e^{-a_\alpha t}\left\{C_I S_D \int_{t_0}^{t} e^{a_\alpha t}\left[\mp S_I W_\alpha(t) + C_I\,(C_D U_\alpha(t) + S_D V_\alpha(t)\right]dt + \right.$$

$$+ C_I\,(C_D \sin\Omega_\alpha t \pm S_I S_D \cos\Omega_\alpha t)\int_{t_0}^{t} e^{a_\alpha t} W_\alpha(t)\cos\Omega_\alpha t\,dt -$$

$$- C_I\,(C_D \cos\Omega_\alpha t \mp S_I S_D \sin\Omega_\alpha t)\int_{t_0}^{t} e^{a_\alpha t} W_\alpha(t)\sin\Omega_\alpha t\,dt -$$

$$
\begin{aligned}
&- (C_I^2 S_D C_D \cos\Omega_\alpha t \mp S_I \sin\Omega_\alpha t) \int_{t_0}^{t} e^{a_\alpha t} U_\alpha(t) \cos\Omega_\alpha t \, dt - \\
&- (C_I^2 S_D C_D \sin\Omega_\alpha t \pm S_I \cos\Omega_\alpha t) \int_{t_0}^{t} e^{a_\alpha t} U_\alpha(t) \sin\Omega_\alpha t \, dt + \\
&+ (1 - C_I^2 S_D) \left(\sin\Omega_\alpha t \int_{t_0}^{t} e^{a_\alpha t} V_\alpha(t) \sin\Omega_\alpha t \, dt + \right. \\
&\left. + \cos\Omega_\alpha t \int_{t_0}^{t} e^{a_\alpha t} V_\alpha(t) \cos\Omega_\alpha t \, dt \right) + \\
&+ e^{-a_\alpha \tau} \left[C_I S_D A + G \sin(\Omega_\alpha \tau + K) \right],
\end{aligned}
\tag{II.3}
$$

where

$$\tau = t - t_0, \quad A = \left[\mp S_I w_{\alpha o} + C_I (C_D u_{\alpha o} + S_D v_{\alpha o}) \right],$$

$$B = C_I \sqrt{\left[C_I w_{\alpha o} \pm S_I (C_D u_{\alpha o} + S_D v_{\alpha o}) \right]^2 + (S_D u_{\alpha o} - C_D v_{\alpha o})^2},$$

$$\tan\delta = \frac{C_I w_{\alpha o} \pm S_I (C_D u_{\alpha o} + S_D v_{\alpha o})}{S_D u_{\alpha o} - C_D v_{\alpha o}},$$

$$F = \sqrt{\left[C_I C_D (\mp S_I w_{\alpha o} - C_I S_D v_{\alpha o}) + (1 - C_I^2 S_D) u_{\alpha o} \right]^2 + (C_I S_D w_{\alpha o} \mp S_I v_{\alpha o})^2},$$

$$\tan\eta = \frac{C_I C_D (\mp S_I w_{\alpha o} + C_I S_D v_{\alpha o}) - (1 - C_I^2 S_D) u_{\alpha o}}{C_I S_D w_{\alpha o} + S_I v_{\alpha o}},$$

$$G = \sqrt{\left[C_I S_D (\mp S_I w_{\alpha o} - C_I C_D u_{\alpha o}) + (1 - C_I^2 S_D) v_{\alpha o} \right]^2 + (C_I C_D w_{\alpha o} \mp S_I u_{\alpha o})^2},$$

$$\tan K = \frac{C_I S_D (\mp S_I w_{\alpha o} - C_I C_D w_{\alpha o}) + (1 - C_I^2 S_D) v_{\alpha o}}{C_I C_D w_{\alpha o} + S_I u_{\alpha o}}.$$

REFERENCES

Alfven H, Fälthammar K G 1967: Cosmic electrodynamics (in Russian). Izd. Mir, Moscow

Boguslavskiy S A 1961: Selected Papers in Physics (in Russian). Fizmattiz, Moscow

Fatkullin M N 1982: In: Results of Science and Technics. Geomagnetism and the upper layers of the atmosphere. Vol. 6, VINITI, Moscow

Fatkullin M N, Zelenova T I, Kozlov V K, Legenka A D, Goboleva T N 1981: Empirical models of the mid-latitude ionosphere (in Russian). Nauka, Moscow

Gershman B N 1974: Dynamics of the ionospheric plasma (in Russian). Nauka, Moscow

Klevtzur S V, Fatkullin M N 1983: Global dynamics of charged particles in a three dimensional, irregular ionosphere (in Russian). Preprint No 3 (416), IZMIRAN, Moscow

Landau L D, Lifshitz E M 1960: Theory of Fields (in Russian). Fizmattiz, Moscow

Schumann W O 1963: In: Hydromagnetic method of the transformation of energy. Fizmattiz, Moscow, 373-380.

Acta Geod. Geoph. Mont. Hung., Vol. 22 (1-2), pp. 155-170 (1987)

ON STABILITY OF THE LOW-FREQUENCY LONGITUDINAL POTENTIAL PERTURBATIONS OF THE CHARGED PARTICLE DISTRIBUTION IN THE F REGION OF THE IONOSPHERE

A M Antonov[1] and M N Fatkullin[1]

[1]Institute of Geomagnetism, Ionosphere and Radio Wave Propagation, Academy of Sciences of the USSR, 142092 Troitsk, Moskovskaya oblast, USSR

The stability of the height distribution of charged particle concentration in the F region of the ionosphere is dealt with from the point of view of low-frequency longitudinal (directed along the magnetic field) potential perturbations. Collisions of a single type of ions (O^+) with neutrals are considered. Conditions for these perturbations becoming unstable are found.

Keywords: dynamics of the ionosphere; F region; irregular structure of the ionosphere; plasma instabilities

In the ionosphere at heights of the F region ($160 \lesssim h \lesssim 1000$ km) a very broad spectrum of space and time scales of electron density irregularities are observed (Erukhimov et al. 1980, Fejer and Kelley 1980, Fatkullin 1982, Hanuise 1983). Unfortunately, there are at present almost no experimental data concerning the scales of irregularities perpendicular ($l_\perp$) and parallel ($l_\parallel$) to the magnetic field. Gershman (1980) mentioned that the separation of very small ratios of $l_\perp/l_\parallel \lesssim 10^{-1}$-$10^{-2}$ is experimentally not sufficiently well founded. According to Fatkullin et al. (1981), Solodovnikov et al. (1984), middle scale irregularities of the electron density with characteristic horizontal scales (l_h) of some hundred kilometers and large scale irregularities of $l_h \simeq 2000$-3000 km can be observed in the outer ionosphere ($h \gtrsim h_mF2$) up to altitudes of $h \lesssim 3000$ km.

The difficulties arising in the explanation of the irregularities in case if a broad spectrum of space and time scales, by a single physical mechanism is considered, have several times been mentioned (Gershman 1974, Gelberg 1977, Erukhimov et al. 1980, Fejer and Kelley 1980, Fatkullin 1982). The mechanisms of

generation of the irregularities at these altitudes, being limited to a given level by certain conditions, i.e. without considering the interaction among them, can be divided into three groups. 1. Processes affecting the redistribution of the charged particles, produced by the motion of the neutral component due to the propagation of internal gravity waves in the upper atmosphere. The sources of generation of the internal gravity waves in the upper atmosphere are auroral phenomena, processes in the vicinity of the terminator, the non-linear decay of the tidal mode and also tropospheric and stratospheric phenomena (atmospheric fronts, storms, tornadoes, earthquakes, volcanic eruptions etc.). 2. Magnetospheric processes, like e.g. generation of ion-acoustic waves with frequencies $\omega \lesssim 10^{-2} s^{-1}$ at heights $h \simeq 1000$ km as a result of the transformation of hydromagnetic waves (Poeverlein 1966). 3. Different instabilities of the ionospheric plasma due to factors like spatial irregularities of different parameters (electron density n_e and electron temperature T_e, ion temperature T_i, velocity of electrons v_e and that of the ions v_i) in "background" state of the ionospheric plasma, fluxes of precipitating charged particles, electric fields and currents and irregularity of the motion of charged particles.

In the following problems of the stability of low-frequency longitudinal (relative to the geomagnetic field) potential disturbances in the distribution of charged particles in the irregular (but undisturbed) F region of the ionosphere are studied. Only small perturbations will be considered. In plasma physics small longitudinal perturbations and the questions related to their stability (or instability) have been investigated several times (e.g. Mikhaylovskiy 1970, 1971, Sreenivasan and Schroeder 1983). Ionospheric conditions at the altitude of the F region have been discussed in a number of papers (Gershman 1963, 1974, 1980, Keskinen and Ossakov 1983, Zhmur 1978).

INITIAL CONDITIONS AND EQUATIONS

1. Only small perturbations of the concentrations and the longitudinal velocity components of electrons and ions are

considered:

$$n_e = n_{eo} + \tilde{n}_e, \quad n_i = n_{io} + \tilde{n}_i, \quad \underline{v}_e^{\parallel} = \underline{v}_{eo}^{\parallel} + \tilde{\underline{v}}_e^{\parallel} \quad \text{and}$$

$$\underline{v}_i^{\parallel} = \underline{v}_{io}^{\parallel} + \tilde{\underline{v}}_i^{\parallel} ,$$

in case of $\tilde{n}_e \ll n_{eo}$, $\tilde{n}_i \ll n_{io}$, $\left| \tilde{\underline{v}}_e^{\parallel} \right| \ll \left| \underline{v}_{eo}^{\parallel} \right|$ and $\left| \tilde{\underline{v}}_i \right| \ll \left| \tilde{\underline{v}}_{io} \right|$.

Here n_{eo}, n_{io}, $\underline{v}_{eo}^{\parallel}$ and $\underline{v}_{io}^{\parallel}$ mean the background electron concentration, the background ion concentration, the longitudinal velocity components of electrons and ions; $N = n_{eo} = n_{io}$, i.e. quasi-neutrality is arbitrarily assumed; for an arbitrary vector $\underline{A}$, $\underline{A}^{\parallel} = \underline{b}\,(\underline{A} \cdot \underline{b})$, with $\underline{b} = \underline{B}/B$ being the unit vector in the direction of the magnetic field.

2. In the quasi-hydrodynamic equations of electrons and ions the gradients of the concentrations (n_e and n_i) and the temperatures (T_e and T_i), the longitudinal velocity component of the undisturbed neutral wind (v_{no}), the gravitational acceleration ($\underline{g}^{\parallel}$), the inner electric field ($\underline{E}_{\parallel}$), the collisions of electrons with ions (γ_{ei}) and the collisions of ions with neutral particles (ν_{in}) are taken into account. Only one type of positive ions (O^+) being predominant in the F region is considered.

3. In an undisturbed state the longitudinal velocity components of electrons and ions are determined by the ambipolar diffusion, i.e.

$$\underline{v}_{eo}^{\parallel} = \underline{v}_{io} \equiv \underline{v}_d^{\parallel} ,$$

where

$$\underline{v}_d^{\parallel} = \underline{v}_{no}^{\parallel} - D_a^{\parallel} \left(\frac{\nabla_{\parallel} N}{N} + \frac{\nabla_{\parallel} T_p}{T_p} - \frac{1}{H_p} \underline{1}\underline{g}^{\parallel} \right) , \tag{2}$$

$$D_a^{\parallel} = \frac{k\,(T_{eo} + T_{io})}{n_{no}\,\Theta_{in}} , \quad T_p = T_{eo} + T_{io} ,$$

$$H_p = \frac{k\,(T_{eo} + T_{io})}{m_i g} , \quad \Theta_{in} = \frac{\nu_{in}}{n_{no}}\,\mu_{in} , \tag{3}$$

$\underline{\underline{1}}\underline{g}^{\parallel} = \underline{g}^{\parallel}/g$, $D_a^{\parallel}$ is the coefficient of the longitudinal ambipolar diffusion, μ_{in} the reduced mass and K the Boltzmann constant.

4. The perturbation of the electric field is considered as potential, i.e.

$$\tilde{\underline{E}}_{\parallel} = -\nabla_{\parallel}\tilde{\varphi} \quad . \tag{4}$$

5. Only low-frequency perturbations are studied for which

$$\left| \frac{\partial \underline{v}_e^{\parallel}}{\partial t} + (\tilde{\underline{v}}_e \cdot \nabla_{\parallel})\underline{v}_{eo}^{\parallel} + (\underline{v}_{eo}^{\parallel} \cdot \nabla_{\parallel})\tilde{\underline{v}}_e^{\parallel} \right| << \left| \nu_{ei}\tilde{\underline{v}}_e \right| ,$$
$$\left| \frac{\partial \tilde{\underline{v}}_i^{\parallel}}{\partial t} + (\tilde{\underline{v}}_i \cdot \nabla_{\parallel})\underline{v}_{io}^{\parallel} + (\underline{v}_{io}^{\parallel} \cdot \nabla_{\parallel})\tilde{\underline{v}}_i \right| \Big| << \nu_{in}\tilde{\underline{v}}_i \Big| \quad . \tag{5}$$

If the conditions mentioned above are valid, the concentration perturbations of electrons and ions are described by

$$\frac{\partial \tilde{N}_i}{\partial t} - D_i^{\parallel} \Delta_{\parallel}\tilde{N}_i + D_i^{\parallel}\left[\frac{\underline{v}_{no}^{\parallel}}{D_i^{\parallel}} - \left(1 + \frac{D_a^{\parallel}}{D_i^{\parallel}}\right) \frac{\nabla_{\parallel}N}{N} - \frac{D_a^{\parallel}}{D_i^{\parallel}} \cdot \frac{\nabla_{\parallel}T_p}{T_p} - \right.$$
$$- \frac{\nabla_{\parallel}D_i^{\parallel}}{D_i^{\parallel}} + \left(\frac{m_e}{m_i} \cdot \frac{1}{H_i} + \frac{D_a^{\parallel}}{D_i^{\parallel}} \cdot \frac{1}{H_p} \right) \underline{\underline{1}}\underline{g}^{\parallel} \Big] \cdot \nabla_{\parallel}\tilde{N}_i +$$
$$+ D_a^{\parallel} \left[\frac{\nabla_{\parallel} \cdot \underline{v}_{no}}{D_a^{\parallel}} - \left(\nabla_{\parallel} + \frac{\nabla_{\parallel}D_a^{\parallel}}{D_a^{\parallel}} + \frac{\nabla_{\parallel}N}{N} \right) \cdot \left(\frac{\nabla_{\parallel}N}{N} + \frac{\nabla_{\parallel}T_p}{T_p} - \frac{1}{H_p} \underline{\underline{1}}\underline{g}^{\parallel} \right) + \right.$$
$$+ \frac{1}{D_a^{\parallel}} \left(\underline{v}_{no}^{\parallel} \frac{\nabla_{\parallel}N}{N} \right) + \frac{1_{io}}{D_a^{\parallel}} + \frac{m_e}{m_i} \frac{1}{H_i} \frac{\nabla_{\parallel}D_i^{\parallel}}{D_a^{\parallel}} \underline{\underline{1}}\underline{g}^{\parallel} - \tag{6}$$
$$- \frac{m_e}{m_i} \frac{D_i^{\parallel}}{D_a^{\parallel}} \nabla_{\parallel} \cdot \left(\frac{\underline{\underline{1}}\underline{g}^{\parallel}}{H_i} \right) + \frac{m_e}{m_i} \frac{1}{H_i} D_i^{\parallel} \left(\frac{\nabla_{\parallel}N}{N} \cdot \underline{\underline{1}}\underline{g}^{\parallel} \right) \Big] \tilde{N}_i -$$
$$- b_i \left(\frac{\nabla_{\parallel}b_i^{\parallel}}{b_i} + \frac{\nabla_{\parallel}N}{N} \right) \cdot \nabla_{\parallel}\tilde{\varphi} - b_i^{\parallel} \Delta_{\parallel}\tilde{\varphi} = 0 \quad ,$$

$$\frac{\partial \tilde{N}_e}{\partial t} - D_e^{\parallel} \Delta_{\parallel}\tilde{N}_e - D_i^{\parallel} \Delta_{\parallel}\tilde{N}_i + D_e^{\parallel}\left[\frac{\underline{v}_{no}^{\parallel}}{D_e^{\parallel}} - \left(1 + \frac{D_a^{\parallel}}{D_e^{\parallel}}\right) \frac{\nabla_{\parallel}N}{N} - \right.$$

$$
\begin{aligned}
&- \left[\frac{\nabla_{\parallel} D_e''}{D_e''} - \frac{D_a''}{D_e''} \cdot \frac{\nabla_{\parallel} T_p}{T_p} + \frac{D_a''}{D_e''} \cdot \frac{1}{H_p} \, \underline{\underline{1}} g'' \right] \cdot \nabla_{\parallel} \tilde{N}_e - \\
&- D_i \left(\frac{\nabla_{\parallel} N}{N} - \frac{m_e}{m_i} \frac{1}{H_i} \, \underline{\underline{1}} g'' \right) \cdot \nabla_{\parallel} \tilde{N}_i + D_a'' \left[\frac{\nabla_{\parallel} \underline{\underline{v}}_{no}}{D_a''} - \right. \\
&- \left(\nabla_{\parallel} + \frac{\nabla_{\parallel} D_a''}{D_a''} + \frac{\nabla_{\parallel} N}{N} \right) \cdot \left(\frac{\nabla_{\parallel} N}{N} + \frac{\nabla_{\parallel} T_p}{T_p} - \frac{1}{H_p} \, \underline{\underline{1}} g'' \right) + \\
&+ \left(\frac{\underline{\underline{v}}_{no}''}{D_a''} \cdot \frac{\nabla_{\parallel} N}{N} \right) + \left. \frac{l_{eo}}{D_a''} \right] \tilde{N}_e + \frac{m_e}{m_i} \frac{D_i''}{H_i} \left[\left(\frac{\nabla_{\parallel} D_i''}{D_i''} \, \underline{\underline{1}} g'' \right) + \right. \\
&+ H_i \nabla_{\parallel} \cdot \left(\frac{\underline{\underline{1}} g''}{H_i} \right) + \left. \left(\underline{\underline{1}} g'' \cdot \frac{\nabla_{\parallel} N}{N} \right) \right] \tilde{N}_i + (b_e'' - b_i) \, \Delta_{\parallel} \tilde{\varphi} + \\
&+ (b_e'' - b_i'') \left[\frac{\nabla_{\parallel} (b_e'' - b_i'')}{b_e'' - b_i''} + \frac{\nabla_{\parallel} N}{N} \right] \cdot \nabla_{\parallel} \tilde{\varphi} = 0 \quad ,
\end{aligned}
\tag{7}
$$

and the potential of the disturbed electric field by the equation

$$
\nabla_{\parallel} \tilde{\varphi} = - 4 \pi e N (\tilde{N}_i - \tilde{N}_e) \, . \tag{8}
$$

In Eqs (6)-(8) the following notations have been used:

$$
\tilde{N}_i = \frac{\tilde{n}_i}{N} \quad , \quad \tilde{N}_e = \frac{\tilde{n}_e}{N} \quad , \quad D_i'' = \frac{k T_{io}}{n_{no} \Theta_{in}} \quad ,
$$

$$
D_e'' = \frac{k T_{eo}}{N \Theta_{ei}} \quad , \quad b_i'' = \frac{e}{n_{no} \Theta_{in}} \quad , \quad b_e'' = \frac{e}{N \Theta_{ei}} \quad ,
$$

$$
H_i = \frac{k T_{io}}{m_i g} \quad , \tag{9}
$$

$$
l_{io} = 2.73 \cdot 10^{-12} \, n_o \, (N_2),
$$

$$
l_{eo} = 4.2 \cdot 10^{-7} \, (T_{eo}/300)^{-0.85} \, n_o \, (NO^+) \quad ,
$$

where m_e is the mass of the electron, D_i, D_e and b_i, b_e are the diffusion and mobility coefficients of ions and electrons.

CONDITIONS OF THE INSTABILITY OF LONGITUDINAL PERTURBATIONS

For the sake of simplicity quasineutrality is assumed, i.e. $\tilde{N}_i = \tilde{N}_e$ and $\nabla\psi = 0$. In this case the investigation can be confined to Eq. (6). Neglecting the terms proportional to the ratio (m_e/m_i), Eq. (6) can be rewritten in the form

$$\frac{\partial N_i}{\partial t} - D_i^{\parallel} \Delta_{\parallel} \tilde{N}_i + D_i \left(\underline{\underline{f}}_1^{\parallel} \cdot \nabla_{\parallel} \tilde{N}_i\right) + D_a^{\parallel} f_2^{\parallel} N_i = 0, \tag{10}$$

where

$$\underline{\underline{f}}_1^{\parallel} = \frac{\underline{\underline{v}}_{no}^{\parallel}}{D_i^{\parallel}} - \left(1 + \frac{D_a^{\parallel}}{D_i^{\parallel}}\right)\frac{\nabla_{\parallel} N}{N} - \frac{D_a^{\parallel}}{D_i^{\parallel}} \cdot \frac{\nabla_{\parallel} T_p}{T_p} - \frac{\nabla_{\parallel} D_i^{\parallel}}{D_i^{\parallel}} + \frac{D_a^{\parallel}}{D_i^{\parallel}} \cdot \frac{1}{H_p} \underline{\underline{1}} \underline{\underline{g}}^{\parallel},$$

$$f_2^{\parallel} = \frac{\nabla_{\parallel} \cdot \underline{\underline{v}}_{no}}{D_a^{\parallel}} - \left(\nabla_{\parallel} + \frac{\nabla_{\parallel} D_a^{\parallel}}{D_a^{\parallel}} + \frac{\nabla_{\parallel} N}{N}\right) \cdot \left(\frac{\nabla_{\parallel} N}{N} + \frac{\nabla_{\parallel} T_p}{T_p} - \right. \tag{11}$$

$$\left. - \frac{1}{H_p} \underline{\underline{1}} \underline{\underline{g}}^{\parallel}\right) + \left(\frac{\underline{\underline{v}}_{no}^{\parallel}}{D_a^{\parallel}} \cdot \frac{\nabla_{\parallel} N}{N}\right) + \frac{\underline{\underline{1}}_{io}}{D_a^{\parallel}} .$$

In general the structure of Eq. (10) is complicated, if the background distribution of the F region parameters depend on latitude and height, and the curvature of the geomagnetic field lines is taken into account. Bearing this in mind, the structure of Eq. (10) in a dipole coordinate system is considered (Fatkullin and Sitnov 1972). In this coordinate system for a scalar quantity f and a vector $\underline{\underline{A}}$

$$\nabla_{\parallel} f = h_\beta^{-1} \frac{\partial f}{\partial \beta} \underline{\underline{e}}_\beta , \qquad \Delta_{\parallel} f = h_\beta^{-2} \frac{\partial^2 f}{\partial \beta 2} ,$$

$$\left(\nabla_{\parallel} \cdot \underline{\underline{A}}^{\parallel}\right) = \frac{\delta^{1/2}}{r^3} \cdot \frac{\partial A_\beta}{\partial \beta} - 3 \frac{\cos\Theta \,(3 + 5\cos^2\Theta)}{r\delta^{3/2}} A_\beta , \tag{12}$$

where

$$\delta = 1 + 3\cos^2\Theta = 1 + 3\beta^2 r^4 , \quad \beta = \frac{\cos\Theta}{r^2} ,$$

$$h_\beta = \frac{r^3}{\delta^{1/2}} , \tag{13}$$

$\underline{e}_\beta$ is the unit vector in the direction of the field lines, h_β is the Lame coefficient, r, Θ are the radial distance and the geomagnetic colatitude.

Taking into account this relations, Eq. (10) can be rewritten in the form.

$$\frac{\partial \tilde{N}_i}{\partial t} + \varphi_2 \frac{\partial^2 \tilde{N}_i}{\partial \beta^2} + \varphi_1 \frac{\partial \tilde{N}_i}{\partial \beta} + \varphi_o \tilde{N}_i = 0 \quad , \tag{14}$$

where

$$\varphi_2 = - D_i'' h_\beta^{-2} \quad ,$$

$$\varphi_1 = D_i'' \left[h_\beta \frac{v_{no\beta}}{D_i''} - \left(1 + \frac{D_a''}{D_i''}\right) \frac{1}{N} \cdot \frac{\partial N}{\partial \beta} - \frac{D_a''}{D_i''} \cdot \frac{1}{T_p} \cdot \frac{\partial T_p}{\partial \beta} - \right.$$

$$\left. - \frac{1}{D_i''} \cdot \frac{\partial D_i''}{\partial \beta} + \frac{D_a''}{D_i''} \cdot \frac{1}{H_p} \cdot \frac{2 \cos\Theta}{\delta^{1/2}} \right] h_\beta^{-2} \quad , \tag{15}$$

$$\varphi_o = D_a'' \left[\frac{1}{D_a''} \cdot \frac{\partial v_{no\beta}}{\partial \beta} - \frac{3 \cos\Theta (3 + 5 \cos^2\Theta)}{r \delta^{3/2} D_a''} h_\beta v_{no\beta} - \right.$$

$$- h_\beta^{-1} \left(\frac{\partial}{\partial \beta} + \frac{1}{D_a''} \cdot \frac{\partial D_a''}{\partial \beta} - \frac{1}{N} \cdot \frac{\partial N}{\partial N\beta} \right) \cdot \left(\frac{1}{N} \frac{\partial N}{\partial \beta} + \frac{1}{T_p} \frac{\partial T_p}{\partial \beta} - \right.$$

$$\left. \left. - \frac{h_\beta g_\beta}{H_i g} \right) + \frac{v_{n\beta}}{D_a'' N} \cdot \frac{\partial N}{\partial \beta} + \frac{1_{io}}{D_a''} \right] h_\beta^{-1} \quad .$$

In a spherical coordinate system the structure of Eq. (10) is the following

$$\frac{\partial \tilde{N}_i}{\partial t} + \varphi_{rr} \frac{\partial^2 \tilde{N}_i}{\partial r^2} + \varphi_{\Theta\Theta} \frac{\partial^2 \tilde{N}_i}{\partial \Theta^2} + \varphi_{r\Theta} \frac{\partial^2 \tilde{N}_i}{\partial r \partial \Theta} +$$

$$+ \varphi_r \frac{\partial \tilde{N}_i}{\partial r} + \varphi_\Theta \frac{\partial \tilde{N}_i}{\partial \Theta} + \varphi \tilde{N}_i = 0 \quad , \tag{16}$$

where

$$\varphi_{rr} = -D_i'' \sin^2 I, \qquad \varphi_{\Theta\Theta} = -D_i'' \frac{\cos^2 I}{r^2},$$

$$\varphi_{r\Theta} = -2 D_i'' \frac{\sin I \cos I}{r},$$

$$\varphi_r = \sin^2 I \cdot v_{nor} + \sin I \cos I \cdot v_{no\Theta} - \frac{D_a''}{H_i} \sin^2 I -$$

$$- D_i'' \sin^2 I \left[\left(1 + \frac{D_a''}{D_i''} \right) \frac{1}{N} \cdot \frac{\partial N}{\partial r} + \frac{1}{T_i} \cdot \frac{\partial T_i}{\partial r} - \frac{1}{n_{no}} \frac{\partial n_{no}}{\partial r} + \right.$$

$$\left. + \frac{D_a''}{D_i''} \cdot \frac{1}{T_p} \cdot \frac{\partial T_p}{\partial r} \right] - D_i'' \cos I \sin I \left[\left(1 + \frac{D_a''}{D_i''} \right) \frac{1}{N} \cdot \frac{\partial N}{\partial \Theta} + \right.$$

$$\left. + \frac{1}{T_i} \cdot \frac{\partial T_i}{\partial \Theta} - \frac{1}{n_{no}} \cdot \frac{\partial n_{no}}{\partial \Theta} + \frac{D_a''}{D_i''} \cdot \frac{1}{T_p} \cdot \frac{\partial T_p}{\partial \Theta} \right] -$$

$$- D_i'' \frac{1}{r} (3 \sin^4 I + 8 \sin^2 I - 2),$$

$$\varphi_\Theta = \frac{\cos I}{r} \left\{ \sin I \cdot v_{nor} + \cos I \, v_{no\Theta} - \frac{D_a''}{H_i} \sin I - \right.$$

$$- D_i'' \sin I \left[\left(1 + \frac{D_a''}{D_i''} \right) \frac{1}{N} \cdot \frac{\partial N}{\partial r} + \frac{1}{T_i} \cdot \frac{\partial T_i}{\partial r} - \frac{1}{n_{no}} \cdot \frac{\partial n_{no}}{\partial r} + \right.$$

$$\left. + \frac{D_a''}{D_i''} \cdot \frac{1}{T_p} \cdot \frac{\partial T_p}{\partial r} \right] - D_i'' \cos I \left[\left(1 + \frac{D_a''}{D_i''} \right) \frac{1}{N} \cdot \frac{\partial N}{\partial \Theta} + \frac{1}{T_i} \cdot \frac{\partial T_i}{\partial \Theta} - \right.$$

$$\left. \left. - \frac{1}{n_{no}} \cdot \frac{\partial n_{no}}{\partial \Theta} + \frac{D_a''}{D_i''} \cdot \frac{1}{T_p} \cdot \frac{\partial T_p}{\partial \Theta} \right] - D_i'' \frac{\sin I}{2r} (11 - 6 \sin^2 I) \right\},$$

$$\varphi = \left\langle r \sin^2 I \frac{\partial v_{nor}}{\partial r} + \cos^2 I \left(\frac{\partial v_{no\Theta}}{\partial \Theta} + \frac{3 \sin^2 I - 4}{2} v_{nor} \right) + \right.$$

$$+ \sin I \cos I \left(r \frac{\partial v_{no\Theta}}{\partial r} + \frac{\partial v_{nor}}{\partial \Theta} + \frac{4 - \sin^2 I}{2} v_{no\Theta} \right) +$$

$$\left. + 3 \sin I (3 - \sin^2 I) \left(\frac{\cos I}{2} v_{no\Theta} + 2 \sin I \, v_{nor} \right) + \right. \quad (17)$$

$$+\frac{1}{rN}\left(r\cdot\sin I\frac{\partial N}{\partial r}+\cos I\frac{\partial N}{\partial\Theta}\right)\left[r\sin I\left(v_{nor}+\frac{D_a''}{n_{no}}\cdot\frac{\partial n_{no}}{\partial r}\right)+\right.$$

$$\left.+\cos I\left(r\,v_{no\Theta}+\frac{D_a''}{n_{no}}\cdot\frac{\partial n_{no}}{\partial\Theta}\right)\right]+\frac{D_a''}{rT_p}\left(r\sin I\frac{\partial T_p}{\partial r}+\right.$$

$$\left.+\cos I\frac{\partial T_p}{\partial\Theta}\right)\left(r\sin I\left(\frac{1}{n_{no}}\cdot\frac{\partial n_{no}}{\partial r}-\frac{2}{N}\cdot\frac{\partial N}{\partial r}\right)+\right.$$

$$\left.+\cos I\left(\frac{1}{n_{no}}\cdot\frac{\partial n_{no}}{\partial\Theta}-\frac{2}{N}\cdot\frac{\partial N}{\partial\Theta}\right)\right)-\frac{D_a''}{rN}\left[r^2\sin^2 I\frac{\partial^2 N}{\partial r^2}+\right.$$

$$+\cos^2 I\frac{\partial^2 N}{\partial\Theta 2}+2r\sin I\cos I\frac{\partial^2 N}{\partial r\partial\Theta}+r\,(3\sin^4 I+8\sin^2 I-$$

$$-2)\frac{\partial N}{\partial r}+\frac{\sin I\cos I}{2}(11-6\sin^2 I)-\frac{D_a''}{rT_p}\left[r^2\sin^2 I\frac{\partial^2 T_p}{\partial r^2}+\right.$$

$$+\cos^2 I\frac{\partial^2 T_p}{\partial\Theta^2}+2r\sin I\cos I\frac{\partial^2 T_p}{\partial r\partial\Theta}+r\,(3\sin^4 I+$$

$$+8\sin^2 I-2)\frac{\partial T_p}{\partial r}+\frac{\sin I\cos I}{2}(11-6\sin^2 I)\frac{\partial T_p}{\partial\Theta}+$$

$$+\frac{D_a''}{H_i}\sin I\left\{r\sin I\left(\frac{1}{n_{no}}\cdot\frac{\partial n_{no}}{\partial r}-\frac{1}{N}\cdot\frac{\partial N}{\partial r}\right)+\right.$$

$$+\cos I\left(\frac{1}{n_{no}}\cdot\frac{\partial n_{no}}{\partial\Theta}+\frac{1}{N}\cdot\frac{\partial N}{\partial\Theta}\right)+\frac{\cos^2 I}{4\sin I}(4-3\sin^2 I)+$$

$$\left.\left.+\frac{1}{2}\sin I\,(3\sin^2 I-5)\right\}+r\,l_{io}\right\rangle\frac{1}{r}\quad,$$

where I is the magnetic dip.

For investigation of the stability, a spherically symmetric distribution of the background F region parameters is taken where all meridional gradients are zero. At $I \gtrsim 60^{o}$ horizontal perturbations can be neglected. Further $v_{nor} = 0$ is taken and the terms comprising the factor $\frac{1}{r}$ are omitted. With these assumptions Eq. (16) has the form

$$\frac{\partial \tilde{N}_i}{\partial t} - \sin^2 I\, D_i'' \frac{\partial^2 \tilde{N}_i}{\partial r^2} + \left\{ \sin I \cos I\, v_{no\Theta} - \frac{D_a''}{H_i} \sin^2 I - \right.$$

$$- \sin^2 I\, D_i'' \left[\left(1 + \frac{D_a''}{D_i''} \right) \frac{1}{N} \cdot \frac{\partial N}{\partial r} + \frac{1}{T_i} \cdot \frac{\partial T_i}{\partial r} - \frac{1}{n_{no}} \cdot \frac{\partial n_{no}}{\partial r} + \right.$$

$$\left. \left. + \frac{D_a''}{D_i''} \cdot \frac{1}{T_p} \cdot \frac{\partial T_p}{\partial r} \right] \right\} \frac{\partial N_i}{\partial r} + \left\{ \sin I \cos I \frac{\partial v_{no\Theta}}{\partial r} + \right. \qquad (18)$$

$$+ \sin I \cos I\, v_{no\Theta} \frac{1}{N} \cdot \frac{\partial N}{\partial r} + \sin^2 I\, D_a'' \left[\frac{1}{N n_{no}} \cdot \frac{\partial N}{\partial r} \cdot \frac{\partial n_{no}}{\partial r} + \right.$$

$$+ \frac{1}{T_p n_{no}} \cdot \frac{\partial T_p}{\partial r} \cdot \frac{\partial n_{no}}{\partial r} - \frac{2}{N T_p} \cdot \frac{\partial N}{\partial r} \cdot \frac{\partial T_p}{\partial r} - \frac{1}{N} \cdot \frac{\partial^2 N}{\partial r^2} - \frac{1}{T_p} \cdot \frac{\partial^2 T_p}{\partial r^2} +$$

$$\left. \left. + \frac{1}{H_p n_{no}} \cdot \frac{\partial n_{no}}{\partial r} - \frac{1}{H_p n_{no}} \cdot \frac{\partial n_{no}}{\partial r} \right] + l_{io} \right\} \tilde{N}_i = 0 \cdot$$

The dependence of the perturbation on space and time is taken into account in the form

$$\tilde{N}_i \sim e^{j(K_r r - \tilde{\omega} t)} \qquad (19)$$

where $\tilde{\omega} = \omega + j\gamma$, $j = \sqrt{-1}$, K_r is the vertical component of the wave vector. Substituting Eqs (19) into Eq. (18) the following relations are obtained for ω and γ

$$\omega = v_f K_r \qquad (20)$$

where

$$v_f = -\sin^2 I \left[-v_{no\Theta} \cot I + \frac{D_i''}{T_i} \cdot \frac{\partial T_i}{\partial r} - \frac{D_i''}{n_{no}} \cdot \frac{\partial n_{no}}{\partial r} + \right.$$

$$\left. + (D_a'' + D_i'') \frac{1}{N} \cdot \frac{\partial N}{\partial r} + \frac{D_a''}{T_p} \cdot \frac{\partial T_p}{\partial r} + \frac{D_a''}{H_p} \right], \qquad (21)$$

$$\gamma = \sin^2 I \left[-\frac{\partial v_{no\Theta}}{\partial r} \cot I - v_{no\Theta} \frac{1}{N} \cdot \frac{\partial N}{\partial r} \cot I - \frac{1_{io}}{\sin^2 I} + \right.$$

$$+ \frac{2D_a''}{NT_p} \cdot \frac{\partial N}{\partial r} \cdot \frac{\partial T_p}{\partial r} - \frac{D_a''}{n_{no}T_p} \cdot \frac{\partial n_{no}}{\partial r} \cdot \frac{\partial T_p}{\partial r} - \frac{D_a''}{n_{no}N} \cdot \frac{\partial n_{no}}{\partial r} \cdot \frac{\partial N}{\partial r} + \quad (22)$$

$$\left. + \frac{D_a''}{N} \frac{\partial^2 N}{\partial r^2} + \frac{D_a''}{T_p} \cdot \frac{\partial^2 T_p}{\partial r^2} + \frac{D_a''}{H_p N} \cdot \frac{\partial N}{\partial r} - \frac{D_a''}{H_p n_{no}} \frac{\partial n_{no}}{\partial r} - D_a'' K_r^2 \right],$$

and v_f if the phase velocity of the wave-like perturbation.

Estimating the values of the quantities v_f and γ for the actual ionospheric conditions, the night-time ionosphere (0100 LT) is considered at heights of the F region (from 170 to 500 km) at a latitude of 60^o in equinoctial months and medium solar activity ($F_{10.7} \leq 100$).

The same height distribution of the plasma parameters as used by Fatkullin et al. (1981) is applied. In this case the neutral wind is directed to the pole ($v_{no\Theta} < 0$) and its velocity is determined according to Stubbe (1972). It is also assumed that all constituents of the ionosphere have the same temperature $T_e = T_i = T_n$. The variation of the concentration and temperature of ions with height is given in Table I. The numerical values for each term in Eq. (21) are also given there. A comparison of these values shows that the motion of the neutral atmosphere (if it is present) is a basic factor, which determines the velocity of propagation of the wave perturbations. Then, in order of decreasing importance at heights below the maximum of the F2 layer follow the concentration gradient of the charged particles and at heights above the maximum the concentration gradients of the neutral and charged particles and the force of gravity. From Table I follows that the wave travels towards the Earth (negative sign of v_f). The phase velocity and frequency increase with increasing height.

In Table II values of the terms of Eq. (22) and the magnitude of the increments for the wave length $\lambda_z = 10$ km are presented. The negative sign of the increment shows that the perturbation is damped. The attenuation is mainly due to ambipolar

Table I

$\frac{h}{km}$	N, cm^{-3}	T^oK	-cot I $v_{no\theta}$	$\frac{D_i^*}{T_i}\cdot\frac{\partial T_i}{\partial r}$	$-\frac{D_i^*}{n_{no}}\cdot\frac{\partial n_{no}}{\partial r}$	$\frac{D_a^*}{T_p}\cdot\frac{\partial T_p}{\partial r}$	$(D_a^*+D_i^*)\frac{1}{N}\frac{\partial N}{\partial r}$	$\frac{D_a^*}{H_p}$	v_f, cms^{-1}	ω, s^{-1}
1	2	3	4	5	6	7	8	9	10	11
170	1.00(3)	680	6.84(3)	7.95(0)	3.48(1)	1.59(1)	4.35(1)	3.90(1)	-5.23(3)	-3.28(-2)
180	1.10(3)	750	8.25(3)	1.13(1)	5.33(1)	2.26(1)	1.00(2)	5.65(1)	-6.36(3)	-3.99(-2)
190	2.29(3)	800	9.12(3)	1.48(1)	7.63(1)	2.96(1)	8.45(2)	7.95(1)	-7.55(3)	-4.75(-2)
200	4.15(3)	850	9.40(3)	2.05(1)	1.09(2)	4.10(1)	4.29(2)	1.07(2)	-7.50(3)	-4.71(-2)
210	5.34(3)	870	1.02(4)	2.66(1)	1.50(2)	5.32(1)	2.81(3)	1.47(2)	-9.97(3)	-6.26(-2)
220	1.25(4)	900	1.08(4)	3.49(1)	2.04(2)	6.98(1)	2.79(3)	1.97(2)	-1.05(4)	-6.59(-2)
230	2.45(4)	940	1.14(4)	4.42(1)	2.70(2)	8.84(1)	2.45(3)	2.54(2)	-1.08(4)	-6.78(-2)
240	4.00(4)	980	1.18(4)	5.82(1)	3.73(2)	1.16(2)	2.04(3)	3.43(2)	-1.10(4)	-6.91(-2)
250	5.50(4)	990	1.24(4)	7.14(1)	4.83(2)	1.42(2)	1.28(3)	4.44(2)	-1.11(4)	-6.97(-2)
260	6.50(4)	1000	1.24(4)	9.13(1)	6.33(2)	1.86(2)	2.17(3)	5.77(2)	-1.20(4)	-7.53(-2)
270	8.05(4)	1050	1.25(4)	1.14(2)	8.49(2)	2.25(2)	1.98(3)	7.43(2)	-1.22(4)	-7.66(-2)
280	9.31(4)	1100	1.28(4)	1.47(2)	1.12(3)	2.94(2)	2.34(3)	9.48(2)	-1.32(4)	-7.72(-2)
290	1.06(5)	1120	1.29(4)	1.82(2)	1.43(3)	3.64(2)	1.23(3)	1.19(3)	-1.38(4)	-8.67(-2)
300	1.12(5)	1150	1.31(4)	2.26(2)	1.84(3)	4.52(2)	2.51(2)	1.50(3)	-1.29(4)	-8.10(-2)
350	8.25(4)	1250	1.31(4)	6.04(2)	6.07(3)	1.20(3)	-6.82(3)	4.67(3)	-1.36(4)	-8.54(-2)
400	5.12(4)	1400	1.31(4)	1.80(3)	1.87(4)	2.60(3)	-2.40(4)	1.31(4)	-1.89(4)	-1.18(-1)
450	3.05(4)	1480	1.31(4)	1.60(3)	5.04(4)	3.20(3)	-5.71(4)	3.37(4)	-3.41(4)	-2.14(-1)
500	1.97(4)	1560	1.31(4)	1.01(4)	1.26(5)	2.02(4)	-9.66(4)	8.23(4)	-1.16(5)	-7.28(-1)

Note: $1.25(4) = 1.25 \cdot 10^4$

Table II

$\frac{h}{km}$	$\cot I \cdot \frac{\partial v_{n\theta}}{\partial r}$	$\cot I \frac{1}{N}\frac{\partial N}{\partial r} v_{no\theta}$	$-\frac{1_{io}}{\sin^2 I}\frac{2D^{\parallel}_a}{NT_p}\cdot\frac{\partial N}{\partial r}\cdot\frac{\partial T_p}{\partial r}$	$-\frac{D^{\parallel}_a}{T_p n_{no}}\cdot\frac{\partial n_{no}}{\partial r}\cdot\frac{\partial T_p}{\partial r}$	$-\frac{D^{\parallel}_a}{n_{no}N}\cdot\frac{\partial n_{no}}{\partial r}\cdot\frac{\partial N}{\partial r}$	$\frac{D^{\parallel}_a}{N}\cdot\frac{\partial^2 N}{\partial r^2}$	$\frac{D^{\parallel}_a}{T_p}\cdot\frac{\partial^2 T_p}{\partial r^2}$	$-\frac{D^{\parallel}_a}{H_p N}\frac{\partial N}{\partial r}$	$-\frac{D^{\parallel}_a}{H_p n_{no}}\cdot\frac{\partial n_{no}}{\partial r}$	$-D^{\parallel}_i \varkappa_r^2$	γ, s^{-1}
1	2	3	4	5	6	7	8	9	10	11	12	13
170	3.0(-3)	6.8(-4)	-4.0(-2)	3.1(-6)	3.8(-6)	6.2(-6)	5.8(-4)	-8.2(-7)	3.9(-6)	8.3(-6)	-5.7(-3)	-3.1(-2)
180	2.6(-3)	1.2(-3)	-1.8(-2)	6.5(-6)	5.2(-6)	1.5(-5)	5.0(-5)	-1.1(-6)	8.1(-6)	1.3(-5)	-9.1(-3)	-1.7(-2)
190	2.5(-3)	7.4(-3)	-1.4(-2)	4.8(-5)	6.5(-6)	1.2(-4)	-1.3(-3)	-1.1(-6)	6.4(-5)	1.7(-5)	-1.4(-2)	-1.5(-2)
200	2.3(-3)	2.7(-3)	-7.0(-3)	2.3(-5)	8.9(-6)	6.2(-5)	-1.6(-4)	-1.5(-6)	3.0(-5)	2.3(-5)	-1.9(-2)	-1.6(-2)
210	1.6(-3)	1.4(-3)	-3.2(-3)	1.4(-4)	1.1(-5)	4.0(-4)	1.5(-3)	-1.6(-6)	7.9(-4)	3.1(-5)	-2.8(-2)	-9.9(-3)
220	1.5(-3)	1.0(-2)	-2.2(-3)	1.3(-4)	1.4(-5)	3.9(-4)	7.2(-4)	-1.9(-6)	7.8(-4)	4.1(-5)	-5.1(-2)	-2.0(-2)
230	1.4(-3)	7.2(-3)	-1.7(-3)	1.1(-4)	1.8(-5)	3.4(-4)	3.6(-4)	-2.3(-6)	1.5(-4)	5.2(-5)	-7.2(-2)	-3.2(-2)
240	1.3(-3)	4.4(-3)	-1.4(-3)	8.7(-5)	2.3(-5)	2.7(-4)	-4.3(-5)	-2.8(-6)	1.2(-4)	7.0(-5)	-9.4(-2)	-5.0(-2)
250	1.2(-3)	2.2(-3)	-8.3(-4)	5.1(-5)	2.5(-5)	1.7(-4)	-4.2(-4)	-3.0(-6)	7.9(-5)	9.0(-5)	-1.2(-1)	-6.8(-2)
260	1.1(-3)	2.8(-3)	-9.0(-4)	8.5(-5)	3.7(-5)	2.9(-4)	5.3(-4)	-3.5(-6)	1.3(-4)	1.1(-5)	-1.6(-1)	-8.9(-2)
270	7.0(-4)	1.9(-3)	-6.0(-4)	7.1(-5)	4.5(-5)	2.6(-4)	-3.0(-4)	-4.0(-6)	1.1(-4)	1.4(-4)	-2.2(-1)	-1.2(-1)
280	4.1(-4)	1.8(-3)	-3.2(-4)	8.1(-5)	5.8(-5)	3.0(-4)	3.6(-5)	-4.5(-6)	1.3(-4)	1.8(-4)	-2.8(-1)	-1.6(-1)
290	3.4(-4)	7.4(-3)	-1.4(-4)	4.1(-5)	7.1(-5)	1.6(-4)	-9.4(-4)	-4.9(-6)	6.7(-5)	2.3(-4)	-3.7(-1)	-2.2(-1)
300	2.2(-4)	1.2(-4)	-1.1(-4)	8.0(-6)	8.8(-5)	3.2(-5)	-5.6(-4)	-5.8(-6)	1.3(-5)	2.9(-4)	-1.2(0)	-2.8(-1)
350	1.1(-4)	-9.4(-4)	-1.8(-4)	-8.5(-5)	2.2(-4)	-8.6(-4)	-5.5(-5)	-8.0(-6)	-3.3(-4)	8.9(-4)	-3.9(0)	-9.4(-1)
400		-1.0(-3)	-3.0(-6)	-4.1(-4)	4.8(-4)	-2.9(-3)	1.6(-3)	-1.2(-5)	-1.0(-3)	2.4(-3)	-3.9(0)	-2.9(0)
450		-9.2(-4)	-3.0(-7)	-4.4(-4)	5.8(-4)	-7.0(-3)	7.0(-3)	-1.4(-5)	-2.3(-3)	6.1(-3)	-1.1(1)	-8.0(0)
500		-6.0(-4)	-6.6(-8)	-1.8(-3)	3.6(-3)	-1.1(-2)	1.5(-2)	-2.7(-5)	-3.7(-3)	1.4(-2)	-2.7(1)	-2.1(1)

Note: $-1.49(-4) = -1.49 \cdot 10^{-4}$

diffusion that suppresses perturbations of wave-length $\lambda_r <$ $< \left(\frac{1}{N}\right)\left(\frac{\partial N}{\partial r}\right)^{-1}$ and to recombination at low altitudes (to 250 km). A substantial contribution to the value of the increment is made by the term containing the second derivative of the charged particle concentration. The term including the second derivative of the temperature is small and its contribution can be neglected.

At heights above the maximum of the F2 layer the increment depends substantially on the force of gravity and on the gradient of the neutral particle concentration, besides the attenuation is enhanced by the terms including the gradient of the neutral particle concentration. At intermediate heights (200-300 km) the stability of the plasma depends strongly on the direction of the neutral wind. If it is directed to the equator, damping is increased, and if it is directed to the pole, then the damping is substantially weakened and in certain conditions it can produce instability. The dependence of the increment on altitude is shown for λ_r = 10 km in Fig. 1. For the maximum of

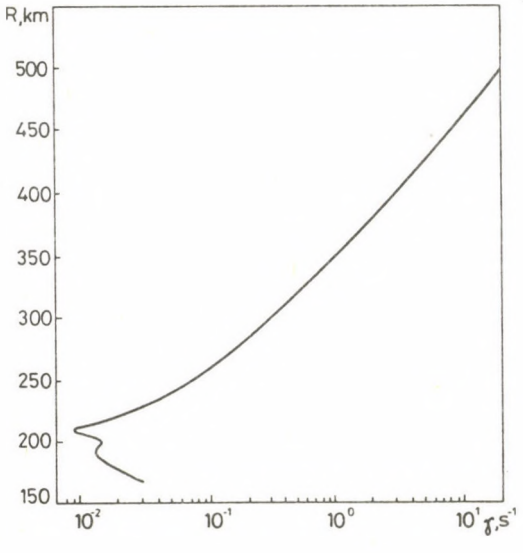

Fig. 1.

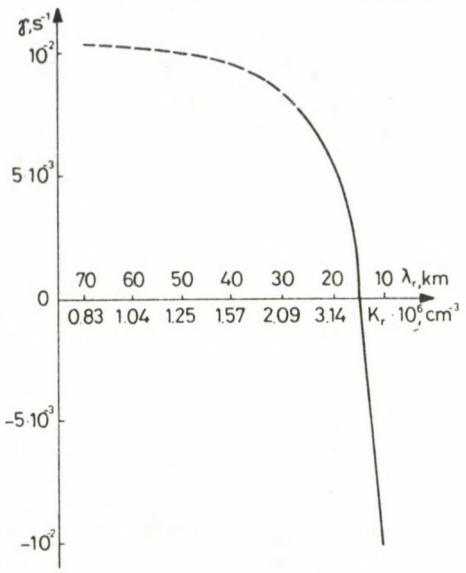

Fig. 2.

$\gamma(h)$ at h = 210 km the dependence of the increment on the wave number has also been plotted (Fig. 2). It shows that perturbations of a wave-length $\lambda_r \gtrsim 15$ km are unstable, however, it should be noted that the approximation (19) is valid only in case of wave-lenghts $\lambda_r < \left(\frac{1}{N} \cdot \frac{\partial N}{\partial r}\right)^{-1}$. Therefore, that part of the curve, which does not correspond to this condition, is indicated by dotted line.

Finally, it is emphasized that the condition of production of instabilities is the presence of a neutral wind directed to the pole.

REFERENCES

Antonov A M, Fatkullin M N 1985: General relations for the description of weak longitudinal potential perturbations in the irregular F region of the ionosphere (in Russian). Preprint IZMIRAN, Moscow

Erukhimov L N, Maksimenko O I, Myasnikov E N 1980: Ionosfernie issledovaniya, 27-48.

Fatkullin M N 1982: Physics of the ionosphere (in Russian). VINITI, Moscow

Fatkullin M N, Sitnov Yu S 1972: Geomagn. i Aeronomiya, 12, 333-335.

Fatkullin M N, Zelenova T I, Kozlov V K, Legenka A D, Soboleva T N 1981: Empirical models of the midlatitude ionosphere (in Russian). Nauka, Moscow

Fejer B G, Kelley M C 1980: Rev. Geophys. and Space Phys., 18, 401-454.

Gelberg M G 1977: In: Propagation of Radio Waves in the Polar Ionospere. Kolsky filial AN SSSR, Apatiti, 3-37.

Gershman B N 1963: Geomagn. i Aeronomiya, 3, 878-886.

Gershman B N 1974: Dynamics of the ionospheric plasma (in Russian). Nauka, Moscow

Gershman B N 1980: Ionosfernie issledovaniya, 30, 17-26.

Hanuise C 1983: Radio Sci., 18, 1093-1121.

Kelley M C, Mc Clure J P 1981: J. Atmos. and Terr. Phys., 43, 427-435.

Keskinen M J, Ossakow S 1983: Radio Sci., 18, 805-807.

Mikhaylovskiy A B 1970: Theory of plasma instabilities 1. Instabilities of the homogen plasma (in Russian). Atomizdat, Moscow

Mikhaylovskiy A B 1971: Theory of plasma instabilities 2. Instabilities of the inhomogen plasma (in Russian). Atomizdat, Moscow

Poeverlein H 1966: J. Atmos. and Terr. Phys., 28, 1111-1123.

Solodovnikov G K, Fatkullin M N, Russkin V M, Krokhmalnikov E B 1984: In: Modeling of the irregular structure of the ionosphere. IZMIRAN, Moscow, 5-41.

Sreenivasan S R, Schroeder M B 1983: Plasma Physics, 25, 925-935.

Stubbe P 1972: J. Atmos. and Terr. Phys., 34, 519-523.

Zhmur M E 1978: To the theory of relaxation process in the ionospheric F region (in Russian). Thesis

Acta Geod. Geoph. Mont. Hung., Vol. 22 (1-2), pp. 171-176 (1987)

GLOBAL ANALYTICAL MODEL OF THE SPORADIC E LAYER FOR RADIO COMMUNICATION

O G Ovezgeldiev[1] and G V Mikhaylova[1]

[1]Physical Technical Institute, Academy of Sciences of the Turkmen SSR
744000 Ashkhabad, Gogol ul. 15, USSR

For the prediction of radio communication a global analytical model of the sporadic E layer is suggested which enables the quantitative estimation of the role of this complex anomalous formation in radio wave propagation.

Keywords: ionospheric sporadic E; probability of sporadic E; radio wave propagation

A global analytical model of the sporadic E layer was developed enabling a reliable determination of the role of this complex anomalous formation in the ionospheric propagation of radio waves. The model is based on a complex investigation of the structure and physics of the Es layer and on the generalization of a large number of experimental data collected in a world-wide network of ionospheric stations. It is analytically described by the following formula (Ovezgeldiev 1970, Ovezgeldiev and Mikhaylova 1976, 1977, 1981, 1983, Mikhaylova 1982).

$$PE_s > f_v = PE_s \left[1 - \Phi(u)\right], \tag{1}$$

where PEs is the general probability of the occurrence of an Es layer, f_v is the equivalent vertical sounding frequency,

$$\Phi(u) = \frac{1}{\sqrt{2\pi}} \int_{-\infty}^{u} \exp\left(-\frac{\xi^2}{2}\right) d\xi \tag{2}$$

is the function of normal distribution, its values are given in tables (Yanko 1961) and

$$u = \frac{\xi_o - \bar{\xi}}{\sigma_\xi} . \qquad (3)$$

The formula of the probability of reflection at frequencies higher than a given arbitrary frequency f_v is:

$$\xi_o = \lg f_v \qquad \bar{\xi} = \overline{\lg f_o E_s} \qquad \sigma_\xi = \sigma_{\lg f_o E_s} \qquad (4)$$

and the probability of screening at frequencies higher than this frequency is:

$$\xi_o = \lg f_v \qquad \bar{\xi} = \overline{\lg f_b E_s} \qquad \sigma_\xi = \sigma_{\lg f_b E_s} . \qquad (5)$$

Thus, the parameters of the analytical model are the general probability of occurrence of an Es layer, PEs, the mean value of the logarithm of the critical frequency, $\overline{\lg foEs}$, the mean value of the logarithm of the blanketing frequency, $\overline{\lg fbEs}$, the mean-square error of the logarithm of foEs, $\sigma_{\lg foEs}$ and the mean-square error of the logarithm of fbEs, $\sigma_{\lg fbEs}$.

Probabilistic-statistical and space-time regularities of the Es layer show that the parameters of the model can be suitably approximated by relations of the form

$$a_o(\delta, x) + \sum_{n=1}^{3} \left[a_n(x) \cos nt + b_n(x) \sin nt \right] , \qquad (6)$$

where δ is the Sun's declination, t the local mean time,

$$x = \operatorname{arc\,tg} \frac{\operatorname{tg} I}{\sqrt{\cos \varphi}} \qquad (7)$$

the modified coordinate and I, φ are respectively the magnetic dip and the geographical latitude. It has to be emphasized that the constant coefficient of disintegration a_o depends on the season and on the coordinate x, while the coefficients of the variable components a_n and b_n depend only on x. The model is made so more compact and its practical use is simplified.

The values of the disintegration coefficients are determined by the experimental data of the world-wide network of ionospheric stations in the northern hemisphere (about five million individual measurements are used) and are presented in a generalized form in 10 summarized tables, for all five parameters of the model 5 tables with the values of the constant component and 5 tables with the values of the variable components. Moreover, in the latitude zone x 5 to 80^{o} the values of the disintegration coefficients are given in steps of 5^{o}, in the equatorial zone (x 0 to 5^{o}) and in the auroral zone as well as at higher latitudes (x 80 to 90^{o}) in steps of 2^{o}. Besides the values of the disintegration constants are given for two levels of the geomagnetic activity, i.e. for geomagnetically quiet (K_p = 1, 0) and geomagnetically disturbed conditions (K_p > 3) in the auroral zone, where the Es layer depends on the level of the geomagnetic activity.

The model has the property of transformation, namely, for its application to the southern hemisphere it is sufficient to shift it in time relative to the northern hemisphere by half year. Therefore, though the values of the disintegration coefficient are determined on the basis of experimental data of the northern hemisphere, the model can be applied in global scales.

The prediction of the influence of the ES layer on the propagation of radio waves enables either to establish the probability of screening of the over-lying ionospheric region by an Es layer, or to determine the probability of the establishment of radio communication and television transmissions through an Es layer with a given sounding frequency. In addition the operating frequency for the oblique incidence sounding f_w, the coordinates of the corresponding points of the transmission paths, the hour of the day and year should be given. Then, the general scheme of the computation consists of the following operations:

1. On the basis of the given coordinates of the points, the geographical coordinates (φ, λ) of the reflection point and the length of the transmission path are determined. The magnetic dip I of the reflection point is also computed.

2. Using Eq. (7) the x coordinate of the reflection point is calculated.

3. The values of the model parameters, i.e. PEs, $\overline{\lg foEs}$, $\overline{\lg fbEs}$, $\sigma_{\lg foEs}$, $\sigma_{\lg fbEs}$ are computed for the given hour of the day and month of the year using Eq. (6) and the values of the disintegration coefficients corresponding to the coordinate of the reflection point of the transmission path given in the tables. It has to be noted that all computations are carried out for the local mean time in the reflection point. Moreover, if the coordinate of the transmission path does not coincide exactly with the value given in the tables, those values of the disintegration coefficient can be used which are nearest to the value of x. In case of a more accurate computation, within the limits of each interval of the coordinate x linear interpolation should be used.

4. In case of reflection from the E region, where as it is known the Es layer is formed, the equivalent vertical frequency f_v corresponding to the given operating frequency of the oblique incidence sounding f_w is determined on the basis of the length of the transmission path. In contrast to the regular layers of the ionosphere the secant law is not always valid at the propagation of radio waves through the Es layer. For frequencies lower than or somewhat higher than fbEs, the secant law is valid, i.e. MEs = M = $\sec\alpha$, where α is the angle of incidence and at higher frequencies, when reflection takes place in the range of the semi-transparency of the Es layer, MEs > M. In the latter case the relation MEs = η M is used in the model calculation. On the basis of the generalization of the experimental data, the value of η has been chosen to 1.56. Thus in model calculations the conversion of the equivalent frequency f_v is carried out according to the following criteria:

$$f_v = \frac{f_w}{ME_s} = \frac{f_w}{M}, \quad \text{if} \quad \overline{\lg f_b E_s} + 1.5\sigma_{\lg f_b E_s} > \lg \frac{f_w}{M}$$

$$f_v = \frac{f_w}{ME_s} = \frac{f_w}{1.56\,M} \quad \text{if} \quad \overline{\lg f_b E_s} + 1.5\sigma_{\lg f_b E_s} < \lg \frac{f_w}{M} \; .$$

Naturally, the value of the coefficient η will be further

improved depending on the availability of new experimental data. In addition, the effect of the energetics of the transmission channel and the directional characteristics of the antenna must also be taken into consideration besides a possible frequency dependence of MEs. It is well known that in case of vertical sounding the characteristics of the Es layer depend on the technical parameters of the equipment.

5. At oblique incidence sounding the probability of reflection and of blanketing of the given operating frequency are determined according to formula (1). The probability of reflection is computed as:

$$u = \frac{\lg f_v - \overline{\lg f_o E_s}}{\sigma_{\lg f_o E_s}},$$

and the probability of blanketing as:

$$u = \frac{\lg f_v - \overline{\lg f_b E_s}}{\sigma_{\lg f_b E_s}}.$$

In case of multi-hop propagation via the Es layer the computation is carried out in the following way. According to the scheme described above the computation is separately executed for each hop. The resultant values of the probability of reflection and of the probability of blanketing by the Es layer are obtained in case of multi-hop propagation as the product of the probabilities of the individual hops.

The computations can be carried out both manually and by computers. In the Physical-Technical Institute, Academy of Sciences of the Turkmen SSR, where the analytical model in question was developed, a Fortran program was prepared.

The suitability of the model calculations has been proved by experimental data obtained both by vertical sounding and at oblique transmission paths. In the majority of the cases, the difference amounts to not more than 15 %, which is usually less than the random fluctuations of the layer from day to day due to

the probabilistic character of its formation.

REFERENCES

Mikhaylova G V 1982: Empirical model of the mid-latitude sporadic E layer (in Russian). Thesis

Ovezgeldiev O G 1970: Structure and formation mechanism of the sporadic E layer at mid-latitudes (in Russian). Thesis

Ovezgeldiev O G, Mikhaylova G V 1976a: Izv. AN TSSR, ser. fiz.-tekhn., khim. i geol. nauk., No 3, 65-72.

Ovezgeldiev O G, Mikhaylova G V 1976b: Izv. AN TSSR, ser. fiz.-tekhn., khim. i geol. nauk., No 6, 48-55.

Ovezgeldiev O G, Mikhaylova G V 1977: Izv. AN TSSR, ser. fiz.-tekhn., khim. i geol. nauk., No 6, 48-52.

Ovezgeldiev O G, Mikhaylova G V 1981: Izv. AN TSSR, ser. fiz.-tekhn., khim. i geol. nauk., No 5, 40-50.

Ovezgeldiev O G, Mikhaylova G V, Myalikguliev B 1983: Izv. AN TSSR, ser. fiz.-tekhn., khim. i geol. nauk., No 6, 24-29.

Yanko Ya 1961: Mathematical-Statistical Tables. Gosstatizdat, Moscow

Acta Geod. Geoph. Mont. Hung., Vol. 22 (1-2), pp. 177-181 (1987)

SPREAD-F AND SPORADIC E LAYER IN THE EQUATORIAL ZONE

A H Depueva[1] and N P Benkova[1]

[1]Institute of Geomagnetism, Ionosphere and Radio Wave Propagation
Academy of Sciences of the USSR, 142092 Troitsk, Moskovskaya oblast, USSR

It is shown that the seasonal and solar cycle variations of spread F and E_{sf} in different longitudinal zones are similar. In an attempt to find the formation mechanisms of irregularities producing these phenomena, the role of metal ions is discussed.

Keywords: spread F; sporadic E; longitudinal variation

Spread F has been an interesting ionospheric problem for a long time and the importance in the last years of this problem augmented. Recently since on the one hand the demand for a knowledge of ionospheric irregularities essential for spotting, radiolocation and operation of different radiosystems had increased, on the other hand spread F is connected to plasma processes in the ionosphere which were investigated more and more. In the followings some experimental results concerning spread F in the equatorial zone are presented which demonstrate its already known properties and show some new features.

One of the interesting properties of the equatorial spread F is the longitudinal effect in its occurrence along the magnetic equator. The longitudinal effect is characterized by the circumstance that in the longitudinal zone near Huancayo the seasonal variation (variation of the probability of observing spread F during the year) is better developed, its amplitude is larger than in the longitudinal zone near Kodaikanal; with a minimum at winter solstice (Nov.-Jan. in the northern hemisphere and June-August in the southern hemisphere) and maximum at summer solstice (June-August in the northern hemisphere and Nov.-Jan. in the southern hemisphere), its form is approximately

the same in all longitudes. Approaching the place, where the magnetic and geographical equators intersect each other (in the Atlantic), the seasonal variation has an intermediate character (Chandra and Rastogi 1970, Benkova and Depueva 1983). The second property of the longitudinal effect is its different dependence on solar activity; in the vicinity of Huancayo it is inversely proportional, in the neighbourhood of Kodaikanal directly proportional to solar activity. This property of the longitudinal effect is illustrated in Fig. 1 taken from Chandra and Rastogi (1970). A similar longitudinal effect is characteristic also of the night-time sporadic E layer. At equatorial stations (and generally at low latitudes) a flat Es layer occurs often and can be both transparent and blanketing.

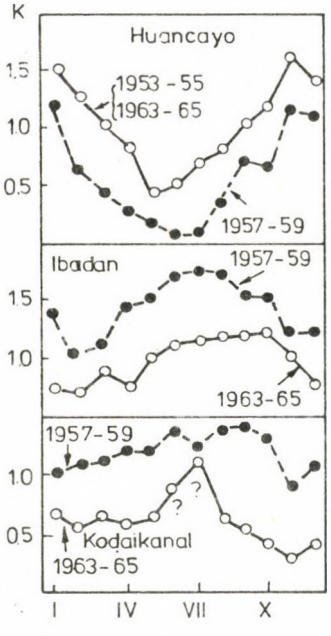

Fig. 1.

In Fig. 2 the seasonal variation of the probability of E_{sf} occurrence in Kodaikanal (Chandra and Rastogi 1974) and the histogram showing the seasonal variation of E_{sf} occurrence in Huancayo (constructed on the basis of data by Rastogi 1977) are presented. The similarity of the seasonal variations of E_{sf} to

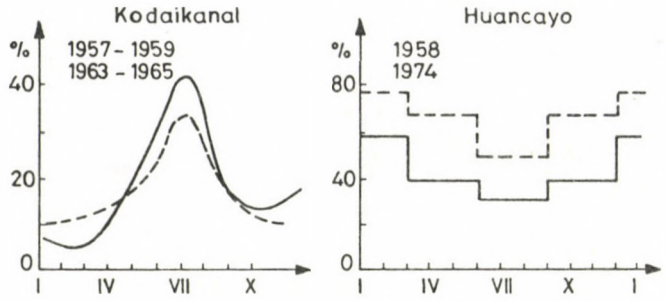

Fig. 2.

the seasonal variations of spread F is striking, i.e. the summer maximum in both hemispheres. Considering the dependence of E_{sf} on solar activity, in the Indian sector it is directly proportional and in the West-American sector inversely proportional to solar activity. In the region of intersection of the magnetic and geographical equators, E_{sf} as spread F has an intermediate seasonal variation. In Fig. 3 the seasonal variation of spread F in this area of the Atlantic taken from Benkova and Depueva (1983) is plotted. In the same figure the probability of E_{sf} in the low latitude zone of the Atlantic in different months are shown by crosses based on data of the vertical sounding on board of the research vessel "Akademik Kurchatov". Although they do not give the whole seasonal trend of the phenomenon, the similarity to the seasonal variation of spread F is evident. Regarding the characteristics of the longitudes between 75 W and 75 E it should additionally be mentioned that at the station Ibadan (Africa) a well defined seasonal variation of spread F and a weak variation of E_{sf} with a low maximum in summer and minima at the equinoxes are observed. The seasonal variation of spread F is directly proportional to solar activity (see Fig. 1), but substantial dependence of E_{sf} on solar activity could not be revealed (Awe 1971).

In an attempt to explain the morphological properties (longitudinal-seasonal variation, relation to solar activity) of spread F the similarity between the behaviour of spread F

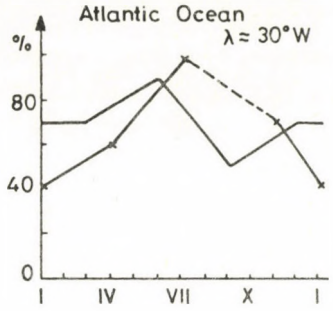

Fig. 3.

and E_{sf} shown above has to be taken into account, in spite of the fact that this similarity appears in general statistical regularities, however in individual cases an unambiguous relation could not be found. The similarity in question proves that for an intensification of irregularities both at the level of the E-region and in the upper ionosphere the same heliogeophysical conditions are favourable. From this point of view the hypothesis relating spread F to long lived metal ions looks promising (e.g. Hanson et al. 1973). The role of metal ions in the formation of Es (including the equatorial area) has been many times demonstrated. In connection with the general increase of electron density and the strengthening of dynamical processes the positive correlation between spread F and E_{sf} is mentioned by many authors. The more complicated question of negative correlation in the relatively narrow West American sector has been studied by Pancheva et al. (1983) from the point of view of confined electric fields affecting the precipitation of particles being especially intense in the South-American region.

REFERENCES

Awe O 1971: J. atmos. terr. Phys., 33, 1209-1222.

Benkova N P, Depueva A H 1983: In: Problems of Physics and Modeling of the Ionosphere. Moscow, 93-97.

Chandra H, Rastogi R G 1970: J. atmos. terr. Phys., 32, 439-443.

Chandra H, Rastogi R G 1974: Curr. Sci., 43, 533-535.

Hanson, McClure, Sterling 1973: J. Geophys. Res., 78.

Pancheva D, Samardzhiev D, Samardzhiev T 1983: Bulg. Geof. Spisanie 9, 51-62.

Rastogi R G 1977: Indian J. Radio and Space Phys., 6, 102-109.

Acta Geod. Geoph. Mont. Hung., Vol. 22 (1-2), pp. 183-190 (1987)

VARIATIONS OF Es PARAMETERS IN DIFFERENT GEOPHYSICAL CONDITIONS

L P Korsunova[1], T A Gorbunova[1], V D Bakaldina[1]

[1]Physical-Technical Institute, Academy of Sciences of the Turkmen SSR, 744000 Ashkhabad, Gogol u. 15, USSR

Dependence of the virtual height of Es layers (h'Es) and that of the range of semi-transparency has been studied on solar and magnetic activity. It was found that h'Es decreases with increasing solar activity at latitudes to the south of 50°N, while at latitudes to the north of it, the opposite relation applies. As regards geomagnetic activity a tendency of increased h'Es values and range of semi-transparency with increasing Kp was revealed in all seasons at latitudes northward of 50°N.

Keywords: ionospheric sporadic E; semi-transparency; turbopause

Considering the Es layer as an indicator of turbulent processes in the lower thermosphere (Ovezgeldiev et al. 1977), regularities of the variations of the virtual height h'Es and of the range of semi-transparency have been studied during the solar cycle, as well as in geomagnetically disturbed periods. For this purpose data of the hourly measurements of Es parameters were used from vertical sounding stations located in the same longitude zone ($\sim 60^{\circ}$E), but at different latitudes of the northern hemisphere [Heiss Island ($\sim 80^{\circ}$N), Moscow ($\sim 56^{\circ}$N), Ashkhabad ($\sim 38^{\circ}$N), Djibouti (12°N)] from the period 1958-68. In order to eliminate the local time effect and for a reliable identification of the height, night-time data (2004 LT) were selected. These data were grouped according to the individual summer (May-August) and winter (November-February) months, then for each of them the monthly mean value of the Es layer virtual height h'Es and that of the range of semi-transparency were calculated.

A comparison of these values with the corresponding Wolf numbers (W) has shown that the variation of the range of semi-

-transparency with solar activity is rather irregular, while in the height change some regularity can be observed.

The character of the relation between the height of the Es layer and the sunspot number was deduced for the winter months from curves of the values h'Es = f(W), (Fig. 1). In spite of a significant scatter of the points at each station a height change of Es layers with solar activity can be traced. The observed scatter may be due either to the quasi-biannual variations of h'Es (Korsunova et al. 1983) or to instrumental errors. It follows from Fig. 1 that there is a positive correlation at $\varphi > 50^{o}$N between h'Es and solar activity while at $\varphi < 50^{o}$N a negative correlation exists; more precisely h'Es increases from 103 to 110 km with increasing solar activity at the station Heiss Island, at the station Moscow it increases from 107 to 115 km, however, at the station Ashkhabad the height of the Es layers decreases from 105 to 100 km. At the low latitude station Djibouti the height of the Es layer also decreases with increasing Wolf numbers from 115 to 107 km. The correlation coefficients computed for the stations Djibouti, Ashkhabad, Moscow

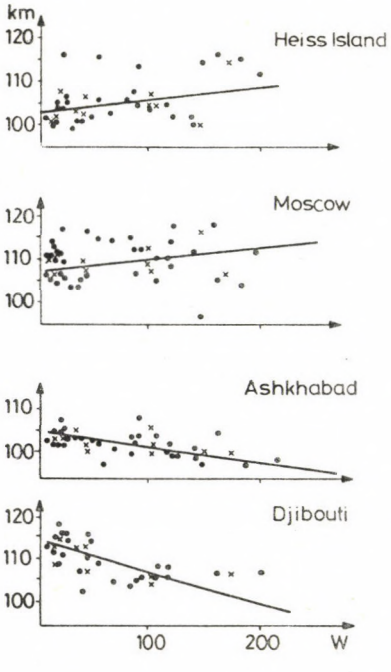

Fig. 1. Relation between h'Es and sunspot number

and Heiss Island from all h'Es and W values amount to -0.56, -0.62, 0.27 and 0.47, respectively. The significance of these coefficients exceeds the 99 % level with the Student-probe in case of stations Ashkhabad and Djibouti, at Heiss Island it reaches the 95 %, while in case of Moscow it does not reach the 90% level of significance. Consequently, a real connection may only exist between h'Es and the sunspot number at latitudes $\varphi < 50^{o}$N. In the latitude range from 10 to 50^{o}N, the variation of h'Es is opposite to that of the sunspot number. Since for the analysis night-time values of h'Es were selected, when absorption is practically absent, the variation of the Es layer heights with the solar cycle is due to internal properties of the layer. As h'Es indicates the height of the turbopause, the turbopause would sink with increasing solar activity at mid--latitude and rise at high-latitudes.

The seasonal and latitudinal variations of the turbopause was deduced in different periods of solar activity for the years of maximum (1958-61) and minimum (1962-66) solar activity from the monthly mean values of h'Es at stations located in the mid-latitude zone ($\varphi < 50^{o}$N), where the significance of the solar cycle variations is high. In case of the station Djibouti data of the years 1967 and 1968 have also been included, since the data of the previous solar activity maximum were not sufficient. In case of the majority of the stations the number of monthly means exceeded 100. For the latitude range 10-50^{o}N the calculated h'Es values are plotted in Fig. 2. The correlation between the height of the sporadic E layers and solar activity is also here negative and the solar cycle variation is maximum at low latitudes. The amplitude of the effect does not depend on the season and the rise of the Es layer is followed at $\varphi < 46^{o}$N in the year of minimum solar activity in summer by an increase of the range of Es semi-transparency. In the vicinity of $\varphi \sim 50^{o}$N the sign of the effect switches to the opposite so that the value of the range of Es semi-transparency becomes larger with increasing solar activity. These results were confirmed by an analogous analysis carried out for stations of the southern hemisphere.

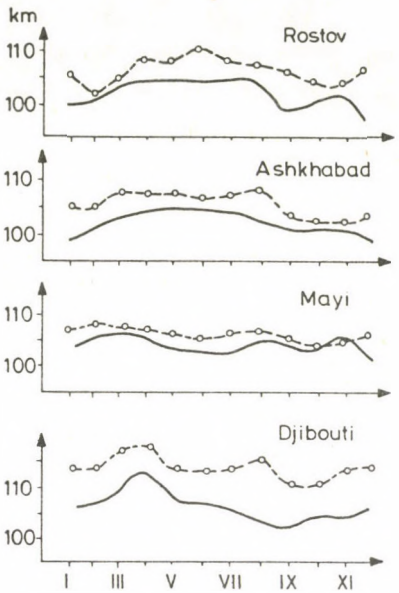

Fig. 2. Seasonal variation of h'Es for different levels of solar activity:
maximum solar activity
(———)
minimum solar activity
(o--o--o)

There are some references that the height of the Es layer h'Es shows some variation during the solar cycle (Samardzhiev and Serafimov 1972). Nevertheless, the solar cycle variation of the Es parameters have formerly been attributed to the conditions of observations, to the changes of absorption in the D region of the ionosphere and to variations of the E region ionization with solar activity. If in the period of maximum solar activity the enhancements of the E and Es layer critical frequencies are due to increases of the solar ionizing radiation, the variation of the height of the Es layer formation indicates that the dynamical conditions, especially the height variation of wind shear change substantially. The possibility of the solar cycle variation of the neutral wind shear and of the corresponding changes of the Es parameters were also mentioned by Reddy and Matsushita (1968).

In so far as the effectivity of the redistribution of ionization due to wind-shears decreases rapidly with decreasing height, the average probability of the Es formation has to

decrease with increasing solar activity at mid-latitudes as it has been observed. Consequently, the variation of PEs during the solar cycle can be partly explained by internal physical processes and not only by variations of the absorption. The conflicting results obtained by different authors on variations of the Es parameters during the solar cycle may be related to the change of sign of the effect with latitude.

Since the sporadic E layer is formed in the zone of the turbopause at mid-latitudes, the results obtained indicate a real decrease of the turbopause height with increasing solar activity at latitudes $< 50^{o}$N and confirm results by Zimmerman and Murphy (1977) and by Danilov et al. (1980) on an inverse relation between the height of the turbopause and solar activity in a limited amount of material.

The influence of the geomagnetic activity on the turbopause has not been studied so far, though it is an important problem. The morphology of the Es layer shows that its relation to changes of the geomagnetic field depends substantially on latitude. Since the Es layer is a tracer of the turbopause, a similar behaviour may be characteristic of the turbopause parameters. This is confirmed by Danilov et al. (1980) and by Bencze and Märcz (1981) on the basis of measurements in Heiss Island and in Juliusruh.

The relation between ionospheric sporadic E and geomagnetic activity has been reviewed by Chavdarov et al. (1975). Here special attention was paid to the probability of Es occurrence. There are indications that the virtual height of the ES layers h'Es is larger on geomagnetically disturbed days than on quiet days. Nevertheless it is difficult to estimate the real variations of h'Es in geomagnetically disturbed periods, because the group retardation of the radio signals is subtantial in day-time. For the elimination of this effect, night-time Es observations were studied when h'Es corresponded to the real height of the layer.

Since variations in h'Es are due to changes in the dynamics of the medium, it had to be taken into consideration that the reaction of the neutral atmosphere is delayed at mid-

-latitude as compared to the main phase of the magnetic storm by at least one day. Thus, night-time measurements of h'Es carried out at the stations Moscow, Rostov, Ashkhabad were selected in the period of maximum solar activity (1958-60) and then grouped according to seasons. As indicator of the geomagnetic activity, the daily sum of Kp indices was used taking into account the effect of the delay ($\Delta\tau \approx 1$ day).

The relation between h'Es and the daily sum of Kp indices is presented at the station Moscow for the different seasons in Fig. 3, where each point represents the mean of the night-time values of h'Es for one day. The h'Es values corresponding to

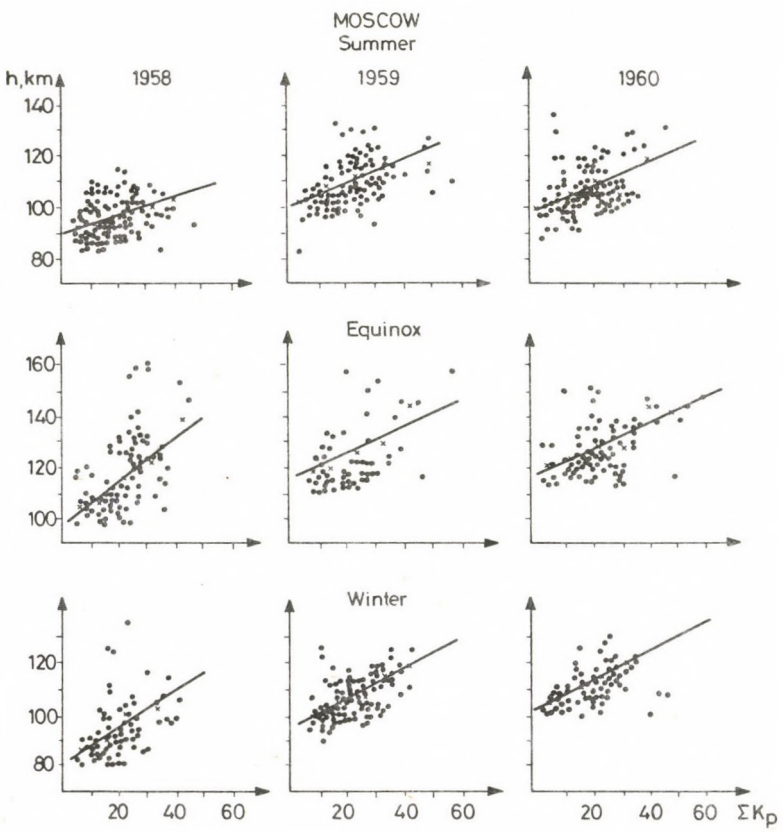

Fig. 3. Relation between h'Es and the daily sum of Kp at the latitude of Moscow for different seasons

certain values of the daily sum of Kp indices are denoted by crosses. h'Es increases continuously with increasing Kp values in all seasons, the scatter of the points is large even in geomagnetically quiet periods. In the period of solar activity studied here the change from year to year is insignificant. The latitudinal boundary of the effects was determined by means of the same method from the behaviour of h'Es in the same years at the stations Rostov and Ashkhabad. A moderate enhancement of h'Es with increasing geomagnetic activity occurs at station Rostov but it is practically missing at Ashkhabad. Consequently, the latitude $\sim 46^{\circ}$N can be considered as the southern boundary for the occurrence of the geomagnetic disturbance effect. As the Es layer is an indicator of the behaviour of the turbopause, the height of the turbopause increases to the north of 50°N in geomagnetically disturbed periods. This fact should be considered when constructing thermospheric models.

Thus, the analyses carried out lead to the following conclusions:

1. h'Es and the range of semi-transparency increases at latitudes $\varphi > 46^{\circ}$N with increasing solar and geomagnetic activity,
2. south of $\varphi = 46^{\circ}$N, the sign of the effect changes to the opposite,
3. similar variations of the height of the turbopause with solar and geomagnetic activity can be inferred from the results obtained here.

REFERENCES

Bencze P, Märcz F 1981: Acta Geod. Geoph. Mont. Hung., 16, 405-414.

Chavdarov S S, Chasovitin Yu K, Chernisheva S P, Sheftel V M 1975: Ionospheric sporadic E at mid-latitudes (in Russian). Nauka, Moscow.

Danilov A D, Kalgin Yu A, Pokhunkov A A 1980: Geomagnetizm i aeronomiya, 30, 474-476.

Korsunova L P, Gorbunova T A, Bakaldina V D 1983: Geomagnetizm i aeronomiya, 23, 113-115.

Ovezgeldiev O G, Korsunova L P, Bakaldina V D 1977: In: Physical processes in the upper atmosphere. Llyim, Ashkhabad

Reddy C A, Matsushita S 1968: J. Geophys. Res., 73, 1600-1641.

Samardzhiev D, Serafimov K 1972: Izv. Geoph. Inst. Bolg. AN, 18, 77-92.

Zimmerman S P, Murphy E D 1977: In: Dynamical and Chemical Coupling Between the Neutral and Ionized Atmosphere, Dordrecht-Holland, 35-47.

Acta Geod. Geoph. Mont. Hung., Vol. 22 (1-2), pp. 191-198 (1987)

THE Es LAYER DURING GEOMAGNETIC SUBSTORMS

O M Pirog[1], Yu I Vakulin[1], E I Nemtsova[1], V D Urbanovich[1]

[1]Sibirian Institute of Geomagnetism, Ionosphere and Radio Wave Propagation (SibIZMIR), 664033 Irkutsk 33, P.O.Box 4, USSR

An analysis of the simultaneous measurements of the geomagnetic field and ionospheric parameters has been carried out, based on the data of the experiment "Taymir 82". Specific features of the behaviour of the Es layer at different latitudes during substorms have been revealed. It has been found on the basis of auroral stations that the development of the substorm is preceded by a reduction of fbEs to the perfect vanishing of the layer. At subauroral latitudes the opposite effect is observed. Before substorms the zone of sporadic ionization in the E region moves in the evening and midnight hours towards the equator, then expands suddenly to the pole with fbEs increasing simultaneously. Comparing the location of the area of maximum fbEs values with the structure of the electrojet the conclusion can be drawn that the westward electrojet is located to the north of the zone of maximum conductivity.

Keywords: auroral electrojet; geomagnetic substorm; sporadic E layer

Geomagnetic and ionospheric disturbances are manifestations of the energy produced during the development of the magnetospheric substorm and are consequently interrelated. In previous papers (Goreliy et al. 1980a, 1980b, Blagoveshchenskaya and Pirog 1982, Zherebtsov et al. 1982) the dependence of the variations of ionospheric parameters on geomagnetic activity has been studied and it was found that at the latitude of Norilsk the Es_r layer appears 0.5-1.5 hours before the onset of the substorm in the H component of the geomagnetic field and the electron density in the layer varies during the substorm simultaneously with the variations of H. At this time the parameters of the F2 layer change insignificantly. Thus in Norilsk the occurrence of the Es_r layer may be a precursor of the substorm (Blagoveshchenskaya and Pirog 1982). Unfortunately, there were no simultaneous geomagnetic and ionospheric measurements at other stations.

Acta Geod. Geoph. Mont. Hung. 22, 1987
Akadémiai Kiadó, Budapest

Nevertheless the variations of $foEs_r$ do not correspond in Dixon to the observations in Norilsk (Goreliy et al. 1980b).

During the experiment "Taymir 82" (Vakulin et al. 1984) in 1982 the variations of the geomagnetic field and that of the state of the ionosphere could be simultaneously recorded at four points located along the meridian $\lambda = 90^{o}$ in the range of latitudes $62^{o} < \Phi < 69^{o}$. This enabled to continue the study of the dynamics of magnetospheric disturbances.

The variations of the ionospheric parameters and the H component of the geomagnetic field were analysed in the whole period of observations (December, 1982 - March, 1983). The analysis confirmed the finding that the state of the F region is determined by its location as compared to the main trough of ionization which depends on the mean level of disturbance characterized by Kp (Zhrebtsov et al. 1982). During the night the critical frequency of the F_{2s} layer varies between 4 and 6 MHz. In case of large disturbances no F region can be seen because of screening by the Es layer or due to total absorption. The behaviour of the Es layer is more interesting.

In Fig. 1 simultaneous variations of fbEs and of the H component are shown for four stations plotted according to decreasing latitude. As examples, typical isolated substorms were selected on a quiet background in the evening hours, at midnight and after midnight. The electron density in the Es layer is characterized by fbEs. If the Es layer is absent, the minimum frequency reflected from the F region can be taken instead of fbEs, in case of total screening or absorption the maximum frequency of the F2 layer observed previously. The most characteristic features of fbEs are the decrease at the auroral stations and the increase at subauroral stations before the onset of negative bays. Moreover, at high latitude the beginning of the decrease of fbEs can be preceded by the beginning of the negative disturbance in the H component which is not observed at subauroral stations where the substorm is preceded by the occurrence of the Es_r layer (Goreliy et al. 1980b, Zherebtsov et al. 1982). That means that within the auroral zone negative disturbances of high intensity develop in case of low E-region ionization (See Fig.1

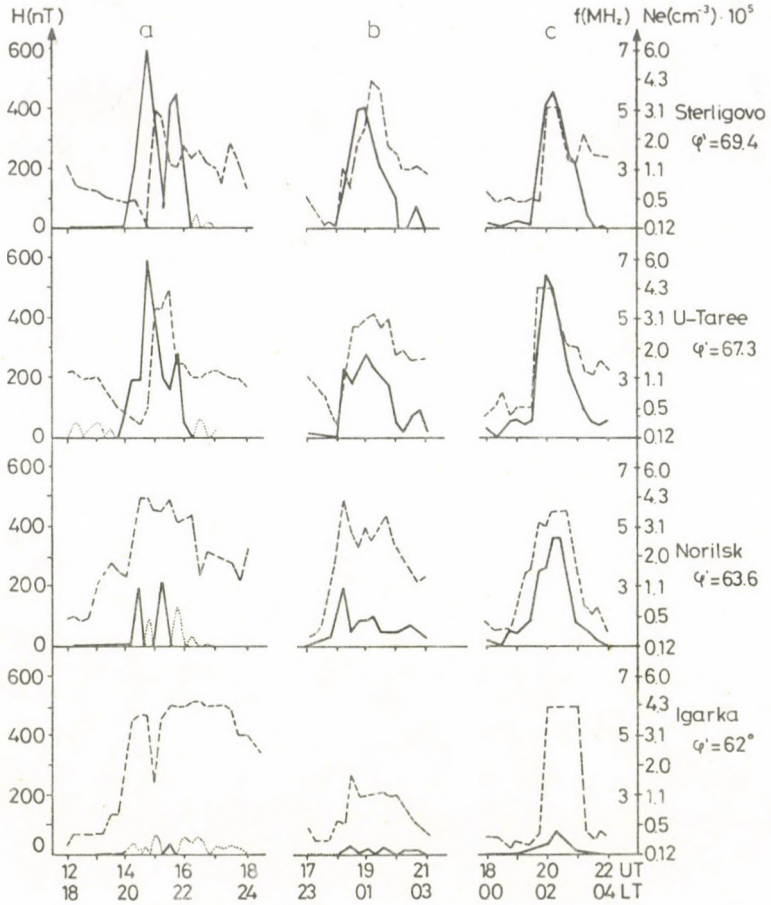

Fig. 1. Variations of ΔH and fbEs during substorms observed at a meridional chain of stations (a) before midnight, (b) at midnight and (c) after midnight. ΔH < 0 (——), ΔH > 0 (.....), fbEs (-----)

ΔH ~ 600 nT, $N_e \sim 10^4$ cm^{-3} in Sterlegovo and Ust-Taree) while at the southern boundary of the zone weak bays are observed in case of $N_e > 10^5$ cm^{-3}. The appearance of an Es layer after the onset of a geomagnetic substorm is more often observed in the evening hours. After midnight the simultaneous development of the geomagnetic and ionospheric disturbances is more probable. All statements above relate to negative disturbances. Positive disturbances are observed at all stations used here in case of

enhanced E region ionization.

The temporal and spatial distribution of Es layers during a substorm are confirmed by the results of a statistical analysis shown in Figs 2 and 3. It follows from Fig. 2 that the probability of a delay of the fbEs growth as compared to the onset of the geomagnetic substorm ($t_0^H < t_0^S$) decreases with decreasing latitude. The increase of fbEs is preceded by the onset of the bay in the H component most often at Sterlegovo, more rarely at

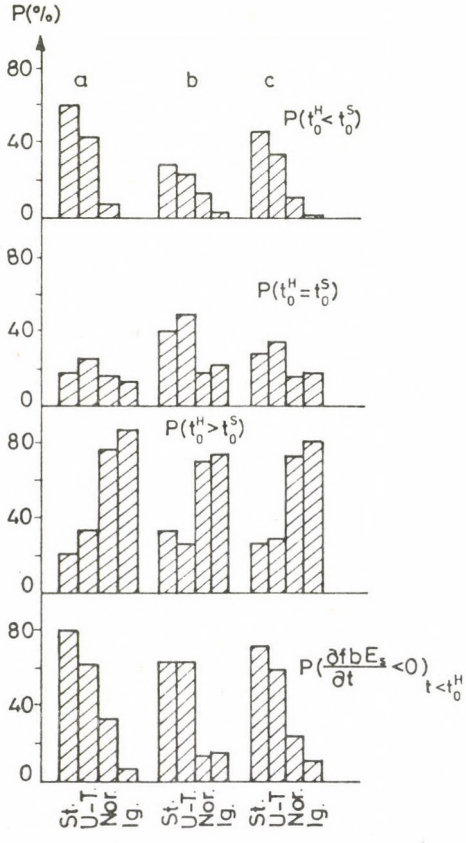

Fig. 2. Variations of the probability of the different type Es layer behaviours as compared to changes of the H component. Here t_0 is the time of the beginning of fbEs growth, t_0^H is the time of onset of the geomagnetic disturbance, (a) before midnight, (b) after midnight and (c) for the whole night

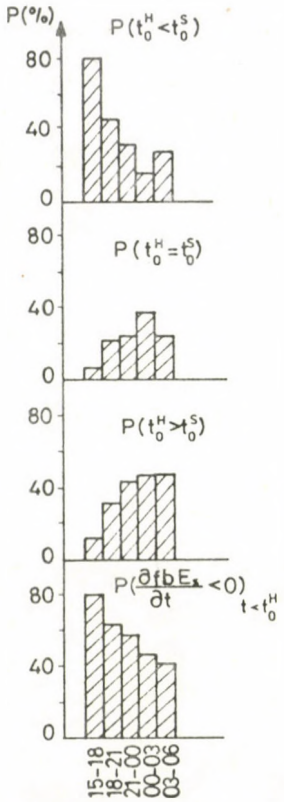

Fig. 3. Variations of the probability from evening to morning, averaged for all stations. The symbols are the same as in Fig. 2.

Ust-Taree and almost never at Igarka. The probability of the simultaneous increase of the geomagnetic intensity H and of fbEs ($t_o^H = t_o^S$) is maximum in Ust-Taree. Cases of the delay of the substorm commencement as compared to the development of the Es layer ($t_o^H > t_o^S$) predominate in Norilsk and Igarka [$P(t_o^H > t_o^S)$ = = 70-85 %]. The decrease of fbEs to the perfect vanishing of the Es layer before the onset of the substorm is observed with the highest probability at Sterlegovo (up to 80 %) and Ust-Taree ($\sim$60 %). In these cases the minimum reflected frequencies decrease to 1-2 MHz. In Norilsk and Igarka the probability of similar cases is significantly lower and fbEs remains more than 3 MHz, i.e. at subauroral latitudes the electron density in the E region is 2-3 times larger than within the zone.

The diurnal variations of the probabilities show that

$P(t_o^H < t_o^S)$ is maximum in the evening hours, decreases toward midnight and then increases again. $P(t_o^H = t_o^S)$ increases toward midnight and has a maximum in the period 0003 LT. $P(t_o^H > t_o^S)$ and $P\left(\frac{\partial fbEs}{\partial t} < 0\right)$ vary oppositely what is obvious, since they are phenomena excluding each other. $P(t_o^H > t_o^S)$ increases from evening to morning and $P\left(\frac{\partial fbEs}{\partial t} < 0\right)_t < t_o^H$ decreases.

The dynamics of the zone of increased ionization in the E region is compared in Fig. 4 with the structure of the electrojet. For the sake of simplicity isolated substorms were selected in the presence of only one westward electrojet shown in Fig. 1, when the positive deviation of the H component from the zero level is less than 50 nT except on December 22, 1982. It follows from the map of contour-lines of ΔH and fbEs that the areas of maximum negative values of ΔH, $\Delta Z = 0$ and of maximum electron density in the Es layer coincide partially, however, the latter is always located equatorwards. Thus the main current in the westward auroral electrojet does not flow in the region of maximum conductivity, but somewhat to the north of it. Before substorms in the evening and at midnight

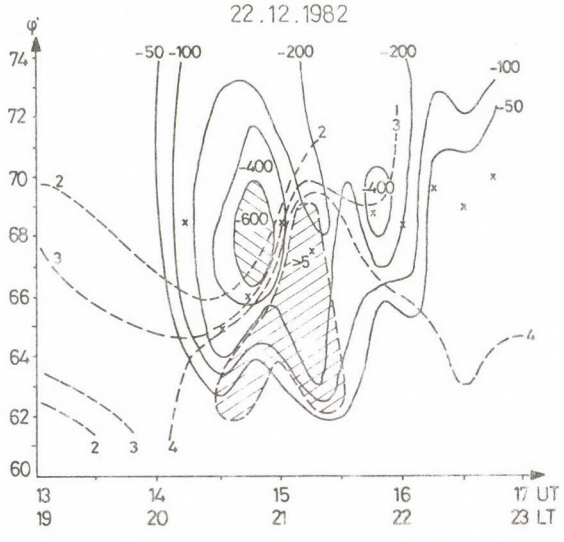

Fig. 4a. Map of the contour lines of the geomagnetic component ΔH and fbEs constructed for substorms on the basis of Fig. 1. Numbers at the contour lines denote ΔH(nT) and fbEs(MHz). ΔH (———), fbEs (-----), $\Delta Z = 0$ (xxxxx)

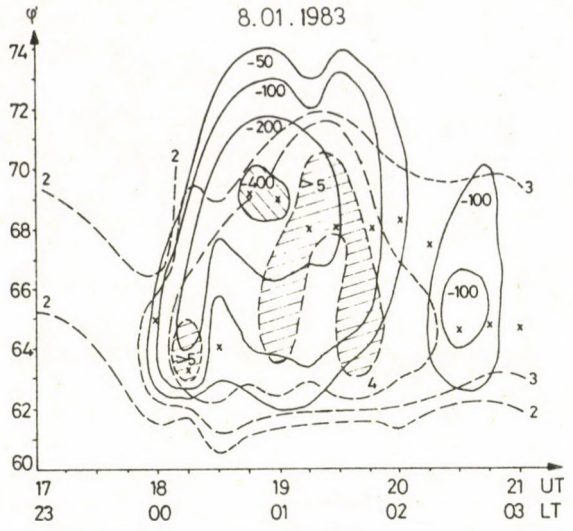

Fig. 4b

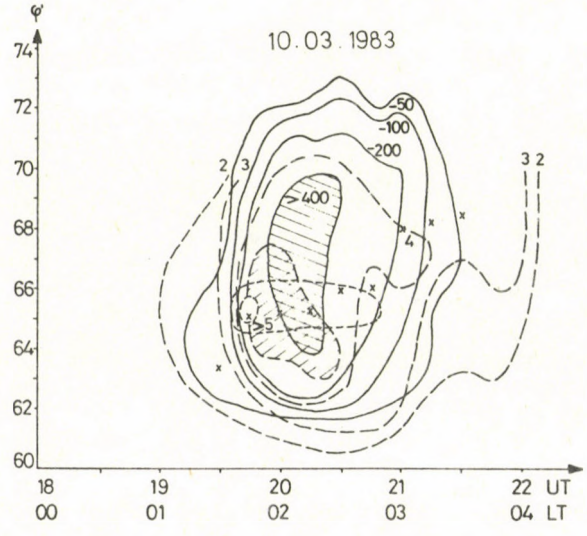

Fig. 4c

the equatorward motion of the zone of sporadic ionization in the E region starts, then the sudden expansion follows to the pole with a simultaneous increase of fbEs. In this process the poleward motion of the Es zone is correlated to the break-up phase of the substorm. The maximum of the sporadic ionization

can be located in the morning or evening side of the maximum of ΔH depending on local time.

The specific features of the variations of fbEs during the development of a substorm correspond to the morphology of the intensity of background airglow in the auroral upper atmosphere (Vakulin et al. 1979).

Thus the results obtained confirm Vakulin et al.'s conclusion (1979) that the electrojet does not flow there where the ionization and conductivity are maximum, but in the region to which the minimum inner resistance of the magnetospheric source is mapped.

Nevertheless, a number of the regularities shown by the variations of the electron density in the Es layer at auroral latitudes demand further investigations and theoretical interpretation during substorms.

REFERENCES

Blagoveshchenskaya N F, Pirog O M 1982. In: Issl. Geomagn. Aeron. Fiz. Solntsa, Nauka, Moscow, No 58, 58-67.

Goreliy K I, Pirog O M, Urbanovich V D 1980a: In: Issl. Geomagn. Aeron. Fiz. Solntsa, Nauka, Noscow, No 50, 81-85.

Goreliy K I, Nemtsova E I, Pirog O M, Urbanovich V D, Ponomarev E A 1980b: In: Issl. Geomagn. Aeron. Fiz. Solntsa, Nauka, Moscow, No 50, 92-98.

Vakulin Yu I et al. 1979: In: Issl. Geomagn. Aeron. Fiz. Solntsa. Nauka, Moscow, No 46, 3-12.

Vakulin Yu I et al. 1984: In: III. All-Union Meeting on "The Polar Ionosphere and Magnetosphere-Ionosphere Relations". Book of Abstracts, Apatiti, 58-59.

Zherebtsov G A, Pirog O M 1982: In: Issl. Geomagn. Aeron. Fiz. Solntsa, Nauka, Moscow, No 59, 148-154.

Zherebtsov G A, Nemtsova E I, Pirog O M, Urbanovich V D 1982: In: Issl. Geomagn. Aeron. Fiz. Solntsa, Nauka, Moscow, No 58, 141-150.

Acta Geod. Geoph. Mont. Hung., Vol. 22 (1-2), pp. 199-209 (1987)

SPORADIC E LAYER IN THE TWILIGHT PERIOD DURING WINTER AND ITS RELATION TO SUNRISE IN THE CONJUGATE AREA

V P Abramchuk[1], V N Oraevsky[1], Yu Ya Ruzhin[1]

[1]Institute of Geomagnetism, Ionosphere and Radio Wave Propagation (IZMIRAN), Academy of Sciences of the USSR, 142092 Troitsk, Moskovskaya oblast, USSR

A maximum in the occurrence probability of sporadic E layers has been found based on the data of the network of ionospheric sounding stations in the twilight period during winter. Conclusions have been drawn on the basis of the analysis of six years' data from the period December-January (symmetrically to the winter solstice equal time intervals have been selected). A definite relation of the occurrence of the sporadic E layer has been revealed with the sunrise in the magnetically conjugate area.

It is suggested that the sporadic E layer formation can be explained by a mechanism due to the magnetospheric propagation of non stationary Alfven waves generated in the ionosphere by the supersonic motion of the terminator in the lower layers of the atmosphere. The occurrence of a sporadic E layer due to the electrostatic interaction of the magnetically conjugate areas of the ionosphere has also been studied.

Keywords: magnetically conjugate area; sporadic E layer; terminator

INTRODUCTION

In the last years the problem of the relation between the processes in the lower atmosphere and in the upper layers of the ionosphere got into the centre of interest. It has been found that earthquakes, lightning discharges, fall of meteorites, the supersonic motion of the terminator (Somsikov and Troitsky 1975) etc. are powerful sources producing disturbances in the neutral component of the ionosphere. In the dynamo region of the ionosphere, where the ion-neutral collision frequency exceeds the ion gyrofrequency, there is a real possibility for the transfer of motion of the neutral component to the ionized, i.e. the motion of the neutrals and ions is strongly interrelated in the weakly ionized plasma of the lower ionospheric layers (Ignatev 1969, Gershman et al. 1976).

If the geomagnetic field lines are considered as equipotentials there is an electrostatical connection between the magnetically conjugate ionospheres resulting in a symmetrical behaviour of the ionospheric layers of the two hemispheres (Mozhaev et al. 1976). The symmetry may be upset in case of unequal illumination of the magnetically conjugate ionospheres especially in the solstice period, when in one of the ends of the geomagnetic field lines the ionosphere is illuminated by the Sun, but the other end is in darkness. In such conditions it is expected that disturbances in the lower layer affect the processes in the magnetically conjugate ionosphere due to the fast motion of the shade boundary.

In the present paper the authors call attention to the energy transfer from the ionosphere of one hemisphere to the other due to the magnetospheric propagation of non-stationary Alfven waves generated in the ionosphere by the supersonic motion of the terminator in the lower layers of the atmosphere. Suitable magnetically conjugate points are the mid-latitude stations Krasnaya Pakhra ($55^{o}28'$N, $37^{o}19'$E) and a point in the Indian Ocean ($42^{o}36'$S, $56^{o}24'$E). As an indicator of the energy transfer the occurrence of a sporadic E layer above the mid-latitude ionospheric station at night in the period of the winter solstice has been selected (Abramchuk and Ruzhin 1985).

EXPERIMENTAL RESULTS

The occurrence probability of a sporadic E layer (PEs) was studied in the winter period on the basis of the data of the ionospheric stations Krasnaya Pakhra, Alma Ata and Karaganda for the time interval from 1976 to 1982. Data symmetrical to the date of the winter solstice were selected in order to enable an analysis of the violation of the symmetry in case of the illumination of the magnetically conjugate area. Moreover, any kind of sporadic E layers was taken into account in the period from 21 hour to 8 hour. Since in the period considered here the variation of the Es occurrence probability is approximately uniform at the above mentioned stations (considering only the difference between the sunrise in the magnetically conjugate

area and the point of observation for these stations), the data of the station Krasnaya Pakhra were only used.

In Fig. 1 the night-time variation of the occurrence probability of an Es layer is shown for the years 1976-1982. Disregarding individual fluctuations in the curve (they are described in more detail in the paper by Abramchuk and Ruzhin 1985) the occurrence probability of a sporadic E layer has two deep minima in the twilight period (the first in the time interval from 2 to 3 h LT and the second in the period from 6 to 7 h LT) having approximately the same magnitude, further a maximum at about 5 h 30 m LT. In the maximum the value of PEs is approximately 20 % greater than the value of PEs in the minima.

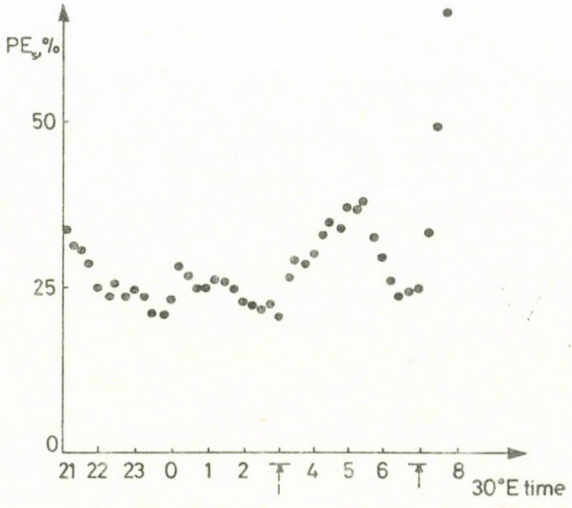

Fig. 1. Occurrence probability of the Es layer for December and January of the period from 1976 to 1982 (on the basis of the data of the station Krasnaya Pakhra)

As computations have shown this phenomenon may be connected to the sunrise at the observing site and in the magnetically conjugate area. In Fig. 1 the variations of the times of the sunrise are shown by thick horizontal lines in the height of the ozone layer for the months December and January at the observing site (thick arrow) and in the magnetically conjugate

area (dashed arrow). This question will be discussed later in more detail. At stations located at latitudes lower than the station Krasnaya Pakhra (e.g. at Alma Ata, Karaganda) the twilight effect is somewhat masked in the occurrence probabilita of Es because of the small time difference between the sunrises at the observing site and at the magnetically conjugate point.

The course of the PEs curves has shown in the months December and January of selected years that the so called twilight effect (on the analogy of the diurnal variation of foF2 (Bukin et al. 1968)) appears in this case less often in the period of solar activity minimum, but it remains detectable (Abramchuk and Ruzhin 1985). The variation of the occurrence probability of the Es layer in years of different solar activity hints at the fact that even if there is a connection between PEs and the level of solar activity, then PEs does not depend on the number of sunspots or on their area rather it depends on the limits of the variations of these parameters.

The experimental data confirmed the twilight time dependence of the critical frequency of the sporadic E layer (foEs). A typical curve demonstrating such a dependence is shown in Fig. 2. The curve presented here indicates this dependence

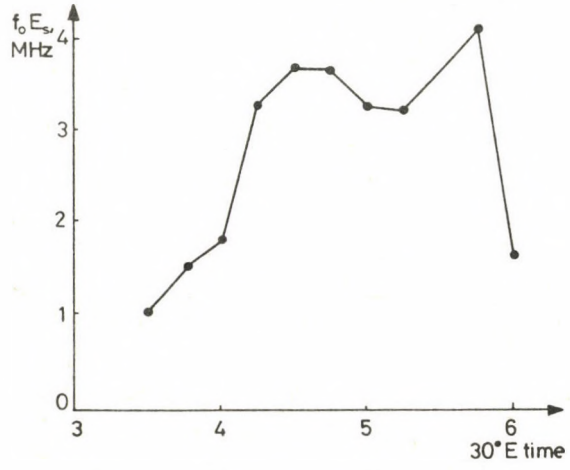

Fig. 2. Critical frequency of the Es layer in the twilight period

quite qualitatively, since for a more detailed study of the time variation of the Es parameters continuous sounding of the ionosphere is needed as according to the observations the sporadic E layer is submitted to fast variations. The time dependences of PEs and foEs (Figs 1 and 2) are similar and the great amount of data enables to conclude that this correlation is not accidental. The correlation between PEs and foEs in the twilight period indicates the change of the effectivity of the mechanism responsible for the formation of Es layers in the same period. During the minima of the occurrence probability of an Es layer its critical frequency does not reach 1 MHz. Obviously, the use of ionosondes with a frequency range extended to lower frequencies and the continuous sounding of the ionosphere would promote the study of these effects and of their relation to other ionospheric parameters.

The following analysis was made for a more reliable clarification of the connection between the formation of sporadic E layers and sunrise in the magnetically conjugate area and in the observing site. Those days of the months December and January were considered at the station Krasnaya Pakhra in the time interval 1976-1982 when the sporadic E layer appeared near or during the twilight period. The days, when an Es layer was observed earlier, were excluded. The points in Fig. 3 indicate the time of occurrence of the Es layer in the period studied. Lines are also plotted showing the sunrise at the horizon and in a height of 60 km in the magnetically conjugate area of the station Krasnaya Pakhra. The greatest part of the data is located above the line showing the sunrise in 60 km altitude what confirms the conclusion drawn above.

Times of vanishing (dots) and formation (triangles) of the sporadic E layer in the morning are plotted in Fig. 4 on the basis of the data of the station Krasnaya Pakhra. In the same figure lines show the sunrise at the horizon and in heights of 60, 200 and 500 km. The steep decrease of PEs before morning may be connected with the sunrise at great altitudes at the observing site, and the morning increase of PEs is due to the sunrise at the height of the ozone layer.

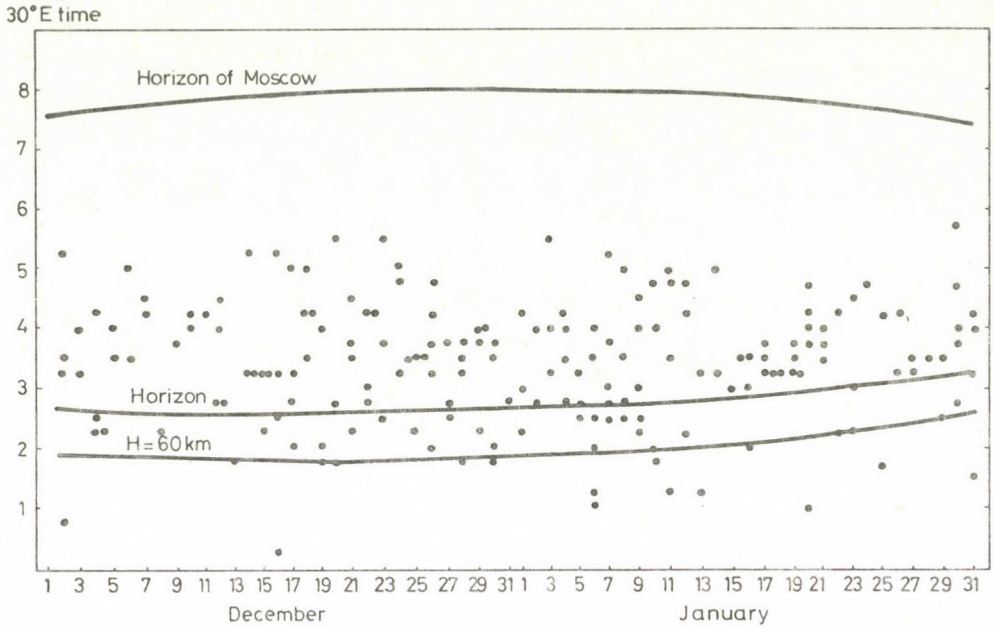

Fig. 3. Time of the appearance of sporadic E layers on ionograms in the twilight period and their relation to the sunrise in the conjugate area (on the basis of the data of the station Krasnaya Pakhra)

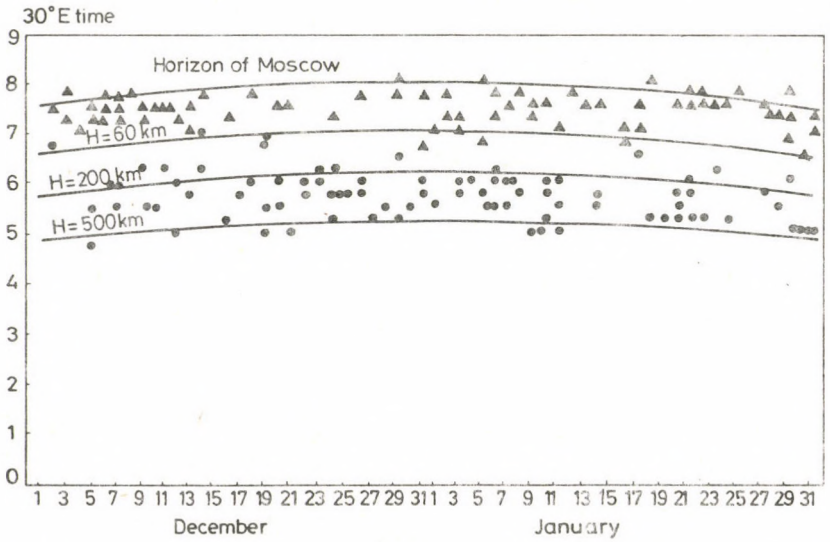

Fig. 4. Time of vanishing (dots) and appearance (triangles) of the sporadic E layer and their relation to the sunrise at the observing site

The virtual height of the sporadic E layer (h'Es) shows also some changes in the period studied here which were considered by Abramchuk and Ruzhin (1985). In the majority of cases an anticorrelation is observed between the values of foEs and h'Es. The strengthening of the Es layer is followed by a decrease of its virtual height, and the reduction of foEs is followed by an increase of h'Es.

This fact and some other phenomena deduced from the experimental data are explained by a mechanism of Es formation in the twilight period suggested below.

Before a discussion of the mechanisms, responsible for the connection of the phenomena in magnetically conjugate areas, the basic features of the phenomenon revealed are listed.

a) The occurrence probability of midlatitude sporadic E layers increases at twilight in the winter solstice period.

b) The increase of the probability is connected with the sunrise in the magnetically conjugate area of the summer hemisphere, and it is due to the appearance of the solar radiation at the height of the ozone layer (below 60 km).

c) The decrease of the occurrence probability of Es layers may be connected with the sunrise above the observing site, but at very great altitudes amounting to 200-500 km.

d) The morning rise of the occurrence probability of Es layers is also connected to the passage of the terminator at the height of the ozone layer, but above the observing station.

e) The relations between the observed effect and the level of solar activity indicates a dependence not on integral characteristics (number of sunspots, their area), but on the dynamics of these parameters in the time interval studied (December-January).

f) The effect appears also at lower latitudes, though, strongly masked by the sunrise at the observing site (see point d).

DISCUSSION

Relations between the magnetically conjugate ionospheres are discussed in a number of papers. This relation appears both

with the occurrence of effects of external, e.g. of magnetospheric origin, and with the transfer of energy from the ionosphere of one hemisphere to the ionosphere of the other hemisphere along geomagnetic field lines. In the latter case, the effects of the energy transfer are most definite during serious violation of the symmetry in illumination of the two areas, especially, if one of the areas is completely illuminated and the other is yet in darkness.

Bukin et al. (1968) discussed the disturbances at the height of the F2 layer produced by the precipitation of photoelectrons coming from the illuminated part of the ionosphere. The conjugate occurrence of sporadic Es formation and variations of their parameters at mid-latitudes may be due to the connection of this layers with the directional fluxes of trapped electrons with energies of 30-100 keV (Ivanov-Kholodny and Lazarev 1966), and to the electrostatic interaction between the magnetically conjugate areas of the ionosphere assuming a high conductivity of the magnetospheric plasma in the magnetic flux tubes and consequently an equipotential character of the geomagnetic field lines (Mozhaev et al. 1976). At mid-latitudes the mechanism connected with directional fluxes of energetic particles is less probable, since fluxes of 10^{10} $cm^{-2}s^{-1}$ are necessary for the formation of sporadic E layers (Ivanov-Kholodny and Lazarev 1966).

The occurrence of sporadic E layers could be explained by an electrostatic link of the conjugate ionospheres. Thus, Kolokolov (1979) studied disturbances of the night-time F2 layer due to the sunrise in the magnetically conjugate area. Because of the electrostatic coupling of the two hemispheres the downward drift of the plasma produced by the westward dynamo field of the summer hemisphere determines in the initial phase the general equilibrium. Later the eastward field connected with the occurrence of steep gradients of the transerve conductivity at the height of the dynamo region increases abruptly with decreasing zenith angle of the Sun in the summer hemisphere. As a result of this the downward drift is gradually substituted by an upward drift. In this case the increase of the probability,

and even more the maximum of the occurrence probability of Es layers at 4-5 h LT refers to the period, when an upward plasma drift has to form due to the electrostatic link in the ionosphere of the night-time hemisphere. According to the wind-shear theory (Gershman et al. 1976) sporadic E layer must not exist in this case. However, in the wind-shear theory the possibility of the formation of a sporadic E layer is considered separately from the turbulence in the dynamo region. Taking into account the turbulent diffusion for the stationary state (sporadic E layer exists) the following relation has been obtained.

$$D\left(\overline{\Delta N'}\right)^2 = D_t\left(\nabla \tilde{N}_o\right)^2 + \frac{\Omega_H}{\nu_{in}}\left(\overline{H}_o \text{ rot } \overline{u}\right)\overline{(\tilde{N}')^2} \ .$$

In normal conditions, regions of increased ionization are formed due to the terms containing the turbulent diffusion coefficient but the effektive molecular diffusion leads to their vanishing. Nevertheless, due to the presence of wind shear and to the effect of the geomagnetic field the term

$$\frac{\Omega_H}{\nu_{in}}\left(\overline{H}_o \text{ rot } \overline{u}\right)\overline{(\tilde{N}')^2} \ ,$$

appears which maintains the irregularities by the wind shear if $\overline{H}_o \text{ rot } \overline{u} > 0$.

Now, we consider the possibility of generation of eddies in the dynamo region due to disturbances in the lower layers of the atmosphere. The source (e.g. the supersonic motion of the terminator at the height of the ozone layer (Somsikov and Troitsky 1975)) can generate a broad spectrum of acoustic waves, however, the longest of them do not reach ionospheric altitudes because of the acoustic cut-off frequency. The same is true for the short waves because of the viscous dissipation. As a result of this atmospheric filtering, the range of periods observed at ionospheric heights is limited to the band from some minutes to some hours. These long wave disturbances of the neutral component propagating from the area of their generation in the near surface layer are dissipated reaching the upper boundary of the

dynamo region due to the transfer of energy to the shorter wave range of the spectrum. An experimental proof is given by Chernisheva et al. (1976), who showed the occurrence of irregular inter-layer formations at altitudes of 150-200 km connected with sunrise.

Eddies developing in the weakly ionized plasma at $\nu_{in} > \Omega_H$, can be the source of Alfven waves (Alfven 1952) in a broad frequency range

$$\omega R \leq 0.5\, u_s,$$

where R is the radius of the eddy, ω its angular frequency and u_s is the velocity of sound.

The Alfven waves are selectively transmitted through the upper layers of the ionosphere to the magnetosphere and reach the conjugate ionosphere nearly without loss (Sen 1971). The small conductivity of the night-time ionosphere allows this flux of waves to get as far as the heights where the wind shear mechanism works. Here, the waves transfer their energy within the skin layer accomplishing the cellular structure of the eddies in the dynamo region of the night-time ionosphere. The "damping" spots are geomagnetically conjugate with the non-stationary eddies of the dynamo region in the other hemisphere. These spots produce either a weak modification (insignificant for ionospheric sounding), or occurrence of chaotic regions of increased ionization forming transparent sporadic E layers depending on their dimensions, on the direction of the eddy electric field, on the height and thickness of the skin layer. In individual cases a stronger layer may also be formed in the E region. Estimates show that the local flux of energy transmitted by Alfven waves is sufficient for the operation of the wind shear in the night-time ionosphere.

Thus the decrease of the occurrence probability of the sporadic E layer after 5 h (30° E time) becomes also clear. The Sun illuminates the upper layers of the ionosphere from 200 to 500 km at this time (Fig. 3), which results in the steep change of the leaking conditions of Alfven waves reaching the conjugate

ionosphere. The increasing conductivity leads to a more effective reflection process in the upper layers of the ionosphere. The morning increase of the occurrence probability of Es may be connected with the increase of turbulence in the dynamo region due to disturbances of the neutral component in the spectrum of acoustic waves propagating from below where they are generated by the fast motion of the shade and by sudden changes of temperature and density in the lower layers of the atmosphere connected with the former in the region of the observing station.

REFERENCES

Abramchuk V P, Ruzhin Yu Ya 1985: Some properties of the night-time mid-latitude sporadic E layer in winter (in Russian). IZMIRAN Preprint No 11 (544), 21.

Alfven H 1952: Cosmical electrodynamics (in Russian). Moscow, 312.

Bukin G V, Evzovich I P, Katsenelson I B 1968: Geomagn. i Aeronomiya, 8, 940-942.

Chavdarov S S, Chasovitin Yu K, Chernisheva S P, Sheftel V M 1975: Mid-latitude sporadic E of the ionosphere (in Russian). Nauka, Moscow

Chernisheva S P, Sheftel V M, Shcharenskaya E G 1976: Geomagn. i Aeronomiya, 16, 809-814.

Gershman B N, Ignatev Yu I, Kamenetskaya G Kh 1976: Mechanisms of formation of ionospheric sporadic E at different latitudes (in Russian). Nauka, Moscow

Ignatev Yu A 1969: Geomagn. i Aeronomiya, 9, 1096-1098.

Ivanov-Kholodny G S, Lazarev V I 1966: Geomagn. i Aeronomiya, 6, 397-400.

Kolokolov L E 1979: Ionospheric effects of the magnetospheric transfer of energy from the conjugate area (in Russian). Thesis

Mozhaev A M, Chernisheva S P, Sheftel V M 1976: Geomagn. i Aeronomiya, 16, 80-83.

Sen A K 1971: Geophys. I., 23, 161-172.

Somsikov V M, Troitsky B V 1975: Geomagn. i Aeronomiya, 15, 856-860.

Acta Geod. Geoph. Mont. Hung., Vol. 22 (1-2), pp. 211-220 (1987)

SOME PROPERTIES OF SPREAD-E IN THE MID-LATITUDE IONOSPHERE

M N Fatkullin[1], K N Vasilev[1], T I Zelenova[1]

[1]Institute of Geomagnetism, Ionosphere and Radio Wave Propagation (IZMIRAN), Academy of Sciences of the USSR, 142092 Troitsk, Moskovskaya oblast, USSR

Results of the sounding of the E region are presented at the station Moscow by means of an SP-3 type ionosonde with improved characteristics. This improvement resulted especially in a broadening of the pass band of the receiver to 100 kHz and in a reduction of the duration of the impulses to 30 μs. Thus, mid-latitude spread-E has been recorded. Typical examples are shown and some characteristics of the spread-E phenomenon are studied.

Keywords: E region; irregular structure of the ionosphere; sounding of the ionosphere; sporadic E layer; traveling ionospheric disturbances

At low and mid-latitudes, spread-E can be observed by bottom-side vertical sounding of the ionosphere using standard equipments. At the same time scattered reflections from sporadic E layers are also recorded. Because of the conditions mentioned these phenomena are studied only in a few publications (Anastassiadis et al. 1970, Chen et al. 1972, Chen 1973). Anastassiadis et al (1970) and Chen et al. (1972) discussed the effect of spread-E and of the scattering by sporadic E layers on the scintillation of radio signals transmitted by satellites at low latitude. Reid (1968) and Chen (1973) attribute the formation of large scale irregularities of the electron density to gradient instability of the plasma in perpendicular electric and magnetic fields.

According to the authors' knowledge spread-E has not been observed yet by vertical sounding at mid-latitudes in natural conditions. This is mainly due to the fact that the usual ionosondes have small height resolving power (~ 30 km) and a receiver of narrow pass band (~ 15 kHz). Because of the latter the low-frequency part of the spectrum passes the receiver and the

impulse is retarded and broadened.

For the investigation of the large scale irregular structure of the ionosphere by means of bottomside sounding an increase of the height and frequency resolving power of the ionosonde, as well as an improvement of the accuracy of the virtual height determination are necessary. In order to increase the resolving power of the ionosonde SP-3, the pass band of the receiver has been extended to 100 kHz and the duration of the transmitted impulse has been reduced to 30 μ s in IZMIRAN (Vasiliev et al. 1978). This enabled to improve the height resolving power to 3-5 km and so to study the fine structure of the mid-latitude E region.

Special experiments have been carried out in IZMIRAN for the investigation of the spread-E phenomenon in 1977-78 and in 1982 by means of the improved SP-3 ionosonde under different helio- and geophysical conditions. Some preliminary results of these investigations are published by Fatkullin et al. (1985). Here a more detailed discussion of the results is presented for typical conditions.

SOUNDING AT A FIXED FREQUENCY

In order to demonstrate the possibilities offered by the improved ionosonde, the virtual height records obtained at the fixed frequency f = 2.2 MHz are shown in Fig. 1 (Fatkullin et al. 1985). Top of the figure shows that by switching the receiver to broad band, the "cloudy" structure of the E region can be observed while individual traces of the reflections from small scale irregularities cannot be distinguished in case of narrow band reception because of the broadening of the impulses in the receiver and their merging into the signal. Moreover, at the time of switching from broad band to narrow band reception, the height of the lower edge of the trace increases suddenly by $\sim$ 2 km and changes depending on the amplitude of the signal. Fig. 1 bottom shows a record of scattered reflections at the same frequency f = 2.2 MHz in case of broad band reception. The cloudy structure can be quite clearly seen.

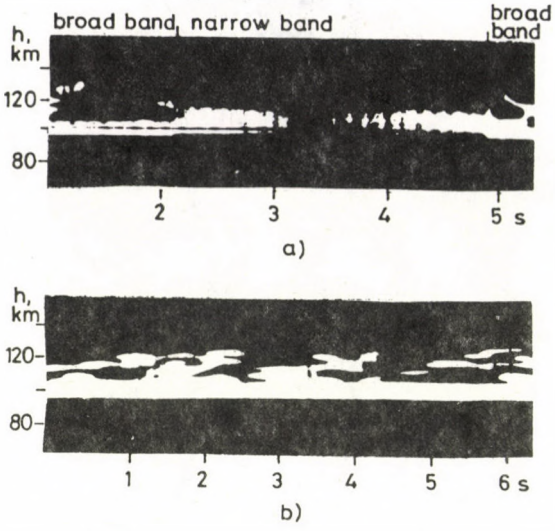

Fig. 1. Variation of the virtual height at the frequency f = 2.2 MHz in Moscow, June 21, 1977. Bottom, (a) the sounding began at 1545 LT. During the first second the station worked with broad band (Δf = = 100 kHz), then during the following 3 seconds with narrow band (Δf = 15 kHz), afterwards broad band reception has been used again. In the lower part (b) the scattered reflections recorded with broad band reception at the same frequency f = 2.2 MHz are shown (July 21, 1977 1546 LT)

SOUNDING WITH SWEPT FREQUENCY

This type of sounding has been carried out only at frequencies $1 \leq f \leq 4$-5 MHz using the improved SP-3 ionosonde. For this reason the state of the ionosphere at heights above the E region was practically not studied in the cases considered below.

In Fig. 2 ionograms are shown recorded by an SP-3 ionosonde simultaneously with improved and usual characteristics. If the ionograms are recorded by the ionosonde with usual parameters practically no spread phenomenon can be observed in the mid-latitude ionosphere.

The following examples illustrate the development of spread-E in time. In Fig. 3 examples of the development and vanishing of the spread-E are presented. At 1509 no spread-E

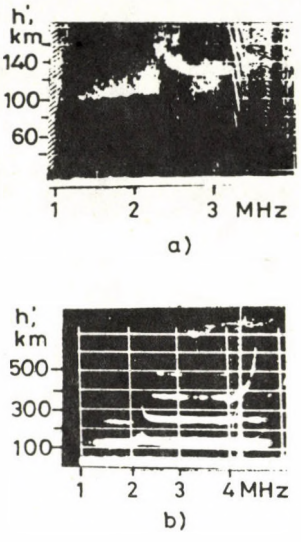

Fig. 2. Comparison of ionograms obtained simultaneously by means of two SP-3 ionosondes, one of which had improved characteristics (a), the other the usual parameters (b). The measurements were carried out in Moscow on July 17, 1977 1800 LT

was recorded. Later spread-E appeared from 1514 to 1559 near the critical frequency of the E layer. Under these conditions a stratification in the E layer has also been observed. At 1559 no spread can be seen in the E region. From 1604 to 1634 a clearly developed spread-E appeared with the difference that it is observed initially only in the vicinity of the E layer critical frequency, then spreads over the whole layer. This phenomenon continues till 1704.

Some typical examples of ionograms showing clearly defined spread-E under different helio- and geophysical conditions are presented in Figs 4 and 5.

An analysis of the results of measurements carried out in different conditions indicated the possibility of its occurrence in different circumstances in the mid-latitude ionosphere.

1. Spread-E in absence of scattering from sporadic E layers and at some indications of traveling ionospheric disturbances (TID) (Figs. 4a and b). In this case spread-E may be observed

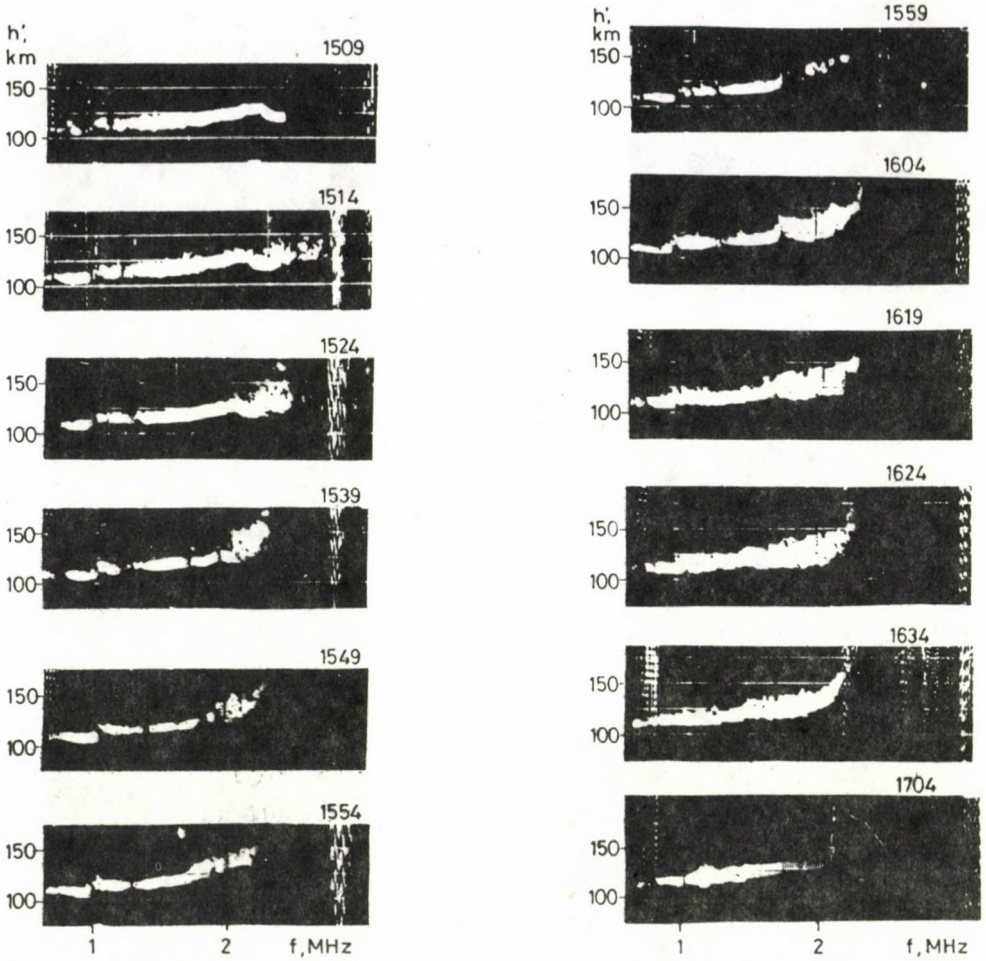

Figs 3a, b. Development and vanishing of spread-E according to the measurements on May 12, 1978

in the vicinity of the E layer critical frequency, but sometimes it spreads practically over the whole range $f \lesssim foE$ (Figs 4d-f).

2. Scattering from sporadic E layers without spread in the E layer (Figs 5b and c and Fig. 6). Figure 6 shows the scattering in the Es layer (type c) to begin at 1200, however, no spread in the E layer is present. In the interval from 1258 to

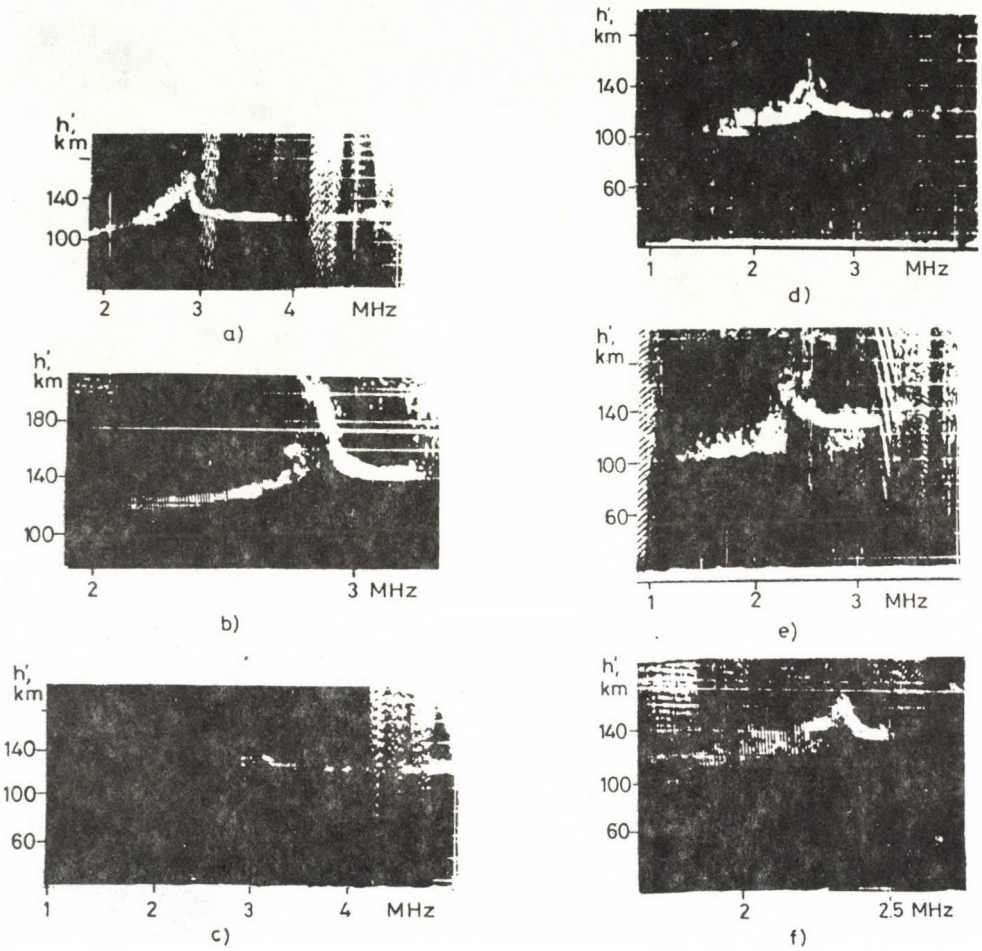

Figs 4a, b. Examples of ionograms showing spread-E in different helio- and geophysical conditions. a - June 9, 1977, 0805 LT, b - February 7, 1978, 1255 LT, c - July 9, 1977, 0900 LT, d - June 15, 1977, 1810 LT, e - June 17, 1977, 1800 LT, f - February 7, 1978, 0950 LT

1312 scattering in both the Es and the E layers is simultaneously observed in the vicinity of the E layer critical frequency. At 1315 scattering is absent both in the Es and the E layers.

3. Scattered reflections are recorded both in the E region and from sporadic E layers of the types c and h (Figs 2a and 6).

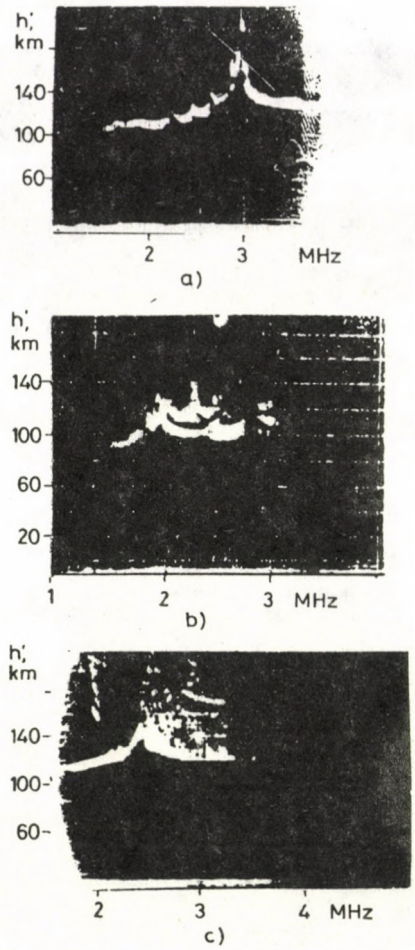

Fig. 5. Typical examples of the simultaneous occurrence of spread-E and scattering from a sporadic E layer. a - June 9, 1977, 1710 LT, b - June 15, 1977, 1925 LT, c - June 9, 1977, 1850 LT

4. Cases of the occurrence of spread-E, when on the ionograms traveling ionospheric disturbances are seen (Fig. 6).

Spread-E is typically observed in geomagnetically quiet conditions ($Kp \lesssim 3$). In day-time (0718 LT) scattered reflections from the E layer can be observed approximately with equal probability independently of the season. In the majority of cases, the frequency band of spread-E amounts to 0.5-0.8 MHz,

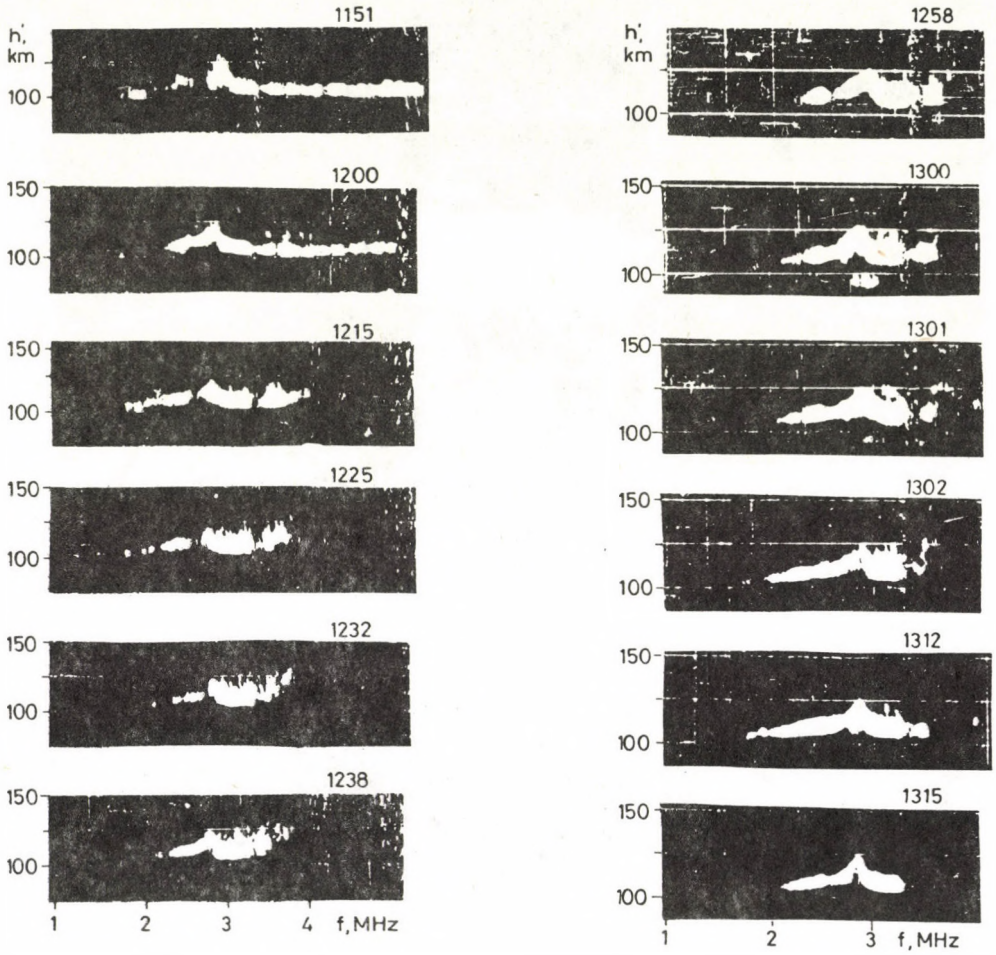

Figs 6a, b. Examples illustrating the development and vanishing of the scattering from a sporadic E layer according to the measurements on June 21, 1977

but some times the range of the frequency spread may reach 2.0-2.4 MHz (Fig. 7a). The virtual height of spread-E extends to an interval of 8 to 30 km, however $\Delta h' \simeq$ 60-80 km or even more is observed in individual cases (Fig. 7b). The duration of the spread-E amounts usually to 15-30 min.

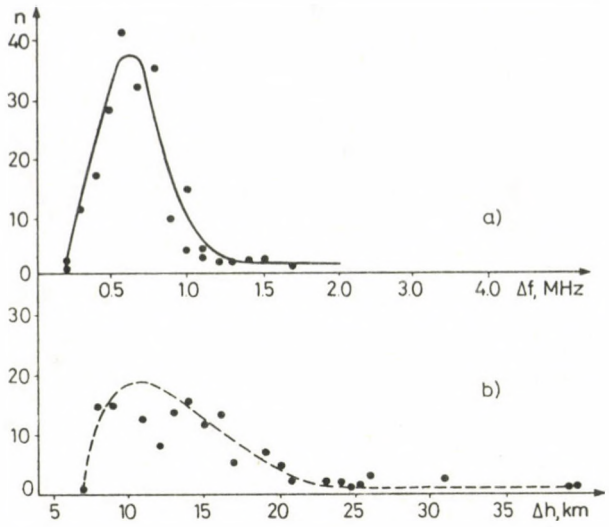

Fig. 7. Distribution of the (a) frequency and (b) height ranges, in which spread-E has been observed under different helio- and geophysical conditions (n - number of observations)

DISCUSSION

The spread-E phenomenon in ionograms of the bottomside vertical sounding is connected with the back scatter of high frequency radio waves from small scale irregularities of the E region, if the ratio of the scale of the irregularity in the direction of the vector of the incident wave to the wave length is $2\pi/K = \lambda_{II} = \lambda/2$. Different cases, when at mid-latitudes spread-E can be observed in vertical sounding ionograms have been discussed by Fatkullin et al. (1985). The role of small scale irregularities in the reflections from mid-latitude sporadic E layers has been discussed by Erukhimov and Savina (1980).

At present the mechanism of the formation of small scale irregularities in the mid-latitude E region cannot be unambiguously specified. The turbulence of the neutral atmosphere may play a role, when the plasma behaves like a passive mixture (Gershman 1974). This mechanism may be effective at heights below the level of the turbopause. Irregularities elongated

along the geomagnetic field are created by gradient instability in perpendicular electric and magnetic fields (Reid 1968, Sato et al. 1968) or by thermal instability (Erukhimov et al. 1983).

REFERENCES

Anastassiadis M, Natsoukas D, Moraitis G 1970: Radio Sci., 5, 953-957.

Chen A A 1973: J. Geophys. Res., 78, 4707-4709.

Chen A A, Chin P N, Chance M P 1972: J. Geophys. Res., 77, 1859-1868.

Erukhimov L M, Savina O N 1980: Ionosfernie issledovaniya, No 30, 80-86.

Erukhimov L M, Kagan L M, Savina O M 1983: Izv. Vuzov (Radiofizika), 26, 1032-1034.

Fatkullin M N, Vasilev K N, Zelenova T I, Savina O N 1985: Geomag. i Aeronomiya, 25.

Gershman B N 1974: Dynamics of the ionospheric plasma (in Russian). Nauka, Moscow

Reid G C 1968: J. Geophys. Res., 73, 1627-1640.

Sato T, Tsuda T, Maeda K 1968: Radio Sci., 3, 529.

Vasilev K N, Vasilev G V, Kryukov A L 1978: In: Fizika ionosferi i magnetosferi. IZMIRAN, Moscow, 43-48.

Acta Geod. Geoph. Mont. Hung., Vol. 22 (1-2), pp. 221-226 (1987)

SIGNALS REFLECTED FROM DIFFERENT TYPE Es LAYERS

T S Kerblay[1], P G Minullin[2], V I Nazarenko[1], G N Nosova[2], O N Sherstyukov[2]

[1]Institute of Geomagnetism, Ionosphere and Radio Wave Propagation, Academy of Sciences of the USSR, 142092 Troitsk, USSR

[2]State University of Kazan, 420008 Kazan, Lenin ul. 18, USSR

The energetic parameters of reflected signals have been investigated by recording the amplitude U of the received signal at the mid-latitude transmission paths Arkhangelsk-Kazan and Moscow-Odessa in the period 1976-80. Two types of Es layers are distinguished, a reflecting and a scattering type one.

The reflection coefficients ϱ_{eff} of Es layers were determined in case of scattering and reflection. It has been found that for frequencies of 15 MHz Es layers with large values of fbEs (>3.5 MHz) result in $\varrho_{eff} \simeq 1.0$, i.e. they are reflecting, but those with low fbEs values give $\varrho_{eff} \simeq 0.5$, i.e. they are semitransparent and scattering. There are cases, when $\varrho_{eff} > 1$, these can be obviously explained by focussing at the reflection of radio waves from the irregular structure of the Es layer.

Es layers can also be divided into "regular" and "occasional" groups. In case of "regular" Es layers the secant law is valid, as for the regular E layer. The "occasional" Es layer is characterized by suddenly increasing and decreasing values of foEs during a period of some tens and hundreds of minutes. Applying corrections of 10-50 %, the secant law can be used.

Keywords: absorption coefficient; oblique incidence sounding of the ionosphere; reflection coefficient; scattering of radio waves; secant law; sporadic E layer

Two types of Es layers can be distinguished: a reflecting and a scattering type. The reflection coefficient ϱ Es and the validity of the secant law for the Es layer are determined by the type of the Es layer. These energetic parameters have been studied by recording the amplitude of the received signal at the mid-latitude transmission paths Arkhangelsk-Kazan and Moscow-Odessa in the years 1976-80. Ionospheric stations worked at about the midpoints of the paths.

In case of radio waves reflected from the Es layer the voltage at the input of the receiver is

$$U = U_o \varrho_{eff} e^{-\Gamma_1} \quad (1)$$

where U_o is the voltage at the input of the receiver without taking into account the losses due to ionospheric absorption and depending on the path length, the power of the transmitter and the antenna-feeder system, Γ_1 is the coefficient of non-deviative absorption in the D region of the ionosphere, ϱ_{eff} is the effective reflection coefficient making allowance for the losses due to absorption in the deviating part of the path and for losses at the reflection of radio waves from the ionospheric layer.

$$\varrho_{eff} = \varrho e^{-\Gamma_2} \quad (2)$$

where ϱ is the coefficient of reflection from the ionosphere, which is in case of reflections from the regular layers of the ionosphere practically equal to one, Γ_2 is the absorption coefficient in the deviative region of the ionosphere. In order of succession

$$\Gamma_1 = \frac{3.0\ f_o^2\ E}{(f+f_g)^2 \cos \varphi_D}, \quad (3)$$

$$\Gamma_2 = \frac{4f \cos^2 \varphi_E}{f_o E} \sqrt{\frac{f}{f+f_g}}, \quad (4)$$

where f_oE is the critical frequency of the E layer, f is the frequency of the signal, f_g is the gyrofrequency, φ_D and φ_E are the angles of incidence at the D and E layers respectively.

For the Es layer the value of Γ_2 could not be determined. Measuring the amplitude at the point of reception, only the ratio

$$\varrho_{eff} = \frac{U}{U_o\ e^{-\Gamma_1}} \quad (5)$$

can be established.

Reflections from the regular E layer have been obtained at a frequency of 9 MHz at the transmission path Arkhangelsk-Kazan from 0600 to 1800 hours. Therefore one mode reflections from the Es layer have been observed from 1800 to 0600 hours. The signals scattered by the ionosphere were less than 15 μV. All signals larger than 15 μV were considered as scattered or reflected from the Es layer.

The value of U_o has been found on the basis of the parameters of the transmission path Arkhangelsk-Kazan. Then, it has been adjusted to the case of reflections from the regular E layer using Eqs (2)-(5). Finally a value of 750 μV was obtained.

For the time interval from 1800 to 0600 hours, when the radio waves of 9 MHz frequency propagate via the Es layer, ϱ_{eff} has been determined on the basis of Eqs (3) and (5). The effective coefficients of reflections from the Es layer obtained for August 1976 are plotted in Fig. 1 as points. In this figure the half hourly values of ϱ_{eff} of the regular E layer, averaged for a month are denoted by crosses.

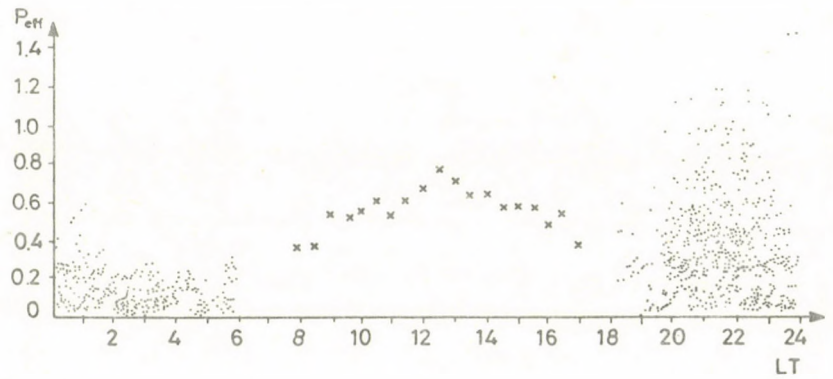

Fig. 1. The effective reflection coefficients referring to the Es (.....) and E (××××) layers at the transmission path Arkhangelsk-Kazan, August, 1976

The value of ϱ_{eff} for the Es layer does not exceed the level 0.4 and only individual values reach the level 0.6 in the postmidnight and morning hours, when scattering is predominant.

In the evening and premidnight hours, when reflection is predominant values of ϱ_{eff} of the Es layer are heavily scattered reaching 1, some times the values of ϱ_{eff} can exceed 1.0. This is probably due to the focussing of radio waves by the Es layer. The coefficients of reflections from individual irregularities of the Es layer have been studied in the transmission path Moscow-Odessa at frequencies of 10 and 15 MHz.

In Fig. 2. the values of the field strength at these frequencies are compared for some measuring periods. In the majority of the cases a simultaneous increase of the field strength at both frequencies is observed. Nevertheless, many points are located in the bottom right part of the Figure when large values of the field at 10 MHz correspond to its small values at 15 MHz, i.e. the Es layer is transparent at 15 MHz, however, it is reflecting at 10 MHz.

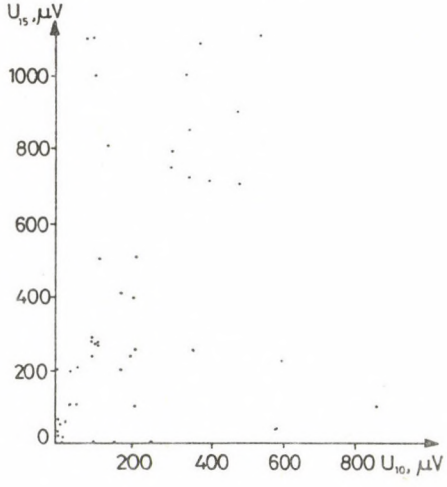

Fig. 2. The connection between the field strengths of signals reflected from Es layers at 10 and 15 MHz at the transmission path Moscow-Odessa in August, 1980

As an example continuous reflections from an Es layer are presented at the frequencies 10 and 15 MHz from 1900 to 2200 hours, August 23, 1980.

On the basis of the method described above ϱ_{eff} was com-

puted in every 15 minutes. The results are presented in Fig. 3a, where ϱ_{eff} is denoted in case of 10 MHz by points, in case of 15 MHz by crosses. For the same time interval the variations of the parameters fbEs and foEs are plotted in Fig. 3b. Figure 3a shows that ϱ_{eff} is equal to 1 in case of 10 MHz during the first hour, while for 15 MHz ϱ_{eff} is small and varies between 0.01 and 0.33. That is in this period radio waves of a frequency of 10 MHz are reflected by the Es layer, however, those of a frequency of 15 MHz are scattered. Large reflection coefficients reaching values of 0.7-1.0 are observed at both frequencies in the time interval 20-22 hour. Some decreases of ϱ_{eff} at 10 MHz may be connected in this period with the structure of the Es layer. A comparison of the values of ϱ_{eff} with those of fbEs shows that the best agreement appears at higher

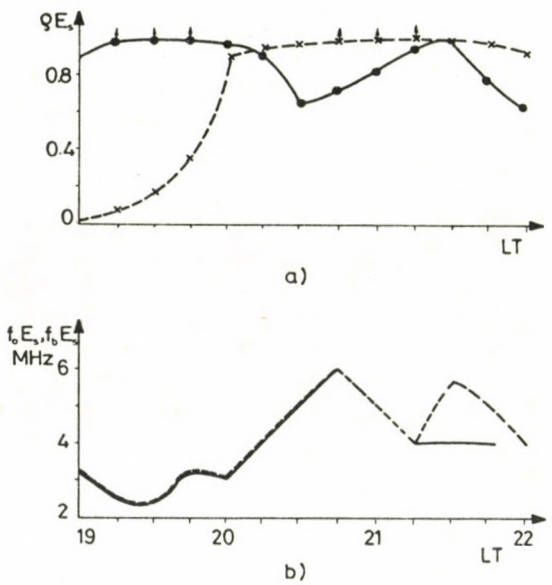

Fig. 3. a) Temporal variations of the reflection coefficient at the frequencies 10 MHz (●—●—●) and 15 MHz (×–×–×) at the transmission path Moscow-Odessa, as well as b) that of the parameters fbEs (———) and foEs (-----)

frequencies. At 15 MHz ϱ_{eff} is directly proportional to fbEs. The increase of fbEs to 4 MHz and higher is followed by high values of the reflection coefficient, though, at 15 MHz it re-reaches the value of 0.9 15 min earlier than an Es layer with fbEs = 4 MHz develops. At the frequency 10 MHz such a clear relation has not been found. In the time interval studied here the magnitude of the reflection coefficient attain values of 0.7 and higher. At the frequency 15 MHz Es layers with large values of fbEs (> 3.5 MHz) result in $\varrho_{eff} \simeq 1.0$, i.e. they are reflecting, while Es layers with small values of fbEs give $\varrho_{eff} \simeq$ 0.5, i.e. they are semitransparent and scattering. At 10 MHz the mean value of ϱ_{eff} is equal to 0.83, at 15 MHz it is equal to 0.71. There are cases, when $\varrho_{eff} > 1$ and this can be obviously explained by the focussing effect of the irregular structure of the Es layer at the reflection of radio waves.

Es layers can be divided into "regular" and "occasional" layers. The "regular" Es layer exhibits a probability of occurrence of 100 % in summer, the variation of its parameters follow the change of the Sun's zenith angle, however, at about 17 hour a second maximum starts. On the basis of summer measurements it has been found that the lowest value of foEs amounts to 1.6 MHz. For the "regular" Es layer the secant law is valid, as in case of the regular layers. Values of foEs suddenly increasing or decreasing within some tens or hundreds of minutes are characteristic of the "occasional" Es layers. The secant law can be applied with corrections of 10-50 %.

Acta Geod. Geoph. Mont. Hung., Vol. 22 (1-2), pp. 227-231 (1987)

AMPLITUDE AND FREQUENCY CHARACTERISTICS OF THE Es LAYER AT OBLIQUE INCIDENCE SOUNDING

T S Kerblay[1] and P G Minullin[2]

[1]Institute of Geomagnetism, Ionosphere and Radio Wave Propagation (IZMIRAN), Academy of Sciences of the USSR, 142092 Troitsk, Moskovskaya oblast, USSR

[2]State University of Kazan, 420008 Kazan, Lenin ul. 18, USSR

The characteristics of Es layers have been studied by means of the mid-latitude transmission paths in the USSR. From the measurements the filling coefficient η Es has been determined as a function of the threshold amplitude at the receiver input U_{th} and the operating frequency f for minimum and maximum solar activities. It is possible to forecast the probability of communication via the Es layer for any season using these relations in case of given f, U_{th} and length of the transmission path.

Keywords: filling coefficient; oblique incidence sounding of the ionosphere; sporadic E layer

The characteristics of the Es layer have experimentally been studied at the mid-latitude transmission paths in the USSR. The list of the paths and their symbols where the measurements were carried out with the parameters are given in Table I. Here f, f_{equ} are the operating frequency and the equivalent frequency corresponding to the vertical sounding ($f_{equ} = f/\sec\varphi$, φ is the angle of incidence at the Es layer), L is the length of the path.

Simultaneously with the signals reflected from the Es layer signals produced by back scatter, spread-F and reflections from meteors are also present in the recording channel. In order to eliminate them a threshold amplitude $U_{th} = 20\ \mu V$ has been set at the receiver input.

At oblique incidence sounding the probability of the presence of an Es layer is characterized by the filling coefficient η Es, which gives in percents the relative time of existence of radio waves reflected from the Es layer at a given sounding frequency.

Table I

No	Transmission path	f MHz	Symbol	L km	f_{equ} MHz
1.	Arkhangelsk-Kazan	9	AK-9	1070	2.4
2.	Moscow-Kazan	10	MK-10	660	3.7
3.	Arkhangelsk-Kazan	14	AK-14	1070	3.7
4.	Moscow-Odessa	15	MO-15	1130	3.8
5.	Moscow-Kazan	15	MK-15	660	5.6
6.	Arkhangelsk-Kazan	24	AK-24	1070	6.3
7.	Salekhard-Tyumen	27	ST-27	1050	7.3
8.	Moscow-Kazan	20	MK-20	660	7.4
9.	Moscow-Odessa	40	MO-40	1130	10.1

As it is shown in Fig. 1 for the path Moscow-Kazan at f = 15 MHz in June, 1979 the magnitude of η Es reaches maxima at about 10-12 and 20 hour during the day. The probability of the presence of an Es layer is maximum in summer and minimum in winter. In Fig. 2 the seasonal variation of η Es at the path Moscow-Odessa is presented in case of a frequency of f = 40 MHz. It can be seen from Fig. 2 that in summer the value of η Es reaches 8 %, while in winter it is less than 1 %.

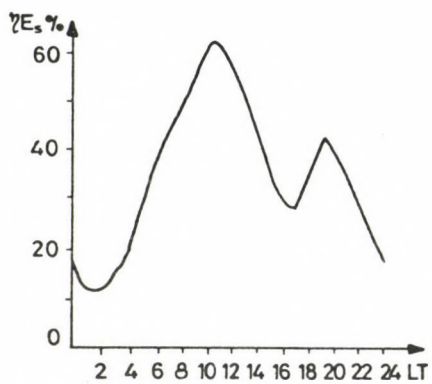

Fig. 1. Diurnal variation of the filling coefficient ηE_s for the transmission path MK, at 15 MHz in June, 1979

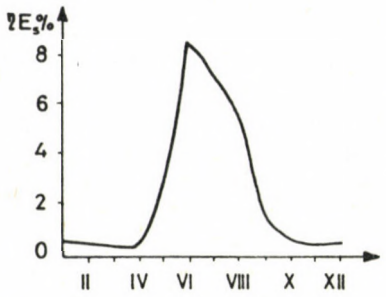

Fig. 2. Seasonal variation of the filling coefficient ηE_s for the transmission path MO, at 40 MHz

Values of η Es have experimentally been determined for the transmission paths listed in Table I by averaging the summer observations at $U_{th} = 20\,\mu V$. For comparison the values of η Es are plotted in Fig. 3 as a function of f_{equ} (see Table I). With increasing f_{equ} the value of η Es decreases. This relation can be approximated by the formula.

$$\eta E_s = 257\ f_{equ}^{-1.61} \quad . \tag{1}$$

If the values of η Es determined at the transmission paths for summer are taken as unit, then the equinox values of η Es are on the average 0.27 and the winter ones -0.13. If formula (1) is used with these factors, then mean values of η Es can be obtained for both the equinoxes and winter for arbitrary paths with arbitrary operating frequency.

For transmitters of an average output of 1-10 kW the amplitude of the signals reflected from the Es layer falls into the range from 1 to 10.000 μV. The distribution of the amplitudes can be approximated by Rayleigh's law.

From the measurements at the transmission paths Arkhangelsk-Kazan, Moscow-Odessa, Moscow-Kazan η Es has been obtained as a function of U_{th} (Fig. 4); values for solar activity maximum are shown by solid lines and for solar activity minimum by dashed lines. The value of η Es decreases with increasing U_{th} and f_{equ} (see Table I). The relationship shown here can be

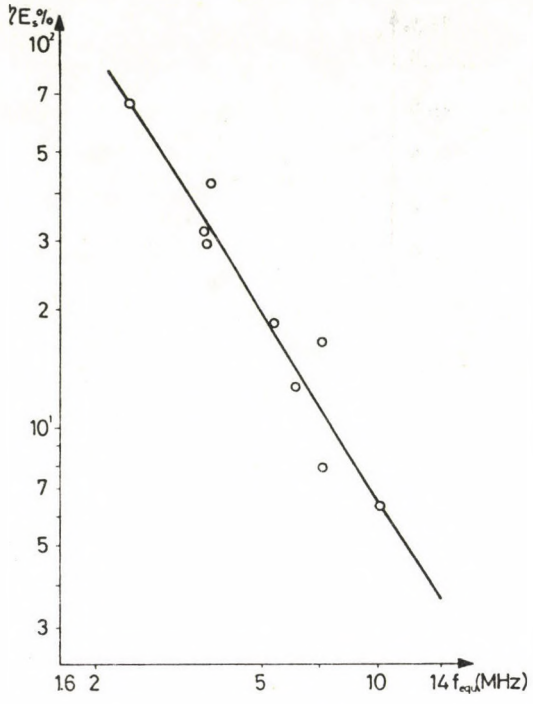

Fig. 3. The filling coefficient ηE_s as a function of the equivalent frequency f_{equ} at mid-latitude transmission paths

approximated by the formula

$$\eta E_s = b\,(\lg U^o_{th} - \lg U_{th}) + \eta E^o_s \qquad (2)$$

where U^o_{th} is the initial threshold amplitude, 20 μV, ηE^o_s is the value of ηE_s at U^o_{th}, which can be found from (1), b is a coefficient determined experimentally and for which values of 0.38 have been obtained at solar activity minimum, and at solar activity maximum values of 0.66. Using the formulas derived above for the particular season the probability of the communication via an Es layer can be forecasted in case of given f, L, U_{th}.

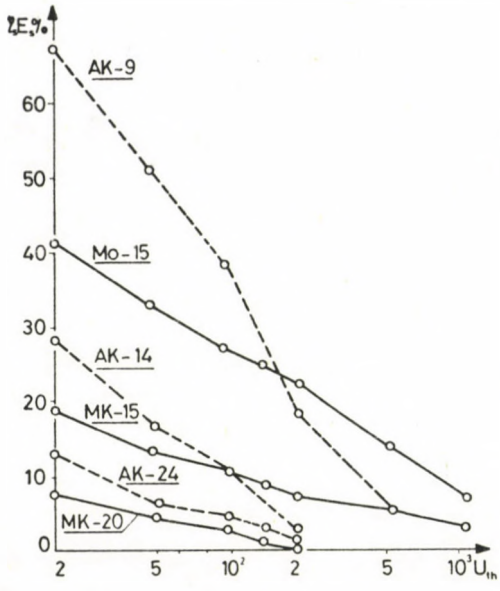

Fig. 4. The filling coefficient ηE_s as a function of the threshold amplitude U_{th} at different transmission paths for solar activity maximum (———) and minimum (-----)

Acta Geod. Geoph. Mont. Hung., Vol. 22 (1-2), pp. 233-240 (1987)

THE IRREGULAR STRUCTURE OF THE MID-LATITUDE Es LAYER ACCORDING TO DATA OF SPECTRAL ANALYSIS

O G Ovezgeldiev[1], L P Korsunova[1], Yu Karadzhaev[1]

[1]Physical-Technical Institute, Academy of Sciences of the Turkmen SSR, 744000 Ashkhabad, Gogol ul. 15, USSR

Time series of Es frequency parameters measured every minute, as well as that of the amplitude of the signal reflected from the Es layer were analyzed statistically and spectrally. The structure of Es layers seems to be characterized by a broad spectrum of irregularities from large scale ones with horizontal dimensions of 150-200 km to small scale ones with horizontal dimensions of 500-100 m generated by stable cellular eddies and turbulence at the level of the turbopause.

Keywords: ionospheric sporadic E; irregular structure of the ionosphere; spectral analysis

Karadzhaev (1982) has shown that the spectral analysis of the time-series of Es characteristics yields data concerning the structure of irregularities in mid-latitude Es layers. As the Es layer is a natural tracer of the turbopause, many possibilities are offered for the study of its dynamical structure, which would be hardly attainable by direct measurements. Here results of an investigation of the irregular structure in Es layers obtained by means of spectral analysis are presented.

The results of Es observations of both a single station (Ashkhabad) and several ionospheric stations spaced 18, 120 and 328 km from each other were used. On the basis of minute measurements of the frequency parameters, a spectral analysis was curried out by means of the maximum entropy method and by Blackman-Tukey filtering with the low frequency ($T > 1$ hour) components eliminated by a simple sliding average filter. It was found from 123 records that the power spectra are characterized by a line structure. In general two types of the spectra can be distinguished, namely spectra with a single maximum

and spectra with two maxima. Sometimes spectra with three maxima do occur, too. Similar results were obtained from the data of the station Moscow (48 spectra). According to the Moscow data, the mean periods are 10 and 48 min, in Ashkhabad, mean periods of 10 and 42 min were obtained what indicates the similarity of the structure of Es layers at latitudes 38^{o} and 60^{o}N (Fig. 1).

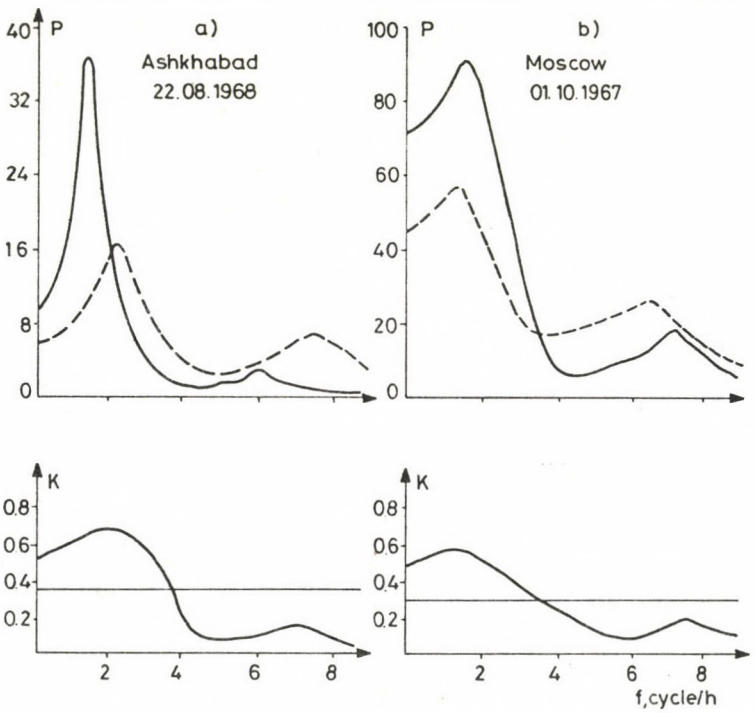

Fig. 1. Power and coherence spectra of the temporal variations of Es frequency parameters on the basis of the data of stations (a) Ashkhabad and (b) (Moscow). Full and dotted lines represent foEs and fbEs, respectively

Based on the results of simultaneous soundings at spaced stations, the spatial coherence spectrum of the Es frequency parameters was computed. The mean coherence spectra determined on the basis of all measurements with spacings of 18, 120 and 328 km are shown in Fig. 2a, b and c. The coherence of the

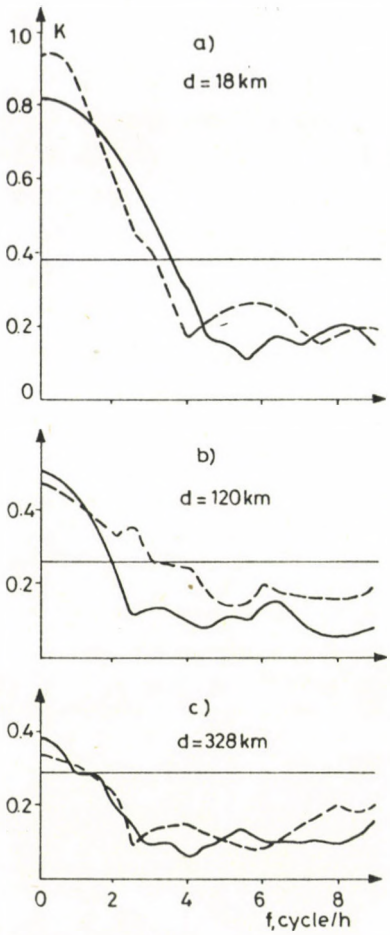

Fig. 2. Spatial spectra of the coherence of foEs (full line) and that of fbEs (dotted line)

frequency parameters decreases with the increase of the spacing and at a distance of 328 km it disappears. Thus the horizontal dimensions of the irregularities responsible for occurrence of these periods are limited to the range 120 km $< l_h <$ 320 km.

Variations of the Es frequency parameters are believed to be due to variations of the dynamical structure of the turbopause; namely the random variations of foEs are produced by small scale turbulent eddies (Gershman and Ovezgeldiev 1973) and those of fbEs by vertical shears of the horizontal wind arising either as a result of internal gravity waves (Miller and Smith 1978) or as the manifestation of large scale cellular

eddies (Barat 1973). Then, the basic periodicities of the spectral analysis are obviously of different nature.

The low frequency maximum with a period $T \approx 40\text{-}50$ min is larger, more stable, it can be found in the majority of the spectra. A larger coherence decreasing with the increase of the spacing belongs to it. From the point of view of the physical mechanism resulting in the formation of Es layers at mid-latitudes, the low frequency maximum is most probably due to cellular eddies with horizontal dimensions of 120 km $< l_h <$ 300 km considered usually as wind-shears. It has to be noted that the same spectral characteristics are possessed by internal gravity waves of the corresponding scale. Nevertheless, in spite of the similarity of the spatial and temporal scales of internal gravity waves to those of cellular eddies, substantial differences exist between these two forms of the meso-scale atmospheric motions comparing the vectors of their phase velocities. In the lower thermosphere the horizontal phase velocity of internal gravity waves is a multiple of the wind velocity and due to the isotropic spatial distribution of the sources of these waves, they have no prevailing direction of propagation (Krasovskiy and Shefov 1976). Two dimensional cells characterized by rising and sinking (i.e. elongated along the wind direction) fluxes are transported by the wind, consequently, their velocities are the same.

In order to explain the nature of the periodicities, the power spectra and coherence spectra of 48 time series of the Es frequency parameters have been computed, which were measured by identical vertical sounding stations located at the vertices of a triangle with legs of 70-90 km (Vasilev et al. 1975). The occurrence and the periods of the spectral components observed at the same base differ substantially in different directions as compared to the wind velocity vector. Namely, the periods coincide and the coherence is large at the leg which is located in east-west direction, coinciding with the direction of the neutral wind (Fig. 3). The results obtained can be hardly interpreted with the location of internal gravity waves in spite of the fact that the presence of the cellular structure of the

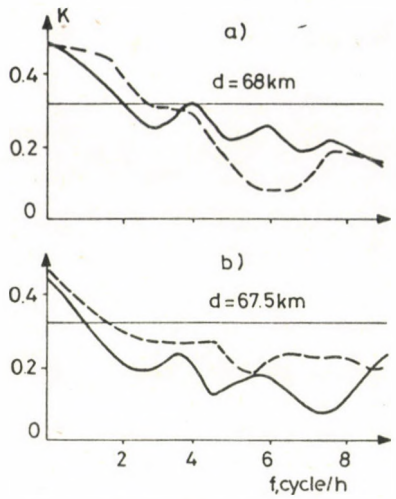

Fig. 3. Dependence of the coherence spectrum of the frequency parameters on the direction of the spacing between the stations a) east-west direction, b) nord-south direction

wind enables to explain the formation of quasiperiodical irregularities which have a prevailing direction of motion coinciding with the wind velocity vector and are elongated along it. Thus the spectral components of the temporal variations of Es frequency parameters with periods $T \sim 40$-50 min are due to cellular eddies with horizontal dimensions of $l_h \approx 150$-200 km.

The vertical structure of the eddies can be estimated by spectral analysis of the temporal variations of two phenomena, i.e. ionospheric sporadic E and OI (5577 Å) emissions observed at the same site, but spaced in height by 10-20 km. The number of periodic components in the frequency range 0.5-5 cph is 1.5 times less in simultaneous fluctuations of the Es frequency parameters than in the intensity variations of the oxygen green line. An analysis of the coherence spectra of the same period has shown that the fluctuations studied here are uncorrelated and a large coherence between fbEs and 5577 Å was only observed in some individual cases (Fig. 4), though, the corresponding variations of foEs and the intensity of the airglow were uncorrelated. The observed lack of correlation in the initial data

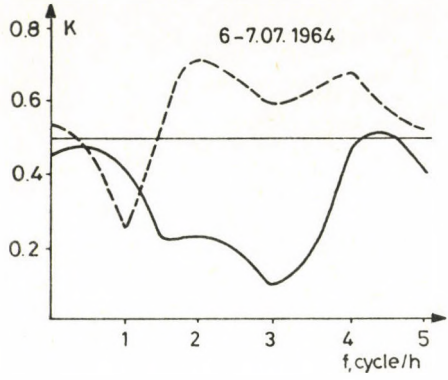

Fig. 4. Relative spectra of coherence of foEs (full line) and that of fbEs (dotted line) with the intensity of OI 5577 A

may be due to the different spatial occurrence of the periodic components (in case of the internal gravity waves), or to a significant anisotropy of the large scale eddies. As periodic components of the variations of the Es layer are caused by cellular eddies, their vertical dimensions can be estimated in $l_z < 15$ km. The results obtained agree with the results of Gorbunova et al. (1982), where simultaneous spectra of h'Es and OI 5577 Å data of 43 nights were studied using the Ashkhabad atlas of the night air glow. In case of observations of the two phenomena at near by heights ($\Delta h \sim 5$ km) a connection between the short period variations of h'Es and intensity of the oxygen green line was found. Moving off in height this connection diminishes so that at a distance of $\sim$ 10 km the events were no more correlated. Thus, large scale cellular eddies of horizontal dimensions of l_h = 150-200 km and vertical extensions of l_z = 5-10 km are present at heights of 100-115 km in the mid-latitude thermosphere. These eddies are the sources of Es irregularities with the corresponding scales.

Time spectra of the structure parameters of the mid-latitude Es layers also show a characteristic high frequency maximum at T = 8-10 min. This maximum is less stable than the low frequency one at T $\approx$ 40-50 min and it can be more frequently observed in foEs spectra. The irregularity, the low power and coherence of the high frequency maximum indicate that its source

can only be turbulence. Using Taylor's frozen turbulence hypothesis and a mean wind velocity of $U \sim 70$ ms^{-1} the high frequency maximum corresponds to turbulent eddies of $l_h \leq 40$ km, supposed to be manifestation of the external scale of the turbulence at the turbopause. In the range of the external scales power spectra of the turbulence normalized to dispersion can be described by the relation $C(f) \sim f^{-m}$, where the mean value of m is 3 from 17 measuring series. Consequently, the theoretical relation obtained by Shur and Lumley (Monin and Yaglom 1967) for a thermally stable stratified atmosphere and a range of scales, where the influence of the mean flow is strongly felt, is confirmed by the spectral relation.

The spectrum of small scale turbulence was investigated using continuous records of the amplitude of radio waves reflected from the Es layer at 4.1 MHz. According to Ovezgeldiev and Babaev (1971) the reflected signal is formed in the range of semi-transparency of the Es layer ($fbEs < f_w < foEs$) by back scatter from small scale irregularities of the electron density, the dimensions of which are equal to the wave-length of the sounding impulse ($l_h \leq \lambda/2 \simeq 40$ m). On the basis of 16 series of amplitude records in the range of semi-transparency of the Es layer, an inverse relation was found between the spectral density and wave number, where the value of m averaged for all series is 1.6 (Fig. 5). The spectral curves have also a slope

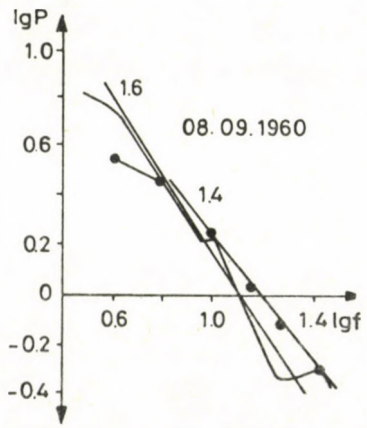

Fig. 5. Power spectra of the amplitude fluctuations of radio waves reflected from the Es layer. $f_w \approx foEs$ (——), $f_w \approx fbEs$ (- · - · -)

of $m \approx 1.6$ for 17 series with $f_w \approx$ fbEs, when in the formation of the reflected signal irregularities of $l_h \geq \lambda$ take part. Consequently, the spectral distribution of energy obeys the law $C(f) \sim f^{-1.6}$ in the range of scales from 40 to 100 m. According to the theory of locally isotropic turbulence (Monin and Yaglom 1967) the spectra of the fluctuations of velocity and density are described by the same power function $C(k) \sim k^{-5/3}$ in the inertial range where, k is the wave number. The approximate coincidence of the slopes of the experimental and theoretical spectral curves (1.6 and 5/3) proves that the irregularities with $l_h \approx$ 40-100 m are formed by turbulent eddies of scales belonging to the inertial range. The smaller eddies are used up by viscous forces so that the internal scale of turbulence is probably 40-50 m in the region of the turbopause.

Thus, a broad spectrum of irregularities of the Es layer has been detected from the anisotropic large scales of l_h = = 150-200 km and l_z = 5-10 km to the small scales of l_h = = 40-100 m, which are formed by cellular eddies and turbulence occurring in the lower thermosphere.

REFERENCES

Barat J 1973: Rech. Spatial., 12, 20-22.

Gershman B N, Ovezgeldiev O G 1973: Proc. Acad. Sci. of the TSSR, Ser. Phys.-Tech., Chem. and Geol. Sci., No. 4, 35-42.

Gorbunova T A, Kuznetsova N Yu, Shved G M 1982: Geomagn. i Aeronomiya,22, 430-434.

Karadzhaev Yu 1982: Proc. Acad. Sci. of the TSSR, Ser. Phys.-Tech., Chem. and Geol. Sci., No. 4, 94-97.

Krasovskiy V I, Shefov N N 1976: Gerl. Beit. Geophys., 85, 175-185.

Miller K L, Smith L G 1978: J. Geophys. Res., 83, 3761-3775.

Monin A S, Yaglom A M 1967: Statistical hydromechanics (in Russian). II. Nauka, Moscow

Ovezgeldiev O G, Babaev A 1971: In: Ionospheric disturbances and their influence on radio communication. Nauka, Moscow, 218-224.

Vasilev K N, Chernisheva S P, Sheftel V M, Shcharenskaya E G 1975: Geomagn. i Aeronomiya,15, 1098-1099.

Acta Geod. Geoph. Mont. Hung., Vol. 22 (1-2), pp. 241-250 (1987)

FORMATION OF THIN Es LAYERS DUE TO THE INFLUENCE OF ELECTRIC FIELDS

O I Razuvaev

Sibirian Institute of Geomagnetism, Ionosphere and Radio Wave Propagation (SibIZMIR), 664033 Irkutsk, P.O.Box 4, USSR

The role of the electric field in the formation of flat sporadic layers at high latitudes is analyzed on the basis of hydromagnetic equation. In the region of field aligned currents leaving the ionosphere the accumulation of metal ions cannot result in the formation of thin layers. No such layer can be formed due to the vertical drift of the metal ions. Starting from electric field models, a zone is found where thin layers can be produced by an electric field. This zone is located in the poleward part of the Harang discontinuity.

Keywords: electric fields; Harang discontinuity; sporadic E layers

INTRODUCTION

The high-latitude ionosphere is characterized not only by a high probability of the occurrence of sporadic E layers, but also by their great variety. Concerning its study the interest is due to the relation of the occurrence of such layers to complicated processes taking place in the magnetosphere, and to practical needs of the telecommunication. Recently, a large material accumulated but an interpretation is lacking. Really, the nature of the formation of thick r type Es layers which are connected with collisional ionization due to charged particle fluxes precipitating from the magnetosphere, is more or less clear. For the explanation of the occurrence of thin f type Es layers at high latitudes there is no suitable theory yet.

In this paper the role of the magnetospheric convection electric field is discussed in the formation of thin Es layers in the presence of metal ions.

Acta Geod. Geoph. Mont. Hung. 22, 1987
Akadémiai Kiadó, Budapest

EFFECT OF THE HORIZONTAL TRANSPORT

Lyatskaya et al. (1978) have shown that ions must be concentrated in the region of outflowing field-aligned currents. This is due to the fact that the carriers of the field-aligned current are electrons while the carriers of the short-circuit current in the ionosphere are ions (Fig. 1). If the mobility of ions along the electric field is maximum at the height of the maximum Pedersen conductivity, then - in a non-stationary case after the sudden strengthening of the field-aligned current - the accumulation of ions at this height proceeds faster than at other altitudes. Thus, a definite maximum can be formed in the electron density profile. For the main ions of the E region the effect of such a process is substantially reduced by recombination. The situation is more favourable in case of metal ions since their recombination coefficient is very small ($\alpha \sim 10^{-12} cm^{-3} s^{-1}$).

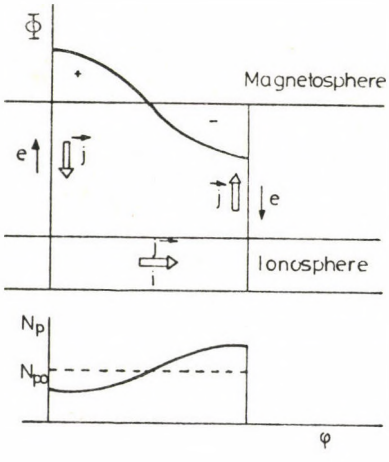

Fig. 1. Scheme explaining the redistribution of the plasma in the ionosphere due to field-aligned currents. Top the distribution of the potential Φ in the magnetosphere, the current system j, as well as the charge carriers and their direction of motion are shown. Bottom the resulting latitudinal variation of the plasma density is plotted

Computations carried out by Lyatskaya et al. (1978) are supplemented here by the study of the horizontal changes in the distribution of ions which produce new effects.

The one-dimensional problem is considered where all quantities change only along the horizontal axis X. Magnetic field lines are considered as equipotential and directed vertically downwards parallel to the Z axis pointing upwards. Then the following equation is obtained from the equations of motion and continuity for the metal ions neglecting diffusion, ionization and recombination:

$$\partial n/\partial t + (e/H)\, f \cdot (E\, \partial n/\partial x + n\, \partial E/\partial x) = 0,$$
$$f = \beta_i/(1+\beta_i^2), \quad \beta_i = \omega_i/\nu_i, \tag{1}$$

where n, ν_i, ω_i are the concentration, the ion-neutral collision frequency and the gyrofrequency of metal ions, β_i is the magnetization parameter of ions. From the continuity equation of current the electric field E can be expressed by the field-aligned current entering the ionosphere as follows

$$j_{\parallel} = \Sigma_p\, \partial E(x)/\partial x .$$

The height integrated Pedersen conductivity Σ_p is assumed to be constant and the distribution of the field-aligned current is given in the simple form:

$$j_{\parallel}(x) = j_o \cos Kx ,$$

where $K = 2\pi/L$, L is the width of the auroral zone. Then in case of the initial condition $n(x,o) = n_o$

$$n(x,t) = 2\, n_o \left[(1 + \cos Kx) \exp(2\, ft/\tau) + (1 - \cos Kx) \exp(-2\, ft/\tau)\right]^{-1}, \tag{2}$$
$$\tau = 2\,(H/c)\, \Sigma_p/j_o .$$

For $Kx = 0$ and π

$$n = n_o \exp (\mp 2\, ft/\tau) ,$$

is obtained, i.e. in the region of the outflowing current the concentration of metal ions increases exponentially and it is reduced in the region of the entering current. $\Sigma_p = 1$ cm and $j_o = 2 + 0.5$ A/km results in $\tau = 50\text{-}200$ s.

From Eq. (2) the width of the horizontal concentration profile is at the level of $n = rn_o$ (r is an arbitrary factor)

$$\frac{d_x}{L} = 1 - \frac{1}{\pi} \arccos \frac{2/r - \exp (2\, ft/\tau) - \exp (-2\, ft/\tau)}{\exp (2\, ft/\tau) - \exp (-2\, ft/\tau)} .$$

The relation $n(x,t)$ enables us the determination of the width $d_z(t)$ of the vertical concentration profile. For this the parameter f has to be determined as a function of z. Considering that the collision frequency is proportional to the concentration of neutrals, which are distributed within the height of the uniform atmosphere H_g according to the barometric law

$$f(z) = (\nu_i/\omega_i) / (1+\nu_i^2/\omega_i^2) \approx \exp (-z/H_g) / [1+\exp (-2z/H_g)] .$$

Then

$$\frac{d_z}{H_g} = \ln \frac{1 + [1 - ((\tau/t) \ln r)^2]^{1/2}}{1 - [1 - ((\tau/t) \ln r)^2]^{3/2}} .$$

In the further calculations $L/H_g = 50$ has been taken.

The curves of d_x and d_z are plotted in Fig. 2 at the level corresponding to the tenfold increase of the concentration. This level was selected because the concentration of metal ions is usually lower by 1-2 orders of magnitude than the electron concentration. The concentration of metal ions increases in the maximum by one order of magnitude from the beginning of the intensification of the field-aligned current in the time of $\sim 2\tau$ (Fig. 2). The formation of the horizontal layer of a width $\sim H_g$ proceeds very fast and remains for $\sim 0.5\,\tau$. From the time $t \approx 3\,\tau$ the width d_x begins to drop, at the same time the width d_z increases steadily. This leads to the degeneration

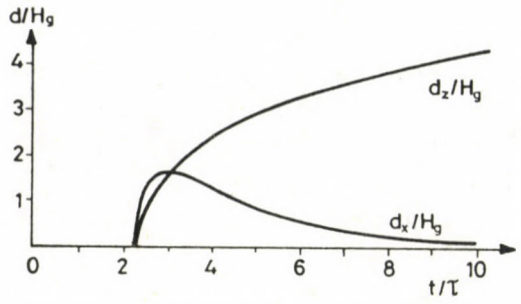

Fig. 2. Variation of the widths d_x, d_z of the horizontal and vertical elecron density profiles with time

of the layer into a thin vertical "wall" of ionization. It is clear that such a mechanism cannot result in the formation of thin (width $\ll H_g$) Es layers.

EFFECT OF THE VERTICAL TRANSPORT

Korenkov (1977) mentioned another possibility of the formation of metal ion layers in the mid-latitude ionosphere due to a vertically non-divergent neutral wind or to an electric field. The mechanism consists substantially of vertical plasma drift in the inclined geomagnetic field. The vertical drift of the plasma is controlled by the component $\underline{\underline{E}}\times\underline{\underline{B}}$ at high altitudes because of the large variation in the degree of magnetization of ions with height, while at low altitudes by the component of the Pedersen drift. In case of a definite direction of the wind or of the electric field at a certain height, the formation of a node of the vertical drift velocity convergence and consequently the development of a layer of increased electron density is possible.

Such a mechanism is sufficiently effective at high latitudes too, where on the one hand the magnetic field lines are almost vertical and this reduces the effect of the vertical drift, however, on the other hand there is a strong magnetospheric convection electric field.

Let the ionosphere be horizontally uniform, but its

properties change with altitude. The ionospheric plasma consists of three components: electrons (index e), molecular (index i1) and metal (index i2) ions. A coordinate system is used with the Z axis directed upwards, the X axis to the north and the Y axis to the west. The vector of the magnetic field $\underline{H}$ lies in the XZ plane, it is directed downward making a small angle χ with the vertical. Let the electric field $\underline{E}$ be uniform. The direction of this field in the horizontal plane relative to north is determined by the angle φ. In a stationary case the following relation is obtained (Razuvaev 1984) from the equations of motion and continuity for the vertical valocity of the metal ions:

$$u_{i2z} = -\frac{1}{2} D_a \left(\frac{dn_{i2}/dz}{n_{i2}} + \frac{dn_e/dz}{n_e} \right) + \frac{e}{H} E \sin\chi \cdot$$

$$\cdot f[\cos\varphi - \beta_i (f+1/\beta_e) \sin\varphi] \quad . \qquad (3)$$

Here n is the concentration, D_a is the coefficient of ambipolar diffusion, the parameters f and β were determined above. The character of the drift of ions is described by the second term in the expression of U_{i2z}. This term is zero, if the electric field has a north-west ($\pi/2 > \varphi > 0$), or south-east ($3\pi/2 > \varphi > \pi$) direction. In the first case the divergence of the velocity is negative which corresponds to a node of the convergence of the velocity, in the second case the divergence is positive. Consequently, the formation of a layer is possible in case of the north-west direction of the electric field and the height of the layer is given by the relation

$$\cot\varphi \approx \beta_i (z_{max}) + 1/\beta_e (z_{max}) \quad .$$

In the latter condition, for the divergence of the drift velocity in the maximum of the layer an expression can be obtained in case of different directions of the electric field. The height profiles of the divergence are presented in Fig. 3 for a certain model of the neutral atmosphere. Curve 1 corresponds to an electric field of 30 mV/m, curve 2 to a field of

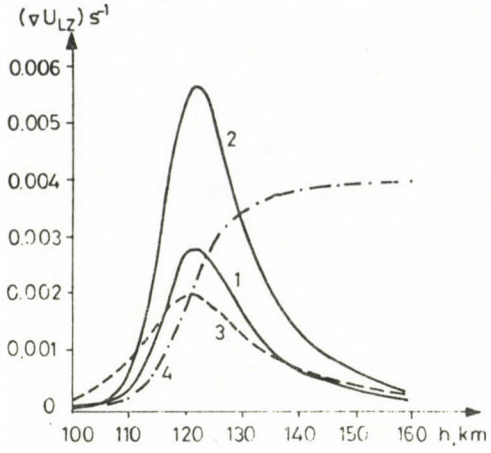

Fig. 3. Height profiles of the divergence of the velocity in case of an electric field and wind-shear

60 mV/m. For comparison profiles of the divergence of the velocity in case of a wind-shear of 0.04 s^{-1} are plotted for east-west shear (curve 3) and for north-south shear (curve 4). At high latitudes the effect of the electric field is comparable or even it surpasses the effect of the wind-shear.

The magnitude of the divergence term can be used for the estimation of the characteristic time of the ionization reduction process $\tau = (dU_{i2z}/dz)^{-1}$. For electric fields occurring in the ionosphere τ varies between 200 and 1000 s and it is minimum at a height of about 121 km, where the magnetization parameter of the ions is $\beta = 1$.

In the state of dynamic equilibrium the ionization reduction process due to the electric field is compensated by diffusion. Therefore, U_{i2z} determined by Eq. (3) must be equal to zero at all heights. Then, assuming photochemical equilibrium of the molecular ions and quasi neutrality the following system of equations is obtained for the determination of the concentration profiles of the different plasma components,

$$\left.\begin{aligned} u_{i2z} &= 0 \\ q - \alpha n_e n_{i1} &= 0 \\ n_e &= n_{i1} + n_{i2} \end{aligned}\right\} .$$

From this one gets

$$\left.\begin{aligned} n_e &= n_{eo} [1 + F(z)]^{1/2} \\ n_{i1} &= n_{eo} [1 + F(z)]^{-1/2} \\ n_{i2} &= n_{eo} F(z) [1 + F(z)]^{-1/2} \end{aligned}\right\} ,$$

$$F(z) = F_o \exp\left\{ 2 \sin\chi \frac{c}{H} E \int (f/D_a) [\cos\varphi - (\beta_i + 1/\beta_e) \sin\varphi] \, dz \right\},$$

where $n_{eo}(z) = \sqrt{q/\alpha}$ is the electron density profile due to collisional ionization, the constant F_o is determined by the total metal ion content, which is taken as 2.10^9 cm^{-2} in this paper.

Results of model calculations are presented in Fig. 4 for two directions of the electric field and three values of the characteristic energy of the precipitating electrons E_o (n_o thick line, n_{i1} dashed line, n_{i2} thin line). The magnitude of the electric field E is 30 mV/m, the flux of precipitating particles 10^7 $cm^{-2}s^{-1}$.

Considering the similarity of the profiles obtained to the profiles computed for the wind-shear mechanism, the conclusion is drawn that the electric field can form thin ($\sim$ 1 km) Es layers in the high latitude ionosphere due to the vertical transport of metal ions. Besides the formation of flat layers of different types (f, l, c and h) is possible.

CONCLUSIONS

The measurement of electric fields in the high latitude ionosphere shows that electric fields of north-west direction are fairly infrequent phenomena. Nevertheless, they can occur

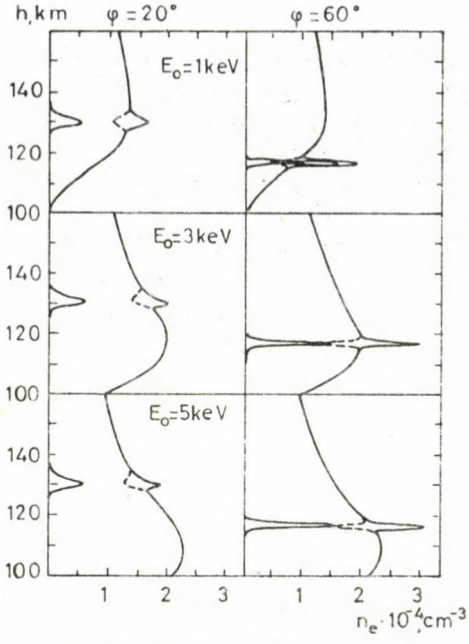

Fig. 4. Profiles of the density of the plasma components computed for different directions of the electric field and for different characteristic energies of the precipitating electrons

in the region of the Harang discontinuity, where the electric field vector rotates counter-clockwise from northern to southern direction (Maynard 1974). Moreover, according to Heppner's (1977) model the configuration of the electric fields in the region of the Harang discontinuity is such that the Pedersen drift of ions has to be directed from the flanks of the Harang discontinuity to its centre and from its southern end to the norhern tip. The results of the first part of this paper show that in the high latitude ionosphere the distribution of metal ions depends considerably on their horizontal transport by electric fields. Thus, the formation of thin Es layers due to the mechanism considered here might be expected in the poleward part of the Harang discontinuity.

The height of such layers should decrease as the station moves below the Harang discontinuity corresponding to the counter-clockwise rotation of the electric field vector.

REFERENCES

Heppner J P 1977: J. Geophys. Res., 82, 1115-1126.

Korenkov Yu I 1977: Investigation of the effect of the neutral atmosphere's motion on the seasonal and diurnal behaviour of the Es layer (in Russian). Prepr. No 24, IZMIRAN

Lyatskaya A M, Lyatsky V B, Maltsev Yu P 1978: Geomag. i Aeronomiya, 18, 228.

Maynard N C 1974: J. Geophys. Res., 79, 4620-4631.

Razuvaev O I, Sheshukov S S 1983: Geomag. i Aeronomiya, 23, 31.

Razuvaev O I 1984: Issl. po Geomagn., Aeron. i Fizike Solntsa, 69, 151.

Acta Geod. Geoph. Mont. Hung., Vol. 22 (1-2), pp. 251-274 (1987)

TURBULENCE AND AERONOMICAL PROCESSES IN THE LOWER THERMOSPHERE

P Bencze

Geodetic and Geophysical Research Institute of the Hungarian Academy of Sciences, H-9401 Sopron, P.O.Box 5, Hungary

Aeronomical processes depend on the transport of atmospheric gases. From the transport processes the turbulent diffusion is the least studied, though, probably the most important. In this paper a method of the determination of the turbulent diffusion coefficient on the basis of sporadic E parameters is discussed. The processes controlling the formation and dispersal of the sporadic E layers (chemistry of metal ions, wind shear and turbulence) are reviewed. The results obtained by this method are presented showing aeronomical applications, too.

Keywords: aeronomical processes; ionospheric sporadic E; turbulence

The composition of the neutral gas mixture and of the ions, thus the properties of the gas in the upper atmosphere depend not only on the production (q) and loss (L), but also on the transport of the gas (div $n\underline{v}$), as shown by the continuity equation

$$\frac{dn}{dt} = q - L \mp \operatorname{div}(n\underline{v}) \ .$$

The transport term comprises the wind, turbulent and molecular diffusion. In the lower thermosphere the turbulent diffusion plays an especially important role. That is, the turbopause forms in the lower thermosphere, where the coefficient of molecular diffusion increasing with height equals the turbulent diffusion coefficient. The gravitational separation of the components of the gas mixture begins above the turbopause and thus the neutral gas composition above it depends on its height.

The determination of the turbulent diffusion coefficient is thus an important problem of the aeronomical investigations. Therefore, a method is needed by means of which the turbulent

diffusion coefficient can be determined regularly at many places, inasmuch as it is possible. At present, only ground based measurements can be taken into consideration from this point of view. As it is known, the vertical sounding of the ionosphere is the most wide-spread ground based method of the study of the upper atmosphere.

During ionospheric soundings parameters are also determined the magnitudes of which depend on the dynamics of the ionosphere, on the kinetic state of the medium. The characteristics of the sporadic E layer are those parameters, which refer to the lower thermosphere and are directly connected with dynamical processes. According to the generally accepted theory of the formation of mid-latitude sporadic E layers, they are produced as a result of the wind-shear. However, the wind shear is only a necessary but not sufficient condition of the sporadic E layer formation. For the persistence of the layer the presence of metal ions of very small recombination coefficient is also necessary. Besides these factors of the layer formation the turbulence is opposed to the persistence of the layer. The presence of metal ions, the wind shear and turbulence determine together the formation of sporadic E layers at mid-latitudes. The height of the layer formation depends on the wind shear. The density of the layer as compared to the background electron density is determined to a certain value by the wind shear. If the magnitude of the wind shear exceeds a certain limit, then turbulence develops, which receives energy from the wind shear. This means that below the limit the wind shear strengthens, then it weakens the layer.

In the lower thermosphere the wind shear is produced by atmospheric gravity waves (other sources of the turbulence are unimportant in the lower thermosphere, in a thermally stable region of the atmosphere). The gravity waves are generated either locally, or in the troposphere. As the waves reach the lower thermosphere they begin to be damped. The energy of the waves is transformed into the energy of eddies of different scale, into turbulent energy and finally into thermal energy. This process is shown by the sporadic E layer. Further, the processes

resulting in the formation, persistance and dispersal of the layer are discussed in connection with aeronomical processes.

CHEMISTRY OF METAL IONS

As it has been shown above, the presence of metal ions is also necessary for the persistance of the layer. Metal ions enter the atmosphere in consequence of the infall of meteors. During the impact of meteors their material is heated due to friction in the dense layers of the atmosphere (<120 km). In this process molecules evaporate from the surface of the meteor. Ions are produced either directly due to collision with the molecules of the atmosphere, or later as a result of charge exchange.

Investigations concerning the relation between the ionization of the sporadic E layer and meteor influx led only gradually to unambiguous results. On the basis of hourly values Hedberg (1974, 1975, 1976) found that the correlation between the parameter fbEs of the Es layer (proportional to the ion density) and the meteor influx is maximum, if the meteor fluxes are correlated with fbEs data measured from 3 to 9 hours after the observation of the meteor flux. The delay of the enhanced ionization in the layer as compared to the increase of the meteor influx depends on season, it is less in summer than in winter. However, this result is due to the different diurnal variations of the quantities compared (see Fig. 1). The investigations of Sinno (1980) based on daily mean values have shown the delay of the enhancement of the ionization as compared to the increase of the meteor flux to be 1-2 weeks and greater in summer than in winter. Finally, on the basis of ionospheric data of 37 years and using daily values Baggaley and Steel (1984) have shown that there is no significant correlation between the parameters of the Es layer and the meteor influx. Thus, the meteor activity establishes a reservoir of metal ions in the lower thermosphere which is steadily replenished by meteors and depleted by the wind shear.

A comparison of Es traces on ionograms with radar reflections from meteor trails has shown that sporadic reflections

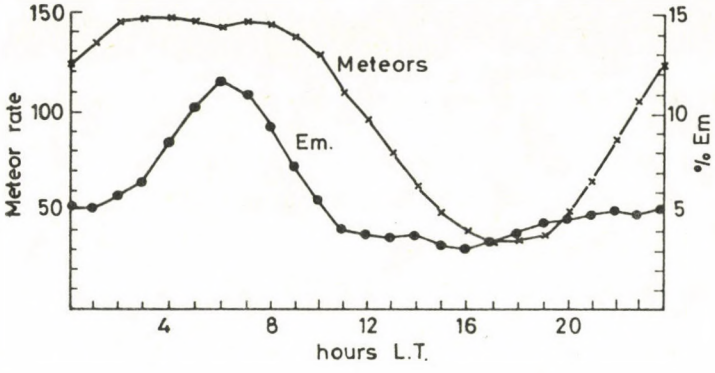

Fig. 1. Diurnal variation of the normalized total hourly percentage occurrence of 1Em type observations (for the period from February, 1964 to January, 1965). The annual averaged hourly diurnal meteor rate is also shown (Goldsbrough and Ellyett 1976)

from the E layer can be divided into three groups; 1. reflections from sporadic ionization produced by a single meteor (type 1 E_m), 2. reflections from sporadic ionization created by meteor showers (type 2 E_m) and 3. reflections from sporadic ionization formed by the concentration of metal ions due to wind shear (type 3 E_m) (Ellyett and Goldsbrough 1976). The types 1 E_m and 2 E_m are the direct consequences of meteor impacts, while the type 3 E_m is only an indirect phenomenon. Type 1 E_m reflections do not influence the critical frequency of the Es layer (fo Es) (Goldsbrough and Ellyett 1976). In Fig. 1 the diurnal variation of the normalized total hourly percentage occurrence of 1 E_m type observations and the diurnal course of the hourly meteor rate are shown. The annual variation of the normalized total percentage occurrence of observed 1 E_m type reflections (influenced by 2 E_m type reflections during meteor showers) and the annual variation of the average hourly meteor rate are presented in Fig. 2. In case of 2 E_m type reflections the greater number of ionized meteor trails may have an effect on foEs, however such cases are seldom. Thus, this result seems to confirm the conclusions drawn by Baggaley and Steel (1984). By comparing the occurrence frequency of 1 E_m and 2 E_m type

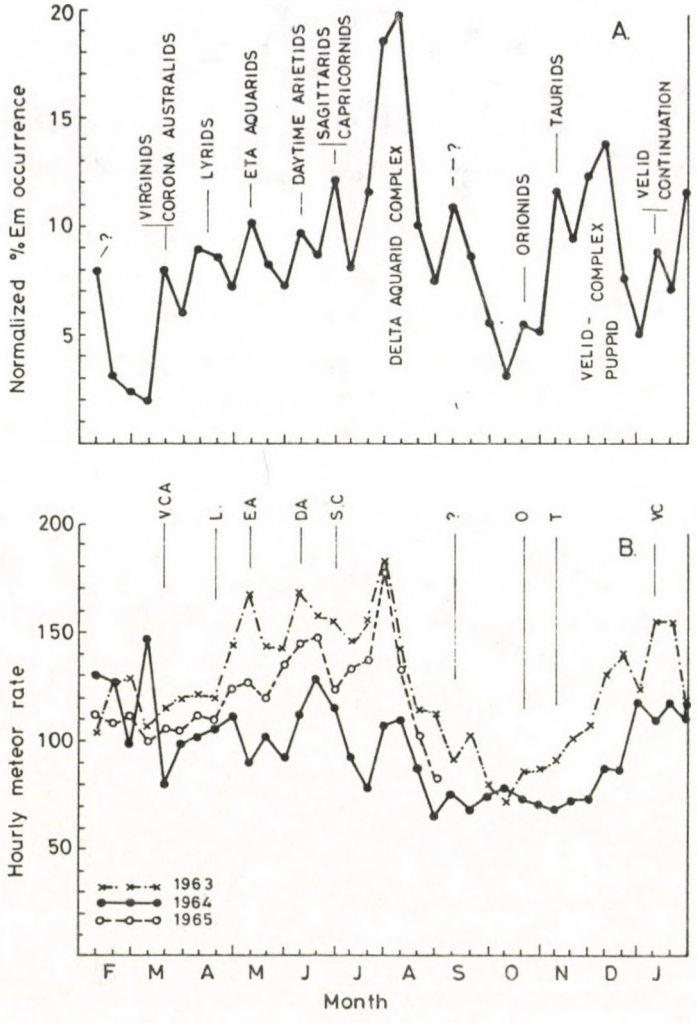

Fig. 2. Annual variation of the normalized total percentage occurrence of 1Em type reflections and the annual variation of the average hourly meteor rate (for the period from February, 1964 to January, 1965) (Goldsbrough and Ellyett 1976)

reflections from sporadic ionization of meteoric origin with 3 E_m reflections it was found that the majority of the reflections belongs to the group 3 E_m, i.e. to the reflections from sporadic stratifications produced by wind shear. Experience

shows that the higher the value of the parameter foEs, or that of fbEs is, above which the changes of the occurrence frequency of the sporadic E layer are studied, the greater is the influence of the meteor activity.

Summarizing, it has to be noted in connection with the interpretation of the correlation between the meteor influx and the ion density in the Es layer that two conditions have to be considered, when searching for correlation between meteor activity and Es, 1. presence of other factors producing sporadic E layers, 2. steady existence of metal ions in the E region. The latter condition can be proved by the comparison of the concentration of metal ions measured in periods without meteor showers with the concentration of these ions observed during meteor showers.

The concentration and distribution of metal ions in the lower thermosphere have been intensively studied in the last years. The metal ions in the F region are in the order of decreasing concentration: Fe^+, Mg^+, Al^+, Si^+, Na^+ and Ca^+. Considering the spatial and temporal variations of the concentration of Fe^+ ions at night, the probability of the concentration being greater than a certain level is maximum below 400 km and at low latitudes ($<20^o$) in the evening hours (Kumar and Hanson 1980). Metal ions are transported by different processes from the lower ionosphere to the upper ionosphere and inversely. If the forces acting on ions (winds, magnetic and electric fields) are known, the diurnal variation of the transport can be determined. In daytime the poleward wind forces the ions to move along the geomagnetic field lines downwards from the F region, while at night the equatorward wind returns them to the F region. During the flight of the satellite OGO-6 measurements have shown the presence of Fe^+ ions at low latitudes to an altitude of 1000 km. Generally, the presence of Fe^+ ions in such large altitudes is explained - in the presence of a steady eastward wind in the E region - by an $\underline{U}\times\underline{b}$ drift. This could raise ions at all latitudes to an altitude, where they are carried by an equatorward wind to the F region. In the vicinity of the magnetic equator the transport is assured by the vertical

$\underline{E}\times\underline{b}$ drift. The detection probability of Mg^+ ions is maximum below 150 km in daytime and in 230 km at night, and at low latitudes near noon (Kumar and Hanson 1980). The concentration of the other metal ions is by an order of magnitude less than that of the ions Fe^+ and Mg^+.

The metal ions in the E region are in the order of decreasing concentration Fe^+, Mg^+, Ni^+, Al^+, Ca^+, K^+, Na^+, Cr^+, Co^+ and Si^+. In the lower ionosphere the metal ions form usually layers and this is due to the wind shear. During periods without meteor showers measurements have shown a distribution of the metal ions presented in Fig. 3. The general characteristic of such profiles is a layer of a half-width of 5-10 km near 93 km containing mostly Fe^+ and Mg^+ ions, but also Na^+, Al^+,

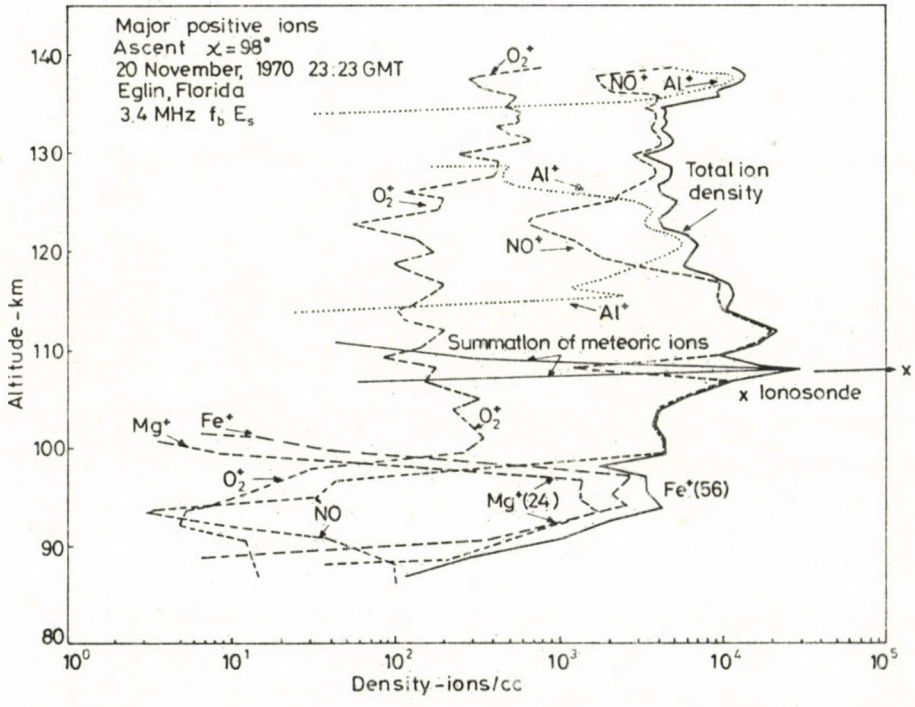

Fig. 3. Ion composition in the E region of the ionosphere after sunset showing a blanketing sporadic E layer (Narcisi 1973, reproduced with permission of D. Reidel Publ. Co., Dordrecht, Holland)

Ca^+, Ni^+ and ions of other metals, as well as other thinner layers at higher altitudes consisting of Si^+, Mg^+ and Fe^+ ions (Narcisi 1968, 1971). In the lower layer the relative abundances of these metals agree with the relative abundance of these metals in chondrite meteorites. The profiles of the different ions are similar. The height of the lower layer and the concentration of ions in it are steadier as compared to the upper layers. A thin layer comprising Si^+ ions at a height of 110 km seems to be a frequent characteristics of the daytime ionosphere, too. The condition that the concentrations of the ions NO^+, O_2^+ in the metal ion layers are less than outside these layers is due to the higher concentration of electrons in these layers accelerating the loss of molecular ions by dissociative recombination. The charge exchange between metal and molecular ions can also contribute to the decreased concentration of molecular ions. The concentration of metal ions amounts to 10 to 100 percent of the total ion density.

During the year the greatest meteor showers are the Perseids in August and the Geminids in December. The results of the measurements carried out during the Geminid meteor shower are shown in Fig. 4 (Zbinden et al. 1975). The concentrations of the metal ions are not higher than in the periods without meteor showers. The ions Na^+, Mg^+, Al^+, Si^+, K^+, Ca^+, Ti^+, Cr^+, Fe^+, Mn^+, Ni^+, Co^+, Zn^+ and the isotopes of Mg^+, Si^+, K^+, Ca^+, Fe^+, Mn^+, Ni^+ were identified. The main metal ion layer exists also in this case. The fact that the density maxima of the heavier metal ions are located at somewhat higher altitudes than the density maxima of the lighter ions can be explained by the different shift, with which these ions follow the nodes of the gravity waves. Computations have shown that only a small part of the metal atoms is ionized. In this case the concentrations of the ions Na^+, Al^+ and Ca^+ relative to that of Mg^+ ions agree well in the region below the main metal layer with the values of the solar system, but the abundances of Fe^+ and Ni^+ are approximately twice as great. In the main metal layer the dominant metal ions are Fe^+ and Mg^+, however, in the

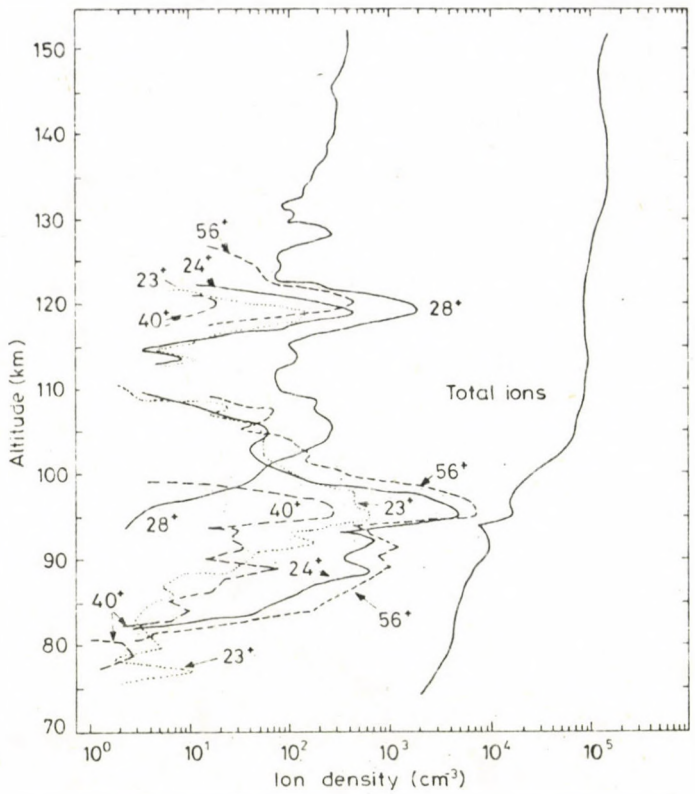

Fig. 4. Height variation of the metal ion densities during the Geminid meteor shower (Reprinted with permission from Planet. Space Sci., vol. 23, Zbinden P A, Hidalgo M A, Eberhardt P, Geiss J, Mass spectrometer measurements of the positive ion composition in the D- and E--regions of the ionosphere, 1975, Pergamon Journals Ltd.)

upper layer the Si^+ ion is the most abundant one as also in periods without meteor showers. The difference between the distribution of Si^+ ions and the profiles of metal ions is due to the fact that the metal oxides can be reduced by atomic oxygen, while in case of SiO this is not possible. The concentrations of alkali ions are twice as great as the usual values. This is probably connected with the low ionization potentials of the alkali metals. The results of the measurements carried out during the Perseid meteor shower are shown in Fig. 5 (Herrmann et al. 1978). The main meteoric layer appears also here in the profile. As in other cases, Na^+, Mg^+, Al^+, Si^+, K^+, Ca^+,

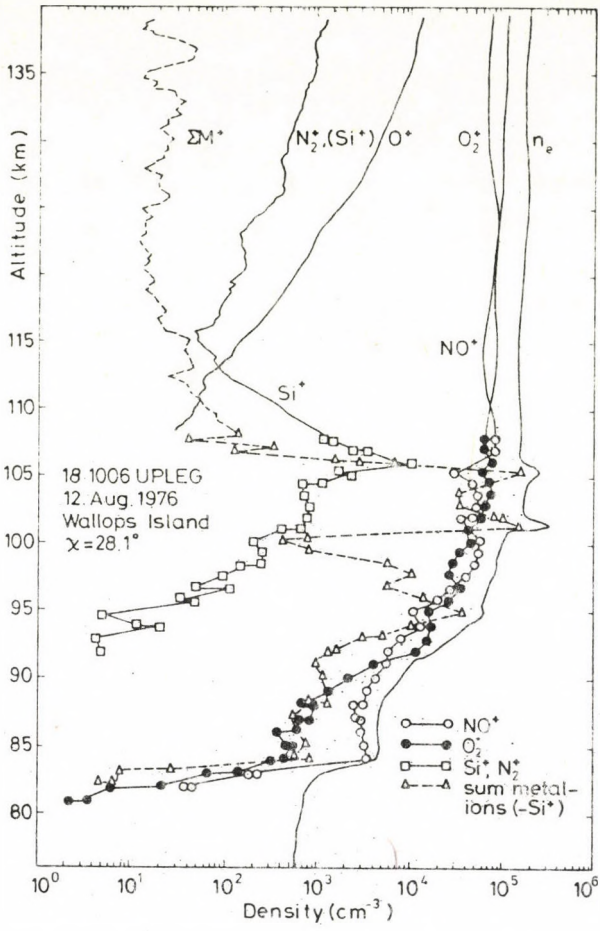

Fig. 5. Height variation of the metal ion densities during the Perseid meteor shower (Reprinted with permission from Space Res. XVIII., Herrmann U, Eberhardt P, Hidalgo M A, Kopp E, Smith L, Metal ions and isotopes in sporadic E layers during the perseid meteor shower, 1978, Pergamon Journals Ltd.)

Ti^+, Cr^+, Mn^+, Fe^+, Co^+ and Ni^+ ions were observed. As in the profile total metal ion concentrations are plotted, the concentrations of these ions are also in this case not higher than in periods without showers. The study of the abundances of the metal ions has shown that the concentration of the iron group ions Ni^+, Cr^+, Co^+ and Mn^+, but also that of Na^+ ions normalized to the concentration of Fe^+ agree with the elemental abundance in carbonaceous chondrites. However, the concentrations of the

Mg^+, Al^+, Ca^+ ions but especially the concentrations of the Ti^+ and Si^+ ions are substantially lower, than in carbonaceous chondrites. This depletion of Ti^+ and Si^+ ions is probably connected with the chemical processes differing from the reactions of other metal ions as it has been demonstrated in case of the Geminid shower. The isotopic ratios showed no substantial difference between the isotopic ratios in the E layer and the terrestrial isotopic abundances.

As regards the existence of the alkali metal ions Na^+ and K^+, observations have shown that the concentration of K^+ ions of meteoric origin does not change during the year, but due to vertical transport the concentration of Na^+ ions of terrestrial origin is greater in winter than in summer (Megie et al. 1978).

In the D and E regions the following reactions participate in the production and loss of metal ions:

$$O_2^+ + M \rightarrow M^+ + O_2 \quad (1)$$

$$NO^+ + M \rightarrow M^+ + NO \quad (2)$$

$$O + M \rightarrow MO^+ + e \quad (3)$$

$$O_2^+ + MO \rightarrow MO^+ + O_2 \quad (4)$$

$$NO^+ + MO \rightarrow MO^+ + NO \quad (5)$$

$$M^+ + O_2 \rightarrow MO^+ + O \quad (6)$$

$$M^+ + O_3 \rightarrow MO^+ + O_2 \quad (7)$$

$$M^+ + O_2 + X \rightarrow MO_2^+ + X \quad (8)$$

$$MO^+ + O \rightarrow M^+ + O_2 \quad (9)$$

$$MO_2^+ + O \rightarrow MO^+ + O_2 \quad (10)$$

$$MO^+ + e \rightarrow M + O \quad (11)$$

where M, X denote respectively metal and a third particle.

Photoionization can be neglected as compared to the charge exchange. Assuming quasi-stationary conditions the following equations are obtained on the basis of these reactions for the metal ions

$$[M^+] = \frac{(k_1[O_2^+] + k_2[NO^+])[M] + k_9[MO^+][O]}{k_6[O_2] + k_7[O_3] + k_8[O_2][X]}$$

$$[MO^+] = \frac{k_3[O][M] + (k_4[O_2^+] + k_5[NO^+])[MO] + (k_6[O_2] + k_7[O_3])[M^+]}{k_9[O] + k_{11}[e]} +$$

$$+ \frac{k_{10}[MO_2^+][O]}{k_9[O] + k_{11}[e]}$$

$$[MO_2^+] = \frac{k_e[M^+][O_2][X]}{k_{10}[O]} .$$

Computations have shown that the concentration of metal oxides is determined erroneusly in the majority of the cases at the processing of mass spectrometer measurements. The concentration established is usually greater than it would be according to the chemical reactions. The erroneus value of the concentration is due on the one hand to a contamination of the mass spectrometer, on the other hand to the conditions that the molecular weight of the metal oxide is equal to the molecular weight of an other component of the ionospheric gas (Murad 1978). As regards SiO, it is noted that though the deposition of the neutral silicon in the E region is similar to the deposition of iron and magnesium, below 100 km due to the reactions

$$Si^+ + H_2O \longrightarrow HSiO^+ + H$$

$$HSiO^+ + e \longrightarrow SiO + H .$$

SiO is produced and thus the concentration of Si^+ is less than the concentrations of other meteor ions. Below 90 km Si^+ ions are lost by reacting with O_2 more quickly than Mg^+ and Fe^+ ions and produce SiO_2 (Ferguson et al. 1981). This is the reason why the concentration of Si^+ is low as compared to the concentrations of Mg^+ and Fe^+ ions in the main layer.

The investigation of the metal dioxides yielded similar results (Murad 1978).

Experimentally found recombination coefficients of the metal ions are very small. These conditions provide for the lasting presence of a layer of an ion density greater than in its surroundings.

WIND-SHEAR

Wind-shear is the other basic factor of the formation of sporadic E layers. However, as it will be explained later, the wind shear promotes not only the formation, but also the dispersal of the layer.

The determination of the wind shear is both directly and indirectly difficult. Therefore, the number of papers dealing with the wind-shear is also small. As regards the direct methods, the wind shear can be determined by means of chemical trails. This method leads to a good height resolution. Rosenberg (1968) collected the data of 70 mid-latitude wind profiles obtained by the method of chemical-release. In Fig. 6 the height profile of the wind shear determined on the basis of these data is shown. The wind shear decreases with increasing height first

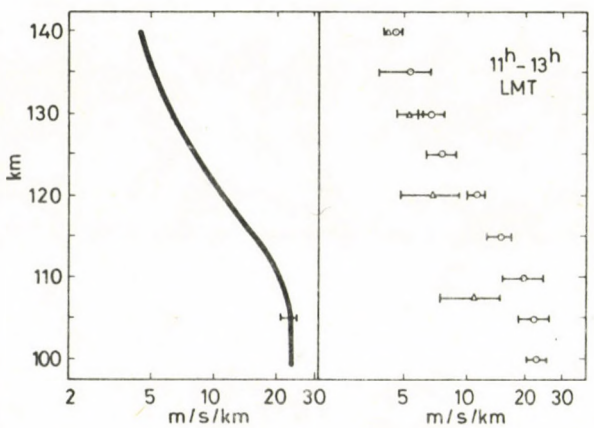

Fig. 6. Height profile of the mean wind-shear determined on the basis of chemical trails (left) (Rosenberg 1968) and computed by means of sporadic E parameters (right) for winter circulation disturbances in the lower thermosphere connected with stratospheric warmings (triangles) and for normal winter conditions (circles) (Bencze 1980)

slowly, then more quickly. Another direct method of the wind--shear determination is the partial reflection method. From the data obtained with this method Manson et al. (1974) inferred the day-time variation of the wind-shear in different height intervals (Fig. 7). Although the day-time variation presented here refers only to April, it is however characteristic of the

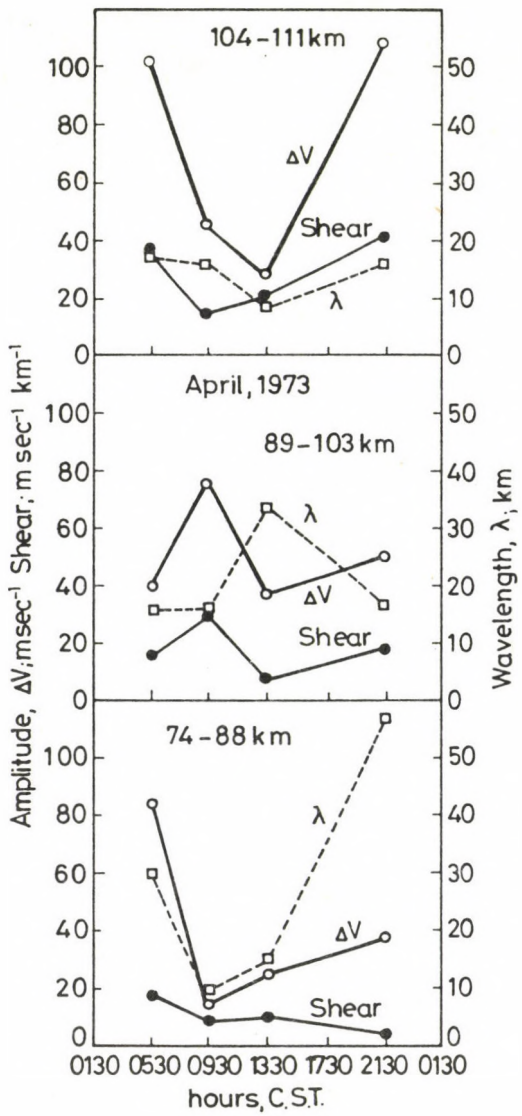

Fig. 7. Day-time variation of the amplitude (ΔV), shear and vertical wave length (λ_z) associated with the irregular wind component (Manson A H, Gregory J B, Stephenson D G, 1974, J. atmos. Sci. 31, 2207-2215, by courtesy of the American Meteorological Society)

other months, too. There is no day-time variation in the height interval 74-88 km. In the height interval 89-103 km the day--time variation is irregular, though near noon a small minimum can be seen. In the height interval 104-111 km the day-time variation shows a minimum about noon with increasing values towards both sunrise and sunset. In summer the wind-shear is significantly less than in winter or during equinoxes.

An indirect method of the wind-shear determination at mid--latitudes is based on the application of the parameters of the sporadic E layer. As it is known from the wind-shear theory of the sporadic E layer formation, the influence of the geomagnetic field on the motion of ions moving with the neutral particles results in stratifications of the ion distribution. From the equation of motion of ions one gets:

$$\vec{V}_i = \frac{1}{1 + \left(\frac{\nu_i}{\omega_i}\right)^2} \left[\left(\frac{\nu_i}{\omega_i}\right)^2 \vec{U} + \left(\frac{\nu_i}{\omega_i}\right) \vec{U}\times\vec{b} + (\vec{U}\times\vec{b})\vec{b} \right]$$

where ν_i, ω_i are respectively the collision frequency and the gyrofrequency, U is the wind velocity and $\underline{b}$ is the unit vector of the geomagnetic field. Since the motion of ions is determined by the motion of the neutral gas and by the geomagnetic field, the velocity of ions has three components, parallel to the velocity of the neutral particles, perpendicular to both the velocity of the neutral particles and the geomagnetic field, and parallel to the geomagnetic field. The factor by which the terms in the equation are multiplied, is the ratio of the collision frequency to the gyrofrequency. Since in the lower thermosphere the collision frequency decreases with height more rapidly than the gyrofrequency, their ratio decreases, too. As a result of this the motion of the ions is determined at the base of the thermosphere by the motion of the neutral particles, i.e. by the wind and the direction of the motion corresponds to that of the wind. With increasing altitude this component becomes insignificant and the motion

becomes predominant, which is determined by the wind and the geomagnetic field, and is perpendicular to both the wind velocity and the geomagnetic field. Finally, also this component loses its importance and the motion determined by the geomagnetic field and parallel to it becomes dominant. Substituting the expression of the ion velocity into the continuity equation

$$\frac{dn_i}{dt} = q - \alpha n_i^2 - \frac{d}{dz}(n_i \vec{V}_i)$$

and neglecting the gradients of the ion density and of the temperature, the vertical and meridional components of the wind, in quasi stationary conditions the effective wind-shear is obtained as

$$\left(\frac{dU_y}{dz}\right)_{eff} = -\frac{1 + \left(\frac{\nu_i}{\omega_i}\right)^2}{\frac{\nu_i}{\omega_i}\cos I} n_{imax}\left(\frac{n_{io}^2}{n_{imax}^2} - 1\right)$$

where n_{io} is the ion density in the absence of the wind-shear (within the layer), n_{imax} is the maximum ion density in the layer and I is the magnetic dip. It is assumed that the recombination coefficient within the layer is equal to the recombination coefficient outside of the layer. Reddy and Matsushita (1968) employed this relation for the determination of the wind-shear. Instead of the undisturbed ion density at the height of the layer (in absence of wind-shear) they used the maximum electron density in the E region (foE^2) multiplied by a factor. In the computations of the collision frequency and of the gyrofrequency the changes of the atmospheric parameters with height were not considered. Their data are mean values of the effective wind-shear referring to the height range, where sporadic E layers occur. In Fig. 8 the diurnal variation of the effective wind-shear constructed by means of these data can be seen which has a day-time maximum and a minimum at night, just

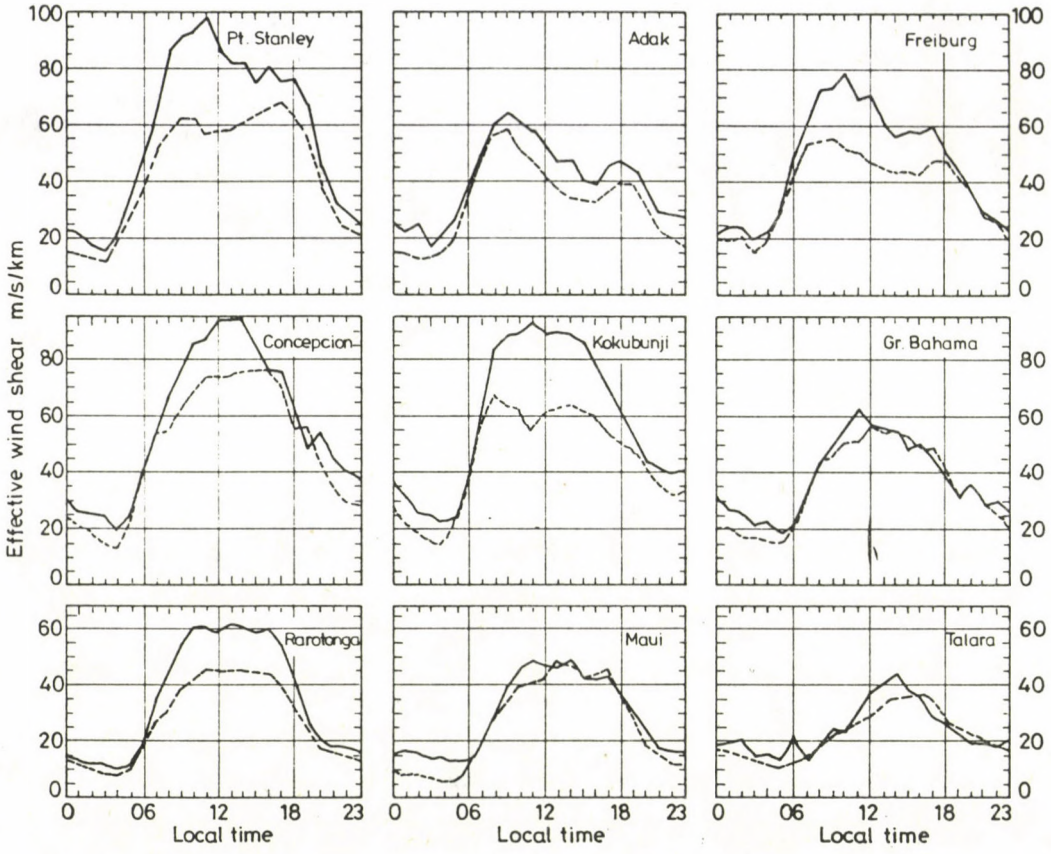

Fig. 8. Diurnal variation of the effective wind-shear deduced from blanketing sporadic E in June-July. The solid curves represent average values for 1958-1961, the broken curves for 1962-1965 (Reprinted with permission from J. atmos. terr. Phys., vol. 30, Reddy C A and Matsushita S, The variations of neutral wind shears in the E-region as deduced from blanketing Es, 1968, Pergamon Journals Ltd.)

contrasted with the results of the partial reflection measurements. This is probably due to the approximations mentioned above. Reddy and Matsushita determined also the seasonal variation and the change of the effective wind-shear with solar activity. They found that the effective wind-shear is larger in summer than in winter, moreover, it decreases with decreasing solar activity.

In order to correct the deficiences of the effective wind--shear determination a method has been developed. The values of

the undisturbed ion density at the height of the sporadic E layer are computed by means of formulas giving the electron (ion) distribution in ionospheric models. In these formulas foE values measured simultaneously with the Es parameters are used. Thus, the computations are limited to day-time hours. In the determination of the collision frequency the decrease of both the neutral gas density and of the molecular weight with height are taken into account using atmospheric models. Computing the gyrofrequency, the decrease of the geomagnetic field and of the molecular weight are also taken into consideration. Thus, it was possible to determine also the height variation of the effective wind-shear (Bencze 1980). According to these results, in the winter months the effective wind-shear decreases with increasing height. At the same time, during winter circulation disturbances in the lower thermosphere connected with stratospheric warmings the effective wind-shear is less to a height of 130 km than in other periods of the winter (Fig. 6). Since the decrease of the wind-shear is due to the increase of the vertical wave length of the gravity waves, it may be assumed that this indicates the decreased damping of atmospheric waves or the increase of the vertical energy flux.

TURBULENCE AND AERONOMICAL PROCESSES IN THE LOWER THERMOSPHERE

The wind-shear can produce not only stratifications, but with its increase a limit is reached where the turbulence produced by the wind-shear promotes the dispersal of the layer. Therefore, the possibility of the development of the turbulence and its intensity have to be determined. As it is known, the criterion of the turbulence can be expressed by the Richardson number. According to experiments, if the gradient Richardson number

$$R_i = \frac{\frac{\partial \Theta}{\partial z}}{\frac{g}{\Theta}\left(\frac{\partial U}{\partial z}\right)^2}$$

is less than 0.25, the motion is turbulent. Here the vertical

temperature gradient, i.e. the stabilizing force is in the numerator, while in the denominator the wind-shear squared, that is the destabilizing force can be found. Computations carried out with model values of the temperature and with wind-shear values obtained by means of sporadic E parameters have shown that in Es layers the motion is always turbulent. This means that the turbulence plays an important role in the formation of sporadic E layers.

This condition can be used in the study of aeronomical reactions, if a relation between the gradient Richardson number and the parameters of the turbulence (intensity, rate of dissipation and coefficient of turbulent diffusion) can be found. Deacon (1959) presented an empirical relation between the gradient Richardson number and the vertical component of the turbulent wind

$$\frac{w}{U} = \mp\ 0.15\ (|R_i|)^{1/2} + 0.08$$

where w is the vertical component of the turbulent wind and U is the horizontal component of the wind. Since the turbulent wind and its square, the turbulent intensity depend on the spectrum of turbulent motions, the intensity and other parameters of the turbulence can be determined, if the dimensions of the eddies arising in the flow are known. The dimensions of the eddies can be estimated from the fact that they are smaller than the wave length of the reflected radio waves. If the dimensions of the eddies are larger than the Kolmogorov microscale and smaller than the Obukhov length, then an inertial subrange exists in the spectrum of turbulence. Investigations show that in our case this is the situation. Then the turbulent parameters can be computed by the formulas (Zimmerman and Murphy 1977)

$$\langle w^2 \rangle = 3.4\ \frac{\varepsilon}{N}\ ; \qquad \varepsilon = \frac{1}{3}\ \langle w^2 \rangle\ N\ ; \quad K = \frac{1}{2}\ \frac{\langle w^2 \rangle}{N}$$

where N is the Brunt-Vaisala frequency, ε and K are respectively the rate of dissipation and the coefficient of turbulent diffusion. Since in aeronomical investigations the turbulent

diffusion coefficient is used in the majority of cases, in the following only the turbulent diffusion coefficient is considered.

Using these formulas the day time and seasonal variations of the turbulent diffusion coefficient have been determined. In Fig. 9 the day-time values of the turbulent diffusion coefficient computed by means of sporadic E parameters are shown at different altitudes (Bencze 1984). There is a good agreement with the results obtained by other methods. In Fig. 10 the day-time variations of the turbulent diffusion coefficient are presented in different altitudes. In agreement with the results obtained by the direct methods the turbulent diffusion coefficient is less in day-time than at night. The seasonal

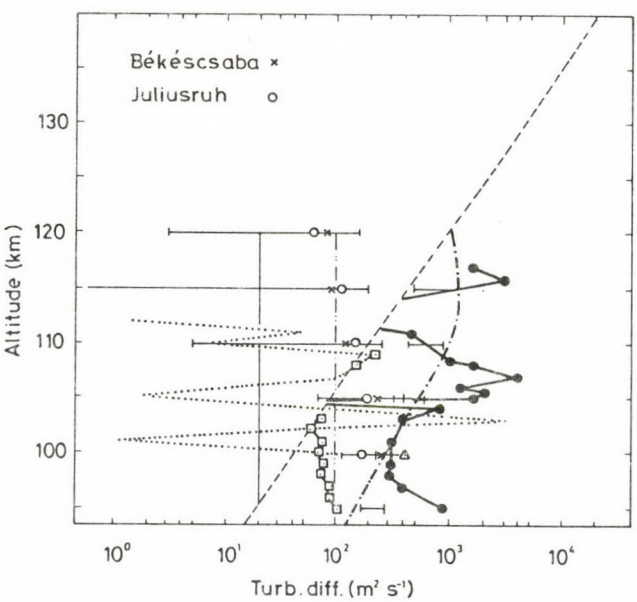

Fig. 9. Day-time values of the turbulent diffusion coefficient at different altitudes computed by means of sporadic E parameters compared with the data of other authors (-·-·- Johnson and Gottlieb 1970, ····· Philbrick et al. 1973, -·-·-·- Hunten 1975, black circles Woomera am, 16 Oct. 1969, squares pm, 17 Oct. 1969, Roper 1977, □ Ebel 1978, ⊢——⊣ Alcayde et al. 1979, ——— Allen et al. 1981, ----- molecular diffusion coefficient) (Bencze 1984)

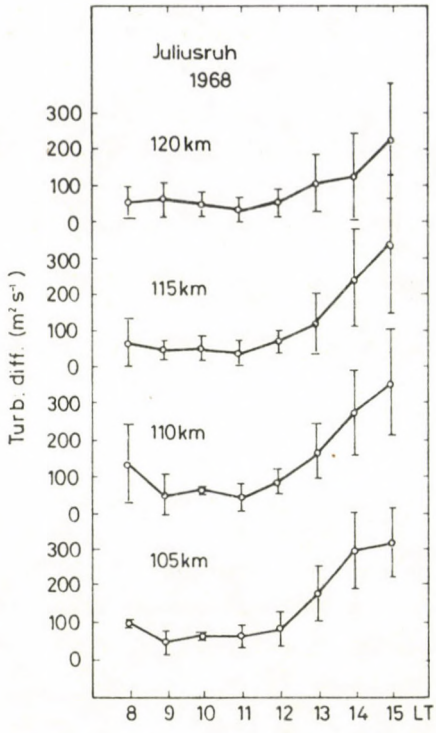

Fig. 10. Day-time variations of the turbulent diffusion coefficient in different altitudes computed by means of sporadic E parameters

variations of the day-time values of the turbulent diffusion coefficient in different heights are shown in Fig. 11. The mean

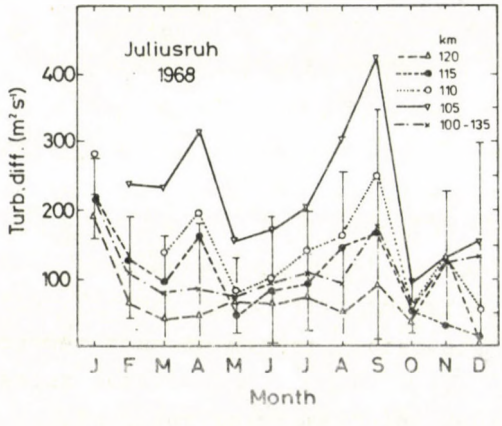

Fig. 11. Seasonal variations of the turbulent diffusion coefficient in different altitudes computed by means of sporadic E parameters

seasonal variation has a minimum in summer and a maximum in winter. This result corresponds to the seasonal variation obtained by other authors. However, as it is indicated by the scattering of the data, the variability of the turbulent diffusion coefficient is large. Since in case of other published data the scattering is not indicated and in the majority of cases the curve is based on individual, or few data, the conclusion might be drawn that the seasonal variation changes from year to year.

On the basis of the computed values of the turbulent diffusion coefficient the height of the turbopause can also be determined (see also Ovezgeldiev et al. 1984). First, using atmospheric models the turbulent and mocelular diffusion coefficients are calculated. As it is known, the turbopause is located at the height, where the molecular diffusion coefficient equals the turbulent diffusion coefficient. If once the height of the turbopause is known, the relative change of the concentration of the atmospheric gases due to the rise or sinking of the turbopause can be obtained on the basis of the formula

$$\frac{\Delta n_j}{n_j} = \left(\frac{1}{H_j} - \frac{1}{H} + \alpha_j \frac{d \ln T}{dz} \right) \Delta z$$

where n_j is the concentration of the atmospheric gas of the type j, H, H_j are the scale height of the j type atmospheric gas and that of the atmosphere, α is the thermal diffusion factor, Δz is the height change of the turbopause, H_j, H and T are obtained from atmospheric models. In Fig. 12 the seasonal variation of the computed relative atomic oxygen concentration is shown. Both the form and the magnitude of the seasonal variation of the relative atomic oxygen concentration agree with the results of mass spectrometer measurements. In this way, the variations of the relative concentration of other atmospheric gases due to height changes of the turbopause can also be determined.

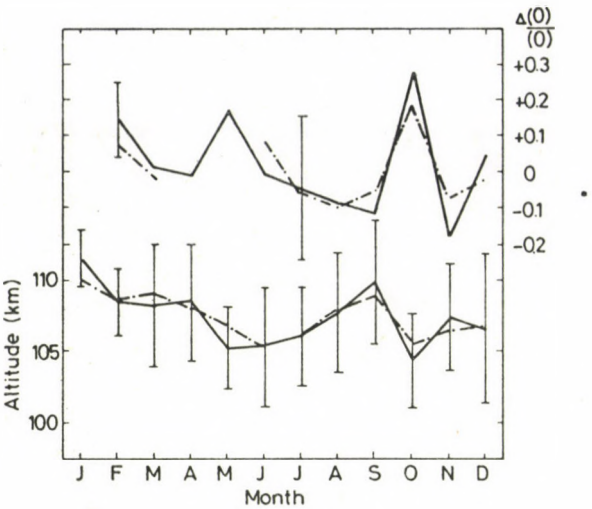

Fig. 12. Seasonal variation of the turbopause (below) and of the relative atomic oxygen concentration due to height changes of the turbopause (above) (The solid curve represents values obtained with the data of the ionospheric station Juliusruh, the dash and dot curve is obtained with the data of the station Békéscsaba)

REFERENCES

Alcayde D, Fontanari J, Kockarts G, Bauer P, Bernard R 1979: Ann. Geophys., 35, 41-51.

Allen M, Yung Y L, Waters J 1981: In: Handbook for MAP, 2, 454-461.

Baggaley W J, Steel D I 1984: Planet. Space Sci., 32, 1533-1539.

Bencze P 1980: Acta Geod. Geoph. Mont. Hung., 15, 247-256.

Bencze P 1984: In: Handbook for MAP, 10, 179-182.

Deacon E L 1959: Intern. J. Air Pollution, 2, 92.

Ebel A 1978: Beitr. Phys. Atmos., 51, 31-43.

Ellyett C D and Goldsbrough P F 1976: J. Geophys. Res., 81, 6131-6134.

Ferguson E E, Fahey D W, Fehsenfeld F C, Albritton D L 1981: Planet. Space Sci., 29, 307-312.

Goldsbrough P F, Ellyett C D 1976: J. Geophys. Res., 81, 6135-6140.

Hedberg A 1974: Kleinheubacher Berichte, 17, 247-254.

Hedberg A 1975: Kleinheubacher Berichte, 18, 261-268.

Hedberg A 1976: J. atmos. terr. Phys., 38, 785-788.

Herrmann U, Eberhardt P, Hidalgo M A, Kopp E, Smith L 1978: Space Res., XVIII, 249-252.

Hunten D M 1975: In: Atmospheres of Earth and the Planets (ed. B M McCormac). D. Reidel Publ. Co., Dordrecht, Holland, 59-72.

Johnson F S, Gottlieb B 1970: Planet. Space Sci., 18, 1707-1718.

Kumar S, Hanson W B 1980: J. Geophys. Res., 85, 6783-6801.

Manson A H, Gregory J B, Stephenson D G 1974: J. atmos. Sci., 31, 2207-2215.

Megie G, Bos F, Blamont J E, Chanin M L 1978: Planet. Space Sci., 26, 27-35.

Murad E 1978: J. Geophys. Res., 83, 5525-5530.

Narcisi R S 1968: Space Res., VIII, 360.

Narcisi R S 1971: In: Physics of the Upper Atmosphere Erice (Italy) 1970 (ed. F Verniani). Editrice Compositori, Bologna, 12-59.

Narcisi R S 1973: In: Physics and Chemistry of Upper Atmospheres (ed. B M McCormac). D. Reidel Publ. Co., Dordrecht, Holland, 171-183.

Ovezgeldiev O G, Korsunova L P, Karadzhaev Yu 1984: In: Handbook for MAP, 10, 183-187.

Philbrick C R, Narcisi R S, Good R E, Hoffman H S, Keneshea T I, MacLeod M A, Zimmerman S P, Reinisch B W 1973: Space Res., XIII, 441-448.

Reddy C A, Matsushita S 1968: J. atmos. terr. Phys., 30, 747-762.

Roper R G 1977: In: The upper-Atmosphere and Magnetosphere. Nat. Acad. Sci., Washington D.C., 117-129.

Rosenberg N W 1968: J. atmos. terr. Phys., 30, 907-917.

Sinno K 1980: J. atmos. terr. Phys., 42, 35-39.

Zbinden P A, Hidalgo M A, Eberhardt P, Geiss J 1975: Planet. Space Sci., 23, 1621-1642.

Zimmerman S P and Murphy E A 1977: In: Dynamical and Chemical Coupling between the Neutral and Ionized Atmosphere (eds. B Grandal and J A Holtet). D. Reidel Publ. Co., Dordrecht, 35-47.

Acta Geod. Geoph. Mont. Hung., Vol. 22 (1-2), pp. 275-281 (1987)

A COMPARISON OF METHODS OF TURBULENCE DETERMINATION BASED ON IONOSPHERIC DATA

L P Korsunova

Institute for Physical and Technical Studies of the Turkmen SSR Academy of Sciences, Gogol st. 15, Ashkhabad, 744000, USSR

The vertical distribution of the turbulent diffusion coefficient K_t determined from ionospheric data on the basis of the "wind-shear" theory of mid-latitude E_s for heights between 95 and 120 km is discussed. Formulae are given, which allow to calculate K_t by means of the frequency parameters of Es and simultaneous wind measurements. It is shown that the annual variation of K_t indicates significant spatial variations.

Keywords: semi-transparence; sporadic E; turbulence; wind-shear

At present it is a commonly accepted fact that mid-latitude sporadic E can be used as an indicator of turbulence in the lower thermosphere. At heights from 95 to 120 km the same vertical shears of the horizontal wind are responsible both for the E_s formation and the generation of turbulence. Due to this several methods based on the wind-shear theory of this layer have been suggested for the determination of turbulent parameters using E_s data (Ovezgeldiev et al. 1977, 1978; Bencze 1983, 1984).

Taking into account the role of eddy diffusion in E_s formation, formulae have been obtained which allow to determine the coefficient of turbulent diffusion K_t, if the simultaneously measured profiles of electron concentration and that of the neutral wind components are given (Ovezgeldiev et al. 1978). For the E_s maximum:

$$K_t = \frac{N^2\, C(Z_m)\, XQ_i}{\pi n_m^2 (I + Q_i^2)} - \frac{2Q_i\,(1 + Z^2 Q_i^2)}{I + Q_i^2}\,\frac{kT}{eB}\,, \qquad (1)$$

where N is the electron content of the Es layer.

n_m and $C(Z_m)$ are respectively the electron concentration and the wind shear at the layer maximum,

$$C(Z_m) = \frac{d}{dz}\left[V - ZQ_i U\right]_{Z_m} ; \quad Q_i = \frac{eB}{m_i \nu_i}$$

(Generally accepted notations are not explained).

In Fig. 1 the average distribution of the vertical turbulent transfer coefficients is shown, which have been calculated by means of Eq. (1) from the published data of rocket measurements of n_e and wind, carried out in Wallops Island, USA at night during the summer months (Korsunova and Ovezgeldiev 1981). These calculations confirmed the existence of turbulence with a layered structure at h = 95-100 km revealed by the observation of chemical releases (Rosenberg et al. 1973), and it made possible to draw the following conclusions:

1. the value of K_t in the mid-latitude lower thermosphere is 10^6-10^7 cm^2/s
2. maximum K_t values are recorded mostly near the height of 110 km.

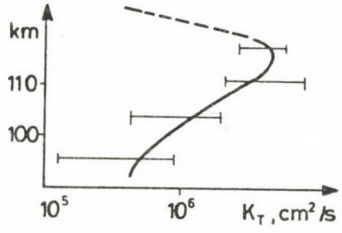

Fig. 1. Vertical distribution of the turbulent diffusion coefficient obtained on the basis of rocket experiments at Wallops Island

It was noted even then that the intensity of turbulent transfer seems to change from day to night and from season to season. However, the reliable determination of these variations by rocket measurements is difficult because of their sporadic and short-lived character. The necessary information can be obtained only by long-lived observations at stations of

vertical ionospheric sounding. It has been shown (Ovezgeldiev et al. 1977) that the range of the semi-transparence of mid-latitude E_s $\left(\frac{\overline{\Delta fb}}{fb}\right)$ due to the scattering of radiowaves on small scale irregularities of electron concentration comprises information on the intensity of turbulent processes in the height of E_s formation. Thus, using the data referring to the range of E_s semitransparence spatial and temporal variations of the turbulence in the lower thermosphere can be studied. In Fig. 2 the annual variations of $\frac{\overline{\Delta fb}}{fb}$ obtained on the basis of E_s observations in Washington (USA) (38.7°N, 77.1°W) and that of K_t calculated by Eq. (1) for published rocket and wind measurements at Wallops Island (USA) (37.9°N, 75.1°W) during low solar activity (Korsunova and Ovezgeldiev 1981) are plotted. As it can be seen the character of the changes of these quantities is similar except the period April-May, which may prove the reality of the relative changes of turbulent intensity obtained by ground-based measurements of the E_s frequency parameters. An analysis of the annual variations of the range of E_s semi-transparence at other ionospheric stations located within the latitude zone of 20-60°N shows that turbulent mixing increases during solstices as compared to equinoxes (Ovezgeldiev et al. 1984).

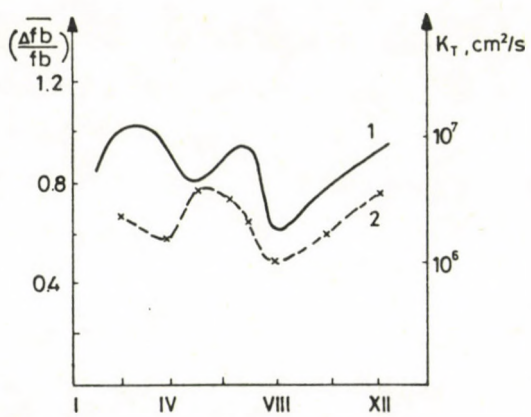

Fig. 2. Annual variation of the range of semi-transparence at Washington (1) and that of the turbulent diffusion coefficient at Wallops Island (2) in 1961-65

For the investigation of aeronomic problems, especially for the determination of the neutral composition it is necessary to turn from the relative changes of the turbulent intensity to the absolute values of the turbulent diffusion coefficient. Such a conversion is possible only for mean statistical distributions of the range of semi-transparence with height. Ovezgeldiev et al. (1977) have shown that the height of the most frequent E_s occurrence is characteristic of the mean height of the turbopause relating to the given conditions, where the condition $K_t = D_m$ is satisfied. In fact, heights of the turbopause determined for $\varphi = 40^oN$ coincide within the range of experimental errors with rocket data referring to the homopause (Ovezgeldiev et al. 1984). Comparing the range of semi-transparence at the height of the turbopause with D_m the value of the coefficient of turbulent diffusion can be estimated to which $\left(\frac{\Delta\bar{f}b}{\bar{f}b}\right)$ observed at other heights within the zone of redistribution (10-15 km) corresponds. In Fig. 3 the mean profiles of K_t (Curve 1) are shown calculated in the above manner for summer day (a) and night (b) conditions in 1966-1967 at the latitude of Ashkhabad (38^oN).

It may be interesting to compare the profile of the turbulent diffusion coefficient determined by means of the above technique with that which is obtained by the method described by Bencze (1983) for one and the same point and time.

According to the latter method (Bencze 1983) K_t is calculated from

$$K_t = \frac{\langle w^2 \rangle}{\left(\frac{g}{\theta}\ \frac{\partial\theta}{\partial Z}\right)^{1/2}} \qquad (2)$$

which is valid for the inertial range of small scale turbulence. Our calculation concerning the energy spectrum of small scale E_s irregularities confirmed the turbulent character of these irregularities and the presence of the inertial range in the spectrum as well (Karadzhayev et al. 1984).

The applicability of formula (2) for the determination of turbulent parameters on the basis of E_s data can be considered as experimentally proved. If the condition $Ri < 0.25$ is satis-

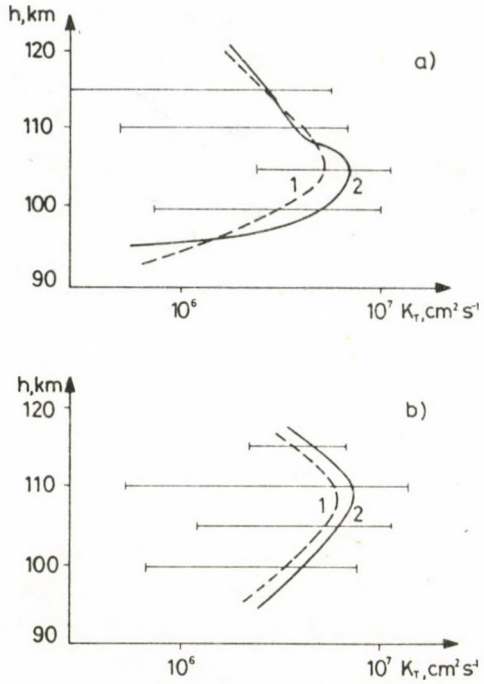

Fig. 3. Vertical distribution of the turbulent diffusion coefficient in summer determined by different methods for Ashkhabad, a) day, b) night

fied, the turbulent intensity $\langle W^2 \rangle$ is calculated using horizontal wind velocity data at E_s heights. The gradient Richardson number (Ri) is calculated taking into account the height variation of temperature and density according to CIRA 72, as well as that of the wind shear computed from measured E_s parameters (suggesting a parabolic form of the layer) and model values of the background electron concentration. The effective wind shears obtained were reduced to true ones by the transformation coefficient K' calculated from the relationship

$$\left(\frac{dU}{dZ}\right)_{exp} = K' \left(\frac{dU}{dZ}\right)_{eff}$$

for each given height (in 5 km intervals) and for all values of effective shears during a season. In this procedure the limiting

values of wind shears observed (Rosenberg and Zimmerman 1971) were taken since E_s formation is connected with the presence of large wind shears. The neutral wind velocity at E_s heights was determined on the basis of simultaneous measurement of the drift velocity of small scale irregularities by the spaced receiver method. In the computations observations of E_s and drifts carried out at Ashkhabad, USSR (38^{O}N, 58^{O}E) in 1966 and 1967 were used. Mean profiles of the turbulent diffusion coefficient calculated according to Eq. (2) for summer day (a) and night (b) conditions are shown in Fig. 3 (Curve 2). Comparison of the profiles in this figure determined by the different methods shows an agreement of the K_t values in case of the statistically sufficiently numerous summer data within the limits of a factor of 1.5-2. The heights of maximum turbulence also coincide within a range of 5 km.

In Fig. 4. the annual variation of the turbulent diffusion coefficient is shown at h = 105 km calculated using the range of E_s semitransparence and turbopause height at the latitude of Ashkhabad.

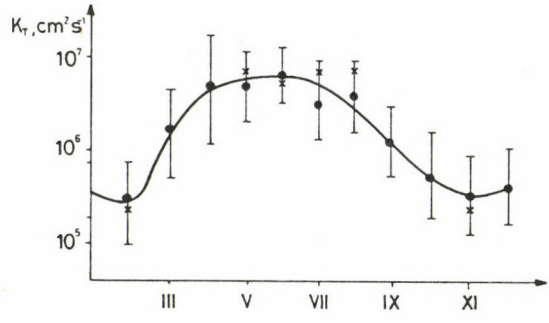

Fig. 4. Annual variation of the turbulent diffusion coefficient at h = 105 km for daytime (Ashkhabad)

Results of daytime ionospheric observations of many years were used. Crosses show K_t values determined by means of the method of Bencze (1983) for simultaneous measurements of E_s and wind carried out in different months of 1966-1967. The agreement

between the two methods of K_t determination is evident and proves the significant change of turbulent intensity from summer to winter (by one order of magnitude).

A comparison of the annual variations of K_t at stations located at the same latitude in the western and eastern hemispheres (Figs 2 and 4) shows some longitudinal effect. This effect is characterized by the occurrence of a second winter maximum of turbulence in the annual variation of K_t in the western hemisphere. The results obtained by Bencze (1984) for 46^{o}N latitude and the data mentioned above show marked spatial changes of the turbulent intensity.

Thus the investigation carried out enables to state that the different methods of turbulent diffusion coefficient determination based on routine measurements of ionospheric parameters and especially that of E_s parameters give results, which are not conflicting and are in agreement with the data obtained by mid-latitude rocket experiments.

REFERENCES

Bencze P 1983: Acta Geod. Geoph. Mont. Hung., 18, 109-117.

Bencze P 1984: In: Middle Atmosphere Program. Handbook for MAP (ed. J Taubenheim), 179-182.

Karadzhayev Yu, Korsunova L P, Ovezgeldiev O G 1984: In: XIV All-Union conference on radiowave propagation. Abstracts, part 1. Nauka, Moscow

Korsunova L D, Ovezgeldiev O G 1981: Geomagn. i Aeronomiya, 21, 124-126.

Ovezgeldiev O G, Korsunova L P, Bakaldina W D 1977: In: Physical processes in the upper atmosphere. Ilym, Ashkhabad, 26-31.

Ovezgeldiev O G, Korsunova L P, Gorbunova T A 1978: Proc. Academy of Sci. of the TSSR, Ser. Phys.-Tech., Chem. and Geolog. Sciences, No 3, 42-45.

Ovezgeldiev O G, Korsunova L P, Karadzhaev Yu 1984: In: Middle Atmosphere Program, Handbook for MAP (ed. J Taubenheim), 183-187.

Rosenberg N W, Zimmerman S P 1971: Third Seminar on the cause and structure of temperate latitude sporadic E., Washington

Rosenberg N W, Golomb D, Zimmerman S P, Vickery W K, Theon J S 1973: Space Research, 13, 435-439.

Acta Geod. Geoph. Mont. Hung., Vol. 22 (1-2), pp. 283-291 (1987)

CHARACTERISTICS OF WIND SHEAR, ATMOSPHERIC GRAVITY WAVES AND TURBULENCE AS DETERMINED BY METEOR RADAR MEASUREMENTS

V V Sidorov, A N Fakhrutdinova, V A Ganin

State University of Kazan, 420008 Kazan, Lenin str. 18, USSR

The results of meteor radar measurements carried out in Kazan are presented, basic relations concerning the variations of wave and turbulent motions with time and height in the lower thermosphere are discussed. In the height variation of the prevailing wind a quasi-sinusoidal wave of a wave length of 14 km has been found. Considering the height profile of the wind and on the basis of the wind-shear theory, the thickness of the Es layer has been estimated.

Keywords: atmospheric waves; meteor radar method; wind-shear; turbulence

The meteor radar investigation of dynamical processes in the height range of 80-110 km is one of the most perspective methods and developed intensively in the last decade both in the USSR and in other countries. The development of the method is promoted by correcting the methodology of observations, by the improvement of the system of radio location, its equipping with height measuring instruments. This assures a reliable determination of the parameters of the prevailing wind, tides, internal gravity waves, turbulence and wind-shear in the lower thermosphere by means of meteor radar measurements.

The knowledge of the wind system of the lower thermosphere including temporal and spatial variations of the wind structure is urgently necessary for the study of the irregular structure of the ionosphere. Based on theoretical and experimental investigations carried out in the last decade, wave like perturbations of the parameters of the neutral atmosphere and ionosphere are brought into connection with the passage of internal gravity waves. The theory of formation of sporadic

stratifications in the lower ionosphere (Es) is directly based on the variability of the wind profile.

The wave-like perturbations of the wind parameters in the range of periods characteristic for internal gravity waves, tides and planetary waves have been studied on the basis of a long series of data obtained in Kazan in the period 1978-1984 by meteor radar measurements. The experimental data were analyzed by means of a method of filtering developed by the authors and published by Sidorov and Fakhrutdinova (1981). The method is based on the application of demodulated reception and zero frequency filters changing the pass band which allows to determine the dynamics of the studied periodicity.

For the separation of short period internal gravity waves wind measurements during intense meteor showers have been selected. In these cases the statistical reliability of the wind measurements for unit time increases, the area of random location of reflecting points in the meteor zone is constricted to the plane (plane of echoes) perpendicular to the radiant of the shower. In consequence of this favourable conditions are produced for the separation of perturbations, the wave front (plane of constant phase) of which is parallel to the plane of the echoes. If there is a definite relation between the inclined propagation and the period of the internal gravity wave, the echo plane of the meteor shower of a given radient plays the role of a filter.

During meteor showers first internal gravity waves in the range of scales corresponding to maximum values in the lower thermosphere have been separated by the meteor radar method (Sidorov et al. 1983). Advancing in chronological order, wave like perturbations of periods $T \gtrsim 4$ min exceeding the level of turbulent noise with a probability ~ 99 % have been separated in the data obtained during the Perseid (August 1978 and 1984) and Geminid (December 1981) meteor showers. The maximum amplitude of the separated wave-like perturbations amounts to 15-20 ms^{-1}. In Fig. 1 the spectral density in the range of periods T = 3-60 min is shown on the basis of measurements on 12 12 1981 (2-4) h, which has been computed for different band

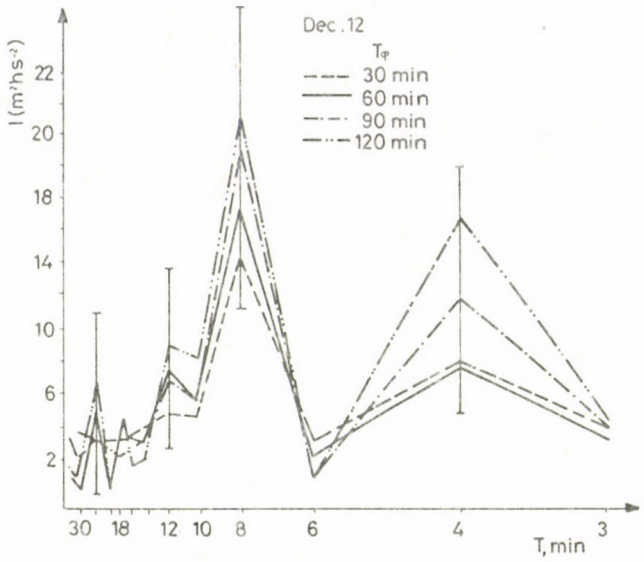

Fig. 1. Spectral density of the wind velocity perturbations at meteor heights in the range of time scales T < 1 h in the period (2-4 h) December 12, 1981

width of the mathematical filters, corresponding to widths of the averaging window of 30, 60, 90 and 120 min. The change of the curves illustrating the spectral density as a function of the width of the averaging window selected enables to estimate the duration of the periodicity in question. According to the results presented in Fig. 1, the duration of the periodicities of T = 4 and 8 min is longer than two hours.

Based on a long series of meteor radar observations carried out in Kazan in 1978 and 1980, the wave like perturbations in the range T = (1-6) h, as well as in the ranges of tidal and planetary waves have been studied. The following results have been obtained.

Practically during all observations a random quasi-periodicity of significant amplitude modulated by long period variations was present in the range of periods analyzed, differences between the spectra of disturbances of the zonal and that

of the meridional circulation have been found.

The spectral density of the zonal and meridional components of the wind velocity shows in all seasons significant peaks in the interval $T \lesssim 3$ h, while in the range $T > 3$ h basically a continuous increase of the spectral density can be observed.

Regarding the diurnal variations the increase of the intensity of disturbances with periods $T < 3$ h in the second half of the day may be mentioned.

In case of the seasonal variations a decrease of intensity of the disturbances from January to June have been recognized, being most definite in the range $T < 3$ h. The seasonal variations of the spectral characteristics I are illustrated by Figs 2 and 3. The presence of disturbances in the range $T \leq 3$ h indicates that the deep mesometeorological minimum in the spectrum of motions observed in the lower troposphere at about 1 hour is weaker developed in the lower thermosphere, as it has been found earlier by the authors based on observations in 1969 with the height finder.

Analyses of the wave like perturbations in the interval of tidal waves have shown a definite modulation of the semidiurnal and diurnal tides by planetary waves. The observed maximum amplitudes of the latter are of the order of 4-16 ms^{-1}. A clear dependence of the amplitude of the modulation on season could not be detected. In consequence of the modulation significant wave like perturbations appear in the form of trains.

The superposition of wave motions in the lower thermosphere produces random fluctuations of the parameters of the atmosphere which can be statistically described by means of the theory of turbulence. Considering the hypothesis of "frozen turbulence" and the meteor radar wind measurements carried out in Kazan in the period from February to June 1969 by the radar equipment fitted with a height finder, the turbulence in the range of horizontal scales from 2 to 200 km has been studied. The limiting scales, which can be investigated by the meteor radar method are determined by the accuracy of the angle measurements and the sensitivity of the radar system within the directional pattern of the applied aerials. On the basis of the

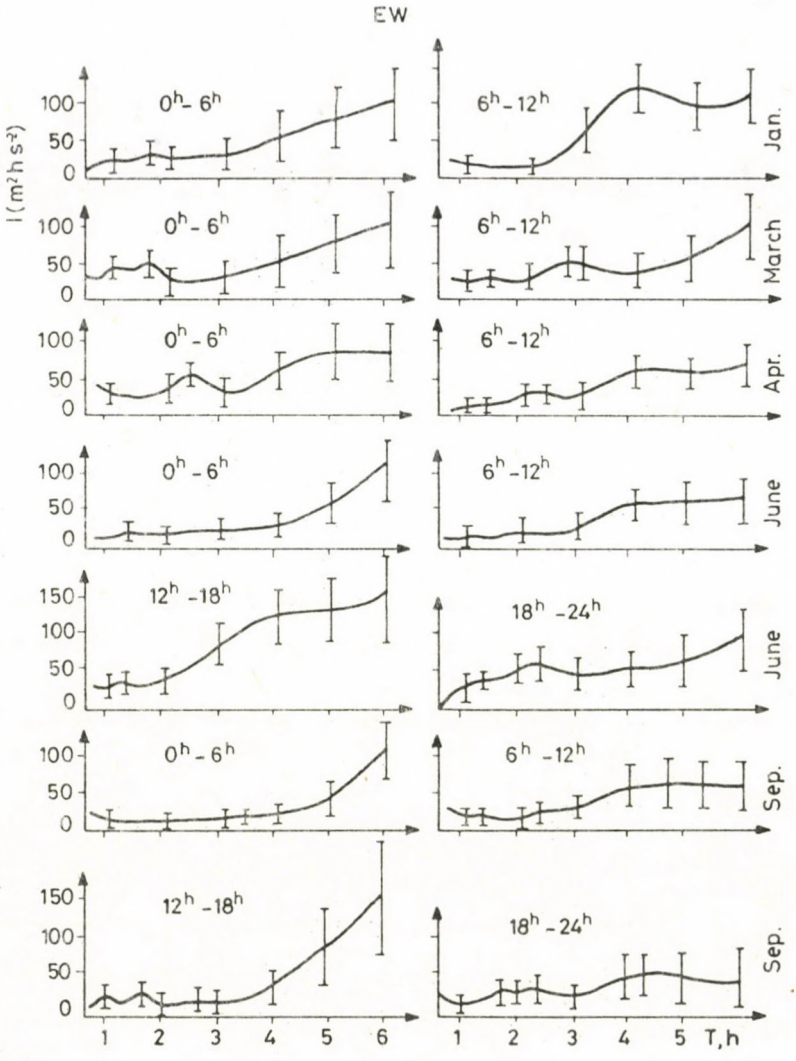

Fig. 2. Diurnal and seasonal variations of the spectral density of perturbations in the zonal circulation for the range of time scales $T \leq 6$ h in 1980

measurements the maximum temporal and spatial scales of the horizontal turbulence have been estimated and found to be respectively 20-30 min and 40 km (Teptin and Fakhrutdinova 1972a, 1972b). These results have recently been confirmed by

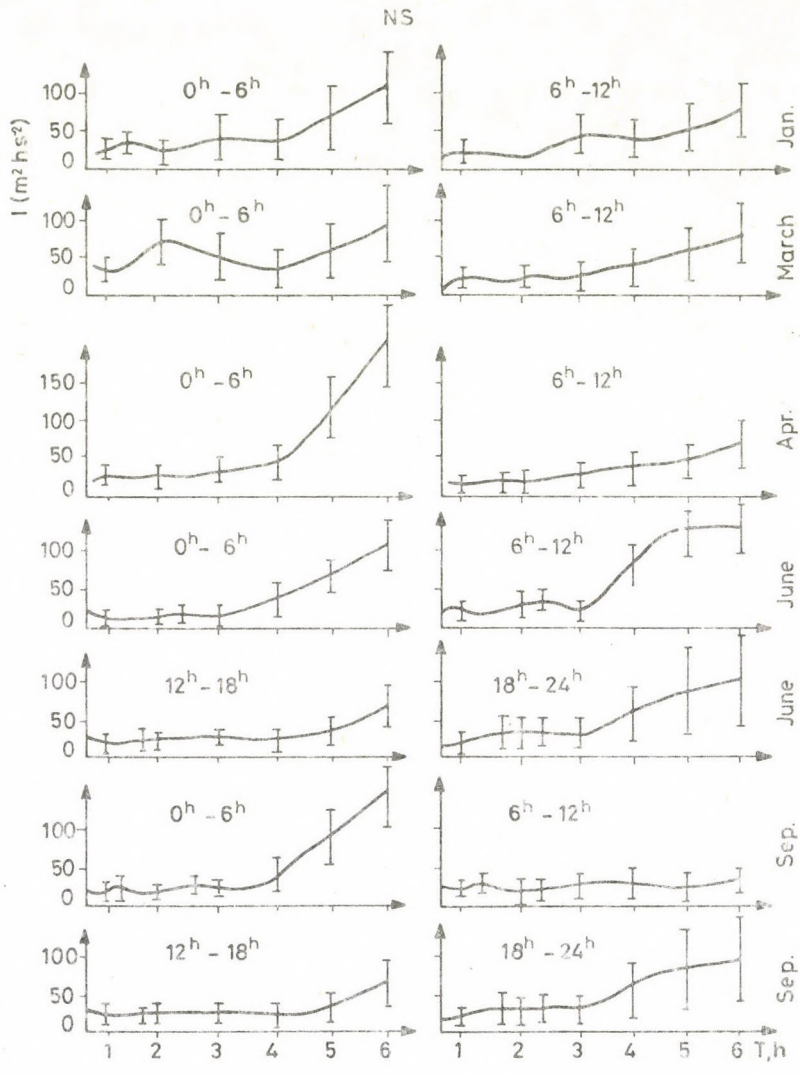

Fig. 3. Diurnal and seasonal variations of the spectral density of perturbations in the meridional circulation for the range of time scales $T \leq 6$ h in 1980

ionospheric data and observations of the intensity variations of the atomic oxygen emission at 557.7 nm.

By the method of measurement of the turbulent parameters based on the analysis of the intensity of long-lived fading

radar reflections in the phase of cessation, the specific turbulent energy dissipation has been estimated and found to be 3300 $cm^2 s^{-3}$ in case of the minimum time scale of 16 s. The detailed results are presented by Teptin and Fakhrutdinova (1972c).

On the basis of meteor radar measurement of the drift velocity carried out by height finder, the height profiles of the zonal component of the prevailing wind U_{EW} and that of irregular motions U'_{EW} in the summer and winter months of 1983 have been determined, internal gravity waves with a period of about one hour, vertical wave length of ~ 13 km and phase velocity of 220 ms^{-1} have been separated. The amplitude of the gravity waves increases with increasing altitude. In Figs 4 and 5 the

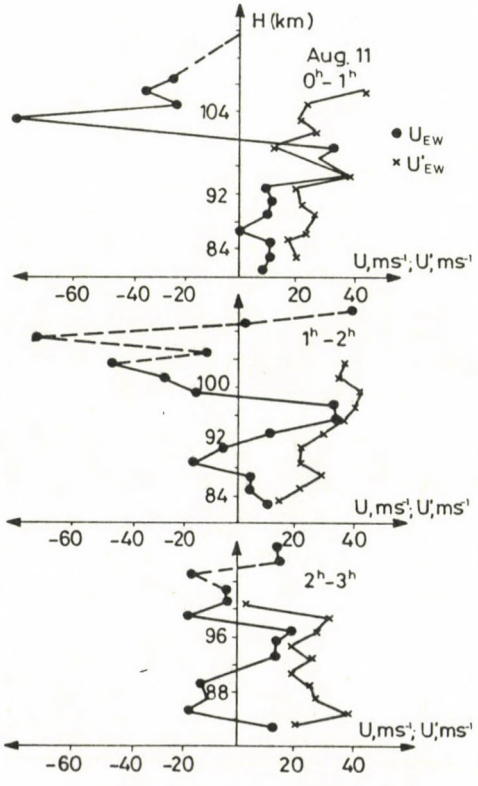

Fig. 4. Vertical profiles of the zonal component of the prevailing and irregular motions on August 11, 1983

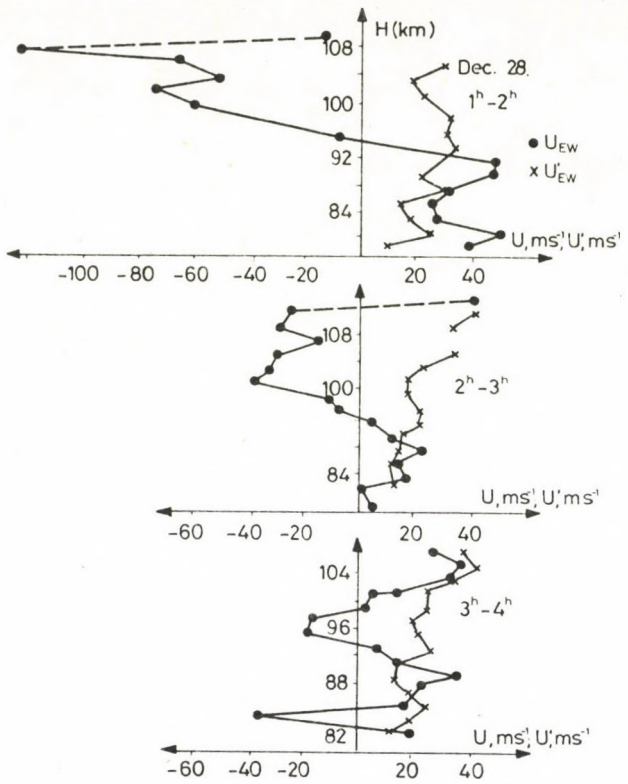

Fig. 5. Vertical profiles of the zonal component of the prevailing and irregular motions on December 28, 1983

variations of the height dependence of U_{EW} and U'_{EW} averaged in the vertical and horizontal plane for an interval of respectively 2 km and 200 km are shown from hour to hour.

The regular variability of the height profile of U_{EW} can clearly be seen. The observed gradients dU_{EW}/dH reach values of 0.05 s^{-1}, they increase with height and decrease with time in the morning from 0 to 4 hours. The wave length of height profiles of U_{EW} presented here varies between 10 and 16 km. Analogous relations are found also in case of the meridional component. The irregular component of the motion tends to increase with height, which is clearly seen in the time intervals

0-2 h, August 11, 1983 and 2-4 h December 28, 1983. This corresponds to an increase of the amplitudes with height of the internal gravity waves propagating in the lower thermosphere.

In agreement with the theory of wind shears (Gershman 1974) the height of formation and the thickness of the Es layer are determined by the height profile of the zonal wind in case of large values of its vertical gradient. Considering the experimental data mentioned above for the formation of Es layers of an effective thickness $\Delta z \simeq \lambda z/2\pi\sqrt{\Delta}$, favourable conditions exist in the height range $\gtrsim 92$ km. Taking as $\lambda_z \simeq 14$ km, for the value of the parameter $\Delta \simeq 10\text{-}50$ (Gershman 1974), $\Delta z \simeq 0.3\text{-}0.7$ km is obtained.

The results regarding the wind system presented in this paper indicate in addition to the prevailing wind the presence of wave-like motions classified as internal gravity waves, tidal and planetary waves in the lower thermosphere, the damping of which produces turbulence; the observed wind-shears can be considered as a consequence of internal gravity waves propagating in the lower thermosphere.

REFERENCES

Gershman B N 1974: Dynamics of the ionospheric plasma (in Russian). Nauka, Moscow

Sidorov V V, Fakhrutdinova A N 1981: In: Meteor investigations. Radio i sviaz, 74-82.

Sidorov V V, Fakhrutdinova A N, Shuvarikov V A 1983: Izv. AN SSSR, ser, FAO, 19, 1201-1202.

Teptin G M, Fakhrutdinova A N 1972a: Meteorologia i Gidrologia, 104-106.

Teptin G M, Fakhrutdinova A N 1972b: Astronomicheskiy cirkular, 691, 4-6.

Teptin G M, Fakhrutdinova A N 1972c: Radiofizika, 15, 1286-1292.

Acta Geod. Geoph. Mont. Hung., Vol. 22 (1-2), pp. 293-299 (1987)

RESULTS OF SIMULTANEOUS MEASUREMENTS OF NEUTRAL WIND AND DRIFT VELOCITY OF THE IONOSPHERIC PLASMA ACCORDING TO THE DOPPLER SHIFT OF THE 630.0 nm [OI] and 731.9 nm [OII] EMISSIONS IN THE AURORA

V A Yugov, V M Ignatiev, A A Fedorov

Institute for Space Research and Aeronomy, 677891 Yakutsk, Lenin str. 31, USSR

In this paper the results of ground based measurements of temperature, neutral wind and drift of ions at the height of the F-region of the ionosphere in auroras are presented. The measurements were carried out by means of Fabry-Perot interferometers in moderately disturbed conditions at Tixie Bay (65.6°N, 194.9°E) in February 1983. The temperature and the neutral wind velocity have been determined by the Doppler broadening and shift of the emission line 630.0 nm [OI]. The drift of ions has been obtained from the Doppler shift of the emission line 731.9 nm [OII]. In the geomagnetic system of co-ordinates the neutral wind and ion drift are directed to the west before midnight and to the east after midnight. It has been found that the change of the direction of the neutral wind velocity is delayed by 40-30 min as compared to that of the ion drift. The maximum zonal velocity of the ion drift is 4-5 times higher than the neutral wind velocity. The meridional wind is directed during the night to the equator, its velocity increases towards the morning hours to ~ 250 ms^{-1}. A decrease of the Doppler temperature from evening to midnight and an increase of it towards the morning hours can be observed. The minimum temperature is reached at 0004 LT. Maximum and minimum temperatures of respectively ~ 1220 K and ~ 960 K have been recorded.

Keywords: Doppler temperature; ion drift; neutral wind

INTRODUCTION

The state of the upper atmosphere at high-latitudes is determined by the temporal and spatial characteristics of the energy input. The main sources of energy are absorption of the solar ultraviolet radiation, electrodynamic (Joule) dissipation, energy yielded by auroral particles, transmission of wave energy from the lower atmosphere, heating due to plasma waves. In perpendicular magnetic and electric fields the motion of neutrals is significantly influenced by the drift of ions. During disturbances the electric field due to the magnetospheric

convection increases which leads to an increased effectivity of this source. Therefore, the simultaneous measurements of temperature, neutral wind and ion drift in the upper atmosphere at high latitudes can give important informations about the physical causes of motions in the auroral ionosphere.

APPARATUS AND METHOD OF THE MEASUREMENTS

For the measurement of the Doppler broadening and shift of the emission lines 630.0 nm [OI] and 731.9 nm [OII], photographic interferometers have been used. Each interferometer consisted of a Fabry-Perot etalon mounted in a barostat and a double thermostat. Before the Fabry-Perot etalon an interference filter has been placed. For the amplification of the illumination three chamber electron optical transducers cooled to a temperature of 40-50^{o}C have been used. The form of the interference pattern was filmed (Yugov et al. 1975). The active surface of the Fabry-Perot etalons was 80 cm^{2}. For the measurement of temperature, neutral winds and ion drift free spectral bands of respectively 0.025 nm, 0.0099 nm and 0.0134 nm have been used. The monochromatization of the light was accomplished by interference filters centered at the wave length 630.0 nm with half widths of 0.9 and 1.18 nm, the transmission coefficients of which were respectively 0.33 and 0.38. The interference filter centered at the wave length 731.9 nm had a half-width of 0.7 nm and a transmission coefficient of 0.38.

The photography of the interference pattern of the emission lines 630.0 nm [OI] and 731.9 nm [OII] has been carried out successively at a zenith angle 60^{o} in the directions north, south, east, west and also in zenith. At the end of every cycle the interference pattern of the laser radiation at 632.8 nm has been photographed which was used as a complementary reference line for the determination of the Doppler shift of the emission lines 630.0 nm [OI] and 731.9 nm [OII]. The instrumental profiles of the interferometers have also been determined by means of the line 632.8 nm. The Doppler shift has been obtained from the diameter of the interference rings observed in the

zenith and at a zenith angle of 60^{o}. The error of measurement of the neutral wind and that of the ion drift amounts to $\pm$ 30 ms^{-1}, in case of the temperature measurement $\pm$ 35 K. Only the zonal component of the drift velocity of ions has been measured.

For the determination of the interference pattern in the area of normal blackening the time of exposure changed from 8 to 3 minute depending on the intensity of the glow of the line 630.0 nm [OI], that of the line 731.9 nm [OII] was 20 min.

RESULTS AND DISCUSSION

Simultaneous measurements of the Doppler temperature and neutral wind have been carried out under moderately disturbed conditions on February 9 (ΣKp = 25+), 10 (ΣKp = 26+) and 11 (ΣKp = 26-) 1983. In Fig. 1 the variations of temperature and neutral wind are shown in a system of geomagnetic coordinates plotted on the basis of points representing twenty minute averages by full lines. It can be seen from Fig. 1a that the scatter of the temperature values is significant from night to night, on the basis of which in all directions a sink of the temperature from evening to midnight and its rise towards the morning hours can be observed. The temperature minimum occurs at 0004 LT. Maximum and minimum temperatures of respectively $\sim$1220 K and $\sim$960 K have been recorded.

The zonal wind (Fig. 1b) is directed to the west before midnight and to the east after midnight. The meridional wind (Fig. 1c) is directed to the equator and its velocity increases towards the morning hour to 250 ms^{-1}.

The measurement of the neutral wind in the period February 9-11, 1983 shows that the basic features of the wind do not differ from the features found on the basis of the observations in College, Alaska (64.8^{o}N, 147.8^{o}W) in the interval January to March 1972 (Hays et al. 1979) and in Tixie Bay in the period February-March 1979 (Yugov et al. 1982). As long as the absolute values of the zonal component according to the measurements in 1979 and 1983 in Tixie Bay are approximately equal, the maximum meridional velocity is approximately 1.2 times less

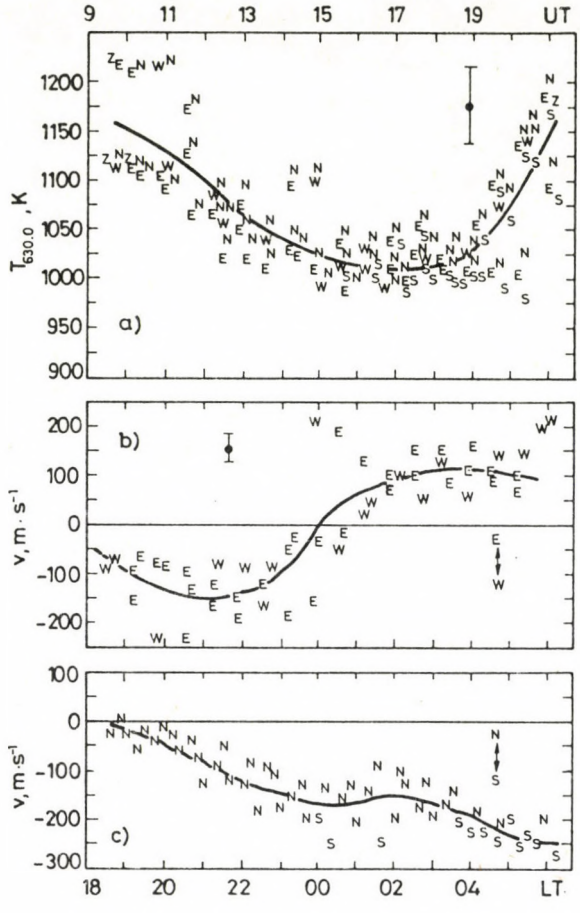

Fig. 1. Results of the temperature and neutral wind measurements on February 9, 10 and 11, 1983. a - temperature, b - zonal velocity, c - meridional velocity. Measurements to the north (N), south (S), east (E) and west (W) are plotted

according to the observations in 1983 than that in 1979. This may be related to the different level of solar activity in the two periods studied here. At the time of observations in 1979 the solar activity was 1.5 times higher than in 1983.

The emission line 731.9 [OII]appears in high altitude auroras. The effective life time of this emission is 2.4-5 s which corresponds to a maximum radiation of 731.9 nm [OII] at

about a height of 200 km.

The interferometric measurement of the ion drift velocity on the basis of 731.9 nm [OII] in the night atmosphere has been carried out in College in February 1972 (Meriwether et al. 1979). The results of these measurements have shown that the emission 731.9 nm [OII] may increase to 100 R. Measurements in the polar cusp have shown that in the auroral spectrum the intensity of the emission 731.9 nm [OII] varies from 20 to 230 R. Spectrometric observations presented in this paper show that the intensity of the line 731.6 nm $P_I(2)$ of the band (8,3) OH, which can be blended with the emission 731.9 [OII] , does not exceed 25 R. The measurement of the motions in auroras in Tixie Bay by means of an infrared three-azimuthal spectrometer using three chamber electron optical transducers (Atlasov et al. 1980, Reshetnikov et al. 1983) showed also that the emission 731.9 nm [OII] can be significantly intensified. On the basis of these data the intensity of 731.9 nm [OII] has been estimated at 20-440 R. In some cases the presence of this line was observed during the whole night.

In Fig. 2 results of the simultaneous measurements of the zonal velocity of neutrals (v_n) and that of ions (v_i), as well as the computed meridional electric field (E) for February 9 and 10, 1983 (Figs. 2a, b) are presented. It can be seen that signs of the zonal velocities of the neutrals and ions to midnight and after midnight coincide. The maximum velocity of the ions is 4-5 times larger than that of the neutrals. A time-lag of 40-50 min in the change of direction of the neutral wind velocity as compared to the ion drift can be observed.

Comparison of the results of the zonal wind measurements with that of the ion drift shows that under moderately disturbed conditions in perpendicular magnetic and electric fields at the height of the F region of the night time auroral zone the motion of the neutrals can be significantly affected by the drift of ions.

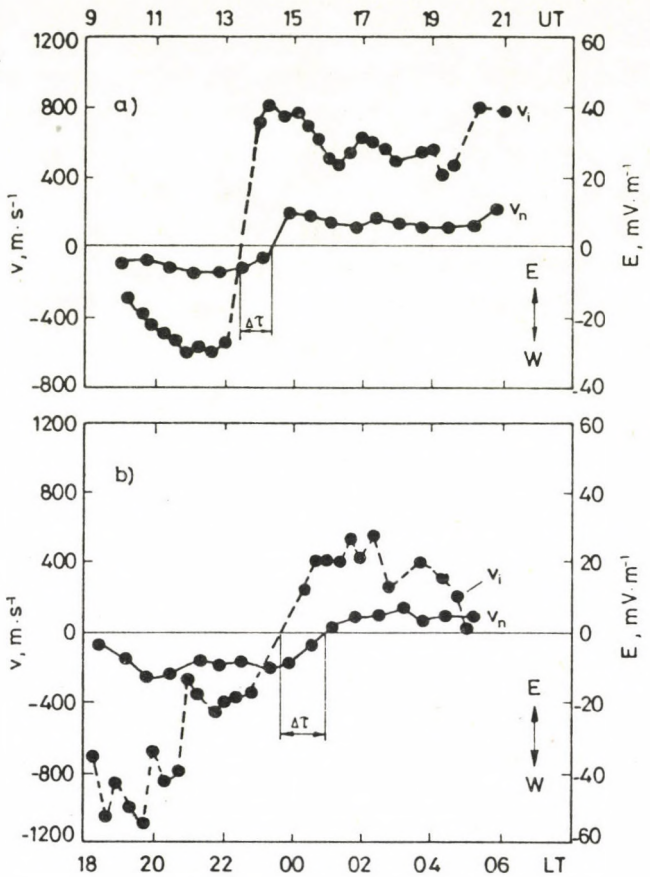

Fig. 2. Zonal components of the neutral wind (v_n) and ion drift (v_i) measured on February 9 (a) and on February 10, 1983. The scale at left corresponds to the velocity, the right hand scale to the meridional component of the electric field computed

REFERENCES

Atlasov K V, Yugov V A, Ignatiev V M 1980: In: Magnetospheric Substorms and Geopnysical Phenomena, Yakutsk, 178-180.

Hays P B, Meriwether I W, Roble R G 1979: J. Geophys. Res., 84, 1905-1913.

Meriwether I W, Hays P B, McWatters K D, Nagy A F 1974: Planet Space Sci., 22, 636-638.

Smith R W, Sivjee G G, Stewart R D, McCormac F G, Deehr C S 1982: J. Geophys. Res., 87, 4455-4460.

Reshetnikov D D, Filippov V M, Yugov V A 1983: Gidrometeoizdat, Moscow, 177-179.

Tolanskiy S 1955: High resolution spectroscopy (in Russian). Moscow, 157-165.

Yugov V A, Ignatiev V M, Atlasov K V, Trofimov N V 1975: In: Physics of the High Latitude Upper Atmosphere, Yakutsk, 157-165.

Yugov V A, Ignatiev V M, Fedorov A A 1982: In: Investigation of ionosphere-magnetosphere coupling at the Yakutsk meridian, Yakutsk, 55-60.

Acta Geod. Geoph. Mont. Hung., Vol. 22 (1-2), pp. 301-311 (1987)

ENFORCED OSCILLATIONS AND RESONANCES DUE TO INTERNAL NON-LINEAR PROCESSES OF PHOTOCHEMICAL SYSTEMS IN THE ATMOSPHERE

G Sonnemann and B Fichtelmann

Academy of Sciences of the GDR, Institute for Space Research,
DDR-2080 Neustrelitz 5, Kalkhorstweg

In order to study the reaction of photochemical systems to periodic stimulation, a model of the photochemistry of ozone has been tested under certain aeronomic conditions and for variable stimulation periods. Non-linear resonance phenomena are observed for stimulation periods of the order of the characteristic times of photochemical systems. Theoretical questions are briefly considered. Conclusions drawn from an empirical ozone model of the mesosphere as derived from measurements of the satellite Interkosmos-16 are discussed in more details.

Keywords: non-linear processes; ozone model of the mesosphere; photochemical system

INTRODUCTION

In this paper possible reactions arising from the periodic stimulation of the atmospheric photochemical systems by the solar radiation energy input are studied. The periodically changing photodissociation and ionization rate constants have different time scales. The most important one is related to the 24 h-period. Others are connected to the 27-day-rotation of the sun, the annual seasonal variation and the 11-year sunspot cycle. We shall discuss the 1-day-period in greater detail. In the following we intend to analyse the particular behaviour of the ozone photochemistry of the upper mesosphere in a manner well known in the study of mechanical or electrical systems. The variable photodissociation rates represent an axciting external force and it is considered how the internal chemical system reacts on the varying frequency of stimulation.

DISCUSSION OF THE MODEL

The upper mesospheric ozone chemistry is essentially determined by the five variable constituents O, O_3, H, OH and HO_2. The odd nitrogen compounds, the hydrogen peroxide, the excited species like O (^1D) and O_2 ($^1\Delta g$) and others are of minor importance. O_2, (Ar) and the number density M can be considered as constant and H_2O is a free parameter within this model varying slowly with regard to chemical processes, which are mainly determined by transport. The initial reaction consists of the photodissociation of O_2. By the subsequent three-body reaction of O with O_2 and a neutral particle, ozone is created. Water vapour undergoes photodissociation producing H and OH, which are the most important ozone destroyers.

Ozone and atomic oxygen will be catalytically removed by the odd hydrogens H, OH and HO_2. These compounds destroy themselves rather unefficiently thereby producing the inactive H_2 or reforming H_2O. A few reactions lead to H_2O_2 being a minor nocturnal OH-store. Due to the fast catalytic destruction of the odd oxygen compounds the odd hydrogen species reach quickly a mutual equilibrium (within minutes). In contrast to this the complete system has a considerably higher characteristic time which is determined by the characteristic time of the odd hydrogen compounds. Figure 1 shows this characteristic time at 81 km height. It is defined by the equation

$$\tau_{H_{ODD}} = \frac{([H] + [OH] + [HO_2])}{(L_6[HO_2] + k_6[M][OH])[H] + (L_8[OH] + L_{10}[HO_2])[OH] + L_{11}[HO_2]^2}[S]. \quad (1)$$

The model assumptions are explained in the next chapter. Table I shows all relevant reactions.

ENFORCED PHOTOCHEMICAL OSCILLATIONS AND RESONANCES DUE TO INTERNAL NON-LINEAR PROCESSES

Development of the problem

A linear second order differential equation with constant coefficients and with a term of external periodic stimulation shows the phenomenon of resonance, if the eigen frequency of the homogeneous equation is equal to the stimulating frequency.

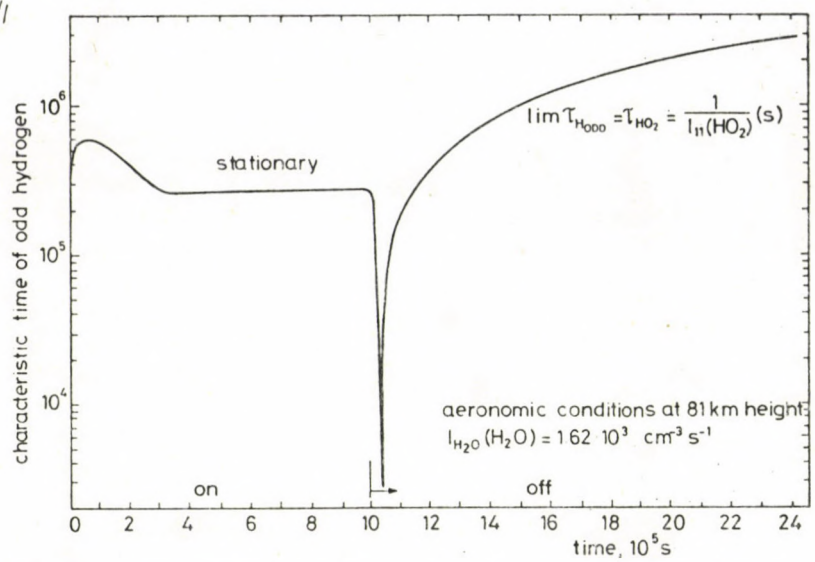

Fig. 1. Characteristic time of odd hydrogen for aeronomic conditions at 81 km height

Table I

List of reactions

$O + O_3 \longrightarrow 2O_2$	$l_1 = 9.08 \cdot 10^{-16}$	$cm^3\ s^{-1}$
$O_3 + H \longrightarrow O_2 + OH$	$l_2 = 1.78 \cdot 10^{-11}$	"
$O + OH \longrightarrow O_2 + H$	$l_3 = 4.40 \cdot 10^{-11}$	"
$O_3 + OH \longrightarrow O_2 + HO_2$	$l_4 = 2.37 \cdot 10^{-14}$	"
$O + HO_2 \longrightarrow O_2 + OH$	$l_5 = 3.50 \cdot 10^{-11}$	"
$H + HO_2 \longrightarrow O_2 + H_2$	$l_6 = 5.40 \cdot 10^{-12}$	"
$H + HO_2 \longrightarrow 2OH$	$l_7 = 2.26 \cdot 10^{-12}$	"
$OH + OH \longrightarrow O + H_2O$	$l_8 = 1.12 \cdot 10^{-12}$	"
$OH + HO_2 \longrightarrow O_2 + H_2O$	$l_{10} = 4.00 \cdot 10^{-11}$	"
$HO_2 + HO_2 \longrightarrow O_2 + H_2O_2$	$l_{11} = 2.50 \cdot 10^{-12}$	"
$O + O_2 + M \longrightarrow O_3 + M$	$k_1 = 1.05 \cdot 10^{-34}$	$cm^6\ s^{-1}$
$O + O + M \longrightarrow O_2 + M$	$k_3 = 8.23 \cdot 10^{-33}$	"
$O + OH + M \longrightarrow HO_2 + M$	$k_4 = 1.40 \cdot 10^{-31}$	"
$O_2 + H + M \longrightarrow HO_2 + M$	$k_5 = 8.08 \cdot 10^{-32}$	"
$OH + H + M \longrightarrow H_2O + M$	$k_6 = 3.31 \cdot 10^{-27}$	"
$O_2 + h\nu \longrightarrow 2O$	$J_{O_2}(\infty) = 1.5 \cdot 10^{-6}$	s^{-1}

Table I (contd)

$H_2O + h\nu \longrightarrow H + OH$	$J_{H_2O}(\infty) = 6.4 \cdot 10^{-6}$	s^{-1}
$O_3 + h\nu \longrightarrow O_2 + O$	$J_{O_3}(\infty) = 7.1 \cdot 10^{-3}$	"

Photochemical systems are generally of non-linear character and linear systems have to be considered as an approximation for certain boundary conditions. Linear mechanical systems have to be considered as a boundary case, too, however the phenomenon of resonance occurs, also in non-linear systems.

Now, an example is presented on the basis of the ozone chemistry, which demonstrates the mathematical isomorphism between mechanical and chemical problems. In a large O_2-supply atomic oxygen is produced by photodissociation. Via a three--body reaction of O and two O_2-molecules, (k_1^*) O_3 is formed again. The O-density compared to the O_2-density is considered negligibly low. The loss of O_3 takes place due to a reaction with atomic hydrogen assumed to be likewise of a sufficiently large amount. Reactions of the kind of $O + O_3 \longrightarrow 2O_2$ or with the products of the reaction $O_3 + H \longrightarrow OH + O_2$, namely: $OH + O_3 \longrightarrow HO_2 + O_2$ and $HO_2 + O \longrightarrow OH + O_2$ etc. may be neglected. This leads to the simple system

$$\frac{d[O]}{dt} = 2 \cdot J_{O_2} [O_2]_0 - k_1^* [O_2]_0^2 [O] \tag{2}$$

$$\frac{d[O_3]}{dt} = k_1^* [O_2]_0^2 [O] - l_2 [H]_0 [O_3] \cdot \tag{3}$$

Differentiating the second equation with respect to time and putting the first equation into the corresponding terms we obtain

$$\frac{d^2[O_3]}{dt^2} + \left(k_1^* [O_2]_0^2 + l_2 [H]_0 \right) \frac{d[O_3]}{dt} + \left(k_1^* [O_2]_0^2 \, l_2 [H]_0 \right) [O_3] = \left(2 \cdot k_1^* [O_2]_0^3 \, J_{O_2} \right) \cdot \tag{4}$$

Making assumptions concerning the dissociation rate (e.g. $J_{O_2} = A\,(1 + \cos(\omega t))$) it is feasible to construct a particular integral of the inhomogeneous equation. Under realistic conditions it is in general not possible to derive an analytical solution, therefore numerical procedures have to be applied.

The eigen frequency of Eq. (4) is given by

$$\begin{aligned} \omega_0^2 &= k_1^* [O_2]_0^2 \, l_2 [H]_0 \\ &= (\tau_0 \cdot \tau_{O_3})^{-1} \\ &= (2\pi\nu_E)^2. \end{aligned} \tag{5}$$

Numerical solution of the model

In order to study the reaction of the described five component photochemical system, for the dissociation rate a rectangular-function of variable period T has been chosen.

$$J_x \equiv \begin{cases} \bar{J}_x & \text{for } 0 < t \leq \frac{T}{2} \\ 0 & \text{for } \frac{T}{2} < t \leq T \end{cases} .$$

The chemical reaction rates have been taken from Hampson (1980) for a temperature corresponding to real upper mesospheric conditions, the O_2-density and the number density M for different altitudes were taken from CIRA (1972). Also the amplitudes of the photodissociation rates J_{O_2} and J_{H_2O} have been calculated using the data of CIRA 72 and real solar radiation flux values. J_{O_3} corresponds to overhead sun. The water vapour concentration has been changed within realistic limits. Figure 2 shows the diurnal maximum ozone concentration (amplitude) via the half period for aeronomic conditions at 75 km height. The figure indicates pronounced resonance phenomena particularly for low H_2O-densities. The resonance frequency occurs at approximately 1 day^{-1}. Depending on the condition $J_x \equiv \bar{J}_x$ or $J_x \equiv 0$, in the following we speak of day or night, and identify the switching time with sunrise and sunset. For sufficiently

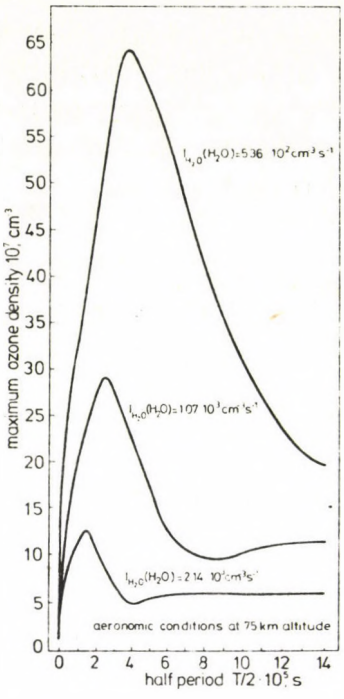

Fig. 2. Diurnal maximum ozone concentration via the half period for aeronomic conditions at 75 km height

long periods the following peculiarities can be observed:

Immediately after the end of a night, with the beginning of the dissociation, the ozone density decreases very fast. From a needlelike minimum shortly after sunrise the ozone concentration begins to increase and reaches a maximum. After this maximum the concentration attains a less pronounced minimum and approaches asymptotically a stationary value. Depending on the water vapour concentration the ozone density increases and reaches the absolute maximum (amplitude) after sunset, thereafter it drops to a faintly marked minimum and approaches a stationary night level. As Fig. 3 shows the diurnal maximum appears the earlier, the more water vapour is contained in the system.

Marked resonances occur in cases if the stimulating time becomes comparable with the internal chemical reaction time. Under non-equilibrium conditions the characteristic chemical time varies, of course, considerably as has been shown in Fig. 1. Hence such a statement has to be accepted with caution and

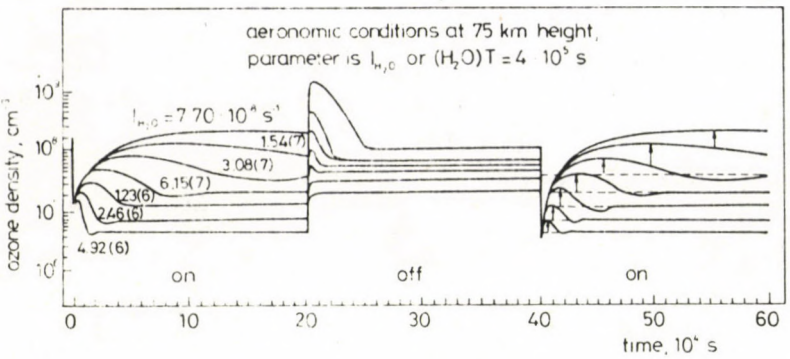

Fig. 3. Diurnal variation of ozone for a period of $4 \cdot 10^5$ s. The water vapour concentration is used as a parameter

it would be better to use an effective diurnal characteristic time. Figure 4 shows model calculations demonstrating that the highest amplitudes will be reached, when the night begins during the diurnal maximum of the ozone concentration. Figure 5 represents the changes of ozone density for a period of 1 day for different water vapour concentrations, if the sunset starts

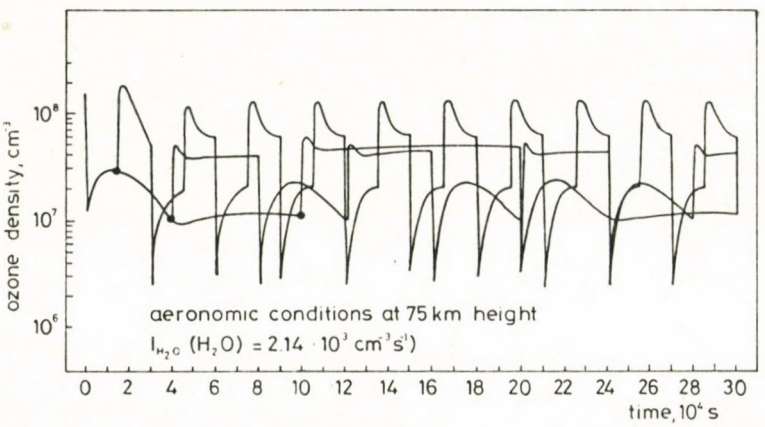

Fig. 4. Diurnal variations of ozone for varying periods that may illustrate the dependence of the amplitude on the time of sunset

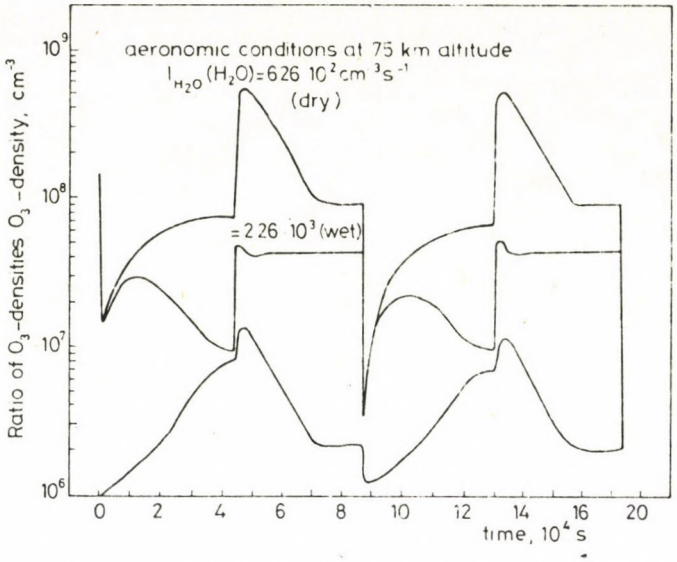

Fig. 5. Top, diurnal variations of ozone for wetnesses occurring, when sunset starts during the diurnal maximum respectively minimum ozone concentrations. Bottom the ratio of both curves is shown

respectively at the diurnal maximum and minimum of the ozone concentration. In the lower part of the figure the ratio of the two cases has been drawn. This ratio shows a remarkable variation with highest values shortly after sunset.

These findings have been confirmed on the basis of a realistic complex model of the photochemistry of the atmosphere including 32 components and more than 200 reactions. The results of these computations will be discussed elsewhere (see Fig. 7).

CONCLUSIONS WITH REGARD TO THE REAL ATMOSPHERE

The natural variability of H_2O within the region of the mesopause is high and can be estimated to vary within the extreme values of 0.5 and 15 ppm, or more realistically between 1 and 10 ppm. Hence, with changing wetness the system will be in or out of resonance, and therefore the variability of the ozone concentration will be most pronounced just during sunset. But the majority of the solar occultation measurements of ozone has been performed during sunset. The same effect as an alteration of

the water vapour concentration is caused by a change of the solar Lyman-α irradiance, becuase within the only production term of odd hydrogen J_{H_2O} [H_2O] both parameters appear. The natural large scale variability of the Lyman-α radiation has been found to be of a factor of about three.

From about 150 sunset measurements of the Interkosmos 16 satellite (launched in 1976) we derived an averaged mesospheric ozone profile (Ohle et al. 1985, Sonnemann et al. 1985) and compared it with the model of Krueger and Minzner (1976). It can be stated as Fig. 6 shows that up to a height of approximately 65 km both profiles are almost identical. Above this height the profiles indicate a discrepancy reaching a factor of two. This may be due to the fact that the Krueger-Minzner-model

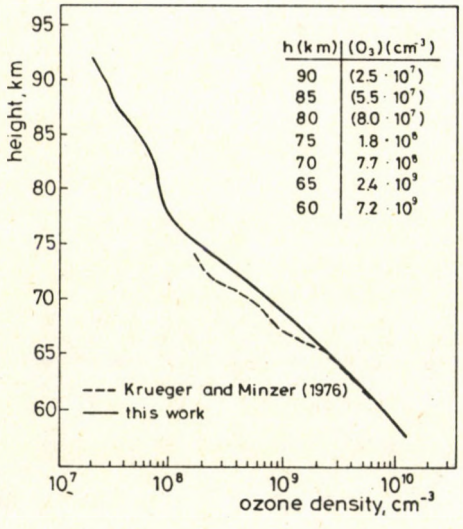

Fig. 6. Empirical ozone model of the mesosphere derived from solar occultation measurements by means of the Interkosmos 16 satellite (launched in 1976) compared with the Krueger-Minzner-model

has been derived from measurements performed at different times of the day. With rising altitude the diurnal ozone maximum is shifted into the evening hours, leading to higher ozone densities than the average daytime value. The low solar activity

in 1976 (less Lyman-α radiation) may be additionally responsible for that behaviour, too. On the other hand our individual profiles show a considerable dispersion within the mesopause region which can be explained by the large variability of the ozone concentration particularly during sunset. Figure 7 shows some of these findings according to calculations using the complex photochemical model.

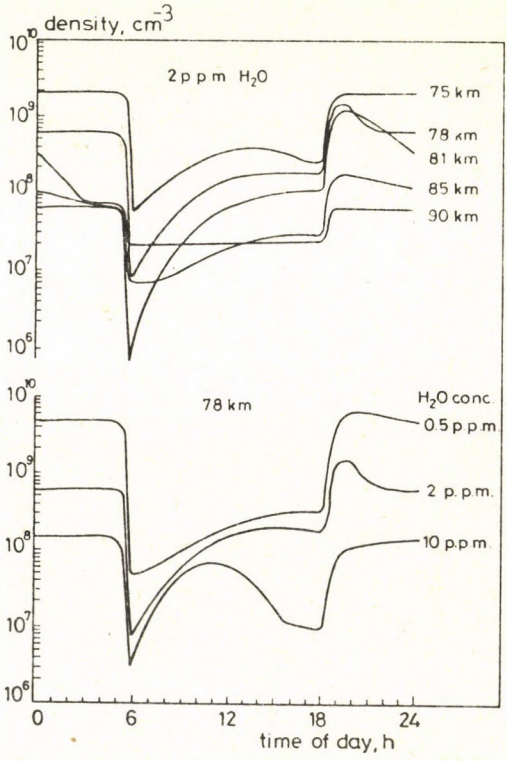

Fig. 7. Model calculations of diurnal variations of the ozone density using a complex photochemical system

REFERENCES

CIRA 1972: Cospar International Reference Atmosphere 1972. Akademie-Verlag, Berlin

Hampson R F 1980: Chemical Kinetic and Photochemical Data Sheets for Atmospheric Reactions, Report No. FAA-EE-80-17,

U.S. Department of Transportation

Krueger A J, Minzner R A 1976: J. Geophys. Res., 81, 4477-4481.

Ohle K-H, Sonnemann G, Fichtelmann B 1985: Space Res. (in press)

Sonnemann G, Fichtelmann B, Ohle K-H 1985: MAP Newsletter (in press)

Acta Geod. Geoph. Mont. Hung., Vol. (1-2), pp. 313-319 (1987)

THE STRANGE ATTRACTOR IN THE PHOTOCHEMISTRY OF OZONE IN THE MESOPAUSE REGION

B Fichtelmann and G Sonnemann

Academy of Sciences of the GDR, Institute for Space Research,
DDR-2080 Neustrelitz 5, Kalkhorstweg

On the basis of a photochemical model of the ozone chemistry of the mesopause region, a non-linear effect has been studied and simulated under realistic conditions. The question is considered here how a photochemical system controlled by the dissociation rate constants responds to periodic stimulations of variable periods. For certain sets of parameters day-to-day variations occur which are controlled by a strange attractor of the densities of the components. Some theoretical questions related to the eigenvalue problem are discussed.

Keywords: mesosphere; ozone; photochemistry

INTRODUCTION TO THE THEORETICAL BACKGROUND

In order to calculate theoretical diurnal variations of the individual components of a photochemical system, proceeding from a certain set of initial conditions the computation has to be continued until two consecutive diurnal curves differ only infinitesimally. That theoretical diurnal variation is called the boundary diurnal variation. The adequate mathematical definition of the existence of such a boundary diurnal variation is given by the following inequality. For an arbitrary $\varepsilon > 0$ exists a μ so that

$$\text{Max} \left| {}^{\mu}[X(t)] - {}^{(\mu+1)}[X(t)] \right| < \varepsilon \qquad (1)$$

$t \in 24$ h.

t is the time between 0 and 24 LT, X denotes the chemical component and μ corresponds to the number of days. The main question arising from Eq. (1) is, does exist a boundary diurnal

variation and if so under which conditions does it occur?

The real photochemical systems contain sets of non-linear first-order differential equations. Especially about sunrise and sunset the system is far from photochemical equilibrium and some constituents increase in a hyperbolic manner. In the particular case of the ozone chemistry there exists a well defined stationary solution of all combinations of the dissociation rates I_{O_2}, I_{O_3} and I_{H_2O} for vanishing dissociation rate constants depending on the conditions during sunset. The stationary solution, of course, is stable in relation to small perturbations.

By analysing the behaviour of the system far from the stationary solution we find time ranges, where these so called dynamical eigenvalues have positive real parts. The solutions of the classical eigenvalue problem using the actual time-depending concentrations of the individual components of the system instead of the densities of the stationary solution are called dynamical eigenvalues. Therefore the eigenvalues calculated so change with time, they have a dynamical character. Positive real parts of the eigenvalues mean also in this case that small superimposed fluctuations increase as compared to the undisturbed variation with time and the value of the positive real part is a measure of the speed of growth.

On the other hand, if none of the eigenvalues has a positive real part, all fluctuations decrease with time. Without considering the theoretical background in this paper, we formulate verbally the condition for the stability of the boundary diurnal variation as follows: The time-balance over a cycle of the real parts of the individual eigenvalues determines the character of the diurnal variation. In case of stability, the rising perturbation within the time-range of the positive real parts of the eigenvalues, increasing the deviations from the boundary diurnal variation must be less efficient than the altering tendency of the negative real parts of the corresponding eigenvalues within the respective time interval. Otherwise the periodically enforced photochemical system shows a chaotic behaviour.

THE STRANGE ATTRACTOR OF THE DIURNAL VARIATION OF OZONE

We consider now the simple model of ozone chemistry developed by Sonnemann and Fichtelmann (1984). Five components O, O_3, H, OH and HO_2 have been taken into account. The dissociation rates I_{O_2}, I_{O_3} and I_{H_2O} have been considered as rectangular functions. The dissociation rates, the concentration of the major component O_2, the number density M and the temperature correspond to real aeronomic conditions of the measopause region in order to calculate the chemical rate constants after Hampson (1980). The system is photochemically stimulated by the dissociation rates periodically switched with a varying period T. We speak of a day, if $I_x \not\equiv 0$ and of a night, if $I_x \equiv 0$. A rectangular function with well defined sunrise and sunset at switching times corresponds strongly (if T = 1 day) to equatorial conditions, but the problem is studied from a theoretical point of view.

Figure 1 shows the results of model calculations for different periods, for aeronomic conditions at 81 km altitude and 2 ppm water vapour concentration. The amount of the highest diurnal ozone concentration is shown as a function of time.

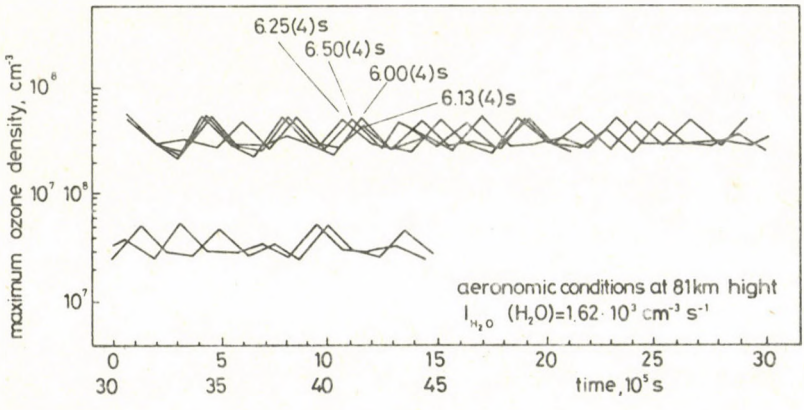

Fig. 1. Model calculations of the ozone concentration for different periods between $T/2 = 6.0 \cdot 10^4$ s and $6.5 \cdot 10^4$ s. The daily maximum values are shown as a function of time

The duration of the half period varies between $6.00 \cdot 10^4$ and $6.50 \cdot 10^4$ s. Whereas in case of the longest period, a clearly pronounced alternating regime of high and low values occurs, the shortest period shows a cycle of distinct low, mean and high values. The intermediate periods show a complicated pattern. For some periods (e.g. for $\frac{T}{2} = 6.25 \cdot 10^4$ s between t = $= 2.4 \cdot 10^6$ and $3.0 \cdot 10^6$ s) the computations indicate no marked changes but amplified values later. In Fig. 2 the trajectory connecting the related values of the two components O_3 and OH has been drawn. This so called "strange attractor" shows clearly the very unsteady behaviour of the solution. Figure 3 shows after an extended initial phase the quasi stationary alternating variation of period doubling for O_3 and OH in case of a period of $1.6 \cdot 10^5$ s.

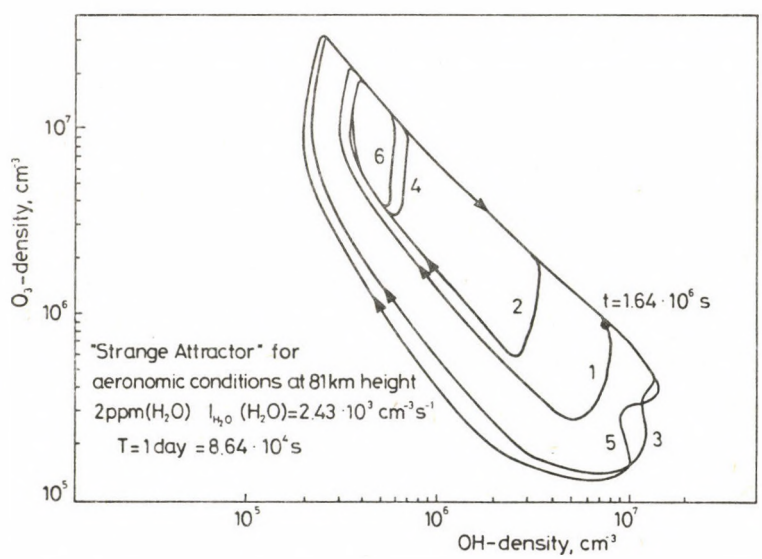

Fig. 2. The trajectory of the components O_3 and OH after a long initial phase of $1.64 \cdot 10^6$ s for a period of one day

It should be noted that the ozone concentration drops at sunrise. The very low nighttime ozone level is reached only during every second cycle. With the beginning of the night a

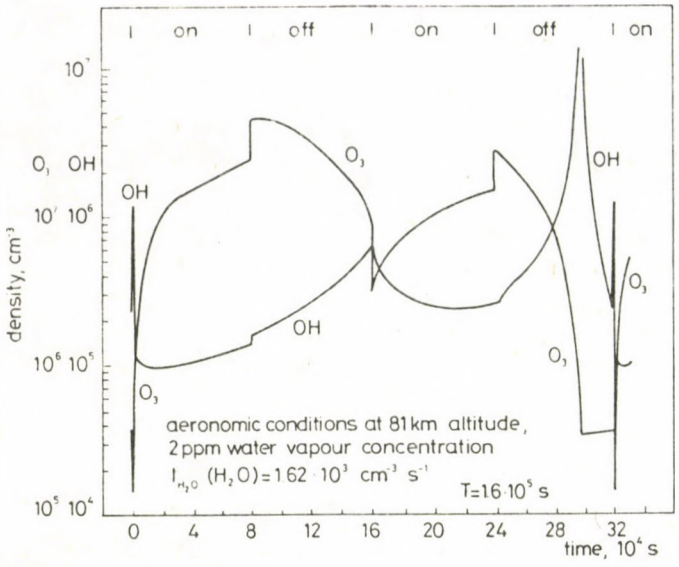

Fig. 3. Quasi stationary alternating variation of the O_3- and OH-concentrations after a long initial phase for a half period of $8.0 \cdot 10^4$ s

strong hyperbolic decrease of the ozone density is coupled with an hyperbolic increase of OH (respectively HO_2) indicating a pronounced internal positive feedback.

CONCLUSIONS

Figure 4 shows on the basis of the complex photochemical model of Sonnemann and Fichtelmann that in middle latitudes under equinoctial conditions an alternating or otherwise chaotic regime may appear even within the real atmosphere at a height of 85 km and for 10 ppm water vapour concentration. Chaotic motions of enforced non-linear systems are known to occur under real conditions in many disciplines but in atmospheric photochemical systems they were unknown so far. Just within the mesopause region we frequently observe a pronounced variability. Another aspect related to this problem is of a mathematical nature and concerns quasi periodic phenomena, in general like the quasi two-day-wave of the zonal prevailing wind at 100 km

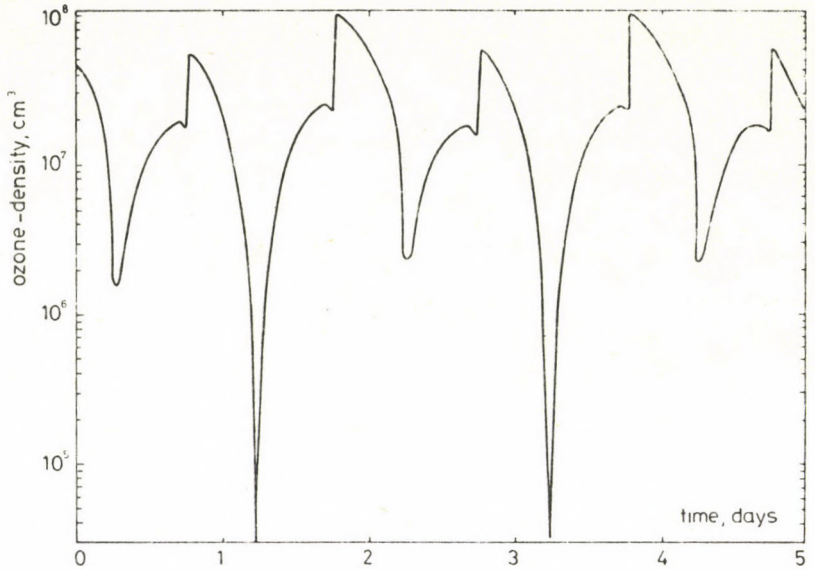

Fig. 4. Ozone density in 85 km height calculated on the basis of a complex photochemical model for 10 ppm water vapour concentration, equinoctial conditions and middle latitudes

height or the quasi biannual oscillation of stratospheric air pressure of the tropics. A doubling of the period is a well known effect in the theory of enforced non-linear systems. Considering some other candidates such as the odd nitrogen system of the thermosphere or the ozone chemistry of the ozone layer having a chemical time scale close to a year, non-linear effects (including diffusion processes) in other enforced photochemical systems are also expected. One of these possible phenomena consists of the formation of spatial-temporal structures in the density distribution of minor constituents (ions and neutrals) first suggested by Sonnemann (1980) and Sonnemann and Fichtelmann (1984).

REFERENCES

Hampson R F 1980: Chemical Kinetic and Photochemical Data Sheets for Atmospheric Reactions, Report No. FAA-EE-80-17, U.S. Department of Transportation

Sonnemann G 1980: Can energy dissipation related to internal chemical oscillations contribute to the occurrence of small scale fluctuations in atmospheric density profiles? Paper presented at the XXIII. COSPAR-Meeting, Budapest

Sonnemann G, Fichtelmann B 1984: Small scale fluctuations of minor constituents caused by photochemical processes. Paper presented at the XXV. COSPAR-Meeting, Graz

Acta Geod. Geoph. Mont. Hung., Vol. (1-2), pp. 321-332 (1987)

IS THERE ANY RELATION BETWEEN GEOMAGNETIC ACTIVITY AND METEOROLOGICAL PROCESSES?

G Sonnemann[1] and J Bremer[2]

[1]Academy of Sciences of the GDR, Institute for Space Research, DDR-2080 Neustrelitz 5, Kalkhorstweg

[2]Heinrich-Hertz-Institute for Atmospheric Research and Geomagnetism, DDR-2565 Kühlungsborn, Mitschurinstr. 4-6

Many reports have been published about the coupling between geomagnetic activity and meteorological phenomena and a control of meteorological parameters (air pressure) by the geomagnetic activity has been suggested. Statistical studies lead to an inverse relation. The mean of the geomagnetic activity indeces Ap referring to the same date of the years between 1932 and 1982 shows clear mesoscale deviations from a smoothed seasonal behaviour. These so called geomagnetic singularities have been statistically analyzed. Taking into consideration the persistence of geomagnetic perturbations it was found, that especially the periods about the equinoxes have a high statistical significance. The Fourier analysis of the mean Ap values shows a marked mode 12 (30.4 days) with a phase of highest activity at the end of the month. This is explained in terms of an aeronomic modulation of the geomagnetic activity induced by processes in the lower atmosphere.

Keywords: coupling between geomagnetic activity and meteorological phenomena; geomagnetic activity; meteorological processes

INTRODUCTION

The assumption that geomagnetic activity influences meteorological processes of the troposphere, has been published as early as 1960 by Macdonald and Roberts and in 1963 by Twitchell. Macdonald and Roberts (1960) found that large troughs at the 300-mb level were formed 2-4 days after the start of significant corpuscular radiation in the 1956/57, 1957/58 and 1958/59 winters in the Gulf of Alaska Aleutian Islands area. As key days the onsets of isolated SC-storms at Cheltenham (Maryland, U S), or the first day of a group of consecutive days have been chosen, on which a strong auroral display was observed at the University of Saskatchewan, Saskatoon, Canada. Twitchell (1963) reported an increase in the 500-mb trough index derived from

the intensity of moving 500-mb troughs approximately 7 and 14 days after SC's. Bucha (1976, 1977, 1983) published several papers about relations between geomagnetic activity and air pressure at the 500-mb level around the geomagnetic north pole 3-6 days after an increase of the geomagnetic activity, the air pressure decreased in that area.

Mustel (1971, 1972, 1973, 1974) investigated the relation between geomagnetic activity and air pressure and reported that large scale areas of increasing and decreasing air pressure occurred after disturbances. These results lead to the suggestion, that there is a relation between meteorological processes and geomagnetic activity. It is worth noting that this relation has been frequently observed in seasons other than the summer months.

Attempts to find a mechanism of the coupling were hitherto very speculative. The published results may give an impression of a very close relation even for the geographic region of Central Europe. However, statistically no significant influence of the geomagnetic activity can be stated on meteorological processes. As shown in Fig. 1 by an autocorrelation analysis of

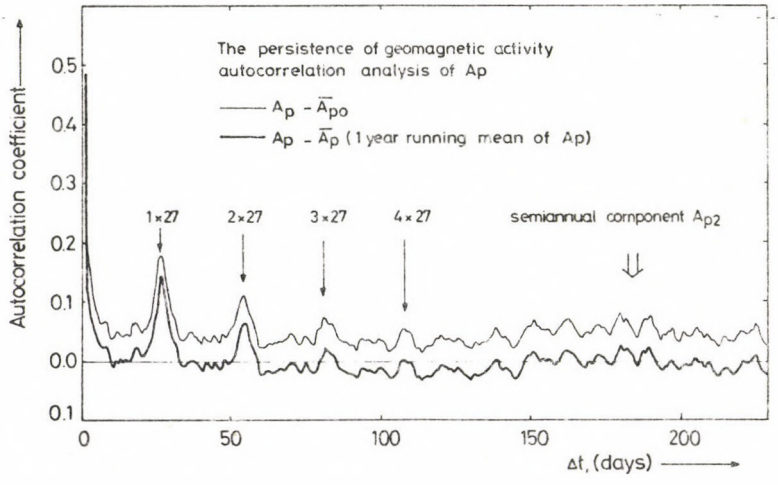

Fig. 1. Autocorrelation analysis of Ap (1932-1982)

Ap (1932-1982), the geomagnetic activity indicates a marked 27 days recurrence tendency. A similar study for the surface air pressure at Potsdam (1893-1982) is shown in Fig. 2. The autocorrelation coefficients should show less recurrence tendency after 27 days independently of the sign of the influence. This is evidently not the case. Obviously the relation must be analyzed in more detail, both with respect to the spatial-temporal structure, as well as to the strength of perturbation.

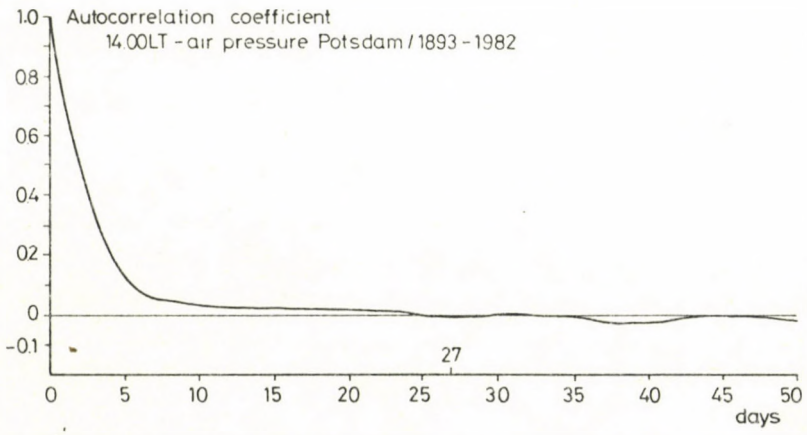

Fig. 2. Autocorrelation analysis of surface air pressure in Potsdam, 14.00 MET (1893-1982)

COUPLING OF METEOROLOGICAL PROCESSES WITH THE UPPER ATMOSPHERE

In the following the inverse relation is considered, i.e. whether processes of the lower atmosphere can influence the geomagnetic activity. In the past the question has been only studied if stratospheric pressure fields affect the ionization of the lower ionosphere. As early as 1965 Shapley and Beynon found a relation between stratwarms and radio wave absorption. Based on an analysis of the data of 12 ionosonde stations between 40^{o}-60^{o}N Deland and Friedmann (1972) found a correlation between f_{min} and pressure in the stratosphere. Brown and Williams (1971) found relations between the 10-mb isobars and

the levels of constant electron density within the E layer. Brown and Johns (1979) studied the heights of constant electron density of the E layer at middle latitudes in an altitude of about 110 km and showed variations of 2-10 km and periods of 5-30 days which have been explained by pressure variations. The correlation is the closest when the stratospheric winds enable the penetration of waves into the upper atmosphere. Otherwise no correlation has been observed. On the basis of numerous studies both theoretically and experimentally, the conclusion was drawn that a coupling via planetary or internal gravity waves is connected with special conditions of the circulation and temperature profile of the middle atmosphere. A particular precondition seems to be the predominance of a winterly cyclonal circulation.

According to the present knowledge, the control by planetary waves may certainly be found up to the lower thermosphere.

Couplings up to the F layer have been excluded for a long time. However, Bauer (1957) indicated that the critical frequency of the ionosphere increased during the passage of hurricanes through the underlaying area. The possibility of a meteorological influence on the critical frequency has been emphasized recently by Kasimirovsky (1982) in a review on "Meteorological Effects and Ionospheric Parameters". The influence of processes of the lower atmosphere on the S_q-system has been first suggested by Hines (1965). Proofs for this hypothesis have been missing until now. A first hint may be a relationship between stratospheric circulation and deviations of the monthly mean S_q-amplitude from the 5 most quiet days of the month shown by Sonnemann et al. (1985) (See Fig. 3). For a superimposed epoch analysis the 24 year period 1958-1981 has been divided into 2 parts of both 12 years according to the lowest and highest stratospheric circulation intensities V_{ZON} in the first decade of February as key time. The wave-like oscillations of the mean S_q-amplitude are of special interest.

SINGULARITIES OF THE GEOMAGNETIC ACTIVITY

Phenomena occurring at the same date with an enhanced

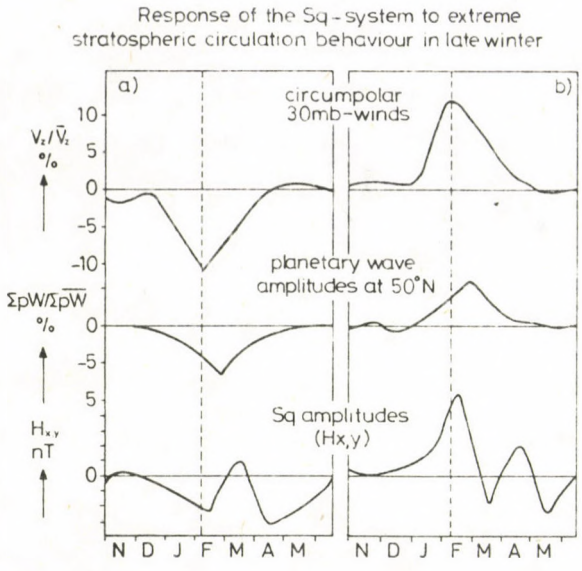

Fig. 3. Comparison between the stratospheric zonal circulation and the deviations of the mean monthly S_q-amplitude from the mean of the 5 most quiet days. The 24 years 1958-1981 have been divided into 2 parts of 12 years according to the lowest and highest stratospheric zonal circulation intensities V_{ZON} in the first decade of February as key time

probability or with an increased or decreased magnitude compared to the seasonal trend should be defined as singularities. Sonnemann (1983, 1984a, 1984b) and Sonnemann and Bremer (1984a, 1984b) studied the question if geomagnetic singularities exist. The starting point was the fact that approximately between October 25, and November 2 rather strong negative ionospheric disturbances occur quite frequently. They appear after the mean seasonal peak of the critical frequency and are often accompanied by moderate geomagnetic disturbances. Simultaneous measurements of the neutral gas density by means of the satellite occultation technique showed pronounced structural variations even down to the lower thermosphere. During the negative phase the strongly disturbed profiles are marked by a resonance-like upwelling of the molecular components, while the density of the thermospheric atomic oxygen decreases below about 250 km and

increases above that height. Internal dynamical processes are obviously of some importance. As it can be derived from simultaneous TEC-measurements the critical frequency has additionally been influenced by plasma transport due to meridional winds (about $E\varphi$ no information was available).

The analysis of the local geomagnetic activity index A_K (26 years) and ΣK_1 (44 years) of Niemegk, GDR, revealed singular periods in its relation to the mean critical frequency. The analysis of the whole year hints at further singular periods, which are in striking conformity with the analysis of the Ap-indices of the years 1932-1982.

STATISTICAL ANALYSIS OF THE Ap-VALUES BETWEEN 1932 AND 1982

The random superposition of strongly scattered values may lead to remarkable deviations from a long-term average. Such pseudosingularities may appear at arbitrary times of the year. An essential task is their elimination so that the computed deviations of the daily Ap-mean values ($\bar{A}p$) from a seasonal trend should not be just random fluctuations. In order to prove the findings statistically, some problems have to be solved.

1. Taking the t-test as a basis the observed data have to be normally distributed. But the Ap-values are extremly unsymmetrically distributed, in practice it follows from this that the periods with more geomagnetically quiet days reach higher significance levels than the disturbed values.

2. The persistence tendency of the geomagnetic activity causes the main problem. If only a single day is considered then the geomagnetic activities of the different years are independent of each other (the persistence of large time-scale is of no importance in this regard). Unfortunately the number of years (N_J) for which the Ap-values are available is not large enough. In order to obtain a sufficiently low significance level under the condition of strong dispersion of the Ap-values ($\bar{s} = 16.47$), it is important to consider the significance of a whole singular period. When grouping several

days (N_T) to a single ensemble of values, the geomagnetic persistence has to be taken into consideration.

Supposing that the autocorrelation function is known, Bartels (1935a, 1935b) derived an equivalent persistence number $\varepsilon(N_T)$. Figure 4 shows this on the basis of Fig. 1. The extent of the statistical random probe decreases according to $N_{eff} = N_T N_J / \varepsilon(N_T)$, at the same time rises the level of significance considerably.

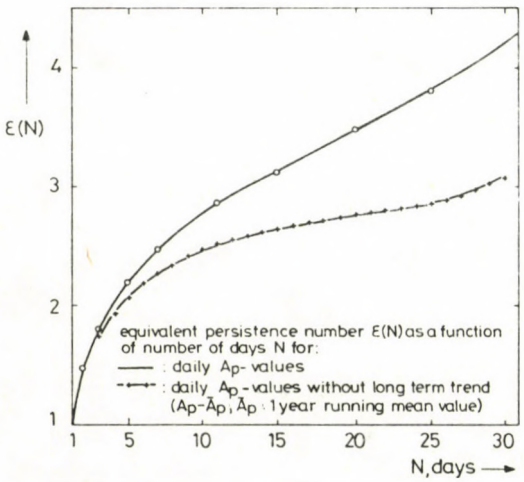

Fig. 4. Equivalent persistence number $\varepsilon(N_T)$ on the basis of the autocorrelation analysis of Fig. 1

3. Regarding the 365 days of the year the 99 % level of significance is reached in 1 % of days, i.e. on 3.65 days in average. The statement on an individual day has to be considered as certain, if the significance level is high enough that the expected value for the whole year is substantially less than 1 day. Although in the other case for (Bartels 1935a, b) an individual day no statement can be made if the amount of 3.65 days is exceeded, it is a distinct indication of the fact, that not all deviations from the seasonal trend can be explained by a superposition of strongly scattered individual values.

In Fig. 5 the results of a statistical significance analysis are shown with and without consideration of the persistence of the deviation which were obtained by calculating the difference between the 9-day running average of the arithmetic mean of Ap and the seasonal trend calculated on the basis of the Fourier analysis of the whole 51 years taking the modes 0, 1 and 2 as seasonal trend. Striking deviations can be recognized only during the equinoxes with a tendency of highest values towards the ends of the months. Due to the smaller scatter of the geomagnetic indices, quiet periods have in general higher significance. The number of significant days is essentially higher than expected. However, most variations do not reach sufficiently high significance, although, as it will be discussed in the next section, there are several hints that some periods with low significance values could also be regarded as singular ones. At present the observation time is insufficient yet.

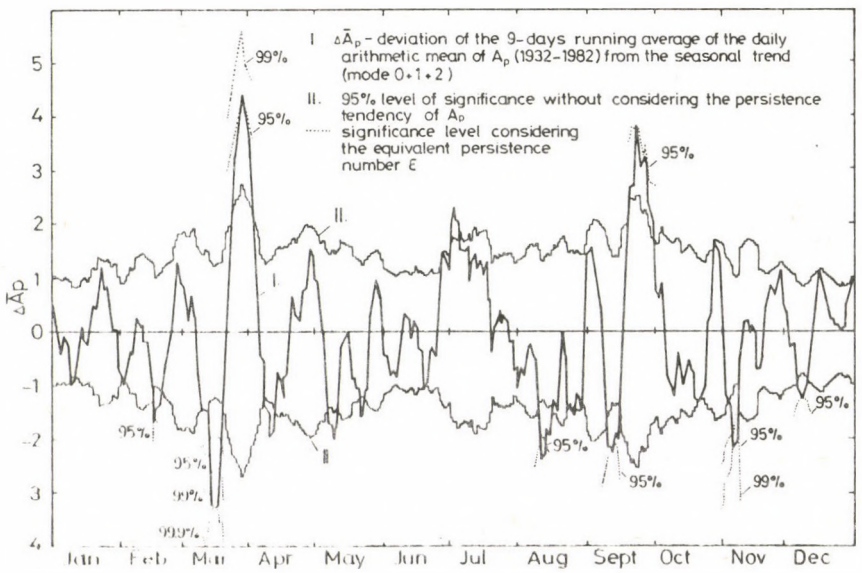

Fig. 5: Deviations of the 9-day running averages of the arithmetic mean of Ap from the seasonal trend derived following a Fourier analysis and the significance level with and without consideration of the geomagnetic persistence

ADDITIONAL RESULTS SUPPORTING THE EXISTENCE OF SINGULAR GEOMAGNETIC EVENTS

Comparing the structural variations of $\bar{A}p$ in two half-years it is found that similar trends exist mainly about and after the equinoxes. After eliminating the seasonal trend a regression analysis of the three day running mean values yielded a relatively high correlation coefficient of $r = 0.655$. The regression between the spring values and the fall values is given by:

$$\Delta\bar{A}p\ (\text{FALL}) = 0.90\ \Delta\bar{A}p\ (\text{SPRING}) + 0.22\ .$$

This means that the spring variations are somewhat more pronounced. This behaviour is shown in Fig. 6. Similar

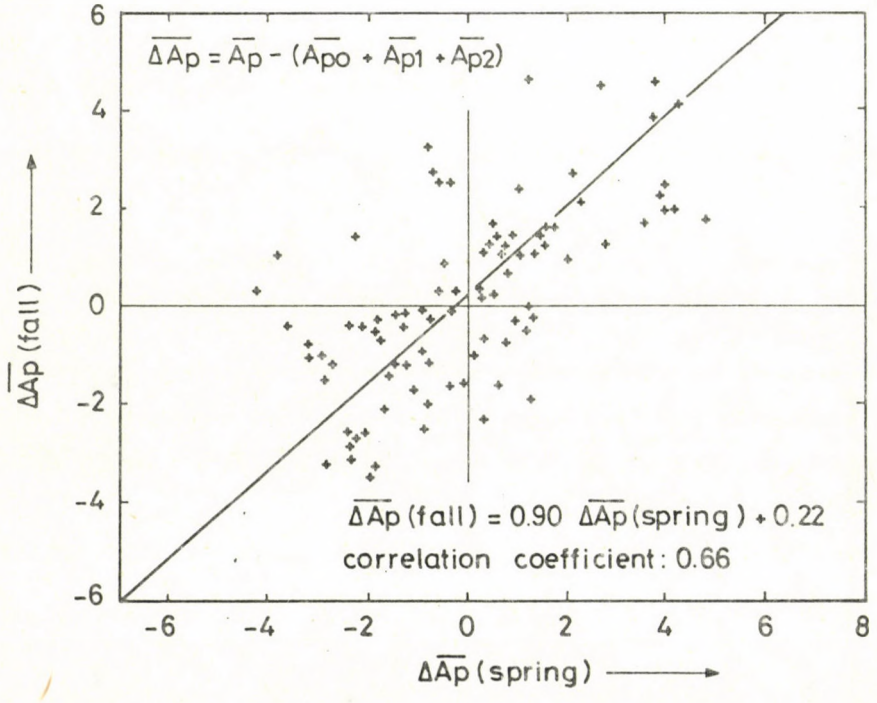

Fig. 6. Regression analysis of mean daily $\overline{\Delta Ap}$ data of the period 1.3.-31.5. and data corresponding to the period 30.8.-29.11. half year later (daily ΔAp-values were calculated from years 1932-1982 and sliding averaged over 5 days after elimination of the mean seasonal variation: $\overline{\Delta Ap} = \overline{Ap} - (\overline{Ap_0} + \overline{Ap_1} + \overline{Ap_2})$)

behaviour is indicated by the local geomagnetic activity $\bar{A}_K$ of Niemegk. The singular periods represent remarkable relative deviations from the seasonal variations. The mechanism of the modulation of the geomagnetic activity is an open question. Dividing the Ap scale into bins and considering the number of days at which Ap had a value within one of these bins, it is found that the modulation has no additional influence, but that there is a certain spread of the scale. This is shown in Fig. 7 for the distribution of the Ap-values on the one hand for the mid-March period and on the other hand for the end of March. The most pronounced differences appear at high Ap-values indicating the efficiency of the modulation process. A modulation of the conductivity of the ionosphere in the dynamo region by aeronomic processes seems feasible, but other possibilities as the influence of the modulated geocoronal neutral gas on the ring current could be responsible, too.

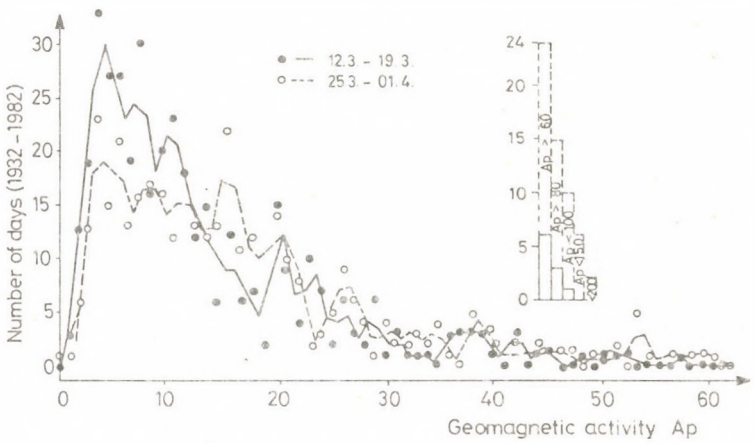

Fig. 7. Distribution of the Ap-values in the mid-March and late-March period

Besides the dominating mode 2 the Fourier analysis of the yearly variation of the mean values indicated a significant mode 12 of 30.4 days with a phase of highest activity at the end of the months being most pronounced around the equinoxes. The mode 12 is even then significant if sets of only 25 random-

ly selected years are considered as shown in Fig. 8.

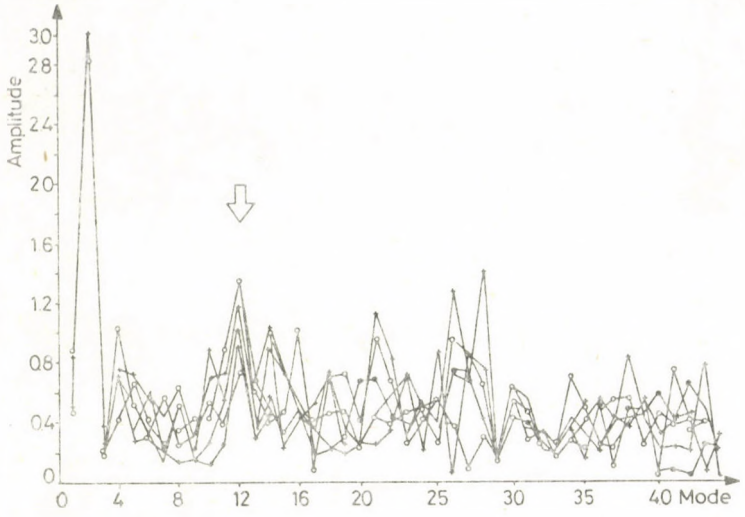

Fig. 8. Fourier analysis of 6 sets of 25 and 26 random years

CONCLUSIONS

It is not very fruitful to speculate about possible sources, coupling mechanisms and influenced current systems as long as the estimations are questionable. From the time scale (mode 12) we may conclude that the source of energy should be located within the lower atmosphere (troposphere-stratosphere). As shown by Schmitz and Grieger (1978), in stratospheric dynamics an energy transfer between V_{ZON} and planetary waves takes frequently place with an oscillation period of about 30 days. A 30-day oscillation was also found in other phenomena. Since only under winter circulation conditions a coupling between the lower and the upper atmosphere seems to be possible, an inter-hemispheric coupling is suggested taking into account the half-yearly symmetric variations of $\bar{A}p$ and $\bar{A}_K$ about the equinoxes.

Besides these general remarks no further conclusions are drawn. The future task consists in an enlargement of the geomagnetic data base and in studying further related phenomena

in order to find support for the results obtained here.

REFERENCES

Bartels J 1935a: S.-B. Preuss. Akad. Wiss. 30, 504.

Bartels J 1935b: Terrestr. Magnetism Atmospher. Electr., 40. 1.

Bauer S J 1957: J.G.R., 62, 425.

Brown G M, Johns J I 1979: J.A.T.P., 41, 379.

Brown G M, Williams D C 1971: J.A.T.P., 33, 1321.

Bucha V 1976: Studia geoph. et geod., 20, 346.

Bucha V 1977: Studia geoph. et geod., 21, 350.

Bucha V 1983: Studia geoph. et geod., 27, 19.

Deland R J, Triedmann R M 1972: J.A.T.P., 34, 295.

Hines C O 1965: J.G.R., 70, 1758.

Kazimirovsky E S 1982: SibIZMIR Preprint 9-82, Irkutsk

Macdonald N J, Roberts W O 1960: J.G.R., 65, 529.

Mustel E R 1971: IUGG Symposium on Solar-Corpuscular Effects in the Troposphere and Stratosphere, Gidrometeoizdat, Leningrad 4.

Mustel E R 1972: Publ. 24, Astron. Sov. Acad. Nauk SSSR, Moscow 8.

Mustel E R 1973: Usp. Fiz. Nauk., 111, No 2, 365.

Mustel E R 1974: Gidrometeozdat, Leningrad 1.

Schmitz G, Grieger N 1978: Z. f. Meteorol., 28, 181.

Shapley A H, Beynon W J G 1965: Nature, 206, 1242.

Sonnemann G 1983a: Gerlands Beitr. Geophysik, 92, 135.

Sonnemann G 1983b: Proceedings of MAP-Symposium, Schwerin - GDR, in press (1984)

Sonnemann G 1983c: Proceedings of INTERCOSMOS-SEMINAR, Stara Zagora - PR Bulgaria, in press (1984)

Sonnemann G, Bremer J 1984a: Proceedings of KAPG-Symposium, Prague - CSSR, in press (1984)

Sonnemann G, Bremer J 1984b: Thesis of papers, IV. KAPG--Symposium on Solar-Terrestrical Physics, Sotschi - USSR

Sonnemann G, Lauter E A, Bremer J 1985: Adv. in Space Res., XXV.

Twitchell P F 1963: Bull. Geophys., Obs. de Geophys. Montreal, No 3, 69.

Acta Geod. Geoph. Mont. Hung., Vol. 22 (3-4) pp. 333-343 (1987)

PROFESSOR JÁNOS ZAMBÓ 70 YEARS - 250th ANNIVERSARY OF HIGHER EDUCATION IN MINING*

In 1985 we commemorated the 250th anniversary of the beginning of higher education in mining in Hungary - which is regarded as the start of technical education, too - and as a part of it, the 215-year jubilee of the Department of Mining Engineering, and special tribute was paid to Professor Zambó, Member of the Hungarian Academy of Sciences on his 70th birthday. The aim of this paper is to commemorate these anniversaries by a brief review on the development of mining science and on the history of the education of mining engineers as well as to express the best birthday-wishes to Professor Zambó.

Mining in Hungary run parallelly with the thousand-year history of the Hungarian people. The country was one of the leading precious-metal-producers in medieval times: in the 13th and 14th centuries, gold and silver mining was important and in the 15th and 16th centuries, copper production also became flourishing. Later, after the Turkish rule Selmecbánya grew to the productive, administrative and intellectual centre of mining and metallurgy.

Mining and metallurgy were pioneers of technical and scientific development in Europe for several centuries: a lot of technical and scientific problems emerged in connection with the extraction of ores and the production of metals. At the beginning of the 18th century a decisive part of engineering knowledge was made up by geology, mineralogy (with special

*Paper presented at the Conference "Fundamentals of the Design of Mining Operations", Miskolc, April 28-30, 1986

Acta Geod. Geoph. Mont. Hung. 22, 1987
Akadémiai Kiadó, Budapest

respect to ores and metals), mine surveying, mining engineering, underground construction, mining machinery, chemical analysis, mineral processing, metallurgy and its machinery, metal forming, minting and machine building. In connection with them the theory of economics, administration and law also developed. Mining strongly relied on the knowledge of mechanical engineering, mechanics, surveying, chemistry, forestry etc. and it was the first to use widely hydraulic energy, steam engine, pumps, mechanical transmission over long distances and machinery of great dimensions. Further development and application of science and engineering made it possible and necessitated to establish the first technical high schools.

Mining education in Hungary started by the "Instructio" of King Charles III, i.e. the founding decree of the predecessor at Selmecbánya (now Banska Stiavnica) of the present University on June 22, 1735. This mining officers' school was the first Hungarian technical school (university in modern terms). The school educated "mining officers", the teaching language was German. The officers were employed as engineers in mines, foundries and forests.

First professor of the Mining Officers' School was Sámuel Mikoviny, a well-known polyhistor of his time. The operation of the institution and curricula offered were regulated by the "Instructio" as well as by the "Organisatio" issued in 1737. Duration of study was two years. In the first year the subject mathematics included arithmetics, geometry, measurement, mechanics, machinery, architecture, drawing and mining knowledge. In the second year education was carried out in five branches: mining engineering and mining law, surveying, ore processing, analysis and metallurgy, minting and money changing. In the first period education was carried out only by a single "department": Sámuel Mikoviny lectured mathematics, mechanics, hydraulics and the fundamentals of mining.

In order to modernize and improve education, Johann Thaddäus Peithner put forward an educational programme and curriculum to the Imperial Treasury. On the basis of his suggestions, Maria Theresia, the Queen of Hungary issued a decree

on October 22, 1762 which prepared the way to establish the first department in 1763 - with Nikolaus Jacquin as head - for chemistry, mineralogy and metallurgy. The second department was founded in 1765 headed by Nikolaus Poda who lectured in mathematics, physics and mechanical engineering including mechanics and hydraulics. The third department, the department of mining - Department of Mining Engineering, as called today - completed the establishment of the Academy of Mining (Bergakademie) on April 3, 1770 and offered a three-year course.

Christof Delius Traugott became the first head of the Department of Mining Engineering. He lectured in mining engineering, mine surveying, ore processing, mining law, mining economics, minting and forestry.

Delius was head of the department from September 4, 1770 till March 1772. During this short period he carried out an outstanding work. He compiled the subject to include practical geology of ore veins and stratified mineral deposits, mining engineering, ore processing, mining machinery, mining law, principles of mining economics and mining policy, mining statistics, forest cultivation and selected topics on metallurgy. He constructed models and equipped the department with drawings and collections of mining law and statistics. He wrote and published the book "Introduction into the theory and practice of mining knowledge" for his students which was used as handbook and compendium in several countries of Europe for more than half a century. The book published in 1773 is divided into four parts: mining geology, mining engineering, ore processing, mining economics and mining policy. The book is even today, after two hundred years an excellent example of style, clear logic, high-level synthetization of knowledge for mining problems and of a technical-economical approach to solve mining tasks. (A Hungarian translation of Delius' book was published in a facsimile edition in 1972 on the 200th anniversary of its first publication and the Hungarian Mining and Metallurgical Society founded at that time the Delius Medal to be granted for scientific achievements in mining and metallurgy.)

Successor of Delius was Professor Johann Thaddäus Peithner

who headed the Department between 1772-1777. Professor Peithner collected many valuable and basic books on mining, metallurgy and sciences, and this became the core of the library of the Academy of Mining at Selmecbánya; more than 200 volumes of them can be found even now in the "Selmec Historic Library" of the Miskolc university.

From 1777 to 1780 visiting professors headed the department, in 1780-88, associate professor János Szeleczky, in 1788-1789 Károly Haidinger, in 1789-90 Mihály Patzier held lectures on mining engineering. Between 1792 and 1798, András Prybilla, from 1798 to 1805, János Möhling and Mihály Patzier and between 1805 and 1812, Ferenc Reichetzer worked at the department. The professors between 1777 and 1812 were first of all experts in mathematics, physics and mechanics, but they lectured in mining and metallurgy, too.

In 1808 the first department of forestry was founded, and the first Professor became Henrik David Wilkens. This indicates the beginning of the specialized education in forestry.

From 1812 till 1840 Johann Nepomuk Lang was head of the mining-department. He was an internationally well-known scientist of mine surveying. He was the first who suggested to use theodolites in (underground) mines and prepared programmes of courses and rules of operation for the Mining Officers' School. In 1841-44 Ferdinánd Landerer lectured in mining as deputy professor.

Between 1844 and 1849 the department was headed by János Adriány a professor of mathematics. His book on mine surveying reached several editions. He carried out extensive investigations about the stratigraphy of the Borsod lignite basin, and played an important role in starting coal mining at Diósgyőr. (A seam and a shaft are named in his honour.)

In 1850-51 Gusztáv Faller was associate professor at the Academy. In 1851-55 Professor Károly Lollok headed the Department of Mining Engineering, Mining Machinery and Mine Surveying.

From 1855 to 1870 Gusztáv Faller (1816-81) led the department as professor. He made internationally known contributions to mining knowledge, in his time he was one of the most

respected mining experts in the Hapsburg empire. The memorial volume published at the 100-years jubilee of the Selmec Academy of Mining was written by him. To cultivate international relations he edited scientific mining and metallurgical bulletins in joint editions with the mining academies at Leoben and Přibram (today Ostrava). He was the first who analyzed in his books the geological and mining conditions of the Dorog coal basin.

After the Austro-Hungarian compromise of 1867, certain reorganizations were made and Hungarian became the language of education. To the responsibilities of the Department of Mining Engineering belonged in addition to mining engineering ore processing, salt and coal mining. Mine surveying was separated from the department: Ottó Cséti (Chrismar) became the first head of the new department.

The Department of Mining Engineering was headed by Lajos Litschauer from 1870 on. He devoted almost whole of his life to write an up-to-date book on mining engineering in Hungarian. The book published in 1890-91 included the full material of mining engineering as lectured at that time: basic concepts of mining, mining stratigraphy, mineral prospecting, drilling, techniques of drilling and blasting as well as mechanized cutting, mining methods, transport of personnel in mines, water control, air transport and ventilation, illumination in mines, natural hazards and rescue operations. He changed the descriptive character of mining engineering by introducing calculation and design methods with practical aims. Lajos Litschauer retired in 1883.

From 1883 to 1904 Professor Gyula Gretzmacher was the head of department. His papers were published in German magazins and the Hungarian Bányászati és Kohászati Lapok (Journal of Mining and Metallurgy). His professional activity was focussed on mine mapping, mine surveying, stratigraphy, cutting and ore processing.

In 1904 the name of the Academy was changed to High School of Mining and Forestry; Géza Réz (Richter) became head of the department which he had until 1926. He recognized and

amphasized the importance of the close connection between scientific research and university education. He showed that the modernization of the education of mining engineers can only be succesful if it is strongly related to the practice of the mining industry. A first volume of his book was only published, but that is an excellent proof of his experience and knowledge gained from study tours abroad and from the technical literature.

In 1923 the Department of Ore and Coal Preparation (predecessor of the Department of Mineral Dressing) headed by Professor József Finkey was founded, thus lecturing in the corresponding subjects was separated from the Department of Mining Engineering. Professor József Finkey published scientific books and papers on mineral processing, but the book "Designing Mines" published by him as a senior lecturer at the Department of Mining, can be regarded as the precursor of the scientific research of mining locations.

Kornél Szoboszlay headed the Department of Mining from 1926 to 1932. He proved his excellent engineering qualities by the reconstruction of the Pécs mining. Professor Szoboszlay made great efforts to modernize the theoretical and practical material of education, and developed a rich collection of mock-ups and visual aids. His far-sighted plans were hampered by his aggravating illness from 1929 on.

Professor Péter Esztó joined the Department of Mining Engineering in 1929 and started to lecture on theory and practice of mining engineering. In 1932 he became head of department in which capacity he continued to lead it until 1954. Professor Esztó was an expert of great practical experience and excellent theoretical knowledge. In his scientific activity the theory of rock motion was of great importance and his contribution is important in starting the research in rock mechanics in Hungary. His achievements are outstanding in mine water control, mine ventilation, mine surveying and mining economics. His lectures and seminars always took account of the needs of mining industry and the requirements of scientific-technical development. His knowledge covered science, mineral processing, mineral

machinery and oil production well illustrated by the fact that his lectures on drilling technology made up the fundamentals of petroleum engineering education in Hungary. In 1954 Professor Péter Esztó handed over the leadership of the Department of Mining Engineering to one of the most outstanding members of the generations of engineers educated by him: to Professor János Zambó. He devoted his remaining time until retirement in 1959 to mineral prospecting, cutting technology, mine ventilation and mining safety. Péter Esztó was not only an excellent professor, but a humanist of deep feeling, too, who esteemed the personality of his students; they returned this attitude by devoted admiration.

In the last three decades, education and research in the Department of Mining Engineering were led by Professor János Zambó, Member of the Hungarian Academy of Sciences. His personal example and creativity ensured high standard and outstanding achievements.

János Zambó was born on May 2, 1916 in Hegykő. He graduated in Sopron with merit. In the academic year 1941-42 he was employed as a lecturer in the Department of Geodesy and Mine Surveying. In 1942 he joined the National Ore Mines as a chief engineer. He returned in 1946 to the university as senior lecturer and wrote several papers on mine surveying and defended his doctor's thesis on mining economics "summa cum laude".

From 1947 to 1953 he was in the coal mining industry, first as first engineer of the Padrag Colliery, then as deputy manager of the Ajka Coal Mines, and finally, as the mining manager of the Middle-Transdanubian Coal Mining Trust. In recognition of his scientific achievements he was awarded the title Ph.D. in 1952. He spent a decade in various leading posts in a period of extreme requirements against mining.

He carried out investigations for the location of several mines, modernized cutting techniques, improved mining methods and increased the level of mine safety. His activity was acknowledged by a lot of awards: Order of Work (1950), Distinguished Worker of Mining Industry (1953), Kossuth Prize Grade 2 (1953), etc.

In 1953-54 he was the director of the Research Institute of Mining and, at the same time, professor and head of the Department of Mining Engineering. From 1955 on he was full-time professor at the Technical University of Heavy Industry and until March 31, 1984, head of the department. In the period 1955-59 he was the dean of the Faculty of Mining Engineering, 1960-61 Pro-rector and between 1961 and 1972 Rector of the Technical University of Heavy Industry.

His activity is primarily characterized by an interaction and unity of theory and practice. From the beginning of his career he made successful efforts to unite the principles of science with practical experience and to solve mining problems with highly effective mathematical skill. This useful amalgamation of knowledge and skill made the results of his practical, teaching and scientific work extremely beneficial for the mining industry.

Professor Zambó headed the Department of Mining Engineering for nearly 30 years and the Research Group of Mining Departments of the Hungarian Academy of Sciences for two decades. His achievements have shown that a department under qualified leadership can significantly contribute to the results of the corresponding branch of economy. His excellent educational abilities and rich practical experience ensured that well-trained young mining engineers graduated at the university. His lectures have always enjoyed top priorities and meant an experience to the audience never to forget. The previous descriptive character of the material of teaching was replaced by modern scientific principles. The research activity of the department under his guidance has achieved international acknowledgement and the department itself became a centre of mining sciences. The main fields of research within the department have been: location and reconstruction of mining and other industrial facilities, mining analysis, mining economics and valuation of workability of useful mineral deposits; prospecting, development and opening, and extraction of solid mineral deposits; solution of problems in rock- and geomechanics, construction of mining and other underground excavations, design

of supports, problems concerning rock motion and mine damage, improving protection methods against natural and mine hazards, mine ventilation and air conditioning, mine and health safety, rescue techniques; cutting and blasting techniques and special cutting methods, nature and environment protection; development and feasibility investigations of new mining technologies; development of computer aided design and its application in planning major mining objects. Research carried out at the department has yielded considerable theoretical and practical results. An active cooperation and advice of the department is required by the leaders of industry in all major problems of development.

Professor Zambó has led and helped his colleagues in their research and inspired them to find their own ways of research. As a result, a highly qualified academic and research staff has grown up under his care.

Apart from heading the department, during his 11-year term as Rector he made his experience, executive ability and resolution profitable for the Technical University of Heavy Industry. He had an outstanding role in the development and execution of the educational reform and long-term development plan in 1963.

The results of his scientific work were published in nearly two hundred papers and six books. After his initial wide interest - mine surveying, rock mechanics and mine water control - his scientific activity became concentrated more and more on mining locations. In his papers published in the Bányászati Lapok (Mining Journal) and in other scientific forums as well as in his books Mining Engineering (Opening and Extraction) (1957, 1965, 1972), Analysis of Mining Locations (1960), Location Theory in Mining (1965) and Fundamentals of Mining Engineering (1985) he created a special Hungarian school in the field of scientific investigation of mining locations which enabled to find the technically and economically optimum solutions even in the most complicated cases of mining locations.

Some of his books were been published abroad and in foreign languages, respectively (Analitichni Metodi pri Projektirovanie na Rudnichi. Publ. Tekhnika, Sofia, 1962; Optimum Location of Mining Facilities, Akadémiai Kiadó, Budapest, 1968).

Professor Zambó's outstanding role in the development of the theory of mining location can be seen on the international recognition reflected by the frequent citation of his books and papers, and the application and adaptation of his methods. He was industrious in introducing analytical calculations for all mining problems in the Hungarian practice. He supervised the team of the department in carrying out the analytical investigations on the location of Eocene mines, the reconstruction of the Mecsek Liassic mines, development of copper ore and bauxite deposits and location of new mines (Dubicsány, Ajka II and open pit mines).

As recognition of his pioneering work in founding the theory of mining locations, Professor Zambó was elected corresponding member of the Hungarian Academy of Sciences in 1961 and ordinary member in 1972. The Moscow Mining University awarded him doctor "honoris causa" in 1971. The Hungarian Mining and Metallurgical Society granted him the Aladár Wahlner medal twice, in 1954 and 1959, and the Kristóf Delius Traugott medal in 1976. His outstanding scientific achievements were acknowledged by the government by granting him Grade I National Prize in 1965.

Professor Zambó has always been a public-spirited man. He was a member of the presidential board of the Hungarian Academy of Sciences over a term, and Chairman of the Committee for Geology, Mining, Surveying and Geophysics for Scientific Qualification over three terms. He was chairman or member of several governmental or academic committees, chairman of a subcommittee of the National and Kossuth Prize Committee and editor of the Mining Section of the Transactions of the Technical University of Heavy Industry.

His awards granted in recognition of his educational, scientific and public activity are: Distinguished Teacher (1959), Order of Work, Grade Gold (1963, 1972), Distinguished Worker of Heavy Industry (1969), Mining Service Medal (Grade Gold 1976, Grade Diamond 1985), Distinguished Miner (1982), order "For Socialist Hungary" (1983).

He is still acting as a professor and participates actively

in the scientific life. He is chairman of the Miskolc Committee of the Academy, member of the Committee of Mining Science of the Hungarian Academy of Sciences, of the National and Kossuth Prize Committee and of the editorial board of Acta Geodaetica, Geophysica et Montanistica Hungarica.

On the occasion of the scientific conference to commemorate the 250th anniversary of the beginning of the Hungarian technical education and the 215-years jubilee of the Department of Mining Engineering we congratulate and wish all the best to Professor János Zambó, Dr. hc., Member of the Academy on his 70th birthday. We wish him good health and hope that the education of mining engineers and the mining industry will continue to benefit from the results of his work for a long time to come.

F Kovács
Head of Department of
Mining Engineering

Acta Geod. Geoph. Mont. Hung., Vol. 22 (3-4), pp. 345-359 (1987)

ECONOMIC ANALYSIS OF PRE-DRAINAGE OF WATER-BEARING SAND LAYERS IN THE BORSOD COAL MINES

B Balogh

Borsod Coal Mines, Miskolc, Karinthy F. u. 19, H-3535

Economic effects of pre-drainage in the workings of Putnok and Farkaslyuk mines have been analyzed. The analysis has proved that the pre-drainage is economical in both mines. The rentability of the pre-drainage depends on the face length and the time of pre-drainage, and it increases as these parameters increase. No correlation has been found, however, between the rentability and the distance between the pre-draining boreholes; that may partly be due to the fact that the borehole distance is mainly based on experience and varies only within a narrow range in each mine. The thickness of protective layers, the time of drainage, and the distance and depth of the pre-draining boreholes in the mines Putnok and Farkaslyuk were almost equal. Calculations have proved that the rentability of pre-drainage is similar, too.

Keywords: Putnok mine; Farkaslyuk mine; pre-drainage; rentability; coal mines

Preventive dewatering of aquifer sand layers above a coal bed has got besides the problems of security, other kinds of advantages. For one part of these advantages a surplus profit can be determined by economic calculation, while for the other part of them the effect of preventive dewatering can be proved, but it cannot be exactly calculated.

Before doing the economic calculations for the first group let us say a few words about the second one.

Two advantages of the second group should be emphasized:

- the feeling of security of the workers which makes their work more tranquil and thus they can reach higher efficiency;
- the production will not be interrupted by water- or mud inrush.

An advantage of the first group is that the speed of longwall advance increases as an effect of the drainage. The present

economic study deals with this matter.

1. DESCRIPTION OF THE ECONOMIC STUDY

The water stored in aquifer layers above the mined coal beds can flow into the set of workings during mining if the aquifer layers were not dewatered at all or not in the required degree before the start of the longwall. The water flown into the set of workings makes the underlaying rock soaked through, decreases its compressive strength and this can lead to the sinking or list of the support, to the decrease of production and to the lower speed of longwall advance.

Preventive dewatering has been applied in several mines, but only in the mines Putnok and Farkaslyuk were registered data correct enough for drawing an unambigous conclusion from them. That is why the calculations are based on these mines.

The expenses of preventive drainage incur before the start of the longwall, while the effect of preventive dewatering arises only after the start of the longwall as the speed of longwall advance increases due to the elimination of the disturbing influence of underground water.

The increase of advance speed of a longwall means surplus production and consequently the rise of income.

The dewatering is profitable if its costs are recovered from the returns of the surplus production; whereby it must be taken into consideration that a previous investment must yield a profit of 12 p.c. pro year according to the economic regulation valid in Hungary for the time being.

Longer or shorter time interval can pass from dewatering till the start of a longwall, i.e. each longwall panel is dewatered in a different degree. In case of shorter draining dewatering has a lower degree, more water remains in the aquifer during the operation of the longwall. Thus, bigger quantity of water flows into the set of workings which hinders the longwall advance more than in case of longer draining.

It often happens in the Borsod Coal-Mining Company that the draining time is shorter than required partly because the

preparation of the longwall works did not reach the required extent, partly due to the lack of drilling capacity. This enables to look for a regressive relation between the time of dewatering and the speed of longwall advance. Naturally, the velocity of longwall advance depends not only on the time of draining, but also on the breast of the longwall.

Since different conditions can affect the speed of advance and the degree of preventive dewatering, each mine had to be investigated separately and not all of them together. It was tried to find regressive relations between the velocity of longwall advance, the breast, the length of dewatering time and the distance of the draining boreholes. A regressive relation was obtained between the speed of longwall advance and the breast, but such a relation could not be found between the speed of advance and the distance of draining boreholes.

The suitable distance of boreholes was chosen in both mines on the basis of the permeability coefficient determined for the aquifer sand layer in the roof; it was 8 m both in Putnok and Farkaslyuk.

In the first step of the study the influence of the breast and draining time on the speed of longwall advance was looked for, then the relation between dewatering time and advance speed was defined in the cases of actual breasts and by means of that the surplus production as consequence of previous dewatering was calculated. The difference between the returns of the surplus production due to dewatering and the costs of dewatering as a sum put out at interest for the period of production yields the profit of preventive dewatering. According to that the following calculations were made.

2. THE EFFECT OF BREAST AND DRAINING TIME ON THE SPEED OF LONGWALL ADVANCE

The connection between the speed of advance, the breast and the draining time can be defined by means of a regression function with two variables. In the estimation the actual data of the speed of advance, of breast and of draining time of each

longwall were used.

The preventive dewatering was implemented from both extraction drifts in the case of longwalls in an unmined area of the mine. In case of such longwalls the time of dewatering was defined as the arithmetic average of the term from the start of draining from the road till the start of mining; and the term from the start of draining from the air opening of the panel till the start of mining. In most cases, however, one side of the longwalls taken into consideration were already extracted, when the longwall was started. The sand-layer above the longwall panel was already partially emptied through this broken area, and this must be taken into consideration at the calculation of the time of dewatering. The draining time of these longwalls was considered as the arithmetical average of the periods from the pass-by of the adjoining longwall till the start of the longwall under discussion; and from the start of draining in the drift being farther from the broken area till the start of our longwall.

The chosen type of correlation function is:

$$y = b_o + b_1X_1 + b_2X_2 \ ,$$

where: y = the speed of longwall advance (m/d),
X_1 = breast or length of longwall face (m),
X_2 = time of dewatering (months),
b_o, b_1, b_2 = wanted coefficients.

The adjustment was done on the basis of the principle of least squares. This function has its minimum where its first derivative with respect to the wanted variables equals to zero.

By solving the obtained equation system with three unknowns with respect to b_o, b_1, b_2 one gets the wanted constants. The calculation was done separately for both mines due to the formerly mentioned reasons.

MINE FARKASLYUK

In case of the mine Farkaslyuk the relation between the speed of longwall advance, breast and draining time was studied on the basis of genuine data of longwalls lying in the southern part of the mine-sector. Breaker-loader machines of the type VOB-HP and KSIK working in these longwalls gave these data.

In this territory a 0.5 m thick protective layer and a 25 m thick sand layer can be found in the roof of the coal bed. The sand layer has to be dewatered in advance in order to assure the undisturbed work of extraction. The breast of the longwalls operating in this area was 60-100 m long, the draining time of them varied between 3 and 36 months. The data of 12 longwalls were used for the investigation.

According to the calculations the approximation function of the speed of longwall advance is:

$$y = 4.670 - 0.029\ X_1 + 0.015\ X_2 \quad (m/d)\ .$$

For the correlation index one gets:

$$I = 0.95\ ;$$

and for the partial correlation coefficients:

$$r_{yx_1} = -0.94\ ,$$

$$r_{yx_2} = 0.91\ .$$

MINE PUTNOK

The respective results are:

$$y = 3.383 - 0.013\ X_1 + 0.015\ X_2\ ;$$

$$I = 0.77\ ;$$

$$r_{yx_1} = -0.25 ,$$

$$r_{yx_2} = +0.70 .$$

3. CALCULATION OF THE RETURN OF SURPLUS PRODUCTION DUE TO PREVENTIVE DEWATERING

The estimated approximation functions show that the dewatering of a longwall, the increase of the draining time augments the speed of longwall advance and the production of the longwall. In the economic study of preventive dewatering the return of the surplus production due to dewatering must be estimated, as draining is only economical if the surplus return covers the surplus production costs, the costs of drilling and pipe fitting, the expenses of the former implementation of productive development (preparation works) as well as the preceding costs of bailing up, whereby it has to be taken into consideration that a part of the costs connected with preventive dewatering has the character of previous capital investment.

The surplus return is calculated from the actual data of the mines for 1980. In the calculation of incomes and costs the prices of 1980 were taken.

The return of the surplus production of a day can be obtained as the product of the specific income of the mine and the quantity of surplus production of a day:

$$P = p \cdot Q ,$$

where: P = the return of the daily surplus production (Ft/d),
p = specific income of the production of the mine (Ft/t),
Q = quantity of surplus production due to preventive dewatering of the longwall panel (t/d);

$$Q = \gamma \cdot m \cdot X_1 \cdot Y_v \qquad (t/d) ,$$

where: γ = density of the extracted product (t/m^3),

m = worked thickness of the coal bed (m),

$Y_v = b_2 X_2$ (m/d), the increase of advance speed due to preventive dewatering (m/d).

MINE FARKASLYUK

In 1980 the genuine value of the specific income was here 773.68 Ft/t, the worked thickness of coal bed 2.49 m, and the density of the extracted coal 1.4 t/m^3.

The daily surplus return due to preventive dewatering was calculated from the following relation:

$$P_f = 40.40 \cdot X_1 \cdot X_2 \quad (Ft/d) .$$

For the estimation of the connection between dewatering time and daily surplus return the breast could be considered unvaried, and it was well measurable.

Hence the daily surplus return was calculated as follows: the term $b_2 \cdot X_2$ of the connection between advance speed of longwall, draining time and breast was multiplied by a constant, i.e. the correlation coefficient of the connection between daily surplus return and draining time is equal with the correlation coefficient r_{yx_2} used above:

$$r_{p_f x_2} = 0.91 .$$

MINE PUTNOK

The following relation gives the daily surplus return due to preventive dewatering:

$$P_p = 41.063 \; X_1 \; X_2 \quad (Ft/d) ,$$

and the correlation coefficient is:

$$r_{p_p x_2} = 0.70 .$$

It can be seen from the results that the surplus return due to dewatering is almost the same in the mine Putnok and in the mine Farkaslyuk.

It should be mentioned that the given functions are valid only within a certain range. Namely the speed of longwall advance is limited by the necessary order of technological process; hence the increase of draining time over a certain limit cannot yield a further increase of the advance speed. Considering the well-determined order of succession of the technological process and the advance of the longwalls on the days of best production in the mines Putnok and Farkaslyuk one can calculate with 4 m/d maximum speed of longwall advance. Consequently the estimated relations can be studied within these ranges.

4. EXPENSES OF DEWATERING AND OF SURPLUS PRODUCTION DUE TO PREVENTIVE DEWATERING

The expenses incurred in course of the surplus production can be divided into four groups:

a) increased production costs due to surplus production;
b) costs of drilling and pipe fitting in the roof;
c) required earning capacity of the costs of longwall preparation for the time of draining before the start of the production;
d) required earning capacity of the former costs of bailing up.

a) The estimation of the increase of production costs was based on the actual specific production costs of 1980. The specific production costs can be divided into two groups, namely:

- Some costs arise independently of the quantity of production. They are the so called fix costs, and have not been taken into consideration in the study as they incur whether the production increases or not.
- The second group of production costs changes proportionally to the quantity of production. According to experimental data they make 53 % of the total production costs. It means that in our economic study we can calculate with 53 % of the genuine production costs of 1980 as the production costs of

the surplus production, i.e. the increase of production causes an exceed of costs only in such a degree.

b) In the economic analysis the costs of drilling and pipe fitting must be considered as a previous capital investment. While the formerly mentioned surplus production costs incur simultaneously with the returns of the surplus product, i.e. the expenses are returned almost at the same time, the costs of dewatering arise longer before it is returned by its result, i.e. by the surplus production.

The present financial regulation in Hungary prescribes a yearly interest rate of 12 % for previous capital investments. Hence the investment is profitable if its result returnes the invested sum and a compound interest of 12 % taken from the beginning of dewatering until the appearance of the result. The cost of the complete work-out of a draining borehole is 642 Ft/m.

The daily expense of dewatering is calculated as the cost of a borehole multiplied by its compound interest and by the daily longwall advance and this product is divided by the usual average distance of boreholes.

$$K_n = 1.12^{\frac{X_2}{12}} \cdot 642 \cdot l \cdot \frac{y}{h} \qquad \text{(Ft/d)}$$

where: K_n = costs of dewatering/day,
l = length of the draining holes (m),
h = average distance between the draining boreholes.

The costs of preventive dewatering do not belong to the total production of a longwall, as draining happens only in the interest of the surplus production.

c) In order to carry out dewatering the extraction drifts have to be driven out a certain time before the start of the longwall; this time is required for draining. Without draining the extraction drifts must be also driven out, but in this case this work can be made later, hence the expenses of longwall preparation incur at an earlier moment alone in the interest of dewatering. Thus the costs of the longwall preparation

itself cannot be considered as belonging to the costs of dewatering but according to point b) the 12 % interest rate of the costs of longwall preparation works must be taken into calculation for the time of draining.

In case of each longwall the required profit rate (i.e. prescribed 12 % interest rate) is calculated only for the costs of driving one drift. The daily cost-effect of the required profit rate of the expenses of production preparation is obtained by the difference between the interest-bearing of the costs of driving a drift-section corresponding to the daily longwall advance for the draining time and the real expenses of driving a drift-section. It is necessary to take this factor into consideration, because without dewatering the production preparation would be done only later. The costs of one meter drift is 20.000 Ft.

The following relation gives the daily expenses corresponding to the required profit rate of the costs of longwall preparation driving:

$$K_e = \left(1.12^{\frac{X_2}{12}} - 1\right) k_e \cdot y \qquad (Ft/d)$$

where: K_e = the daily outlay corresponding to the required profit rate of the costs of production preparation (Ft),

k_e = driving cost of one meter drift (Ft).

d) The water quantity stored in the aquifer sand layer above the coal bed has to be pumped out earlier than the surplus production due to dewatering appears. The effect of costs corresponding to the required profit rate must be included into the calculation. The cost of bailing up itself cannot be considered as a cost of dewatering, because the water in the sand above the coal bed must be pumped out from the mine in any case. In case of preventive dewatering, however, bailing up can be done during draining while without preventive dewatering it is done during the work of the longwall.

This water quantity is approximated by the specific water spring of the mine and the surplus production due to dewatering.

It has been supposed in the calculation that during dewatering the daily water quantity flowing from the draining boreholes is equal with the product of the daily surplus production and the specific bailing up of the mine. It is supposed hereby that during dewatering the water quantity belonging to the surplus production is bailed up. The corresponding effect of the required profit rate of dewatering expenses is calculated from the following relation:

$$K_v = \left(1.12^{\frac{X_2}{12}} - 1\right) \Big/ q \cdot k_v \cdot \gamma m \cdot x_1 \cdot Y_v \qquad (Ft/d) \ ,$$

where: K_v = daily effect corresponding to the required profit rate of dewatering expenses (Ft/d),
q = specific bailing up of the mine (m^3/t),
k_v = cost of bailing up of one m^3 water (Ft/m^3).

The above mentioned costs connected with dewatering are estimated as follows:

MINE FARKASLYUK

a) Increase of production costs

In the mine Farkaslyuk the actual specific production costs in 1980 amounted to 603.30 Ft/t, 53 % of it were proportionally variable costs.

The total increase of production costs in order to reach a surplus production was calculated by the following relation:

$$K_t = 16.72 \ X_1 \ X_2 \qquad (Ft/d) \ .$$

b) Costs of roof-drilling and pipe fitting

In the mine Farkaslyuk draining boreholes are drilled in every 8 m in the extraction drifts on the basis of experiences. The length of each draining hole is 8 m. The costs of drilling and pipe fitting are estimated by the following relation according to 4/b:

$$K_n = 1.12^{\frac{X_2}{12}} \; 642 \; (4.670 - 0.029 \, X_1 + 0.015 \, X_2) \quad (\text{Ft/d}).$$

c) Required profit rate of the costs of production preparation

According to the relation deduced in 4/c the daily effect of an earlier implementation of the extraction drifts is the following:

$$K_e = \left(1.12^{\frac{X_2}{12}} - 1\right) \; 2000 \; (4.670 - 0.029 \, X_1 + 0.015 \, X_2) \; (\text{Ft/d}).$$

d) Required profit rate of the costs of a previous bailing up

In the mine Farkaslyuk the production of 1980 was 378 054 metric tons, the water bailed up was 1 487 711 m^3, and the cost of bailing up of one m^3 water was 3.50 Ft. On the basis of that written previously, the daily effect of the required profit rate of the costs of preventive bailing up is given by the following relation:

$$K_{vp} = \left(1.12^{\frac{X_2}{12}} - 1/0.27 \, X_1 X_2\right) \quad (\text{Ft/d}) \; .$$

e) Total expenses of preventive dewatering

The total costs of dewatering at Farkaslyuk is given by summing up the costs estimated in a, b, c, and d of section 4. After summing up the cost-factors and doing the possible reductions the following relation is obtained:

$$K_f = 1.12^{\frac{X_2}{12}} \; (96398 - 598 \, X_1 + 309.63 \, X_2 + 0.72 \, X_1 X_2) +$$

$$+ 16 \, X_1 X_2 - 93400 + 580 \, X_1 - 300 \, X_2 \quad (\text{Ft/d}) \; .$$

MINE PUTNOK

The increase of costs due to preventive dewatering is giv-

en by the following relation:

$$K_p = 1.12^{\frac{X_2}{12}} (69831 - 268.35\ X_1 + 309.63\ X_2 + 1.38\ X_1X_2) -$$

$$- 67660 + 260\ X_1 - 300\ X_2 + 16.95\ X_1X_2 \qquad (Ft/d).$$

5. ECONOMIC RESULTS OF PREVENTIVE DEWATERING

The estimation of the economic results of preventive dewatering in the mine Farkaslyuk is presented in Fig. 1 in case of different breasts as functions of draining time. The expected daily surplus production due to dewatering depends on the length of draining time and of the breast. In case of longer faces the quantity of surplus production and through it the income is higher then in case of shorter faces.

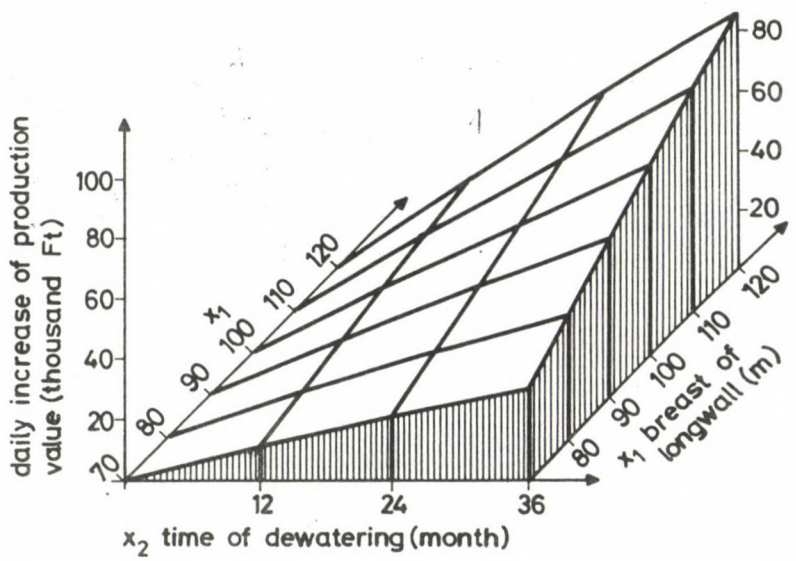

Fig. 1. Daily increase of the production return (in Ft) as the function of X_1 and X_2

The possible income increases with increasing draining time. The degree of income increase decreases with the increase of draining time, but within the range of a planned draining time the function has no optimum; it increases monotonously within this range.

In case of the mines Putnok and Farkaslyuk the income increase was estimated for 36 months of dewatering.

Prognostics for longer draining times cannot be set up as the function was determined from real data of recently operated longwalls and the draining time of them varied within this range; thus the estimated functions are valid only within this range.

SUMMARY

The economical effects of preventive dewatering of longwall panels were studied in case of the mines Putnok and Farkaslyuk. The study proved that preventive dewatering was an economical activity in both mines. The economical result of dewatering depends on the breasts and on the draining time.

The economical result i.e. the income increases with the increase of the breast and the draining time. No correlation could be found between the distance of draining boreholes and the economical result of dewatering; the explanation is that in both mines the distance of boreholes yielding the best draining results varies only within a narrow interval, it was defined on the basis of practical experiences.

In the mines Putnok and Farkaslyuk the thickness of the protective layer and the sand, the applied draining time, the distance and depth of the draining boreholes are almost the same. Our study verifies that the economical result of preventive dewatering remains also nearly on the same level.

REFERENCES

Balogh B 1973: Bányászati és Kohászati Lapok, Bányászat 106, 306-314.

Balogh B 1982: Underground methods and results of preventive dewatering of aquifer sand layers near to the coal beds in Borsod brown coal basin. VIII. Conference of Mine-Water Prevention, Budapest

Balogh B 1983: Problems of preventive drainage of aquifer sand layers near to the coal beds in Borsod brown coal basin. Doctoral Dissertation, Miskolc

Jeney-Jambrik R, Kovács F, Schmotzer I 1985: Bányászati és Kohászati Lapok, Bányászat 115, 147-154.

Jeney-Jambrik R 1985: Földtani Kutatás 18, No 3, 21-30.

Köves P, Párnitzky G 1973: Általános statisztika. Közgazdasági és Jogi Könyvkiadó. Budapest

Acta Geod. Geoph. Mont. Hung., Vol. 22 (3-4), pp. 361-369 (1987)

ABOUT THE POSSIBILITIES OF INVESTIGATING AND IMPROVING THE SOURCE-PATTERN OF COAL PRODUCTION

G Faller[1] and M Tóth[2]

[1]Ministry of Industry, Budapest, Markó u. 16, H-1055

[2]Mining Corporation, Budapest, Arany J. u. 10, H-1051

An index is introduced which enables to design the economically optimum mining pattern of a country or a coal basin. An investigation method is given by means of which the economy of the mechanization of workings can be determined within different natural and technical conditions. The method enables a comparison of rentability between mechanization and advance working expenses and savings, respectively.

Keywords: optimum mining pattern; longwall mechanization; profit; mine model

Zambó was the first to mention in his report at the session of Section 10 of the Hungarian Academy of Sciences during the Congress of the Academy in 1967 the investigations for the optimization of the production structure of coal mining which were carried out in the former Ministry of Heavy Industry. In the discussion the present authors emphasized that the study was based on the determination of the cost-functions for individual mines what belonged to the location theory of mines. The change of prime-costs in function of capacity was the fundamental parameter that defined the capacity with which each mine investigated was taken into regard for satisfying the coal demands in the analyzed long-term period. The most important conclusion of the study was that by maintaining the yearly coal production of 1965, i.e. roughly 100 Pcal/year, the yearly profit of coal production could be increased by about 1.2 billion Ft for the year 1973 if an uneconomical capacity of about 20 Pcal/year can be replaced by the same capacity of economical mines till that time, what would mean an improvement of the total coal mining effectivity by 40 p.c.

Acta Geod. Geoph. Mont. Hung. 22, 1987
Akadémiai Kiadó, Budapest

This is not recalled here for the sake of the result of the study (as this program has not been realized after all), but due to its implication that the mentioned total economical result can be achieved about in half by a change of the mining pattern within a coal basin, and only in half by changing the production rate among different coal basins.

Possibilities to improve the mining pattern within a basin are in general easier to realize than those among different basins. Nevertheless, the efficiency of the production units shows even now a very high scattering within a basin. Thus it is an important task to look for means of improving the source pattern within a basin or an enterprise. Theoretical considerations in this connection belong to the fundamentals of planning mining operations.

The high scattering of the profit data of mines belonging to the same basin are present by the primary data. For different comparisons, however, it is more informative to calculate and analyze complex indices. Such an index is introduced in the first part of this paper, while in the second part conclusions are drawn from the combined investigation of the mechanization of longwalls and the design of mining patterns about the strategy of the enterprises.

DESIGN OF OPTIMUM MINING PATTERNS

As mentioned, the profits of the mines, i.e. the production units show a high scattering. The scattering of profit data of 32 underground coal mines in Hungary can be represented in a "step" diagram, on the ordinate of which the heat equivalents of the coal production (PJ pro year) were plotted by starting from the origin with the mine having the highest profit (in Ft/GJ), followed in decreasing sequence by the heat equivalents of the other mines. The heights of steps on the abscissa are the profits (Ft/GJ) of the mines. Steps representing mines with a deficit lie below the ordinate. Within the sequence according to decreasing profit the mines of different basins show no regularity according to their location.

Taking this as a probability distribution, several types

of functions can be fitted to it. For the sake of analogies applied in the followings, from the point of interest and as a basis of further discussions, the Boltzmann function of a form

$$E_N = E_0 e^{-bN} + E_E$$

was chosen. Due to mines with deficit the function is increased by E_E along the axis E_N. In order to justify the choice of the function type let us refer to the analogy of thermodynamics in a very simplified manner:

E_0 is the energy of the gas molecule of highest energy if the function relates e.g. to the distribution of energy among the molecules of the gas enclosed in a box; in our case it means the specific profit of the "most profitable production" of the unit heat equivalent;

e is the basis of natural logarithms;

b is a number characterizing the inclination of the curve; if it would be zero, there would be a completely uniform energy distribution among the molecules; in our case each production expressed in PJ would have the same efficiency;

N is the serial number of gas molecules; in our case it is the "serial number" of the heat production of the mines moving off from the origin;

E_N is the energy of the Nth molecule; in our case it is the profit (Ft/GJ) characteristic for the Nth heat production unit (PJ).

If the gas in the box is subdivided into several parts than the situation with respect to the energy content of the molecules of the highest and the lowest energy must be similar in each part to the original situation, i.e. the value of b expressed in the function of the individual parts must be greater than the value b referring to the "undivided" gas. When arranging the studied mines into groups, whereby each group contains the mines belonging to one basin, then just the opposite behaviour would be expected from the values b of such groups, even if the analogy is imperfect in the respect that the most profitable mines and those with the highest deficit of the

different groups must not have the same profit or loss, respectively. An opposite behaviour is expected because theoretically the conditions within a basin are less heterogeneous than over the country, thus the more the study is restricted to a certain region, the value b should the more approximate zero. The curve of the overall data set as well as the curves of data sets divided to three coal basins, however, show in a good approximation just the opposite (Table I).

Table I. Data about production units of different basins

	Investigated underground coal mines	Coal mines in Transdanubia	Coal mines in Northern Hungary	Coal mines in the Mecsek Mts
Number of production units investigated	32	14	12	6
Value b characterizing the distribution ("decreasing speed" of the function)	0.0030	0.0049	0.0156	0.0107
Closeness of the function	0.88	0.81	0.93	0.83
Relative error in p.c.	0.0	8.5	11.4	8.0

It is remarkable that the value b characterizing the Transdanubian coal mines hardly exceeds that of the total (underground) coal mining of the country, that of the coal mines of the Mecsek district is three times greater and that of the coal mines in Northern Hungary is five times greater than the overall value of b. These b values indicate that the improvement of the production pattern within the last two regions is a task of paramount importance.

Of course, the pattern analysis by means of the Boltzmann function is rather a matter of curiosity with respect to analogies and cannot be regarded as a method for drawing far-reaching conclusions. Nevertheless, it is worth mentioning

that by applying such unfamiliar investigation methods in economy, on the one hand the pattern analysis can be made more comprehensive, on the other conclusions drawn by familiar economical methods can be checked by them. Here it also can be used to emphasize the actuality of the pattern improvement within certain coal basins.

ESTIMATION OF THE ECONOMICAL EFFICIENCY OF WORKINGS MECHANIZATION

A study of the possibilities to improve the production pattern within a basin has to cover utilization and efficiency of the mechanization of the workings as well as the natural conditions among which these living workings are operated and which determine in a high degree the former ones. In our investigation the starting point is the recently almost common experience that the production of a mine, i.e. the utilization of an existing production capacity is not or only slightly increased by a full mechanization of the longwalls.

One of the main reasons of that is that, due to the general shortage in manpower, the mines are satisfied by a saving in manpower in consequence of mechanization, and by striving at a concentration of the production within the mine, they decrease - in some cases they are forced to decrease - the number of simultaneously producing workings and their face widths, respectively. Thus, the production increasing effect of the higher advance speed of longwalls is more or less compensated by the simultaneous reduction of the total face width, and the area extracted during the time unit, and thus the production in the mine does not increase or at least it does not in a sufficient degree.

Besides a few exceptions a similar situation and trend can be observed in the fully mechanized workings: the speed of face advance is increased due to the higher level of technics and organization, the face width is decreased with the same rate, mainly due to the general shortage in manpower or due to lower technical level and consequently capacity shortages in the elements of the production chain subsequent to the face. Moreover,

in consequence of restrictions in wages and of low-level organization, the utilization of the very expensive heading machines is usually low, in other works the speed of face advance and the working productivity do not reach the optimum.

The dependence of the rentability of working mechanization on the production of the studied mines and the suitable design of their production patterns, respectively, can be illustrated by a model in which the economical parameters of two mines with different natural conditions are compared in several versions:

- with unmechanized or only traditionally mechanized workings (version 0),
- the full mechanization of the workings does not influence the production (version a),
- the full mechanization of the workings goes together with a production increase of 50 p.c. (version b),

as well as in production pattern combinations from these versions for the mines "A" and "B".

As for the two mines in the model, it is supposed that the coal seams in mine "A" are of medium thickness and free of faults disturbing the mining, while the coal seams in the mine "B" are thin and cut by faults disturbing the mining. For the sake of simplicity the coal quality was supposed the same in both mines. The natural conditions of mine "B" were taken as the basis to determine the costs of a possible substitution by import or by some other unadvantageous energy source.

The results of the model-study are summarized in Table II.

By combining these basic versions the sequences in Table III are obtained depending on whether the pattern combinations covering the original coal demand of 800 + 400 = 1200 kt/year were taken into account or all combinations, namely those too which yield a production surplus.

According to the results a mechanization of workings substituting only manpower and not increasing the production is only just acceptable from the point of view of rentability, as consequence of the relatively high costs of machines and energy besides a relatively low expense for wages, because the possible savings in wages are almost compensated by the amortization and by the high costs of operation and maintenance of the

Table II. Results of the model study with respect to the individual mines "A" and "B"

			Mine A			Mine B		
			0	a	b	0	a	b
Quantity of coal	production	kt/year	800	800	1200	400	400	600
Price per unit	quantity	Ft/t	1200	1200	1200	1200	1200	1200
Productivity	in workings	t/man/year	3200	5300	5300	2000	3300	3300
	total	t/man/year	500	600	800	300	350	450
Specific prime costs	in workings	Ft/Ft	200	250	250	350	450	450
	total	Ft/Ft	950	950	800	1350	1350	1200
Rentability	index	Ft/Ft	1.25	1.25	1.50	0.90	0.90	1.00
Profit		million Ft/year	+200	+200	+480	-60	-60	0
Specific prime costs of production growth		Ft/t	-	-	500	-	-	850

Table III: Rentability sequence of the combinations of the basic versions

Pattern combinations	Coal production kt/year	Rentability index Ft/Ft	Sequence of rentability	
			between combinations just covering coal demands	between combinations just covering and exceeding coal demands
A/0 + B/o	1200	1.10	2	6
A/0 + B/a	1200	1.10	3	7
A/0 + B/b	1400	1.15	-	5
A/a + B/o	1200	1.10	4	8
A/a + B/a	1200	1.10	5	9
A/a + B/b	1400	1.15	-	10
A/b + B/0	1600	1.25	-	3
A/b + B/a	1600	1.25	-	4
A/b + B/b	1800	1.35	-	2
A/b	1200	1.50	1	1

machines. Thus in such a case the amortization period of the investment is very long, almost infinite.

From the results of the modelling it is clearly visible that by far the most rentable solution is to create in mine "A", having advantageous conditions, as many fully mechanized workings or longwall faces and to reach an advance speed that the resulting surplus production (50 p.c. in our example) should substitute the production of mine "B" (or the equivalent import of coal). This solution yields according to the model a yearly surplus profit of 500 million Ft with respect to the original situation, thus the investment needed would be returned within about 1 year.

A relatively favourable profit can be achieved in the case too, if the actual coal demand exceeds the original one in an extent that market could be found for the coal production of the mine "B" with disadvantageous natural conditions, whereby

this production is increased also by mechanization and thus it is made profitable with respect to the imported coal. The necessary investment has a return time of 3 years in the mine "A", whereas the time of return in mine "B" may reach even 10 years.

The detailed results of the model study show that the rentability of workings mechanization which substitutes manpower but does not increase the production, may be in a special case even independent of the natural conditions of the seams, and it may occur that in a mine with disadvantageous conditions the mechanization substituting only manpower should prove to be more profitable than in a mine with more advantageous conditions, where the required manpower is automatically less. Since the cost increase of a surplus production is, however, certainly lower in a mine with advantageous conditions, i.e. where production costs are lower, the mechanization can yield in such a mine a many times higher profit, if it goes together with the increase of the production, too. (According to our model, e.g. the cost increase to reach a double higher production in mine "A" is only 60 p.c. of that in the mine "B", while the profit increase is nearly five times higher.)

This regularity must be emphasized, because a lack of its knowledge may lead very easily to wrong decisions and erroneous developments, respectively which seem otherwise to be sound.

Though a possible drop of the price of machines or increase of wages (or simply a more realistic consideration of them) can make profitable a mechanization aimed only to manpower substitution, nevertheless, a production increasing effect of mechanization should be a primary task, especially and first of all in mines with advantageous conditions, as far as the coal production of the mine does not reach a level when its production capacity can be only increased by too high investments. Thus in mines with advantageous conditions a production increase must be striven at by a better utilization of the machines and by an increase of the face advance speed even if restrictions of the capacity pattern, of manpower management and of consumers must be overcome in a rational way.

Acta Geod. Geoph. Mont. Hung., Vol. 22 (3-4), pp. 371-389 (1987)

THE DEPOSIT AS A PRODUCTION FACTOR OF MINING

G B Fettweis[1], W A Brandstätter[1], F Hruschka[1]

Institute of Mining Engineering and Mineral Economics,
Montanuniversität Leoben, Leoben, Franz-Josef Strasse 18, A-8700

In the mining production process, the deposit has equal rank as the production factor materials - be it raw material, basic material or semi-finished product - in the processing industry. As is the case for all production factors, therefore, deposits enter into economic considerations not only with their factor inputs but also with their factor qualities. The deposit quality, the deposit quantity and the deposit bonitaet, which have to be distinguished from each other in this respect, are first dealt with using a mathematical expression; then the principal influences of these factors on the economic mineability of the occurrences of mineral raw materials are discussed. This is followed by an investigation of the principal influence of the deposit bonitaet on the output and therefore on the productivity of mines. This is done by discussing and evaluating the economic production theory.

Keywords: bonitaet; deposit; deposit quality; economic mineability; production factors

INTRODUCTION

1. As Tóth and Faller (1974) reported to the World Mining Congress (Tóth et al. 1982), in Hungary mineable occurrences - and therefore deposits - are distinguished from uneconomic occurrences of minerals by means of the mineability characteristic figure m in Eq. (1).

$$m = \frac{w}{k} \quad [-] \tag{1}$$

w - production costs limit, Ft/t
k - real costs, Ft/t
Ft - Forint.

The production costs limit w is derived from the costs of

the most expensive raw material unit produced in or imported to Hungary which is necessary for satisfying the demand of the Hungarian economy. The real costs k are the calculated costs for the raw material unit to be mined and processed. If the mineability characteristic figure m for an occurrence is $\geqq 1$, it is classified as economically mineable.

2. The mineability characteristic figure can be compared to the "operating ratio" in relation to the product quantity, e.g. the concentrate (Busse von Colbe 1983, Gabler's Wirtschaftslexikon 1984, Staehle 1969). The derivation of the operating ratio will illustrate this Eq. (2).

$$w = \frac{LEA}{AK} = \frac{\frac{LEA}{AM}}{\frac{AK}{AM}} = \frac{LER}{KR} \qquad [-] \qquad (2)$$

w - operating ratio [-]
LEA - period returns, GE/ZE
LER - output returns, GE/ME
AK - period costs, GE/ZE
AM - period output, ME/ZE
KR - cost rate, GE/ME
GE - money units
ME - material units
ZE - time period.

In contrast to the mineability characteristic figure, the numerator of operating ratio does not contain a general upper limit for the costs but does contain the returns planned or actually achieved by the individual operation. It is mainly determined by the market price for the produced goods. The denominator of both characteristic figures comprises the planned or actual costs of an operation.

3. Equation (3) characterizes the operating ratio of a mining operation producing only one product (one-product operation). Operation includes the steps of extraction and mineral processing. All factors of the quotient therefore refer to the

product of the total operation, e.g. to the concentrate of an ore mine. See (Fettweis et al. 1986) for the derivation.

$$w = \frac{LER}{KR_G + KR_A} = \frac{g_P \cdot q \cdot PR - KR_V - KR_T}{\frac{1}{AM_P} \cdot \left(\sum_{i=1}^{n} M_{Gi} \cdot p_i + \sum_{i=1}^{n} M_{Ai} \cdot p_i \right)} \quad [-] \qquad (3)$$

PR - market price of the commodity, GE/WE

g_p - grade of the mining product, WE/ME

q - quality factor [-]

KR_V - cost rate of metallurgical processing before price fixing (e.g. smelting), GE/ME

KR_T - cost rate of transport between mine and market, GE/ME

KR_A - cost rate of mineral processing, GE/ME

KR_G - cost rate of extraction, GE/ME

AM_p - period output of the mining product, ME/ZE

$\sum_{i=1}^{n} M_{Gi} \cdot p_i$ - period costs of extraction, GE/ZE

$\sum_{i=1}^{n} M_{Ai} \cdot p_i$ - period costs of mineral processing, GE/ZE

M_{Gi} - quantities of production factor types i in extraction, GE/ZE

M_{Ai} - quantities of production factor types i in processing, ME/ZE

p_i - price of the factor type, GE/ME

WE - value matter unit, ME .

The output returns LER are calculated from the product of the market price PR for the standard quality of the commodity, the grade of the mining product g_p and a quality factor q for value-increasing or value-decreasing properties of the mining product, reduced by the metallurgical processing costs KR_V and the transport costs KR_T to the market.

The denominator comprises the costs for producing the mining product which are the cost rates for extraction KR_G and mineral processing KR_A. The cost rates themselves are quotients from the period costs, i.e. from the sum of valued consumptions

of production factors during the time period under consideration $\sum_{i=1}^{n} M_i p_i$ and the produced output AM_p.

4. Production factors are material or immaterial goods used for production, for technical and economic reasons whose input is required for producing other economic goods. The production factors can be allocated to the following cost types: material costs, personnel costs, capital costs, nonpersonnel costs, external costs, taxes and rates.

Basically, when considering production factors, a clear distinction must be made between the respective factor types, the factor input and the factor quality. The factor quality influences both the selection of factor types i, the factor input M and also the price p of the production factor.

The relationships which determine the factor inputs M_i are very complex. Besides the factor quality, other influences include the size of the operation, the capacity utilization and the respective production programs. Not only these influencing factors designated as x_{ij} have to be taken into account, but also the interdependences of the factor inputs. According to Oberhoffer (1984), the following general system of equations can be established for describing these interdependences:

$$
\begin{aligned}
M_1 &= f\,(x_{11},x_{12},\ldots,x_{1j},\ldots,x_{1m},\ M_2,M_3,\ldots\ldots\ldots\ldots\ldots,M_n)\\
M_2 &= f\,(x_{21},x_{22},\ldots,x_{2j},\ldots,x_{2m},\ M_1,M_3,\ldots\ldots\ldots\ldots\ldots,M_n)\\
&\vdots \quad \vdots\\
M_i &= f\,(x_{i1},x_{i2},\ldots,x_{ij},\ldots,x_{im},\ M_1,M_2,\ldots,M_{i-1}.M_{i+1},\ldots,M_n)\\
&\vdots \quad \vdots\\
M_n &= f\,(x_{n1},x_{n2},\ldots,x_{nj},\ldots,x_{nm},\ M_1,M_2,\ldots\ldots\ldots\ldots\ldots,M_{n-1}).
\end{aligned}
\qquad (4)
$$

Oberhofer refers explicitly to difficulties in recognizing the influencing factors and in determining their effects on the costs.

5. The deposit is the most important and necessary production factor of a mine. It takes the same place as the production factor materials in the processing industry, which may be

a raw material, a basic material or a semi-finished product (Dorstewitz 1967, Nötstaller 1982, von Wahl 1973).

Narrowly defined, however, this applies only to the subprocess of extraction. Its objective is the deposit as a body immediately created by nature, its product is the run of mine (ROM) material. Therefore only extraction is primary production. The subprocess of mineral processing, however, takes the ROM material as a semifinished product in the transformation from nature to finished product, such as in the case of ores the subsequent smelting.

6. The deposit as production factor can therefore be best discussed not by taking the mining product as reference quantity but rather the ROM material; thereby the deposit itself becomes the indirect object of economic considerations.

Based on Eq. (3), the operating ratio has to be established for the subprocess extraction. All factors must be calculated to fit the product of this process which is the ROM material. The cost rate of mineral processing in this case is subtracted from the returns.

According to miners' usage, the operating ratio of the subprocess extraction is defined as the economic mineability b of the deposit (Eq. 5).

7. In order to illustrate the complex influences of the deposit on the economic mineability, a version of Eq. (5) is required which - in agreement with paragraph 4 - also contains variables dependent on each other. This is not only true for the influence of deposit conditions on the factor inputs and therefore on the costs of extraction according to the following paragraphs 12 to 27. It is also valid for the relationships between the processibility of the ROM material, the processing recovery and the mineral processing costs; this, however, is not dealt with in detail in the following.

Equation (5) may therefore be considered only together with Eqs 5a-5f. It refers only to the completely planned or occurring operation process with constant values of the variables for the life span of the operation.

$$b = \frac{m \cdot g_R \cdot (1-d) \cdot q \cdot PR - v \cdot (KR_A + KR_T + KR_V)}{\frac{Y}{R \cdot \frac{(1-l)}{(1-d)}} \cdot (M_R \cdot p_R + \sum_{i=2}^{n} M_{Gi} \cdot p_i)} \quad [-] \; . \qquad (5)$$

The following is valid:

$$g_H = g_R \cdot (1-d), \quad WE/ME \qquad (5a)$$

$$v = g_H \cdot \frac{m}{g_p} \quad [-] \qquad (5b)$$

$$Y = \frac{R \cdot \frac{(1-l)}{(1-d)}}{AM_H} \; , \quad ZE \qquad (5c)$$

$$M_R = \frac{R}{Y} \; , \quad ME/ZE \qquad (5d)$$

$$KR_A = f\,(m,\ v,\ AM_H,\ processibility) \qquad (5e)$$

$$M_{Gi} = f\,(l,\ d,\ AM_H) \qquad (5f)$$

$$KR_V = f(g_p) = const. \qquad (5g)$$

The following definitions supplement the legend of Eq. (3):

AM_H - run of mine material, ME/ZE
R - resources in situ, ME
Y - mine life ZE,
m - recovery in the mineral processing plant in shares [-]
v - yield by weight in the mineral processing plant in shares [-]
g_H - grade of the ROM material, WE/ME
g_R - grade of the resources in situ, WE/ME
d - dilution in shares [-]
l - losses during extraction in shares [-]
$M_R = M_{G1}$ - input of the production factor deposit, ME/ZE
$p_R = p_1$ - price of the production factor deposit, GE/ME .

8. The characteristics of the production factor deposit which are relevant for the economic mineability can be divided into quality, quantity and bonitaet. On the basis of Eq. (5), this can be illustrated by the following statements.

Deposit quality

9. "Quality" comprises the raw material properties, that is, all geologically given characteristics of an occurrence which go into the product of extraction, i.e. to the ROM material, and which are relevant as factor quality for further use. Equation (5) has these values in the numerator; this means that they determine the returns of extraction.

In detail, these are the following:

- the type of raw material which is expressed in the market price of the commodity PR, GE/WE ,
- the quality factor q [-] for value-increasing or value-decreasing properties of the mined product,
- the average grade of the resource in situ g_R, WE/ME ,
- the processibility of the ROM material, which is expressed by the following quantities:
  - value matter recovery in the mineral processing plant m in shares [-],
  - yield by weight in the mineral processing plant v in shares [-],
  - cost rate of mineral processing KR_A, GE/ME ,
- the metallurgical processibility of the mining product which is reflected in the cost rate KR_V [GE/ME] if the price PR is fixed only after a further processing step, e.g. smelting.

10. The quality of a deposit therefore has a decisive influence on mineral processing, and on its substantial and financial result. It determines correspondingly the reference price for extraction. Quality therefore is - as already stated - the essential deposit characteristic for the returns of extraction.

11. Apart from the deposit quality, the factor quality of the ROM material and thereby mineral processing and its result can be additionally determined by the dilution d of the deposit content in the course of extraction.

Deposit quantity

12. Despite their essential similarity according to paragraphs 4 and 5, the production factor 'deposit' of a mining operation differs from the production factor 'material' in the production sequence of the subsequent industry by its quantity, i.e. by its limited resources. In contrast to industrial enterprises, mining operations on principle have a limited life time.

According to Eq. (5c), the mine life Y [ZE] is in a mutual relationship with the given quantity of resources in situ R [ME] - which is to be corrected by the mining losses l and the dilution d - and with the average output AM_H [ME/ZE].

13. From the quantity and the mine life there results the factor input of the production factor deposit M_R belonging to the output AM_H according to Eq. (5d).

In Eq. (5) the period costs for the factor input $M_R \cdot p_R$ are shown separately. In the factor price p_R both the proportional costs for prospecting and exploration have to be remunerated and also possible royalties, etc.

14. The considerable influence of the quantity of a deposit on its economic mineability results from its influence on the size of the respective mine. The size of operation in turn determines - as already discussed in paragraph 4 - essentially the factor input and thereby the costs of an operation.

This influence can be illustrated by four facts, supported by the principal relationships shown qualitatively in Fig. 1.

15. First, it must be stated that the operation size of a mine at normal capacity utilization corresponds to its output AM_H [ME/ZE].

16. Second, according to Eq. (5c) the output AM_H is inversely proportional to the mine life Y at given resources in situ and constant values for the mining losses l and the dilution d. The output and the operation size can therefore be expressed by the values R and Y, as in Eq. (5) and Eq. (5c).

In the three-dimensional representation of Fig. 1, R and Y therefore form one coordinate each. The third coordinate is

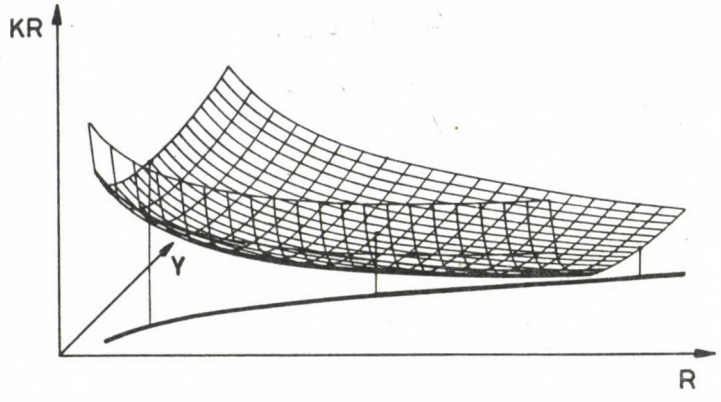

Fig. 1. Qualitative representation of the principal relationships between the cost rate KR, the mine life Y and the deposit quantity R of mines

the corresponding cost rate.

17. The third fact reflects two mining-specific experiences which were theoretically confirmed mainly by von Wahl (1970). These are:

a) For each given resource quantity there is an optimal mine life and a corresponding optimal operation size with respect to the cost rate of a mine. In Fig. 1 this is expressed by the U-shape of the cost rate as a function of the mine life.
b) With increasing given resources in situ the optimal size of a mine generally also increases. This, however, is less than proportional so that the optimal mine life also becomes longer. Correspondingly, in Fig. 1 the respective minima of cost functions for given R values shift.

The optimal combination of production factors and thereby the optimal life and size of a mine must be assessed by separate calculations for each given resource quantity.

A statistical relationship was established by Taylor on the basis of mining plans over three decades (von der Linden 1981):

$$\text{Optimal size} \quad AM_H = \frac{R \cdot \frac{(1-l)}{(1-d)}}{0.2 \cdot \sqrt[4]{R \cdot \frac{(1-l)}{(1-d)}}} \text{ , ME/ZE .} \qquad (6)$$

18. The fourth fact refers to mines in the same way as to producing firms in other economic sectors. It says that the cost rates generally sink with increasing operation size (economy of scale). "Larger machines and plants generally function with a better technical efficiency and a lower demand of capital and personnel, and thereby with decreasing overall costs of production facilities per production unit" (Oberhofer 1984).

As stated in paragraph 17, operation size and resources have an analog behaviour. Accordingly, the minima of cost curves over the mine life decrease with increasing resources in the principal diagram of Fig. 1.

As demonstrated above, there exists a complex influence of the quantity of a deposit on the costs of its mining. This relationship, however, is not expressed in Eq. (5) which refers only to certain states of operation. It rather has to be assessed separately. In Eq. (5), accordingly, $\sum_{i=1}^{n} M_{Gi} p_i$ is a variable depending on R and Y.

20. Independently of this, however, it follows from the above mentioned facts that mines with large resources and correspondingly larger optimal operation sizes can generally work with lower costs than those with smaller resources. Figure 1 illustrates this qualitatively. Accordingly, the economic mineability of deposits increases with the deposit quantity.

21. Be it noted additionally that the demonstrated influence of the deposit quantity always refers to the cost rate of extraction according to the denominator of Eq. (5). If - as in the normal case - the ROM material is not a product to be sold or is not transferred to a central mineral processing plant, this influence also refers to the cost rate of mineral processing KR_A in the numerator of this equation. In this case the optimal operation size of extraction and mineral processing

together results depending on the respective deposit quantity.

22. The above considerations are based in a simplified form on given resources in situ R. Actually the "quantity" of a deposit is no original geological figure. The quantity is derived from the characteristics of the deposit belonging to bonitaet and quality.

If an occcurrence of a mineral raw material consists of geological bodies with a fairly constant sequence of different qualities, such as in the case of a disseminated deposit, the deposit quantity can be assessed only by separate mineral-economic considerations to determine the cut-off-grade. These considerations include circular reasoning: all factors appearing in the denominator of Eq. (5) as dependent variables are both connected with each other and also with the values of quality in the numerator of the equation. Therefore, these considerations can only be carried out iteratively.

Deposit bonitaet

23. As already explained in paragraph 13, the denominator of Eq. (5) also contains the period costs for the factor input of the factor type deposit used per time period, i.e. the consumption of resources M_R valued at the respective period p_R. This factor input M_R of the factor type deposit is connected with a factor quality. It is designated as 'bonitaet'.

24. 'Bonitaet' is a collective term. It includes the geometric, geomechanic, hydrological, geochemical and geothermal conditions of the deposit and of the surrounding rock relevant for mining, and in some cases the composition of the deposit body from blocks with different quality values, e.g. grades. A varying distribution of grades is significant if one has to supply the mineral processing plant with ROM material as uniform as possible, and therefore extraction must be selective. This causes additional costs.

25. The influence of bonitaet on the period costs $\sum_{i=1}^{n} M_{Gi} \cdot p_i$ results from the relationships explained in paragraph 4. In

Eq. (5), $\sum_{i=2}^{n} M_{Gi} \cdot p_i$, therefore, is a variable dependent on $M_R \cdot p_R$. These relationships are extraordinarily complex; they can be assessed only by separate calculations for each case.

The costs $\sum_{i=1}^{n} M_{Gi} \cdot p_i$ are in any case inversely connected with the bonitaet of the production factor deposit.

26. The effects originating from differences in the bonitaet on the consumption of production factors may be much more significant with respect to the period costs $\sum_{i=2}^{n} M_{Gi} \cdot p_i$ than the immediate costs of the factor input of the factor type deposit $M_R \cdot p_R$.

27. The bonitaet is therefore the factor quality of the production factor deposit for the subprocess of extraction. It includes all geologically given characteristics of occurrences or deposits which determine, in addition to the quantity, the input of production factors to be used for supplying a certain amount of products, and thus determine the cost rate of extraction KR_G.

28. The bonitaet corresponds to the "other conditions of extraction", whose significance was referred to by Tóth and Faller (1974): "Earlier the mineability of mineral raw material was characterized, among the natural parameters, above all or even almost exclusively, by the quality (in the case of ores by the grade, in the case of coal by the calorific value). With regard to expenditure, there was no principal difference in connection to extraction. As time went on, however, as a consequence of scientific and technical progress, the extraction techniques for mineral raw materials became differentiated to such an extent that expenditure differences of great magnitude may occur. Therefore mineability conditions expressed by quality can nowadays be fixed only in connection with extraction technologies determined by other conditions of extraction" (translation from German).

Bonitaet and production theory

29. The influence of bonitaet on the economic mineability of mineral occurrences can be made clearer by means of production theory. For this purpose it is necessary first to deal with this theory and then to evaluate it with regard to our problem.

30. Production theory deals with the quantity relationships between the production factors (input) and the product quantities (output) of production processes. The product quantities are also designated as returns.

31. The production function for a one-product operation is generally:

$$X = f(M_1, M_2 \ldots M_n) \qquad (7)$$

X - output, ME/ZE

M_i - input of factor types i, (i=1,2,...n), ME/ZE .

32. For our discussion it is relevant that even detailed production functions - such as the Cobb-Douglas function, the Leontief function and the CES function - and their discussions are based on a constant factor quality of production factors, such as, for example, a constant training level of employees.

33. The production factors can be distinguished according to different criteria (Busse von Colbe and Lassmann 1983).

The individual production factors can be combined to production factor packages according to certain technical processes (Stobbe 1983). In order to simplify the discussion, the authors will generally only speak about production factors in the following.

A distinction immediately relevant for production theory is that between substitutive (for "substituting" and "substitutable") and limitative factors (Stobbe 1983).

Substitutive production factors are those which allow the output to be kept constant if the input of factor i is reduced, and compensated by the increased input of another factor j.

This means at the same time that it is possible to increase the output by increasing the input of one factor while all other factor inputs remain constant. However, if there is an inverse, unambiguous relationship between the product output and the input of a factor, which means that at constant consumption of one factor the output cannot be increased by raising the input of the other factors, this factor is designated as limitative (or limiting).

34. All production factors can be derived from the three factors land, labour and capital. In the case of mining, the deposit is land; the use of labour and capital is determined by the chosen mining technology and can be considered as a factor package.

35. Prerequisites for the following discussion of production functions are:

- The function be differentiable, i.e. product and production factors can be divided at will.
- All production factors can be combined into two factors.
- The production factors are substitutive.
- The factor quality of production factors is constant.

36. Figure 2 shows a two-dimensional representation of three production functions with different courses at varied inputs of only one production factor and constant input of the second factor.

Each point of the production functions symbolizes the complete course of a process during the planning period; this means a factor combination is realized which excludes all other cases (Stobbe 1983).

Figure 2a shows a "classical" production function, Figs 2b and 2c represent "neoclassical" production functions. The neoclassical production functions differ from the classical ones in that they assume, at increasing factor input, only increasing outputs and decreasing output growth rates.

The marginal output is geometrically the gradient of the tangent to each point of the production function. It indicates which additional output is made possible by infinitesimal

factor input increase.

The average output is the output produced per unit of variable production factor input. The average output of the classical production function shows a maximum. It is in each case the best suitable combination of inputs from constant and variable factors.

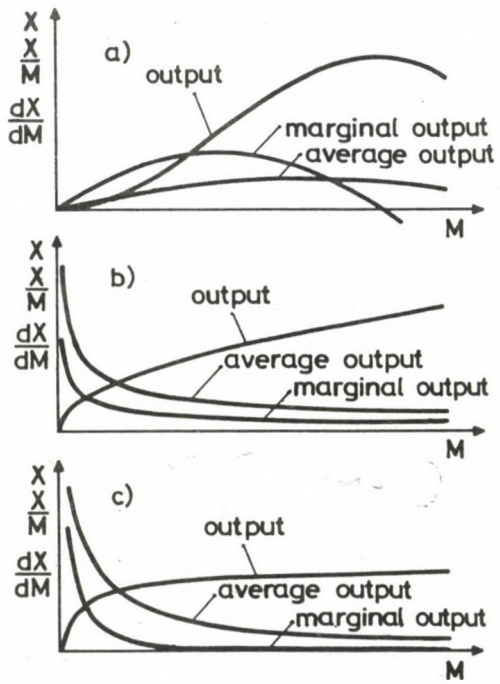

Fig. 2. Principal course of the classical production function (a) and the neoclassical production functions (b and c). X = output, M = factor input

37. If one allows a variation of both production factors considered, the production function represents an area; in German it is referred to as "output mountain". The isoquants - "contour lines" of the output mountain - connect points of equal output, which can be realized by different factor combinations (Fig. 3).

38. Thus the output of a mine can be represented as "output mountain" depending on the input of the selected factor package "mining technology" (= labour + capital) and the production factor "deposit" for each time period. The output mountain has a shape as in Fig. 3; M_1 is formed by the production factor deposit and M_2 by the production factor mining technology.

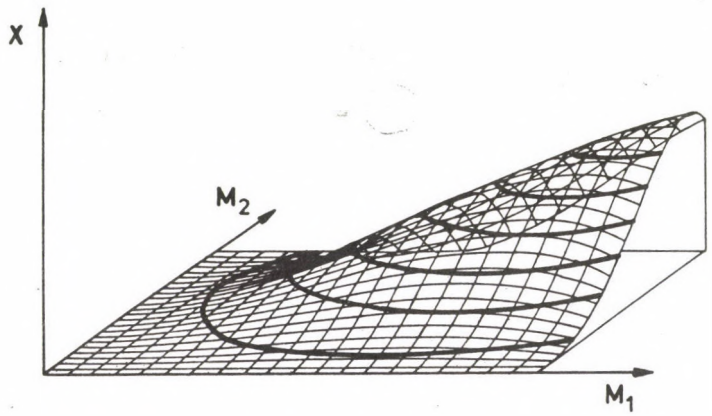

Fig. 3. Output mountain of a classical production function

39. For both factor types a course following the classical production function can be applied. This means that only in the first range an increasing factor input leads to increasing output while the other factor is kept constant. In the second range the opposite holds true.

This corresponds to the production-technological fact that the quantity variation of the factor deposit must be understood as a change in the availability of faces and therefore working area sizes within the time period considered.

At a given deposit input, therefore, the operation faces and equipments interfere with each other, as soon as a certain input of mining technology is exceeded. This at first causes diminishing marginal output and, as the mining technology input becomes higher, finally a negative development of output.

The development is similar if the input of the factor

package mining technology remains constant while the factor input of deposit is varied. The marginal output decreases as soon as the concentration of operation falls below a certain level by increasing the factor input deposit.

The growing working area size and the subsequently increased demand on the given factor input mining technology for the "unproductive" processes, such as man-riding, conveying, mine maintenance, etc. can lead to diminishing output.

40. The production theory outlined here does not differentiate the factor quality, as stated in the premise of paragraph 35. This restriction is not acceptable for the production factor deposit. The 'bonitaet' is arbitrarily given by nature and generally cannot be influenced. In the following we therefore integrate the variation of bonitaet into the production theory.

41. Simultaneous variation of factor input and factor quality, i.e. of the bonitaet, on the axis of the production factor deposit in Fig. 3 is not possible. Instead, one can apply several deposits with differing bonitaet over this axis and construct a number of output mountains.

42. Figure 4 shows average output functions derived from

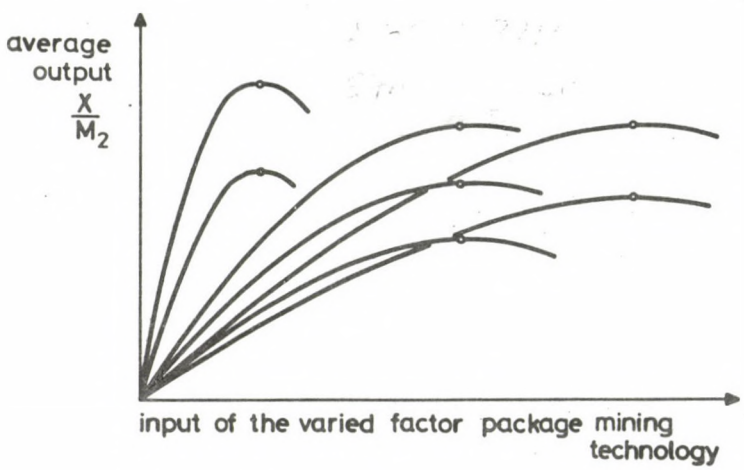

Fig. 4. Average output of mines depending on differences in the bonitaet of deposits at constant input of deposit

these output mountains while the factor input deposit is kept constant. On the abscissa the input of the factor package mining technology is varied, on the ordinate the average output is indicated. One can clearly recognize the influence of bonitaet on the position of optima, i.e. the best suitable combination of constant and variable factors.

43. The average output is frequently defined as productivity. Productivity is a ratio of economy and - in contrast to the operating ratio - shows the relationship between physical output and input. Both ratios are closely related to each other because the operating ratio can be understood as valued productivity (Staehle 1969).

The productivity ratio of labour in tons per man and shift is widely used in mining. Together with the productivity ratio of capital it allows conclusions about the bonitaet of deposits for the purpose of making comparisons between time periods or between different mines.

44. Actually, in many branches of mining all over the world considerable differences of productivity in tons per man and shift can be found even if we can calculate with a nearly similar level of mining technology. These differences amount to 1:25 or even more, such as in coal mining in the Soviet Union, between the large surface mines in Asia and the difficult underground mines in the Ukraine. The decisive influence arises mainly from differences in the bonitaet of deposits, but partly also from differences in the deposit quantities.

REFERENCES

Busse von Colbe W, Lassmann G 1983: Betriebswirtschaftstheorie. Band 1: Grundlagen, Produktions- und Kostentheorie. Heidelberger Taschenbücher, Band 156. 2. Auflage. Berlin/Heidelberg, Springer Verlag

Dorstewitz G 1967: Glückauf 103, 921-929.

Fettweis G B, Brandstätter W A, Hruschka F 1986: Mitteilungen der österreichischen geologischen Gesellschaft, Wien, 78 (1985), 23-40.

Gabler's Wirtschaftslexikon, Wiesbaden, Betriebswirtschaftlicher Verlag Dr.Th.Gabler GmbH, 1984

Nötstaller R 1982: Zur Frage der geeigneten Bergtechnik für Bergwerksprojekte in Entwicklungsländern unter besonderer Berücksichtigung des zweckmässigen Mechanisierungsgrades untersucht am Beispiel des Kohlenbergbaues. Dissertation. Montanuniversität Leoben

Oberhofer A F 1984: Planung und Kosten. Wirtschaftspraxis für Ingenieure, Band 1. Düsseldorf, Verlag Stahleisen mbH

Staehle W H 1969: Kennzahlen und Kennzahlensysteme als Mittel der Organisation und Führung von Unternehmen. Wiesbaden, Betriebswirtschaftlicher Verlag Dr. Th Gabler

Stobbe A 1983: Volkswirtschaftslehre II. Mikroökonomik. Heidelberger Taschenbücher, Berlin/New York/Tokyo, Springer Verlag, Band 227

Tóth M, Faller G 1974: Untersuchungen zur Bestimmung des heutigen und zukünftigen ökonomischen Wertes der Mineral-Vorräte Ungarns. In: Proceedings of the VIII. World Mining Congress, Lima, Peru

Tóth M, Faller G, Pruzsina J, Tóth J 1982: Principles of the Economy of Mineral Resources (in Hungarian). Műszaki Könyvkiadó, Budapest

von der Linden E 1981: Development and Expansion of Small Underground Mines. In: The First International Symposium on Small Mine Economics and Expansion. Taxco, Mexico

Wahl S von 1970: Die optimale Betriebsgrösse. Gundlagen, Modelle für den Bergbau. Essen, Verlag Glückauf

Wahl S von 1978: Bergwirtschaft als einzel- und gesamtwirtschaftliches Problem. Erzmetall 31, 554-560.

Acta Geod. Geoph. Mont. Hung., Vol. 22 (3-4), pp. 391-408 (1987)

PRESENT SITUATION AND TRENDS IN BLASTING TECHNOLOGY IN UNDERGROUND MINING OF THE GDR

H Gerhardt

Bergakademie Freiberg, Section Geotechnics and Mining, Freiberg, GDR-9200

The paper reviews the present situation of blasting technology, the used jumbos, the function of large holes, the selection of ignition sequences, the initiation of ANFO columnar charges, the used ANFO explosive Dekamon, the achieved efficiency of round, the ignition method, the efficiency and the construction of drilling and explosion plans in the potash- and copper mines of the GDR, and it surveys the future trends to be expected.

Keywords: ANFO-explosive; blasting; copper mining; GDR; potash mining; underground mining

1. INTRODUCTORY REMARK

The extraction of solid minerals by the use of underground mining methods is concentrated to potash and ore mining in the GDR. Compared to this, the extraction of spar, schist and limestone in underground mining is of less importance. In potash mining the GDR takes the third place in the world. Its annual crude salt output yields more than 34 Mt. In ore mining the annual output is smaller, however, it is important for the national economy. Thus, a steady output can be expected in potash as well as ore mining in the years to come. At present the extraction of potash is carried out in the GDR exclusively by means of drilling and blasting. This is similar to tin mining. Only copper and some other ores are extracted by means of partly mechanized and geotechnological methods (Fig. 1). Drilling and blasting is therefore the most important extraction process in underground mining in the GDR. Below, a general review is given on the present situation of blasting technology

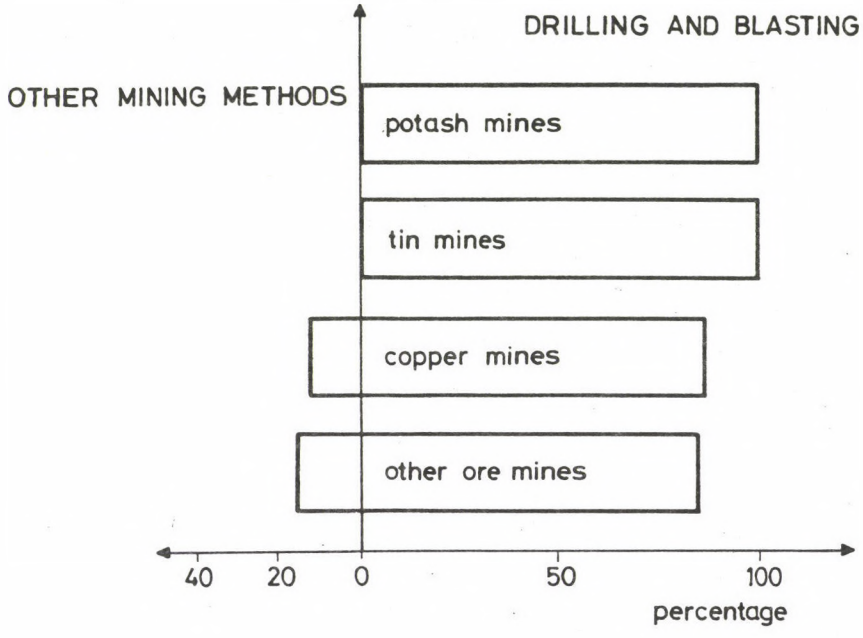

Fig. 1. Percentage of extraction methods in underground mining of the GDR

in potash and copper mining and future trends.

2. BLASTING TECHNOLOGY IN POTASH MINING IN THE GDR

In potash mining of the GDR flat deposition is prevailing. The room- and pillar working is the dominant extraction method. The relatively regular composition of the salt rocks and their good drillability - depending on the type of salt, the drilling velocity yields 4 to 12 m per minute with rotary drilling and using wet-air-circulation with a hole diameter of 37 mm - result in two peculiarities which have to be underlined in contrast to ore mining:

1. It is possible to use drilling patterns which are standardized to a great extent in certain types of salt.
2. Drilling is subordinated in the complex of drilling and

blasting.

Considerable results have been achieved by the introduction of drill jumbos with carriages reaching hole lengths of 5.4 m and 7.2 m, respectively. The general introduction of ANFO--explosives - their portion amounts to 95 % - as well as the mechanization of charging have resulted in considerable rationalization effects in the mines. The present situation can be characterized as follows:

1. Parallel cuts with large holes are exclusively used. 2 to 4 large holes with diameters of 280 mm are set in horizontal and vertical directions (Gerhardt et al. 1985a, Duchrow and Gerhardt 1984). The cut is performed by a corresponding order of the blast holes for the first group of shots in form of centre, box or spiral cuts (Fig. 2b, 2c). All these cut forms have advantages and disadvantages, thus, the decision on a certain cut form is influenced by subjective factors in the different mines (Table I). The centre cut has the simplest drilling pattern, but the greatest number of holes and highest explosive consumption. Therefore, it has the highest costs compared to the other forms. The spiral or double-spiral cut offers the lowest costs in drilling and blasting. But the necessary preconditions (exact position of boreholes, parallelism of the holes) can not be fulfilled in every case. Thus, the box cut is used most often (Table I).

2. The large holes fulfil several functions:
- provide additional free space and thus reflection faces for the pressure waves,
- reduce the internal tension behind the face,
- provide free space for the movement of the rock which is blast in the first round of shots (burden cut).

3. It is very important for a successful round that the correct delay pattern should be chosen. Detonators of the "Kaliserie" are used with a pattern shown in Table II. The combined usage of millisecond-delay, quartersecond-delay and half-second-delay firing adapted to the rock conditions offers the following advantages:
- Use of the advantages of millisecond-delay firing in the

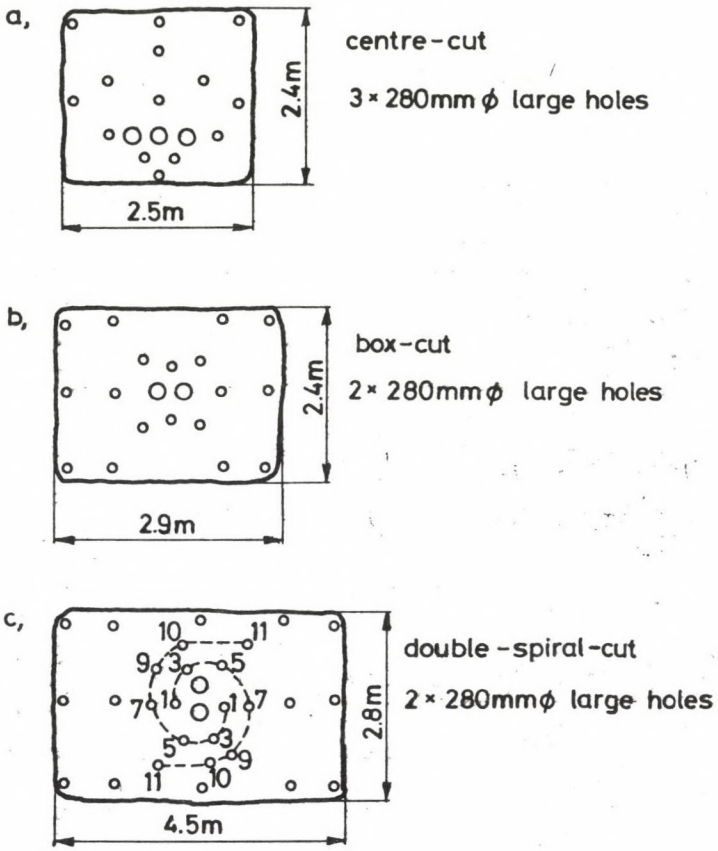

Fig. 2. Usual cuts in potash mining in the GDR

immediate cut area (mutual influence of the charges, avoidance of "deadpressing"-effects, good propulsive effect and providing free space for the following detonations, reduce of misfires, regularly and well crushed blast rock).

- Reduction of the number of ignite steps by igniting the charges in pairs considering the blasted space (Fig. 2c). In doing so, a relatively large driving cross section can be made by the available delay pattern.

4. The ANFO-columnar charges are initiated to a greater extent without additional gelatin primers or detonating fuse

Table I. Used variants of cuts in potash mining

	Cut Centre	Box	Spiral
Complication of patterns and firing orders	○	◐	●
Exact positions for bore holes	○	◐	●
Exact drilling work	○	◐	●
Adaptation at diverse conditions	◐	◐	●
Number of bore holes	●	◐	○
Relation between blasted and drilled advance per round	●	◐	○
Costs for drilling and blasting	●	◐	○

● unfavourable
○ favourable

Table II. Detonators of the "Kaliserie"

Number of delay steps	1 ... 8	9 ... 18	19 ... 24
Delay interval between two steps (ms)	80	250	500

only by the detonators of the above mentioned "Kaliserie". This differs from conventional methods, but is based on corresponding investigations (Ullrich 1985, Kahmann and Moye 1984). The advantages are as follows:

- shorter charging time,
- reduction of explosive costs and
- increasing safety in explosive storage and transport.

5. The employed ANFO-explosive Dekamon 1 PK-14-339 is characterized by the following parameters:

Portion of ammonium nitrate 80 %, portion of calcium ammonium nitrate 14.2 %, portion of diesel 5.8 %, detonating heat $3.6 \cdot 10^6$ J/kg, gas ratio 960 dm^3/kg, detonation velocity 1970 m/s. If it is used in boreholes with a diameter of 37 mm, the optimum charging density is 0.80 kg dm^{-3} to 0.83 kg dm^{-3} with the desired value of critical charging density of 0.6 to 0.9. Under these conditions "dead-pressing"-effects can surely be avoided (Cook 1974, Krebs 1985). It goes without saying that greater charging densities within these limits lead to better results. This has been verified previously by Richter (1985). However, the achieved better blasting effect is not adequate to the simultaneously rising explosive consumption in every case. The mentioned charging densities are implemented by means of blow pressures of approximately 230 kPa in the pressure boiler.

6. The achieved efficiency of round amounts with the mentioned hole length 80 to 90 %. An important factor which influences the efficiency is the quality of drilling. The dependence of the efficiency or round on the hole length is described by the following equation, in which a reference value of 5.40 m hole length is used (Schmiedel 1985).

$$\eta_r = \eta_{r\ 5.4} - 0.7\ \% \ (l_{bh} - 5.4\ m)$$

η_r = efficiency of round
l_{bh} = length of bore hole.

Due to this, the efficiency of round decreases by 0.7 %/m for hole lengths longer than 5.4 m. The value 0.7 % is relatively favourable concerning the quality of drilling.

7. Due mainly to safety reasons (dangerous gas formation) the charges are generally ignited only at the end of the shift from central places when the staff had left the face. Power--circuit firing is applied which is nowadays equipped with condenser-type ignition devices. By means of a control transformer a secondary voltage of 620 V is generated from the 500-V-circuit by the use of which the condenser is charged up to 1755 V. The condenser feeds a firing circuit for 8 seconds each, by means of a step relay several firing circuits are connected one after the other. With series connection of 0.45-A-detonators the maximum permissible resistance is 510 Ω.

8. After introducing ANFO-explosives into the mines, nowadays 300 to 600 kg explosives are charged per man-shift (before 20 to 35 kg per man-shift with simultaneous drilling). Blasting is specialized. The charging vehicles contain pressure vessels with a volume of 345 and 1130 l, respectively being adequate to 270 and 883 kg explosives (Fig. 3). A very low-built charging vehicle has been developed for particular mining conditions. It contains four pressure boilers with 350 l volume each. Under normal conditions it has a charging performance of 15 to 18 kg/min and 1200 kg per man-shift. The explosive consumption is

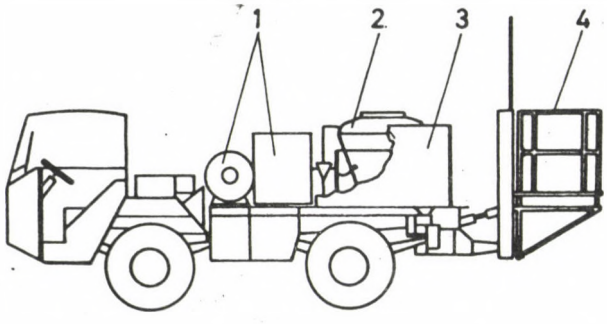

Fig. 3. Charging vehicle. 1 - compressor, compressed air container, 2 - pressure boiler for explosives, 3 - explosive material container, 4 - platform

0.6 kg/t crude salt. Transportation and transloading have been fully mechanized. For example, in one shaft the explosive is transported by means of tubes. As shown in Fig. 4, the explosive delivered by train is pneumatically discharged into a bunker and afterwards piped by two parallel tubes into underground bunkers. The effectiveness of such systems results from the reduction of transport space, packing material and labour consumption (Moye 1982, Moye 1984). The total labour consumption of blasting in the potash mines could be reduced to ap-

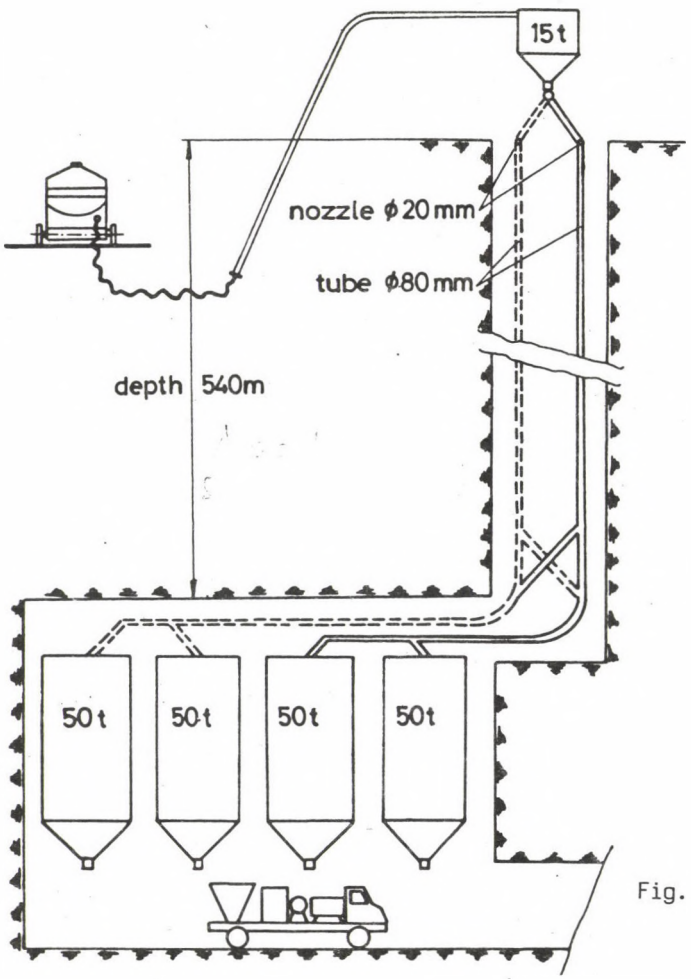

Fig. 4. Tube for vertical transport of ANFO-explosive in potash mining

proximately 20 %.

9. Under particular mining conditions elements of smooth blasting are used. The aim is to utilize the existing explosives and blasting accessories and to avoid special explosive materials. Tests with modified ANFO-explosives - addition of inert material - as well as the use of only the detonating fuse in the roof holes presented considerable results. Under geomechanically unfavourable conditions decisive improvements have been reached in the stability of the contour, in the reduction of rock-bolt density and in explosive consumption by a simultaneous reduction of the hole intervals, ignition in one step and vault of the roof (Kaule 1983, Koch 1984, Jonek 1985, Moye et al. 1981). It has been realized as follows:

- The admixture of polystyrene to the ANFO-explosive enables a reduction of the explosive amount in the borehole and thus the desired effect of reduced blasting force while the charging techniques remains unchanged (use of jumbos with pressure boilers). Even with an admixture ratio of 60 %, detonation velocities of > 1800 m/s could be indicated and a stable process of detonation was verified. The data given in Fig. 5 (based on Heltzen 1974), turned out to be correct.
- The employed modified ANFO-explosives can be initiated by detonators without additional primers.
- The maximum permissible values of toxic gases (CO, N_xO_y) are not exceeded up to a portion of 50 % polystyrene. The lesser admixture ratios of 20 to 30 % polystyrene result in pollution by harmful substances even less than with the use of pure ANFO-explosive. Moreover, these modified ANFO-explosives offer the same blasting performance as pure ANFO-explosives (detonation velocity and gas ratio are nearly the same). Therefore, the combined usage of modified ANFO-explosives with 20 to 30 % polystyrene and 60 to 80 % polystyrene in the cut and roof area results in a totally less pollution by harmful substances.

10. For some time computer programmes have been used for the construction of the drilling and blasting pattern considering the maximum burden for the different salt types in the cut,

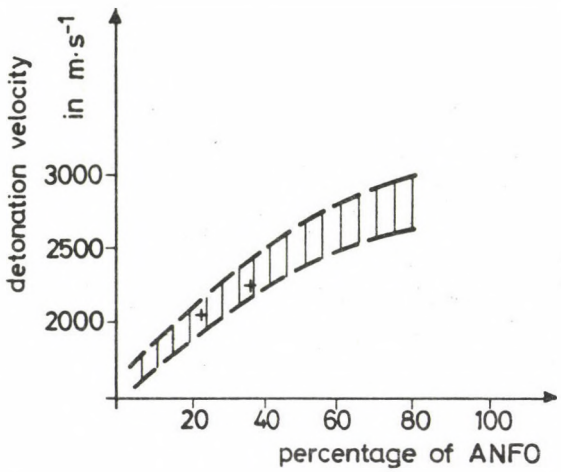

Fig. 5. Detonation velocity depending on the polystyrene portion in the ANFO--explosive

the crater angle, the coefficient of bulk increase and the face height. This results in lower costs (Gerhardt et al. 1985a, b, c, Richter 1985a, b) (Fig. 6). The digital simulation of blast drivings in potash mining enables the handling of the following questions of individual and complex optimizing:

- Determination of the driving cross-section,
- Determination of the number and diameter of the large holes,
- Determination of the optimum blast-hole diameter,
- Determination of the optimum hole length,
- Determination of the utilization coefficient of the drilling equipment.

Based on Richter (1985a) the determined explosive costs and total extraction costs are shown in Fig. 7 depending on the number of large holes. Based on these results and further investigations the extension of the large holes from 280 mm diameter to 500 mm is not favourable. In the area of 5 to 8 m driving with to 2 blast holes less are necessary with the use

number of bore holes = 28

bore holes per m^2 = 1.56 m^{-2}

number of detonators = 28

explosive consumption = 120.4 kg DEKAMON 1PK 14-339

explosive per t blast rock = 0.61 kg/t

advance per round = 4.95 m

blast rock = 196 t

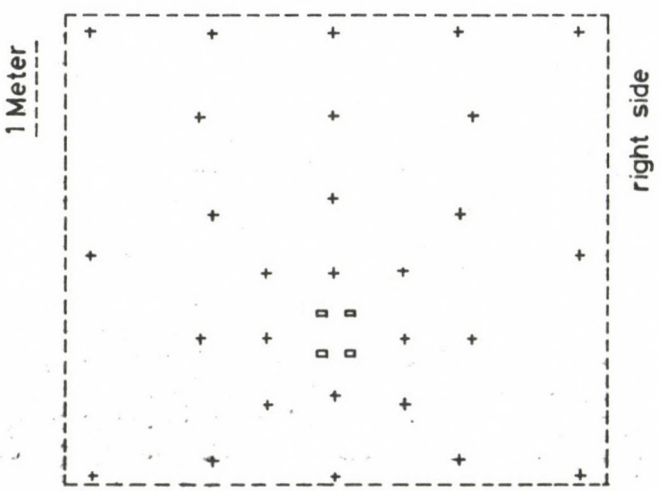

Fig. 6. Computer-printed blasting pattern with four large holes of 280 mm diameter

of two large holes of 280 mm diameter than with one large hole of 500 mm diameter for the provision of free space.

3. BLASTING TECHNOLOGY IN COPPER MINING

In contrast to potash mining the development and design of blasting techniques and methods in ore mining is not equally

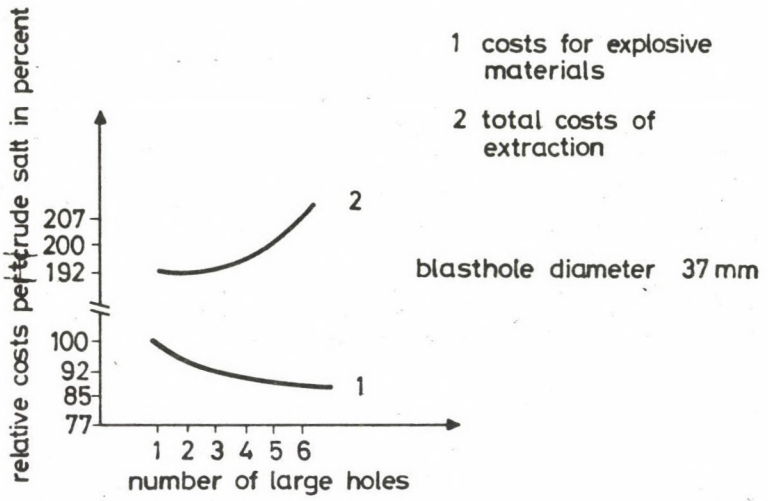

Fig. 7. Explosive costs and total extraction costs depending on the number of large holes

uniform because of alternating geological and technological conditions. Below, copper mining is dealt with in detail. In copper mining blasting plays a more significant role in extraction than in driving.

In copper mining of the GDR a thin, slighty inclined seam is worked in longwall working. About 90 % of the annual worked seam area is extracted by means of intensive blasting. The following geological-technological factors have to be considered with regard to blasting (Fig. 8):

- With a thickness of the ore-bearing layers of 0.20 to 0.35 m, the average height of the face yields only 1 m. They are extracted selectively. The faces are in average 60 m long and are divided into two parts by a conveying road.
- The waste rock is used as filling material immediately in the face. It is the aim to blast the whole waste rock directly into the filling space. Afterwards the seam is extracted and the ore hauled.
- Although blasting is very intensive, the quality of the blast

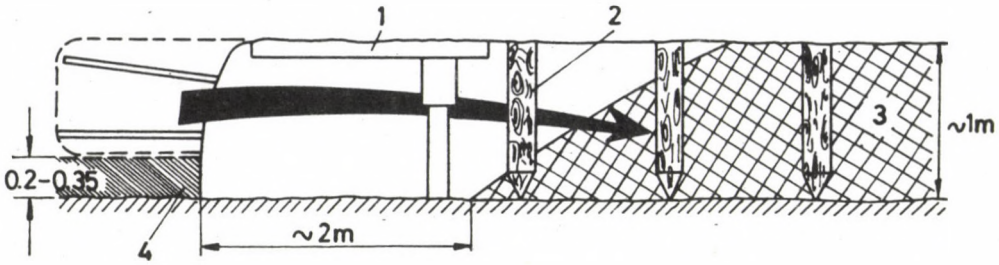

Fig. 8. Schematic view of a face in copper mining. 1 - hydraulic prop, roof bar, 2 - wood prop, 3 - fitting, 4 - seam

rock (dilution) and ore losses shall not be affected. The effectiveness of the used hydraulic-prop-support has to be retained as well.

Considering all these conditions a blasting technique has been developed for extraction methods with intensive blasting in copper mining which can be characterized as follows:

1. Because of the existing geometric conditions small-diameter blast holes with a diameter of 26 mm are used. The hole lengths are 0.7 to 1.0 m.

2. The holes are set into two lines; a sit is shown in Fig. 9 (Gerhardt and Schäfer 1972). The hole intervals in the upper line amount to 0.4 m, in the lower line they are 0.8 to 1.2 m. In the upper line wedge cuts are set in both parts of the face. The other holes are drilled with an angle of 50 to 70^{o}. Thus, the desired effect - blasting of the waste rock directly into the filling space - is supported. The holes in the lower line are fired after the holes in the upper one, thus, cuts are not necessary. These holes are drilled with a 90^{o}-angle. Deviations in the hole pattern are possible and depend on the position of the face in relation to the old man, the thickness of the ore-bearing layers and so on. At the end of the face, the holes are set in a slabbing position.

3. Depending on the above mentioned conditions, the number of detonators per round amounts to 110 to 140 per 30 m face. Therefore, the portion of detonator costs in the total

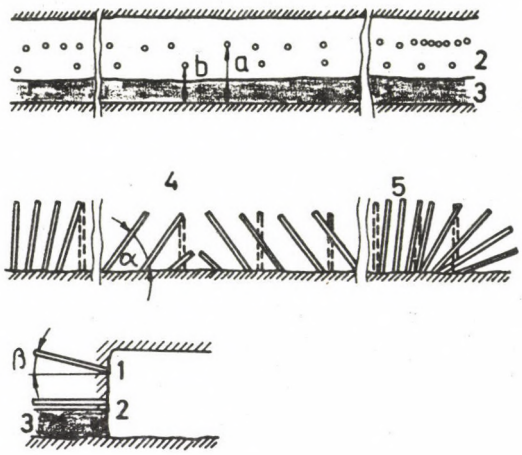

Fig. 9. Blasting pattern in the face. 1 - upper blast holes, 2 - lower blast holes, 3 - seam, 4 - wedge cut, 5 - slabbing in the end of face, $\alpha = 60^{o}$, $\beta = 15^{o}$, a = 0.7 m, b = 0.3 m

explosive costs is high. The following technical parameters are achieved:

drilling metre	3.6 to 5 Bm/m^2
explosive consumption	about 1.7 to 2.2 kg/m^2
number of detonators	4 to 7 per m^2

with 1 m^2 seam area corresponding approximately to 1 t crude ore and to 2.7 t blast rock, respectively.

4. The tests verified that even with the small hole diameter ANFO-explosives can be fired safely if gelatin primers are used for initiation. However, economic calculations have shown that under the above mentioned conditions - low costs of ANFO-explosives and high costs of detonators and primers - the economic results are not better than with the use of only gelatinized explosive (Gerhardt et al. 1975). For this reason, ANFO-explosive is not used in the face. Cartriged gelatins are employed with a cartrige diameter of 16 mm.

5. In the upper line the holes are fired by means of

millisecond-delay detonators with a delay of the ignite steps of 23 ms. Compared to other methods it can be seen that such a delay interval result in optimum conditions, since with

$$\Delta_t = 46.68 - 2.44 \cdot f_{Pr} \qquad \text{(ms)}$$

f_{Pr} (Protodyakonov coefficient) = 8 ... 12

detonators are fully effective in the rock which is to be extracted. Particularly the propulsive effect is used to blast the waste rock directly into the filling space and to avoid additional manual removal.

6. Because of the large number of charges which have to be fired at the same time - under extreme conditions up to 290 charges have to be fired in one round of shots - in the late seventies an ignition device was developed using insensitive detonators. These detonators response only to an amperage of more than 0.45 A. From a central place up to six faces can be fired one after the other at the end of the shift. This ignition device has proved to be worthwhile. To run this plant a voltage of 500 V/50 Hz is necessary. The maximum voltage at the condenser was determined to 1.75 kV and the storage capacity to 48 µF. The maximum permissible resistance with series connection of these 0.45-A-detonators is 625 Ω .

For driving in copper mining (cross-cuts, drifts, inclines) parallel or so-called toe cuts are used. A toe cut is a slabbing cut which is directed into the floor (Fig. 10). With parallel cuts uncharged holes with a diameter of 56 or 75 mm are used for the provision of free space. The blast holes have a diameter of 36 mm. Although the slabbing cut offers disadvantages in drilling, it is still used because of its advantages in blasting. As shown in Fig. 10, the utilization of the geomechanic properties of the seam allows a lower explosive consumption. Moreover, the slabbing cut permits partly simulfaneous drilling and loading. ANFO-explosive is used and, latest investigations verified that it can be fired immediately by the used quartersecond-delay detonators without primers (Kahmann and Moye 1984).

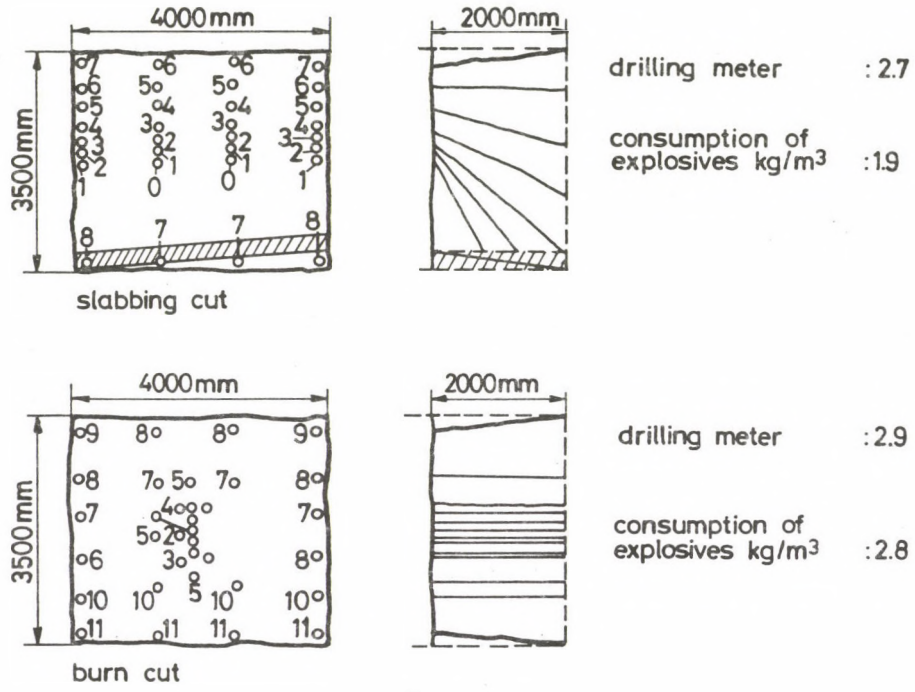

Fig. 10. Blasting patterns in driving in copper mining (parallel cut and toe cut)

4. PROSPECTS AND TRENDS

In underground mining of the GDR drilling and blasting will dominate in extraction of raw materials even in future, although the extraction is partly mechanized and geotechnological methods are applied. Moreover, blasting methods are used in open-cast mining and some other branches as well. Therefore, the development of blasting technology is of general interest.

Explosives: The explosive production of the GDR meets the domestic demand, in addition to this, explosives are exported as well. By the construction of a new plant for the production of ammonium nitrate (operation started in 1985) the industrial demand for this basic material of the production of ANFO-explo-

sive could be covered as well. At present, investigations are undertaken for the production of expansive explosives which can also be used in underground mining. Moreover, the development of slurry-explosives is taken into account in order to reduce the usage of gelatinized explosives in wet mines. Modified ANFO-explosives for special use (smooth blasting) will also in future be produced by the users themselves.

Detonators: The presently used detonators which are made by domestic producers and imported from the CSSR, will be sufficient also in the years to come. Modern nonelectrical ignition methods (NONEL etc.) will not be applied because of the unfavourable cost proportions. Due to the general introduction of insensitive detonators the power-circuit firing will more and more dominate the scene.

Blasting technology: Charging has to be mechanized to a greater extend in case of large charging amounts per working place, great hole lengths and unfavourable climatic conditions (use of manipulators). The use of computers for the construction of drilling and blasting patterns in order to optimize blasting is extended. In addition to this, parallel run jumbos are introduced. Thus, the preconditions are provided for partly or fully automatic drilling of the entire pattern by means of jumbos which are controlled by microprocessors (closed CAD/CAM--system). Moreover, the application of computers result in better and better mastering the relation between rock conditions and blasting process. Thus, it renders a contribution to the development of blasting technology.

REFERENCES

Cook M A 1974: The Science of Industrial Explosives. Ireco Chamicals, Salt Lake City

Duchrow G, Gerhardt H 1984: Berg- und Hüttenmännische Monatshefte 129, 444-452.

Gerhardt H, Schäfer E 1972: Neue Bergbautechnik, 2, No. 1. 27-37.

Gerhardt H, Schäfer E, Ehricht W 1975: Neue Bergbautechnik, 5, No. 11, 836-847.

Gerhardt H, Kahmann H J, Wakan R 1981: Neue Bergbautechnik, 11, No. 5, 287-291.

Gerhardt H, Baumann K, Richter E 1985a: Neue Bergbautechnik, 15, No. 2, 45-54.

Gerhardt H, Baumann K, Richter E, Krebs H 1985b: Sprengtechnologie und Rechentechnik. Proceedings of the VII. International Conference on Blasting, Balatonfüred

Gerhardt H, Richter E, Baumann K 1985c: Sprengvortrieb Kali ein CAD-Model. Paper at the Conference of Kali-Mining, Magdeburg (unpublished)

Heltzen A M 1974: World mining, 27, No. 5, 43.

Jonek R 1985: Erprobung modifizierter ANO-Sprengstoffe, Thesis, Bergakademie Freiberg (unpublished)

Kahmann H J, Moye U 1984: Neue Bergbautechnik, 14, No. 7, 253-256.

Kaule D 1983: Ermittlung der Detonationseigenschaften von ANO--Sprengstoffen. Thesis, Freiberg (unpublished)

Koch H 1984: "Firstschonende Sprengverfahren". Thesis, Bergakademie Freiberg (unpublished)

Krebs H 1985: Sprengtechnische und sprengtechnologische Untersuchungen zum Mischladen von losen Sprengstoffen. Thesis A, Freiberg

Moye U, Michalzik A, Hölzke W, Seidel H 1981: Neue Bergbautechnik, 11, No. 5, 287-291.

Moye U 1984: Rationalisierung des Sprengstofftransportes im Kalibergbau. Paper presented at the IX. Conference Blasting, Gera (unpublished)

Richter E 1985a: Beitrag zur Optimierung des Sprengvortriebes im Kalibergbau. Thesis A, Freiberg (unpublished)

Richter E 1985b: Thesis "Sprengingenieurwesen". Freiberg (unpublished)

Schmiedel K 1985: Erfassung von Bohr- und Sprengparametern beim Abbau und Streckenvortrieb. Freiberg (unpublished manuscript)

Ullrich E 1985: Neue Bergbautechnik 15, No. 5, 185-189.

Acta Geod. Geoph. Mont. Hung., Vol. 22 (3-4), pp. 409-419 (1987)

WATER PREVENTION OF THE PLANNED VADNA I OPEN COAL MINE

R Jeney Jambrik

Technical University for Heavy Industry, Miskolc, Egyetemváros, H-3515

Out of the characteristic five coal seams the lowest, developed in the Vadna brown coal territory belongs to the East-Borsod brown coal basin. This coal bed being near to the surface is planned to be mined with stripping in two parts. The hydrogeological and hydrological conditions of the territory are discussed in the paper, and a proposal is given for the protection of part 1 of the surface mining against surface and underground water.

Keywords: Vadna coal territory; coal stripping; Borsod coal basin; protection against water

HYDROLOGICAL CONDITIONS

The most important surface water source of the territory is the Sajó river which springs in the Slovak Ore-Mountains. A rightside branch of it is the Bán streamlet that reaches the river at the section marked by 100.280 km (Fig. 1). Upwards from the mouth of the Bán streamlet the Sajó river has a catchment area of 3964 km^2; its length is 123 km. The width of the valley varies from 2.0 to 7.0 km, the fall of the river is 50-70 cm/km in the area of the planned open cut mine. The water level may change between 284 and 496 cm due to floods and dry periods. Maximum water level comes about in March-April, minimum in September-October. The percentual probability rates of water flow in the section of the mouth of the Bán streamlet are:

$$P_{1\ \%} = 590\ m^3/s$$

$$P_{3\ \%} = 470\ m^3/s$$

Acta Geod. Geoph. Mont. Hung. 22, 1987
Akadémiai Kiadó, Budapest

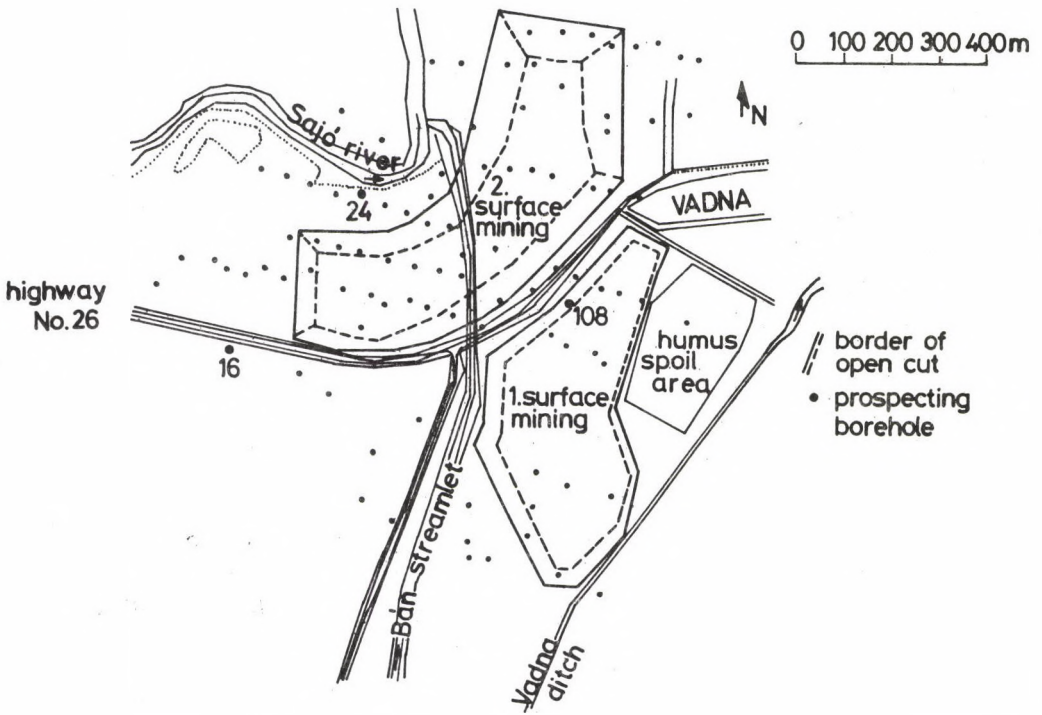

Fig. 1. Map of the planned open pit near the village Vadna

$$P_{10\ \%} = 360\ m^3/s$$
$$P_{50\ \%} = 185\ m^3/s.$$

Flood control works are only besides of a 17 km upper reach of the river, but there is no embankment in the area of the planned open cut mine. The northern part of the territory is an open flood area.

The construction of the about 1 km long mouth of Bán streamlet belonging to the territory of surface mine allows a water discharge of $Q_{10\ \%} = 43\ m^3/s$, that of the highway No 26 in the section 0+566 of the streamlet $Q_{1\ \%} = 85\ m^3/s$. Although the Lázbérc Water Basin having put in operation in 1969; significantly influences the water level fluctuation of the Bán streamlet by its flood-regulating effect, nevertheless - according to the flood prevention instructions - the standard flood level is higher than the surface level of part 1 of the open pit mine being close to the bridge, hence for protection against surface waters embankment building is unambiguously required.

The Vadna ditch branching out of the Bán streamlet and flowing into the Sajó river has a length of 2570 m, its catching area is 3.2 km^2, and its characteristic water discharges are:

$$Q_{1\ \%} = 3.4\ m^3/s$$
$$Q_{3\ \%} = 2.7\ m^3/s$$
$$Q_{10\ \%} = 1.7\ m^3/s\ .$$

The channel section of the ditch is constructed for $Q_{10\ \%}$, in the outer area and for $Q_{1\ \%}$ in the municipal area of the village Vadna. The dike drain at the branching point of the Vadna ditch and the Bán streamlet renders to pass a water discharge of 1.3 m^3/s and at the same time it means a connection between the Bán streamlet and the Vadna ditch.

HYDROGEOLOGICAL CONDITIONS

The average depth of the coal series i.e. the average thickness of overlying strata is 21.6 m in the territory of part 1 of the open pit mine. The seat rock under of the coal bed is an impermeable one, but in the covering layers, there are two aquifer layers.

The upper aquifer layer which contains the groundwater is the terrace gravel of the Sajó river. It has an average thickness 3.7 m, and lies under a soil of 2.4 m average thickness. From pumping tests of the group V-3/108 of wells 24.2 m/d, ($2.8 \cdot 10^{-4}$ m/s) was found as permeability coefficient of this level. For the planning of drainage the accepted gravitational porosity was n_o = 0.15, and the hydrostatic water level was 3.0-3.5 m under the surface.

The lower aquifer layer in the overlying strata of the coal series is a sand layer under the terrace gravel developed in one or two benches, but from hydraulic point of view it can be considered homogeneous. In the eastern and south-eastern part of the exploration the impremeable or badly permeable formations between gravel and sand were destroyed, thus the young terrace gravel is directly bedded on the aquifer sand. Hence the two water bearing levels are in a hydraulic connection with each other.

The permeability coefficient of the sand - defined by pumping tests - is 0.6 m/d, ($6.9 \cdot 10^{-6}$ m/s) the value of the gravitational porosity is n_o = 0.1, and the hydrostatic level is identical with the level of groundwater.

Impermeable aleurites, clayey aleurites were opened up by every borehole in the roof of the coal beds with a 7.5 m average thickness.

The average sequence of strata in part 1 of the open pit mine, taken as the basis of the planned dewatering, is shown in Fig. 2.

Water bearing formations get a constant water supply from the Sajó river, with an intensity of 15 l/s defined from the evaluation of tests of group of wells.

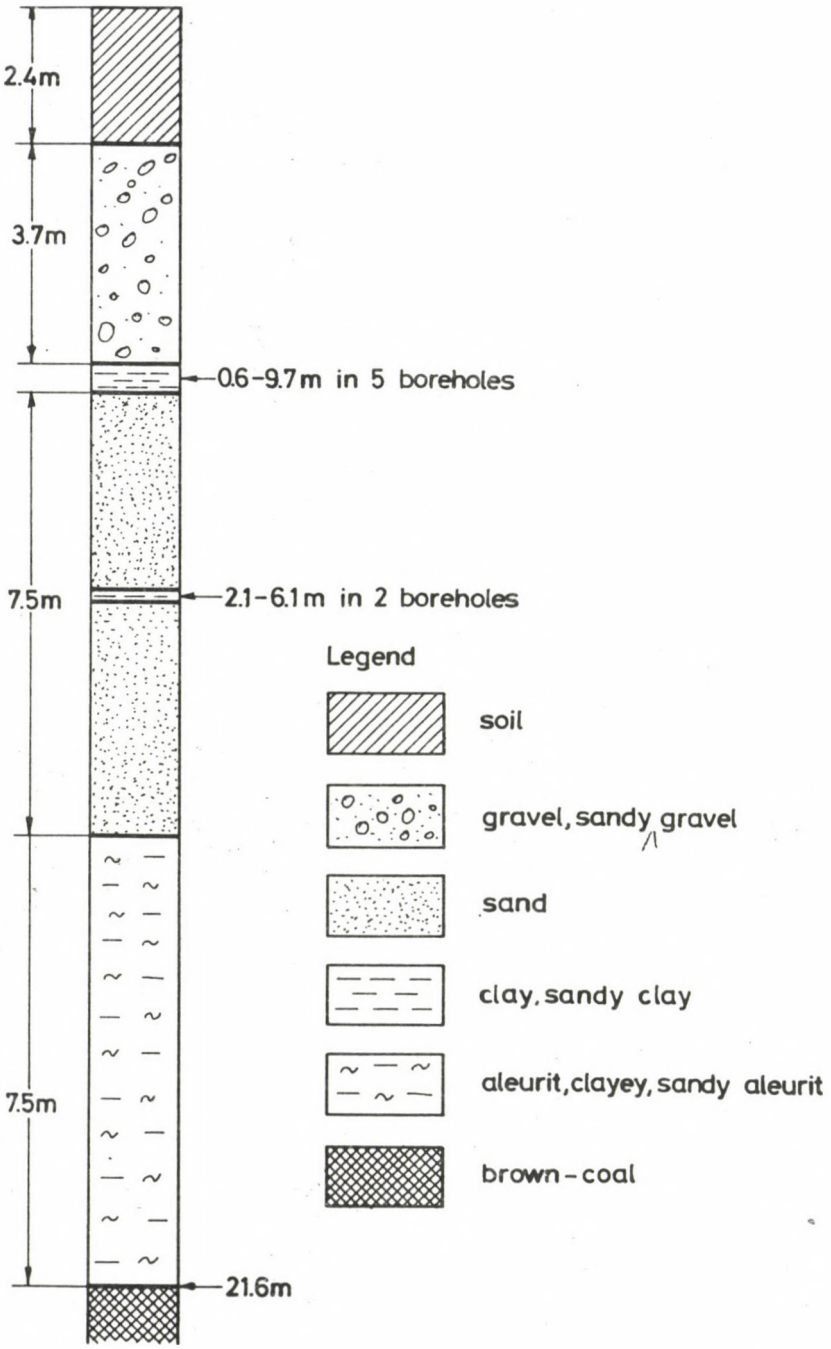

Fig. 2. Average layer sequence of the Vadna I open-pit mine

With regard to the technical conditions of the channel of Bán streamlet and the practical experiences obtained at the open pit mines of the Borsod Coal Mining Company, in the Sajó valley the effect of dewatering the subsurface aquifers on the Bán streamlet can be neglected. The drawndown of water table probably does not cause leakage from the considerably mudded up and colmative channel of the streamlet.

PROTECTION AGAINST SURFACE WATERS

The protection against surface water of part 1 of the open mine means outside of the open pit on one hand the diversion of rainfall water and on the other hand the prevention of water inflow from the Bán streamlet and the Sajó river.

The water running down from the hills surrounding the territory from the South and South-East is collected and diverted into the Sajó river by the Vadna ditch. As the mudded sections of the channel were dredged its present condition is suitable for the safe diverting of the collected rainfall from the catching area of the Vadna ditch. On case of floods on the Bán streamlet the 600 mm diameter dike drain at the mouth section of the Vadna ditch has to be closed in order to avert the danger of flood for the open cut through the Vadna ditch.

The standard flood level of the Bán streamlet ($Q_{1\ \%}$) at the reach above the bridge crossing the highway No. 26 is higher than the surface level, thus an embankment must be built on the western shore for the protection of the open pit. The corona level of the bank is 1 m higher than the flood level of 1 % probability, the length of the bank is 650 m. The 0+000 section of the required embankment starts from the highway No. 26 and ends at the Vadna ditch (Fig. 3).

On the northwestern side the highway itself can be used as an embankment against the floods of the Sajó river in a length of 240 m. To protect from the North, North-East and East a 630 m long embankment is necessary to be built up (Fig. 3) against the floods of the Sajó river with a height forming according to the section shown in Fig. 4.

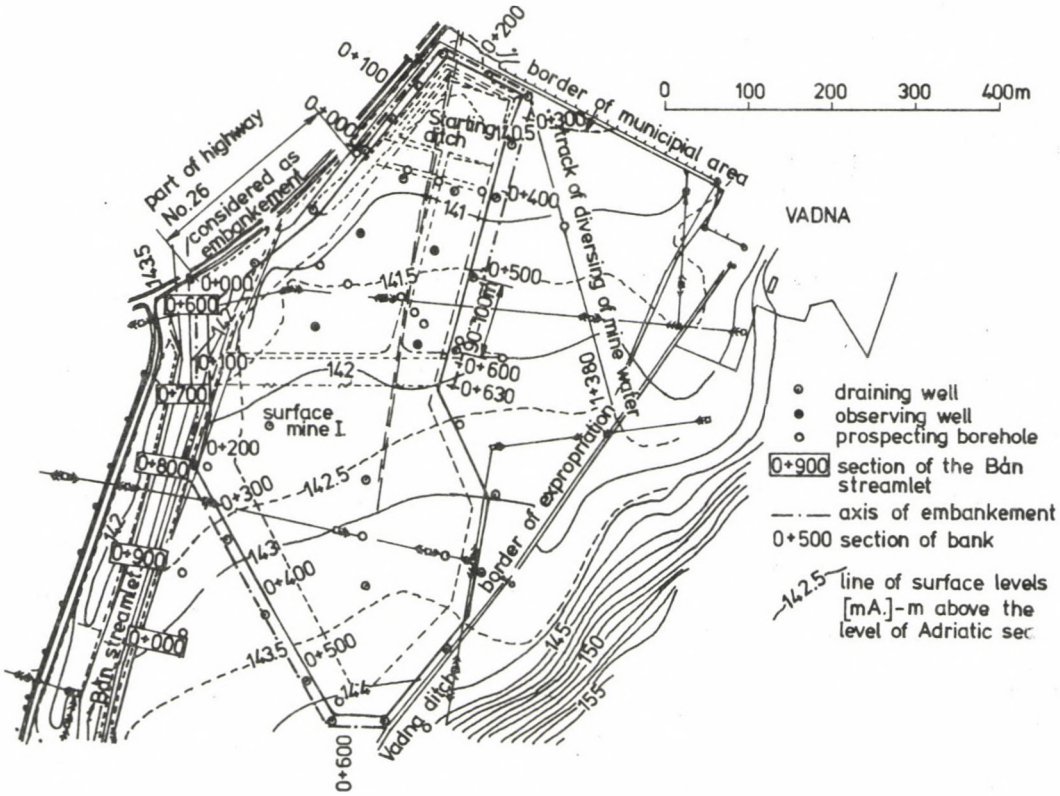

Fig. 3. Establishment of draining system and solution of flood control

The suggested width of bank-corona is 3.0 m, the bank slope is 1:2.

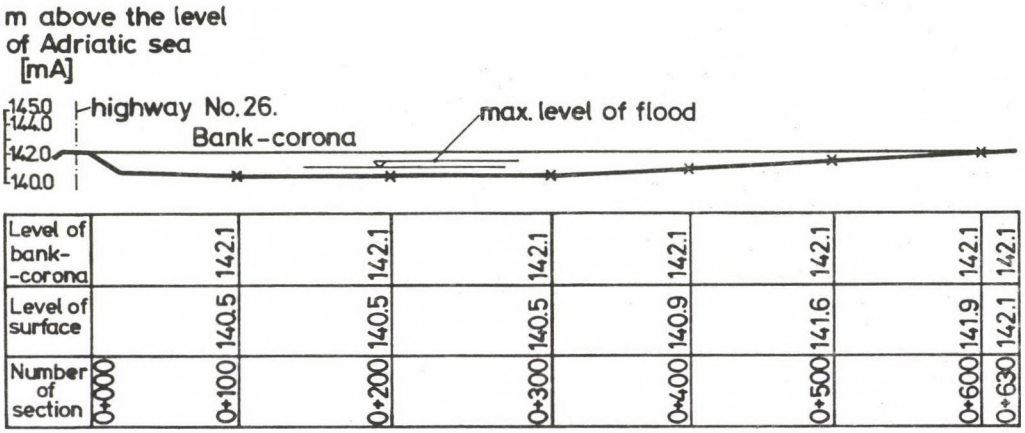

Fig. 4. Longitudinal section of the eastern embankment

DRAINAGE OF THE AQUIFER LAYERS IN THE OVERLYING

In order to protect the open mine the drainage of both water bearing layers in the overlying is necessary. The water discharge to be lifted during dewatering is given in Table I whereby the hydraulic parameters, the depth of bedding, the distance from the Sajó river, and dimensions of the oper mine are taken into account.

The water discharge calculated for the total area is a theoretical maximum, since the opened area in a certain moment is always less than the total area.

According to the hydraulic tests the capacity of the wells to be established has to be 210 l/min in gravel, 40 l/min in sand, i.e. 250 l/min maximum water discharge can be expected in the wells draining the whole permeable strata. Thus, by taking

Table I

stratum	water discharge to be lifted m^3/min	
	starting ditch	whole area
gravel	1.4	3.2
sand	0.5	0.6
total	1.9	3.8

a safety of 20 %, 10 wells are required to protect the starting ditch and at least 19 to protect the whole territory. In case of a uniform distribution of wells along the ramp slope the distance between the established wells must be 57 m around the starting ditch, and 96 m around the whole territory.

A change of the regular arrangement of wells can be necessary due to following reasons:

a) In order to take more advantage of the dip of layers and coal seams the wells can be established closer to each other on the western side of the surface mine.
b) If the foot of the sand layer is not plane due to tectonics, ditch-like areas may remain filled with water in case of a regular distribution of the wells, and supplementary wells are needed to dewater them.
c) Along the eastern boundary of the open pit mine the sand layer becomes thin or pinches out; here the protection of the open pit can be solved by the drainage of the gravel.

Further on the following points of view are to be considered for an effective water prevention:

1. It is practical to filter the wells both in gravel and in sand as the low rate of water flow from the sand would disturb the operation of pumps.
2. The water column still left in the sand after draining due to capillarity can be higher than 3.0 m, therefore in order to make the protection work more effective inside of the

open pit, it is proposed to dredge the sand in a supplementary cut which precedes the removal of the direct overburden of coal till a depth of at least 10 m. Thus the water can be easily collected in a conduit and lifted without disturbing the coal breaking work.

3. To control the effectiveness of water prevention along the boundary at least 4 observer wells must be established separately for both layers.

The scheme of establishment of the suggested draining and observing system is shown in Fig. 3. (It is to be noted that the discharge of the already operating wells which protect the starting ditch, varies from 70 to 230 l/min; the wells at the eastern border have lower water flow rates.)

THE PROBABLE EFFECTS OF WATER DRAINAGE FOR THE ENVIRONMENT

The probable radius of influence of the draining system after 2.0-2.5 years i.e. at the planned end of mining activity can be estimated as 1.5-2.0 km. The drawdown of the water table can be observed in the dug wells in the municipal area of the village Vadna as well as in the well of the waterworks of Nagybarca; the depth of this well is 8.0 m, it is filtered between 3.1-7.0 m. Owing to the distance of the established wells the depression decreasing logarithmically with the distance can cause not more than some ten cm drawdown of water level in the wells of Vadna, and only some cm in the well of the waterworks of Nagybarca. The drawdown of water table can be controlled by continuous observation of the 3 dug-wells of the village Vadna and of the 4 formerly established observing wells in the waterworks of Nagybarca.

The degree of the surface depression due to drainage was determined by taking into consideration the modulus of compression defined on the core-samples from the territory. The actual thickness of the strata according to the cross-section of the line of the highway No. 26 is shown in Fig. 2:

soil: 2.0 m,
gravel: 2.5 m,

sand: 3.5 m.

The probable value of surface depression in case of total dewatering calculated from the strata characteristics determined in laboratory and from a hydrostatic water level lying 3 m under the surface, will be 7-8 mm along the highway.

Taking into consideration the average succession of layers of the Vadna I open pit mine and the average thickness of each layer in the territory, 10-12 m is obtained for the compression of strata in case of a complete empty of reservoirs.

The estimated compression of 1 cm, however, can be regarded as the maximum extreme value, as it belongs to the maximum drawdown, i.e. to a complete empty of the water bearing layers, but the state of complete dewatering can be brought about only in the immediate surrounding of the draining wells till some ten cm even in case of an ideal operation of the wells. With increasing distance from the working-pit the value of surface depression decreases logarithmically.

The working-pit formed during coal mining will be filled up with the removed overburden; the closing-ditch will be filled up till the original surface level with the overburden of part 2 of the open mines of the Borsod Coal Mining Company. The territory of the open-pit mine will be set up in a way that it will be suitable again for agricultural cultivation.

REFERENCES

Jeney-Jambrik R, Szilágyi G, Nagy F 1986: Hydrogeological study of open-pit mining in Vadna. Study report, Technical University for Heavy Industry (NME), Miskolc

Acta Geod. Geoph. Mont. Hung., Vol. 22 (3-4), pp. 421-433 (1987)

PERFORMANCE CHANGE OF ELEVATOR DREDGERS IN SELECTIVE EXPLOITATION

F Kovács

Technical University of Heavy Industry, Miskolc, Egyetemváros, H-3515

A new efficiency factor is introduced by the author for the performance calculations of dredgers. The efficiency of selectivity characterizes the reduction of the efficiency of a dredger used for separating barren interstratifications. A regression function is determined on the basis of data obtained with elevator dredgers working at the Thorez mining plant to describe the variation of efficiency. The relation between dredging efficiency, time utilization factor, and selection is also discussed.

Keywords: barren interstratification; dredgers; efficiency; Visonta mine

One of the essential drawbacks of selective production is the capacity reduction of breakers and of the whole system of machines (haulage, immediate reloading, refuse disposal, second cut), respectively, the decrease of dredging efficiency and the reduction of time utilization factor. The reduction of performance of machines arises even then if the oberburden removing machines break also coal. The situation is similar when coal-breakers are set in for removing overburden. The decrease of efficiency of dredgers depends not only on the selection ratio, but also on the theoretical performance of them (dimension and type of machine). It is not usual to set in the machines of burden removing levels (bucketwheel dredger) for selective exploitations, as on one hand bigger machines have significant capacity reduction in selective operation and on the other hand due to the dimensions of the machines thin beds or interstratifications can be only extracted with a higher rate of deadrocks than allowed. Usually elevator dredgers (ladder bucket dredgers) of lower capacity are used in selective exploitation.

Acta Geod. Geoph. Mont. Hung. 22, 1987
Akadémiai Kiadó, Budapest

In selective production the operation of dredgers is characterised by the selectivity factor (S) in order to determine the capacity decrease of them. The selectivity factor is the double of the stripping rate of the auxiliary rock(s); in case of overburden removing machines it is the stripping rate of coal, in case of coal breakers it is the rate of the extracted overburden or interbeddings. The "s" rate of breaking shows how much is the proportion of auxiliary rock stripping of the full working time of a machine. If the value of s is higher than 50 %, the definition of the main and the auxiliary rock changes. It follows from the above definition that $0 = s = 0.50$, and $0 = S = 1.00$, as well $S = 2s$. The theoretical performance (Q_{theo}) of the continuous operation dredgers applied in open pit mines is essentially determined by the parameters of the machine (bucket volume, number of emptying) and by the slacking factor of the stripped material. When calculating the actual or effective capacity of dredgers in operation, i.e. when only one kind of rock is stripped, the features of loading, the value of dredging efficiency (η_d), and the effect of time utilization factor (η_t) must be taken into consideration, too. Hence, the relation between the actual and theoretical capacity is:

$$Q_{eff} = Q_{theo} \cdot \eta_d \cdot \eta_t = Q_{theo} \cdot \eta_e ,$$

where: η_d - dredging efficiency in case of breaking one kind of rocks,

η_t - time utilization factor,

η_e - total efficiency of a dredger operating in selective exploitation.

In case of selective production the capacity reduction can be defined by means of the efficiency of selectivity. The efficiency of selectivity is:

$$\eta_s = 1 - S\,(1 - \eta_r) ,$$

where: η_r - reduction factor.

The η_s factor expresses the effect of selective exploitation on the time utilization factor and on the capacity of

dredgers of different type, or operating under different conditions due to other capacity decreasing factors. The actual capacity of a dredger in a case characterised by the selectivity factor S is:

$$Q_{eff,s} = Q_{theo} \cdot \eta_d \cdot \eta_t \cdot \eta_s = Q_{theo} \cdot \eta_e$$

$$Q_{eff,s} = Q_{theo} \cdot \eta_d \cdot \eta_t \cdot \left[1 - S\,(1 - \eta_r)\right] .$$

The dredging factor (η_d) and the time utilization factor (η_t) are not absolutely constant parameters in the practice. In case of a dredger working in selective operation the values of the factors depend both on the natural and on the technical conditions of stripping. Hence, for calculating the capacities, a formula can be applied in which both the dredging and the time utilization factors are considered to be variables depending on the ratio of selective production.

Naturally, in this case the η_s efficiency of selectivity represents only the primary capacity decreasing effects of selective stripping. The actual performance of the dredger on these terms is:

$$Q_{eff,s} = Q_{theo} \cdot \eta_{ds} \cdot \eta_{ts} \cdot \eta_s = Q_{theo} \cdot \eta_{ds} \cdot \eta_{ts}\left[1 - S\,(1 - \eta_r)\right] .$$

As shown by Kovács (1984 and 1985) the reduction factor η_r depends on the parameters of the stripping-machines and on the conditions of operation. The relation is as follows:

$$\eta_r = \frac{C}{v_b}$$

where: C - a constant characterising the conditions of operations

v_b - the volume of the bucket of dredger (litre).

The value of C is 233 as given by Kovács (1984).

Considering the reduction factor the total efficiency and the capacity of a dredger working in selective operation is:

$$\eta_t = \eta_{ds} \cdot \eta_{ts} \left[1 - S\left(1 - \frac{C}{v_b}\right)\right],$$

and

$$Q_{eff,s} = Q_{theo} \cdot \eta_{ds} \cdot \eta_{ts} \left[1 - S\left(1 - \frac{C}{v_b}\right)\right].$$

Besides the theoretical study of this problem real data taken from the Thorez mining plant of the Mátraalja Coal Mining Company of the year 1984 were analysed, too. The effects of selective exploitation were examined by processing the data of the HM-2 dredgers of the type ERs-560, the HM-3 dredgers of the type ERs-500, and the HM-5 dredgers of the type ERs-700. The quantities of the stripped coal (t, m^3) of the overburden extracted from the first (I) and second (II) cut and the total quantity of moved rock (coal and overburden) (m^3) were determined and calculated for each month. The rock quantity coming from the first cut was considered as the selected overburden. The ratio of selective production (s) was also calculated. The monthly time of dredging (of coal, of first cut and the total time), the dredging capacities, the useful basis of time of a month and of a year, as well as the value of time utilization factor (η_t) were determined, too. The product of the dredging factor and the time utilization factor ($\eta_d \cdot \eta_t$) as well as the efficiency of selectivity were calculated, too.

Following data were determined on the basis of the total efficiency (η_t):

HM-2 0.397; HM-3 0.256; HM-5 0.228;

on the basis of the theoretical performance (Q_{theo}):

HM-2 1100 m^3/h; HM-3 1250 m^3/h; HM-5 1680 m^3/h;

and on the basis of the actual performance of the dredgers ($Q_{eff,s}$):

HM-2 437 m^3/h; HM-3 320 m^3/h; HM-5 383 m^3/h .

According to the calculations the yearly average dredging efficiency of each dredger is:

$$HM\text{-}2 \cong 0.60; \qquad HM\text{-}3 \cong 0.45; \qquad HM\text{-}5 \cong 0.50 \ .$$

The results of our calculation are presented in figures. Figures 1-3 show the increase of actual performances is function of the ratio of selective production (s) based on monthly data. The increase of the ratio of selective production means a definite reduction of the average value of the hourly effective performance of the dredgers.

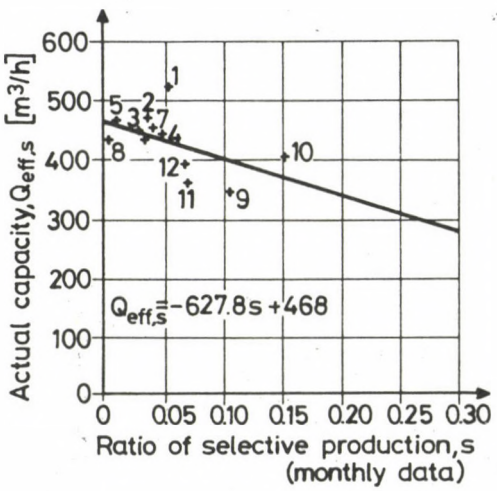

Fig. 1. Change of the actual dredging capacity of the HM-2 dredger in function of the rate of selective production

On the basis of monthly data it was not possible to define an exact trend between the rate of selective production (s) and the time utilization factor (η_t).

Figures 4-7 illustrate the development of the efficiency of selectivity in function of the rate of selective production. On the basis of the three dredgers and the summarized data one can find the obvious trend, i.e. the efficiency of selectivity decreases with the increase of the rate of selective stripping. The values of C determined for the three dredgers are almost the same (242, 305, 281), all the three are higher than the

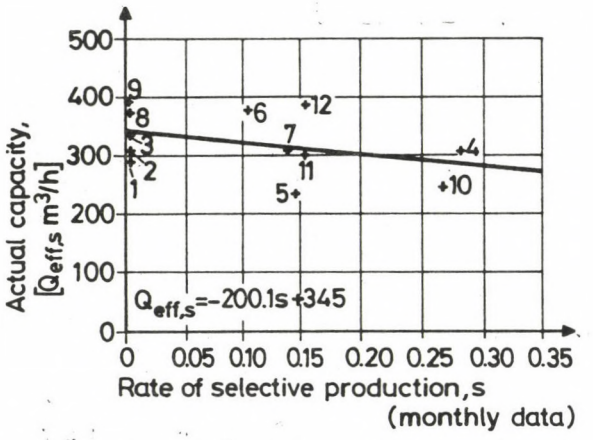

Fig. 2. Change of the actual dredging capacity of the HM-3 dredger in function of the rate of selective production

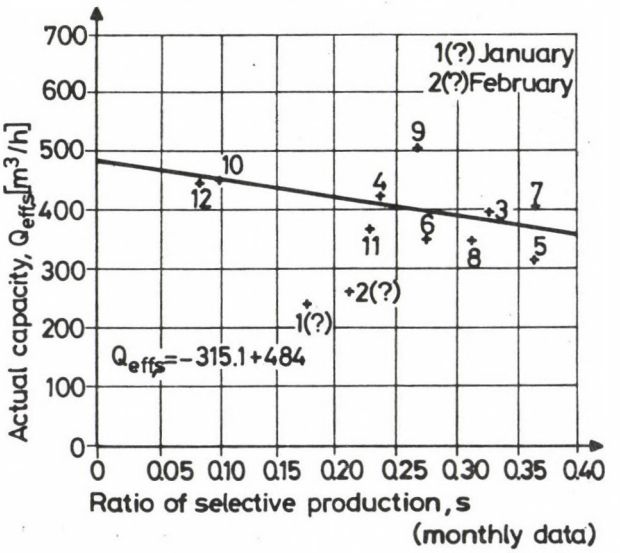

Fig. 3. Change of the actual dredging capacity of the HM-5 dredger in function of the rate of selective production

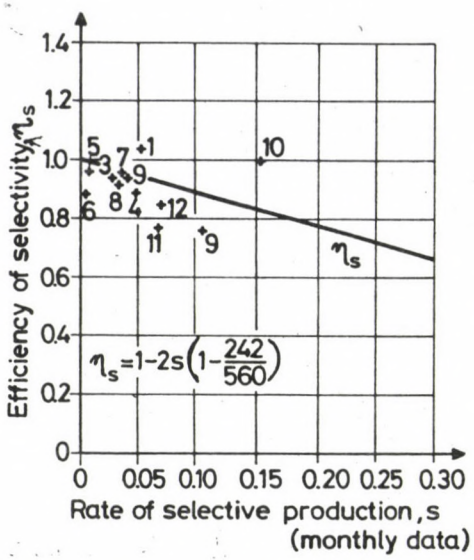

- Fig. 4. Change of the efficiency of selectivity of the HM-2 dredger in function of the rate selective production

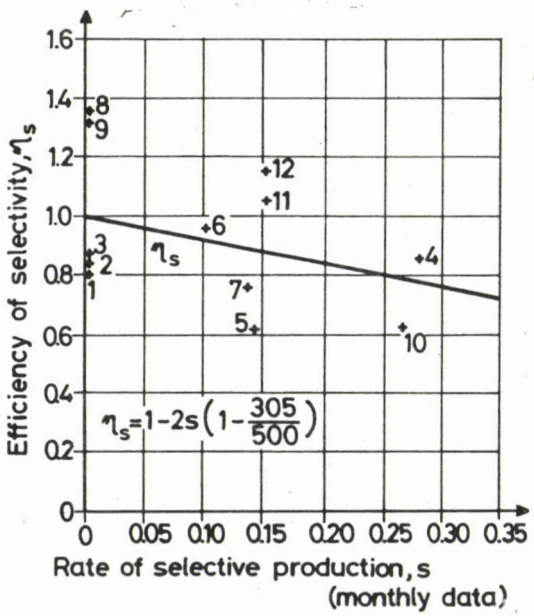

Fig. 5. Change of the efficiency of selectivity of the HM-3 dredger in function of the rate selective production

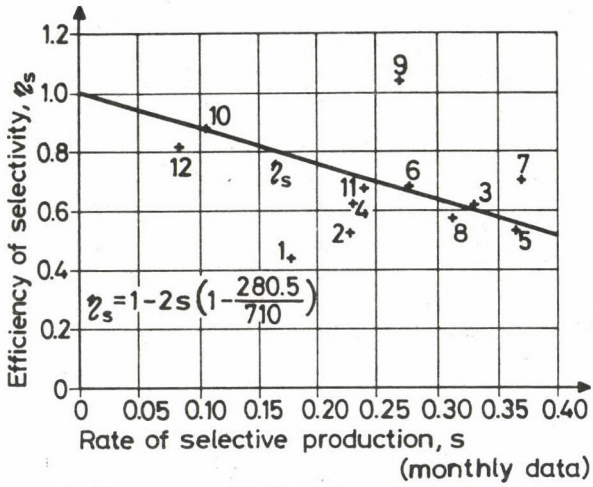

Fig. 6. Change of the efficiency of selectivity of the HM-5 dredger in function of the rate selective production

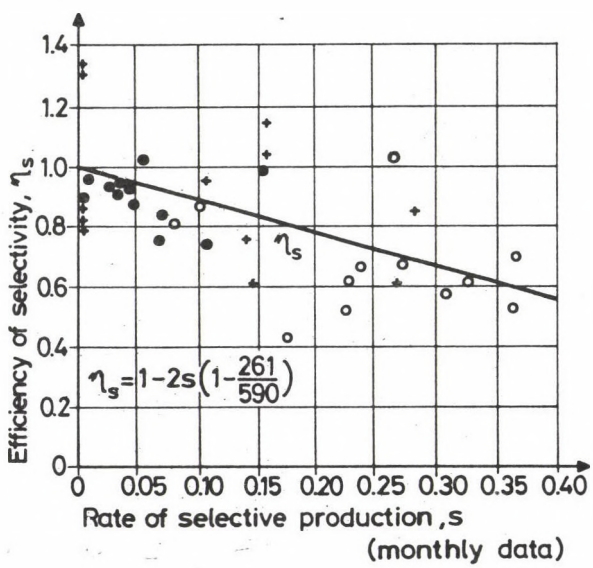

Fig. 7. Change of efficiency of selectivity in function of the rate of selective production (HM-2 ● , HM-3 + , HM-5 o)

C = 233 given by the references. On the basis of Fig. 7 C = 261 (the average bucket volume of 590 l).

The efficiency value has been also examined on the basis of the yearly data of dredgers.

In Fig. 8 the tendency of η_{ds} decrease with the increasing s is clearly visible. Selective operation reduces the dredging efficiency. On the basis of this figure two more facts appear. One is that the straight line connecting the data of the HM-5 and the HM-3 dredgers yields η_{ds} = 55 % dredging efficiency at s = 0.051; while the actual data of HM-2 dredger is η_{ds} = 60 %. It means that the dredging efficiency of HM-2 is 5 % higher - evidently first of all it is the result of the special technical parameters of it, as this dredger is outfitted with a stabilizer - further the trend line yields a selective production rate of 0.051. The other thing is that the efficiency (η_{ds} = 50 %) of HM-5 dredger having a bigger bucket is lower than the value yielded by the trend line determined by the data of the HM-2 and HM-3 dredgers.

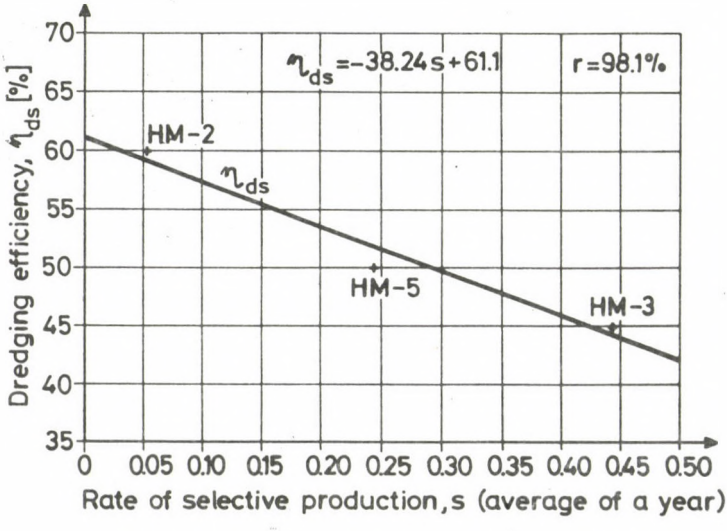

Fig. 8. Change of dredging efficiency in function of the rate of selective production

The change of dredging efficiency in function of the rate of selective production is:

$$\eta_{ds} = 0.611 - 0.3824\ s\ .$$

The change of yearly averages of the time utilization factor is illustrated in Fig. 9. Based on the regression relation for the change of time utilization factor in function of the rate of selective production one has:

$$\eta_{ts} = 0.715 - 0.1759\ s\ .$$

It can be also seen in this figure that the HM-2 machine achieved a more advantageous efficiency than yielded by the value s, while the efficiency of the HM-5 machine is lower than that.

In Fig. 10 the "efficiency" values of dredging efficiency and time utilization factor are united in one straight line in

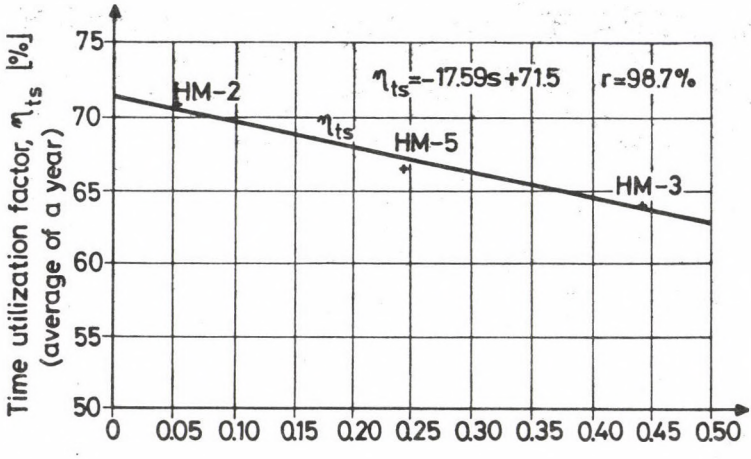

Fig. 9. Variation of the time utilization factor in function of the rate of selective production

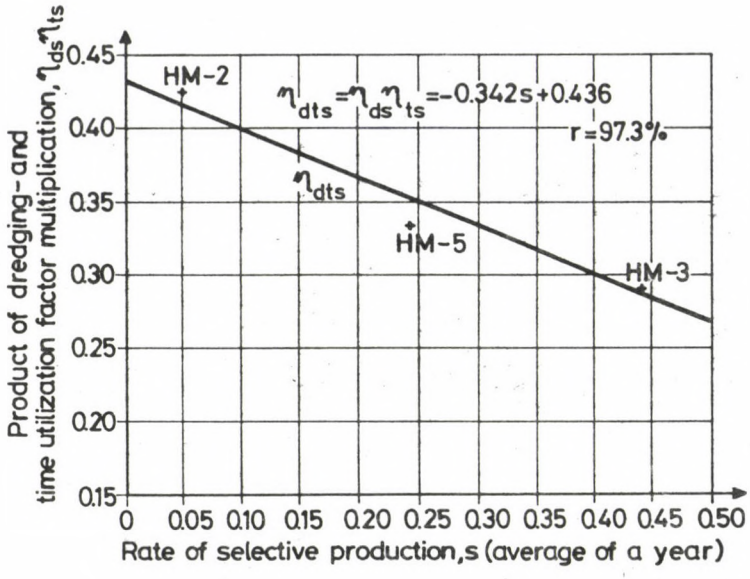

Fig. 10. Variation of the product of multiplication of the dredging and time utilization factor in function of the rate of selective production

case of a linear regression. Naturally, the η_{dts} can be derived as the product of η_{ds} and η_{ts}, then the result is a quadratic function. It can be seen on the basis of Fig. 10, too that the HM-2 machine can be applied with a relatively advantageous efficiency (even the effect of s is eliminated).

In the economical evaluation of selective production a primary question is how the efficiency factor changes with the independent variable s; here the effects of machine parameters (v_b) and the effect of operation conditions (C) must be taken into account.

On the basis of the above facts the total efficiency of dredgers working in selective production is:

$$\eta_t = \eta_{dts} \cdot \eta_s = (0.436 - 0.342\ s) \left[1 - 2\ s \left(1 - \frac{261}{v_b}\right)\right].$$

Hence, the two fundamental parameters defining the total dredging efficiency are the dimensions of the dredger (v_b) and

the rate of selective production (s). The given relation is generally valid, but the constants in it refer to the natural (thickness of coal seams, quality of rocks) and technical (elevator dredgers, band conveyor) conditions of the coal-mine Visonta.

Figure 11 illustrates the value of total efficiency defined by the data of 1984 of the capacity of the three dredgers. This figure also shows that the HM-5 machine - as the efficiency of selectivity is essentially lower due to its larger dimensions - achieved a lower overall efficiency in selective exploitation than the two other machines of smaller sizes. The total efficiency of the HM-5 machine is almost 10 % lower than would be reasonable on the basis of the rate of selective production (s).

On the basis of this investigation it can be stated with general validity that in selective exploitation the dredging efficiency, the time utilization factor and the efficiency of

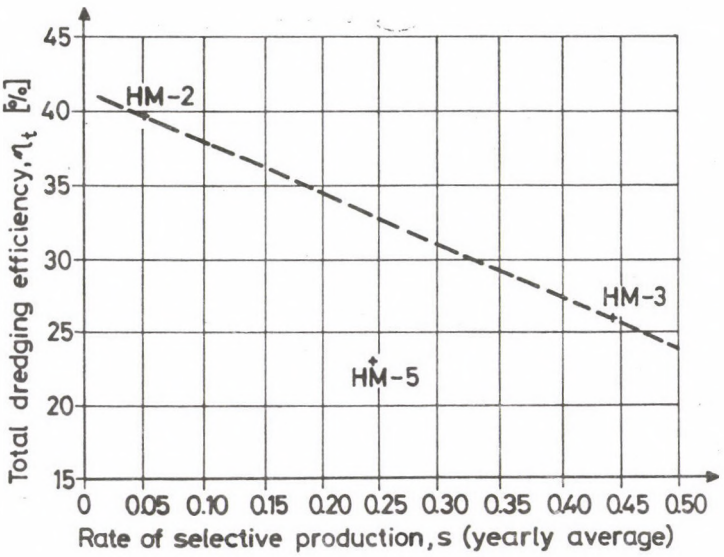

Fig. 11. Change of overall efficiency of dredging in function of the rate of selective production

selective production decrease with the increase of the dredger sizes. It is well-known, however, that the specific theoretical capacity increases within certain limits with the increase of machine dimensions. On the basis of these two opposed effects an optimum dimension of dredgers can be defined for a given rate of selection (s), i.e. for a given geological condition or for a certain coal series. In exploitation of a dislocated deposit (a formation with more coal beds, or coal seams with interbeddings) the application of smaller dredgers is economical, they can reach higher dredging efficiency with lower theoretical specific performance. In case of regular bedding (with one coal seam without interbeddings) the use of dredgers of bigger dimensions (it means higher capacity) is economical.

REFERENCES

Chair of Mining at Technical University for Heavy Industry 1985: Optimisation of parameters of selective production. Study report provided on behalf of Mátraalja Coal Mining Company, Miskolc

Kovács F 1984: Journal of Mining and Metallurgy, Mining. 117, 289-301.

Acta Geod. Geoph. Mont. Hung., Vol. 22 (3-4), pp. 435-451 (1987)

OVERBURDEN CONVEYOR BRIDGES AND DIRECT-DUMPING COMBINATIONS IN THE GDR'S OPEN-CAST LIGNITE MINES

K Strzodka

Institute of Open-Cast Mining and Water Economy, Bergakademie Freiberg, DDR-9200

The paper emphasizes the importance of lignite for the energy economy of the GDR. The lignite production by open-cast mines is described, including geological-geotechnical conditions of the application of overburden conveyor bridges, the development of direct-dumping combinations. A survey of development trends concludes the review.

Keywords: bench haulage; conveyor bridge; dumping; GDR; lignite; overburden excavation

1. THE IMPORTANCE OF LIGNITE FOR THE ENERGY ECONOMY OF THE GDR

The GDR has extensive lignite deposits at its disposal which formed the basis for the development of an independent energy economy after 1945 and which will retain their significance well beyond the year 2000.

In 1946 lignite output was about $110 \cdot 10^6$ t, in 1984 $296.3 \cdot 10^6$ tons were produced and in 1985 the planned output will be more than $310 \cdot 10^6$ t. Thus, the domestic production of lignite covers more than 70 % of the GDR's primary energy requirements. More than 80 % of the electrical energy is generated by the use of lignite and about 12 % by nuclear energy (Table I). In addition to this, about $20 \cdot 10^6$ t/an mineral oil and about $6 \cdot 10^9$ m^3/an natural gas are imported, especially from the Soviet Union.

The lignite deposits of the GDR (Fig. 1) are of Tertiary origin and are mined in open-cast mining exclusively. They are deposited in two large areas:

- in the region East of the river Elbe (Cottbus/Senftenberg)

Table I. Structure of energy suppliers in the GDR, in percent

	1960	1965	1975	1980	1983
solid fuels	96.9	92.5	76.5	69.0	72.8
among these lignite	83.2	79.6	69.2	64.2	71.0
nuclear energy and water-power	-	0.1	0.5	1.4	1.4
mineral oil and natural gas	3.1	7.4	23.0	29.6	25.8

and

- in the region West of the river Elbe (Halle/Leipzig/Magdeburg).

These deposits differ in geological age and conditions of deposition, consequently there are differences in their chemical and physical composition and, thus, in their uses. The younger Miocene coals of the main region East of the river Elbe belong to the epirogenetic type and have a low content of ash and sulphur. Among other things, they are suitable for the production of brown coal high-temperature coke (Lauchhammer and Schwarze Pumpe). The older Oligocene coals of the Halle/Leipzig region are bitumenous in certain areas. Therefore, they form the basis for production in low-temperature carbonizing and chemical plants. In the Halle/Magdeburg region, where the lignite is in contact with the underlying Zechstein, so-called "salt coals" are found.

2. THE EXTRACTION OF LIGNITE

The extraction of lignite in open-cast mining requires the removal of the rock which overlies the lignite known as "overburden". The effectiveness of an open-cast mine is evaluated by the ratio overburden volume to mass of raw material (lignite) $V_o : m_1$ which indicates how much overburden (in m^3) has to be handled for extracting one ton of lignite. If the overburden consists of unsolidated rock (e.g. sand) deposited by Pleistocene watercourses, water must also be raised the mass of which

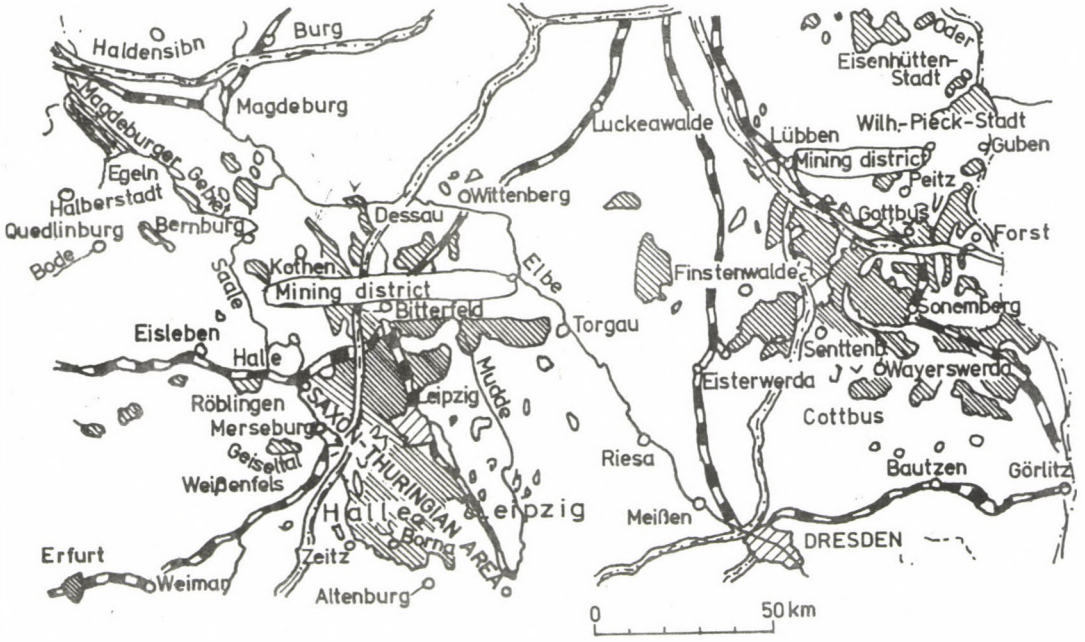

Fig. 1. Lignite occurrences in the GDR

is many times that of the mass of lignite extracted. At this time, in the GDR's open-cast mines the ratio V_o: m_1 is about 5:1, and in average about 7 m^3 of water have to be raised per ton of lignite (Table II).

Table II. Prognosis of performance development in open-cast lignite mining of the GDR

		1980	1983	1985	1990	2000
lignite output	10^6 t/a	285	278	310	>320	~330
overburden removal	10^6 m^3/a	1100	1275	1550	1600	1900
ratio V_o:m_1	m^3/t	4.3	4.6	5.0	>5.0	~5.8
water hoisting	10^6 m^3/a	1500	1720	2200	2400	2800
ratio V_o:m_1	m^3/t	5.8	6.2	7.3	7.6	8.8
average mine depth	m	68	72	77	80	90
average field size	10^6 t	230	225	215	205	190

The handling of these "secondary masses" has an important influence on the production costs of lignite. In the GDR's average the handling of overburden comes up to about 50 % and mine drainage to about 25 % of the total production costs.

Consequently, overburden excavation and its methods are a significant part of the economy of GDR open-cast mines. The oberburden is transported by trains, belt conveyors, overburden conveyor bridges or direct-dumping combinations. Due to these methods of transportation (haulage) the open-cast mines are called e.g. train type open-cast mines and conveyor bridge type open-cast mines.

Excavation, haulage and dumping are the main processes of overburden removal. Haulage plays a significant role in this production chain, since the haulage distance heavily influences the efficiency of an open-cast mine. In principle, two kinds of haulage are differenciated: bench haulage and direct haulage.

In bench haulage (Fig. 2) the loosened overburden dug by excavators (bucket-chain and bucket-wheel excavators and shovels resp.) is loaded into wagons, onto belt conveyors or into

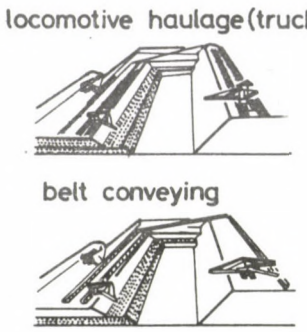

Fig. 2. Haulage methods in overburden removal - bench haulage

trucks and transported on the bench around the pit to be dumped at a part of the open-cast mine which has already been worked--out. Usually, the haulage distance is long (6 to 8 km). This results in high transportation costs. In each of the three stages (excavation, haulage and dumping) special devices and technological approaches are used.

In direct haulage (Fig. 3) the overburden extracted by excavator units (mostly continuously working ones) is transported

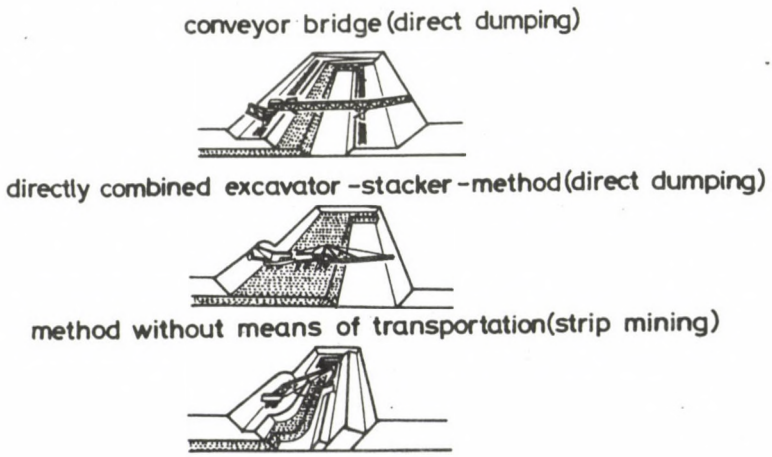

Fig. 3. Haulage methods in overburden removal - direct haulage

by the shortest path over the exposed mineral by means of a mobile conveyor system which follows the excavator units in the direction of face advance. Then the overburden is discharged immediately onto the exposed, worked-out floor. In addition to overburden conveyor bridges (OCB) which have been used in the area of the GDR for more than 60 years, directly combined excavator-stacker-systems (DDC) have been developed in the last fews years. The OCBs, mostly equipped with bucket-chain excavators work in frontal digging (Fig. 4) while the whole system has to move steadily, but DDCs, where a bucket-wheel excavator is mainly combined directly with a specially designed stacker, work in block digging (Fig. 5) and move only in stages.

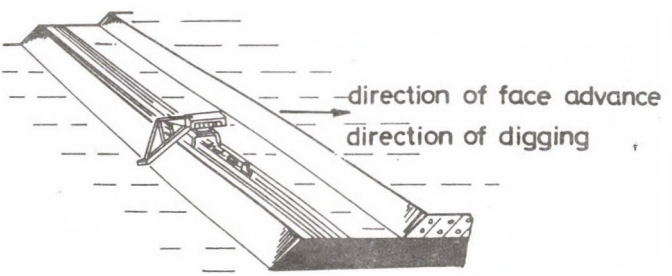

Fig. 4. Frontal digging

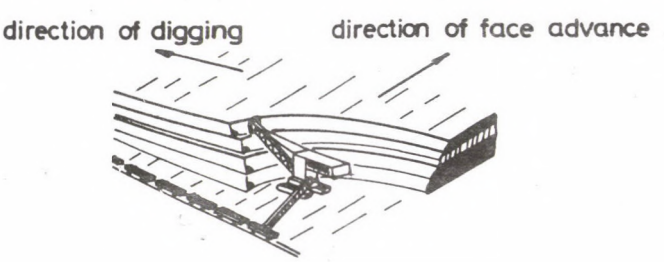

Fig. 5. Head block digging

In direct haulage the haulage distance is as short as possible and the overburden is immediately dumped by means of transportation. While in bench haulage in the open-cast lignite mines of the GDR the average haulage distance is about 5 or 6 km, in direct haulage, e.g. with overburden conveyor bridges, it does not exceed 500 or 600 m. This relatively short haulage distance and the combination of several working stages of the technological chain (excavation - haulage - dumping) result in relatively high labour productivity of the conveyor bridge (Table III). However, the production costs of direct haulage are between a quarter and a third that of bench haulage (Fig. 6). Therefore, the trend in overburden technology is to use direct-haulage methods where it is geotechnically possible.

Table III. Labour productivity and prime costs of some haulage method in open-cast lignite mining of the GDR (1980)

	Labour productivity in m^3/h (maximum) form I	form II	Costs in Mark/m^3 (minimum)
conveyor bridge	109 (188)	52 (85)	105 (62)
belt conveying - overburden -	66 (100)	25 (37)	244 (154)
locomotive haulage - overburden -	19 (30)	11 (22)	333 (122)

In order to adapt to the steadily increasing overburden thicknesses, from the middle fifties till the middle of the seventies the overburden conveyor bridges developed for open-cast mining in the GDR were improved in cutting-height capability from 34 m (F 34) to 60 m (F 60). There are the types F 34, F 45, and F 60 (Fig. 7).

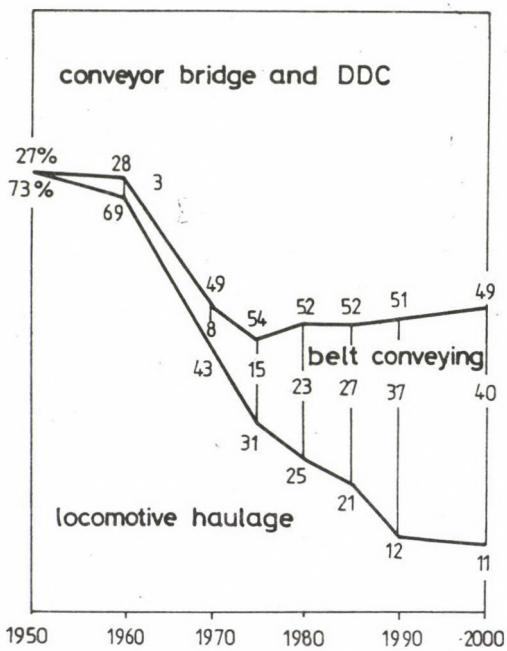

Fig. 6. Development of methods of overburden haulage in open-cast lignite mining of the GDR

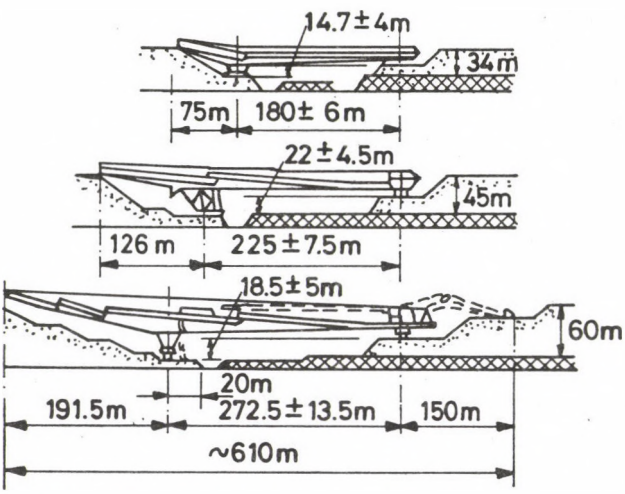

a: 2Es 1120
b: 2700t
c: $44 \cdot 10^6 m^3$
d: 1:2.6

a: 2Es 1600
b: 6400t
c: $>50 \cdot 10^6 m^3$
d: 1:3

a: 3Es 3150 and 3750
b: 15900t
c: 115 to $120 \cdot 10^6 m^3$
d: 1:3.3

a – attached excavator
b – service weight (without exc.)
c – annual output volume
d – general inclination of slope system

Fig. 7. Comparison of the conveyor bridge units

The greater the thickness to be excavated the higher is the

dump. To ensure the dump stability a geotechnically calculated dump system has to be established. This requires a span of 272.5 m with ± 13.5 m telescopic length and a boom of 191.5 m length with three discharge points with the F 60 type. The boom of the F 34 type was only 75 m long and was extended by 20 m to improve the geotechnical stability of the dump. The F 45 type has a boom of 125 m length and an intermediate discharge point.

3. THE GEOLOGICAL-GEOTECHNICAL CONDITIONS FOR THE USE OF OVERBURDEN CONVEYOR BRIDGES

The geological conditions under which a lignite deposit was formed are significant for the selection of the open-cast mining method to be used. The autochthonous formation of a lignite deposit is effected by the growth of a lignite bog, under special climatic conditions and also by surface subsidence. With the epirogenetic type of deposit the subsidence covers a vast area. In most cases, there was steady velocity of subsidence which was nearly as high as the rate of growth of the bog. Therefore, the epirogenetic lignite seams are characterized by an undisturbed deposition with most regular, but relatively small thicknesses (5 to 20 m). We find a considerable number of such seams in the Niederlausitz region (East of the river Elbe).

In the case of the tectonic type, the subsidence is a tectonic process, mostly a trough fault which is characterized by short-term subsidences in a small area which are temporally shifted (Fig. 8). Consequently, lignite seams of the tectonic type cover only a small area which is as big as the tectonic unit, but they are of great thickness. Because of the unevenness and great extent of the tectonic subsidence, clastic material is often alluviated. For these intercalations of sand and clay the ash content is very high. The flanks of such a basin and the numerous uneven intercalations form geotechnical slickensides and, thus, endanger the large open-cast mining units, although they rest predominantly on horizontal working levels. In the case of the salt-tectonic type (Fig. 9) of deposit, the surface subsidence necessary for seam formation is caused when, due to rock tensions and the plastic nature of salt, salt

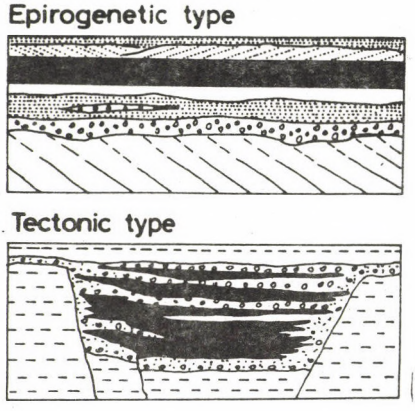

Fig. 8. Genetic types of lignite deposits: a) epirogenetic type, b) tectonic type

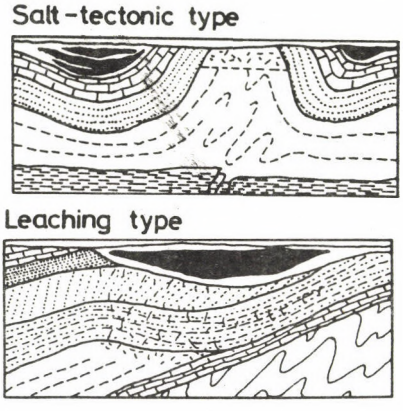

Fig. 9. Genetic types of lignite deposits: c) salt-tectonic type, d) leaching type

masses move in the underground into a near-by developing salt anticline or salt diapir. At the flanks of the salt anticline synclines are formed which can be filled by a lignite bog. If the velocity of subsidence is greater than the rate of growth of the bog, clastic sediments can be alluviated.

Moreover, the surface subsidence necessary for seam formation can be caused by leaching of salt or other dissolvable rock, e.g. gypsum. These deposits, belonging to the leaching type of deposit (Fig. 9), are found only in areas with a great thickness of the Zechstein subdivision. Such synclinical deposits are mostly of great thickness (up to 100 m). The flanks of the basin of such a synclinical deposit formed by salt leaching and salt movement respectively are mostly very steep and, therefore, areas of weakness, in the geotechnical sense.

The epirogenetic type of deposit is particularly suitable for the use of overburden conveyor bridges (Fig. 10). This unit spans the exposed mineral with a bridge and usually rests on two railmounted supports. The excavator-side support rests on the working level, where one or two bucket-chain excavators operate. The support on the tipping side mostly rests on a preliminary dump. This preliminary dump is formed by excavated

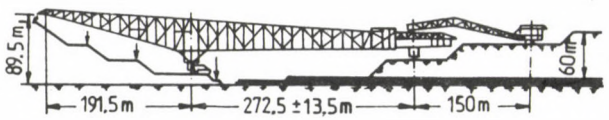

Fig. 10. Overburden conveyor bridge for 60 m thickness to be excavated

overburden material discharged from the overburden conveyor bridge and consequently, it is a part of the whole dump system. The main dump has to be formed with a calculated angular position of slope in order to guarantee geotechnical stability. This requires a discharge boom the length of which depends on the height of the dump.

Overburden conveyor bridges have a service weight up to 10000 t (F 60), including the excavator up to 25000 t. For this reason, they can work only under special geological conditions, i.e. the overburden has to consist of 50 % sand and the preliminary dump, on which the travel gear rests, has to be formed by sand. Working levels with very low inclines (transverse inclination) are necessary and the difference between the heights of the supports is limited (longitudinal inclination). Therefore, overburden conveyor bridges can be used only with very even deposits. Such epirogenetic depositions with thick Pleistocene overburden exist in the Niederlausitz region, where 11 of the total 15 overburden conveyor bridges operating in the GDR are working.

As a rule, an overburden conveyor bridge can work only one seam at a time. It is even difficult to select thin interbedded layers. If two seams divided by a thick interbedded layer are to be worked, a multi-supported overburden conveyor bridge is necessary. This means an upper bridge has to be combined with the lower main bridge.

The floor of lignite seams consists mostly of clays which differ from sandy dumps in their soil-mechanical parameters. The clay has a smaller angle of inner friction than the dump bottom. In order to prevent the dumped material which has a

naturally established angular position of slope of 30^{o} from slipping onto the clayey floor, the slope system has to be shaped to a suitable size. Consequently, the dump system of the F 60 type contains two intermediate dumps in addition to the preliminary dump.

Overburden conveyor bridges are units with a high concentration of operation. The F 60 type conveyor bridge yields an annual output volume of about $126 \cdot 10^{6}$ m^{3}, its conveyor belts are designed for a maximum volume flow of 10 m^{3}/s. These great mass flows cause other geotechnical problems: the excess pore water pressure in the floor caused by sudden high speed loading. If a clay bed with a low permeability and fully water-saturated pores is suddenly loaded, the whole additional pressure is temporally absorbed by the water. Thus, an excess pore water pressure is caused reducing the strength of the clay. This excess pressure decreases only in accordance with the possible speed of the water running-off (consolidation). Due to their high concentration of operations at the slewing end of the mine, overburden conveyor bridges can have a daily face advance up to 4 m. The speed of load and the dynamics of decreasing excess pore water pressure have to be known and taken into consideration in determining the size of the dump and the dumping method.

Usually, it is necessary to reduce the pressure in artesic aquifers of the floor, in case of the F 60 type overburden conveyor bridge the floor has to be drained up to a depth of 25 m.

The use of units of this size causes new problems which were earlier unknown. It is no longer possible to control the distribution of the mass flow (max. 10 m^{3}/s) united at the tipping-end support onto the preliminary dump and the three discharge points of the main dump by conventional manual methods. Therefore, the three F 60 type overburden conveyor bridges in operation (Welzow-Süd, Nochten and Jaenschwalde open-cast mines) which will be soon followed by another two, were equipped with computer processors. These processors control the material distribution at the different discharge points by means of a programme according to the angular position and the siting of the overburden conveyor bridge at the bench. In doing so, a

dump system is established which meets the soilmechanic requirements and will prevent the dump from becoming too high. Thus, the dumping space is used for optimum performance and simultaneously, an even dump surface is achieved.

The design of the overburden conveyor bridges requires that the opening trench, where the OCB is assembled, is dug separately (mostly in bench haulage). Consequently, the opening--up of an open-cast mine using overburden conveyor bridges takes a much longer time - up to 3 years. The re-locating of an OCB from a worked-out field to a new one is only possible after the OCB has been dismantled. However, some attempts have been made to re-locate an OCB directly without dismantling.

Due to these pecularities overburden conveyor bridges have to be used in fields with large reserves to ensure a full amortization of the investments which requires an operating period of some 20 years. This means, if the annual output of an open--cast mine using a F 60 type OCB yields approximately $25 \cdot 10^6$ t, the field reserve has to be about $500 \cdot 10^6$ t. But in the GDR there are only a few connected fields which meet the demands for the use of an OCB.

4. THE DEVELOPMENT OF DIRECT-DUMPING COMBINATIONS

As mentioned above, overburden conveyor bridges can only be used under special geological, geotechnical and technological conditions. Where these conditions are not entirely fulfilled, another kind of direct haulage can be applied: the directly combined excavator-stacker-method, also called "direct-dumping combination" (DDC) (Fig. 11). With such a DDC, - mostly a caterpillar-mounted bucket-wheel excavator which works in block digging and feeds the belt stacker directly or by means of a mobile transfer conveyor - the belt stacker spans the exposed mineral by means of a boom (with a length of up to 225 m). The operation of such a unit combination - block digging of bucket--wheel excavator, block discharge of belt stacker, possible angular position and distance of units to each other and so on - requires special technological knowledge and experience.

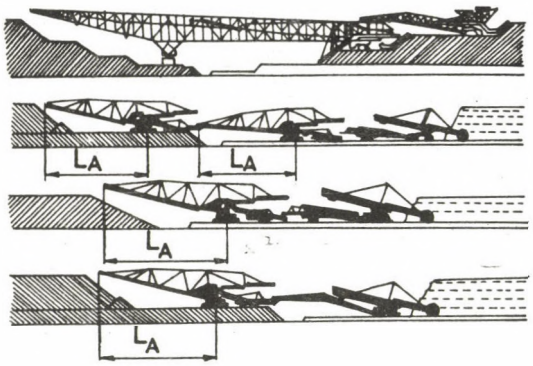

Fig. 11. Comparison of direct-dumping combinations with an overburden conveyor bridge

In the open-cast mine Thorez/Visonta of the Mátra lignite combine Gyöngyös, Hungary this type pf DDC has been used sucessfully for several years.

In contrast to overburden conveyor bridges direct-dumping combinations are usually most suitable for excavating small thicknesses, i.e. not more than 35 m. According to the size of unit their annual output yields 30 to 40 $\cdot 10^6$ m^3 and does not reach, for example, that of a F 60 type OCB.

The greatest advantages of a DDC are as follows: It can be applied to geologic-geotechnical conditions not suitable for overburden conveyor bridges. It is mobile (caterpillar mounted) and excavator and stacker can be assembled separately at the same time at an assembly site away from the opening trench. Afterwards they can be moved into the opening trench. Thus, the period of opening-up is reduced considerably. Moreover, since they are mobile, these unit combinations can be relocated from a worked-out pit to another pit much faster than overburden conveyor bridges (Fig. 12). This is particularly important for mining smaller fields with fewer reserves in highly concentrated operations. A DDC can also be used to open up a field cutting into the depth with a slicing action. In doing so, the time and more particularly the costs of opening-up can be

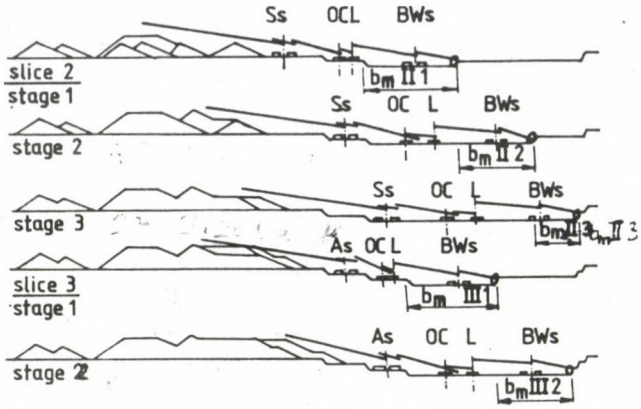

Fig. 12. Opening-up of an open-cast mine by means of direct-dumping combination - slicing overburden excavation and slicing overburden dumping

reduced substantially.

5. TRENDS

Overburden conveyor bridges will continue to dominate the scene even in the years to come; they handle about 50 % of the total overburden volume excavated in the open-cast mines of the GDR. Two further F 60 type bridges will be put into operation in the open-cast mines Reichwalde and Klettwitz-Nord which were opened up recently, thus, five F 60 type bridges will be in operation handling an overburden of $600 \cdot 10^6$ m^3/an, which amounts to about a third of the rising total overburden volume. In addition to that, direct-dumping combinations will gain increasing importance, even if they handle no more than 10 % of the total overburden volume.

The cutting height of overburden conveyor bridges and particularly that of direct-dumping combinations is limited. With OCBs it is twice that of DDCs. Therefore, OCBs will be used more often. In order to make use of the advantages of direct haulage for thicknesses to be excavated greater than 60 m, in technological research work so-called "slant mining"

has been developed (Fig. 13). In slant mining a multi-supported shiftable belt conveyor is installed at a slope with an inclination of 1:7 up to 1:10 at both the excavator and tipping sides. The overburden is dug out in block digging by an excavator which can be levelled and it can be discharged by a stacker which can also be levelled. The bucket-wheel excavator

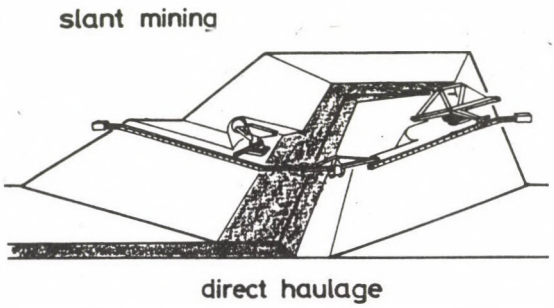

Fig. 13. Haulage methods in overburden removal - direct haulage

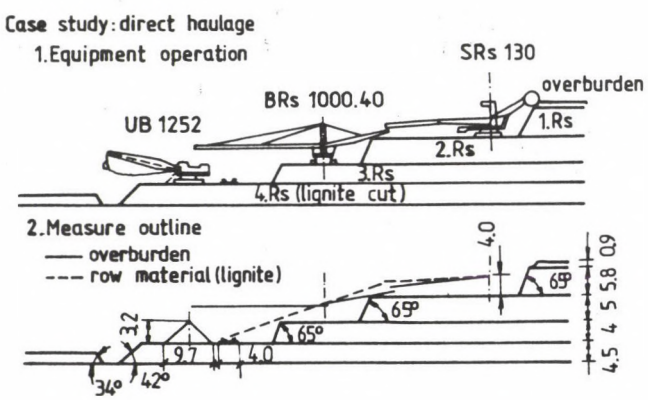

Fig. 14. Case study: Direct haulage in small open-cast mines

excavates blocks of relatively small heights, thus it can be constructed as a compact excavator with a relatively short bucket-wheel boom.

Such an arrangement of units allows various thicknesses to be excavated.

At first sight the developed open-cast mining field seems to be relatively large in case of an inclination of 1:10. Compared to an open-cast mine with several benches arranged according to the necessary general inclination, the pit turns out to be larger than conventional open pits by only 10 %.

The short-distance direct haulage method can be used in smaller open-cast mines (Fig. 14), for example in building materials industry, to have the shortest haulage distance from face to dump and to reduce production costs which are strongly affected by the overburden volume to be handled.

Acta Geod. Geoph. Mont. Hung., Vol. 22 (3-4), pp. 453-460 (1987)

AIRFLOW MODELLING BY THE AVERAGE VELOCITY OF AIR

K Z Ushakov

Mining University, Moscow, USSR

Problems of air flow in drifts of mines are dealt with in the study. Using the modelling law, the criteria of fluid flow with medium velocity are analyzed, and a relationship is experimentally established between air resistance and the Reynolds number. It has been found that the friction on the walls of drifts is most reliably described by the Reynolds number.

Keywords: airflow in mines; drift-type working; fluid flow; modelling; Reynolds number; ventilation

To get the similarity criteria for the Reynolds equation of the unsteady-state turbulent motion one may take only one of its projections, e.g. on the Ox axis; only gravity is taken into consideration of the volumetric forces. One has:

$$\frac{\partial u}{\partial t} + u\frac{\partial u}{\partial x} + v\frac{\partial u}{\partial y} + w\frac{\partial u}{\partial z} = g - \frac{1}{\varrho}\frac{\partial p}{\partial x} + \nu\Delta u + \frac{1}{\varrho}\frac{\partial}{\partial x}\left(-\varrho\overline{u_p u_p}\right) + \frac{1}{\varrho}\frac{\partial}{\partial y}\left(-\varrho\overline{v_p u_p}\right) + \frac{1}{\varrho}\frac{\partial}{\partial z}\left(-\varrho\overline{w_p u_p}\right), \quad (1)$$

where u, v, w are the components of the average velocity along the coordinates; t - time; g - acceleration due to gravity; ϱ - density of the fluid; p - pressure; ν - kinematic viscosity coefficient; Δ - Laplacian operator; u_p, v_p, w_p - components of pulsing velocity along the coordinates; x, y, z - coordinates.

Similarity criteria are obtained by the method of integral analogues, thus by choosing the characteristic time of the process θ as time in Eq. (1); the absolute value of its

vector V as the component of the average velocity; the hydraulic diameter D of the working as coordinate; the pressure difference H of the motion area as pressure; the absolute value of the vector V_p of pulsing velocity as component of the pulsing velocity. Having replaced in Eq. (1) the values t, u, v, w, x, y, z by the adopted integral analogues one gets the following proportional dimensional expressions:

$$V/\Theta \sim V^2/D \sim g \sim H/\varrho D \sim \nu V/D^2 \sim V_p^2/D . \qquad (2)$$

By dividing each term in Eq. (2) by V^2/D, the following dimensionless expressions or similarity criteria are obtained:

$V\Theta/D$ = Ho - homochronism criterion;

dD/V^2 = Fr - Froude number;

$H/\varrho V^2$ = Eu - Euler number;

VD/ν = Re - Reynolds number;

$\sqrt{\overline{V_p^2}}/V = V_p'/V = \varepsilon$ - intensity of turbulence.

Here V_p' is the mean-square value of the pulsing velocity vector.

The criteria Ho, Fr, Eu, Re are obvious. Let us envisage criterion ε in detail. First of all it defines the relationship between the turbulent friction forces τ and the inertial forces $\varrho u_a^2/2$.

For the turbulent tangential stresses in a two-dimensional flow, one has

$$\tau_T = \varrho \varepsilon_I (\partial u/\partial y) = \varepsilon_I u_a \left[\partial(u/u_a)/\partial(y/D)\right]/D , \qquad (3)$$

where ε_I is the coefficient of the turbulent exchange for an impulse; u_a the average velocity of the flow and D its hydraulic diameter.

Thus the relationship between frictional and inertial forces is

$$\tau_T/(\varrho u_a^2/2) = 2\,\varepsilon_I\,\left[\partial(u/u_a)/\partial(y/D)\right]/u_a D\ . \qquad (4)$$

For kinematically and geometrically similar flows the relations u/u_a and y/D are in corresponding points equal. The derivative in brackets in Eq. (4) is also constant. Therefore the relationship between forces of turbulent friction and inertia is defined only by the following dimensionless expression:

$$u_a D/\varepsilon_I = U\ . \qquad (5)$$

It is evident that the criterion U is equivalent to the Reynolds number. The only difference is the denominator, where the kinematic viscosity is replaced by the coefficient of turbulent exchange of impulse (kinematic coefficient of turbulent viscosity) ε_I. The criterion U may be considered as a turbulent analogue of the number Re; it defines the relation of molecular friction forces and inertial forces.

The theory of mixing length shows that

$$\varepsilon_I = -\overline{L_m u_p} = k_1 L_m' u_p'\ , \qquad (6)$$

where L_m is a momentary value of Prandtl's mixing length for the impulse; L_m' its mean-square value; u_p a momentary value of the pulsing velocity along the axis Ox; u_p' its mean-square value; k_1 the proportionality coefficient.

Having in view that the mixing length L_m' is proportional to the diameter D of the working and does not depend on Re (Shlikhting 1969, Ushakov 1975) i.e. $L_m' = k_2 D$, and $u_p' = k_3 v_p$, Eqs (5) and (6) yield

$$T = K/\varepsilon\ , \qquad (7)$$

where $K = 1/k_1 k_2 k_3$ is a proportionality coefficient.

Thus the criterion ε defines the relation between turbulent friction forces and inertial forces and is identical to criterion U.

The similarity conditions of two flows by the action of turbulent friction forces and inertial forces is in corresponding

points of the flows accordingly:

$$\varepsilon = \text{inv.} , \tag{8}$$

or

$$U = \text{inv.} \tag{9}$$

In Eq. (5) the coefficient of the turbulent exchange for the impulse can be defined by the tangential stresses according to Eq. (3):

$$\varepsilon_I = \tau / \left[\varrho \left(\partial u / \partial y \right) \right] .$$

Accepting the tangential stresses on the wall as a scale unit for τ

$$\tau_w = \alpha u_a^2 ,$$

where α is the friction coefficient of the mine airway. By taking an average velocity in the working u_a as velocity, and the hydraulic diameter of the working D as distance one gets:

$$\varepsilon_I \sim \alpha u_a D / \varrho .$$

Then Eq. (5) yields

$$T \sim \alpha / \varrho = \beta , \tag{10}$$

where β is the dimensionless friction coefficient of the airway.

Thus the friction coefficient β is a similarity criterion of the forces of turbulent friction and inertial forces and its invariance for the corresponding points of the object and the model may serve as the condition of similarity:

$$\beta = \text{inv.} \tag{11}$$

Equation (10) shows that the relationship between the model velocity and the object velocity does not influence the

similarity of turbulent friction forces and inertial forces. The only condition which is required is the existence of the turbulent character of the flow. The motion velocity in the model and that in the object can be sometimes equal.

The condition

$$u = \text{inv.} \tag{12}$$

expresses the principle of modelling "by velocity" which does not contradict Eq. (11) and it is used nowadays in turbulent flow modelling.

Jones and Hinsley (1959) define with reference to Marfy the lower limit of modelling by the average velocity in a value of $Re = 3 \cdot 10^4$.

This limit may also be defined by the expression

$$\lambda = \tau_T / \tau_M = \varrho \varepsilon_I \left(\partial u / \partial y \right) / \left[\varrho \nu \left(\partial u / \partial y \right) \right] = \varepsilon_I / \nu \ , \tag{13}$$

where τ_T, τ_M are the turbulent and molecular (viscous) stresses in the flow, respectively; ν is the kinematic viscosity coefficient.

That value of λ in Eq. (13), where the turbulent friction is equal to the viscous friction, should be denoted by Λ. If $\lambda \ll \Lambda$, the viscous stresses predominate in the flow and the modelling should be made according to the criterion U. In the particular case if the airway resistance is being modelled with $\lambda \gg \Lambda$, the modelling must be made "by velocity". If the forces of molecular and turbulent friction have the same order of magnitude, none of the mentioned criteria ensures the similarity of the action of frictional and inertial forces; modelling by any of the criteria Re or U causes considerable errors. That is why a modelling in the vicinity of Λ is undesirable. Thus when modelling of the action of frictional and inertial forces in a flow, the parameter Λ defines the region of applicability of the criteria Re and U.

Three main regions of the frictional and inertial forces modelling are given in Table I according to the value of λ. Corresponding similarity criteria are indicated, too.

Table I

Regions of modelling	I	II	III
Value of	$\ll \Lambda$	$\Lambda \gg$	Λ
Similarity criterion	Re	-	U

Region II can be defined experimentally by comparing the results of airway resistance modelling according to Re and U (or u_a) with the real object.

According to Eq. (13), $\varepsilon_I = \lambda \nu$

In the case if $\lambda = 10$ and $\nu = 1.5 \cdot 10^{-5}$ m^2/s, one gets

$$\varepsilon_I = 1.5 \cdot 10^{-4} \ m^2/s \ .$$

It is necessary to determine the limits of the value in natural conditions in order to define the regions of modelling in accordance with these similarity criteria.

The expression $\varepsilon_I / v^* D = \overline{\varepsilon}_I$ does not depend on Re (Ushakov 1975). Thus taking into account

$$v^* = u_a \sqrt{\alpha/\varrho} = u_a \sqrt{\beta}$$

(see Eq. 3) one has

$$\varepsilon_I = \overline{\varepsilon_I} \nu \sqrt{\beta/2} \ \mathrm{Re} \ ,$$

resulting in

$$\lambda = \overline{\varepsilon_I} \sqrt{\beta/2} \ \mathrm{Re} \qquad (14)$$

λ depends linearly on the relative turbulent exchange of the impulse coefficient $\overline{\varepsilon}_I$, on Re, and on the square root of the friction coefficient. This relation may be controlled experimentally for different types of workings. It is necessary to take into account that in general cases λ is a function of the coordinates, if the flow does not change along its length, it is a function of the cross coordinates. The region of model-

ling should be estimated according to the average value of λ . That is why the value of ε_I in Eq. (14) must be accepted as average for the whole flow or for its cross-section.

Figure 1 shows the relation $\lambda(Re)$ with a friction coefficient $\alpha = 24.1 \cdot 10^{-3}$ M s^2/m^4, $\beta = 3.95 \cdot 10^{-2}$ and a turbulent exchange coefficient of the impulse $\varepsilon_I = 2.18 \cdot 10^{-2}$, as arithmetic average from average values of ε_I for two directions through the centre of the cross-section; one of the directions is perpendicular to the roof and floor, the other to the walls of the working.

Figure 2 shows the relation λ (Re) for the model of drift-type working supported by timber with the parameters α and β . Similar relations may be obtained for workings with other types of support.

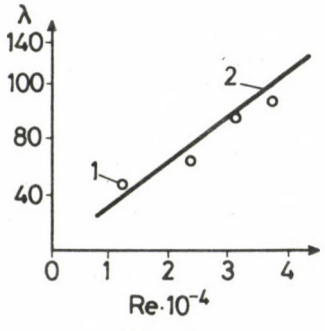

Fig. 1

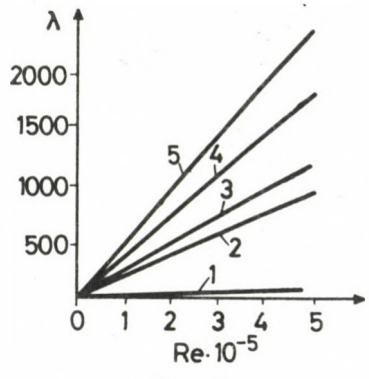

Fig. 2

Fig. 1. The function $\lambda(Re)$ for the model of a drift-type working with a rectangular cross-section; 1 - according to measurements, 2 - according to Eq. (14)

Fig. 2. The function $\lambda(Re, \beta, \alpha)$ for the model of a drift-type working: 1,2,3,4,5 - $\alpha \cdot 10^3$ and $\beta \cdot 10^2$; 3N s^2/m^4 and 0.492; 10N s^2/m^4 and 1.64; 20N s^2/m^4 and 3.28; 35N s^2/m^4 and 5.74; 50N s^2/m^4 and 8.20, respectively

The principle of modelling "by velocity" widens the technical possibilities of modelling, as it does not require a sometimes impracticable increase in the velocity of fluid

motion in the model relatively the object, as in the case of the use of the similarity conditions according to the Reynolds number. The main advantage of the method is, however, that it makes experiments more precise.

REFERENCES

Jones J D, Hinsley F B 1959: Colliery Guardian, 199, No 5131, 31-38.

Shlihting A 1969: Theory of the boundary layer. Moscow, Nauka

Ushakov K Z 1975: Aeromechanics of ventilation flows in mine workings. Moscow, Nedra

Ushakov K Z (ed.-in-chief) 1977: Reference-book in mine ventilation. Moscow, Nedra

Acta Geod. Geoph. Mont. Hung., Vol. 22 (3-4), pp. 461-467 (1987)

FORECASTING OF METHANE EMISSION DYNAMICS WITH COMBINED METHOD

L Szirtes

Information and Computing Services Company for the Mining Industry (BISZT), Tatabánya, Hungary

Efficient and reliable forecasting methods for firedamp prevention are needed for gassy coal mines. Both production control and mine safety underline the importance of effective forecasting because mining of coal is performed at greater and greater depth and this results in constant increase in methane emission into workings. The use of computation intensive algorithms in mine information and dispatching systems became feasible through widespread use of mini and micro computers in coal mines. In a case history various forecasting models are described and evaluated for a gassy coal mine in Hungary. The proposed forecasting methodology can be applied for both short and medium-range computer aided emission control (Szirtes 1984).

Keywords: coal mines; firedamp prevention; forecasting; methane emission

INTRODUCTION. TIME SCALES OF METHANE EMISSION

Both production control and mine safety need efficient and reliable methane emission forecasts in longwall faces of gassy coal mines. Prediction of methane emission is generally performed on three time scales, reflecting three aspects of production and adjacent seam and rock strata interaction:

- Long-term forecasting is based on general description of zones of gas emission. All gassy coal seams and strata lying within the effected zone are considered, and typical forecasts are made for a year ahead. Predictions are made for a whole mine field. Used mainly for mine planning, and only static relations are formulated.
- Medium-term forecasting produces estimates of gas emission on a monthly or weekly basis. Both methods reflect the influence of production rate on gas emission, but only in

weekly estimation is the production variation between working days considered. Medium-term forecasts are used for ventilation and production control.

- Short-term forecasting is based on real-time measurement of methane concentration and of some ventilation parameters. Forecasts are made for some minutes/hours. Direct use in safety and production control.

Both forecasting model structure needed and forecasting error produced are influenced by geologic structure, dimensions, mining methods used in a given coal mine. The relations are well known for static forecasting, where no time variations are considered. A very thorough summary of methods used in Europe was published by Curl (1978). For complicated geology no use of rule-of-thumb methods, or simple equations are possible. The forecasting model developed for the Mecsek coal mines describes the influence of 30 coal seams in 40-55 m neighborhood of a longwall face.

While fairly good estimation is possible for long-term planning, the nature of rock failure, and so the dynamics of gas emission can not be estimated by these methods. A combined method is suggested for monthly forecasting, for modeling the gas dynamics in outlet air concentration measuring production rate at the face. Steps of this combined method:

1. Using geology (stratigraphy), surveying and mining information assumptions are derived on forecasting model structure.
2. Model parameters are estimated using statistically analysed measurement data. Monthly average methane concentration and average production rate data as time series can be used for the estimation.
3. Steps 1 and 2 are repeated until minimum degree model is attained at acceptable error limits.

MODEL DECOMPOSITION AND THE DYNAMICS OF EMISSION

Model development for gas emission can be illustrated using the storage, potentiometer and delay elements of systems dynamics simulation. Storage reflects gas reservoir (coal seam or gassy strata). Potentiometer is needed for modelling the

complex relationship of gas emission from adjacent coal seams and its distance to coal face. The use of storage and potentiometer is well founded by the research in long-term forecasting, but very few has been done on estimation of delay parameters in nonlinear models. It is well known that different potentiometers are needed for different coal mines. The parameters of the potentiometers may change within a coal mine and they may vary with position of the face as well. The degree of gas emission is described within an ellipsoid of influence in most cases. All models use ellipsoids but the parameters are usually not estimated by measured data. A less geometry dependent model was developed by Tarasov in the USSR using several parameters of mine geometry, geology and technology.

DYNAMIC EMISSION MODEL ALTERNATIVES

For delay mechanism determination the notion of transfer function can be borrowed from control engineering. The delay is a function of several variables of a given face e.g. seam thickness, face advance rate, mining methods. It is clear that in most cases the variation in the face advance rate is the only variable which can be controlled for a producing face. For determination of gas emission delays in faces using measurement data two methods can be recommended:

1. Using rock mechanical properties of surrounding rock types, their geometrical parameters and failure characteristics failure-rate-ratios are derived. Simulating the presence of various ratios the best fit (e.g. the smallest absolute error) of measured data on simulated results is searched for.
2. Reaction rates are estimated between production and gas emission using cross correlations of the data. Reaction rates as lags on production data are used in multivariate discrete time models. Using methods of time-series analysis cyclic behavior or trend can also be estimated or eliminated from measured data.

Using either methods a fairly extensive preliminary engineering and statistical data analysis is needed to produce

input for simulation and/or regression analysis. All mining activities, their influence on gas content of seams, effects of degasification are to be considered in producing input data. Analysing the effects of gas drainage a correction is usually needed in measured data, or the amount of gas drained has to be considered in the forecasting model.

A CASE HISTORY

For illustration of the proposed method corrected gas emission data were analysed for István shaft in the Mecsek collieries. All the data from mine surveying, production, ventilation services were acquired and analysed for a period of one year. Monthly gas emission, average daily production rate, volume of gas drained are shown on Fig. 1. Figure 2 gives a summary of forecasting model parameters, fitted corrected gas emission data, relative value of residuals (in %) and the sum of residuals for a 4 parameter regression model using monthly production and three time lags on production for gas emission forecasts. Because of correction in gas emission emission forecasts can be produced using four production rate data and one degasification rate data. Degasification data are needed only for the last month, because gas drained at István shaft effects only neighbouring coal seams (Bánhegyi and Radó 1984).

ENTRY	CORRGAS	2	PROD	1
DRGAS	6			
1	66.7000	45.0000		4.90000
2	117.600	56.0000		30.4000
3	272.000	108.000		54.5000
4	224.700	182.000		91.4000
5	380.800	185.000		94.2000
6	413.300	111.000		110.000
7	198.800	52.0000		87.8000
8	227.300	112.000		56.6000
9	285.800	136.000		84.6000
10	211.000	89.0000		43.0000
11	192.500	64.0000		28.5000
12	129.500	.000000		.000000

Fig. 1. Input data of gas emission forecasting models

NO.	LABEL	VAR	LAG	COEFFICIENT
***	*******	***	***	**********
1	PROD	1	0	.4993482
2	PROD	1	1	1.537733
3	PROD	1	2	-.1400626
4	PROD	1	3	.3640341

ENTRY	FITTED	10 REPROC	11 SUM4
15			
4	265.495	18.1551	84.3345
5	377.506	-.865039	87.6285
6	353.733	-14.4127	147.196
7	236.997	19.2138	185.393
8	187.688	-17.4270	225.005
9	273.262	-4.38700	237.543
10	256.816	21.7139	283.359
11	190.540	-1.01828	285.319
12	135.458	4.60074	291.277

Fig. 2. Model structure and forecasted emission rate for a four parameter model

Effects of gas drainage for longer time periods were not detected.

On Fig. 3. comparative results can be seen for four emission forecasting model structures. Symbol A represents cumulative absolute forecasting error for a 3 parameter regression model using production rate and its 2 previous values. Symbol B depicts results for a 6 parameter model using 3 regression coefficients on production rate and 3 on squared production rate. (Squared production rate is an alternative model independent variable, because some theory on gas emission states a heavy influence of advance rate on emission as well.) Symbol C represents model results for a model using 3 terms for production and 3 for long term simulated (static forecast) emission values. Symbol D stands for cumulative absolute forecasting error of the model in Fig. 2. Symbol E shows results for a 5 parameters model using production rate and 4 lags on it.

Symbols C, D and E represent better models than A or B. Because models marked by symbols C and E use one and two more parameters then model D we have chosen model D for future predictions.

```
SYMBOL A: SERIES   12      SUM1
SYMBOL B: SERIES   13      SUM2
SYMBOL C: SERIES   14      SUM3
SYMBOL D: SERIES   15      SUM4
SYMBOL E: SERIES   16      SUM5

MIN VALUE    43.54      MAX VALUE    417.53     SPACING     7.632

    +++++++++++++++++++++++++++++++++++++++++++++++++++++++++++++
  3 &  B   A                                                  + CDE
  4 C    & D          A                                      + DE
  5 +C    DB E          A                                     +
  6 +       C   B D E          A                            +
  7 +          C B     D E          A                       +
  8 +            CB          &         A                    + DE
  9 +             C  B        &            A                + DE
 10 +                         C  EB  D           A          +
 11 +                           C  E BD             A       +
 12 +                              CE D      B              A
    +++++++++++++++++++++++++++++++++++++++++++++++++++++++++++++
```

Fig. 3. Summary of cumulated absolute forecasting error for five models

After a fairly long engineering and statistical preparatory work model estimation was performed within half a minute on an IBM PC microcomputer, and forecasting took less then a second.

FUTURE RESEARCH NEEDED

Preliminary simulation results indicated that the same method can be used for short-term forecasting as well. Some simulation runs were made using directly measured gas concentration and production rate data. Results indicated that combined data series are needed for return air velocity and barometric pressure as well. Methodology for setting digital filter parameters also has to be elaborated for short-term methane emission forecasts.

REFERENCES

Bánhegyi M, Rado A 1984: Gas outburst problems in the Mecsek

coal mining basin. Paper presented for the Mine Ventilation Congress, Harrogate

Curl ed. 1978: Methane prediction in coal mines. IEA Coal Research, Report Number ICTIS/TR 04, London

Szirtes L 1984: Computer control of mining processes: what is to come from computer and control engineering. Paper presented for the VII. ICAMC, Budapest

BOOK REVIEWS

P O BAUMGARTNER: Jurassic Sedimentary Evolution and Nappe Emplacement in the Argolis Peninsula (Peloponnesus, Greece). (Denkschriften der Schweizerischen Naturforschenden Gesellschaft, Bd. 99), Birkhäuser, Basel, 1985, 111 p., 34 figs., 7 Pls.

The Argolis Peninsula is not large but its geological complexity gives an opportunity to solve many general problems of the Mesozoic stratigraphy and paleogeography of the Mediterranean region. Peter Baumgartner made the best of this opportunity. His work is concise though the studies were very detailed and precise from field-work to X-ray diffractometry and from radiolarian stratigraphy to ophiolite petrography. His conclusions are strictly on the subject though his extensive knowledge and experience reach far beyond the Mediterranean region.

The introductory chapter gives a review of the tectonic units studied (an external Adhami Composite Unit, an internal Dhidhimi-Trapezona Composite Unit and a younger Akros Unit) and of the main results. The section "History of Research" is especially instructive. From this, the reader learns that the German school working previously in the area (Jacobshagen, Bachmann, Risch, etc.) oversimplified the stratigraphy and structure of the Argolis peninsula and lumped together the stratigraphical columns of several, different, superimposed tectonic units. The author followed the ideas of the French school (Dercourt, Vrielynck) in differentiating the Mesozoic nappe structure but he stepped well beyond their results in more precise dating of the important sedimentary and tectonic events (ages of radiolarian cherts in different units; timing of Mesozoic nappe emplacements). This may remind the reader to the fact that good sedimentological and/or tectonic analysis is impossible without precise krono(=bio)stratigraphy.

Chapter B is the backbone of the work; it deals with the stratigraphy and paleogeographic evolution of the study area.

The Basal Sequences mirror an evolution of a passive continental margin from Late Triassic to mid-Late Jurassic. The deepest formation is the Pantokrator Limestone with characteristic shallow-water carbonate platform development. Its age is Late Triassic in the Adhami Unit and in the most part of the Dhidhimi-Trapezone Unit but in a restricted region the platform conditions remained stable up to the Middle Liassic. The subsequent pelagic limestones and Rosso Ammonitico show considerable variation in space. In the Adhami Unit the base of the pelagic sequence is associated with deep neptunian dykes and the Rosso Ammonitico is characterized by pelagic stromatolites. In the western part of the Dhidhimi-Trapezona Unit the pelagic sequence is extremely condensed and is underlain by "young" (Middle Liassic) platform limestones. In the eastern (internal) part the sequence begins with thick, crinoidal and cherty, redeposited limestones (Siniais Limestones) or, in some places, with slump breccias and limestone turbidites. From the Oxfordian (or Callovian?) onwards radiolarites were laid down everywhere (Aiyos Nikolaos Chert in the Adhami Unit and Angelokastron Chert in the Dhidhimi-Trapezone Unit). Suddenly, within the Kimmeridgian, coarse detrital sediments follow (Kandhia Breccia, Potami Formation) with chrome spinel and ophiolite detritus. They appear earlier and contain more ophiolite fragments in the internal than in the external units; this points to an ophiolite nappe emplacement prograding from the east to the west during Kimmeridgian times.

The Overlying Late Jurassic Nappes are partly sedimentary partly ophiolitic in composition. The Asklipion Unit consists of Middle Triassic

to Middle Jurassic pelagic limestones (thick and cherty: Adhami Limestones - condensed and ammonitic: Asklipion Limestones). In the Middle Jurassic (Bathonian) radiolarites (Koliaki Chert) developed. In the Early Kimmeridgian clastic formations rich in ophiolite detritus follow and close the succession. On the basis of these facts, the Asklipion Unit is placed palinspastically to a more internal position than the Basal Sequences. The Ophiolites form the highest nappes and the most internal paleogeographic unit. Their Jurassic age is based on intercalated radiolarites. Incorporated exotic blocks imply vicinity to a continental margin.

One of the most substantial improvements of Baumgartner's work is the timing of events by biostratigraphy. (This means first of all radiolarian biostratigraphy of which he is a well-known expert.) Yet, the only shortcoming worth mentioning lies in the field of biostratigraphy. Notably, the age of deposition of pelagic limestone series of the Basal Sequences is delimited from bottom and top by fossils from the Pantokrator Limestones and from the Angelokastron and Aiyos Nikolaos Cherts, respectively. Direct biostratigraphical evidence is, however, missing or scarce from the pelagic limestones themselves therefore the stratigraphic gaps (cf. Fig. 53) are of unknown extent or only supposed. This remark does not touch Baumgartner's merits since collecting ammonoids and other megafossils is a tiresome and time-consuming task in itself. However, it points to something what remained to be done.

Chapter C is devoted to ophiolite petrography and geochemistry. This and the next chapter on chrome spinel and clay mineralogy are of appendix character, nevertheless, they are profusely and marvellously illustrated and provide substantial conclusions. From the acknowledgements it appears clearly that the author was helped by numerous colleagues in carrying out the mineralogical and geochemical studies, yet the reviewer is captivated by this versatility, unusual among stratigraphers.

In the Conclusions the general evolution, the palinspastic position and the emplacement history of different units are given accompanied by a very informative and fascinating cartoon (Plate 7). The author's brilliant way of thinking about Mesozoic paleogeography clearly reflects his fruitful contact with Daniel Bernoulli (Basel) who is among the giants of the subject.

The book is wonderful in all respects. The cover pictures are spectacular and witty. The figures (photographs and line drawings) are of excellent quality just as the printing of the text. All these harmonize well with the concise, intelligent and genuine content.

Baumgartner's work should be read by everyone working on Mesozoic stratigraphy and sedimentology in the Mediterranean region.

A Vörös

SVEN MAALØE: Principles of Igneous Petrology, Springer Verlag, 1985, p 371, figs 291

The theory of magma origin based on plate-tectonics and the rapid development of the analysis of trace elements and of isotope-geochemistry in the last 25 years revealed a data amount and produced theoretical approximations in magma petrology which enables a quantitative description of the process of origin and development of magmas. This needs a physico-chemical and thermodynamical approximation in petrology. The handbook and compendium, respectively, applies this type of approximation and is thus the most outstanding petrology written in recent years.

One of the most useful parts of the book is the presentation of the theory of phase-diagrams of moner, bimer, terner and multicomponent systems, always connected to examples taken from the nature.

The Chapter discussing systems with gas-content converts the new experimental data of petrology emphasizing the study of rock-melts containing water and CO_2. Author spends an extra chapter to the role of oxigene fugacity in the fractional crystallization of the magma and in the determination of paleothermobarometric conditions of the magma.

The main point of the coming into being and development of magmas is enlightened in the chapters discussing partial melting and fractional crystallization. The first explains the composition of primary magmas showing the process on the example of partial melting of lherzolites and granites. Author shows here the most modern discrimination method based on geochemistry.

In the chapter dealing with magma kinetics one gets a picture about the diffusive processes taking place in gas, liquid, and solid phase, about the thermodynamic conditions of undercooling, about crystal growth and about the importance of the crystal-habit in the revealing of magma crystallization processes.

In the chapter: Magma dynamics one can read about the connection between density and viscosity, and between temperature-pressure and chemical behaviour, about the gravitational sinking of phenocrystals, about the thermodynamics of convection currents in magmas, about the theory of mantle-diapir-origin and about the calculation of upward penetration of magmas. The dynamics of laminar and turbulent lava-flow is described here, too.

In the chapter dealing with isotope geology a review is given about radiogene age-determination and about the application of strontium-, neodium-, and samarium isotopes as well as the isotope combinations of inert gases for the solution of magma-genetical problems. The changes of oxigene isotopes enables to trace the cooling of the magma and thus to trace the path of magma in the crust.

A list of nearly 500 references from the most up-to-date topics completes the book.

The book is recommended to geologists and students, but it can be useful for experts in silikate-chemistry, too.

T Póka

T BÁLDI: Mid-Tertiary Stratigraphy and Palaeogeographic Evolution of Hungary. Akadémiai Kiadó, Budapest, 1986, 201 p., 95 figs, 16 tables, 134 photographs on 11 plates. ISBN 963 05 3945 4, 290,- Ft (for socialist countries), 24,- US $ (rest of the world)

Professor Tamás Báldi was among the few geologists, who realized at the beginning of the 1980s, that the Palaeogene history of the Carpathian-Pannonian region cannot be understood in the present-day tectonic framework; and certainly he was the first one, who draw mobilistic palaeogeographic reconstructions with solid stratigraphic background. To achieve these ambitious aims, he has organized the activities of a team of specialists of calcareous nannoplankton, dinoflagellates, higher plants, foraminifers, ostracods, and of sedimentologists, petrologists, magnetostratigraphers, etc. He himself, as an internationally well-known expert on molluscs, provided the palaeoecological data and directed the investigations towards a large-scale synthesis. This book presents the final results of more than

twenty years' research work, while details have been published in dozens of journal papers.

The first half of the book contains the stratigraphic description of Upper Eocene to Lower Miocene formations in the Transdanubian Midmountains and Northern Hungary, with extensive listings of the mollusc fauna. A palaeoecological evaluation and palaeobiogeographical characters (e.g. Boreal, Paratethyan, Mediterranean, or endemic) of the altogether 100 bivalve and gastropod genera are given. The descriptions are illustrated by sediment distribution maps and by outcrop and subcrop profiles. Special emphasis is laid on biological and sedimentological events at the boundary between the Kiscellian and Egerian regional stages and at the Oligocene/Miocene boundary.

After giving the stratigraphic data with detailed facies interpretations, the conclusions on tectonics and palaeogeography are drawn in the second chapter. A series of sediment distribution maps, and another on the tectonic framework displays the complicated history of the region from Middle Eocene to Earliest Miocene, when a general SW to NE displacement of several crustal fragments occurred, leading to the formation of the sinuous Carpathian arc. The geological part is closed by a review of the surrounding regions: four small-scale palaeogeographic maps display the positions of seaways and lands in a wide belt from the German Plain to the Caspian Sea.

While the final conclusions are embedded in their regional context, an introductory chapter providing geographical and geological overview would have been useful for those who are unfamiliar with the Carpathian-Pannonian region.

An appendix contains brief descriptions of 6 mollusc species from the Lower Oligocene Tard Clay and of 52 taxa from the Middle Oligocene Kiscell Clay, supplemented by 134 photographs on 11 plates. Heavily compacted pelitic sediments are not the best media for preserving minute details of the embedded fossils: the photographer, L Klinda can only be praised for the excellent results of his patient work.

Some comments have to be mentioned on the form of the book. The octavo format is good, the linen binding with the nice dust-cover will stand any kind of treatment. The layout is fine and printer's errors are few. However, a major drawback of the book is that all 95 line drawings are piled up at the end of the volume, while tables listing dozens of mollusc taxa are embedded in the text. This action of the publisher, applied in the Hungarian edition also, is probably explained by lower production costs. However, a publisher who wants to get results in the international book market, cannot allow himself this kind of negligence.

The publication of Báldi's monograph is a significant gain to the understanding of a major epoch in the history of the Carpathian-Pannonian region. The book can be recommended to those, who are interested in the Palaeogene and Miocene history of SE-Europe, and to those, who study Tertiary molluscs.

M Kázmér

G BRANDSTÄTTER: Die "Very Long Baseline Interferometry" und ihre geodätische Anwendung. Mitteilungen der Geodätischen Institute der Technischen Universität Graz. Folge 50, Graz 1985, p. 22, öS 50.-

In spite of the fact that Brandstätter's lecture had been delivered at

the Technical University Braunschweig in the Year 1971, its actuality remained in these 15 years due to a rapid development of satellite technics, by the introduction of the base interferometry and of the GPS satellites.

The paper prepared from this lecture calls attention to the uptodate technical solution of the very long baseline interferometry (VLBI), it gives the physical principles by presenting the equation for the additive and crosscorrelated superposition of the signals and deduces the equation for the determination of the numbers of the interference stripes firstly for the monochromatic radiointerferometry, then for the actual frequency range. At the end of the publication the author enumerates the possibilities of the method in geodesy: in geodynamics, in global triangulation and in national surveys.

Gy Szádeczky-Kardoss

treble underlining: bold-face italics
red underlining: Greek letters
green underlining: script letters

Rules for mathematical-physical notations:

trigonometric, logarithmic, analytic symbols, symbols for units and functions are in roman type (not underlined)

letter symbols in mathematical and physical formulas, scalars, and subscripts of algebraic and physical quantities are in italics (underlined)

vectors, matrices, operators in probability theory are in bold-face roman type (double underlining) tensors, operators and some special functions are in script letters (green underlining). These cannot be bold.

Greek letters (red underlining) cannot be bold or extra bold type (thus they cannot be used for vectors or tensors)

void upper lines e.g. for vectors

avoid possible confusion between o (letter) and 0 (zero), l (letter) and 1 (one), ν (Greek nu) and v.u. (letters) etc.

explain ambiguous or uncommon symbols by making marginal notes in pencil

be careful about superscripts and subscripts

formulae must be numbered consecutively with the number in parentheses to the right of the formula. References in text to the equations may then usually be made by the number in parenthesis. When the word equation is used with a number, it is to be abbreviated. Eq. or Eqs in the plural the International System of Units (SI) should be used.

Authors are liable for the cost of alteration in the *proofs.* It is, therefore, the responsibility of the author to check the text for errors of facts before submitting the paper for publication.

3. *References* are accepted only in the Harvard system. Citations in the text should be as:

... (Bomford 1971) ... or Bomford (1971)

... (Brosche and Sündermann 1976) ...

... (Gibbs et al. 1976b) ...

The list of references should contain names and initials of all authors (the abbreviation et al. is not accepted here); for *journal articles* year of publication, the title of the paper, title of the journal abbreviated, volume number, first and last page.

For *books* or *chapters in books,* the title is followed by the publisher and place of publication.

All items must appear both in the text and references.

Examples:

Bomford G 1971: Geodesy. Clarendon Press, Oxford

Brosche P, Sündermann J 1976: Effects of oceanic tides on the rotation of the earth. Manuscript. Univ. of Bonn

Buntebarth G 1976: Temperature calculations on the Hungarian seismic profile-section NP–2. In: *Geoelectric and Geothermal Studies (East-Central Europe. Soviet Asia), KAPG Geophysical Monograph.* Akadémiai Kiadó, Budapest, 561–566.

Gibbs N E, Poole W G, Stockmeyer P K 1976a: An algorithm for reducing the bandwidth and profile of a sparse matrix. *SIAM J. Number. Anal.,* 13, 236–250.

Gibbs N E, Poole W G, Stockmeyer P K 1976b: A comparison of several bandwidth and profile reduction algorithms. *ACM Trans. on Math. Software.* 2, 322–330.

Szarka L 1980: Potenciáltérképezés analóg modellezéssel (Analogue modeling of potential mapping). *Magyar Geofizika,* 21, 193–200.

4. *Footnotes* should be typed on separate sheets.

5. *Legends* should be short and clear. The place of the tables and figures should be indicated in the text, on the margin.

6. *Tables* should be numbered serially with Roman numerals. Vertical lines are not used.

All the illustrations should contain the figure number and author's name in pencil on the reverse.

Figures will be redrawn. Therefore the most important point is clearness of the figures, even pencil-drawings are accepted (with a duplicate).

Photographs and *half-tone* illustrations should be sharp and well contrasted.

If a specific reduction or enlargement is required, please indicate this in blue pencil on the figure.

The editors will send information to the first author about the *arrival* and acceptance of the papers. A galley proof is also sent to the first author for *correction.* Hundred *offprints* are supplied free of charge.

Periodicals of the Hungarian Academy of Sciences are obtainable at the following addresses:

AUSTRALIA
C.B.D. LIBRARY AND SUBSCRIPTION SERVICE
Box 4886, G.P.O., *Sydney N.S.W. 2001*
COSMOS BOOKSHOP, 145 Ackland Street
St. Kilda (Melbourne), Victoria 3182

AUSTRIA
GLOBUS, Hochstädtplatz 3, *1206 Wien XX*

BELGIUM
OFFICE INTERNATIONAL DES PERIODIQUES
Avenue Louise, 485, *1050 Bruxelles*
E. STORY-SCIENTIA P.V.B.A.
P. van Duyseplein 8, *9000 Gent*

BULGARIA
HEMUS, Bulvar Ruszki 6, *Sofia*

CANADA
PANNONIA BOOKS, P.O. Box 1017
Postal Station "B", *Toronto, Ont. M5T 2T8*

CHINA
CNPICOR, Periodical Department, P.O. Box 50
Peking

CZECHOSLOVAKIA
MAD'ARSKA KULTURA, Národni třida 22
115 66 Praha
PNS DOVOZ TISKU, Vinohradská 46, *Praha 2*
PNS DOVOZ TLAČE, *Bratislava 2*

DENMARK
EJNAR MUNKSGAARD, 35, Nørre Søgade
1370 Copenhagen K

FEDERAL REPUBLIC OF GERMANY
KUNST UND WISSEN ERICH BIEBER
Postfach 46, *7000 Stuttgart 1*

FINLAND
AKATEEMINEN KIRJAKAUPPA, P.O. Box 128
00101 Helsinki 10

FRANCE
DAWSON-FRANCE S.A., B.P. 40, *91121 Palaiseau*
OFFICE INTERNATIONAL DE DOCUMENTATION ET LIBRAIRIE, 48 rue Gay-Lussac
75240 Paris, Cedex 05

GERMAN DEMOCRATIC REPUBLIC
HAUS DER UNGARISCHEN KULTUR
Karl Liebknecht-Straße 9, *DDR-102 Berlin*

GREAT BRITAIN
BLACKWELL'S PERIODICALS DIVISION
Hythe Bridge Street, *Oxford OX1 2ET*
BUMPUS, HALDANE AND MAXWELL LTD.
Cowper Works, *Olney, Bucks MK46 4BN*
COLLET'S HOLDINGS LTD., Denington Estate,
Wellingborough, Northants NN8 2QT
WM DAWSON AND SONS LTD., Cannon House
Folkstone, Kent CT19 5EE
H. K. LEWIS AND CO., 136 Gower Street
London WC1E 6BS

GREECE
KOSTARAKIS BROTHERS INTERNATIONAL BOOKSELLERS, 2 Hippokratous Street, *Athens-143*

HOLLAND
FAXON EUROPE, P.O. Box 167
1000 AD Amsterdam
MARTINUS NIJHOFF B. V.
Lange Voorhout 9–11, *Den Haag*
SWETS SUBSCRIPTION SERVICE
P.O. Box 830, 2160 Sz Lisse

INDIA
ALLIED PUBLISHING PVT. LTD.
750 Mount Road, *Madras 600002*
CENTRAL NEWS AGENCY PVT. LTD.
Connaught Circus, *New Delhi 110001*
INTERNATIONAL BOOK HOUSE PVT. LTD.
Madame Cama Road, *Bombay 400039*

ITALY
D. E. A., Via Lima 28, *00198 Roma*
INTERSCIENTIA, Via Mazzé 28, *10149 Torino*
LIBRERIA COMMISSIONARIA SANSONI
Via Lamarmora 45, *50121 Firenze*
SANTO VANASIA, Via M. Macchi 58
20124 Milano

JAPAN
KINOKUNIYA COMPANY LTD.
Journal Department, P.O. Box 55
Chitose, *Tokyo 156*
MARUZEN COMPANY LTD., Book Department
P.O. Box 5050 Tokyo International, *Tokyo 100-31*
NAUKA LTD., Import Department
2-30-19 Minami Ikebukuro, Toshima-ku, *Tokyo 171*

KOREA
CHULPANMUL, *Phenjan*

NORWAY
TANUM-TIDSKRIFT-SENTRALEN A.S.
Karl Johansgata 43, *1000 Oslo*

POLAND
WĘGIERSKI INSTYTUT KULTURY
Marszalkowska 80, *00-517 Warszawa*
CKP I W, ul. Towarowa 28, *00-958 Warszawa*

ROUMANIA
D. E. P., *Bucuresti*
ILEXIM, Calea Grivitei 64–66, *Bucuresti*

SOVIET UNION
SOYUZPECHAT — IMPORT, *Moscow*
and the post offices in each town
MEZHDUNARODNAYA KNIGA, *Moscow G-200*

SPAIN
DIAZ DE SANTOS Lagasca 95, *Madrid 6*

SWEDEN
ESSELTE TIDSKRIFTSCENTRALEN
Box 62, *101 20 Stockholm*

SWITZERLAND
KARGER LIBRI AG, Petersgraben 31, *4011 Basel*

USA
EBSCO SUBSCRIPTION SERVICES
P.O. Box 1943, *Birmingham, Alabama 35201*
F. W. FAXON COMPANY, INC.
15 Southwest Park, *Westwood Mass. 02090*
MAJOR SCIENTIFIC SUBSCRIPTIONS
1851 Diplomat, P.O. Box 819074,
Pallas, Tx. 75381-9074
READ-MORE PUBLICATIONS, INC.
140 Cedar Street, *New York, N. Y. 10006*

YUGOSLAVIA
JUGOSLOVENSKA KNJIGA, Terazije 27, *Beograd*
FORUM, Vojvode Mišića 1, *21000 Novi Sad*